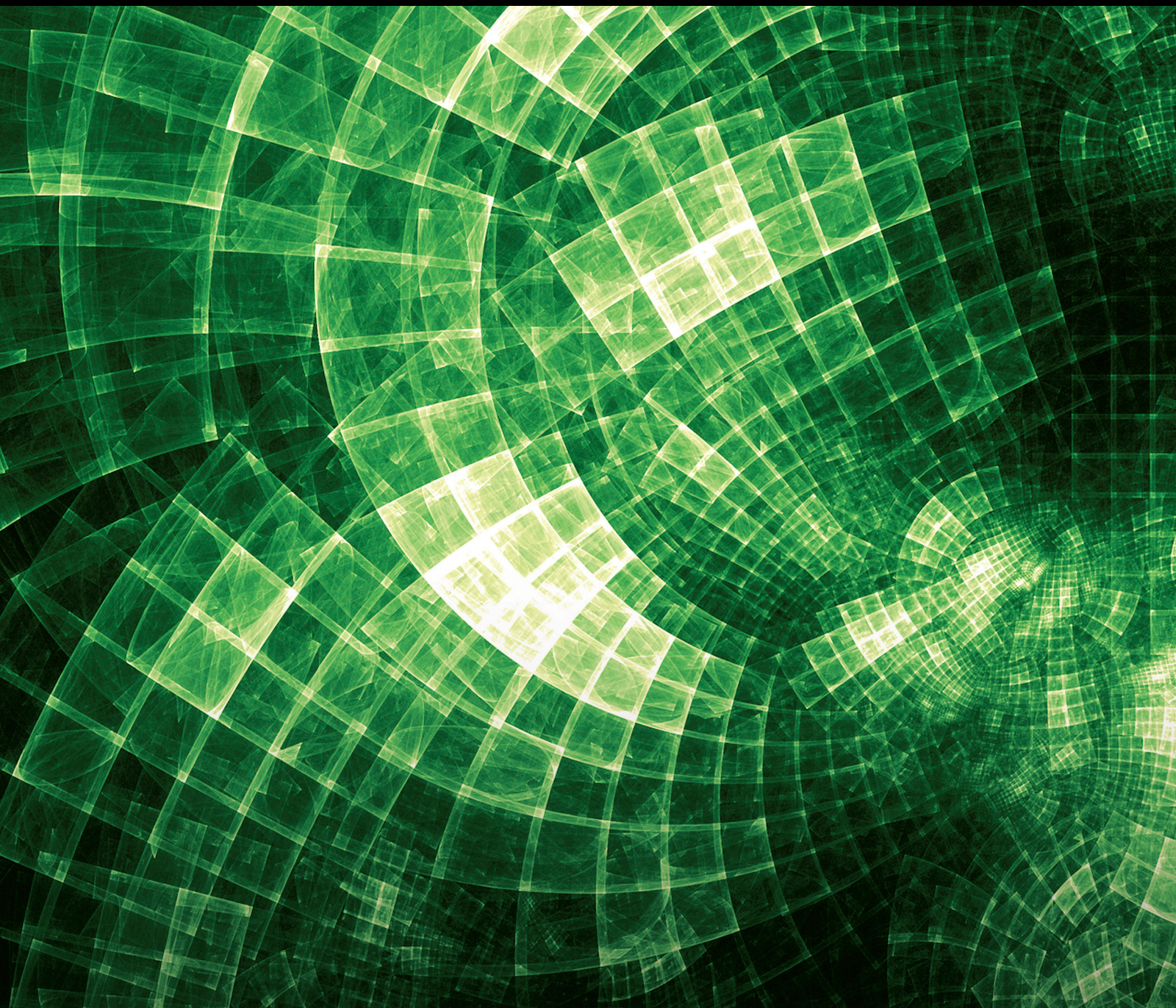


Nonlinear Hybrid Systems and Their Applications

Lead Guest Editor: Watcharaporn Cholamjiak

Guest Editors: Suhel Ahmad Khan, Rehan Ali, and Ovidiu Bagdasar





Nonlinear Hybrid Systems and Their Applications

Nonlinear Hybrid Systems and Their Applications

Lead Guest Editor: Watcharaporn Cholamjiak

Guest Editors: Suhel Ahmad Khan, Rehan Ali, and
Ovidiu Bagdasar



Copyright © 2023 Hindawi Limited. All rights reserved.

This is a special issue published in "Journal of Mathematics." All articles are open access articles distributed under the Creative Commons Attribution License, which permits unrestricted use, distribution, and reproduction in any medium, provided the original work is properly cited.

Chief Editor

Jen-Chih Yao, Taiwan

Algebra

SEÇİL ÇEKEN , Turkey
Faranak Farshadifar , Iran
Marco Fontana , Italy
Genni Fragnelli , Italy
Xian-Ming Gu, China
Elena Guardo , Italy
Li Guo, USA
Shaofang Hong, China
Naihuan Jing , USA
Xiaogang Liu, China
Xuanlong Ma , China
Francisco Javier García Pacheco, Spain
Francesca Tartarone , Italy
Fernando Torres , Brazil
Zafar Ullah , Pakistan
Jiang Zeng , France

Geometry

Tareq Al-shami , Yemen
R.U. Gobithaasan , Malaysia
Erhan Güler , Turkey
Ljubisa Kocinac , Serbia
De-xing Kong , China
Antonio Masiello, Italy
Alfred Peris , Spain
Santi Spadaro, Italy

Logic and Set Theory

Ghous Ali , Pakistan
Kinkar Chandra Das, Republic of Korea
Jun Fan , Hong Kong
Carmelo Antonio Finocchiaro, Italy
Radomír Halaš, Czech Republic
Ali Jaballah , United Arab Emirates
Baoding Liu, China
G. Muhiuddin , Saudi Arabia
Basil K. Papadopoulos , Greece
Musavarah Sarwar, Pakistan
Anton Setzer , United Kingdom
R Sundareswaran, India
Xiangfeng Yang , China

Mathematical Analysis

Ammar Alsinai , India
M.M. Bhatti, China
Der-Chen Chang, USA
Phang Chang , Malaysia
Mengxin Chen, China
Genni Fragnelli , Italy
Willi Freeden, Germany
Yongqiang Fu , China
Ji Gao , USA
A. Ghareeb , Egypt
Victor Ginting, USA
Azhar Hussain, Pakistan
Azhar Hussain , Pakistan
Ömer Kişi , Turkey
Yi Li , USA
Stefan J. Linz , Germany
Ming-Sheng Liu , China
Dengfeng Lu, China
Xing Lü, China
Gaetano Luciano , Italy
Xiangyu Meng , USA
Dimitri Mugnai , Italy
A. M. Nagy , Kuwait
Valeri Obukhovskii, Russia
Humberto Rafeiro, United Arab Emirates
Luigi Rarità , Italy
Hegazy Rezk, Saudi Arabia
Nasser Saad , Canada
Mohammad W. Alomari, Jordan
Guotao Wang , China
Qiang Wu, USA
Çetin YILDIZ , Turkey
Wendong Yang , China
Jun Ye , China
Agacik Zafer, Kuwait

Operations Research

Ada Che , China
Nagarajan Deivanayagam Pillai, India
Sheng Du , China
Nan-Jing Huang , China
Chiranjibe Jana , India
Li Jin, United Kingdom
Mehmet Emir Koksal, Turkey
Palanivel M , India

Stanislaw Migorski , Poland
Predrag S. Stanimirović , Serbia
Balendu Bhooshan Upadhyay, India
Ching-Feng Wen , Taiwan
K.F.C. Yiu , Hong Kong
Liwei Zhang, China
Qing Kai Zhao, China

Probability and Statistics

Mario Abundo, Italy
Antonio Di Crescenzo , Italy
Jun Fan , Hong Kong
Jiancheng Jiang , USA
Markos Koutras , Greece
Fawang Liu , Australia
Barbara Martinucci , Italy
Yonghui Sun, China
Niansheng Tang , China
Efthymios G. Tsionas, United Kingdom
Bruce A. Watson , South Africa
Ding-Xuan Zhou , Hong Kong

Contents

Modeling the Spread of COVID-19 Using Nonautonomous Dynamical System with Simplex Algorithm-Based Optimization for Time-Varying Parameters

Kevin Yotongyos  and Somchai Sriyab 






Research Article (12 pages), Article ID 6156749, Volume 2023 (2023)

Solvability of the System of Extended Nonlinear Mixed Variational-Like Inequalities and Proximal Dynamical System

Iqbal Ahmad  and Mijanur Rahaman 


Research Article (25 pages), Article ID 7414514, Volume 2023 (2023)

On New Solutions of Fuzzy Hybrid Differential Equations by Novel Approaches

Prasantha Bharathi Dhandapani , Jayakumar Thippan , Bundit Unyong , R. Vadivel , and P. Hammachukiattikul 

Research Article (18 pages), Article ID 7865973, Volume 2023 (2023)

Convergence Analysis of Two Parallel Methods for Common Variational Inclusion Problems Involving Demicontractive Mappings

Thanasak Mouktonglang, Kanyuta Poochinapan, Pariwate Varnakovida, Raweerote Suparatulorn , and Sompop Moonchai


Research Article (19 pages), Article ID 1910411, Volume 2023 (2023)

Bifurcations in a Plant-Pollinator Model with Multiple Delays

Long Li , Yanxia Zhang , Jianfei Yao, and Xiuxing Wu



Research Article (21 pages), Article ID 9950187, Volume 2023 (2023)

Mann Hybrid Deepest-Descent Extragradient Method with Line-Search Process for Hierarchical Variational Inequalities for Countable Nonexpansive Mappings

Yun-Ling Cui, Lu-Chuan Ceng , Fang-Fei Zhang, Liang He, Jie Yin, Cong-Shan Wang, and Hui-Ying Hu





Research Article (18 pages), Article ID 6177912, Volume 2023 (2023)

Novel Approximations to the Damped Parametric Driven Pendulum Oscillators

Weaam Alhejaili, Alvaro H. Salas , and S. A. El-Tantawy 


Research Article (14 pages), Article ID 6294798, Volume 2023 (2023)

An Efficient Iterative Algorithm for Solving the Split Feasibility Problem in Hilbert Spaces Applicable in Image Deblurring, Signal Recovering, and Polynomiography

Lanchakorn Kittiratanawasin , Damrongsak Yambangwai , Chonjaroen Chairatsiripong , and Tanakit Thianwan 




Research Article (15 pages), Article ID 4934575, Volume 2023 (2023)

Oblique Flow of Shear Thinning Fluid through an Absorptive Radiative Medium with Hall Effect

S. Rana, K. Mahmud, R. Mehmood, and M. M. Bhatti 



Research Article (16 pages), Article ID 3210794, Volume 2023 (2023)

New Existence and Stability Results for $[\psi, \omega]$ -Caputo–Fabrizio Fractional Nonlocal Implicit Problems

Mohammed S. Abdo , Wafa Shammakh , and Hadeel Z. Alzumi 

Research Article (11 pages), Article ID 6123608, Volume 2023 (2023)

Comparative Analysis of the Time-Fractional Black–Scholes Option Pricing Equations (BSOPE) by the Laplace Residual Power Series Method (LRPSM)

Muhammad Imran Liaqat  and Eric Okyere 

Research Article (18 pages), Article ID 6092283, Volume 2023 (2023)

On a Mathematical Model of Tumor-Immune Interaction with a Piecewise Differential and Integral Operator

Shahram Rezapour , Chernet Tuge Deressa , Robert G. Mukharlyamov, and Sina Etemad 

Research Article (18 pages), Article ID 5075613, Volume 2022 (2022)

Research Article

Modeling the Spread of COVID-19 Using Nonautonomous Dynamical System with Simplex Algorithm-Based Optimization for Time-Varying Parameters

Kevin Yotongyos  and Somchai Sriyab 

Department of Mathematics, Faculty of Science, Chiang Mai University, Chiang Mai, Thailand

Correspondence should be addressed to Somchai Sriyab; somchai.sriyab@gmail.com

Received 5 October 2022; Revised 4 July 2023; Accepted 20 July 2023; Published 9 August 2023

Academic Editor: Francisco J. Garcia Pacheco

Copyright © 2023 Kevin Yotongyos and Somchai Sriyab. This is an open access article distributed under the Creative Commons Attribution License, which permits unrestricted use, distribution, and reproduction in any medium, provided the original work is properly cited.

The SIRDV (Susceptible, Infected, Recovered, Death, Vaccinated) compartmental model along with time-varying parameters is used to model the spread of COVID-19 in the United States. Time-varying parameters account for changes in transmission rates, people's behaviors, safety precautions, government regulations, the rate of vaccinations, and also the probabilities of recovery and death. By using a parameter estimation based on the simplex algorithm, the system of differential equations is able to match real COVID-19 data for infections, deaths, and vaccinations in the United States of America with relatively high precision. Autoregression is used to forecast parameters in order to forecast solutions. Van den Driessche's next-generation approach for basic reproduction number agrees well across the entire time period. Analyses on sensitivity and elasticity are performed on the reproduction number with respect to transmission, exit, and natural death rates in order to observe the changes from a small change in parameter values. Model validation through the Akaike Information Criterion ensures that the model is suitable and optimal for modeling the spread of COVID-19.

1. Introduction

The Kermack–McKendrick SIR-type model and its variants have become one of the most useful tools for modeling the spread of infectious diseases. Much research has been done on exploring the capabilities and extensions of SIR-type models through applications in many infectious diseases [1]. The SIR and SEIR model variants are commonly used to analyze the spread of infectious diseases in population. The SIR model divides the population into three compartments: Susceptible (S), Infected (I), and Recovered (R). It assumes that individuals can be categorized into one of these compartments, with recovered individuals gaining lifelong immunity. The model tracks the transitions between compartments, such as susceptible individuals becoming infected and infected individuals recovering. The SEIR model expands on this by adding an Exposed (E)

compartment to represent individuals in the incubation period. It accounts for the fact that individuals can transmit the infection before showing symptoms [2]. Both models help researchers understand disease dynamics, evaluate interventions, and make predictions. While these models simplify real-world complexities, they provide valuable insights into how diseases spread and can inform public health strategies.

Due to COVID-19, mathematical epidemiology, particularly the use of the SIR model, has gained popularity and is used by many researchers throughout the world who are interested in studying the topic [3–13]. Since COVID-19 is a disease with a latent period, some include the exposed compartment in the SIR model [2]. SEIR models are also suitable and popular amongst epidemiologists to study the outbreak of COVID-19 in different countries and regions [8]. On December 31, 2020, WHO issues its first emergency

use validation for a COVID-19 vaccine [14]. The vaccinated compartment, along with other compartments such as quarantined and death, is added to the SEIR or SIR model [15]. However, while the models previously mentioned are able to simulate and match real COVID-19 data for a relatively short span of time of around a few weeks to months, they fail to compare to the data over a long period of time due to many factors changing and affecting the disease. These models often assume constant, time-independent parameters for transmission, death, and recovery rates, which would be sufficient for a short time span; however, it is not realistic due to the changes in safety regulations set by the government, the behavior of people, the ability to cure COVID-19 patients, and the rate at which people are getting vaccinated.

There are several publications with similar interests in modeling the spread of COVID-19 over a long period of time using varying parameters. An example of a model using time-varying parameters for a longer time span include Nastasi's use of nine different time-dependent transmission frequency parameter values throughout the span of 400 days in order to account for different policy measures in Great Britain and Israel [16]. Similarly, Girardi and Gaetan apply the concept of time-varying parameters to the transmission rate, which is able to qualitatively describe the number of cases over the span of several months in three different countries [17]. Another research explores the same notion of time-varying parameters in the sense of parameter estimation through deep learning on the transmission rate and deceased rate [18]. Furthermore, a study involving the estimation of the time-varying reproduction number has been done based on various cities in China [19]. From these works, it can be seen that the time-varying parameters are what make SIR-type models capable of modeling COVID-19 over a longer period of time, accounting for changes that affect the spread of the disease.

The objective of this research is to use an SIRDV model to match the United State's real COVID-19 data with high precision. The compartments compared with real data are infected (I), death (D), and vaccinated (V). In order to achieve high precision, this model varies the transmission rate β , death probability p , and vaccination rates σ on a daily basis. The method used for parameter estimation is developed based on MATLAB's *fminsearch* function and the simplex algorithm. Specifically, the *fminsearch* function in MATLAB utilizes the Nelder–Mead simplex algorithm, a derivative-free optimization method, to find the minimum value of a given function. It constructs a simplex in the parameter space, iteratively updating its vertices based on function evaluations, aiming to converge towards the minimum. *fminsearch* is particularly useful for optimizing functions without readily available derivative information or in cases where computing derivatives is challenging. Since the simplex algorithm is lightweight and fast, all three parameters with over 800 final values each after 10 attempts of optimization are able to be obtained in under 6 minutes. The solutions are plotted against real active cases data from Worldometer [20], deaths, and fully vaccinated people on Our World in Data [21].

The parameters obtained by the method are used to compute time-varying basic reproduction numbers and are compared to reproduction rates presented by Our World in Data [21]. Sensitivity analysis is performed by day since different parameter values yield different values for sensitivity. Elasticity values are calculated in order to observe the basic reproduction numbers' response to each parameter. Error analysis is performed, and Akaike Information Criterion (AIC) values are also computed on a daily basis in order to show that the model is indeed valid when compared to similar models [22].

2. Model

The constructed SIRDV model is similar to a typical SIR-type model, with the same compartments being susceptible (S), infected (I), and recovered (R); however, with the addition of deaths (D) due to COVID-19 and vaccinated (V), the infected class has the same exit rate for recovery and death, with the difference being the death probability p . It is allowed for recovered people to become susceptible again at the rate of α and for fully vaccinated people to become infected, but with a probability factor of r . The diagram and the nonlinear differential equation for the SIRDV model are represented in Figure 1 and equations (1)–(5), respectively.

$$\frac{dS}{dt} = \mu N - \frac{\beta SI}{N} - (\sigma + \mu)S + \alpha R, \quad (1)$$

$$\frac{dI}{dt} = \frac{\beta SI}{N} + r \frac{\beta VI}{N} - (\gamma + \mu)I, \quad (2)$$

$$\frac{dR}{dt} = (1 - p)\gamma I - (\alpha + \mu)R, \quad (3)$$

$$\frac{dD}{dt} = p\gamma I. \quad (4)$$

When the vaccinated compartment is considered, there are two differential equations used for vaccinations, (5) and (6). When optimizing for compartments other than V , equation (5) is used. Since the vaccination data are only a count of who has received the vaccine (not accounting for people who are infected or died after the vaccination), equation (6) must be used for optimizing the vaccination compartment. Equation (6) is a modification of equation (5), where all negative terms denoting the population exiting the vaccination compartment are omitted.

$$\frac{dV}{dt} = -r \frac{\beta VI}{N} + \sigma S - \mu V, \quad (5)$$

$$\frac{dV}{dt} = \sigma S. \quad (6)$$

The term N denotes the current population, in which only the alive population takes into account, thus excluding people in compartment D .

$$N = S + I + R + V. \quad (7)$$

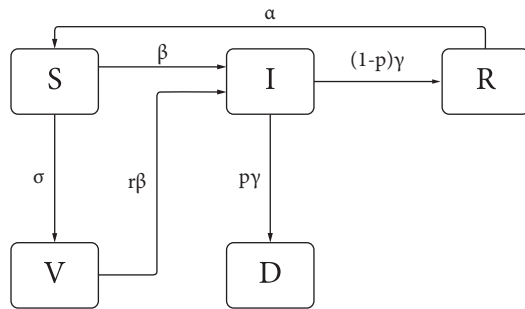


FIGURE 1: Diagram of the SIRDV model.

3. Parameter Estimation

3.1. Parameters. Constant parameters are kept as a single value throughout the simulation under the assumption that there are no significant changes in the values over the entire time span. It is assumed that the average exit rate from infectious, recovery to susceptible, natural death rate, and probability of infection from being vaccinated do not change over the entire time span. Constant parameter values are listed in Table 1; meanwhile, varying parameters will attain many different values upon optimization, their values will not be presented within Table 1.

3.2. Time-Varying Parameter Estimation. Constant parameter values are not realistic due to the changes in safety regulations set by the government, behavior of people, ability to cure COVID-19 patients, and vaccination rate; hence, there are many previous studies implementing the time-varying parameters in the models [16–19]. Therefore, the time-varying parameter estimation is an essential technique to optimize the parameter in the SIRDV model. Parameters γ , α , μ , and r are kept constant throughout all time steps, as there are no reported significant changes in the rate at which people recover, become susceptible again, die of other causes, or change in the probability of being infected after being fully vaccinated. The transmission rate, probability of death, and vaccination rate are expected to change throughout the course of the pandemic, and will also have the greatest impact when attempting to match the solutions of the model to the real data. Therefore, only parameters β , p , and σ vary with time and undergo the parameter estimation method.

MATLAB's built-in *fminsearch* function which is based on the simplex algorithm is used to minimize the sum of squared errors (SSE) of the solution computed by MATLAB's *ode45* based on the Runge–Kutta numerical scheme and the real data in time steps of a single day by one parameter at a time. In MATLAB, *ode45* is a numerical integration algorithm used to solve ODEs. It employs a variable step-size, Runge–Kutta method of order 4(5), meaning it combines the fourth and fifth-order Runge–Kutta methods to achieve higher accuracy. *ode45* subdivides the integration interval into smaller intervals and approximates the solution by iteratively computing intermediate values using the Runge–Kutta formulae. It

dynamically adjusts the step-size based on the estimated error, aiming to maintain accuracy while efficiently integrating the ODE. *ode45* is a popular choice for solving a wide range of ODE problems due to its balance between accuracy and computational efficiency.

The *fminsearch* function in MATLAB is a numerical optimization algorithm that aims to find the minimum value of a given function without requiring derivative information. It utilizes the Nelder–Mead simplex algorithm, which constructs a geometric figure called a simplex in the parameter space. The algorithm iteratively adjusts the simplex's vertices based on function evaluations, such as reflecting, expanding, contracting, or shrinking, in order to converge towards the minimum. By iteratively updating the simplex, *fminsearch* searches for the optimal solution within the parameter space, making it useful for optimizing functions where derivatives are not readily available or difficult to compute.

In the parameter estimation method in Figure 2, the initial parameter value guesses are improved upon via the simplex algorithm, leading to the optimal parameter values by minimizing the error between the real data and the numerical solution. The parameters can be estimated in any order and will yield the same results; however, choosing the order from left to right in the model results in less time and optimization attempts are needed. After performing the optimization algorithm for one time step, the optimized parameter value and its corresponding solution value are then stored in the parameters and solution arrays, respectively. The process is then repeated by taking the endpoint of the solution array as the initial condition for when the dynamical system is to be solved and optimized again, and the next initial guess for the parameter is reset to 0.

The *fminsearch* function is highly efficient, however unconstrained; therefore, it may return values that are invalid for being less than 0 or greater than 1 for certain parameters. In order to avoid negative parameters, a lower bound condition is placed such that the dynamical system is solved with the assumption that the parameter is 0 if the optimal parameter returned by the algorithm is negative. An upper bound condition is also in place for p and σ , since those parameters must be strictly less than 1. Since *fminsearch* operates by searching for a local minimum in the neighborhood of the initial guess, the initial guess for every parameter is 0. The optimization procedure is applied multiple times to yield the best results for all classes.

3.3. Results of Estimated Parameters. The values of β , p , and σ obtained from the parameter estimation technique are plotted starting from January 1st, 2020, in Figure 3, in order to demonstrate the change in people's behavior over the time span, as well as to observe any trends that may be present.

The estimated parameter values appear to generally follow a nonlinear trend with very few outliers, which lead to the ability to analyze people's behavior over the course of the pandemic. The transmission rate β appears to take a drop significantly during the months of COVID-19 lockdown,

TABLE 1: Parameter interpretation and values.

Parameters	Description	Values (da y ⁻¹)	Types
β	Transmission rate	—	Varying
γ	Infectious exit rate	1/14	Constant
α	Recovery to susceptible rate	1/30	Constant
p	Probability of death	—	Varying
σ	Vaccination rate	—	Varying
μ	Natural death rate	0.0000248	Constant
r	Probability of infection after vaccinated	0.01	Constant

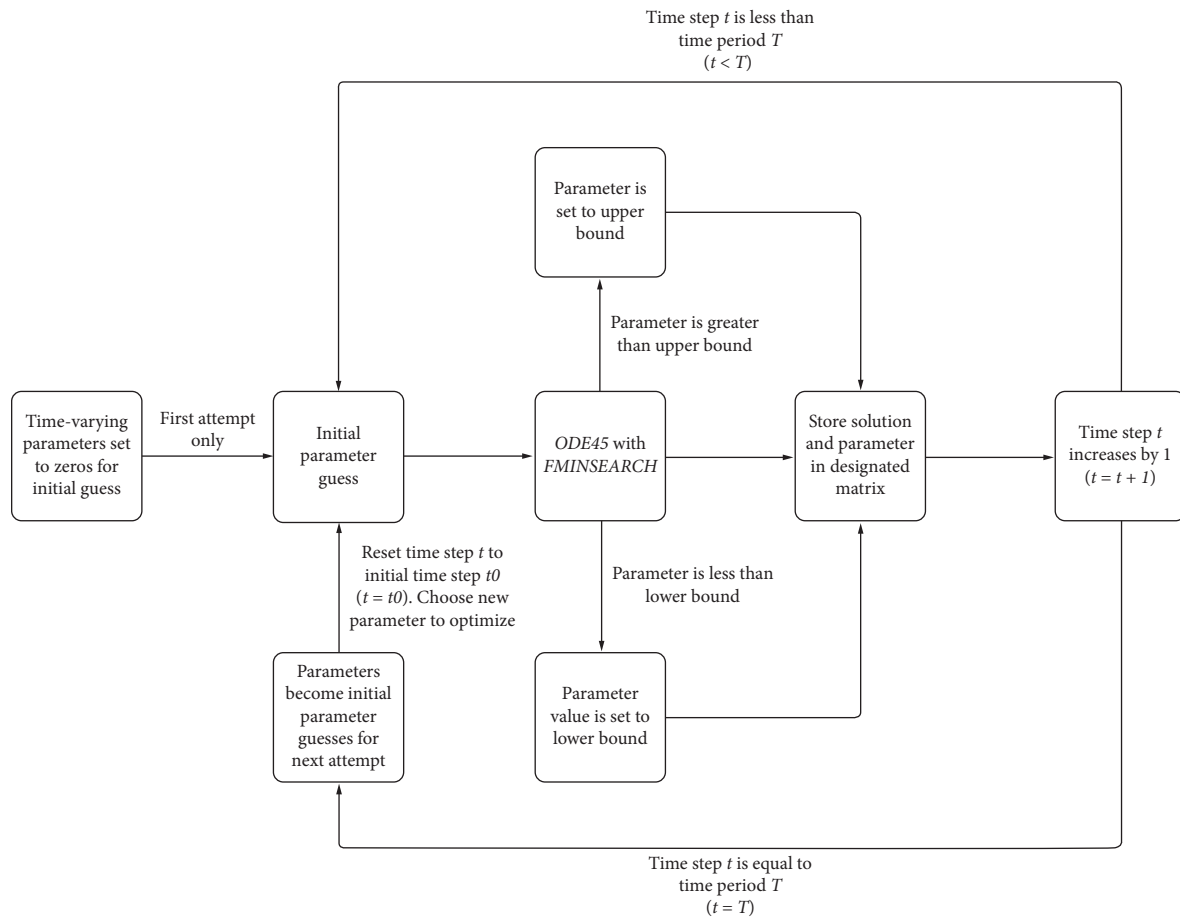


FIGURE 2: Parameter estimation flowchart.

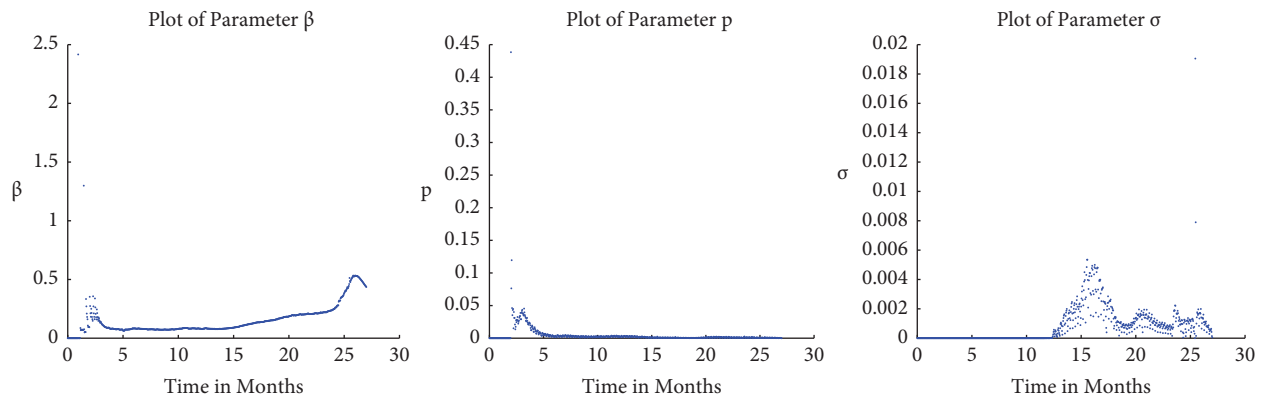


FIGURE 3: Plots of parameters used in order to attain optimized solutions.

which is around late March to late May of 2020 (dates of lockdown vary by state). The parameter β steadily increases between March 2021 and February 2022, then rapidly increases after, which corresponds well to the real behavior of people practicing strict safety precautions during lockdown, then gradually increasing transmission, and currently having little to no safety precautions after month 25. The death probability p was initially high in the first few days of COVID-19, then quickly dropped to less than 0.05 and eventually converged to 0 around May 2020. The vaccination rate increases rapidly from around January until May 2021, which was when vaccines were first issued to the public in the United States.

The first peak in the vaccination rate likely corresponds to when the COVID-19 vaccines were first released to the public, where large numbers of people were receiving the vaccines at around the same time. Following that first peak, there are smaller peaks that follow, which suggests that there are people who became vaccinated in the months following the period in which the vaccines were first rolled out. The vaccination rate in later months was significantly lower than the vaccines that were first available, suggesting that everyone who wanted the vaccine had received it. The parameter values yielded from the parameter estimation method correlate well with people's behavior over the course of the pandemic.

4. Basic Reproduction Number

The basic reproduction number denoted by \mathcal{R}_0 is the expected number of cases from one infected case. Since the parameters are functions of time, the basic reproduction number is also computed as a function of time. Here, \mathcal{R}_0 is computed using two different methods, one based on the transmission rate and mean infectious time, while the other uses Van den Driessche's next-generation approach [23]. It is able to be observed that the next-generation approach yields better results when compared to the reproduction rate data [21].

4.1. Computing Basic Reproduction Number with Transmission Rate and Infectious Period. The basic reproduction number \mathcal{R}_0 is often approximated using the simple definition of the transmission rate multiplied by the exit rate from the infectious compartment.

$$\mathcal{R}_0 = \beta\tau, \tag{8}$$

where

$$\tau = (\gamma + \mu)^{-1}. \tag{9}$$

The \mathcal{R}_0 values obtained from the transmission rate and mean infectious time agree with the reproduction rate data up until around month 15 in Figure 4. Its inability to match the trend of the data throughout the entire time span suggests another method may be able to yield results closer to the data.

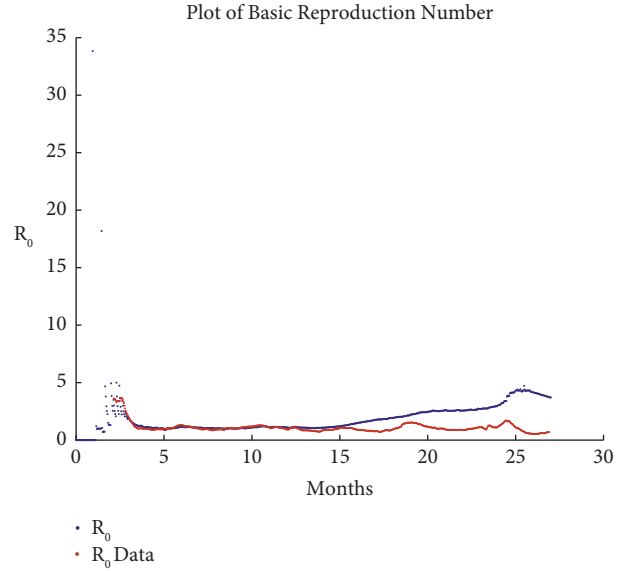


FIGURE 4: Plot of basic reproduction number obtained by the transmission rate and the mean infectious time.

4.2. Basic Reproduction Number (Van den Driessche and Watmough Next Generation). In the attempt to obtain better results for \mathcal{R}_0 , Van den Driessche's next-generation approach is used [23]. Let \mathcal{F} denote the terms entering the infected compartment and \mathcal{V} be the exiting terms from the infected compartment.

$$\mathcal{F} = \frac{\beta SI}{N} + r \frac{\beta VI}{N}, \tag{10}$$

$$\mathcal{V} = (\gamma + \mu)I.$$

Let F and V be partial derivatives with respect to the active infected cases I at initial value x_0 .

$$F = \frac{\partial \mathcal{F}(x_0)}{\partial I} = \frac{\beta S_0}{N} + r \frac{\beta V_0}{N}, \tag{11}$$

$$V = \frac{\partial \mathcal{V}(x_0)}{\partial I} = (\gamma + \mu),$$

where \mathcal{R}_0 is defined as FV^{-1} . Therefore, substituting F and V yields

$$\mathcal{R}_0 = FV^{-1} = \frac{\beta(S_0 + rV_0)}{N(\gamma + \mu)}. \tag{12}$$

The \mathcal{R}_0 values obtained from the transmission rate and mean infectious time in Figure 5 are able to agree with the reproduction rate data for only around the first year. The next-generation approach, however, agrees well with the reproduction rate data throughout the entire two years. The dynamical system is solved repeatedly with different parameters at each time step; the initial values S_0 and V_0 are considered to be the endpoints of the previous solution values. Since the \mathcal{R}_0 values from the next-generation

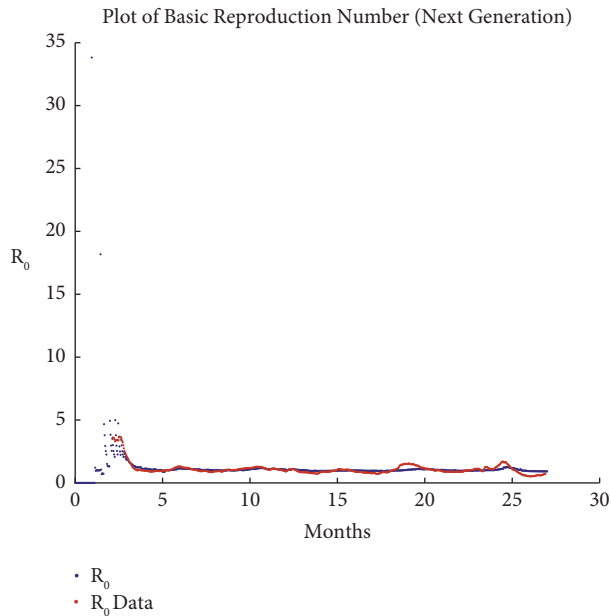


FIGURE 5: Plot of the basic reproduction number obtained by Van den Driessche's next-generation approach.

approach agree well with the data, it can be stated that the estimated values of the time-varying parameter β and the chosen constant parameters r , γ , and μ are suitable.

5. Results and Discussion

5.1. Numerical Solutions and Data Comparison. The data for active infected cases, deaths from COVID-19, and vaccinations are available by day; therefore, numerical results of compartments I , D , and V are able to be compared to real data.

After obtaining the solutions for active infected cases, deaths, and vaccinations, each class is plotted against their respective real data for visual comparison (Figure 6). The solutions for all three compartments seem to agree well with the real data across the entire time span. The major advantage of varying parameter values by day is the ability to capture every detail such as small and large peaks in active infected cases and to account for sudden increases or decreases. It can also be seen that the plots for vaccinations and deaths are able to capture changes in rates despite being monotonically increasing solutions. The plot of vaccinations here is the count for the number of vaccinations, which neglects the population that has exited the compartment and has become infected or died (from reasons other than COVID-19) after vaccinations.

5.2. Numerical Solutions for All Compartments. The solutions for all compartments are plotted in the same figure in order to compare the populations in each compartment and the magnitude of each trajectory relative to one another.

The numerical solutions shown in the plot of all solutions (Figure 7) are representative of the population currently in each class. It should be noted that the solution curve for the vaccinated class V here represents the number of vaccinated people who have not become infected after vaccination, not to be confused with the vaccinated plot previously shown (Figure 6), which is the count of the number of people who are fully vaccinated. Similarly, the solution curve for the recovered class R represents the number of people who have recently recovered and are not yet susceptible to reinfection.

The rapid decline of the solutions to the susceptible class S suggests that the number of susceptible people will soon approach 0, which suggests the number of COVID-19 infections would likely also reach 0 at around the same time. Although the vaccinated class V is similar to the susceptible class S in the way that people in both compartments are able to become infected, the plots show that significantly more people are protected by the vaccine, since at the moment the solution for V is significantly higher than the solution for S .

Despite the high number of deaths, the magnitude of the solution curve for deaths is relatively low throughout the entire time span when compared to solutions of the other compartments. The curve of recovered class R follows the same trends as the curve of infected class I , confirming the fact that most people who are infected with COVID-19 do indeed recover, keeping in mind that R is continuously losing its population to S at the rate of α .

6. Forecasting Parameters and Solutions

6.1. Forecasting Parameters. An autoregressive (AR) model based on MATLAB's *ar* function is used on the parameters β , p , and σ in order to predict the future parameter values for the next 365 days based on all past respective parameter values. Previous research utilizing the AR model used the method directly on the solutions of the dynamical system [24]. Meanwhile, in this research, it is applied to the parameters, which are then used when solving the dynamical system. White noise is then added to the forecasted parameters in order to simulate the noise present in the parameter values obtained through the parameter estimation method.

6.2. Forecasting Solutions. Past parameter values and forecasted parameter values are shown together on the same plots in Figure 8. The forecasted parameter values are then used in the model in order to forecast the solutions for I , D , and V . The prediction shows that all parameter values will eventually converge rapidly to 0.

Additional data corresponding to these compartments are added in order to evaluate the performance of the forecasting method in Figure 9. From the plot of active infected cases, it is able to be observed that the solution using the forecasted parameters follows the same trend as the real

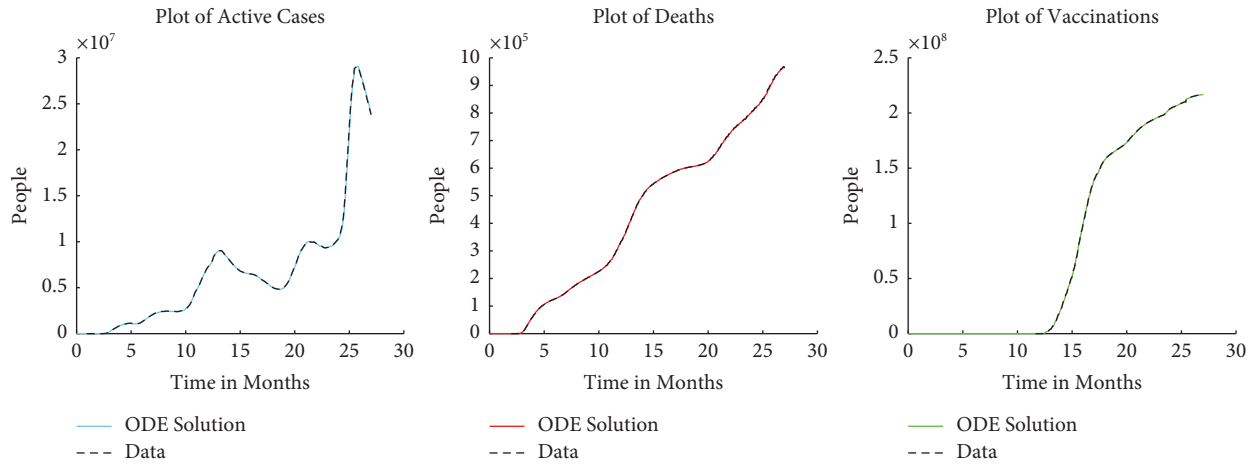


FIGURE 6: Plots of solutions compared to real data.

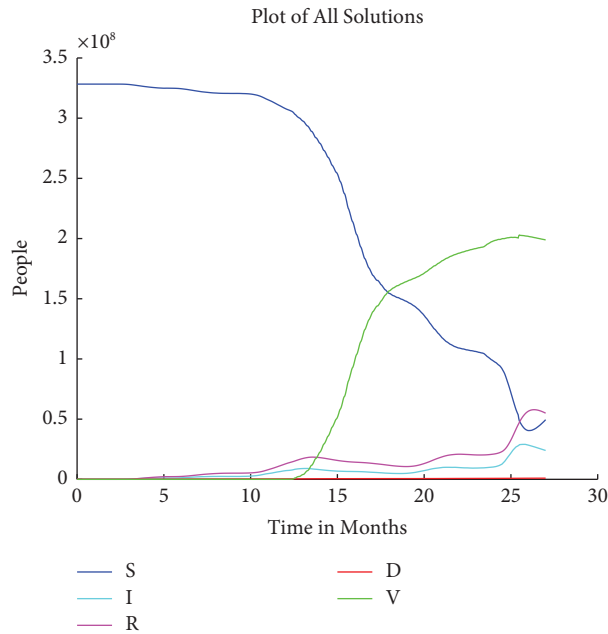


FIGURE 7: Plot of numerical solutions for all compartments.

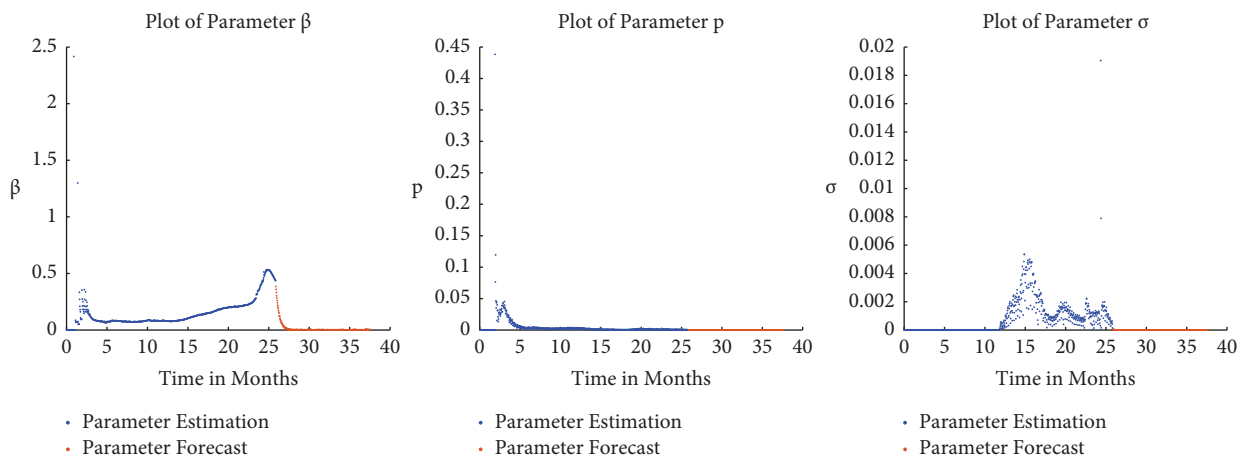


FIGURE 8: Forecast of parameter values.

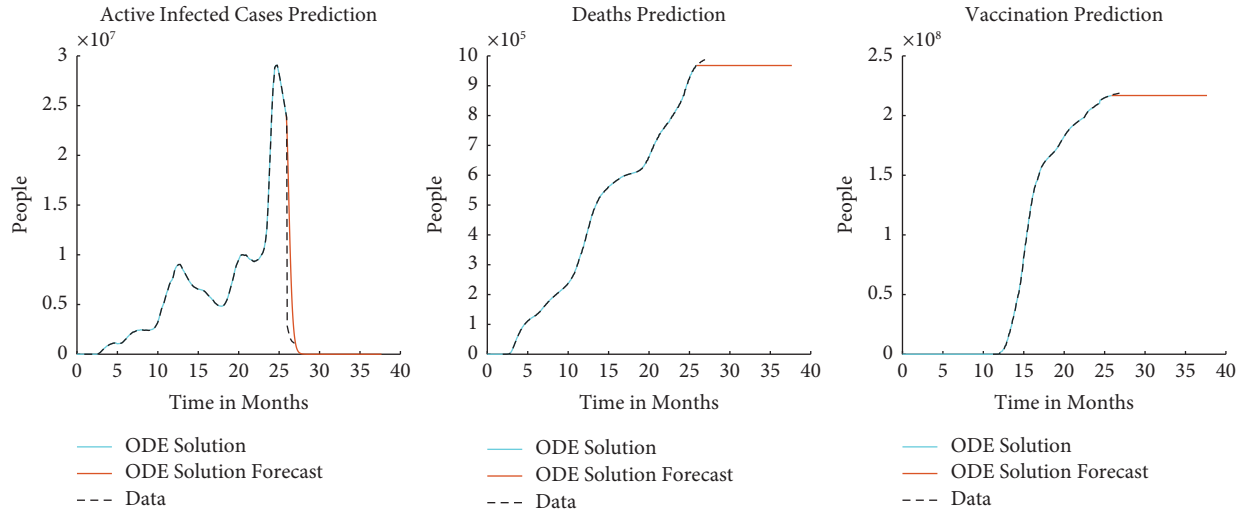


FIGURE 9: Forecast of solutions.

data, except the real data decrease at a slightly faster rate. The predictions for deaths and vaccinations suggest that both classes will no longer increase due to the parameter values for p and σ being 0 in the forecast.

7. Sensitivity and Elasticity Analysis

7.1. *Sensitivity.* The objective of the sensitivity analysis is to determine which parameters are most influential on the solution of the model. Sensitivity is defined as follows:

$$S = \frac{\partial Q}{\partial P}. \tag{13}$$

In which the sensitivity of quantity Q is being analyzed with respect to the parameter P . The reproduction number \mathcal{R}_0 obtained by the next-generation method is the quantity whose sensitivity is chosen to be analyzed. Let the disease-free equilibrium be $\mathcal{E} = (S^*, I^*, R^*, D^*, V^*) = (N, 0, 0, 0, 0)$. The reproduction number at disease-free equilibrium is

$$\mathcal{R}_0 = \frac{\beta}{\gamma + \mu}. \tag{14}$$

Taking the partial derivative of \mathcal{R}_0 with respect to each parameter yields

$$S_{\mathcal{R}_0}^\gamma = \frac{\partial \mathcal{R}_0}{\partial \gamma} = -\frac{\beta}{(\gamma + \mu)^2}, \tag{15}$$

$$S_{\mathcal{R}_0}^\mu = \frac{\partial \mathcal{R}_0}{\partial \mu} = -\frac{\beta}{(\gamma + \mu)^2}, \tag{16}$$

$$S_{\mathcal{R}_0}^\beta = \frac{\partial \mathcal{R}_0}{\partial \beta} = \frac{1}{\gamma + \mu}. \tag{17}$$

Since $S_{\mathcal{R}_0}^\beta$ only depends on constant parameters, it may be easily computed as a constant scalar value.

$$S_{\mathcal{R}_0}^\beta = 0.9998. \tag{18}$$

However, $S_{\mathcal{R}_0}^\gamma$ and $S_{\mathcal{R}_0}^\mu$ depend on β , which is a variable parameter which can be a wide range of values. Many different values of sensitivity will arise from this simple formula. Therefore, a range of sensitivity values may be observed.

$$\begin{aligned} \max_\beta S_{\mathcal{R}_0}^\gamma &\leq S_{\mathcal{R}_0}^\gamma \leq \min_\beta S_{\mathcal{R}_0}^\gamma, \\ \max_\beta S_{\mathcal{R}_0}^\mu &\leq S_{\mathcal{R}_0}^\mu \leq \min_\beta S_{\mathcal{R}_0}^\mu. \end{aligned} \tag{19}$$

Since $S_{\mathcal{R}_0}^\gamma = S_{\mathcal{R}_0}^\mu$, upon substituting with appropriate values for sensitivity formulae (15) or (16), yields the sensitivity range

$$-473.2930 \leq S_{\mathcal{R}_0}^\gamma, S_{\mathcal{R}_0}^\mu \leq 0. \tag{20}$$

The average values of $S_{\mathcal{R}_0}^\gamma$ and $S_{\mathcal{R}_0}^\mu$ are obtained by letting β be the mean value of all the β values.

$$\overline{S_{\mathcal{R}_0}^\gamma}, \overline{S_{\mathcal{R}_0}^\mu} = -18.6214. \tag{21}$$

In order for the model to match the data towards the beginning of the pandemic, the transmission rate β had to be significantly higher due to the small initial infected population I_0 . Therefore, when computing $S_{\mathcal{R}_0}^\gamma$ and $S_{\mathcal{R}_0}^\mu$ which depend on β , the sensitivity spikes all the way to -473.2930 . To demonstrate the sensitivity of each parameter, a perturbation of $+0.001$ is applied to one parameter (β, γ , or μ), while the other parameters, both variables and constants, are kept at their original values after optimization. The solutions using the perturbed parameter values are then plotted in Figure 10 against the real data for all three classes in order to observe the effects of the perturbation.

The active cases and deaths are greatly affected by the small changes in parameter values. Vaccinations, however, experience slight changes throughout perturbations of all three parameters, although they are still visually observable. As expected, the solutions exhibit the same characteristics as the original parameter values, although they increase and decrease at different rates.

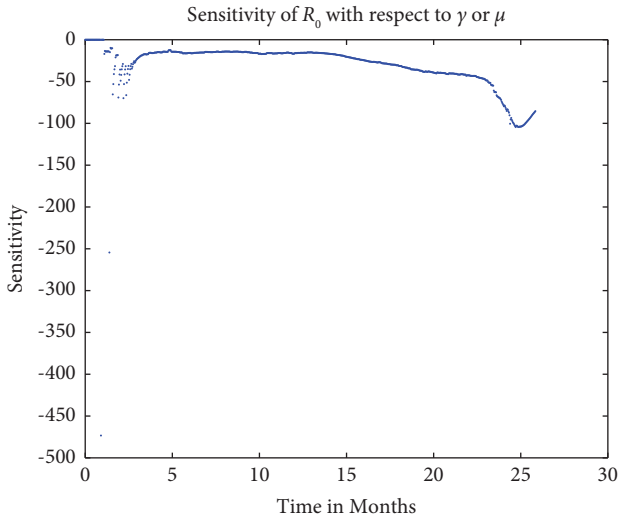


FIGURE 10: Plot of the sensitivity of \mathcal{R}_0 with respect to γ or μ .

7.2. *Elasticity.* Since the sensitivity analysis is local, it does not take into account the range of values that can be input as parameters [2]. Therefore, the more useful concept elasticity is computed, where elasticity is defined as follows:

$$E_Q^P = \frac{\partial Q}{\partial P} \frac{P}{Q}. \quad (22)$$

Using the results previously obtained from the section on sensitivity, elasticity may be computed. Since formulae obtained for elasticity are dependent only on constant parameters, singular scalar values for elasticities may be obtained.

$$\begin{aligned} E_{\mathcal{R}_0}^\gamma &= \frac{\partial \mathcal{R}_0}{\partial \gamma} \frac{\gamma}{\mathcal{R}_0} = -\frac{\beta}{(\gamma + \mu)^2} \frac{\gamma}{\mathcal{R}_0} = -\frac{\gamma}{\gamma + \mu} = -0.9998, \\ E_{\mathcal{R}_0}^\mu &= \frac{\partial \mathcal{R}_0}{\partial \mu} \frac{\mu}{\mathcal{R}_0} = -\frac{\beta}{(\gamma + \mu)^2} \frac{\mu}{\mathcal{R}_0} = -\frac{\mu}{\gamma + \mu} = -2.4794 \times 10^{-4}, \\ E_{\mathcal{R}_0}^\beta &= \frac{\partial \mathcal{R}_0}{\partial \beta} \frac{\beta}{\mathcal{R}_0} = \frac{1}{(\gamma + \mu)} \frac{\beta}{\mathcal{R}_0} = 1. \end{aligned} \quad (23)$$

The value obtained for $E_{\mathcal{R}_0}^\beta$ is 1, which is expected. The \mathcal{R}_0 observes a 0.9998% decrease after a 1% increase in γ . Similarly, \mathcal{R}_0 decreases by $2.4794 \times 10^{-4}\%$ after a 1% increase in μ . The impacts of β and γ are very similar, meanwhile μ has a significantly less significance (Figure 11).

8. Model Validation

Model validation is used in order to check accuracy and performance of a certain model. Since the nature of this research is able to be interpreted as a model solved separately over small time steps or as one large model covering a long period of time, the validation process is performed using both interpretations.

8.1. *Error Analysis.* In order to measure the error between the solution and the data, some basic regression analysis techniques are used [25]. The sum of squared errors (SSE) and the sum of squared total (SST) are computed. Points where there are no data present are excluded from the computation of SSE. Let x_i denote the value of the class at time step i and \hat{x}_i denote corresponding data at the same time step. Furthermore, let \bar{x} be the mean of the corresponding data. The time step i is a single day.

$$\begin{aligned} \text{SSE} &= \sum_{i=1}^N (x_i - \hat{x}_i)^2, \\ \text{SST} &= \sum_{i=1}^N (x_i - \bar{x})^2, \end{aligned} \quad (24)$$

$$\text{FVU} = \frac{\text{SSE}}{\text{SST}},$$

$$R^2 = 1 - \text{FVU}.$$

Table 2 shows the SSE, SST, R^2 , and FVU of infected, deaths, and vaccinated compartments. The SSE values computed for each class are notably high for infected and vaccinated classes, which is contributed by several different factors. The model handles very large populations; therefore, relatively small errors between the solutions and the real data are in reality quite large when compared to models that work with smaller populations. The model covers a long time span and therefore contains more data, which are prone to having higher SSE values. The parameter estimation also has limitations, as the optimized solution is the best possible solution obtained by *fminsearch*, which is inferior to more sophisticated optimization techniques in machine learning. The R^2 values, however, are approximately 1 for all classes, with the fraction of variance unexplained (FVU) being insignificantly small.

8.2. *Single Time Step AIC.* The Akaike Information Criterion (AIC) is applied to the model and data in order to determine the validity of the model. Since the model is solved multiple times in small time steps, the SSE and AIC values are calculated for every time step j . Let m denote the number of data points and k denote the number of parameters. For a single time step, $m = 2$ and $k = 7$.

$$\text{AIC}_j = m \log\left(\frac{\text{SSE}_j}{m}\right) + 2k. \quad (25)$$

From the plot of AIC values (Figure 12), the range of AIC values from where the spread of COVID-19 started in the United States appears to be in the typical range of AIC values for SIR-type models [2].

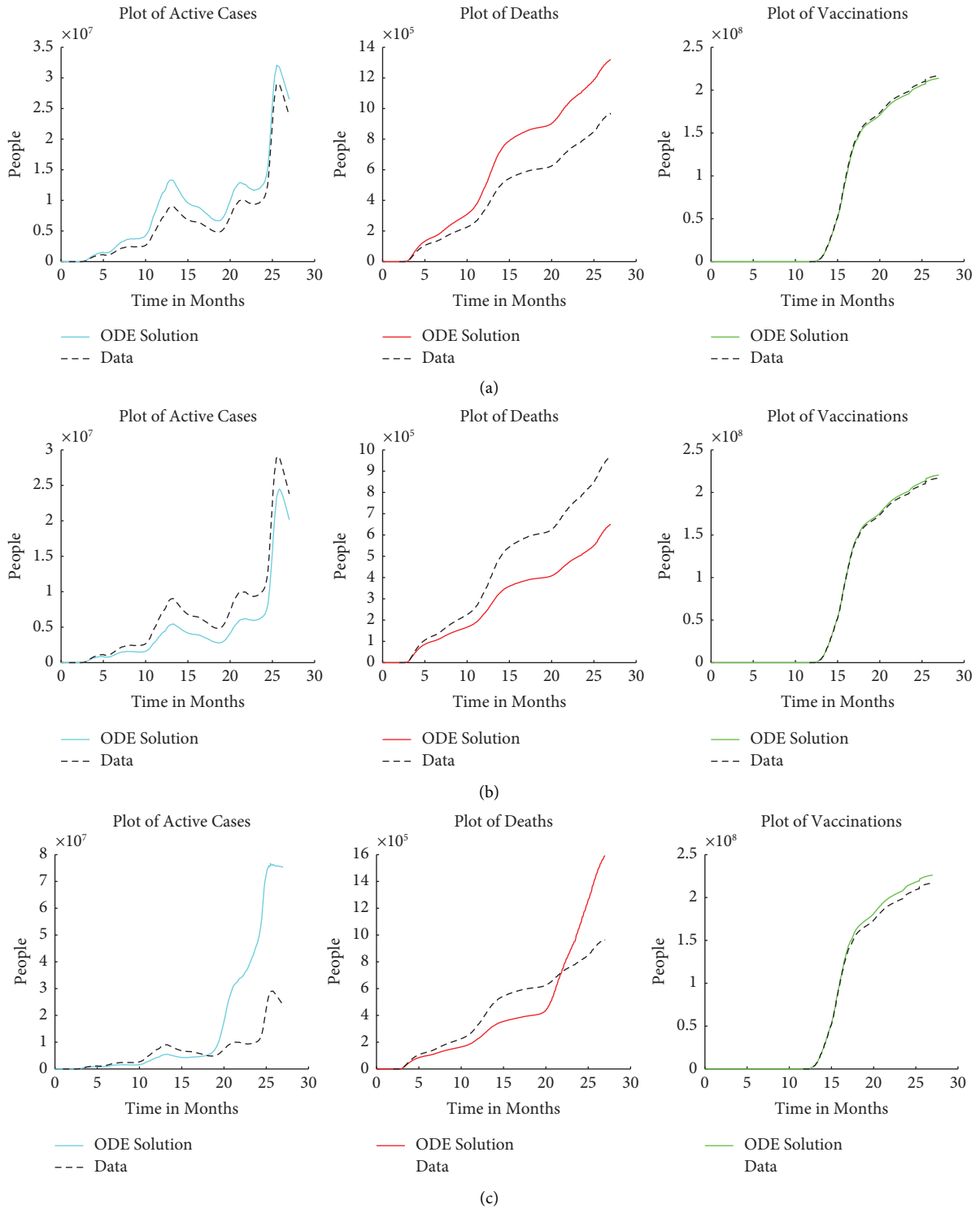


FIGURE 11: Solutions after perturbing each parameter value by +0.001: (a) perturbation of β , (b) perturbation of γ , and (c) perturbation of μ .

TABLE 2: Error.

Class	SSE	SST	R^2	FVU
Infected	3.3845×10^{11}	3.7574×10^{16}	1.0000	9.2507×10^{-6}
Deaths	6.3502×10^7	7.1267×10^{13}	1.0000	8.9103×10^{-7}
Vaccinated	6.5550×10^{12}	9.1546×10^{18}	1.0000	7.1663×10^{-7}

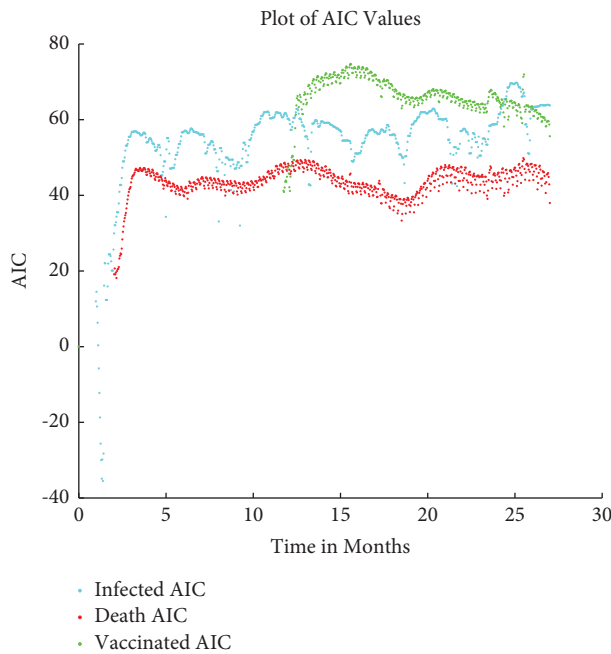


FIGURE 12: Plot of AIC values.

TABLE 3: Total AIC.

Class	Total AIC
Infected	20826
Deaths	13897
Vaccinated	23191

8.3. *Total AIC.* The total AIC is calculated using the SSE between the solutions and respective data over the entire time span previously calculated in Section 7.1, along with the total number of parameters used, which account for every single value for each varying parameter. For total AIC, $m = 805$ and $k = 3(805) + 4 = 2410$ (3 sets of varying parameters and 4 constant parameters).

The total AIC values are similar to those calculated based on the study of dynamic epidemic models via iterated filtering [26]. The AIC values for all three in Table 3 are significantly high due to the large sample size and number of parameters used in total.

9. Conclusion

By allowing the parameters to vary, the numbers of infections, deaths, and vaccinations are able to be matched relatively well to the real data on a daily basis for over two years by a very simple model and optimization technique. A major advantage of using the simplex algorithm for optimization of many thousand parameter values is its ability to yield satisfactory results within merely a few minutes on a personal machine. The basic reproduction number calculated based on the parameter values obtained by the parameter estimation method agrees well with the reproduction rate data. However, the model may be vulnerable to data overfitting, as the solutions depend heavily on the parameter values, where future parameter values may not be

precisely determined, possibly leading to the future solutions being inaccurate.

Performing the sensitivity analysis shows that there is a wide range of sensitivity due to the many values of the transmission rate β . Elasticity may be computed as singular scalar values due to not depending on any variable parameters. The SSE along with the AIC values falls within the typical range for models of similar nature. From the results, it can be concluded that the model along with the parameter estimation algorithm is able to handle the United States' COVID-19 data well and therefore should be able to handle simulating the spread of other infectious diseases with more intricate behavior, in which models with constant parameters are unable to. A limitation worth mentioning is that the model is designed around COVID-19 data in the United States, which makes the use of this model applicable only to similar types of data. The model may be modified and adjusted accordingly in order to be applied to other infectious diseases that are similar in nature.

Data Availability

The data used to support the findings of this study are included within the website, <https://www.worldometers.info/coronavirus/country/us/> [14].

Conflicts of Interest

The authors declare that they have no conflicts of interest.

Acknowledgments

We would like to thank Dr. Casey Diekman and Soheil Sagafhi of New Jersey Institute of Technology for assisting in the groundwork and initial structure of the project. This research is supported by Ph.D Degree Program in Mathematics, Faculty of Science, Chiang Mai University, under the CMU Presidential Scholarship and Chiang Mai University.

References

- [1] F. Brauer, *Mathematical Models in Epidemiology*, Springer, New York, NY, USA, 2019.
- [2] M. Martcheva, *An Introduction to Mathematical Epidemiology*, Springer, New York, NY, USA, 2015.
- [3] S. A. Alanazi, M. M. Kamruzzaman, M. Alruwaili, N. Alshammari, S. A. Alqahtani, and A. Karime, "Measuring and preventing COVID-19 using the SIR model and machine learning in smart health care," *Journal of Healthcare Engineering*, vol. 2020, Article ID 8857346, 12 pages, 2020.
- [4] C. J. Wang, C. Y. Ng, and R. H. Brook, "Response to COVID-19 in Taiwan: big data analytics, new technology, and proactive testing," *JAMA*, vol. 323, no. 14, pp. 1341-1342, 2020.
- [5] B. Tang, X. Wang, Q. Li et al., "Estimation of the transmission risk of the 2019-nCoV and its implication for public health interventions," *Journal of Clinical Medicine*, vol. 9, no. 2, p. 462, 2020.
- [6] M. Alenezi, F. Al-Anzi, and H. Alabdulrazzaq, "Building a sensible SIR estimation model for COVID-19 outbreak in

- Kuwait,” *Alexandria Engineering Journal*, vol. 60, no. 3, pp. 3161–3175, 2021.
- [7] I. Cooper, A. Mondal, and C. G. Antonopoulos, “A SIR model assumption for the spread of COVID-19 in different communities,” *Chaos, Solitons and Fractals*, vol. 139, Article ID 110057, 2020.
- [8] L. Lopez and X. Rodo, “A modified SEIR model to predict the COVID-19 outbreak in Spain and Italy: simulating control scenarios and multi-scale epidemics,” *Results in Physics*, vol. 21, Article ID 103746, 2021.
- [9] L. Peng, “Epidemic analysis of COVID-19 in China by dynamical modeling,” p. 6563, 2020, <https://arxiv.org/abs/2002.06563>.
- [10] K. Prem, Y. Liu, T. W. Russell et al., “The effect of control strategies to reduce social mixing on outcomes of the COVID-19 epidemic in Wuhan, China: a modelling study,” *The Lancet Public Health*, vol. 5, no. 5, pp. e261–e270, 2020.
- [11] N. M. Ferguson, “Impact of non-pharmaceutical interventions (NPIs) to reduce COVID-19 mortality and healthcare demand,” *Imperial College London*, vol. 16, no. 16, pp. 1–20, 2020.
- [12] G. Giordano, F. Blanchini, R. Bruno et al., “Modelling the COVID-19 epidemic and implementation of population-wide interventions in Italy,” *Nature Medicine*, vol. 26, no. 6, pp. 855–860, 2020.
- [13] J. M. Read, J. R. E. Bridgen, D. A. T. Cummings, A. Ho, and C. P. Jewell, “Novel coronavirus 2019-nCoV (COVID-19): early estimation of epidemiological parameters and epidemic size estimates,” *Philosophical Transactions of the Royal Society B: Biological Sciences*, vol. 376, pp. 1–4, 2021.
- [14] M. Harris, “WHO issues its first emergency use validation for a COVID-19 vaccine and emphasizes need for equitable global access,” 2020, <https://www.who.int/news/item/31-12-2020-who-issues-its-first-emergency-use-validation-for-a-covid-19-vaccine-and-emphasizes-need-for-equitable-global-access>.
- [15] R. Ghostine, M. Gharamti, S. Hassrouny, and I. Hoteit, “An extended SEIR model with vaccination for forecasting the COVID-19 pandemic in Saudi arabia using an ensemble kalman filter,” *Mathematics*, vol. 9, no. 6, p. 636, 2021.
- [16] G. Nastasi, C. Perrone, S. Taffara, and G. Vitanza, “A time-delayed deterministic model for the spread of COVID-19 with calibration on a real dataset,” *Mathematics*, vol. 10, no. 4, p. 661, 2022.
- [17] P. Girardi and C. Gaetan, “An SEIR model with time-varying coefficients for analyzing the SARS-CoV-2 epidemic,” *Risk Analysis*, vol. 43, no. 1, pp. 144–155, 2021.
- [18] A. Bousquet, W. H. Conrad, S. O. Sadat, N. Vardanyan, and Y. Hong, “Deep learning forecasting using time-varying parameters of the SIRD model for Covid-19,” *Scientific Reports*, vol. 12, no. 1, p. 3030, 2022.
- [19] C. You, Y. Deng, W. Hu et al., “Estimation of the time-varying reproduction number of COVID-19 outbreak in China,” *International Journal of Hygiene and Environmental Health*, vol. 228, Article ID 113555, 2020.
- [20] W. Worldometer’s, “COVID-19 data,” 2022, <https://www.worldometers.info/coronavirus/country/us/>.
- [21] H. Ritchie, “Our world in data COVID-19 dataset,” 2022, <https://ourworldindata.org/coronavirus/country/united-states>.
- [22] W. C. Roda, M. B. Varughese, D. Han, and M. Y. Li, “Why is it difficult to accurately predict the COVID-19 epidemic?” *Infectious Disease Modelling*, vol. 5, pp. 271–281, 2020.
- [23] P. Van den Driessche, “Reproduction numbers of infectious disease models,” *Infectious Disease Modelling*, vol. 2, no. 3, pp. 288–303, 2017.
- [24] S. K. Yadav and Y. Akhter, “Statistical modeling for the prediction of infectious disease dissemination with special reference to COVID-19 spread,” *Frontiers in Public Health*, vol. 9, 2021.
- [25] J. O. Rawlings, S. G. Pantula, and D. A. Dickey, *Applied Regression Analysis: A Research Tool*, Springer, New York, NY, USA, Second edition, 1998.
- [26] T. Stocks, T. Britton, and M. Höhle, “Model selection and parameter estimation for dynamic epidemic models via iterated filtering: application to rotavirus in Germany,” *Biostatistics*, vol. 21, no. 3, pp. 400–416, 2020.

Research Article

Solvability of the System of Extended Nonlinear Mixed Variational-Like Inequalities and Proximal Dynamical System

Iqbal Ahmad ¹ and Mijanur Rahaman ²

¹Department of Mechanical Engineering, College of Engineering, Qassim University, P.O. Box 6677, Buraidah 51452, Al-Qassim, Saudi Arabia

²Department of Mathematics, Syamaprasad College, Kolkata 700026, India

Correspondence should be addressed to Mijanur Rahaman; mrahaman96@yahoo.com

Received 17 August 2022; Revised 29 November 2022; Accepted 20 April 2023; Published 29 June 2023

Academic Editor: Rehan Ali

Copyright © 2023 Iqbal Ahmad and Mijanur Rahaman. This is an open access article distributed under the Creative Commons Attribution License, which permits unrestricted use, distribution, and reproduction in any medium, provided the original work is properly cited.

In this article, our goal is to study the system of extended nonlinear mixed variational-like inequalities (in short, SENMVLI) with a nonconvex functional in the setting of real Hilbert spaces and discuss the existence of solution of our considered problem. We propose a three-step iterative algorithm to calculate the approximate solutions of SENMVLI and investigate the convergence analysis as well as stability analysis of the proposed algorithm. Furthermore, we also study the proximal dynamical system for SENMVLI and prove that the trajectory of the solution of the extended proximal dynamical system converges globally exponentially to a unique solution of SENMVLI. Our suggested iterative algorithm and results have become the significant improvement, enhancement, and generalization of many previously known results in the literature.

1. Introduction

In prior 1960s, the concept of variational inequality originated by Hartmann and Stampacchia [1] has appeared as a fruitful and methodical mechanism to study a wide range of applications in economics, finance, pure and applied sciences, and optimization, see, e.g. [2–5]. Using novel and regenerated techniques, several extensions and generalizations of variational inequalities have been explored and developed in recent years. The functional, pivotal, and applicable generalizations of variational inequalities are variational-like inequalities and mixed variational-like inequalities which have significant applications in nonconvex optimizations and mathematical programming problems. For details, we refer to [6–8] and references therein.

In classical variational inequality theory, ones have been failing to exploit the projection method and its modified forms to analyze the existence of solutions of mixed variational-like inequalities involving the nonlinear term. To vanquish this flaw, it is assumed that the nonlinear term involving the mixed variational-like inequalities is a proper,

convex, and lower-semicontinuous functional. It is well-known that the subdifferential of a proper, convex, and lower-semicontinuous functional is a maximal monotone operator. This characterization enables to define the resolvent operator associated with the maximal monotone operator. The resolvent operator technique is used to establish the equivalence between the mixed variational-like inequalities and fixed point problems. Such type of methods is called the operators splitting methods. For recent development of the subject, we refer to [9–12]. Noor [13, 14] has used the resolvent operator technique to propose and study some two-step forward-backward splitting methods. It has been noticed that the convergence of such type of splitting algorithms needs relatively relaxed strong monotonicity, which is a weaker constraint than cocoercivity. Glowinski and Tallec [15] and many authors have suggested and analyzed some three-step forward-backward splitting methods for solving various classes of variational inequalities by using the Lagrangian multipliers and auxiliary principle techniques. They have shown that three-step splitting methods are numerically more efficient and handy as compared with

one-step and two-step splitting methods. They have studied the convergence of these splitting methods under the assumption that the underlying operators are monotone and Lipschitz continuous. For the convergence analysis of iterative-type splitting methods and their applications, we refer to [16–19] and references therein.

The dynamical system has appeared as a feasible substitute for solving variational inequalities with a specific interest on optimization problems. Dupuis and Nagurney [20], Friesz et al. [21], Noor [22], and many authors introduced and studied many projected dynamical systems associated with variational inequalities. In these dynamical systems, discontinuity appears due to the discontinuity of the projection operator which occurs on the right side of the ordinary differential equation. The novel importance of projected dynamical systems is that the set of stationary points of the projected dynamical systems is the set of solutions of the associated variational inequalities and all those problems which can be studied in the structure of variational inequalities. Since proximal dynamical systems are generalization of projected dynamical systems, therefore clearly the results enhance to global stability of modified projected dynamical systems. Moreover, a vast category of optimization problems can be considered as special cases of mixed variational inequalities (variational-like inequalities) and, therefore, can be solved by using the proximal dynamical systems.

Inspired and motivated by the research works mentioned above, in this article, we introduce and study a system of extended nonlinear mixed variational-like inequalities in real Hilbert space and discuss the existence of solution of our problem. Next, we propose and analyze a new three-step iterative scheme for solving the system of extended nonlinear mixed variational-like inequalities. The convergence and stability analysis for the system of extended nonlinear mixed variational-like inequalities are established. We also study proximal dynamical system associated with the system of extended nonlinear mixed variational-like inequalities. Finally, we show that the trajectory of the solution of extended nonlinear mixed variational-like proximal dynamical system converges globally exponentially to a unique solution of system of extended nonlinear mixed variational-like inequalities.

2. Preliminaries

Throughout this article, we assume that \mathcal{H} is a real Hilbert space whose norm and inner product are denoted by $\|\cdot\|$ and $\langle \cdot, \cdot \rangle$, respectively.

Let us recall the following well-known concepts and results.

Definition 1 (see [9, 23]). Let $g, T: \mathcal{H} \rightarrow \mathcal{H}$ and $\zeta: \mathcal{H} \times \mathcal{H} \rightarrow \mathcal{H}$ be the single-valued mappings. Then,

- (i) ζ is said to be τ -Lipschitz continuous if, there exists a constant $\tau > 0$ such that

$$\|\zeta(p, q)\| \leq \tau \|p - q\|, \quad \forall p, q \in \mathcal{H}. \quad (1)$$

- (ii) ζ is said to be δ -strongly monotone if, there exists a constant $\delta > 0$ such that

$$\langle \zeta(p, q), p - q \rangle \geq \delta \|p - q\|^2, \quad \forall p, q \in \mathcal{H}. \quad (2)$$

- (iii) g is said to be μ_g -strongly monotone if, there exists a constant $\mu_g > 0$ such that

$$\langle g(p) - g(q), p - q \rangle \geq \mu_g \|p - q\|^2, \quad \forall p, q \in \mathcal{H}. \quad (3)$$

- (iv) g is said to be λ_g -Lipschitz continuous if, there exists a constant $\lambda_g > 0$ such that

$$\|g(p) - g(q)\| \leq \lambda_g \|p - q\|, \quad \forall p, q \in \mathcal{H}. \quad (4)$$

- (v) T is said to be ζ -relaxed Lipschitz continuous if, there exists a constant $\alpha > 0$ such that

$$\langle T(p) - T(q), \zeta(p, q) \rangle \leq -\alpha \|p - q\|^2, \quad \forall p, q \in \mathcal{H}. \quad (5)$$

- (vi) T is said to be μ_T -strongly monotone with respect to g if, there exists a constant $\mu_T > 0$ such that

$$\begin{aligned} \langle T(g(p)) - T(g(q)), g(p) - g(q) \rangle \\ \geq \mu_T \|p - q\|^2, \quad \forall p, q \in \mathcal{H}. \end{aligned} \quad (6)$$

Definition 2 (see [9]). For each $i = 1, 2, \dots, m$, let $h_i: \mathcal{H}_i \rightarrow \mathcal{H}_i$ and $A_i: \prod_{i=1}^m \mathcal{H}_i \rightarrow \mathcal{H}_i$ be the single-valued mappings. Then, A_i is said to be

- (i) γ -Lipschitz continuous in the i^{th} -argument if, there exist a constant $\gamma > 0$ such that

$$\|A_i(p_1, p_2, \dots, p_{i-1}, p_i, p_{i+1}, \dots, p_m) - A_i(p_1, p_2, \dots, p_{i-1}, \hat{p}_i, p_{i+1}, \dots, p_m)\|_i \leq \gamma \|p_i - \hat{p}_i\|_i, \quad \forall p_i, \hat{p}_i \in \mathcal{H}_i. \quad (7)$$

- (ii) ϱ -strongly monotone in the i^{th} -argument if, there exists a constant $\varrho > 0$ such that

$$\langle A_i(p_1, p_2, \dots, p_{i-1}, p_i, p_{i+1}, \dots, p_m) - A_i(p_1, p_2, \dots, p_{i-1}, \hat{p}_i, p_{i+1}, \dots, p_m), p_i - \hat{p}_i \rangle \geq \varrho \|p_i - \hat{p}_i\|_i^2, \quad \forall p_i, \hat{p}_i \in \mathcal{H}_i. \quad (8)$$

- (iii) μ_{g_i} -strongly monotone with respect to g_i in the i^{th} -argument if, there exists a constant $\mu_{g_i} > 0$ such that

$$\begin{aligned} & \langle A_i(p_1, p_2, \dots, p_{i-1}, p_i, p_{i+1}, \dots, p_m) - A_i(p_1, p_2, \dots, p_{i-1}, \widehat{p}_i, p_{i+1}, \dots, p_m), g_i(p_i) - g_i(\widehat{p}_i) \rangle \\ & \geq \mu_{g_i} \|g_i(p_i) - g_i(\widehat{p}_i)\|_i^2, \quad \forall p_i, \widehat{p}_i \in \mathcal{H}_i. \end{aligned} \tag{9}$$

Definition 3 (see [24]). A functional $f: \mathcal{H} \times \mathcal{H} \rightarrow \mathbb{R}$ is said to be 0-diagonally quasi-concave (inshort, 0-DQCV) in p if, for any finite set $\{p_1, p_2, \dots, p_n\} \subset \mathcal{H}$ and for any $q = \sum_{i=1}^n t_i p_i$ with $t_i \geq 0$ and $\sum_{i=1}^n t_i = 1$,

$$\min_{1 \leq i \leq n} f(p_i, q) \leq 0. \tag{10}$$

Definition 4 (see [24]). Let $\zeta: \mathcal{H} \times \mathcal{H} \rightarrow \mathcal{H}$ be a mapping and $\psi: \mathcal{H} \rightarrow \mathbb{R} \cup \{\infty\}$ be a proper functional. A vector $f^* \in H$ is called an ζ -subgradient of ψ at $p \in \text{dom} \psi$ if

$$\langle f^*, \zeta(q, p) \rangle \leq \psi(q) - \psi(p), \quad \forall q \in \mathcal{H}. \tag{11}$$

Each ψ can be associated with the following map $\partial_\zeta \psi$, called ζ -subdifferential of ψ at p , defined by

$$\partial_\zeta \psi(p) = \begin{cases} f^* \in \mathcal{H}: \langle f^*, \zeta(q, p) \rangle \leq \psi(q) - \psi(p), \forall q \in \mathcal{H}, & p \in \text{dom} \psi, \\ \emptyset, & p \notin \text{dom} \psi. \end{cases} \tag{12}$$

Definition 5 (see [12]). Let $\psi: \mathcal{H} \rightarrow \mathbb{R} \cup \{+\infty\}$ be a proper, ζ -subdifferential (may not be convex) functional, $\zeta: \mathcal{H} \times \mathcal{H} \rightarrow \mathcal{H}$, $T: \mathcal{H} \rightarrow \mathcal{H}$ be the mappings, and $I: \mathcal{H} \rightarrow \mathcal{H}$ be an identity mapping. If for any given $z \in \mathcal{H}$ and $\rho > 0$, there exists a unique point $p \in \mathcal{H}$ satisfying

$$\langle (I - T)p - z, \zeta(q, p) \rangle \geq \rho \psi(p) - \rho \psi(q), \quad \forall q \in \mathcal{H}, \tag{13}$$

then the mapping $z \mapsto p$, denoted by $\mathcal{F}_{\rho, T}^{\partial_\zeta \psi}(z)$, is said to be relaxed ζ -proximal operator of ψ . We have $z - (I - T)p \in \rho \partial_\zeta \psi(p)$, and it follows that

$$\mathcal{F}_{\rho, T}^{\partial_\zeta \psi}(z) = [(I - T) + \rho \partial_\zeta \psi]^{-1}(z). \tag{14}$$

Definition 6 (see [25]). Let $S, T: \mathcal{H} \rightarrow \mathcal{H}$ be the single-valued mappings, $p_0 \in \mathcal{H}$ and

$$p_{n+1} = S(T, p_n), \tag{15}$$

defines an iterative sequence which yields a sequence of points $\{p_n\}$ in \mathcal{H} . Suppose that $\text{Fix}(T) = \{p \in \mathcal{H}: Tp = p\} \neq \emptyset$ and $\{p_n\}$ converges to a fixed point p^* of T . Let $\{u_n\} \subset \mathcal{H}$ and

$$\vartheta_n = \|u_{n+1} - S(T, u_n)\|. \tag{16}$$

If $\lim_{n \rightarrow \infty} \vartheta_n = 0$, which implies that $u_n \rightarrow p^*$, then the iterative sequence $\{p_n\}$ is said to be T -stable or stable with respect to T .

Theorem 1 (see [12]). Let $\zeta: \mathcal{H} \times \mathcal{H} \rightarrow \mathcal{H}$ be a δ -strongly monotone and τ -Lipschitz continuous mapping such that $\zeta(p, q) = -\zeta(q, p)$, for all $p, q \in \mathcal{H}$. Let $T: \mathcal{H} \rightarrow \mathcal{H}$ be ζ -relaxed Lipschitz continuous mapping with constant α and $I: \mathcal{H} \rightarrow \mathcal{H}$ be an identity mapping. Let $\psi: \mathcal{H} \rightarrow \mathbb{R} \cup$

$\{+\infty\}$ be a proper, lower-semicontinuous, ζ -subdifferential functional which may not be convex, and for any $z, p \in \mathcal{H}$, the mapping $f(q, p) = \langle z - (I - R)p, \zeta(q, p) \rangle$ is 0-DQCV in q . Then, for any $\rho > 0$, and any $z \in \mathcal{H}$, there exists a unique $p \in \mathcal{H}$ such that $p = \mathcal{F}_{\rho, T}^{\partial_\zeta \psi}(z)$, and hence, the relaxed ζ -proximal operator $\mathcal{F}_{\rho, T}^{\partial_\zeta \psi}$ of ψ is well-defined and $(T/(\alpha + \delta))$ -Lipschitz continuous, i.e.,

$$\|\mathcal{F}_{\rho, T}^{\partial_\zeta \psi}(p) - \mathcal{F}_{\rho, T}^{\partial_\zeta \psi}(q)\| \leq \frac{\tau}{(\alpha + \delta)} \|p - q\|, \quad \forall p, q \in \mathcal{H}. \tag{17}$$

Lemma 1 (see [26]). Let $\{\varrho_n\}$, $\{\gamma_n\}$, and $\{\varrho_n\}$ be nonnegative real sequences satisfying the following condition: there exists a natural number n_0 such that

$$\varrho_{n+1} \leq (1 - \omega_n)\varrho_n + \gamma_n \omega_n + \varrho_n, \quad \forall n \geq n_0, \tag{18}$$

where $\omega \in [0, 1]$, $\sum_{n=0}^\infty \omega_n = \infty$, $\lim_{n \rightarrow \infty} \gamma_n = 0$, $\sum_{n=0}^\infty \varrho_n < \infty$. Then, $\lim_{n \rightarrow \infty} \varrho_n = 0$.

3. Formulation of the Problem and Existence Result

For each $i \in \Lambda = \{1, 2, 3, \dots, m\}$, let \mathcal{H}_i be a real Hilbert space equipped with the norm $\|\cdot\|_i$, and let $h_i, g_i, T_i: \mathcal{H}_i \rightarrow \mathcal{H}_i$, $\zeta_i: \mathcal{H}_i \times \mathcal{H}_i \rightarrow \mathcal{H}_i$, and $A_i: \prod_{j=1}^m \mathcal{H}_j \rightarrow \mathcal{H}_i$ be the nonlinear single-valued mappings, respectively. Let $\psi_i: \mathcal{H}_i \times \mathcal{H}_i \rightarrow \mathbb{R} \cup \{+\infty\}$ be such that for each fixed $p_i \in \mathcal{H}_i$, $\psi_i(\cdot, p_i)$ is lower semicontinuous, ζ_i -subdifferential, proper functional on $\mathcal{H}_i \times \mathcal{H}_i$ (may not be convex) satisfying $h_i(\mathcal{H}_i) \cap \text{dom}(\partial \psi_{\zeta_i}(\cdot, p_i)) \neq \emptyset$, where $\partial \psi_{\zeta_i}(\cdot, p_i)$ is a ζ_i -subdifferential of $\psi_i(\cdot, p_i)$. We consider the following system of extended nonlinear mixed variational-like inequalities (in short, SENMVLi).

For each $\rho_i > 0$, find $(p_1, p_2, \dots, p_m) \in \prod_{i=1}^m \mathcal{H}_i$ such that $h_i(p_i) \in \text{dom}(\partial_{\zeta_i} \psi_i(\cdot, p_i))$ and for all $q_i \in \mathcal{H}_i$

$$\left\{ \begin{aligned} \langle h_1(p_1) - (g_1(p_1) - \rho_1 A_1(p_1, p_2, \dots, p_m)), \zeta_1(q_1, h_1(p_1)) \rangle &\geq \rho_1 \psi_1(h_1(p_1), p_1) - \rho_1 \psi_1(q_1, p_1), \\ \langle h_2(p_2) - (g_2(p_2) - \rho_2 A_2(p_1, p_2, \dots, p_m)), \zeta_2(q_2, h_2(p_2)) \rangle &\geq \rho_2 \psi_2(h_2(p_2), p_2) - \rho_2 \psi_2(q_2, p_2), \\ \langle h_3(p_3) - (g_3(p_3) - \rho_3 A_3(p_1, p_2, \dots, p_m)), \zeta_3(q_3, h_3(p_3)) \rangle &\geq \rho_3 \psi_3(h_3(p_3), p_3) - \rho_3 \psi_3(q_3, p_3), \\ &\vdots \\ \langle h_m(p_m) - (g_m(p_m) - \rho_m A_m(p_1, p_2, \dots, p_m)), \zeta_m(q_m, h_m(p_m)) \rangle &\geq \rho_m \psi_m(h_m(p_m), p_m) - \rho_m \psi_m(q_m, p_m). \end{aligned} \right. \quad (19)$$

Equivalently, for each $i \in \Lambda$, above system can be written as

$$\begin{aligned} \langle h_i(p_i) - (g_i(p_i) - \rho_i A_i(p_1, p_2, \dots, p_m)), \zeta_i(q_i, h_i(p_i)) \rangle \\ \geq \rho_i \psi_i(h_i(p_i), p_i) - \rho_i \psi_i(q_i, p_i). \end{aligned} \quad (20)$$

Some special cases of problem (19) are as follows:

- (i) If $\rho_i = 1, \psi_i = 0, h_i, g_i = I_i$ (identity mappings) and $\psi_i(q_i, p_i) = \psi_i(q_i)$, for each $i \in \Lambda$, then problem (20) reduces to the problem of finding $(p_1, p_2, \dots, p_m) \in \prod_{i=1}^m \mathcal{H}_i$ such that

$$\langle A_i(p_1, p_2, \dots, p_m), \zeta_i(q_i, p_i) \rangle \geq \psi_i(p_i) - \psi_i(q_i). \quad (21)$$

Problem (21) was considered and studied by Balooee [27].

- (ii) If $\rho_i = 1, \psi_i = 0, h_i, g_i = I_i$ (identity mappings), and $\zeta_i(q_i, h_i(p_i)) = q_i - p_i$, for each $i \in \Lambda$, then problem (19) reduces to the problem of finding $(p_1, p_2, \dots, p_m) \in \prod_{i=1}^m \mathcal{H}_i$ such that

$$\left\{ \begin{aligned} \langle A_1(p_1, p_2, \dots, p_m), q_1 - p_1 \rangle &\geq 0, \\ \langle A_2(p_1, p_2, \dots, p_m), q_2 - p_2 \rangle &\geq 0, \\ \langle A_3(p_1, p_2, \dots, p_m), q_3 - p_3 \rangle &\geq 0, \\ &\vdots \\ \langle A_m(p_1, p_2, \dots, p_m), q_m - p_m \rangle &\geq 0. \end{aligned} \right. \quad (22)$$

Problem (22) was considered and studied by Tang et al. [28].

By taking suitable choices of the mappings $g_i, h_i, T_i, \psi_i, \zeta_i$ and the space \mathcal{H}_i , for each $i \in \Lambda$, in above problem (19), one can easily obtain the problems considered and studied in [9, 13, 14, 22, 29, 30] and references therein.

Example 1. Let $\mathbb{R} = (-\infty, \infty), \mathcal{H}_i = [a, b]$. Let $G(p_1, p_2, \dots, p_m)$ be a continuous real m -variable function with $G \in C^1(\mathcal{H}_i)$. Then, there exists an element $p_0 = (p_{0,1}, p_{0,2}, \dots, p_{0,m}) \in \prod_{i=1}^m \mathcal{H}_i$ such that

$$G(p_{0,1}, p_{0,2}, \dots, p_{0,m}) = \min_{(p_1, p_2, \dots, p_m) \in \prod_{i=1}^m \mathcal{H}_i} G(p_1, p_2, \dots, p_m). \quad (23)$$

This element p_0 must be a solution of the following system of variational inequalities:

$$\left\{ \begin{aligned} \left\langle \frac{\partial G}{\partial p_1}(p_1, p_2, \dots, p_m), q_1 - p_1 \right\rangle &\geq 0, \\ \left\langle \frac{\partial G}{\partial p_2}(p_1, p_2, \dots, p_m), q_2 - p_2 \right\rangle &\geq 0, \\ \left\langle \frac{\partial G}{\partial p_3}(p_1, p_2, \dots, p_m), q_3 - p_3 \right\rangle &\geq 0, \\ &\vdots \\ \left\langle \frac{\partial G}{\partial p_m}(p_1, p_2, \dots, p_m), q_m - p_m \right\rangle &\geq 0. \end{aligned} \right. \quad (24)$$

If fact, we have

$$\frac{\partial G}{\partial p_i}(p_1, p_2, \dots, p_m) \begin{cases} = 0, p_{0,i} \in (a, b), \\ \geq 0, p_{0,i} = a, \\ \leq 0, p_{0,i} = b, \end{cases} \quad (25)$$

for all $i = 1, 2, \dots, m$. Hence, p_0 must satisfy (24). In addition, the system of variational inequalities (24) is equivalent to

$$\langle \text{grad } G(p), q - p \rangle \geq 0, \quad (26)$$

where $\text{grad } G(x) = ((\partial G/\partial p_1), (\partial G/\partial p_2), \dots, (\partial G/\partial p_m))$. This example is special case of a practical background of problem (19), where $A_i = (\partial G/\partial p_i), h_i, g_i = I_i, \rho_i = 1$ and $\psi_i = 0$, for all $i = 1, 2, \dots, m$ and $\text{grad } G(x) = A^*$.

The following lemma ensures the equivalence between the system of extended nonlinear mixed variational-like inequalities (19) and fixed point problem.

Lemma 2. For each $i \in \Lambda$, let $(p_1, p_2, \dots, p_m) \in \prod_{i=1}^m \mathcal{H}_i$ is a solution of the system of extended nonlinear mixed

variational-like inequalities (19) if and only if (p_1, p_2, \dots, p_m) satisfies the following equation:

$$h_i(p_i) = \mathcal{F}_{\rho_i, T_i}^{\partial_{\zeta_i} \psi_i(\cdot, p_i)} [g_i(p_i) - (T_i(h_i(p_i)) + \rho_i A_i(p_1, p_2, \dots, p_m))], \quad (27)$$

where $\mathcal{F}_{\rho_i, T_i}^{\partial_{\zeta_i} \psi_i(\cdot, p_i)} = [(I_i - T_i) + \rho_i \partial_{\zeta_i} \psi_i(\cdot, p_i)]^{-1}$, T_i is ζ_i -relaxed Lipschitz continuous mapping with constant α_i , and I_i is the identity mapping on \mathcal{H}_i .

Proof. Assume that $(p_1, p_2, \dots, p_m) \in \prod_{i=1}^m \mathcal{H}_i$ satisfies relation (27), i.e.,

$$h_i(p_i) = \mathcal{F}_{\rho_i, T_i}^{\partial_{\zeta_i} \psi_i(\cdot, p_i)} [g_i(p_i) - (T_i(h_i(p_i)) + \rho_i A_i(p_1, p_2, \dots, p_m))]. \quad (28)$$

Since $\mathcal{F}_{\rho_i, T_i}^{\partial_{\zeta_i} \psi_i(\cdot, p_i)} = [(I_i - T_i) + \rho_i \partial_{\zeta_i} \psi_i(\cdot, p_i)]^{-1}$, the above equality holds if and only if

$$\begin{aligned} &g_i(p_i) - (T_i(h_i(p_i)) + \rho_i A_i(p_1, p_2, \dots, p_m)) \\ &\in h_i(p_i) - T_i(h_i(p_i)) + \rho_i \partial_{\zeta_i} \psi_i(h_i(p_i), p_i). \end{aligned} \quad (29)$$

By using the definition of ζ_i -subdifferential of $\psi_i(\cdot, p_i)$, the above relation holds if and only if

$$\begin{aligned} &\langle (g_i(p_i) - \rho_i A_i(p_1, p_2, \dots, p_m)) - h_i(p_i), \zeta_i(q_i, h_i(p_i)) \rangle \\ &\leq \rho_i \psi_i(q_i, p_i) - \rho_i \psi_i(h_i(p_i), p_i). \end{aligned} \quad (30)$$

Hence, we have

$$\begin{aligned} &\langle h_i(p_i) - (g_i(p_i) - \rho_i A_i(p_1, p_2, \dots, p_m)), \zeta_i(q_i, h_i(p_i)) \rangle \\ &\geq \rho_i \psi_i(h_i(p_i), p_i) - \rho_i \psi_i(q_i, p_i), \end{aligned} \quad (31)$$

i.e., (p_1, p_2, \dots, p_m) is a solution of system of extended nonlinear mixed variational-like inequalities (19). \square

In the next theorem, we discuss the existence and uniqueness of the solution of the SENMVLI (19).

Theorem 2. For each $i \in \Lambda$, let $g_i, h_i, T_i: \mathcal{H}_i \rightarrow \mathcal{H}_i$, $\zeta_i: \mathcal{H}_i \times \mathcal{H}_i \rightarrow \mathcal{H}_i$, and $A_i: \prod_{i=1}^m \mathcal{H}_i \rightarrow \mathcal{H}_i$ be the nonlinear single-valued mappings such that g_i is λ_{g_i} -Lipschitz continuous and μ_{g_i} -strongly monotone, h_i is λ_{h_i} -Lipschitz continuous and μ_{h_i} -strongly monotone such that $h_i(\mathcal{H}_i) = \mathcal{H}_i$, T_i is λ_{T_i} -Lipschitz continuous, relaxed α_i -Lipschitz continuous, and μ_{T_i} -strongly monotone with respect to h_i , ζ_i is τ_i -Lipschitz continuous, and ζ_i is δ_i -strongly monotone such that $\zeta_i(p_i, q_i) = -\zeta_i(q_i, p_i)$, for each $p_i, q_i \in \mathcal{H}_i$, A_i is λ_{A_i} -Lipschitz continuous in the i^{th} -argument

and $\nu_{i,j}$ -Lipschitz continuous in the j^{th} -argument for each $j \in \Lambda, i \neq j$, and μ_{A_i} -strongly monotone in the i^{th} -argument with respect to g_i , respectively. Let $\psi_i: \mathcal{H}_i \times \mathcal{H}_i \rightarrow \mathbb{R} \cup \{+\infty\}$ be such that for each fixed $p_i \in \mathcal{H}_i$, $\psi_i(\cdot, p_i)$ is lower-semicontinuous, ζ_i -subdifferential, proper functional on $\mathcal{H}_i \times \mathcal{H}_i$ (may not be convex) satisfying $h_i(\mathcal{H}_i) \cap \text{dom}(\partial \psi_{\zeta_i}(\cdot, p_i)) \neq \emptyset$, where $\partial \psi_{\zeta_i}(\cdot, p_i)$ is a ζ_i -subdifferential of $\psi_i(\cdot, p_i)$. Suppose that there exist constants $\rho_i > 0$, $\xi_i > 0$ such that for each $z_i \in \mathcal{H}_i$

$$\left\| \mathcal{F}_{\rho_i, T_i}^{\partial_{\zeta_i} \psi_i(\cdot, p_i)}(z_i) - \mathcal{F}_{\rho_i, T_i}^{\partial_{\zeta_i} \psi_i(\cdot, q_i)}(z_i) \right\| \leq \xi_i \|p_i - q_i\|, \quad (32)$$

and the following conditions are satisfied:

$$\left\{ \begin{aligned} &\theta_i = \xi_i + \sqrt{(1 - 2\mu_{h_i} + \lambda_{h_i}^2)} + \sum_{k \in \Lambda, k \neq i} \frac{\tau_k \rho_k}{\alpha_k + \delta_k} \nu_{k,i} < 1, \\ &\tau_i \sqrt{(\lambda_{g_i}^2 - 2\rho_i \mu_{A_i} + \rho_i^2 \lambda_{A_i}^2)} < [(1 - \theta_i)(\alpha_i + \delta_i) - \tau_i \lambda_{T_i} \lambda_{h_i}], \\ &2\mu_{h_i} < 1 + \lambda_{h_i}^2, \\ &2\rho_i \mu_{A_i} < \lambda_{g_i}^2 + \rho_i^2 \lambda_{A_i}^2. \end{aligned} \right. \quad (33)$$

Then, the SENMVLI (19) admits a unique solution $(p_1^*, p_2^*, \dots, p_m^*)$.

Proof. By Lemma 2, it is sufficient to prove that there exist $(p_1^*, p_2^*, \dots, p_m^*)$ which satisfying (27). For each $i \in \Lambda$, we define $\phi_i: \prod_{i=1}^m \mathcal{H}_i \rightarrow \mathcal{H}_i$ by

$$\phi_i(p_1, p_2, \dots, p_m) = p_i - h_i(p_i) + \mathcal{F}_{\rho_i, T_i}^{\partial_{\zeta_i} \psi_i(\cdot, p_i)} [g_i(p_i) - (T_i(h_i(p_i)) + \rho_i A_i(p_1, p_2, \dots, p_m))], \quad (34)$$

for all $(p_1, p_2, \dots, p_m) \in \prod_{i=1}^m \mathcal{H}_i$. Define $\|\cdot\|_*$ on $\prod_{i=1}^m \mathcal{H}_i$ by

$$\|(p_1, p_2, p_3, \dots, p_m)\|_* = \sum_{i=1}^m \|p_i\|_i, \forall (p_1, p_2, \dots, p_m) \in \prod_{i=1}^m \mathcal{H}_i. \quad (35)$$

It is easy to see that $(\prod_{i=1}^m \mathcal{H}_i, \|\cdot\|_*)$ is a Hilbert space. Also, define $G: \prod_{i=1}^m \mathcal{H}_i \rightarrow \prod_{i=1}^m \mathcal{H}_i$ as follows:

$$G(p_1, p_2, \dots, p_m) = (\phi_1(p_1, p_2, \dots, p_m), \phi_2(p_1, p_2, \dots, p_m), \dots, \phi_m(p_1, p_2, \dots, p_m)), \quad (36)$$

for all $(p_1, p_2, \dots, p_m) \in \prod_{i=1}^m \mathcal{H}_i$. First of all, we prove that G is a contraction mapping.

Let $(p_1, p_2, \dots, p_m), (\widehat{p}_1, \widehat{p}_2, \dots, \widehat{p}_m) \in \prod_{i=1}^m \mathcal{H}_i$ be given. By using (32) and (34) and Theorem 1, for each $i \in \Lambda$, we have

$$\begin{aligned} & \|\phi_i(p_1, p_2, \dots, p_m) - \phi_i(\widehat{p}_1, \widehat{p}_2, \dots, \widehat{p}_m)\|_i \\ &= \left\| \left[p_i - h_i(p_i) + \mathcal{F}_{\rho_i, T_i}^{\partial_{\xi} \Psi_i(\cdot, p_i)} [g_i(p_i) - (T_i(h_i(p_i)) + \rho_i A_i(p_1, p_2, \dots, p_m))] \right] - \left[\widehat{p}_i - h_i(\widehat{p}_i) + \mathcal{F}_{\rho_i, T_i}^{\partial_{\xi} \Psi_i(\cdot, \widehat{p}_i)} [g_i(\widehat{p}_i) - (T_i(h_i(\widehat{p}_i)) + \rho_i A_i(\widehat{p}_1, \widehat{p}_2, \dots, \widehat{p}_m))] \right] \right\|_i \\ &\leq \left\| (p_i - h_i(p_i)) - (\widehat{p}_i - h_i(\widehat{p}_i)) \right\|_i + \left\| \mathcal{F}_{\rho_i, T_i}^{\partial_{\xi} \Psi_i(\cdot, p_i)} [g_i(p_i) - (T_i(h_i(p_i)) + \rho_i A_i(p_1, p_2, \dots, p_m))] - \mathcal{F}_{\rho_i, T_i}^{\partial_{\xi} \Psi_i(\cdot, \widehat{p}_i)} [g_i(\widehat{p}_i) - (T_i(h_i(\widehat{p}_i)) + \rho_i A_i(\widehat{p}_1, \widehat{p}_2, \dots, \widehat{p}_m))] \right\|_i \\ &\quad + \left\| \mathcal{F}_{\rho_i, T_i}^{\partial_{\xi} \Psi_i(\cdot, \widehat{p}_i)} [g_i(p_i) - (T_i(h_i(p_i)) + \rho_i A_i(p_1, p_2, \dots, p_m))] - \mathcal{F}_{\rho_i, T_i}^{\partial_{\xi} \Psi_i(\cdot, \widehat{p}_i)} [g_i(\widehat{p}_i) - (T_i(h_i(\widehat{p}_i)) + \rho_i A_i(\widehat{p}_1, \widehat{p}_2, \dots, \widehat{p}_m))] \right\|_i \leq \|p_i - h_i(p_i) - (\widehat{p}_i - h_i(\widehat{p}_i))\|_i + \xi_i \|p_i - \widehat{p}_i\|_i \\ &\quad + \left\| \mathcal{F}_{\rho_i, T_i}^{\partial_{\xi} \Psi_i(\cdot, \widehat{p}_i)} [g_i(p_i) - (T_i(h_i(p_i)) + \rho_i A_i(p_1, p_2, \dots, p_m))] - \mathcal{F}_{\rho_i, T_i}^{\partial_{\xi} \Psi_i(\cdot, \widehat{p}_i)} [g_i(\widehat{p}_i) - (T_i(h_i(\widehat{p}_i)) + \rho_i A_i(\widehat{p}_1, \widehat{p}_2, \dots, \widehat{p}_m))] \right\|_i \\ &\quad + \frac{\tau_i}{\alpha_i + \delta_i} \left\| [g_i(p_i) - (T_i(h_i(p_i)) + \rho_i A_i(p_1, p_2, \dots, p_m))] - [g_i(\widehat{p}_i) - (T_i(h_i(\widehat{p}_i)) + \rho_i A_i(\widehat{p}_1, \widehat{p}_2, \dots, \widehat{p}_m))] \right\|_i \leq \|p_i - h_i(p_i) - (\widehat{p}_i - h_i(\widehat{p}_i))\|_i + \xi_i \|p_i - \widehat{p}_i\|_i \\ &\quad + \frac{\tau_i}{\alpha_i + \delta_i} \left\| [(g_i(p_i) - g_i(\widehat{p}_i)) - (T_i(h_i(p_i)) - T_i(h_i(\widehat{p}_i)))] - \rho_i [A_i(p_1, p_2, \dots, p_{i-1}, p_i, p_{i+1}, \dots, p_m) - A_i(p_1, p_2, \dots, p_{i-1}, \widehat{p}_i, p_{i+1}, \dots, p_m)] \right\|_i \\ &\quad + \frac{\tau_i \rho_i}{\alpha_i + \delta_i} \left[\left\| A_i(p_1, p_2, \dots, p_{i-1}, p_i, p_{i+1}, \dots, p_m) - A_i(p_1, p_2, \dots, p_{i-1}, p_i, p_{i+1}, \dots, \widehat{p}_m) \right\|_m + \left\| A_i(p_1, p_2, \dots, p_{i-1}, p_i, p_{i+1}, \dots, \widehat{p}_m) - A_i(p_1, p_2, \dots, p_{i-1}, p_i, p_{i+1}, \dots, \widehat{p}_m) \right\|_{m-1} \right. \\ &\quad \left. + \left\| A_i(p_1, p_2, \dots, p_{i-1}, p_i, p_{i+1}, \dots, \widehat{p}_m) - A_i(p_1, p_2, \dots, p_{i-1}, p_i, p_{i+1}, \dots, \widehat{p}_m) \right\|_{m-2} \dots + \left\| A_i(p_1, \widehat{p}_2, \dots, \widehat{p}_{i-1}, p_i, \widehat{p}_{i+1}, \dots, \widehat{p}_m) - A_i(\widehat{p}_1, \widehat{p}_2, \dots, \widehat{p}_{i-1}, p_i, \widehat{p}_{i+1}, \dots, \widehat{p}_m) \right\|_1 \right] \\ &\leq \|p_i - h_i(p_i) - (\widehat{p}_i - h_i(\widehat{p}_i))\|_i + \xi_i \|p_i - \widehat{p}_i\|_i \\ &\quad + \frac{\tau_i}{\alpha_i + \delta_i} \left\| [(g_i(p_i) - g_i(\widehat{p}_i)) - (T_i(h_i(p_i)) - T_i(h_i(\widehat{p}_i)))] - \rho_i [A_i(p_1, p_2, \dots, p_{i-1}, p_i, p_{i+1}, \dots, p_m) - A_i(p_1, p_2, \dots, p_{i-1}, \widehat{p}_i, p_{i+1}, \dots, p_m)] \right\|_i \\ &\quad + \frac{\tau_i \rho_i}{\alpha_i + \delta_i} \sum_{j \in \Lambda, j \neq i} \left(\left\| A_i(p_1, p_2, \dots, p_{j-1}, p_j, p_{j+1}, \dots, p_m) - A_i(p_1, p_2, \dots, p_{j-1}, \widehat{p}_j, p_{j+1}, \dots, \widehat{p}_m) \right\|_i \right) \leq \|p_i - \widehat{p}_i\|_i - (h_i(p_i) - h_i(\widehat{p}_i))\|_i + \xi_i \|p_i - \widehat{p}_i\|_i \\ &\quad + \frac{\tau_i}{\alpha_i + \delta_i} \left[\|T_i(h_i(p_i)) - T_i(h_i(\widehat{p}_i))\|_i + \left\| (g_i(p_i) - g_i(\widehat{p}_i)) - \rho_i [A_i(p_1, p_2, \dots, p_{i-1}, p_i, p_{i+1}, \dots, p_m) - A_i(p_1, p_2, \dots, p_{i-1}, \widehat{p}_i, p_{i+1}, \dots, p_m)] \right\|_i \right] \\ &\quad + \frac{\tau_i \rho_i}{\alpha_i + \delta_i} \sum_{j \in \Lambda, j \neq i} \left(\left\| A_i(p_1, p_2, \dots, p_{j-1}, p_j, p_{j+1}, \dots, p_m) - A_i(p_1, p_2, \dots, p_{j-1}, \widehat{p}_j, p_{j+1}, \dots, \widehat{p}_m) \right\|_i \right) \leq \|p_i - \widehat{p}_i\|_i - (h_i(p_i) - h_i(\widehat{p}_i))\|_i + \xi_i \|p_i - \widehat{p}_i\|_i \\ &\quad + \frac{\tau_i}{\alpha_i + \delta_i} [\lambda_{T_i} \lambda_{h_i} \|p_i - \widehat{p}_i\|_i + \left\| (g_i(p_i) - g_i(\widehat{p}_i)) - \rho_i [A_i(p_1, p_2, \dots, p_{i-1}, p_i, p_{i+1}, \dots, p_m) - A_i(p_1, p_2, \dots, p_{i-1}, \widehat{p}_i, p_{i+1}, \dots, p_m)] \right\|_i] \\ &\quad + \frac{\tau_i \rho_i}{\alpha_i + \delta_i} \sum_{j \in \Lambda, j \neq i} \left(\left\| A_i(p_1, p_2, \dots, p_{j-1}, p_j, p_{j+1}, \dots, p_m) - A_i(p_1, p_2, \dots, p_{j-1}, \widehat{p}_j, p_{j+1}, \dots, \widehat{p}_m) \right\|_i \right). \end{aligned} \quad (37)$$

It follows from μ_{h_i} -strongly monotonicity and λ_{h_i} -Lipschitz continuity of h_i that

$$\begin{aligned} \|p_i - \widehat{p}_i - (h_i(p_i) - h_i(\widehat{p}_i))\|_i^2 &= \|p_i - \widehat{p}_i\|_i^2 - 2 \langle h_i(p_i) - h_i(\widehat{p}_i), p_i - \widehat{p}_i \rangle + \|h_i(p_i) - h_i(\widehat{p}_i)\|_i^2 \\ &\leq \|p_i - \widehat{p}_i\|_i^2 - 2\mu_{h_i} \|p_i - \widehat{p}_i\|_i^2 + \lambda_{h_i}^2 \|p_i - \widehat{p}_i\|_i^2 \\ &= (1 - 2\mu_{h_i} + \lambda_{h_i}^2) \|p_i - \widehat{p}_i\|_i^2, \end{aligned} \quad (38)$$

i.e.,

$$\|p_i - \widehat{p}_i - (h_i(p_i) - h_i(\widehat{p}_i))\|_i \leq \sqrt{(1 - 2\mu_{h_i} + \lambda_{h_i}^2)} \|p_i - \widehat{p}_i\|_i. \quad (39)$$

By using the $\lambda_{A_{ii}}$ -Lipschitz continuity of A_i and $\mu_{A_{ii}}$ -strongly monotonicity of A_i with respect to g_i and λ_{g_i} -Lipschitz continuity of g_i , respectively, we evaluate

$$\begin{aligned} & \| (g_i(p_i) - g_i(\widehat{p}_i)) - \rho_i [A_i(p_1, p_2, \dots, p_{i-1}, p_i, p_{i+1}, \dots, p_m) - A_i(p_1, p_2, \dots, p_{i-1}, \widehat{p}_i, p_{i+1}, \dots, p_m)] \|_i^2 \\ & \leq \| (g_i(p_i) - g_i(\widehat{p}_i)) \|^2 - 2\rho_i \langle A_i(p_1, p_2, \dots, p_{i-1}, p_i, p_{i+1}, \dots, p_m) - A_i(p_1, p_2, \dots, p_{i-1}, \widehat{p}_i, p_{i+1}, \dots, p_m), (g_i(p_i) - g_i(\widehat{p}_i)) \rangle \\ & \quad + \rho_i^2 \| A_i(p_1, p_2, \dots, p_{i-1}, p_i, p_{i+1}, \dots, p_m) - A_i(p_1, p_2, \dots, p_{i-1}, \widehat{p}_i, p_{i+1}, \dots, p_m) \|_i^2 \\ & \leq \lambda_{g_i}^2 \|p_i - \widehat{p}_i\|_i^2 - 2\rho_i \langle A_i(p_1, p_2, \dots, p_{i-1}, p_i, p_{i+1}, \dots, p_m) - A_i(p_1, p_2, \dots, p_{i-1}, \widehat{p}_i, p_{i+1}, \dots, p_m), g_i(p_i) - g_i(\widehat{p}_i) \rangle \\ & \quad + \rho_i^2 \lambda_{A_{ii}}^2 \|p_i - \widehat{p}_i\|_i^2 \\ & \leq \lambda_{g_i}^2 \|p_i - \widehat{p}_i\|_i^2 - 2\rho_i \mu_{A_{ii}} \|p_i - \widehat{p}_i\|_i^2 + \rho_i^2 \lambda_{A_{ii}}^2 \|p_i - \widehat{p}_i\|_i^2 \\ & = (\lambda_{g_i}^2 - 2\rho_i \mu_{A_{ii}} + \rho_i^2 \lambda_{A_{ii}}^2) \|p_i - \widehat{p}_i\|_i^2, \end{aligned} \quad (40)$$

which implies that

$$\begin{aligned} & \| (g_i(p_i) - g_i(\widehat{p}_i)) - \rho_i [A_i(p_1, p_2, \dots, p_{i-1}, p_i, p_{i+1}, \dots, p_m) - A_i(p_1, p_2, \dots, p_{i-1}, \widehat{p}_i, p_{i+1}, \dots, p_m)] \|_i \\ & \leq \sqrt{(\lambda_{g_i}^2 - 2\rho_i \mu_{A_{ii}} + \rho_i^2 \lambda_{A_{ii}}^2)} \|p_i - \widehat{p}_i\|_i, \end{aligned} \quad (41)$$

Since for $i \in \Lambda$, A_i is $\nu_{i,j}$ -Lipschitz continuous in the j^{th} argument ($j \in \Lambda, j \neq i$), we have

$$\|A_i(p_1, p_2, \dots, p_{j-1}, p_j, p_{j+1}, \dots, p_m) - A_i(p_1, p_2, \dots, p_{j-1}, \widehat{p}_j, p_{j+1}, \dots, p_m)\|_i \leq \nu_{i,j} \|p_j - \widehat{p}_j\|_j. \quad (42)$$

Substituting (39)–(42) in (37), for $i \in \Lambda$, we deduce that

$$\begin{aligned} \| \phi_i(p_1, p_2, \dots, p_m) - \phi_i(\widehat{p}_1, \widehat{p}_2, \dots, \widehat{p}_m) \|_i & \leq \left[\xi_i + \sqrt{(1 - 2\mu_{h_i} + \lambda_{h_i}^2)} + \frac{\tau_i (\lambda_{T_i} \lambda_{h_i} + \sqrt{(\lambda_{g_i}^2 - 2\rho_i \mu_{A_{ii}} + \rho_i^2 \lambda_{A_{ii}}^2)})}{\alpha_i + \delta_i} \right] \|p_i - \widehat{p}_i\|_i \\ & \quad + \frac{\tau_i \rho_i}{\alpha_i + \delta_i} \sum_{j \in \Lambda, i \neq j} \nu_{i,j} \|p_j - \widehat{p}_j\|_j, \end{aligned} \quad (43)$$

i.e.,

$$\| \phi_i(p_1, p_2, \dots, p_m) - \phi_i(\widehat{p}_1, \widehat{p}_2, \dots, \widehat{p}_m) \|_i \leq \Theta_i \left\| p_i - \widehat{p}_i + \frac{\tau_i \rho_i}{\alpha_i + \delta_i} \sum_{j \in \Lambda, i \neq j} \nu_{i,j} \|p_j - \widehat{p}_j\|_j \right\|, \quad (44)$$

where $\Theta_i = \xi_i + \sqrt{(1 - 2\mu_{h_i} + \lambda_{h_i}^2) + \sqrt{(\lambda_{g_i}^2 - 2\rho_i\mu_{A_{ii}} + \rho_i^2\lambda_{A_{ii}}^2)}/\alpha_i + \delta_i}$ $\tau_i(\lambda_{T_i}\lambda_{h_i} +$

From (36) and (42), we get

$$\begin{aligned} \|G(p_1, p_2, \dots, p_m) - G(\hat{p}_1, \hat{p}_2, \dots, \hat{p}_m)\|_* &= \sum_{i=1}^m \|\phi_i(p_1, p_2, \dots, p_m) - \phi_i(\hat{p}_1, \hat{p}_2, \dots, \hat{p}_m)\|_i \\ &\leq \sum_{i=1}^m \left(\Theta_i \|p_i - \hat{p}_i\|_i + \frac{\tau_i \rho_i}{\alpha_i + \delta_i} \sum_{j \in \Lambda, i \neq j} \nu_{i,j} \|p_j - \hat{p}_j\|_j \right) \\ &= \left(\Theta_1 + \sum_{k=2}^m \frac{\tau_k \rho_k}{\alpha_k + \delta_k} \nu_{k,1} \right) \|p_1 - \hat{p}_1\|_1 \\ &\quad + \left(\Theta_2 + \sum_{k \in \Lambda, k \neq 2} \frac{\tau_k \rho_k}{\alpha_k + \delta_k} \nu_{k,2} \right) \|p_2 - \hat{p}_2\|_2 + \dots + \left(\Theta_m + \sum_{k=1}^{m-1} \frac{\tau_k \rho_k}{\alpha_k + \delta_k} \nu_{k,m} \right) \|p_m - \hat{p}_m\|_m \\ &\leq \max \left\{ \Theta_i + \sum_{k \in \Lambda, k \neq i} \frac{\tau_k \rho_k}{\alpha_k + \delta_k} \nu_{k,i}; i \in \Lambda \right\} \sum_{i=1}^m \|p_i - \hat{p}_i\|_i, \end{aligned} \tag{45}$$

i.e.,

$$\|G(p_1, p_2, \dots, p_m) - G(\hat{p}_1, \hat{p}_2, \dots, \hat{p}_m)\|_* \leq \Omega \| (p_1, p_2, \dots, p_m) - (\hat{p}_1, \hat{p}_2, \dots, \hat{p}_m) \|_*, \tag{46}$$

where $\Omega = \max \{ \Theta_i + \sum_{k \in \Lambda, k \neq i} (\tau_k \rho_k) / (\alpha_k + \delta_k) \nu_{k,i}; i \in \Lambda \}$. The condition (33) guarantees that $0 \leq \Omega < 1$. By the inequality (44), we note that G is a contraction mapping. Therefore, there exists a unique point $(p_1^*, p_2^*, \dots, p_m^*) \in$

$\prod_{i=1}^m \mathcal{H}_i$ such that $G(p_1^*, p_2^*, \dots, p_m^*) = (p_1^*, p_2^*, \dots, p_m^*)$. From (34) and (36), it follows that $(p_1^*, p_2^*, \dots, p_m^*)$ satisfies in equation (27), i.e., for each $i \in \Lambda$,

$$h_i(p_i^*) = \mathcal{F}_{\rho_i, T_i}^{\delta_{\tau_i}, \psi_i}(\cdot, p_i^*) [g_i(p_i^*) - (T_i(h_i(p_i^*)) + \rho_i A_i(p_1^*, p_2^*, \dots, p_m^*))]. \tag{47}$$

By Lemma 2, we conclude that $(p_1^*, p_2^*, \dots, p_m^*) \in \prod_{i=1}^m \mathcal{H}_i$ is a unique solution of SENMVL I (19). This completes the proof. \square

4. Proximal Iterative Schemes and Stability Analysis

In this section, we first recall some definitions related to nearly uniformly Lipschitzian mapping. Furthermore, we use a nearly uniformly Lipschitzian mapping $Q_i, i \in \Lambda$, to define a self-mapping $S = (Q_1, Q_2, \dots, Q_m)$ on $\prod_{i=1}^m \mathcal{H}_i$, by using the equivalent alternative formulation (27) to suggest and analyze some proximal iterative algorithms for finding an element of the set of the fixed points of S which is the unique solution of the problem SENMVL I (19).

Definition 7 (see [9]). A nonlinear mapping $Q: \mathcal{H} \rightarrow \mathcal{H}$ is said to be

(i) generalized Lipschitzian if, there exists a constant $k' > 0$ such that

$$\|Q(p) - Q(q)\| \leq k' (\|p - q\| + 1), \quad \forall p, q \in \mathcal{H}, \tag{48}$$

(ii) uniformly k -Lipschitzian if, there exists a constant $k > 0$ such that for each $n \in \mathbb{N}$,

$$\|Q^n(p) - Q^n(q)\| \leq k \|p - q\|, \quad \forall p, q \in \mathcal{H}, \tag{49}$$

(iii) nearly Lipschitzian with respect to the sequence $\{\alpha_n\}$ if, for each $n \in \mathbb{N}$, there exists a constant $\kappa_n > 0$ such that

$$\|Q^n(x) - Q^n(y)\| \leq \kappa_n(\|p - q\| + \alpha_n), \quad \forall p, q \in \mathcal{H}, \tag{50}$$

where $\{\alpha_n\}$ is a fixed sequence in $[0, \infty]$ with $\alpha_n \rightarrow 0$ as $n \rightarrow \infty$.

For an arbitrary, but fixed $n \in \mathbb{N}$, the infimum of constants κ_n in (50) is called nearly Lipschitz constant and it is denoted by $\beta(Q^n)$. Notice that

$$\beta(Q^n) = \sup \left\{ \frac{\|Q^n(p) - Q^n(q)\|}{\|p - q\| + \alpha_n} : p, q \in \mathcal{H}, p \neq q \right\}. \tag{51}$$

Definition 8 (see [9]). A nearly Lipschitzian mapping $Q: \mathcal{H} \rightarrow \mathcal{H}$ with the sequence $\{\alpha_n, \beta(Q^n)\}$ is said to be nearly uniformly K -Lipschitzian mapping if, $\beta(Q^n) < K$, for all $n \in \mathbb{N}$. In other words, $\alpha_n = K$, for all $n \in \mathbb{N}$.

For each $i \in \Lambda$, let $Q_i: \mathcal{H}_i \rightarrow \mathcal{H}_i$ be a nearly uniformly K_i -Lipschitzian mapping with the sequence $\{l_{i,n}\}$. We define the self-mapping S of $\prod_{i=1}^m \mathcal{H}_i$ by

$$S(p_1, p_2, \dots, p_m) = (Q_1 p_1, Q_2 p_2, \dots, Q_m p_m), \quad \forall (p_1, p_2, \dots, p_m) \in \prod_{i=1}^m \mathcal{H}_i. \tag{52}$$

Then, $S = (Q_1, Q_2, \dots, Q_m): \prod_{i=1}^m \mathcal{H}_i \rightarrow \prod_{i=1}^m \mathcal{H}_i$ is a nearly uniformly $\max\{K_i: i \in \Lambda\}$ -Lipschitzian mapping with the sequence $\{\sum_{i=1}^m l_{i,n}\}_{n=1}^\infty$ with respect to the norm $\|\cdot\|_*$

in $\prod_{i=1}^m \mathcal{H}_i$. To see this fact, let $(p_1, p_2, \dots, p_m), (\hat{p}_1, \hat{p}_2, \dots, \hat{p}_m) \in \prod_{i=1}^m \mathcal{H}_i$ be given. Then for any $n \in \mathbb{N}$, we have

$$\begin{aligned} \|S^n(p_1, p_2, \dots, p_m) - S^n(\hat{p}_1, \hat{p}_2, \dots, \hat{p}_m)\|_* &= \|(Q_1^n p_1, Q_2^n p_2, \dots, Q_m^n p_m) - (Q_1^n \hat{p}_1, Q_2^n \hat{p}_2, \dots, Q_m^n \hat{p}_m)\|_* \\ &= \|(Q_1^n p_1 - Q_1^n \hat{p}_1, Q_2^n p_2 - Q_2^n \hat{p}_2, \dots, Q_m^n p_m - Q_m^n \hat{p}_m)\|_* \\ &= \sum_{i=1}^m \|Q_i^n p_i - Q_i^n \hat{p}_i\| \leq \sum_{i=1}^m K_i (\|p_i - \hat{p}_i\| + l_{i,n}) \\ &\leq \max\{K_i: i \in \Lambda\} \sum_{i=1}^m (\|p_i - \hat{p}_i\| + l_{i,n}) \\ &= \max\{K_i: i \in \Lambda\} \left(\|(p_1, p_2, \dots, p_m) - (\hat{p}_1, \hat{p}_2, \dots, \hat{p}_m)\|_* + \sum_{i=1}^m l_{i,n} \right). \end{aligned} \tag{53}$$

We denote the sets of all the fixed points of $Q_i, i \in \Lambda$ and S by $\text{Fix}(Q_i)$ and $\text{Fix}(S)$, respectively, and the set of all the solutions of SENMVLI (19) by $\text{SENMVLI}(\mathcal{H}_i, g_i, h_i, T_i, \psi_i, A_i, i \in \Lambda)$. In view of (52), for any $(p_1, p_2, \dots, p_m) \in \prod_{i=1}^m \mathcal{H}_i, (p_1, p_2, \dots, p_m) \in \text{Fix}(S)$ if and only if

$$p_i \in \text{Fix}(Q_i), i \in \Lambda, \quad \text{i.e.,} \quad \text{Fix}(S) = \text{Fix}(Q_1, Q_2, \dots, Q_m) = \prod_{i=1}^m \text{Fix}(Q_i).$$

If $(p_1^*, p_2^*, \dots, p_m^*) \in \text{Fix}(S) \cap \text{SENMVLI}(\mathcal{H}_i, g_i, h_i, T_i, \psi_i, A_i, i \in \Lambda)$, then by using Lemma 2, one can easily see that for each $i \in \Lambda$ and for all $n \in \mathbb{N}$,

$$\begin{cases} p_i^* = Q_i^n p_i^* = p_i^* - h_i(p_i^*) + \mathcal{F}_{\rho_i, T_i}^{\partial_{\zeta_i} \psi_i(\cdot, p_i^*)} [g_i(p_i^*) - (T_i(h_i(p_i^*)) + \rho_i A_i(p_1^*, p_2^*, \dots, p_m^*))] \\ = Q_i^n [p_i^* - h_i(p_i^*) + \mathcal{F}_{\rho_i, T_i}^{\partial_{\zeta_i} \psi_i(\cdot, p_i^*)} [g_i(p_i^*) - (T_i(h_i(p_i^*)) + \rho_i A_i(p_1^*, p_2^*, \dots, p_m^*))]] \end{cases} \tag{54}$$

The fixed point formulation (54) enables us to suggest the following proximal iterative algorithm with mixed errors for finding an element of the set of the fixed points of the nearly uniformly Lipschitzian mapping $S = (Q_1, Q_2, \dots, Q_m)$ which is also a unique solution of SENMVLI (19).

Iterative Algorithm 1. For each $i \in \Lambda$, let $\mathcal{H}_i, g_i, h_i, T_i, \psi_i, \zeta_i$ and $\rho_i > 0$ be the same as in SENMVLI (19). For any given $(p_{1,1}, p_{2,1}, \dots, p_{m,1}) \in \prod_{i=1}^m \mathcal{H}_i$, compute the iterative sequences $\{p_{i,n}\}_{n=1}^\infty = \{(p_{1,n}, p_{2,n}, \dots, p_{m,n})\}_{n=1}^\infty <i>, </i>$, $\{u_{i,n}\}_{n=1}^\infty = \{(u_{1,n}, u_{2,n}, \dots, u_{m,n})\}_{n=1}^\infty <i>, </i>$ $\{v_{i,n}\}_{n=1}^\infty =$

$\{(v_{1,n}, v_{2,n}, \dots, v_{m,n})\}_{n=1}^\infty \langle /i \rangle, \langle //i \rangle \{s_{i,n}\}_{n=1}^\infty = \{(s_{1,n}, s_{2,n}, \dots, s_{m,n})\}_{n=1}^\infty$ by the following iterative process:

$$\begin{cases} p_{i,n+1} = (1 - \sigma_n - \varepsilon_n)p_{i,n} + \sigma_n \left[Q_i^n \left(u_{i,n} - h_i(u_{i,n}) + \mathcal{F}_{\rho_i, T_{i,n}}^{\partial_{\zeta_i} \Psi_i(\cdot, u_{i,n})} [g_i(u_{i,n}) - (T_i(h_i(u_{i,n})) + \rho_i A_i(u_{1,n}, u_{2,n}, \dots, u_{m,n}))] \right) + \eta_{i,n} \right] + \varepsilon_n \vartheta_{i,n} + r_{i,n}, \\ u_{i,n} = (1 - \sigma'_n - \varepsilon'_n)p_{i,n} + \sigma'_n \left[Q_i^n \left(v_{i,n} - h_i(v_{i,n}) + \mathcal{F}_{\rho_i, T_{i,n}}^{\partial_{\zeta_i} \Psi_i(\cdot, v_{i,n})} [g_i(v_{i,n}) - (T_i(h_i(v_{i,n})) + \rho_i A_i(v_{1,n}, v_{2,n}, \dots, v_{m,n}))] \right) + \eta'_{i,n} \right] + \varepsilon'_n \vartheta'_{i,n} + r'_{i,n}, \\ v_{i,n} = (1 - \sigma''_n - \varepsilon''_n)p_{i,n} + \sigma''_n \left[Q_i^n \left(p_{i,n} - h_i(p_{i,n}) + \mathcal{F}_{\rho_i, T_{i,n}}^{\partial_{\zeta_i} \Psi_i(\cdot, p_{i,n})} [g_i(p_{i,n}) - (T_i(h_i(p_{i,n})) + \rho_i A_i(p_{1,n}, p_{2,n}, \dots, p_{m,n}))] \right) + \eta''_{i,n} \right] + \varepsilon''_n \vartheta''_{i,n} + r''_{i,n}. \end{cases} \tag{55}$$

Let $\{z_{i,n}\}_{n=1}^\infty = \{(z_{1,n}, z_{2,n}, \dots, z_{m,n})\}_{n=1}^\infty$, $\{s_{i,n}\}_{n=1}^\infty = \{(s_{1,n}, s_{2,n}, \dots, s_{m,n})\}_{n=1}^\infty$ and $\{t_{i,n}\}_{n=1}^\infty = \{(t_{1,n}, t_{2,n}, \dots, t_{m,n})\}_{n=1}^\infty$ be

the sequences in $\prod_{i=1}^m \mathcal{H}_i$, and define $\{\varphi_{i,n}\}_{n=1}^\infty = \{(\varphi_{1,n}, \varphi_{2,n}, \dots, \varphi_{m,n})\}_{n=1}^\infty$ by

$$\begin{cases} \varphi_{i,n} = \left\| z_{i,n+1} - \left[(1 - \sigma_n - \varepsilon_n)z_{i,n} + \sigma_n \left(Q_i^n \left(s_{i,n} - h_i(s_{i,n}) + \mathcal{F}_{\rho_i, T_{i,n}}^{\partial_{\zeta_i} \Psi_i(\cdot, s_{i,n})} [g_i(s_{i,n}) - (T_i(h_i(s_{i,n})) + \rho_i A_i(s_{1,n}, s_{2,n}, \dots, s_{m,n}))] \right) + \eta_{i,n} \right) + \varepsilon_n \vartheta_{i,n} + r_{i,n} \right] \right\|_i, \\ s_{i,n} = (1 - \sigma'_n - \varepsilon'_n)z_{i,n} + \sigma'_n \left[Q_i^n \left(t_{i,n} - h_i(t_{i,n}) + \mathcal{F}_{\rho_i, T_{i,n}}^{\partial_{\zeta_i} \Psi_i(\cdot, t_{i,n})} [g_i(t_{i,n}) - (T_i(h_i(t_{i,n})) + \rho_i A_i(t_{1,n}, t_{2,n}, \dots, t_{m,n}))] \right) + \eta'_{i,n} \right] + \varepsilon'_n \vartheta'_{i,n} + r'_{i,n}, \\ t_{i,n} = (1 - \sigma''_n - \varepsilon''_n)z_{i,n} + \sigma''_n \left[Q_i^n \left(z_{i,n} - h_i(z_{i,n}) + \mathcal{F}_{\rho_i, T_{i,n}}^{\partial_{\zeta_i} \Psi_i(\cdot, z_{i,n})} [g_i(z_{i,n}) - (T_i(h_i(z_{i,n})) + \rho_i A_i(z_{1,n}, z_{2,n}, \dots, z_{m,n}))] \right) + \eta''_{i,n} \right] + \varepsilon''_n \vartheta''_{i,n} + r''_{i,n}, \end{cases} \tag{56}$$

where $S_i: \mathcal{H}_i \rightarrow \mathcal{H}_i$ $i \in \Lambda$ is nearly uniformly Lipschitzian mapping, and the sequences $\{\sigma_n\}, \{\varepsilon_n\}, \{\sigma'_n\}, \{\varepsilon'_n\}, \{\sigma''_n\}, \{\varepsilon''_n\}$ and $\{\varepsilon''\}$ satisfy the conditions $0 < \sigma_n + \varepsilon_n, \sigma'_n + \varepsilon'_n, \sigma''_n + \varepsilon''_n < 1$, $\sum_{n=0}^\infty \varepsilon_n < \infty$, and $\sum_{n=0}^\infty \sigma_n = \infty$. For each $i \in \{1, 2, \dots, m\}$ and for all $n \in \mathbb{N}$, $\{\vartheta_{i,n}\}, \{\vartheta'_{i,n}\}$, and $\{\vartheta''_{i,n}\}$ are bounded sequences

in \mathcal{H}_i , and $\{\eta_{i,n}\}, \{\eta'_{i,n}\}, \{\eta''_{i,n}\}, \{r_{i,n}\}, \{r'_{i,n}\}$, and $\{r''_{i,n}\}$ are six sequences in \mathcal{H}_i to take into account the possible inexact computation satisfying the following conditions:

$$\begin{cases} \eta_{i,n} = \widehat{\eta}_{i,n} + \overline{\eta}_{i,n}, \eta'_{i,n} = \widehat{\eta}'_{i,n} + \overline{\eta}'_{i,n}, \eta''_{i,n} = \widehat{\eta}''_{i,n} + \overline{\eta}''_{i,n}, \\ \left\| (\widehat{\eta}_{1,n}, \widehat{\eta}_{2,n}, \dots, \widehat{\eta}_{m,n}) \right\|_* = \lim_{n \rightarrow \infty} \left\| (\widehat{\eta}'_{1,n}, \widehat{\eta}'_{2,n}, \dots, \widehat{\eta}'_{m,n}) \right\|_* = \lim_{n \rightarrow \infty} \left\| (\widehat{\eta}''_{1,n}, \widehat{\eta}''_{2,n}, \dots, \widehat{\eta}''_{m,n}) \right\|_* = 0, \\ \sum_{n=1}^\infty \left\| (\overline{\eta}_{1,n}, \overline{\eta}_{2,n}, \dots, \overline{\eta}_{m,n}) \right\|_* < \infty, \sum_{n=1}^\infty \left\| (\overline{\eta}'_{1,n}, \overline{\eta}'_{2,n}, \dots, \overline{\eta}'_{m,n}) \right\|_* < \infty, \sum_{n=1}^\infty \left\| (\overline{\eta}''_{1,n}, \overline{\eta}''_{2,n}, \dots, \overline{\eta}''_{m,n}) \right\|_* < \infty, \\ \sum_{n=1}^\infty \left\| (r_{1,n}, r_{2,n}, \dots, r_{m,n}) \right\|_* < \infty, \sum_{n=1}^\infty \left\| (r'_{1,n}, r'_{2,n}, \dots, r'_{m,n}) \right\|_* < \infty, \sum_{n=1}^\infty \left\| (r''_{1,n}, r''_{2,n}, \dots, r''_{m,n}) \right\|_* < \infty. \end{cases} \tag{57}$$

Now, we establish the following strong convergence result for the sequences generated by the proximal iterative Algorithm 1 and stability analysis under some suitable conditions.

Theorem 3. For each $i \in \Lambda$, let $\mathcal{H}_i, g_i, h_i, T_i, \psi_i, \zeta_i$ and $\rho_i > 0$ be the same as in Theorem 2, and let all the conditions of Theorem 2 hold. For each $i \in \Lambda$, suppose that $Q_i: \mathcal{H}_i \rightarrow \mathcal{H}_i$ is a nearly uniformly K_i -Lipschitzian mapping with the sequence $\{l_{i,n}\}$, and $S: \prod_{i=1}^m \mathcal{H}_i \rightarrow \prod_{i=1}^m \mathcal{H}_i$ is a nearly uniformly $\max \{K_i; i \in \Lambda\}$ -Lipschitzian mapping with the sequence $\{l_{i,n}\}_{i=1}^m$ defined by (52) such that $\text{Fix}(S) \cap \text{SENMVLI}(\mathcal{H}_i, g_i, h_i, T_i, \psi_i, A_i, i \in \Lambda) \neq \emptyset$. Suppose

that $\Omega < \min \{1, 1/K_i\}$, for each $i \in \Lambda$, where Ω is same as in (44). Then,

- (i) the iterative sequence $\{(p_{1,n}, p_{2,n}, \dots, p_{m,n})\}_{n=1}^\infty$ generated by Algorithm 1 converges strongly to a unique element of $\text{Fix}(S) \cap \text{SENMVLI}(\mathcal{H}_i, g_i, h_i, T_i, \psi_i, A_i, i \in \Lambda)$
- (ii) Furthermore, if $0 < \kappa < \sigma_n$, then $\lim_{n \rightarrow \infty} (z_{1,n}, z_{2,n}, \dots, z_{m,n}) = (p_1^*, p_2^*, \dots, p_m^*)$ if and only if $\lim_{n \rightarrow \infty} (\sum_{i=1}^m \varphi_{i,n}) = 0$, where $\varphi_{i,n}$ is given in (55); i.e., the sequence $\{(p_{1,n}, p_{2,n}, \dots, p_{m,n})\}_{n=1}^\infty$ generated by (55) is $\mathcal{F}_{\rho_i, T_i}^{\partial_{\zeta_i} \Psi_i(\cdot, p_i)}$ -stable, for each $i \in \Lambda$

Proof

(i) Suppose $(p_1^*, p_2^*, \dots, p_m^*)$ is a unique solution of SENMVL I (19). For each $i \in \Lambda$, we have

$$h_i(p_i^*) = \mathcal{F}_{\rho_i, T_{i,n}}^{\partial_{\zeta_i} \Psi_i(\cdot, p_i^*)} [g_i(p_i^*) - (T_i(h_i(p_i^*)) + \rho_i A_i(p_1^*, p_2^*, \dots, p_m^*))]. \quad (58)$$

Since SEMVLI $(\mathcal{H}_i, g_i, h_i, T_i, \psi_i, A_i, i \in \Lambda)$ is a singleton set and $\text{Fix}(S) \cap \text{SEMVLI}(\mathcal{H}_i, g_i, h_i, T_i, \psi_i, A_i, i \in \Lambda) \neq \emptyset$, we conclude that for each $i \in \Lambda$,

$p_i^* \in \text{Fix}(Q_i)$. Hence, for each $n \in \mathbb{N}$ and for each $i \in \Lambda$, we can write

$$\begin{aligned} p_i^* &= (1 - \sigma_n - \varepsilon_n)p_i^* + \sigma_n \left[Q_i^n \left(p_i^* - h_i(p_i^*) + \mathcal{F}_{\rho_i, T_{i,n}}^{\partial_{\zeta_i} \Psi_i(\cdot, p_i^*)} [g_i(p_i^*) - (T_i(h_i(p_i^*)) + \rho_i A_i(p_1^*, p_2^*, \dots, p_m^*))] \right) \right] + \varepsilon_n p_i^*, \\ &= (1 - \sigma'_n - \varepsilon'_n)p_i^* + \sigma'_n \left[Q_i^n \left(p_i^* - h_i(p_i^*) + \mathcal{F}_{\rho_i, T_{i,n}}^{\partial_{\zeta_i} \Psi_i(\cdot, p_i^*)} [g_i(p_i^*) - (T_i(h_i(p_i^*)) + \rho_i A_i(p_1^*, p_2^*, \dots, p_m^*))] \right) \right] + \varepsilon'_n p_i^*, \\ &= (1 - \sigma''_n - \varepsilon''_n)p_i^* + \sigma''_n \left[Q_i^n \left(p_i^* - h_i(p_i^*) + \mathcal{F}_{\rho_i, T_{i,n}}^{\partial_{\zeta_i} \Psi_i(\cdot, p_i^*)} [g_i(p_i^*) - (T_i(h_i(p_i^*)) + \rho_i A_i(p_1^*, p_2^*, \dots, p_m^*))] \right) \right] + \varepsilon''_n p_i^*, \end{aligned} \quad (59)$$

where the sequences $\{\sigma_n\}$, $\{\varepsilon_n\}$, $\{\sigma'_n\}$, $\{\varepsilon'_n\}$, $\{\sigma''_n\}$, and $\{\varepsilon''_n\}$ are same as in Algorithm 1.

$\{\sup_{n \geq 1} \|\vartheta_{i,n} - p_i^*\|_i, i \in \Lambda\}$. Using Algorithm 1 and (44), it follows that

Now, let $L = \max \{\sup_{n \geq 1} \|\vartheta_{i,n} - p_i^*\|_i, i \in \Lambda\}$, $L' = \max \{\sup_{n \geq 1} \|\vartheta'_{i,n} - p_i^*\|_i, i \in \Lambda\}$ and $L'' = \max$

$$\begin{aligned} \|p_{i,n+1} - p_i^*\|_i &= \left\| \left[(1 - \sigma_n - \varepsilon_n)p_{i,n} + \sigma_n \left(Q_i^n \left(u_{i,n} - h_i(u_{i,n}) + \mathcal{F}_{\rho_i, T_{i,n}}^{\partial_{\zeta_i} \Psi_i(\cdot, u_{i,n})} [g_i(u_{i,n}) - (T_i(h_i(u_{i,n})) + \rho_i A_i(u_{1,n}, u_{2,n}, \dots, u_{m,n}))] \right) \right) + \eta_{i,n} \right] + \varepsilon_n \vartheta_{i,n} + r_{i,n} \right\|_i \\ &\quad - \left[(1 - \sigma_n - \varepsilon_n)p_i^* + \sigma_n \left[Q_i^n \left(p_i^* - h_i(p_i^*) + \mathcal{F}_{\rho_i, T_{i,n}}^{\partial_{\zeta_i} \Psi_i(\cdot, p_i^*)} [g_i(p_i^*) - (T_i(h_i(p_i^*)) + \rho_i A_i(p_1^*, p_2^*, \dots, p_m^*))] \right) \right] + \varepsilon_n p_i^* \right] \right\|_i \\ &\leq (1 - \sigma_n - \varepsilon_n) \|p_{i,n} - p_i^*\|_i + \sigma_n \left\| \begin{aligned} &Q_i^n \left(u_{i,n} - h_i(u_{i,n}) + \mathcal{F}_{\rho_i, T_{i,n}}^{\partial_{\zeta_i} \Psi_i(\cdot, u_{i,n})} [g_i(u_{i,n}) - (T_i(h_i(u_{i,n})) + \rho_i A_i(u_{1,n}, u_{2,n}, \dots, u_{m,n}))] \right) \\ &- Q_i^n \left(p_i^* - h_i(p_i^*) + \mathcal{F}_{\rho_i, T_{i,n}}^{\partial_{\zeta_i} \Psi_i(\cdot, p_i^*)} [g_i(p_i^*) - (T_i(h_i(p_i^*)) + \rho_i A_i(p_1^*, p_2^*, \dots, p_m^*))] \right) \end{aligned} \right\|_i \\ &\quad \cdot \|\vartheta_{i,n} - p_i^*\|_i + \sigma_n \|\eta_{i,n}\|_i + \|r_{i,n}\|_i \\ &\leq (1 - \sigma_n - \varepsilon_n) \|p_{i,n} - p_i^*\|_i + \sigma_n K_i \left\{ \left\| \begin{aligned} &(u_{i,n} - h_i(u_{i,n}) + \mathcal{F}_{\rho_i, T_{i,n}}^{\partial_{\zeta_i} \Psi_i(\cdot, u_{i,n})} [g_i(u_{i,n}) - (T_i(h_i(u_{i,n})) + \rho_i A_i(u_{1,n}, u_{2,n}, \dots, u_{m,n}))]) \\ &- (p_i^* - h_i(p_i^*) + \mathcal{F}_{\rho_i, T_{i,n}}^{\partial_{\zeta_i} \Psi_i(\cdot, p_i^*)} [g_i(p_i^*) - (T_i(h_i(p_i^*)) + \rho_i A_i(p_1^*, p_2^*, \dots, p_m^*))]) \end{aligned} \right\|_i + L_{i,n} \right\} \\ &\quad \cdot \|\vartheta_{i,n} - p_i^*\|_i + \sigma_n \|\eta_{i,n}\|_i + \|r_{i,n}\|_i \\ &\leq (1 - \sigma_n - \varepsilon_n) \|p_{i,n} - p_i^*\|_i + \sigma_n K_i \left\| \begin{aligned} &(u_{i,n} - h_i(u_{i,n}) + \mathcal{F}_{\rho_i, T_{i,n}}^{\partial_{\zeta_i} \Psi_i(\cdot, u_{i,n})} [g_i(u_{i,n}) - (T_i(h_i(u_{i,n})) + \rho_i A_i(u_{1,n}, u_{2,n}, \dots, u_{m,n}))]) \\ &- (p_i^* - h_i(p_i^*) + \mathcal{F}_{\rho_i, T_{i,n}}^{\partial_{\zeta_i} \Psi_i(\cdot, p_i^*)} [g_i(p_i^*) - (T_i(h_i(p_i^*)) + \rho_i A_i(p_1^*, p_2^*, \dots, p_m^*))]) \end{aligned} \right\|_i \\ &\quad + \sigma_n K_i L_{i,n} + \varepsilon_n L + \sigma_n (\|\widehat{\eta}_{i,n}\|_i + \|\overline{\eta}_{i,n}\|_i) + \|r_{i,n}\|_i \end{aligned}$$

$$\begin{aligned}
&\leq (1 - \sigma_n - \varepsilon_n) \|p_{i,n} - p_i^*\|_i + \sigma_n K_i \left(\Theta_i \|u_{i,n} - \hat{p}_i\|_i + \frac{\tau_i \rho_i}{\alpha_i + \delta_i} \sum_{j \in \Lambda, i \neq j} \nu_{i,j} \|u_{j,n} - \hat{p}_j\|_j \right) \\
&\quad + \sigma_n K_i l_{i,n} + \varepsilon_n L + \sigma_n (\|\hat{\eta}_{i,n}\|_i + \|\bar{\eta}_{i,n}\|_i) + \|r_{i,n}\|_i \\
&\leq (1 - \sigma_n - \varepsilon_n) \|p_{i,n} - p_i^*\|_i + \sigma_n K_i \left(\Theta_i \|u_{i,n} - \hat{p}_i\|_i + \frac{\tau_i \rho_i}{\alpha_i + \delta_i} \sum_{j \in \Lambda, i \neq j} \nu_{i,j} \|u_{j,n} - \hat{p}_j\|_j \right) \\
&\quad + \sigma_n K_i l_{i,n} + \sigma_n (\|\hat{\eta}_{i,n}\|_i + \|\bar{\eta}_{i,n}\|_i) + \|r_{i,n}\|_i + \varepsilon_n L.
\end{aligned} \tag{60}$$

Using the similar arguments of (60), we can establish that for each $i \in \Lambda$,

$$\|u_{i,n+1} - p_i^*\|_i \leq (1 - \sigma'_n - \varepsilon'_n) \|p_{i,n} - p_i^*\|_i + \sigma'_n K_i \left(\Theta_i \|v_{i,n} - p_i^*\|_i + \frac{\tau_i \rho_i}{\alpha_i + \delta_i} \sum_{j \in \Lambda, i \neq j} \nu_{i,j} \|v_{j,n} - \hat{p}_j\|_j \right) \|\hat{\eta}'_{i,n}\|_i + \|\bar{\eta}'_{i,n}\|_i + \|r'_{i,n}\|_i + \varepsilon'_n L', \tag{61}$$

$$\begin{aligned}
\|v_{i,n+1} - p_i^*\|_i &\leq (1 - \sigma''_n - \varepsilon''_n) \|p_{i,n} - p_i^*\|_i + \sigma''_n K_i \left(\Theta_i \|p_{i,n} - p_i^*\|_i + \frac{\tau_i \rho_i}{\alpha_i + \delta_i} \sum_{j \in \Lambda, i \neq j} \nu_{i,j} \|p_{j,n} - \hat{p}_j\|_j \right) \\
&\quad + \sigma''_n K_i l_{i,n} + \sigma''_n \|\hat{\eta}''_{i,n}\|_i + \|\bar{\eta}''_{i,n}\|_i + \|r_{i,n}''\|_i + \varepsilon''_n L''.
\end{aligned} \tag{62}$$

Let $K = \max \{K_i : i \in \Lambda\}$. Combining (60)–(62), we obtain

$$\begin{aligned}
\|(p_{1,n+1}, p_{2,n+1}, \dots, p_{m,n+1}) - (p_1^*, p_2^*, \dots, p_m^*)\|_* &\leq (1 - \sigma_n - \varepsilon_n) \|(p_{1,n}, p_{2,n}, \dots, p_{m,n}) - (p_1^*, p_2^*, \dots, p_m^*)\|_* \\
&\quad + \sigma_n K \sum_{i=1}^m \left(\Theta_i \|u_{i,n} - \hat{p}_i\|_i + \frac{\tau_i \rho_i}{\alpha_i + \delta_i} \sum_{j \in \Lambda, i \neq j} \nu_{i,j} \|u_{j,n} - \hat{p}_j\|_j \right) \\
&\quad + \sigma_n K \sum_{i=1}^m l_{i,n} + \sigma_n (\|\hat{\eta}_{1,n}, \hat{\eta}_{2,n}, \dots, \hat{\eta}_{m,n}\|_*) \\
&\quad + (\|\bar{\eta}_{1,n}, \bar{\eta}_{2,n}, \dots, \bar{\eta}_{m,n}\|_* + \|r_{1,n}, r_{2,n}, \dots, r_{m,n}\|_* \\
&\quad + m \varepsilon_n L = (1 - \sigma_n - \varepsilon_n) \|(p_{1,n}, p_{2,n}, \dots, p_{m,n}) - (p_1^*, p_2^*, \dots, p_m^*)\|_*.
\end{aligned}$$

$$\begin{aligned}
 & + \left[\left(\Theta_1 + \sum_{k=2}^m \frac{\tau_k \rho_k}{\alpha_k + \delta_k} \nu_{k,1} \right) \|u_{1,n} - p_1^*\|_1 \right. \\
 & + \left. \text{left} \left(\Theta_2 + \sum_{k \in \Lambda, k \neq 2}^m \frac{\tau_k \rho_k}{\alpha_k + \delta_k} \nu_{k,2} \right) \|u_{2,n} - p_2^*\|_2 + \dots + \left(\Theta_m + \sum_{k=1}^{m-1} \frac{\tau_k \rho_k}{\alpha_k + \delta_k} \nu_{k,m} \right) \|u_{m,n} - p_m^*\|_m \right] \\
 & + \sigma_n K \sum_{i=1}^m l_{i,n} + \sigma_n \left\| (\hat{\eta}_{1,n}, \hat{\eta}_{2,n}, \dots, \hat{\eta}_{m,n}) \right\|_* + \left\| \bar{\eta}_{1,n}, \bar{\eta}_{2,n}, \dots, \bar{\eta}_{m,n} \right\|_* + \left\| (r_{1,n}, r_{2,n}, \dots, r_{m,n}) \right\|_* + m \varepsilon_n L \\
 \leq & (1 - \sigma_n - \varepsilon_n) \left\| (p_{1,n}, p_{2,n}, \dots, p_{m,n}) - (p_1^*, p_2^*, \dots, p_m^*) \right\|_* + \sigma_n K \Omega \sum_{i=1}^m \|u_{i,n} - p_i^*\|_i + \sigma_n K \sum_{i=1}^m l_{i,n} \tag{63} \\
 & + \sigma_n \left\| (\hat{\eta}_{1,n}, \hat{\eta}_{2,n}, \dots, \hat{\eta}_{m,n}) \right\|_* + \left\| \bar{\eta}_{1,n}, \bar{\eta}_{2,n}, \dots, \bar{\eta}_{m,n} \right\|_* + \left\| (r_{1,n}, r_{2,n}, \dots, r_{m,n}) \right\|_* + m \varepsilon_n L \\
 = & (1 - \sigma_n - \varepsilon_n) \left\| (p_{1,n}, p_{2,n}, \dots, p_{m,n}) - (p_1^*, p_2^*, \dots, p_m^*) \right\|_* \\
 & + \sigma_n K \Omega \left\| (u_{1,n}, u_{2,n}, \dots, u_{m,n}) - (p_1^*, p_2^*, \dots, p_m^*) \right\|_* + \sigma_n K \sum_{i=1}^m l_{i,n} \\
 & + \sigma_n \left\| (\hat{\eta}_{1,n}, \hat{\eta}_{2,n}, \dots, \hat{\eta}_{m,n}) \right\|_* + \left\| \bar{\eta}_{1,n}, \bar{\eta}_{2,n}, \dots, \bar{\eta}_{m,n} \right\|_* + \left\| (r_{1,n}, r_{2,n}, \dots, r_{m,n}) \right\|_* + m \varepsilon_n L.
 \end{aligned}$$

Applying equivalent logics of (63), we can compute that

$$\begin{aligned}
 \left\| (u_{1,n+1}, u_{2,n+1}, \dots, u_{m,n+1}) - (p_1^*, p_2^*, \dots, p_m^*) \right\|_* & \leq (1 - \sigma'_n - \varepsilon'_n) \left\| (p_{1,n}, p_{2,n}, \dots, p_{m,n}) - (p_1^*, p_2^*, \dots, p_m^*) \right\|_* \\
 & + \sigma'_n K \Omega \left\| (v_{1,n}, v_{2,n}, \dots, v_{m,n}) - (p_1^*, p_2^*, \dots, p_m^*) \right\|_* \\
 & + \sigma'_n K \sum_{i=1}^m l_{i,n} + \sigma'_n \left\| (\hat{\eta}'_{1,n}, \hat{\eta}'_{2,n}, \dots, \hat{\eta}'_{m,n}) \right\|_* \\
 & + \left\| (\bar{\eta}'_{1,n}, \bar{\eta}'_{2,n}, \dots, \bar{\eta}'_{m,n}) \right\|_* + \left\| (r'_{1,n}, r'_{2,n}, \dots, r'_{m,n}) \right\|_* + m \varepsilon'_n L', \tag{64}
 \end{aligned}$$

$$\begin{aligned}
 \left\| (v_{1,n+1}, v_{2,n+1}, \dots, v_{m,n+1}) - (p_1^*, p_2^*, \dots, p_m^*) \right\|_* & \leq (1 - \sigma''_n - \varepsilon''_n) \left\| (p_{1,n}, p_{2,n}, \dots, p_{m,n}) - (p_1^*, p_2^*, \dots, p_m^*) \right\|_* \\
 & + \sigma''_n K \Omega \left\| (p_{1,n}, p_{2,n}, \dots, p_{m,n}) - (p_1^*, p_2^*, \dots, p_m^*) \right\|_* \\
 & + \sigma''_n K \sum_{i=1}^m l_{i,n} + \sigma''_n \left\| (\hat{\eta}''_{1,n}, \hat{\eta}''_{2,n}, \dots, \hat{\eta}''_{m,n}) \right\|_* \\
 & + \left\| (\bar{\eta}''_{1,n}, \bar{\eta}''_{2,n}, \dots, \bar{\eta}''_{m,n}) \right\|_* + \left\| (r''_{1,n}, r''_{2,n}, \dots, r''_{m,n}) \right\|_* + m \varepsilon''_n L''. \tag{65}
 \end{aligned}$$

Since $(1 - \sigma''_n(1 - K\Omega)) \leq 1$, therefore (65) becomes

$$\begin{aligned}
\| (v_{1,n+1}, v_{2,n+1}, \dots, v_{m,n+1}) - (p_1^*, p_2^*, \dots, p_m^*) \|_* &\leq (1 - \sigma_n''(1 - K\Omega)) \| (p_{1,n}, p_{2,n}, \dots, p_{m,n}) - (p_1^*, p_2^*, \dots, p_m^*) \|_* \\
&\quad + \sigma_n'' K \sum_{i=1}^m l_{i,n} + \sigma_n'' \| (\hat{\eta}_{1,n}'', \hat{\eta}_{2,n}'', \dots, \hat{\eta}_{m,n}'') \|_* + \| (\bar{\eta}_{1,n}'', \bar{\eta}_{2,n}'', \dots, \bar{\eta}_{m,n}'') \|_* \\
&\quad + \| r_{1,n}'', r_{2,n}'', \dots, r_{m,n}'' \|_* + m \varepsilon_n'' L'' \\
&\leq \| (p_{1,n}, p_{2,n}, \dots, p_{m,n}) - (p_1^*, p_2^*, \dots, p_m^*) \|_* + \sigma_n'' K \sum_{i=1}^m l_{i,n} \\
&\quad + \sigma_n'' \| (\hat{\eta}_{1,n}'', \hat{\eta}_{2,n}'', \dots, \hat{\eta}_{m,n}'') \|_* + \| (\bar{\eta}_{1,n}'', \bar{\eta}_{2,n}'', \dots, \bar{\eta}_{m,n}'') \|_* \\
&\quad + \| r_{1,n}'', r_{2,n}'', \dots, r_{m,n}'' \|_* + m \varepsilon_n'' L'' .
\end{aligned} \tag{66}$$

Since $(1 - \sigma_n''(1 - K\Omega)) \leq 1$, therefore using (64) and (66) becomes

$$\begin{aligned}
\| (u_{1,n+1}, u_{2,n+1}, \dots, u_{m,n+1}) - (p_1^*, p_2^*, \dots, p_m^*) \|_* &\leq (1 - \sigma_n' - \varepsilon_n') \| (p_{1,n}, p_{2,n}, \dots, p_{m,n}) - (p_1^*, p_2^*, \dots, p_m^*) \|_* \\
&\quad + \sigma_n' K \Omega \left[\| (p_{1,n}, p_{2,n}, \dots, p_{m,n}) - (p_1^*, p_2^*, \dots, p_m^*) \|_* \right. \\
&\quad + \sigma_n'' \| (\hat{\eta}_{1,n}'', \hat{\eta}_{2,n}'', \dots, \hat{\eta}_{m,n}'') \|_* + \| \bar{\eta}_{1,n}'', \bar{\eta}_{2,n}'', \dots, \bar{\eta}_{m,n}'' \|_* \\
&\quad \left. + \sigma_n'' K \sum_{i=1}^m l_{i,n} + \| (r_{1,n}'', r_{2,n}'', \dots, r_{m,n}'') \|_* + m \varepsilon_n'' L'' \right] \\
&\quad + \sigma_n' K \sum_{i=1}^m l_{i,n} + \sigma_n' \| (\hat{\eta}_{1,n}', \hat{\eta}_{2,n}', \dots, \hat{\eta}_{m,n}') \|_* + \| (\bar{\eta}_{1,n}', \bar{\eta}_{2,n}', \dots, \bar{\eta}_{m,n}') \|_* \\
&\quad + \| r_{1,n}', r_{2,n}', \dots, r_{m,n}' \|_* + m \varepsilon_n' L' \\
&\leq (1 - \sigma_n'(1 - K\Omega)) \| (p_{1,n}, p_{2,n}, \dots, p_{m,n}) - (p_1^*, p_2^*, \dots, p_m^*) \|_* \\
&\quad + \sigma_n' \sigma_n'' K \Omega \| (\hat{\eta}_{1,n}'', \hat{\eta}_{2,n}'', \dots, \hat{\eta}_{m,n}'') \|_* + \sigma_n' \sigma_n'' K^2 \Omega \sum_{i=1}^m l_{i,n} \\
&\quad + \sigma_n' K \Omega \| (r_{1,n}'', r_{2,n}'', \dots, r_{m,n}'') \|_* + \sigma_n' K \Omega \| \bar{\eta}_{1,n}'', \bar{\eta}_{2,n}'', \dots, \bar{\eta}_{m,n}'' \|_* \\
&\quad + \sigma_n' K \sum_{i=1}^m l_{i,n} + \sigma_n' \| (\hat{\eta}_{1,n}', \hat{\eta}_{2,n}', \dots, \hat{\eta}_{m,n}') \|_* + \| (\bar{\eta}_{1,n}', \bar{\eta}_{2,n}', \dots, \bar{\eta}_{m,n}') \|_* \\
&\quad + \| r_{1,n}', r_{2,n}', \dots, r_{m,n}' \|_* + m \sigma_n' \varepsilon_n'' K \Omega L'' + m \varepsilon_n' L' \\
&\leq \| (p_{1,n}, p_{2,n}, \dots, p_{m,n}) - (p_1^*, p_2^*, \dots, p_m^*) \|_* \\
&\quad + \sigma_n' \sigma_n'' K \Omega \| (\hat{\eta}_{1,n}'', \hat{\eta}_{2,n}'', \dots, \hat{\eta}_{m,n}'') \|_* + \sigma_n' \sigma_n'' K^2 \Omega \sum_{i=1}^m l_{i,n} \\
&\quad + \sigma_n' K \Omega \| (r_{1,n}'', r_{2,n}'', \dots, r_{m,n}'') \|_* + \sigma_n' K \Omega \| \bar{\eta}_{1,n}'', \bar{\eta}_{2,n}'', \dots, \bar{\eta}_{m,n}'' \|_* \\
&\quad + \sigma_n' K \sum_{i=1}^m l_{i,n} + \sigma_n' \| (\hat{\eta}_{1,n}', \hat{\eta}_{2,n}', \dots, \hat{\eta}_{m,n}') \|_* \\
&\quad + \| (\bar{\eta}_{1,n}', \bar{\eta}_{2,n}', \dots, \bar{\eta}_{m,n}') \|_* + \| r_{1,n}', r_{2,n}', \dots, r_{m,n}' \|_* + m \sigma_n' \varepsilon_n'' K \Omega L'' + m \varepsilon_n' L' .
\end{aligned} \tag{67}$$

Using (63) and (67) becomes

$$\begin{aligned}
& \|(p_{1,n+1}, p_{2,n+1}, \dots, p_{m,n+1}) - (p_1^*, p_2^*, \dots, p_m^*)\|_* \leq (1 - \sigma_n - \varepsilon_n) \|(p_{1,n}, p_{2,n}, \dots, p_{m,n}) - (p_1^*, p_2^*, \dots, p_m^*)\|_* \\
& + \sigma_n K \Omega \left[\|(p_{1,n}, p_{2,n}, \dots, p_{m,n}) - (p_1^*, p_2^*, \dots, p_m^*)\|_* + \sigma_n' \sigma_n'' K \Omega \|\widehat{\eta}_{1,n}, \widehat{\eta}_{2,n}, \dots, \widehat{\eta}_{m,n}\|_* + \sigma_n' \sigma_n'' K^2 \Omega \sum_{i=1}^m l_{i,n} + \sigma_n' K \Omega \|r_{1,n}, r_{2,n}, \dots, r_{m,n}\|_* + \sigma_n' K \Omega \|\overline{\eta}_{1,n}, \overline{\eta}_{2,n}, \dots, \overline{\eta}_{m,n}\|_* \right. \\
& \left. + \sigma_n' K \sum_{i=1}^m l_{i,n} + \sigma_n' \|\widehat{\eta}'_{1,n}, \widehat{\eta}'_{2,n}, \dots, \widehat{\eta}'_{m,n}\|_* + \|\overline{\eta}'_{1,n}, \overline{\eta}'_{2,n}, \dots, \overline{\eta}'_{m,n}\|_* + \|r'_{1,n}, r'_{2,n}, \dots, r'_{m,n}\|_* + m \sigma_n' \varepsilon_n'' K \Omega L' + m \varepsilon_n' L' \right] \\
& + \sigma_n K \sum_{i=1}^m l_{i,n} + \|\overline{\eta}_{1,n}, \overline{\eta}_{2,n}, \dots, \overline{\eta}_{m,n}\|_* + \|r_{1,n}, r_{2,n}, \dots, r_{m,n}\|_* + m \varepsilon_n L \\
& \leq (1 - \sigma_n (1 - K \Omega)) \|(p_{1,n}, p_{2,n}, \dots, p_{m,n}) - (p_1^*, p_2^*, \dots, p_m^*)\|_* \\
& + \sigma_n (1 - K \Omega) \left[\frac{1}{(1 - K \Omega)} \left(\sigma_n' \sigma_n'' K^2 \Omega^2 \|\widehat{\eta}_{1,n}, \widehat{\eta}_{2,n}, \dots, \widehat{\eta}_{m,n}\|_* + \sigma_n' K^2 \Omega^2 \|\overline{\eta}_{1,n}, \overline{\eta}_{2,n}, \dots, \overline{\eta}_{m,n}\|_* + \sigma_n' K^2 \Omega^2 \|r_{1,n}, r_{2,n}, \dots, r_{m,n}\|_* + \sigma_n' K \Omega \|\widehat{\eta}'_{1,n}, \widehat{\eta}'_{2,n}, \dots, \widehat{\eta}'_{m,n}\|_* + K \Omega \|\overline{\eta}'_{1,n}, \overline{\eta}'_{2,n}, \dots, \overline{\eta}'_{m,n}\|_* \right) \right. \\
& \left. + K \Omega \|r'_{1,n}, r'_{2,n}, \dots, r'_{m,n}\|_* + \|\widehat{\eta}_{1,n}, \widehat{\eta}_{2,n}, \dots, \widehat{\eta}_{m,n}\|_* + (\sigma_n' \sigma_n'' K^3 \Omega^2 + \sigma_n' K^2 \Omega + K) \sum_{i=1}^m l_{i,n} + m \sigma_n' \varepsilon_n'' K^2 \Omega^2 L' + m \varepsilon_n' K \Omega L' \right. \\
& \left. + \|\overline{\eta}_{1,n}, \overline{\eta}_{2,n}, \dots, \overline{\eta}_{m,n}\|_* + \|r_{1,n}, r_{2,n}, \dots, r_{m,n}\|_* + m \varepsilon_n L \right] \tag{68}
\end{aligned}$$

On setting,

$$\wp_{n+1} = \|(p_{1,n+1}, p_{2,n+1}, \dots, p_{m,n+1}) - (p_1^*, p_2^*, \dots, p_m^*)\|_*; \quad \omega_n = \sigma_n (1 - K \Omega); \tag{69}$$

$$\varrho_n = \|\overline{\eta}_{1,n}, \overline{\eta}_{2,n}, \dots, \overline{\eta}_{m,n}\|_* + \|r_{1,n}, r_{2,n}, \dots, r_{m,n}\|_* + m \varepsilon_n L,$$

$$\gamma_n = \left[\frac{1}{(1 - K \Omega)} \left(\begin{aligned} & \sigma_n' \sigma_n'' K^2 \Omega^2 \|\widehat{\eta}_{1,n}, \widehat{\eta}_{2,n}, \dots, \widehat{\eta}_{m,n}\|_* + \sigma_n' K^2 \Omega^2 \|\overline{\eta}_{1,n}, \overline{\eta}_{2,n}, \dots, \overline{\eta}_{m,n}\|_* + \sigma_n' K^2 \Omega^2 \|r_{1,n}, r_{2,n}, \dots, r_{m,n}\|_* \\ & + \sigma_n' K \Omega \|\widehat{\eta}'_{1,n}, \widehat{\eta}'_{2,n}, \dots, \widehat{\eta}'_{m,n}\|_* + K \Omega \|\overline{\eta}'_{1,n}, \overline{\eta}'_{2,n}, \dots, \overline{\eta}'_{m,n}\|_* + K \Omega \|r'_{1,n}, r'_{2,n}, \dots, r'_{m,n}\|_* + \|\widehat{\eta}_{1,n}, \widehat{\eta}_{2,n}, \dots, \widehat{\eta}_{m,n}\|_* \\ & + (\sigma_n' \sigma_n'' K^3 \Omega^2 + \sigma_n' K^2 \Omega + K) \sum_{i=1}^m l_{i,n} + m \sigma_n' \varepsilon_n'' K^2 \Omega^2 L' + m \varepsilon_n' K \Omega L' \end{aligned} \right) \right]. \tag{70}$$

Equation (68) can be written as

$$\wp_{n+1} \leq (1 - \omega_n) \wp_n + \gamma_n \omega_n + \varrho_n, \tag{71}$$

where $\Omega = \max \{ \Theta_i + \sum_{k \in \Lambda, k \neq i} (\tau_k \rho_k) / (\alpha_k + \delta_k) \nu_{k,i} : i \in \Lambda \}$. Since $\lim_{n \rightarrow \infty} l_{i,n} = 0$, for each $i \in \Lambda$, and $\sum_{i=1}^m \varepsilon_n < \infty$, in view of (57), it follows that the conditions of Lemma 1 are satisfied. Therefore, using Lemma 1 and (68), we deduce that $(p_{1,n+1}, p_{2,n+1}, \dots, p_{m,n+1}) \rightarrow (p_1^*, p_2^*, \dots, p_m^*)$, as $n \rightarrow \infty$, and so the sequence $\{(p_{1,n+1}, p_{2,n+1}, \dots,$

$p_{m,n+1})\}_{n=1}^{\infty}$ generated by Algorithm 1 converges strongly to the only element $(p_1^*, p_2^*, \dots, p_m^*)$ of the singleton set $\text{Fix}(S) \cap \text{SEMVI}(\mathcal{H}_i, g_i, h_i, T_i, \psi_i, A_i, i \in \Lambda)$. This completes the part (I).

(ii) Next, we prove the second conclusion. Let $H(p_i^*) = S_i^n(p_i^* - h_i(p_i^*) + \mathcal{F}_{\rho_i, T_i, \psi_i}^{\partial_i, \psi_i}(\cdot, p_i^*)) [g_i(p_i^*) - (T_i(h_i(p_i^*)) + \rho_i A_i(p_1^*, p_2^*, \dots, p_m^*))]$. Using (59) and Algorithm 1, we have

$$\begin{aligned}
\|z_{i,n+1} - p_i^*\|_i & \leq \|z_{i,n+1} - [(1 - \sigma_n - \varepsilon_n) z_{i,n} + \sigma_n (H(s_{i,n}) + \eta_{i,n}) + \varepsilon_n \vartheta_{i,n} + r_{i,n}]\| \\
& + \|[(1 - \sigma_n - \varepsilon_n) z_{i,n} + \sigma_n (H(s_{i,n}) + \eta_{i,n}) + \varepsilon_n \vartheta_{i,n} + r_{i,n}] - [(1 - \sigma_n - \varepsilon_n) p_i^* + \sigma_n H(p_i^*) + \varepsilon_n p_n^*]\|_i \\
& \leq \varphi_{i,n} + (1 - \sigma_n - \varepsilon_n) \|z_{i,n} - p_i^*\|_i + \sigma_n K_i \left(\Theta_i \|s_{i,n} - p_i^*\|_i + \frac{\tau_i \rho_i}{\alpha_i + \delta_i} \sum_{j \in \Lambda, i \neq j} \nu_{i,j} \|s_{j,n} - p_j^*\|_j \right) \\
& + \sigma_n K_i l_{i,n} + \sigma_n \|\widehat{\eta}_{i,n}\|_i + \|\overline{\eta}_{i,n}\|_i + \|r_{i,n}\|_i + \varepsilon_n L. \tag{72}
\end{aligned}$$

On similar manner of (73), we can deduce that

$$\begin{aligned} \|s_{i,n+1} - p_i^*\|_i &\leq (1 - \sigma'_n - \varepsilon'_n) \|z_{i,n} - p_i^*\|_i + \sigma'_n K_i \left(\Theta_i \|t_{i,n} - p_i^*\|_i + \frac{\tau_i \rho_i}{\alpha_i + \delta_i} \sum_{j \in \Lambda, i \neq j} \nu_{i,j} \|t_{j,n} - p_j^*\|_j \right) \\ &\quad + \sigma'_n K_i l_{i,n} + \sigma'_n \|\hat{\eta}'_{i,n}\|_i + \|\bar{\eta}'_{i,n}\|_i + \|r'_{i,n}\|_i + \varepsilon'_n L, \end{aligned} \quad (73)$$

$$\begin{aligned} \|t_{i,n+1} - p_i^*\|_i &\leq (1 - \sigma''_n - \varepsilon''_n) \|z_{i,n} - p_i^*\|_i + \sigma''_n K_i \left(\Theta_i \|p_{i,n} - p_i^*\|_i + \frac{\tau_i \rho_i}{\alpha_i + \delta_i} \sum_{j \in \Lambda, i \neq j} \nu_{i,j} \|z_{j,n} - p_j^*\|_j \right) \\ &\quad + \sigma''_n K_i l_{i,n} + \sigma''_n \|\hat{\eta}''_{i,n}\|_i + \|\bar{\eta}''_{i,n}\|_i + \|r''_{i,n}\|_i + \varepsilon''_n L. \end{aligned} \quad (74)$$

Using the similar arguments of (63) and combining (72)–(74), we obtain that

$$\begin{aligned} &\| (z_{1,n+1}, z_{2,n+1}, \dots, z_{m,n+1}) - (p_1^*, p_2^*, \dots, p_m^*) \|_* \\ &\leq \sum_{i=1}^m \left[\varphi_{i,n} + (1 - \sigma_n - \varepsilon_n) \|z_{i,n} - p_i^*\|_i + \sigma_n K_i \left(\Theta_i \|s_{i,n} - p_i^*\|_i + \frac{\tau_i \rho_i}{\alpha_i + \delta_i} \sum_{j \in \Lambda, i \neq j} \nu_{i,j} \|s_{j,n} - p_j^*\|_j \right) \right. \\ &\quad \left. + \sigma_n K_i l_{i,n} + \sigma_n \|\hat{\eta}_{i,n}\|_i + \|\bar{\eta}_{i,n}\|_i + \|r_{i,n}\|_i + \varepsilon_n L \right] \\ &\leq \sum_{i=1}^m \varphi_{i,n} + (1 - \sigma_n - \varepsilon_n) \| (z_{1,n}, z_{2,n}, \dots, z_{m,n}) - (p_1^*, p_2^*, \dots, p_m^*) \|_* \\ &\quad + \sigma_n K \Omega \| (s_{1,n}, s_{2,n}, \dots, s_{m,n}) - (p_1^*, p_2^*, \dots, p_m^*) \|_* + \sigma_n K \sum_{i=1}^m l_{i,n} \\ &\quad + \sigma_n \| (\hat{\eta}_{1,n}, \hat{\eta}_{2,n}, \dots, \hat{\eta}_{m,n}) \|_* + \| (\bar{\eta}_{1,n}, \bar{\eta}_{2,n}, \dots, \bar{\eta}_{m,n}) \|_* \\ &\quad + \| (r_{1,n}, r_{2,n}, \dots, r_{m,n}) \|_* + m \varepsilon_n L. \end{aligned} \quad (75)$$

Similarly, we have

$$\begin{aligned} \| (s_{1,n+1}, s_{2,n+1}, \dots, s_{m,n+1}) - (p_1^*, p_2^*, \dots, p_m^*) \|_* &\leq (1 - \sigma'_n - \varepsilon'_n) \| (z_{1,n}, z_{2,n}, \dots, z_{m,n}) - (p_1^*, p_2^*, \dots, p_m^*) \|_* \\ &\quad + \sigma'_n K \Omega \| (t_{1,n}, t_{2,n}, \dots, t_{m,n}) - (p_1^*, p_2^*, \dots, p_m^*) \|_* \\ &\quad + \sigma'_n K \sum_{i=1}^m l_{i,n} + \sigma'_n \| (\hat{\eta}'_{1,n}, \hat{\eta}'_{2,n}, \dots, \hat{\eta}'_{m,n}) \|_* + \| \bar{\eta}'_{1,n}, \bar{\eta}'_{2,n}, \dots, \bar{\eta}'_{m,n} \|_* \\ &\quad + \| (r'_{1,n}, r'_{2,n}, \dots, r'_{m,n}) \|_* + m \varepsilon'_n L. \end{aligned} \quad (76)$$

Since $(1 - \sigma_n''(1 - K\Omega)) \leq 1$, therefore we obtain

$$\begin{aligned}
 \|(t_{1,n+1}, t_{2,n+1}, \dots, t_{m,n+1}) - (p_1^*, p_2^*, \dots, p_m^*)\|_* &\leq (1 - \sigma_n'' - \varepsilon_n'') \|(z_{1,n}, z_{2,n}, \dots, z_{m,n}) - (p_1^*, p_2^*, \dots, p_m^*)\|_* \\
 &\quad + \sigma_n'' K \Omega \|(z_{1,n}, z_{2,n}, \dots, z_{m,n}) - (p_1^*, p_2^*, \dots, p_m^*)\|_* \\
 &\quad + \sigma_n'' K \sum_{i=1}^m l_{i,n} + \sigma_n'' \left\| (\hat{\eta}_{1,n}'', \hat{\eta}_{2,n}'', \dots, \hat{\eta}_{m,n}'') \right\|_* + \|\bar{\eta}_{1,n}'', \bar{\eta}_{2,n}'', \dots, \bar{\eta}_{m,n}''\|_* \\
 &\quad + \left\| (r_{1,n}'', r_{2,n}'', \dots, r_{m,n}'') \right\|_* + m\varepsilon_n'' L'' \\
 &\leq (1 - \sigma_n''(1 - K\Omega)) \|(z_{1,n}, z_{2,n}, \dots, z_{m,n}) - (p_1^*, p_2^*, \dots, p_m^*)\|_* \\
 &\quad + \sigma_n'' \left\| (\hat{\eta}_{1,n}'', \hat{\eta}_{2,n}'', \dots, \hat{\eta}_{m,n}'') \right\|_* + \|\bar{\eta}_{1,n}'', \bar{\eta}_{2,n}'', \dots, \bar{\eta}_{m,n}''\|_* \\
 &\quad + \left\| (r_{1,n}'', r_{2,n}'', \dots, r_{m,n}'') \right\|_* + \sigma_n'' K \sum_{i=1}^m l_{i,n} + m\varepsilon_n'' L'' \\
 &\leq \|(z_{1,n}, z_{2,n}, \dots, z_{m,n}) - (p_1^*, p_2^*, \dots, p_m^*)\|_* \\
 &\quad + \sigma_n'' K \sum_{i=1}^m l_{i,n} + \sigma_n'' \left\| (\hat{\eta}_{1,n}'', \hat{\eta}_{2,n}'', \dots, \hat{\eta}_{m,n}'') \right\|_* + \|\bar{\eta}_{1,n}'', \bar{\eta}_{2,n}'', \dots, \bar{\eta}_{m,n}''\|_* \\
 &\quad + \left\| (r_{1,n}'', r_{2,n}'', \dots, r_{m,n}'') \right\|_* + m\varepsilon_n'' L'' .
 \end{aligned} \tag{77}$$

Since $(1 - \sigma_n'(1 - K\Omega)) \leq 1$, therefore using (76) and (77) becomes

$$\begin{aligned}
 \|(s_{1,n+1}, s_{2,n+1}, \dots, s_{m,n+1}) - (p_1^*, p_2^*, \dots, p_m^*)\|_* &\leq \|(z_{1,n}, z_{2,n}, \dots, z_{m,n}) - (p_1^*, p_2^*, \dots, p_m^*)\|_* \\
 &\quad + \sigma_n' \sigma_n'' K \Omega \left\| (\hat{\eta}_{1,n}'', \hat{\eta}_{2,n}'', \dots, \hat{\eta}_{m,n}'') \right\|_* + \sigma_n' \sigma_n'' K^2 \Omega \sum_{i=1}^m l_{i,n} \\
 &\quad + \sigma_n' K \Omega \left\| (r_{1,n}'', r_{2,n}'', \dots, r_{m,n}'') \right\|_* + \sigma_n' K \Omega \|\bar{\eta}_{1,n}'', \bar{\eta}_{2,n}'', \dots, \bar{\eta}_{m,n}''\|_* \tag{78} \\
 &\quad + \sigma_n' K \sum_{i=1}^m l_{i,n} + \sigma_n' \left\| (\hat{\eta}_{1,n}', \hat{\eta}_{2,n}', \dots, \hat{\eta}_{m,n}') \right\|_* + \left\| (\bar{\eta}_{1,n}', \bar{\eta}_{2,n}', \dots, \bar{\eta}_{m,n}') \right\|_* \\
 &\quad + \left\| (r_{1,n}', r_{2,n}', \dots, r_{m,n}') \right\|_* + m\sigma_n' \varepsilon_n'' K \Omega L'' + m\varepsilon_n' L' .
 \end{aligned}$$

Using (77) and (78), (75) implies that

$$\begin{aligned}
 & \left\| (z_{1,n+1}, z_{2,n+1}, \dots, z_{m,n+1}) - (p_1^*, p_2^*, \dots, p_m^*) \right\|_* \leq \sum_{i=1}^m \varphi_{i,n} + (1 - \sigma_n - \varepsilon_n) \left\| (z_{1,n}, z_{2,n}, \dots, z_{m,n}) - (p_1^*, p_2^*, \dots, p_m^*) \right\|_* \\
 & + \sigma_n K \Omega \left[\begin{aligned} & \left\| (z_{1,n}, z_{2,n}, \dots, z_{m,n}) - (p_1^*, p_2^*, \dots, p_m^*) \right\|_* + \sigma_n' \sigma_n'' K \Omega \left\| (\hat{\eta}_{1,n}'', \hat{\eta}_{2,n}'', \dots, \hat{\eta}_{m,n}'') \right\|_* + \sigma_n' \sigma_n'' K^2 \Omega \sum_{i=1}^m l_{i,n} \\ & + \sigma_n' K \Omega \left\| (r_{1,n}'', r_{2,n}'', \dots, r_{m,n}'') \right\|_* + \sigma_n' K \Omega \left\| (\bar{\eta}_{1,n}'', \bar{\eta}_{2,n}'', \dots, \bar{\eta}_{m,n}'') \right\|_* + \sigma_n' K \sum_{i=1}^m l_{i,n} + \sigma_n' \left\| (\hat{\eta}_{1,n}', \hat{\eta}_{2,n}', \dots, \hat{\eta}_{m,n}') \right\|_* + \left\| \bar{\eta}_{1,n}', \bar{\eta}_{2,n}', \dots, \bar{\eta}_{m,n}' \right\|_* + \left\| (r_{1,n}', r_{2,n}', \dots, r_{m,n}') \right\|_* + m \sigma_n' \varepsilon_n'' K \Omega L'' + m \varepsilon_n' L' \end{aligned} \right] \\
 & + \sigma_n K \sum_{i=1}^m l_{i,n} + \sigma_n \left\| (\eta_{1,n}, \eta_{2,n}, \dots, \eta_{m,n}) \right\|_* + \left\| (r_{1,n}, r_{2,n}, \dots, r_{m,n}) \right\|_* + m \varepsilon_n L \\
 & \leq (1 - \sigma_n (1 - K \Omega)) \left\| (z_{1,n}, z_{2,n}, \dots, z_{m,n}) - (p_1^*, p_2^*, \dots, p_m^*) \right\|_* + \sigma_n (1 - K \Omega) \\
 & \left[\frac{\sum_{i=1}^m \varphi_{i,n}}{\kappa(1 - K \Omega)} + \frac{1}{(1 - K \Omega)} \left(\begin{aligned} & \sigma_n' \sigma_n'' K^2 \Omega^2 \left\| (\hat{\eta}_{1,n}'', \hat{\eta}_{2,n}'', \dots, \hat{\eta}_{m,n}'') \right\|_* + \sigma_n' K^2 \Omega^2 \left\| (\bar{\eta}_{1,n}'', \bar{\eta}_{2,n}'', \dots, \bar{\eta}_{m,n}'') \right\|_* + \sigma_n' K^2 \Omega^2 \left\| (r_{1,n}'', r_{2,n}'', \dots, r_{m,n}'') \right\|_* + \sigma_n' K \Omega \left\| (\hat{\eta}_{1,n}', \hat{\eta}_{2,n}', \dots, \hat{\eta}_{m,n}') \right\|_* + K \Omega \left\| (\bar{\eta}_{1,n}', \bar{\eta}_{2,n}', \dots, \bar{\eta}_{m,n}') \right\|_* \\ & + K \Omega \left\| (r_{1,n}', r_{2,n}', \dots, r_{m,n}') \right\|_* + \left\| \bar{\eta}_{1,n}', \bar{\eta}_{2,n}', \dots, \bar{\eta}_{m,n}' \right\|_* + (\sigma_n' \sigma_n'' K^3 \Omega^2 + \sigma_n' K^2 \Omega + K) \sum_{i=1}^m l_{i,n} + m \sigma_n' \varepsilon_n'' K^2 \Omega^2 L'' + m \varepsilon_n' K \Omega L' \end{aligned} \right) \right] \\
 & + \left\| (\bar{\eta}_{1,n}', \bar{\eta}_{2,n}', \dots, \bar{\eta}_{m,n}') \right\|_* + \left\| (r_{1,n}', r_{2,n}', \dots, r_{m,n}') \right\|_* + m \varepsilon_n' L, \tag{79}
 \end{aligned}$$

Since it is given that $\lim_{n \rightarrow \infty} \sum_{i=1}^m \varphi_{i,n} = 0$, therefore, $\lim_{n \rightarrow \infty} (z_{1,n+1}, z_{2,n+1}, \dots, z_{m,n+1}) = (p_1^*, p_2^*, \dots, p_m^*)$, and the result follows.

Conversely, assume that $\lim_{n \rightarrow \infty} (z_{1,n+1}, z_{2,n+1}, \dots, z_{m,n+1}) = (p_1^*, p_2^*, \dots, p_m^*)$. From (59) and $\lim_{n \rightarrow \infty} l_{i,n} = 0$, we have

$$\begin{aligned}
 \varphi_{i,n} &= \left\| z_{i,n+1} - \left[(1 - \sigma_n - \varepsilon_n) z_{i,n} + \sigma_n (H(t_{i,n}) + \eta_n) + \varepsilon_n \vartheta_{i,n} + r_n \right] \right\|_i \\
 &\leq \left\| z_{i,n+1} - p_i^* \right\|_i + \left\| \left[(1 - \sigma_n - \varepsilon_n) z_{i,n} + \sigma_n (H(t_{i,n}) + \eta_n) + \varepsilon_n \vartheta_{i,n} + r_n \right] - p_i^* \right\|_i \\
 &\leq \left\| z_{i,n+1} - p_i^* \right\|_i + \left\| \left[(1 - \sigma_n - \varepsilon_n) z_{i,n} + \sigma_n (H(t_{i,n}) + \eta_n) + \varepsilon_n \vartheta_{i,n} + r_n \right] - \left[(1 - \sigma_n - \varepsilon_n) p_i^* + \sigma_n H(p_i^*) + \varepsilon_n p_i^* \right] \right\|_i \tag{80} \\
 &\quad \cdot \left\| z_{i,n+1} - p_i^* \right\|_i + (1 - \sigma_n - \varepsilon_n) \left\| z_{i,n} - p_i^* \right\|_i + \sigma_n \left\| H(t_{i,n}) - H(p_i^*) \right\|_i \\
 &\quad + \sigma_n \left\| \hat{\eta}_{i,n} \right\|_i + \left\| \bar{\eta}_{i,n} \right\|_i + \varepsilon_n \left\| \vartheta_{i,n} - p_i^* \right\|_i + \left\| r_{i,n} \right\|_i
 \end{aligned}$$

By using (80), we have

$$\begin{aligned}
 \sum_{i=1}^m \varphi_{i,n} &\leq \sum_{i=1}^m \left\| z_{i,n+1} - p_i^* \right\|_i + (1 - \sigma_n - \varepsilon_n) \left\| z_{i,n} - p_i^* \right\|_i + \sigma_n \left\| H(t_{i,n}) - H(p_i^*) \right\|_i \\
 &\quad + (\sigma_n \left\| \hat{\eta}_{i,n} \right\|_i + \left\| \bar{\eta}_{i,n} \right\|_i + \varepsilon_n \left\| \vartheta_{i,n} - p_i^* \right\|_i + \left\| r_{i,n} \right\|_i) \\
 &\leq \left\| (z_{1,n+1}, z_{2,n+1}, \dots, z_{m,n+1}) - (p_1^*, p_2^*, \dots, p_m^*) \right\|_* \\
 &\quad + (1 - \sigma_n (1 - K \Omega)) \left\| (z_{1,n}, z_{2,n}, \dots, z_{m,n}) - (p_1^*, p_2^*, \dots, p_m^*) \right\|_* \\
 &\quad + \sigma_n \left(\sigma_n' \sigma_n'' K^2 \Omega^2 \left\| (\hat{\eta}_{1,n}'', \hat{\eta}_{2,n}'', \dots, \hat{\eta}_{m,n}'') \right\|_* \right. \\
 &\quad + \sigma_n' K^2 \Omega^2 \left\| (\bar{\eta}_{1,n}'', \bar{\eta}_{2,n}'', \dots, \bar{\eta}_{m,n}'') \right\|_* + \sigma_n' K^2 \Omega^2 \left\| (r_{1,n}'', r_{2,n}'', \dots, r_{m,n}'') \right\|_* \\
 &\quad + \sigma_n' K \Omega \left\| (\hat{\eta}_{1,n}', \hat{\eta}_{2,n}', \dots, \hat{\eta}_{m,n}') \right\|_* + K \Omega \left\| (\bar{\eta}_{1,n}', \bar{\eta}_{2,n}', \dots, \bar{\eta}_{m,n}') \right\|_* \\
 &\quad + K \Omega \left\| (r_{1,n}', r_{2,n}', \dots, r_{m,n}') \right\|_* + \left\| (\hat{\eta}_{1,n}', \hat{\eta}_{2,n}', \dots, \hat{\eta}_{m,n}') \right\|_* \\
 &\quad + (\sigma_n' \sigma_n'' K^3 \Omega^2 + \sigma_n' K^2 \Omega + K) \sum_{i=1}^m l_{i,n} + m \sigma_n' \varepsilon_n'' K^2 \Omega^2 L'' + m \varepsilon_n' K \Omega L' \\
 &\quad \left. + \left\| (\bar{\eta}_{1,n}', \bar{\eta}_{2,n}', \dots, \bar{\eta}_{m,n}') \right\|_* + \left\| (r_{1,n}', r_{2,n}', \dots, r_{m,n}') \right\|_* + m \varepsilon_n' L, \tag{81}
 \end{aligned}$$

which implies that $\lim_{n \rightarrow \infty} (\sum_{i=1}^m \varphi_{i,n}) = 0$.
Hence, the sequence $\{(p_{1,n}, p_{2,n}, \dots, p_{m,n})\}_{n=1}^{\infty}$ generated by (56) is $\mathcal{F}_{\rho_i, T_i}^{\partial_{\zeta_i} \psi_i(\cdot, p_i)}$ -stable, for each $i \in \Lambda$.
This completes the proof. \square

5. Proximal Dynamical System

In this section, we consider the proximal dynamical system technique to study the existence and uniqueness of the

$$\mathcal{E}_i(p_i) = h_i(p_i) - \mathcal{F}_{\rho_i, T_i}^{\partial_{\zeta_i} \psi_i(\cdot, p_i)} [g_i(p_i) - (T_i(h_i(p_i)) + \rho_i A_i(p_1, p_2, \dots, p_m))]. \tag{82}$$

It is evident from Lemma 2 that SENMVLI (19) has a solution $(p_1, p_2, \dots, p_m) \in \prod_{i=1}^m \mathcal{H}_i$ if and only if (p_1, p_2, \dots, p_m) is a zero of the equation

$$\mathcal{E}_i(p_i) = 0, \text{ for each } i \in \Lambda. \tag{83}$$

$$\begin{aligned} \frac{dp_i}{dt} &= -\omega_i \mathcal{E}_i(p_i) \\ &= \omega_i \left\{ \mathcal{F}_{\rho_i, T_i}^{\partial_{\zeta_i} \psi_i(\cdot, p_i)} [g_i(p_i) - (T_i(h_i(p_i)) + \rho_i A_i(p_1, p_2, \dots, p_m))] - h_i(p_i) \right\}, p_i(t_0) = c_i \in \mathcal{H}_i, \end{aligned} \tag{84}$$

associated with SENMVLI (19), where $\omega_i > 0$ is parameter. We call the proximal dynamical system (84) as extended nonlinear mixed variational-like proximal dynamical system. Here, the right hand side is related to the proximal operator and is discontinuous on the boundary of \mathcal{H}_i . From the definition, it is definite that the solution of the extended nonlinear mixed variational-like proximal dynamical system (84) belongs to the constraint set \mathcal{H}_i . This points out that the approximate results such as the existence, uniqueness, and continuous dependence of the solution of (84) can be investigated.

To state our results, we need the following well-known concepts.

Definition 9 (see [23]). The dynamical system is said to be converge to the solution set Γ^* of the problem (19), if, irrespective of the initial point, the trajectory of the dynamical system satisfies

$$\lim_{t \rightarrow \infty} \text{dist}(p_i(t), \Gamma^*) = 0, \tag{85}$$

where $\text{dist}(p_i(t), \Gamma^*) = \inf_{q_i \in \Gamma^*} \|p_i - q_i\|$.

If the solution set Γ^* has a unique solution $(p_1^*, p_2^*, \dots, p_m^*) \in \prod_{i=1}^m \mathcal{H}_i$, then (84) implies that $\lim_{t \rightarrow \infty} (p_1(t), p_2(t), \dots, p_m(t)) = (p_1^*, p_2^*, \dots, p_m^*)$.

Definition 10 (see [23]). The dynamical system is said to be globally exponentially stable with degree θ at p^* , if, irrespective of the initial point, the trajectory of the dynamical system satisfies

solution of SENMVLI (19). In Section 3, we have shown that the SENMVLI (19) is equivalent to a fixed point problem. By using this equivalent result, we suggest and analyze the following proximal dynamical system associated with the SENMVLI (19). For each $i \in \Lambda$, we define the residue vector as follows:

Using the residue vector equations (82) and (83) and fixed point formulation (27), we suggest the following proximal dynamical system:

$$\|p(t) - p^*\| \leq c_0 \|p(t_0) - p^*\| \exp(-\theta(t - t_0)), \forall t \geq t_0, \tag{86}$$

where c_0 and θ are positive constants, independent of the initial point.

Lemma 3 (see [23]). *Let \hat{p} and \hat{q} be real-valued nonnegative continuous functions with domain $\{t: t \geq t_0\}$ and let $\alpha(t) = \alpha_0(|t - t_0|)$, where α_0 is a monotone increasing function. If, for all $t \geq t_0$,*

$$\hat{p}(t) \leq \alpha(t) + \int_{t_0}^t \hat{p}(s) \hat{q}(s) ds, \tag{87}$$

holds, then

$$\hat{p}(t) \leq \alpha(t) \exp \left\{ \int_{t_0}^t \hat{q}(s) ds \right\}. \tag{88}$$

The existence and uniqueness of the solution of SENMVLI (19) is shown in Theorem 2. Now, by combining Lemma 3 and Theorem 2, we obtain the unique solution of extended nonlinear mixed variational-like proximal dynamical system (84).

Theorem 4. *For each $i \in \Lambda$, let $\mathcal{H}_i, g_i, h_i, T_i, \psi_i, \zeta_i$ and $\rho_i > 0$ be the same as in Theorem 2 and let all the conditions of Theorem 2 hold. For each $i \in \Lambda$, suppose that $Q_i: \mathcal{H}_i \rightarrow \mathcal{H}_i$ K_i -Lipschitzian mapping with the sequence $\{l_{i,n}\}$, and $S: \prod_{i=1}^m \mathcal{H}_i$ is a nearly uniformly $\rightarrow \prod_{i=1}^m \mathcal{H}_i$ is*

a nearly uniformly $\max\{K_i: i \in \Lambda\}$ -Lipschitzian mapping with the sequence $\{\sum_{i=1}^m l_{i,n}\}_{n=1}^\infty$ defined by (52) such that $\text{Fix}(S) \cap \text{SEMVLI}(\mathcal{H}_i, g_i, h_i, T_i, \psi_i, A_i, i \in \Lambda) \neq \emptyset$. Suppose that $\Omega < \min\{1, 1/K_i\}$, for each $i \in \Lambda$, where Ω is the same as in (42). Then, there exists a unique continuous solution $(p_1(t), p_2(t), \dots, p_m(t))$ of extended nonlinear mixed

variational-like proximal dynamical system (84) with $p_i(t_0) = c_i$ over $[t_0, \infty]$.

Proof. By Lemma 2, we have $h_i(p_i) = \mathcal{F}_{\rho_i, T_i}^{\partial_{\xi_i} \psi_i(\cdot, p_i)} [g_i(p_i) - (T_i(h_i(p_i)) + \rho_i A_i(p_1, p_2, \dots, p_m))]$ is a solution of SENMVLI (19). For each $i \in \Lambda$, we define $\mathcal{F}_i: \prod_{i=1}^m \mathcal{H}_i \rightarrow \mathcal{H}_i$ by

$$\mathcal{F}_i(p_1, p_2, p_3, \dots, p_m) = \omega_i \left\{ \mathcal{F}_{\rho_i, T_i}^{\partial_{\xi_i} \psi_i(\cdot, p_i)} [g_i(p_i) - (T_i(h_i(p_i)) + \rho_i A_i(p_1, p_2, \dots, p_m))] - h_i(p_i) \right\}, \tag{89}$$

for all $(p_1, p_2, \dots, p_m) \in \prod_{i=1}^m \mathcal{H}_i$. Define $\|\cdot\|_*$ on $\prod_{i=1}^m \mathcal{H}_i$ by

$$\|(p_1, p_2, p_3, \dots, p_m)\|_* = \sum_{i=1}^m \|p_i\|, \forall (p_1, p_2, \dots, p_m) \in \prod_{i=1}^m \mathcal{H}_i. \tag{90}$$

It is easy to see that $(\prod_{i=1}^m \mathcal{H}_i, \|\cdot\|_*)$ is a Hilbert space. Also, define $G: \prod_{i=1}^m \mathcal{H}_i \rightarrow \prod_{i=1}^m \mathcal{H}_i$ as follows:

$$\mathcal{G}(p_1, p_2, \dots, p_m) = (\mathcal{F}_1(p_1, p_2, \dots, p_m), \mathcal{F}_2(p_1, p_2, \dots, p_m), \dots, \mathcal{F}_m(p_1, p_2, \dots, p_m)), \tag{91}$$

for all $(p_1, p_2, \dots, p_m) \in \prod_{i=1}^m \mathcal{H}_i$.

To prove that $\mathcal{G}(p_1, p_2, \dots, p_m)$ is a locally Lipschitz continuous mapping, suppose that $(p_1, p_2, \dots, p_m) \neq$

$(\hat{p}_1, \hat{p}_2, \dots, \hat{p}_m) \in \prod_{i=1}^m \mathcal{H}_i$ are given. By using (32) and (34) and Theorem 1, for each $i \in \Lambda$, we have

$$\begin{aligned} & \|\mathcal{F}_i(p_1, p_2, \dots, p_m) - \mathcal{F}_i(\hat{p}_1, \hat{p}_2, \dots, \hat{p}_m)\|_i \\ &= \omega_i \left\| \left[\mathcal{F}_{\rho_i, T_i}^{\partial_{\xi_i} \psi_i(\cdot, p_i)} [g_i(p_i) - (T_i(h_i(p_i)) + \rho_i A_i(p_1, p_2, \dots, p_m))] - h_i(p_i) \right] \right. \\ & \quad \left. - \left[\mathcal{F}_{\rho_i, T_i}^{\partial_{\xi_i} \psi_i(\cdot, \hat{p}_i)} [g_i(\hat{p}_i) - (T_i(h_i(\hat{p}_i)) + \rho_i A_i(\hat{p}_1, \hat{p}_2, \dots, \hat{p}_m))] - h_i(\hat{p}_i) \right] \right\|_i \\ &\leq \omega_i \|p_i - \hat{p}_i\|_i + \omega_i \left\| \left(p_i - h_i(p_i) + \mathcal{F}_{\rho_i, T_i}^{\partial_{\xi_i} \psi_i(\cdot, p_i)} [g_i(p_i) - T_i(h_i(p_i)) \right. \right. \\ & \quad \left. \left. + \rho_i A_i(p_1, p_2, \dots, p_m)] \right) - \left(\hat{p}_i - h_i(\hat{p}_i) + \mathcal{F}_{\rho_i, T_i}^{\partial_{\xi_i} \psi_i(\cdot, \hat{p}_i)} [g_i(\hat{p}_i) - (T_i(h_i(\hat{p}_i)) \right. \right. \\ & \quad \left. \left. + \rho_i A_i(\hat{p}_1, \hat{p}_2, \dots, \hat{p}_m))] \right) \right\|_i. \end{aligned} \tag{92}$$

Using the same technique of (35)–(39) and (42) and (92) becomes

$$\begin{aligned} & \|\mathcal{F}_i(p_1, p_2, \dots, p_m) - \mathcal{F}_i(\hat{p}_1, \hat{p}_2, \dots, \hat{p}_m)\|_i \\ &\leq \omega_i \|p_i - \hat{p}_i\|_i + \omega_i \left(\Theta_i \|p_i - \hat{p}_i\|_i + \frac{\tau_i \rho_i}{\alpha_i + \delta_i} \sum_{j \in \Lambda, i \neq j} \nu_{i,j} \|p_j - \hat{p}_j\|_j \right), \end{aligned} \tag{93}$$

where $\Theta_i = \xi_i + \sqrt{(1 - 2\mu_{h_i} + \lambda_{h_i}^2) + (\tau_i (\lambda_{T_i} \lambda_{h_i} + \sqrt{(\lambda_{g_i}^2 - 2\rho_i \mu_{A_{ii}} + \rho_i^2 \lambda_{A_{ii}}^2)}) / (\alpha_i + \delta_i))}$. Applying the similar arguments of (36) and (44), we have

$$\begin{aligned} & \|\mathcal{G}(p_1, p_2, \dots, p_m) - \mathcal{G}(\hat{p}_1, \hat{p}_2, \dots, \hat{p}_m)\|_* \\ &= \sum_{i=1}^m \|\mathcal{F}_i(p_1, p_2, \dots, p_m) - \mathcal{F}_i(\hat{p}_1, \hat{p}_2, \dots, \hat{p}_m)\|_i \\ &\leq \max\{\omega_i: i \in \Lambda\} \left(\sum_{i=1}^m \|p_i - \hat{p}_i\|_i + \max\{\Theta_i \right. \\ & \quad \left. + \sum_{k \in \Lambda, k \neq i} \frac{\tau_k \rho_k}{\alpha_k + \delta_k} \nu_{k,i}: i \in \Lambda\} \sum_{i=1}^m \|p_i - \hat{p}_i\|_i \right) \\ &\leq \omega \left(\sum_{i=1}^m \|p_i - \hat{p}_i\|_i + \Omega \sum_{i=1}^m \|p_i - \hat{p}_i\|_i \right), \end{aligned} \tag{94}$$

i.e.,

$$\|\mathcal{G}(p_1, p_2, \dots, p_m) - \mathcal{G}(\widehat{p}_1, \widehat{p}_2, \dots, \widehat{p}_m)\|_* \leq \omega(1 + \Omega) \|(p_1, p_2, \dots, p_m) - (\widehat{p}_1, \widehat{p}_2, \dots, \widehat{p}_m)\|_*, \quad (95)$$

where $\Omega = \max \{\Theta_i + \sum_{k \in \Lambda, k \neq i} (\tau_k \rho_k) / (\alpha_k + \delta_k) \nu_{k,i} : i \in \Lambda\}$ and $\omega = \max \{\omega_i : i \in \Lambda\}$. Therefore, \mathcal{G} is a locally Lipschitz continuous mapping. Hence, for each $(c_1, c_2, \dots, c_m) \in \prod_{i=1}^m \mathcal{H}_i$, there exists a unique and continuous solution $(p_1(t), p_2(t), \dots, p_m(t))$ of the extended nonlinear mixed variational-like proximal dynamical system

(84), defined in an interval $t_0 \leq t \leq \mathcal{B}$ with the initial condition $p_i(t_0) = c_i$, for each $i \in \Lambda$. Suppose that $[t_0, \mathcal{B}]$ is the maximal interval of the existence of the solutions of (84). Now, we have to show that $\mathcal{B} = \infty$. For any $(p_1, p_2, \dots, p_m) \in \prod_{i=1}^m \mathcal{H}_i$, we have

$$\begin{aligned} \left\| \frac{dp_i}{dt} \right\|_i &= \|\mathcal{F}_i(p_1, p_2, \dots, p_m)\|_i \\ &= \omega_i \left\| \mathcal{F}_{\rho_i, T_i}^{\partial_{\rho_i} \Psi_i(\cdot, p_i)} [g_i(p_i) - (T_i(h_i(p_i)) + \rho_i A_i(p_1, p_2, \dots, p_m))] - h_i(p_i) \right\|_i \\ &\leq \omega_i \left\| \mathcal{F}_{\rho_i, T_i}^{\partial_{\rho_i} \Psi_i(\cdot, p_i)} [g_i(p_i) - (T_i(h_i(p_i)) + \rho_i A_i(p_1, p_2, \dots, p_m))] \right. \\ &\quad \left. - \mathcal{F}_{\rho_i, T_i}^{\partial_{\rho_i} \Psi_i(\cdot, p_i^*)} [g_i(p_i^*) - (T_i(h_i(p_i^*)) + \rho_i A_i(p_1^*, p_2^*, \dots, p_m^*))] \right\|_i \\ &\quad + \omega_i \|p_i - p_i^*\|_i \\ &\leq \omega_i \left[\left\| \mathcal{F}_{\rho_i, T_i}^{\partial_{\rho_i} \Psi_i(\cdot, p_i)} [g_i(p_i) - (T_i(h_i(p_i)) + \rho_i A_i(p_1, p_2, \dots, p_m))] \right. \right. \\ &\quad \left. \left. - \mathcal{F}_{\rho_i, T_i}^{\partial_{\rho_i} \Psi_i(\cdot, p_i^*)} [g_i(p_i) - (T_i(h_i(p_i)) + \rho_i A_i(p_1, p_2, \dots, p_m))] \right\|_i \right. \\ &\quad \left. + \left\| \mathcal{F}_{\rho_i, T_i}^{\partial_{\rho_i} \Psi_i(\cdot, p_i)} [g_i(p_i) - (T_i(h_i(p_i)) + \rho_i A_i(p_1, p_2, \dots, p_m))] \right. \right. \\ &\quad \left. \left. - \mathcal{F}_{\rho_i, T_i}^{\partial_{\rho_i} \Psi_i(\cdot, p_i^*)} [g_i(p_i^*) - (T_i(h_i(p_i^*)) + \rho_i A_i(p_1^*, p_2^*, \dots, p_m^*))] \right\|_i \right] \\ &\leq \omega_i \|p_i - p_i^*\|_i + \omega_i \left(\Theta_i \left\| p_i - p_i^* \right\|_i + \frac{\tau_i \rho_i}{\alpha_i + \delta_i} \sum_{j \in \Lambda, i \neq j} \nu_{i,j} \left\| p_j - p_j^* \right\|_j \right). \end{aligned} \quad (96)$$

Now, we calculate

$$\begin{aligned}
 \|\mathcal{G}(p_1, p_2, \dots, p_m)\|_* &= \sum_{i=1}^m \|\mathcal{F}_i(p_1, p_2, \dots, p_m)\|_i = \sum_{i=1}^m \left\| \frac{dp_i}{dt} \right\|_i \\
 &\leq \sum_{i=1}^m \omega_i \left(\|p_i - p_i^*\|_i + \left(\Theta_i \|p_i - p_i^*\|_i + \frac{\tau_i \rho_i}{\alpha_i + \delta_i} \sum_{j \in \Lambda, i \neq j} \nu_{i,j} \|p_j - p_j^*\|_j \right) \right) \\
 &\leq \max \{ \omega_i : i \in \Lambda \} \left(\sum_{i=1}^m \|p_i - p_i^*\|_i + \max \{ \Theta_i \right. \\
 &\quad \left. + \sum_{k \in \Lambda, k \neq i} \frac{\tau_k \rho_k}{\alpha_k + \delta_k} \nu_{k,i} : i \in \Lambda \} \sum_{i=1}^m \|p_j - p_j^*\|_i \right) \tag{97} \\
 &\leq \omega \left(\sum_{i=1}^m \|p_i - p_i^*\|_i + \Omega \sum_{i=1}^m \|p_i - p_i^*\|_i \right) \\
 &\leq \omega(1 + \Omega) \sum_{i=1}^m \|p_i - p_i^*\|_i \\
 &= \omega(1 + \Omega) \|(p_1, p_2, \dots, p_m) - (p_1^*, p_2^*, \dots, p_m^*)\|_* \\
 &\leq \omega(1 + \Omega) \|(p_1, p_2, \dots, p_m)\|_* + \omega(1 + \Omega) \|(p_1^*, p_2^*, \dots, p_m^*)\|_*,
 \end{aligned}$$

and therefore,

$$\begin{aligned}
 \|(p_1(t), p_2(t), \dots, p_m(t))\|_* &\leq \|(p_1(t_0), p_2(t_0), \dots, p_m(t_0))\|_* \\
 &\quad + \int_{t_0}^t \|\mathcal{G}(p_1(s), p_2(s), \dots, p_m(s))\|_* ds \\
 &\leq (\|(p_1(t_0), p_2(t_0), \dots, p_m(t_0))\|_* + k_1(t - t_0)) \\
 &\quad + k_2 \int_{t_0}^t \|(p_1(s), p_2(s), \dots, p_m(s))\|_* ds, \tag{98}
 \end{aligned}$$

where $k_1 = \omega(1 + \Omega) \|(p_1^*, p_2^*, \dots, p_m^*)\|_*$ and $k_2 = \omega(1 + \Omega)$. Using Lemma 3, we have

$$\|(p_1(t), p_2(t), \dots, p_m(t))\|_* \leq (\|(p_1(t_0), p_2(t_0), \dots, p_m(t_0))\|_* + k_1(t - t_0)) e^{k_2(t - t_0)}, \forall t \in [t_0, \mathcal{B}]. \tag{99}$$

Hence, the solution is bounded for $t \in (t_0, \mathcal{B})$, if \mathcal{B} is finite. Thus, $\mathcal{B} = \infty$. This completes the proof. \square

Applying the approach of Xia and Feng [31, 32], we now show that the trajectory of the solution of extended non-linear mixed variational-like proximal dynamical system (84) converges to a unique solution of SENMVL (19).

Theorem 5. For each $i \in \Lambda$, let $\mathcal{H}_i, g_i, h_i, T_i, \psi_i, \zeta_i$, and $\rho_i > 0$ be the same as in Theorem 2 and let all the

conditions of Theorem 2 hold. If the following conditions are satisfied:

$$\begin{cases} \chi_i = \mu_{h_i} + \frac{\tau_i \rho_i}{\alpha_i + \delta_i} \sum_{j \in \Lambda, i \neq j} \nu_{i,j}, \\ \tau_i \sqrt{(\lambda_{g_i}^2 - 2\rho_i \mu_{A_{ii}} + \rho_i^2 \lambda_{A_{ii}}^2)} < [(\chi_i - \xi_i)(\alpha_i + \delta_i) - \tau_i \lambda_{T_i} \lambda_{h_i}], \end{cases} \tag{100}$$

then, the extended nonlinear mixed variational-like proximal dynamical system (84) converges globally exponentially to a unique solution of SENMVLI (19).

Proof. In Theorem 2, we prove the existence of a unique solution $(p_1^*, p_2^*, \dots, p_m^*)$ of the problem SENMVLI (19). By Lemma 2, we have $h_i(p_i^*) = \mathcal{F}_{\rho_i, T_i}^{\partial_{c_i} \Psi_i(\cdot, p_i^*)} [g_i(p_i^*) - (T_i(h_i(p_i^*)) + \rho_i A_i(p_1^*, p_2^*, \dots, p_m^*))]$. Also, in

view of Theorem 4, the extended mixed variational-like resolvent dynamical system (82) has a unique solution $(p_1(t), p_2(t), \dots, p_m(t))$ over $[t_0, \mathcal{B}]$ for any fixed $c_i \in \mathcal{H}_i$, for each $i \in \Lambda$. Let $(p_1(t), p_2(t), \dots, p_m(t)) = (p_1(t, t_0; c_1), p_2(t, t_0; c_2), \dots, p_m(t, t_0; c_m))$ be the solution of the initial value problem (84) with $p_i(t_0) = c_i$, for each $i \in \Lambda$. Now, we consider the Lyapunov function \mathcal{L} defined on $\prod_{i=1}^m \mathcal{H}_i$ by

$$\mathcal{L}(p_1, p_2, \dots, p_m) = \|(p_1, p_2, \dots, p_m) - (p_1^*, p_2^*, \dots, p_m^*)\|_*^2, \forall (p_1, p_2, \dots, p_m) \in \prod_{i=1}^m \mathcal{H}_i. \tag{101}$$

For each $i \in \Lambda$, from (82), (91)–(95), and (101), and using μ_{h_i} -strongly monotonicity of h_i , we have

$$\begin{aligned} \frac{\partial \mathcal{L}}{\partial p_i} \frac{dp_i}{dt} &= 2 \left\langle p_i(t) - p_i^*, \frac{dp_i}{dt} \right\rangle_i \\ &= 2\omega_i \langle p_i(t) - p_i^*, \mathcal{F}_{\rho_i, T_i}^{\partial_{c_i} \Psi_i(\cdot, p_i)} [g_i(p_i) - (T_i(h_i(p_i)) + \rho_i A_i(p_1, p_2, \dots, p_m))] - h_i(p_i) \rangle_i \\ &= -2\omega_i \langle p_i(t) - p_i^*, h_i(p_i) - h_i(p_i^*) \rangle_i \\ &\quad + 2\omega_i \langle p_i(t) - p_i^*, \mathcal{F}_{\rho_i, T_i}^{\partial_{c_i} \Psi_i(\cdot, p_i)} [g_i(p_i) - (T_i(h_i(p_i)) + \rho_i A_i(p_1, p_2, \dots, p_m))] - h_i(p_i^*) \rangle_i \\ &\leq -2\omega_i \mu_{h_i} \|p_i(t) - p_i^*\|_i^2 + 2\omega_i \|p_i(t) - p_i^*\|_i \left\| \mathcal{F}_{\rho_i, T_i}^{\partial_{c_i} \Psi_i(\cdot, p_i)} g_i(p_i) - (T_i(h_i(p_i)) \right. \\ &\quad \left. + \rho_i A_i(p_1, p_2, \dots, p_m) - \mathcal{F}_{\rho_i, T_i}^{\partial_{c_i} \Psi_i(\cdot, p_i^*)} g_i(p_i^*) - (T_i(h_i(p_i^*)) + \rho_i A_i(p_1^*, p_2^*, \dots, p_m^*)) \right\|_i \\ &\leq -2\omega_i \left(\mu_{h_i} - \frac{\xi_i(\alpha_i + \delta_i) + \tau_i(\lambda_{T_i} \lambda_{h_i} + \sqrt{(\lambda_{g_i}^2 - 2\rho_i \mu_{A_{ii}} + \rho_i^2 \lambda_{A_{ii}}^2)})}{\alpha_i + \delta_i} \right) \|p_i(t) - p_i^*\|_i^2 \\ &\quad - \omega_i \frac{\tau_i \rho_i}{\alpha_i + \delta_i} \sum_{j \in \Lambda, i \neq j} \nu_{i,j} \|p_j - \hat{p}_j\|_j^2 \\ &\leq -2\omega_i \left(\Phi_i \|p_i(t) - p_i^*\|_i^2 + \frac{\tau_i \rho_i}{\alpha_i + \delta_i} \sum_{j \in \Lambda, i \neq j} \nu_{i,j} \|p_j(t) - p_j^*\|_j^2 \right), \end{aligned} \tag{102}$$

where $\Phi_i = \mu_{h_i} - \xi_i(\alpha_i + \delta_i) + \tau_i(\lambda_{T_i} \lambda_{h_i} + \sqrt{(\lambda_{g_i}^2 - 2\rho_i \mu_{A_{ii}} + \rho_i^2 \lambda_{A_{ii}}^2)}) / (\alpha_i + \delta_i)$. By using (102), we have

$$\begin{aligned} \frac{d\mathcal{L}}{dt} &= \sum_{i=1}^m \frac{\partial \mathcal{L}_i}{\partial p_i} \frac{dp_i}{dt} = 2 \sum_{i=1}^m \langle p_i(t) - p_i^*, \frac{dp_i}{dt} \rangle_i \\ &\leq -2 \sum_{i=1}^m \left[\omega_i \Phi_i \|p_i(t) - p_i^*\|^2 + \omega_i \frac{\tau_i \rho_i}{\alpha_i + \delta_i} \sum_{j \in \Lambda, i \neq j} \nu_{i,j} \|p_j - \hat{p}_j\|_j^2 \right], \\ &\leq -2\omega \max \left\{ \Phi_i + \frac{\tau_i \rho_i}{\alpha_i + \delta_i} \sum_{j \in \Lambda, i \neq j} \nu_{i,j}; i = 1, 2, \dots, m \right\} \sum_{i=1}^m \|p_i(t) - p_i^*\|_i^2, \end{aligned} \tag{103}$$

i.e.,

$$\frac{d}{dt} \|(p_1, p_2, \dots, p_m) - (p_1^*, p_2^*, \dots, p_m^*)\|_*^2 \leq -2\omega\Delta \|(p_1, p_2, \dots, p_m) - (p_1^*, p_2^*, \dots, p_m^*)\|_*^2, \tag{104}$$

where $\Delta = \max \{ \Phi_i + (\tau_i \rho_i) / (\alpha_i + \delta_i) \sum_{j \in \Lambda, i \neq j} \nu_{i,j}; i \in \Lambda \}$ and $\omega = \{ \omega_i; i \in \Lambda \}$. Therefore, we have

$$\|(p_1, p_2, \dots, p_m) - (p_1^*, p_2^*, \dots, p_m^*)\|_* \leq \|(p_1, p_2, \dots, p_m) - (p_1^*, p_2^*, \dots, p_m^*)\|_* e^{-\omega\Delta(t-t_0)}. \tag{105}$$

Using the conditions (32) and (100), we conclude that $\Delta > 0$. Hence, the trajectory of the solution of extended nonlinear mixed variational-like inequalities involving different nonlinear mappings in the setting of real Hilbert spaces. Using the proximal operator technique, we have shown that the system of extended nonlinear mixed variational-like inequalities is equivalent to the corresponding fixed point problem, and applying this equivalent result, we have proved the existence and uniqueness of solution of the system of extended nonlinear mixed variational-like inequalities. Making use of equivalent fixed point formulation and nearly uniformly Lipschitzian mapping, we have proposed a new three-step iterative algorithm with mixed errors to examine the convergence and stability analysis of the suggested iterative algorithm under some suitable conditions. Finally, we have analyzed and suggested a proximal dynamical system associated with the system of extended nonlinear mixed variational-like inequalities. We have shown that the trajectory of the solution of the proximal dynamical system converges globally exponentially to a unique solution of the considered problem. We would like to emphasize that the problem considered in this article can be further investigated from different aspects such as sensitivity analysis, well-posedness, approximation, and numerical analysis. The concepts and method of the

proposed operator splitting scheme may be extended for solving the system of quasi variational-like inequalities, system of equilibrium problems, and other related generalized systems.

Data Availability

No data were used to support the findings of this study.

Conflicts of Interest

The authors declare that they have no conflicts of interest.

Acknowledgments

The researcher(s) would like to thank the Deanship of Scientific Research, Qassim University for funding the publication of this project.

References

- [1] P. Hartman and G. Stampacchia, "On some nonlinear elliptic differential functional equations," *Acta Mathematica*, vol. 115, no. 0, pp. 271–310, 1966.
- [2] J. Eckstein and D. P. Bertsekas, "On the Douglas-Rachford splitting method and the proximal point algorithm for maximal monotone operators," *Mathematical Programming*, vol. 55, no. 1-3, pp. 293–318, 1992.
- [3] R. Glowinski, J. Lions, and R. Tremolieres, *Numerical Analysis of Variational Inequalities*, North-Holland, Amsterdam, Netherlands, 1981.
- [4] S. Haubruge, V. H. Nguyen, and J. J. Strodiot, "Convergence analysis and applications of the glowinski-le Tallec splitting method for finding a zero of the sum of two maximal

6. Conclusion

In this work, we have studied a new system of extended nonlinear mixed variational-like inequalities involving different nonlinear mappings in the setting of real Hilbert spaces. Using the proximal operator technique, we have shown that the system of extended nonlinear mixed variational-like inequalities is equivalent to the corresponding fixed point problem, and applying this equivalent result, we have proved the existence and uniqueness of solution of the system of extended nonlinear mixed variational-like inequalities. Making use of equivalent fixed point formulation and nearly uniformly Lipschitzian mapping, we have proposed a new three-step iterative algorithm with mixed errors to examine the convergence and stability analysis of the suggested iterative algorithm under some suitable conditions. Finally, we have analyzed and suggested a proximal dynamical system associated with the system of extended nonlinear mixed variational-like inequalities. We have shown that the trajectory of the solution of the proximal dynamical system converges globally exponentially to a unique solution of the considered problem. We would like to emphasize that the problem considered in this article can be further investigated from different aspects such as sensitivity analysis, well-posedness, approximation, and numerical analysis. The concepts and method of the

- monotone operators,” *Journal of Optimization Theory and Applications*, vol. 97, no. 3, pp. 645–673, 1998.
- [5] X. L. Weng, “Fixed point iteration for local strictly pseudo-contractive mapping,” *Proceedings of the American Mathematical Society*, vol. 113, no. 3, pp. 727–731, 1991.
 - [6] A. Bnouhachem and M. A. Noor, “Numerical comparison between prediction-correction methods for general variational inequalities,” *Applied Mathematics and Computation*, vol. 186, no. 1, pp. 496–505, 2007.
 - [7] X. P. Ding and C. L. Lou, “Perturbed proximal point algorithms for general quasi-variational-like inclusions,” *Journal of Computational and Applied Mathematics*, vol. 113, no. 1-2, pp. 153–165, 2000.
 - [8] X. P. Ding, J. C. Yao, and L. C. Zeng, “Existence and algorithm of solutions for generalized strongly nonlinear mixed variational-like inequalities in Banach spaces,” *Computers & Mathematics with Applications*, vol. 55, no. 4, pp. 669–679, 2008.
 - [9] J. Balooee and Y. J. Cho, “Algorithms for solutions of extended general mixed variational inequalities and fixed points,” *Optics Letters*, vol. 7, no. 8, pp. 1929–1955, 2013.
 - [10] M. Farid, R. Ali, and W. Cholamjiak, “An inertial iterative algorithm to find common solution of a split generalized equilibrium and a variational inequality problem in Hilbert spaces,” *Journal of Mathematics*, vol. 2021, Article ID 3653807, pp. 1–17, 2021.
 - [11] M. Farid, W. Cholamjiak, R. Ali, and K. R. Kazmi, “A new shrinking projection algorithm for a generalized mixed variational-like inequality problem and asymptotically quasi- ϕ -nonexpansive mapping in a Banach space ϕ -nonexpansive mapping in a Banach space,” *RACSAM*, vol. 115, no. 3, p. 114, 2021.
 - [12] M. Rahaman, R. Ahmad, M. Dilshad, and I. Ahmad, “RELAXED H-PROXIMAL OPERATOR FOR SOLVING A VARIATIONAL-LIKE INCLUSION PROBLEM η -proximal operator for solving a variational-like inclusion problem,” *Mathematical Modelling and Analysis*, vol. 20, no. 6, pp. 819–835, 2015.
 - [13] M. A. Noor, “Projection-splitting algorithms for monotone variational inequalities,” *Computers & Mathematics with Applications*, vol. 39, no. 9-10, pp. 73–79, 2000.
 - [14] M. A. Noor, “Splitting methods for pseudomonotone mixed variational inequalities,” *Journal of Mathematical Analysis and Applications*, vol. 246, no. 1, pp. 174–188, 2000.
 - [15] G. Glowinski and P. L. Tallec, *Augmented Lagrangian and Operator Splitting Methods in Nonlinear Mechanics*, SIAM, Philadelphia, PA, USA, 1989.
 - [16] D. V. Hieu and P. K. Quy, “An inertial modified algorithm for solving variational inequalities,” *RAIRO - Operations Research*, vol. 54, no. 1, pp. 163–178, 2020.
 - [17] S. S. Irfan, M. Rahaman, I. Ahmad, R. Ahmad, and S. Husain, “Generalized nonsmooth exponential-type vector variational-like inequalities and nonsmooth vector optimization problems in Asplund spaces,” *Mathematics*, vol. 7, p. 345, 2019.
 - [18] H. Y. Lan, “Convergence analysis of new over-relaxed proximal point algorithm frameworks with errors and applications to general A-monotone nonlinear inclusion forms,” *Applied Mathematics and Computation*, vol. 230, pp. 154–163, 2014.
 - [19] Y. Q. Qiu, J. Z. Chen, and L. C. Ceng, “Auxiliary principle and iterative algorithm for a system of generalized set-valued strongly nonlinear mixed implicit quasi-variational-like inequalities,” *Journal of Inequalities and Applications*, vol. 2016, no. 1, p. 38, 2016.
 - [20] P. Dupuis and A. Nagurney, “Dynamical systems and variational inequalities,” *Annals of Operations Research*, vol. 44, no. 1, pp. 7–42, 1993.
 - [21] T. L. Friesz, D. Bernstein, and R. Stough, “Dynamic systems, variational inequalities and control theoretic models for predicting time-varying urban network flows,” *Transportation Science*, vol. 30, no. 1, pp. 14–31, 1996.
 - [22] M. A. Noor, “Implicit dynamical systems and quasi variational inequalities,” *Applied Mathematics and Computation*, vol. 134, no. 1, pp. 69–81, 2003.
 - [23] M. A. Noor, “A Wiener-Hopf dynamical system for variational inequalities,” *New Zealand J. Math.* vol. 31, pp. 171–182, 2002.
 - [24] J. X. Zhou and G. Chen, “Diagonal convexity conditions for problems in convex analysis and quasi-variational inequalities,” *Journal of Mathematical Analysis and Applications*, vol. 132, no. 1, pp. 213–225, 1988.
 - [25] S. Simson, “From Hahn-Banach to monotonicity,” *Lecture Notes in Math*, Springer, New York, NY, USA, 2nd edition, 2008.
 - [26] L. S. Liu, “Ishikawa and Mann iterative process with errors for nonlinear strongly accretive mappings in Banach spaces,” *Journal of Mathematical Analysis and Applications*, vol. 194, no. 1, pp. 114–125, 1995.
 - [27] J. Balooee, “Resolvent algorithms for system of generalized nonlinear variational inclusions and fixed point problems,” *Afrika Matematika*, vol. 25, no. 4, pp. 1023–1042, 2014.
 - [28] Y. Tang, J. Guan, Y. Xu, and Y. Su, “A kind of system of multivariate variational inequalities and the existence theorem of solutions,” *Journal of Inequalities and Applications*, vol. 2017, no. 1, p. 208, 2017.
 - [29] N. J. Huang, “Generalized nonlinear variational inclusions with noncompact valued mappings,” *Applied Mathematics Letters*, vol. 9, no. 3, pp. 25–29, 1996.
 - [30] R. U. Verma, “On generalized variational inequalities involving relaxed Lipschitz and relaxed monotone operators,” *Journal of Mathematical Analysis and Applications*, vol. 213, no. 1, pp. 387–392, 1997.
 - [31] Y. S. Xia and G. Feng, “On convergence conditions of an extended projection neural network,” *Neural Computation*, vol. 17, no. 3, pp. 515–525, 2005.
 - [32] Y. S. Xia and J. Wang, “A recurrent neural network for solving linear projection equations,” *Neural Networks*, vol. 13, no. 3, pp. 337–350, 2000.
 - [33] Z. Liu, Z. S. Chen, S. M. Kang, and J. S. Ume, “Existence and iterative approximations of solutions for mixed quasi-variational-like inequalities in Banach spaces,” *Nonlinear Analysis: Theory, Methods & Applications*, vol. 69, no. 10, pp. 3259–3272, 2008.

Research Article

On New Solutions of Fuzzy Hybrid Differential Equations by Novel Approaches

Prasanth Bharathi Dhandapani ¹, Jayakumar Thippan ², Bundit Unyong ³,
R. Vadivel ⁴, and P. Hammachukiattikul ⁴

¹Department of Mathematics, Sri Eshwar College of Engineering, Coimbatore-641202, Tamilnadu, India

²Department of Mathematics, Sri Ramakrishna Mission Vidyalaya College of Arts and Science, Coimbatore-641020, Tamilnadu, India

³Department of Mathematics, School of Science, Walailak University, Tha Sala, Nakhon Si Thammarat 80160, Thailand

⁴Department of Mathematics, Faculty of Science and Technology, Phuket Rajabhat University, Phuket 83000, Thailand

Correspondence should be addressed to Bundit Unyong; bundit.un@wu.ac.th

Received 7 November 2022; Revised 25 December 2022; Accepted 22 March 2023; Published 12 June 2023

Academic Editor: Watcharaporn Cholamjiak

Copyright © 2023 Prasanth Bharathi Dhandapani et al. This is an open access article distributed under the Creative Commons Attribution License, which permits unrestricted use, distribution, and reproduction in any medium, provided the original work is properly cited.

The goal of this paper is to find the best of two sixth-order methods, namely, RK-Huta and RK-Butcher methods for solving the fuzzy hybrid systems. We state a necessary definition and theorem in terms of consistency for convergence, and finally, we compare the obtained numerical results of two different methods with analytical solution using two different numerical examples. In addition to that, we generalize the solutions obtained by RK-6 Huta and RK-6 Butcher methods (same order different stage methods) for both the problems we handled. We are proposing these two methods in order to reduce the error in accuracy and to establish these two methods are better than any other existing numerical methods. The best of two sixth-order methods are found by the error analysis study for both the problems. Also, we show whether the change in number of stages of same order methods affects the accuracy of the approximation or not.

1. Introduction

The hybrid systems are the dynamic systems which involve both continuous and discrete actions. We shall discuss about the hybrid systems in detail. The term hybrid is not a new thing to the world. We are using the term hybrid everywhere knowingly or unknowingly. The botanist often used this term while some plants, fruits, and vegetables are produced by the technique of hybridization. This hybrid plantation is quite common in all the developing countries. The people are used to compare these hybrid products and original organic products though some of the hybrid products are even organic. The industrialists often use this term hybrid in making of innovative technologies. Nowadays, we are offered to use the hybrid cars which are making use of two different fuels as a combination of liquid fuel and electric motor.

Now, in mathematics, it is used to call some functions as hybrid functions. The system which is involving two or more functions are termed as hybrid systems. The functions which are both continuous and discrete depending upon the interval of time being considered as hybrid functions. Sometimes, we have to call a function as a hybrid function when it exhibits continuous discontinuities such as modulus functions and trigonometric functions.

The hybrid system is often modeled with the aid of differential equations. Obviously, we can easily grasp that it should be a nonlinear equations. Since it is tedious to obtain the exact solutions, we prefer to apply the concept of numerical techniques to adopt the solutions. After achieving the approximate solutions, it is our prior most duty to assure the readers that our method is providing the better approximations. For that, we can take two

different methods but one can easily say higher order method will automatically provide better approximation. So instead of taking two different order methods, we are using same sixth-order methods and going to compare them in order to find the method providing better approximations.

These dynamic behaviors with Zadeh’s fuzzy theory [1] paved a way to fuzzy differential equations [2–5] and fuzzy hybrid differential equations (FHDEs) [5–15]. In the present paper, two sixth-order methods called RK-Huta and RK–Butcher, respectively, having eight stages and seven stages are used to obtain approximate solutions of FHDE. Since they are the higher-order methods, the solution converges rapidly to exact solutions than any other numerical methods. Numerical solutions of FHDE are studied over a period of time using various methods such as Euler and Runge–Kutta, by various authors like Pederson and Sambandham [16, 17] and Jayakumar and Kanagarajan [18, 19]. Other than them, Salahshour along with Allahviranloo and Ahmadian et al. made remarkable contributions in hybrid fuzzy differential equations [20, 21]. The readers are encouraged to go through the various applications of numerical methods to solve various types of differential equations through [4–15, 22–24].

We are eager to present one such study of FHDE for the benefit of the authors. Two different sixth-order methods such as RK-Huta and Bucher methods are presented and compared while solving these types of nonlinear differential equations.

The whole study was split as four sections in which FHDE and two RK-6 methods such as Huta and Butcher methods are presented in Section 2. Section 3 contains numerical examples, and finally, the study is concluded in Section 4.

2. Fuzzy Hybrid Differential Equations (FHDEs) and RK-6 Methods

The picture of the hybrid system is shown in Figure 1 in a way as P.B. Dhandapani et al. showed it in the discontinuity between continuity or continuity between discontinuity in [15].

Following the preliminaries of [16], the hybrid systems are treated via the continuous and discrete parameters.

E^n represents the set of $y_H: R^n \longrightarrow [0, 1]$ in the following manner:

- (i) y_H is always normal, as there exists an $t_0 \in R^n$ such that $y_H(t_0) = 1$
- (ii) y_H is convex under fuzzy definitions, as for $t_1, t_2, y_H \in R^n$ and $0 \leq \alpha \leq 1$

$$y_H(\alpha t_1 + (1 - \alpha)t_2) \geq \min [y_H(t_1), y_H(t_2)]. \quad (1)$$
- (iii) y_H is always upper-semi continuous
- (iv) $[y_H]^0 \equiv$ the closure of $[t \in R^n: y_H(t) > 0]$ is compact

For $0 < \alpha \leq 1$, we define $[y_H(2t)]^\alpha = [t \in R^n: y_H(t) \geq \alpha]$. The α -level sets of $y_H(t)$ throughout the paper are given by the following equation:

$$y_H(t; \alpha) = [\underline{y}_H(t; \alpha), \overline{y}_H(t; \alpha)]. \quad (2)$$

Here, H is used to represent the association of hybrid systems in the system. Since we are dealing with fuzzy functions, we are defining below the minimum and maximum of $y_H(t)$, i.e.,

$$\begin{aligned} \underline{y}_H(t; \alpha) &= [0.75 + 0.25\alpha]y_H(t), \\ \overline{y}_H(t; \alpha) &= [1.125 - 0.125\alpha]y_H(t). \end{aligned} \quad (3)$$

Consider the FHDE, similar to [16, 18, 19]

$$\begin{cases} \Delta y_H(t) = \delta(t, y_H(t), \omega_k(y_{H_k})), & t \in [t_k, t_{k+1}], \\ y_H(t_k) = y_{H_k}, \end{cases}$$

$$\omega_k(u_k) = \begin{cases} \hat{0}, & \text{if } k = 0, \\ u_k, & \text{if } k \in \{1, 2, \dots\}, \end{cases} \quad (4)$$

where Δ denotes Seikkala’s differentiation, $0 \leq t_0 < t_1 < \dots < t_r < \dots, t_r \longrightarrow \infty$,

$$\delta \in C[R^+ \times E^1 \times E^1, E^1], \omega_r \in C[E^1, E^1]. \quad (5)$$

We may alter (4) by an equivalent system

$$\begin{cases} \Delta \underline{y}_H(t) = \underline{\delta}(t, y_H, \omega_k(y_{H_k})) \equiv P_k(t, \underline{y}_H, \overline{y}_H), \underline{y}_H(t_k) = \underline{y}_{H_k}, \\ \Delta \overline{y}_H(t) = \overline{\delta}(t, y_H, \omega_k(y_{H_k})) \equiv Q_k(t, \underline{y}_H, \overline{y}_H), \overline{y}_H(t_k) = \overline{y}_{H_k}, \end{cases} \quad (6)$$

$[\underline{y}_H(t; \alpha), \overline{y}_H(t; \alpha)]$ is a fuzzy number, and also the solutions of the parametric form given by the following equation:

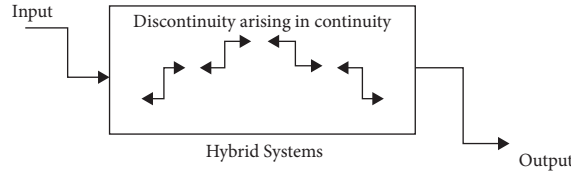


FIGURE 1: Hybrid systems.

$$\begin{cases} \Delta \underline{y}_H(t; \alpha) = P_k \left[t, \underline{y}_{H_k}(t; \alpha), \overline{y}_H(t; \alpha) \right], & \Delta \underline{y}_H(t_k; \alpha) = \underline{y}_{H_k}(\alpha), \\ \Delta \overline{y}_H(t; \alpha) = Q_k \left[t, \underline{y}_{H_k}(t; \alpha), \overline{y}_H(t; \alpha) \right], & \overline{y}_H(t_k; \alpha) = \overline{y}_{H_k}(\alpha), \alpha \in [0, 1], \end{cases} \quad (7)$$

where $P_k[t, \underline{y}_{H_k}(t; \alpha), \overline{y}_H(t; \alpha)]$ and $Q_k[t, \underline{y}_{H_k}(t; \alpha), \overline{y}_H(t; \alpha)]$ are the parametric forms to represent the function.

2.1. Convergence. From the notes of [25], the general single-step method for (4) is given by $y_{m+1} = y_m + \phi(t_m, y_m, h)$, $m = 0, 1, \dots, M-1$. Here, $\phi(t_m, y_m, h)$ is the increment function. The true value of $y(t_m)$ will satisfy $y(t_{m+1}) = y(t_m) + h\phi(t_m, y(t_m), h) + T_n$, $n = 0, 1, 2, \dots, N-1$. Here, T_n is the truncation error.

Definition 1 (see [25]). The general single-step method $y_{m+1} = y_m + \phi(t_m, y_m, h)$, $m = 0, 1, \dots, M-1$ is said to be consistent if $\phi(t, y, 0) = \psi(t, y)$

Theorem 1 (see [25]). *A necessary and sufficient condition for the convergence of a single step method which is regular of order $p \geq 1$ is consistency.*

Proof 1. According to Jain [25], "there exist a unique solution $y(t)$ on $[t_0, h]$ where $a \leq t_0 \leq t \leq t_0 + h \leq b$ and also $y(t) \in C^{p+1}[t_0, b]$, for $p \geq 1$. The solution $y(t)$ can be expanded in a Taylor series about any point t_n .

$$\begin{aligned} y(t) &= y(t_n) + (t - t_n)\Delta y(t_n) + \frac{1}{2!}(t - t_n)^2 \Delta^2 y(t_n) + \dots \\ &+ \frac{1}{p!}(t - t_n)^p \Delta^p y(t_n) + \frac{1}{(p+1)!}(t - t_n)^{p+1} \Delta^{p+1} y(t_n) \epsilon_n f. \end{aligned} \quad (8)$$

This expansion holds good for $t \in [t_0, b]$, $t_n < \epsilon < t$. Substituting $t = t_{n+1}$ in (8), we obtain the following equation:

$$y(t_{n+1}) = y(t_n) + h\Delta y(t_n) + \frac{h^2}{2!} \Delta^2 y(t_n) + \dots + \frac{h^p}{p!} \Delta^p y(t_n), \quad (9)$$

and $h\phi(t_n, y(t_n), h)$ is to be obtained from $h\phi(t_n, y(t_n), h)$ by using an approximate value y_n in place of the exact value $y(t_n)$. We compute $y_{n+1} = y_n + h\phi(t_n, y_n, h)$, $n = 0, 1, 2, \dots, N-1$ to approximate $y(t_{n+1})$. This is called Taylor's series method of order p . When $p = 1$, the Taylor series method becomes Euler's method as $y_{n+1} = y_n + hf(t_n, y_n)$, $n = 0, 1, 2, \dots, N-1$. The values of $\delta^2(y(t_n))$ and higher derivatives can be computed by substituting $t = t_n$. Therefore, we can compute $y(t_{n+1})$ with an error

$$\frac{h^{p+1}}{(p+1)! y^{(p+1)}(\epsilon_n)}, t_n < \epsilon_n < t_{n+1}. \quad (10)$$

By which consistency could be established since number of terms in Taylor's series is fixed by means of permissible error. From the theorem, the result ensures that the approximate solution converges to the exact solution since the convergence of Euler's method and Runge-Kutta method for hybrid fuzzy differential equations are proved by Pederson et al., [16, 17]. Also from the theorem of [16, 17], the point-to-point convergence for all k in α is fixed. \square

2.2. Numerical Methods. In order to get better clarity about the terms involved in Runge-Kutta methods, we shall present here the fourth-order Runge-Kutta method. When the hybrid term involves, the representation will change accordingly which will be shown on following sixth-order RK-Huta method.

2.3. Fourth-Order Runge-Kutta Method for ODE. For non-fuzzy ODE,

$$\begin{cases} \Delta y_H(t) = \delta(t, y(t)), t \in [t_k, t_{k+1}], \\ y(t_k) = y_k, \end{cases} \quad (11)$$

TABLE 1: Sixth-order RK-Huta [25].

1/9	1/9							
1/6	1/24	3/24						
1/3	1/6	-3/6	4/6					
1/2	-5/8	27/8	-24/8	6/8				
2/3	221/9	-981/9	867/9	-102/9	1/9			
5/6	-183/48	678/48	-472/48	-66/48	80/48	3/48		
1	716/82	-2079/82	1002/82	834/82	-454/82	-9/82	72/82	
	41/840	0	216/840	27/840	272/840	27/840	216/840	41/840

TABLE 2: Sixth-order RK-Butcher [25].

1/3	1/3							
2/3	0	2/3						
1/3	1/12	1/3	-1/12					
1/2	-1/16	9/8	-3/16	-3/8				
1/2	0	9/8	-3/8	-3/4	1/2			
1	9/44	-9/11	63/44	18/11	0	-16/11		
	11/120	0	27/40	27/40	-4/15	-4/15		11/120

we have

$$\begin{aligned}
 k_1 &= h\delta(t, y_k), \\
 k_2 &= h\delta\left(t + \frac{h}{2}, y_k + \frac{k_1}{2}\right), \\
 k_3 &= h\delta\left(t + \frac{h}{2}, y_k + \frac{k_2}{2}\right), \\
 k_4 &= h\delta(t + h, y_k + k_3), \\
 y_{n+1} &= y_n + \frac{1}{6}(k_1 + 2k_2 + 2k_3 + k_4),
 \end{aligned}
 \tag{12}$$

where k_1, k_2, \dots represents stages. y_n represents previous stage when y_{n+1} represents present iteration. The number of iterations to move from y_n to y_{n+1} is decided by the factor called step size h ; i.e., if we take $h=0.1$, then to reach $y(1)$ from $y(0)$, we have 11 iterations such that $y(0), y(0.1), y(0.2), \dots, y(1)$.

Since it is too complex to show these two sixth-order methods in stage form involving terms like $y_{H_{k,n}}(\alpha)$, $y_{H_{k,n+1}}(\alpha)$, and k_i (which is explained previously), we are just giving the coefficients involved in these two sixth-order methods, namely, Huta method and Butcher method from the study of [25]. With the belief that the reader may be familiar with conversion from the coefficient form to the stage form of numerical methods, we present that coefficient terms involved in sixth-order RK-Butcher and RK-Huta methods. The readers may refer basic studies like [18, 25] given in reference. Tables 1 and 2 represent the Sixth Order RK-Huta and Butcher values, which can be expanded as the following equation:

$$\begin{aligned}
 \underline{y}_{H_{k,n+1}}(\alpha) - \underline{y}_{H_{k,n}}(\alpha) &= \sum_{i=1}^8 v_i \underline{k}_i(t_{k,n}; y_{H_{k,n}}(\alpha)), \\
 \overline{y}_{H_{k,n+1}}(\alpha) - \overline{y}_{H_{k,n}}(\alpha) &= \sum_{i=1}^8 v_i \overline{k}_i(t_{k,n}; y_{H_{k,n}}(\alpha)),
 \end{aligned}
 \tag{13}$$

Next, we are defining

$$\begin{aligned}
\check{\zeta}_{k_1}(t_{k,n}, y_{H_{k,n}}(\alpha)) &= \underline{y}_{H_{k,n}}(\alpha) + \frac{1}{9}k_1(t_{k,n}, y_{H_{k,n}}(\alpha)), \\
\bar{\zeta}_{k_1}(t_{k,n}, y_{H_{k,n}}(\alpha)) &= \overline{y}_{H_{k,n}}(\alpha) + \frac{1}{9}\bar{k}_1(t_{k,n}, y_{H_{k,n}}(\alpha)), \\
\check{\zeta}_{k_2}(t_{k,n}, y_{H_{k,n}}(\alpha)) &= \underline{y}_{H_{k,n}}(\alpha) + \frac{1}{24}k_1(t_{k,n}, y_{H_{k,n}}(r)) + \frac{3}{24}k_2(t_{k,n}, y_{H_{k,n}}(\alpha)), \\
\bar{\zeta}_{k_2}(t_{k,n}, y_{H_{k,n}}(\alpha)) &= \overline{y}_{H_{k,n}}(r) + \frac{3}{24}\bar{k}_1(t_{k,n}, y_{H_{k,n}}(r)) + \frac{3}{24}\bar{k}_2(t_{k,n}, y_{H_{k,n}}(r)), \\
\check{\zeta}_{k_3}(t_{k,n}, y_{H_{k,n}}(\alpha)) &= \underline{y}_{H_{k,n}}(r) + \frac{1}{6}k_1(t_{k,n}, y_{H_{k,n}}(\alpha)) \\
&\quad - \frac{3}{6}k_2(t_{k,n}, y_{H_{k,n}}(\alpha)) + \frac{4}{6}k_3(t_{k,n}, y_{H_{k,n}}(\alpha)), \\
\bar{\zeta}_{k_3}(t_{k,n}, y_{H_{k,n}}(\alpha)) &= \overline{y}_{H_{k,n}}(\alpha) + \frac{1}{6}\bar{k}_1(t_{k,n}, y_{H_{k,n}}(\alpha)) \\
&\quad - \frac{3}{6}\bar{k}_2(t_{k,n}, y_{H_{k,n}}(\alpha)) + \frac{4}{6}\bar{k}_3(t_{k,n}, y_{H_{k,n}}(\alpha)), \\
\check{\zeta}_{k_4}(t_{k,n}, y_{H_{k,n}}(\alpha)) &= \underline{y}_{H_{k,n}}(\alpha) - \frac{5}{8}k_1(t_{k,n}, y_{H_{k,n}}(\alpha)) \\
&\quad + \frac{27}{8}k_2(t_{k,n}, y_{H_{k,n}}(\alpha)) - \frac{24}{8}k_3(t_{k,n}, y_{H_{k,n}}(\alpha)) + \frac{6}{8}k_4(t_{k,n}, y_{H_{k,n}}(\alpha)), \\
\bar{\zeta}_{k_4}(t_{k,n}, y_{H_{k,n}}(\alpha)) &= \overline{y}_{H_{k,n}}(\alpha) - \frac{5}{8}\bar{k}_1(t_{k,n}, y_{H_{k,n}}(\alpha)) \\
&\quad + \frac{27}{8}\bar{k}_2(t_{k,n}, y_{H_{k,n}}(\alpha)) - \frac{24}{8}\bar{k}_3(t_{k,n}, y_{H_{k,n}}(\alpha)) + \frac{6}{8}\bar{k}_4(t_{k,n}, y_{H_{k,n}}(\alpha)), \\
\check{\zeta}_{k_5}(t_{k,n}, y_{H_{k,n}}(\alpha)) &= \underline{y}_{H_{k,n}}(\alpha) + \frac{221}{9}k_1(t_{k,n}, y_{H_{k,n}}(\alpha)) - \frac{981}{9}k_2(t_{k,n}, y_{H_{k,n}}(\alpha)) \\
&\quad + \frac{867}{9}k_3(t_{k,n}, y_{H_{k,n}}(\alpha)) - \frac{102}{9}k_4(t_{k,n}, y_{H_{k,n}}(\alpha)) + \frac{1}{9}k_5(t_{k,n}, y_{H_{k,n}}(\alpha)), \\
\bar{\zeta}_{k_5}(t_{k,n}, y_{H_{k,n}}(\alpha)) &= \overline{y}_{H_{k,n}}(\alpha) + \frac{221}{9}\bar{k}_1(t_{k,n}, y_{H_{k,n}}(\alpha)) + \frac{981}{9}\bar{k}_2(t_{k,n}, y_{H_{k,n}}(\alpha)) \\
&\quad + \frac{867}{9}\bar{k}_3(t_{k,n}, y_{H_{k,n}}(\alpha)) + \frac{102}{9}\bar{k}_4(t_{k,n}, y_{H_{k,n}}(\alpha)) - \frac{1}{9}\bar{k}_5(t_{k,n}, y_{H_{k,n}}(\alpha)), \\
\check{\zeta}_{k_6}(t_{k,n}, y_{H_{k,n}}(\alpha)) &= \underline{y}_{H_{k,n}}(\alpha) - \frac{183}{48}k_1(t_{k,n}, y_{H_{k,n}}(\alpha)) + \frac{678}{48}k_2(t_{k,n}, y_{H_{k,n}}(\alpha)) \\
&\quad - \frac{472}{48}k_3(t_{k,n}, y_{H_{k,n}}(\alpha)) - \frac{66}{48}k_4(t_{k,n}, y_{H_{k,n}}(\alpha)) + \frac{80}{48}k_5(t_{k,n}, y_{H_{k,n}}(\alpha)) \\
&\quad + \frac{3}{48}k_6(t_{k,n}, y_{H_{k,n}}(\alpha)), \\
\bar{\zeta}_{k_6}(t_{k,n}, y_{H_{k,n}}(\alpha)) &= \overline{y}_{H_{k,n}}(\alpha) + \frac{183}{48}\bar{k}_1(t_{k,n}, y_{H_{k,n}}(\alpha)) + \frac{678}{48}\bar{k}_2(t_{k,n}, y_{H_{k,n}}(\alpha)) \\
&\quad + \frac{472}{48}\bar{k}_3(t_{k,n}, y_{H_{k,n}}(\alpha)) + \frac{66}{48}\bar{k}_4(t_{k,n}, y_{H_{k,n}}(\alpha)) - \frac{80}{48}\bar{k}_5(t_{k,n}, y_{H_{k,n}}(\alpha)) \\
&\quad + \frac{3}{48}\bar{k}_6(t_{k,n}, y_{H_{k,n}}(\alpha)), \\
\check{\zeta}_{k_7}(t_{k,n}, y_{H_{k,n}}(\alpha)) &= \underline{y}_{H_{k,n}}(\alpha) - \frac{716}{82}k_1(t_{k,n}, y_{H_{k,n}}(\alpha)) \\
&\quad - \frac{2079}{82}k_2(t_{k,n}, y_{H_{k,n}}(\alpha)) + \frac{1002}{82}k_3(t_{k,n}, y_{H_{k,n}}(\alpha)) + \frac{834}{82}k_4(t_{k,n}, y_{H_{k,n}}(\alpha)) \\
&\quad - \frac{454}{82}k_5(t_{k,n}, y_{H_{k,n}}(\alpha)) - \frac{9}{82}k_6(t_{k,n}, y_{H_{k,n}}(r)) + \frac{72}{82}k_7(t_{k,n}, y_{H_{k,n}}(\alpha)), \\
\bar{\zeta}_{k_7}(t_{k,n}, y_{H_{k,n}}(\alpha)) &= \overline{y}_{H_{k,n}}(\alpha) + \frac{716}{82}\bar{k}_1(t_{k,n}, y_{H_{k,n}}(\alpha)) \\
&\quad - \frac{2079}{82}\bar{k}_2(t_{k,n}, y_{H_{k,n}}(\alpha)) + \frac{1002}{82}\bar{k}_3(t_{k,n}, y_{H_{k,n}}(\alpha)) + \frac{834}{82}\bar{k}_4(t_{k,n}, y_{H_{k,n}}(\alpha)) \\
&\quad - \frac{454}{82}\bar{k}_5(t_{k,n}, y_{H_{k,n}}(\alpha)) - \frac{9}{82}\bar{k}_6(t_{k,n}, y_{H_{k,n}}(\alpha)) + \frac{72}{82}\bar{k}_7(t_{k,n}, y_{H_{k,n}}(\alpha)).
\end{aligned} \tag{15}$$

Next, we define

$$\begin{aligned} S_k \left[t_{k,n}, \underline{y}_{H_{k,n}}(\alpha), \overline{y}_{H_{k,n}}(\alpha) \right] &= 41\underline{k}_1 + 0\underline{k}_2 + 216\underline{k}_3 + 27\underline{k}_4 + 272\underline{k}_5 + 27\underline{k}_6 + 216\underline{k}_7 + 41\underline{k}_8, \\ T_k \left[t_{k,n}, \underline{y}_{H_{k,n}}(\alpha), \overline{y}_{H_{k,n}}(\alpha) \right] &= 41\overline{k}_1 + 0\overline{k}_2 + 216\overline{k}_3 + 27\overline{k}_4 + 272\overline{k}_5 + 27\overline{k}_6 + 216\overline{k}_7 + 41\overline{k}_8, \end{aligned} \tag{16}$$

where k_1, k_2, \dots represents the stages involved in Runge–Kutta methods. The exact solution at $t_{k,n+1}$ is given by

$$\begin{cases} \underline{Y}_{H_{k,n+1}}(\alpha) \approx \underline{y}_{H_{k,n}}(\alpha) + \frac{1}{840} S_k \left[t_{k,n}, \underline{y}_{H_{k,n}}(\alpha), \overline{y}_{H_{k,n}}(\alpha) \right], \\ \overline{Y}_{H_{k,n+1}}(\alpha) \approx \overline{y}_{H_{k,n}}(\alpha) + \frac{1}{840} T_k \left[t_{k,n}, \underline{y}_{H_{k,n}}(\alpha), \overline{y}_{H_{k,n}}(\alpha) \right]. \end{cases} \tag{17}$$

The approximate solution is given by

$$\begin{cases} \underline{y}_{H_{k,n+1}}(\alpha) \approx \underline{y}_{H_{k,n}}(\alpha) + \frac{1}{840} S_k \left[t_{k,n}, \underline{y}_{H_{k,n}}(\alpha), \overline{y}_{H_{k,n}}(\alpha) \right], \\ \overline{y}_{H_{k,n+1}}(\alpha) \approx \overline{y}_{H_{k,n}}(\alpha) + \frac{1}{840} T_k \left[t_{k,n}, \underline{y}_{H_{k,n}}(\alpha), \overline{y}_{H_{k,n}}(\alpha) \right]. \end{cases} \tag{18}$$

In the similar fashion of RK-Huta expansion, we can also expand RK–Butcher method. As it is similar, we are not providing the expansion here. These methods are fuzzified and treated for fuzzy hybrid differential equations as followed by Pederson and Sambandham in [16, 17]. Then, from theory of [18, 19], we solve a numerical example from which these two RK-6 methods can be easily understood.

3. Numerical Example

Example 1. Similar to [16], the fuzzy hybrid IVP is taken.

$$\begin{cases} \Delta y_H(t) = y_H(t) + \xi_H(t)\omega_k y_H(t_k), & t \in [t_k, t_{k+1}], t_k = k, k = 0, 1, 2, 3, \dots, \\ y_H(0; \alpha) = \left[\left(\frac{750}{1000} + \frac{250\alpha}{1000} \right), \left(\frac{1125}{1000} - \frac{125\alpha}{1000} \right) \right], & 0 \leq \alpha \leq 1, \end{cases} \tag{19}$$

where

$$\begin{aligned} \xi_H(t) &= \begin{cases} \frac{10}{5}(1 - t \pmod{1}), & \text{for } t \pmod{1} > \frac{5}{10}, \\ \frac{10}{5}(t \pmod{1}), & \text{for } t \pmod{1} \leq \frac{5}{10}, \end{cases} \\ \omega_k(u_k) &= \begin{cases} \widehat{0}, & \text{if } k = 0, \\ u_k, & \text{if } k \in \{1, 2, \dots\}. \end{cases} \end{aligned} \tag{20}$$

In (19), $y_H(t_k) + \xi_H(t_k)\omega_k(y_H(t_k))$ is continuous function of t, y and $\omega_k(y_H(t_k))$.

$$\begin{cases} \Delta y_H(t) = y_H(t) + \xi_H(t)\omega_k(y_H(t_k)), & t \in [t_k, t_{k+1}], t_k = k, \\ y_H(t_k) = y_{Ht_k}, \end{cases} \tag{21}$$

$\Delta y_H(t)$ has a continuous solution on $[t_k, t_{k+1}]$.

3.1. Numerical Solution by RK–Butcher. For numerically solving the Fuzzy Hybrid IVP (19), let $\delta: [0, \infty) \times R \times R \rightarrow R$ be given by the following equation:

$$\delta(t, y_H, \omega_k(y_H(t_k))) = y_H(t) + \xi_H(t)\omega_k(y_H(t_k)), \tag{22}$$

$$t_k = k, k = 0, 1, 2, \dots,$$

where $\omega_k: R \rightarrow R$ is given by the following equation:

$$\omega_k(y_H)(t_k) = \begin{cases} 0, & \text{if } k = 0, \\ y_H(t_k), & \text{if } k \in \{1, 2, \dots\}. \end{cases} \tag{23}$$

By example 3 of [2], (19) gives

$$y_{H1}\left(\frac{10}{10}, \alpha\right) = \left[\left(\frac{750}{1000} + \frac{250\alpha}{1000} \right) (D_{1,0})^{10}, \left(\frac{1125}{1000} - \frac{125\alpha}{1000} \right) (D_{1,0})^{10} \right]. \tag{24}$$

Now, we define

$$\begin{aligned} L_k \left[t_{k,n}, \underline{y}_{H_{k,n}}(\alpha), \overline{y}_{H_{k,n}}(\alpha) \right] &= 11\underline{k}_1 + 0\underline{k}_2 + 810\underline{k}_3 - 32\underline{k}_4 + 11\underline{k}_5, \\ M_k \left[t_{k,n}, \underline{y}_{H_{k,n}}(\alpha), \overline{y}_{H_{k,n}}(\alpha) \right] &= 11\overline{k}_1 + 0\overline{k}_2 + 810\overline{k}_3 - 32\overline{k}_4 + 11\overline{k}_5. \end{aligned} \quad (25)$$

From which, we obtain

$$\begin{aligned} \underline{y}_{H_1} \left(\frac{11}{10}; \alpha \right) &= \underline{y}_{H_1} \left(\frac{10}{10}; \alpha \right) + \frac{1}{120} L_k \left[\frac{10}{10}, \underline{y}_{H_1} \left(\frac{10}{10}; \alpha \right), \overline{y}_{H_1} \left(\frac{10}{10}; \alpha \right) \right], \\ \overline{y}_{H_1} \left(\frac{11}{10}; \alpha \right) &= \overline{y}_{H_1} \left(\frac{10}{10}; \alpha \right) + \frac{1}{120} M_k \left[\frac{10}{10}, \underline{y}_{H_1} \left(\frac{10}{10}; \alpha \right), \overline{y}_{H_1} \left(\frac{10}{10}; \alpha \right) \right]. \end{aligned} \quad (26)$$

To obtain $y_{H_1}((20/10); \alpha)$,

$$\begin{aligned} D_{1,0} &= 1 + d + d^2 + \frac{d^3}{3} + \frac{d^4}{24} + \frac{d^5}{120} + \frac{d^6}{720} - \frac{d^7}{2160}, \\ D_1 &= d^2 + \frac{d^3}{3} + \frac{d^4}{12} + \frac{d^5}{60} + \frac{d^6}{360} + \frac{d^7}{1080}, \\ D_2 &= 3d^2 + \frac{4d^3}{3} + \frac{5d^4}{12} + \frac{6d^5}{60} + \frac{7d^6}{360} + \frac{8d^7}{540} - \frac{d^8}{1080}, \\ D_3 &= 5d^2 + \frac{7d^3}{3} + \frac{3d^4}{4} + \frac{11d^5}{60} + \frac{13d^6}{360} + \frac{d^7}{216} - \frac{d^8}{540}, \\ D_4 &= 7d^2 + \frac{10d^3}{3} + \frac{13d^4}{12} + \frac{4d^5}{60} + \frac{19d^6}{360} + \frac{d^7}{135} - \frac{d^8}{360}, \\ D_5 &= 9d^2 + \frac{13d^3}{3} + \frac{17d^4}{12} + \frac{7d^5}{20} + \frac{5d^6}{72} + \frac{11d^7}{1080} - \frac{d^8}{270}, \\ D_6 &= 2d - 10d^2 - 5d^3 - \frac{5d^4}{3} - \frac{5d^5}{12} - \frac{d^6}{12} - \frac{d^7}{72} + \frac{d^8}{216}, \\ D_7 &= 2d - 12d^2 - 6d^3 - 2d^4 - \frac{d^5}{2} - \frac{d^6}{10} - \frac{d^7}{60} + \frac{d^8}{180}, \\ D_8 &= 2d - 14d^2 - 7d^3 - \frac{7d^4}{3} - \frac{7d^5}{12} - \frac{7d^6}{60} - \frac{7d^7}{360} + \frac{7d^8}{1080}, \\ D_9 &= 2d - 16d^2 - 8d^3 - \frac{8d^4}{3} - \frac{5d^5}{12} - \frac{d^6}{12} - \frac{d^7}{72} + \frac{d^8}{216}, \\ D_{10} &= 2d - 10d^2 - 5d^3 - \frac{5d^4}{3} - \frac{5d^5}{12} - \frac{d^6}{12} - \frac{d^7}{72} + \frac{d^8}{216}, \\ y_{H_1} \left(\frac{i}{10}; \alpha \right) &= \left[\left(\frac{750}{1000} + \frac{250\alpha}{1000} \right) (D_{1,0})^i, \left(\frac{1125}{1000} - \frac{125\alpha}{1000} \right) (D_{1,0})^i \right], i = 1, 2, \dots, 10, \\ y_{H_1} \left(\frac{i}{10}; \alpha \right) &= (D_{1,0})^i + (D_{1,0})^{10} (D_{i-10}), i = 11, 12, \dots, 20. \end{aligned} \quad (27)$$

3.2. Numerical Solution by RK-Huta. To numerically solve the Fuzzy Hybrid IVP (19),

$$\delta(t, y_H, \omega_r(y_H(t_k))) = y_H(t) + \xi_H(t)\omega_k(y_H(t_k)), \quad (28)$$

$$t_k = k, k = 0, 1, 2, \dots,$$

where $\omega_k: R \rightarrow R$ is given by the following equation:

$$\omega_k(u_k) = \begin{cases} 0, & \text{if } k = 0, \\ u_k, & \text{if } k \in \{1, 2, \dots\}. \end{cases} \quad (29)$$

By example 3 of [2], (19) gives

$$y_{H_1}\left(\frac{10}{10}; \alpha\right) = \left[\left(\frac{750}{1000} + \frac{250\alpha}{1000} \right) (D_{1,0})^{10}, \left(\frac{1125}{1000} - \frac{125\alpha}{1000} \right) (D_{1,0})^{10} \right], \quad (30)$$

where

$$D_{1,0} = 1 + d + \frac{d^2}{2} + \frac{d^3}{6} + \frac{d^4}{24} + \frac{d^5}{120} + \frac{d^6}{720} + \frac{d^7}{4480} + \frac{d^8}{483840},$$

$$\underline{y}_{H_1}\left(\frac{11}{10}; \alpha\right) = \underline{y}_{H_1}\left(\frac{10}{10}; \alpha\right) + \frac{1}{840} S_k \left[\frac{10}{10}; \underline{y}_{H_1}\left(\frac{10}{10}; \alpha\right), \overline{y}_{H_1}\left(\frac{10}{10}; \alpha\right) \right], \quad (31)$$

$$\overline{y}_{H_1}\left(\frac{11}{10}; \alpha\right) = \overline{y}_{H_1}\left(\frac{10}{10}; \alpha\right) + \frac{1}{840} T_K \left[\frac{10}{10}; \underline{y}_{H_1}\left(\frac{10}{10}; \alpha\right), \overline{y}_{H_1}\left(\frac{10}{10}; \alpha\right) \right].$$

To obtain $y_{H_1}\left(\frac{20}{10}; \alpha\right), i = 1, 2, 3, 4, 5$

$$\underline{y}_H\left(1 + \frac{i}{10}; \alpha\right) = \underline{y}_H\left(1 + \frac{i-1}{10}; \alpha\right) D_{1,0} + \left[(2i-1)d^2 + \frac{(3i-2)d^3}{3} + \frac{(4i-3)d^4}{12} \right. \\ \left. + \frac{(5i-4)d^5}{60} + \frac{(6i-1)d^6}{360} + \frac{(56i-47)d^7}{20160} + \frac{(108i-107)d^8}{241920} \right. \\ \left. + \frac{(5i-5)d^9}{120960} \right] \underline{y}_H\left(\frac{10}{10}; \alpha\right), \quad (32)$$

$$\overline{y}_H\left(1 + \frac{i}{10}; \alpha\right) = \overline{y}_H\left(1 + \frac{i-1}{10}; \alpha\right) D_{1,0} + \left[(2i-1)d^2 + \frac{(3i-2)d^3}{3} + \frac{(4i-3)d^4}{12} \right. \\ \left. + \frac{(5i-4)d^5}{60} + \frac{(6i-1)d^6}{360} + \frac{(56i-47)d^7}{20160} + \frac{(108i-107)d^8}{241920} \right. \\ \left. + \frac{(5i-5)d^9}{120960} \right] \overline{y}_H\left(\frac{10}{10}; \alpha\right).$$

Then, for $i = 6, 7, 8, 9, 10$,

$$\begin{aligned}
 \underline{y}_H\left(1 + \frac{i}{10}; \alpha\right) &= \underline{y}_H\left(1 + \frac{i-1}{10}; \alpha\right)D_{1,0} + \left[\frac{1}{5} - \left((2i-2)d^2 + (i-1)d^3 + \frac{(i-1)d^4}{3}\right.\right. \\
 &\quad \left.+\frac{(i-1)d^5}{12} + \frac{(i-1)d^6}{60} + \frac{(i-1)d^7}{360} + \frac{(i-1)d^8}{2240}\right. \\
 &\quad \left.+\frac{(i-1)d^9}{241920}\right] \underline{y}_H(10/10; \alpha), \\
 \bar{y}_H\left(1 + \frac{i}{10}; \alpha\right) &= \bar{y}_H\left(1 + \frac{i-1}{10}; \alpha\right)D_{1,0} + \left[\frac{1}{5} - \left((2i-2)h^2 + (i-1)h^3 + \frac{(i-1)h^4}{3}\right.\right. \\
 &\quad \left.+\frac{(i-1)h^5}{12} + \frac{(i-1)h^6}{60} + \frac{(i-1)h^7}{360} + \frac{(i-1)h^8}{2240}\right. \\
 &\quad \left.+\frac{(i-1)h^9}{241920}\right] \bar{y}_H\left(\frac{10}{10}; \alpha\right).
 \end{aligned}
 \tag{33}$$

3.3. *Exact Solution.* The analytically obtained solution of (19) for $t \in [1, 1.5]$ is

$$\begin{aligned}
 y_H(t; \alpha) &= y_H(1; \alpha)(3e^{t-1} - 2t), 0 \leq \alpha \leq 1, \\
 y_H(1.5; \alpha) &= y_H(1; \alpha)(3\sqrt{e} - 3), 0 \leq \alpha \leq 1.
 \end{aligned}
 \tag{34}$$

Then, $y_H(1.5; 1)$ is nearly approximate to 5.290221725637059, and $y_{H_1}(1.5, 1)$ is approximately nearer to 5.290221725881617.

Since the exact solution of (19) for $t \in [1.5, 2]$ is

$$y_H(t; \alpha) = y_H(1; \alpha)(2t - 2 + e^{t-1.5}(3\sqrt{e} - 4)), 0 \leq \alpha \leq 1.
 \tag{35}$$

Therefore, $y_H(2.0; \alpha) = y_H(1; \alpha)(2 + 3e - 4\sqrt{e})$.

Then, $y_H(2.0; 1)$ is nearly approximate to 9.67697567235778, and $y_{H_1}(2.0; 1)$ is nearly approximate to 9.676975672823584.

The approximate solution by RK-Huta is plotted at $t \in [0, 2], \alpha \in [0, 1]$ (see Figure 2), and the error analysis has also been shown (see Table 3). The comparison of approximately obtained solutions by sixth-order methods and exact solutions are plotted at $t = 2, \alpha \in [0, 1]$ (see Tables 4 and 5 and Figure 3).

Next, consider the following hybrid fuzzy IVP.

Example 2

$$\begin{cases} \Delta y_H(t) = y(t) + \xi(t)\omega_k y_H(t_k), & t \in [t_k, t_{k+1}], t_k = k, k = 0, 1, 2, 3, \dots, \\ y_H(0, \alpha) = [(0.75 + 0.25\alpha), (1.125 - 0.125\alpha)], & 0 \leq \alpha \leq 1, \end{cases}
 \tag{36}$$

where $\xi(t) = |\sin(\pi t)|, k = 0, 1, 2, \dots,$

$$\omega_k(u_k) = \begin{cases} 0, & \text{if } k = 0, \\ u_k, & \text{if } k \in \{1, 2, \dots\}. \end{cases}
 \tag{37}$$

Then, $y_H(t) + \xi_H(t)\omega_k(y_H(t_k))$ is continuous function of t, y and $\omega_k(y(t_k))$. Therefore, by example 6.1 of Kaleva [3], for each $k = 0, 1, 2, \dots,$ the fuzzy IVP

$$\begin{cases} \Delta y_H(t) = y_H(t) + \xi_H(t)\omega_k(y_H(t_k)), & t \in [t_k, t_{k+1}], t_k = k, \\ y(t_k) = y_{Ht_k}, \end{cases}
 \tag{38}$$

has a unique solution on $[t_k, t_{k+1}]$.

3.4. *Numerical Solution by RK-Butcher.* For numerically solving the hybrid fuzzy IVP (36), we will apply the RK-Butcher method of order six for hybrid fuzzy differential

equations with $N = 10$. To obtain $y_{H_1}(2.0, \alpha), y_{H_1}(2.0; \alpha)$ is approximated. Let $\delta: [0, \infty) \times R \times R \rightarrow R$ be given by the following equation:

$$\begin{aligned}
 \delta(t, y_H, \omega_k(y_H(t_k))) &= y_H(t) + \xi_H(t)\omega_k(y_H(t_k)), \\
 t_k &= k, k = 0, 1, 2, \dots,
 \end{aligned}
 \tag{39}$$

where $\omega_k: R \rightarrow R$ is given by the following equation:

$$\omega_k(u_k) = \begin{cases} 0, & \text{if } k = 0, \\ u_k, & \text{if } k \in \{1, 2, \dots\}. \end{cases}
 \tag{40}$$

By example 3 of [2], (36) gives

$$y_{H_1}(1.0, \alpha) = \left[(0.75 + 0.25\alpha)(D_{1,0})^{10}, (1.125 - 0.125\alpha)(D_{1,0})^{10} \right].
 \tag{41}$$

Then,

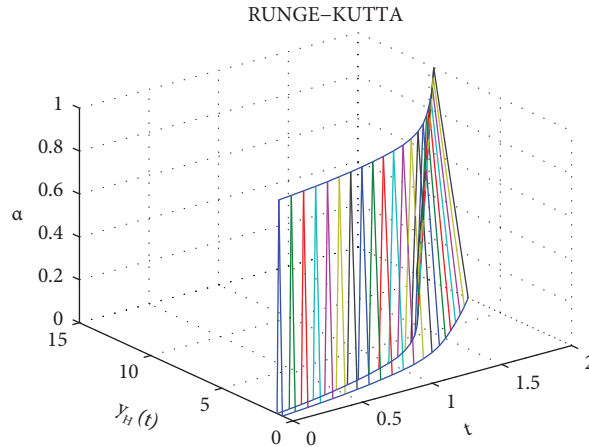


FIGURE 2: Approximate solution by sixth-order RK-Huta method (for $h=0.1$) in Example 1.

TABLE 3: Approximate solutions by RK-Butcher and RK-Huta in Example 1.

α	Sixth-order RK-Butcher method		Sixth-order RK-Huta method	
	$\underline{y}_H(t_i; \alpha)$	$\bar{y}_H(t_i; \alpha)$	$\underline{y}_H(t_i; \alpha)$	$\bar{y}_H(t_i; \alpha)$
0	7.25773174395989	10.8865976159398	7.25773175461769	10.8865976319265
0.1	7.49965613542523	10.7656354202072	7.49965614643828	10.7656354360162
0.2	7.74158052689056	10.6446732244745	7.74158053825887	10.6446732401059
0.3	7.98350491835588	10.5237110287418	7.98350493007946	10.5237110441956
0.4	8.22542930982121	10.4027488330092	8.22542932190005	10.4027488482854
0.5	8.46735370128655	10.2817866372765	8.46735371372064	10.2817866523751
0.6	8.70927809275187	10.1608244415439	8.70927810554123	10.1608244564648
0.7	8.95120248421720	10.0398622458112	8.95120249736182	10.0398622605545
0.8	9.19312687568253	9.91890005007852	9.19312688918240	9.91890006464417
0.9	9.43505126714786	9.79793785434586	9.43505128100300	9.79793786873388
1.0	9.67697565861319	9.67697565861319	9.67697567282358	9.67697567282358

TABLE 4: Exact solution in Example 1.

α	Exact solution	
	$\underline{y}_H(t_i; \alpha)$	$\bar{y}_H(t_i; \alpha)$
0	7.25773175426834	10.8865976314025
0.1	7.49965614607728	10.7656354354980
0.2	7.74158053788623	10.6446732395936
0.3	7.98350492969517	10.5237110436891
0.4	8.22542932150411	10.4027488477846
0.5	8.46735371331306	10.2817866518801
0.6	8.70927810512201	10.1608244559757
0.7	8.95120249693095	10.0398622600712
0.8	9.19312688873989	9.91890006416673
0.9	9.43505128054884	9.79793786826225
1.0	9.67697567235778	9.67697567235778

TABLE 5: Error in sixth-order RK-Butcher method and sixth-order RK-Huta method in Example 1.

α	Sixth-order RK-Butcher method		Sixth-order RK-Huta method	
	$\underline{Y}_H(t_i; \alpha)$	$\bar{Y}_H(t_i; \alpha)$	$\underline{Y}_H(t_i; \alpha)$	$\bar{Y}_H(t_i; \alpha)$
0	1.03085×10^{-8}	1.54627×10^{-8}	3.49350×10^{-10}	5.24000×10^{-10}
0.1	1.06520×10^{-8}	1.52908×10^{-8}	3.61000×10^{-10}	5.18201×10^{-10}
0.2	1.09957×10^{-8}	1.51191×10^{-8}	3.72641×10^{-10}	5.12301×10^{-10}
0.3	1.13393×10^{-8}	1.49473×10^{-8}	3.84290×10^{-10}	5.06500×10^{-10}
0.4	1.16829×10^{-8}	1.47754×10^{-8}	3.95939×10^{-10}	5.00799×10^{-10}

TABLE 5: Continued.

α	Sixth-order RK-Butcher method		Sixth-order RK-Huta method	
	$\underline{Y}_H(t_i; \alpha)$	$\overline{Y}_H(t_i; \alpha)$	$\underline{Y}_H(t_i; \alpha)$	$\overline{Y}_H(t_i; \alpha)$
0.5	1.20265×10^{-8}	1.46036×10^{-8}	4.07580×10^{-10}	4.95000×10^{-10}
0.6	1.23701×10^{-8}	1.44318×10^{-8}	4.19220×10^{-10}	4.89100×10^{-10}
0.7	1.27138×10^{-8}	1.42600×10^{-8}	4.30870×10^{-10}	4.83301×10^{-10}
0.8	1.30574×10^{-8}	1.40882×10^{-8}	4.42510×10^{-10}	4.77440×10^{-10}
0.9	1.34010×10^{-8}	1.39164×10^{-8}	4.54159×10^{-10}	4.71630×10^{-10}
1.0	1.37446×10^{-8}	1.37446×10^{-8}	4.65800×10^{-10}	4.65800×10^{-10}

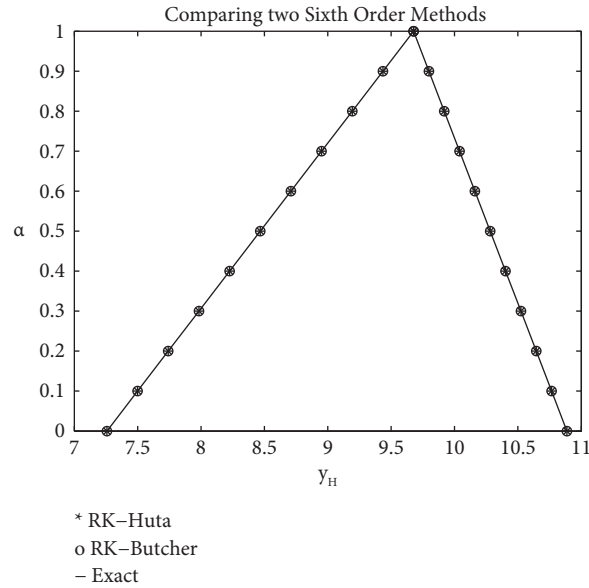


FIGURE 3: Comparison of approximate solution with exact solution (for $h = 0.1$) in Example 1.

$$\begin{aligned} \underline{y}_{H_1}(1.1; \alpha) &= \underline{y}_{H_1}(1.0; \alpha) + \frac{1}{120}L_k \left[1.0, \underline{y}_{H_1}(1.0; \alpha), \overline{y}_{H_1}(1.0; \alpha) \right], \\ \overline{y}_{H_1}(1.1; \alpha) &= \overline{y}_{H_1}(1.0; \alpha) + \frac{1}{120}M_k \left[1.0, \underline{y}_{H_1}(1.0; \alpha), \overline{y}_{H_1}(1.0; \alpha) \right]. \end{aligned} \tag{42}$$

To obtain $y_{H_1}(2.0; \alpha)$ for $h = 0.1$, let

$$\begin{aligned} y_{H_1}\left(\frac{i}{10}; \alpha\right) &= (D_{1,0}), i = 1, 2, \dots, 10 \\ y_{H_1}\left(\frac{i}{10}; \alpha\right) &= (D_{1,0})^i + (D_{1,0})^{10} \left(\sin\left(1 + \frac{h}{3}\right)\pi \right) (A_1) - \left(\sin\left(1 + \frac{h}{2}\right)\pi \right) (A_2) + \left(\sin\left(1 + \frac{2h}{3}\right)\pi \right) (A_3) + \sin(1+h)\pi (A_4) i = 11 \\ y_1\left(\frac{i}{10}; \alpha\right) &= (D_{1,0})^i + \left((D_{1,0})^{10} \right) (D_{i-10}) i = 12, 13, \dots, 20 \end{aligned} \tag{43}$$

$$\begin{aligned} D_{i-10} &= \sin\left((1 + (i-11)h)\pi \right) B_1 + \sin\left(\left(1 + \frac{((i-8+2j)h)}{3} \right) \pi \right) B_2 + \sin\left(\left(1 + \frac{((i-9+j)h)}{3} \right) \pi \right) B_3 + \\ &\sin\left(\left(1 + \frac{((i-8+2j)h)}{3} \right) \pi \right) A_3 + \sin\left((1 + (i-10)h)\pi \right) A_4 \text{ for } i = 11, 12, \dots, 20, j = i - 12, \end{aligned}$$

for $i = 11, 12, \dots, 20, j = i - 12$ where

$$\begin{aligned}
 A_1 &= \frac{27h}{40} + \frac{9h^2}{20} + \frac{3h^3}{20} + \frac{h^4}{40} + \frac{h^5}{120} + \frac{h^6}{720} \\
 A_2 &= \frac{8h}{15} + \frac{4h^2}{15} + \frac{h^3}{15} \\
 A_3 &= \frac{27h}{40} + \frac{9h^2}{40} + \frac{3h^3}{80} - \frac{h^5}{480} \\
 A_4 &= \frac{11h}{120} \\
 B_1 &= \frac{11h}{120} + \frac{11h^2}{120} + \frac{11h^3}{240} + \frac{h^4}{60} + \frac{h^5}{480} + \frac{h^6}{360} + \frac{h^7}{2160} \\
 B_2 &= \frac{27h}{40} + \frac{9h^2}{40} + \frac{3h^3}{80} + \frac{h^4}{40} + \frac{h^5}{120} - \frac{h^6}{720} \\
 B_3 &= \frac{-8h}{15} - \frac{4h^2}{15} - \frac{h^3}{15}
 \end{aligned} \tag{44}$$

3.5. *Numerical Solution by RK-Huta.* For numerically solving the hybrid fuzzy IVP (36), we will apply the RK-Huta method of order six for hybrid fuzzy differential equations with $N = 10$. To obtain $y_1(2.0; \alpha)$, $y(2.0; \alpha)$ is approximated. Let $\delta: [0, \infty) \times R \times R \rightarrow R$ be given by the following equation:

$$\begin{aligned}
 \delta(t, y_H, \omega_k(y(t_k))) &= y(t) + \xi(t)\omega_k(y(t_k)), \\
 t_k &= k, k = 0, 1, 2, \dots,
 \end{aligned} \tag{45}$$

where $\omega_k: R \rightarrow R$ is given by the following equation:

$$\omega_k(u_k) = \begin{cases} 0, & \text{if } k = 0, \\ u_k, & \text{if } k \in \{1, 2, \dots\}. \end{cases} \tag{46}$$

By example 3 of [2], (36) gives

$$y_{H_1}(1.0, \alpha) = \left[(0.75 + 0.25\alpha)(D_{1,0})^{10}, (1.125 - 0.125\alpha)(D_{1,0})^{10} \right], \tag{47}$$

where

$$D_{1,0} = 1 + h + \frac{h^2}{2} + \frac{h^3}{6} + \frac{h^4}{24} + \frac{h^5}{120} + \frac{h^6}{720} + \frac{h^7}{4480} + \frac{h^8}{483840},$$

$$\underline{y}_{H_1}(1.1; \alpha) = \underline{y}_1(1.0; \alpha) + \frac{1}{840} S_k \left[1.0, \underline{y}_1(1.0; \alpha), \overline{y}_{H_1}(1.0; \alpha) \right], \tag{48}$$

$$\overline{y}_1(1.1; \alpha) = \overline{y}_1(1.0; \alpha) + \frac{1}{840} T_k \left[1.0; \underline{y}_1(1.0; \alpha), \overline{y}_1(1.0; \alpha) \right].$$

To obtain $y_1(2.0; \alpha)$ for $h = 0.1$, let

$$\begin{aligned}
 D_1 &= 23616h + 23616h^2 + 5328h^3 + 7920h^4 + 1872h^5 - 264h^6 + 99h^7 + h^8, \\
 D_2 &= -5292h^5 + 864h^6 + 99h^7, \\
 D_3 &= 124416h + 103680h^2 + 67392h^3 + 432h^4 + 7344h^5 + 72h^6, \\
 D_4 &= 15552h + 103680h^2 - 28512h^3 + 11664h^4 + 108h^5, \\
 D_5 &= 156672h + 78336h^2 + 35136h^3 + 144h^4, \\
 D_6 &= 15552h + 5184h^2 + 1296h^3, \\
 D_7 &= 124416h + 20736h^2, \\
 D_8 &= 23616h,
 \end{aligned} \tag{49}$$

$$\begin{aligned}
 \underline{y}(1.1; \alpha) &= \underline{y}(1.0; \alpha)(D_{1,0}) + \frac{1}{483840} \left[D_2 \sin \frac{\pi}{90} + D_3 \sin \frac{\pi}{60} + D_4 \sin \frac{\pi}{30} \right. \\
 &\quad \left. + D_5 \sin \frac{\pi}{20} + D_6 \sin \frac{2\pi}{30} + D_7 \sin \frac{5\pi}{60} + D_8 \sin \frac{\pi}{10} \right] \underline{y}(1.0; \alpha),
 \end{aligned}$$

$$\begin{aligned}
 \overline{y}(1.1; \alpha) &= \overline{y}(1.0; \alpha)(D_{1,0}) + \frac{1}{483840} \left[D_2 \sin \frac{\pi}{90} + D_3 \sin \frac{\pi}{60} + D_4 \sin \frac{\pi}{30} \right. \\
 &\quad \left. + D_5 \sin \frac{\pi}{20} + D_6 \sin \frac{2\pi}{30} + D_7 \sin \frac{5\pi}{60} + D_8 \sin \frac{\pi}{10} \right] \overline{y}(1.0; \alpha).
 \end{aligned}$$

Then, for $i = 1, 2, 3, \dots, 10$,

$$\begin{aligned} \underline{y}\left(1 + \frac{i}{10}; \alpha\right) &= \underline{y}\left(1 + \frac{i-1}{10}; \alpha\right)(D_{1,0}) + \frac{1}{483840} \left[D_1 \sin \frac{(i-1)\pi}{10} + D_2 \sin \frac{(9i-8)\pi}{90} \right. \\ &\quad + D_3 \sin \frac{(6i-5)\pi}{60} + D_4 \sin \frac{(3i-2)\pi}{30} + D_5 \sin \frac{(2i-1)\pi}{20} \\ &\quad \left. + D_6 \sin \frac{(3i-1)\pi}{30} + D_7 \sin \frac{(6i-1)\pi}{60} + D_8 \sin \frac{(i)\pi}{10} \right] \underline{y}(1.0; \alpha), \\ \bar{y}\left(1 + \frac{i}{10}; \alpha\right) &= \bar{y}\left(1 + \frac{i-1}{10}; \alpha\right)(D_{1,0}) + \frac{1}{483840} \left[D_1 \sin \frac{(i-1)\pi}{10} + D_2 \sin \frac{(9i-8)\pi}{90} \right. \\ &\quad + D_3 \sin \frac{(6i-5)\pi}{60} + D_4 \sin \frac{(3i-2)\pi}{30} + D_5 \sin \frac{(2i-1)\pi}{20} \\ &\quad \left. + D_6 \sin \frac{(3i-1)\pi}{30} + D_7 \sin \frac{(6i-1)\pi}{60} + D_8 \sin \frac{(i)\pi}{10} \right] \bar{y}(1.0; \alpha). \end{aligned} \tag{50}$$

Let

$$\begin{aligned} D_{2,0} &= (D_{1,0})^{10} + \sum_{k=1}^{10} (D_{1,0})^{10-k} \frac{1}{483840} \left[D_1 \sin \frac{(k-1)\pi}{10} + D_2 \sin \frac{(9k-8)\pi}{90} \right. \\ &\quad + D_3 \sin \frac{(6k-5)\pi}{60} + D_4 \sin \frac{(3k-2)\pi}{30} + D_5 \sin \frac{(2k-1)\pi}{20} \\ &\quad \left. + D_6 \sin \frac{(3k-1)\pi}{30} + D_7 \sin \frac{(6k-1)\pi}{60} + D_8 \sin \frac{(k)\pi}{10} \right]. \end{aligned} \tag{51}$$

Then,

$$\begin{aligned} \mathcal{Y}_{2,0;\alpha} &= D_{2,0} \mathcal{Y}_1(1.0; \alpha) \\ &= \left[D_{2,0} (0.75 + 0.25\alpha)(D_{1,0})^{10}, D_{2,0} (1.125 - 0.125\alpha)(D_{1,0})^{10} \right], 0 \leq \alpha \leq 1, \end{aligned} \tag{52}$$

for $t \in [1, 2]$.

3.6. *Exact Solution.* The exact solution of (36) satisfies

$$\begin{aligned} \underline{y}_H(t; \alpha) &= \underline{y}_H(1; \alpha) \left[\frac{\pi \cos(\pi t) + \sin(\pi t)}{\pi^2 + 1} + e^{t-1} \left(1 + \frac{\pi}{\pi^2 + 1} \right) \right], \\ \bar{y}_H(t; \alpha) &= \bar{y}_H(1; \alpha) \left[\frac{\pi \cos(\pi t) + \sin(\pi t)}{\pi^2 + 1} + e^{t-1} \left(1 + \frac{\pi}{\pi^2 + 1} \right) \right]. \end{aligned} \tag{53}$$

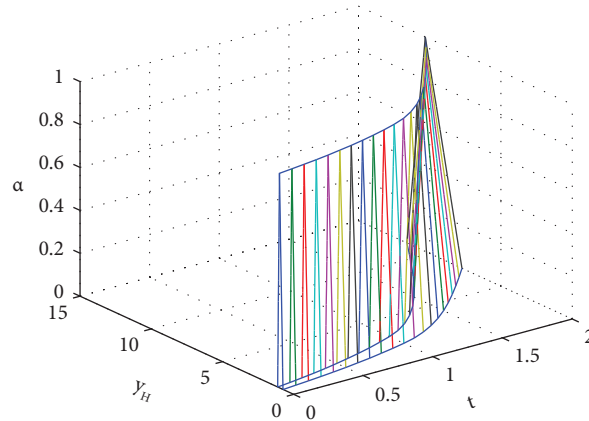


FIGURE 4: Approximate solution by sixth-order RK-Huta method (for $h=0.1$) in Example 2.

TABLE 6: Approximate solutions by RK-Butcher and RK-Huta in Example 2.

α	Sixth-order RK-Butcher method		Sixth-order RK-Huta method	
	$\underline{y}_H(t_i; \alpha)$	$\bar{y}_H(t_i; \alpha)$	$\underline{y}_H(t_i; \alpha)$	$\bar{y}_H(t_i; \alpha)$
0	7.73275073110805	11.5991260966621	7.73275073776977	11.5991261066547
0.1	7.99050908881165	11.4702469178103	7.99050909569543	11.4702469276918
0.2	8.24826744651526	11.3413677389585	8.24826745362109	11.3413677487290
0.3	8.50602580421886	11.2124885601067	8.50602581154675	11.2124885697662
0.4	8.76378416192246	11.0836093812549	8.76378416947241	11.0836093908033
0.5	9.02154251962606	10.9547302024031	9.02154252739807	10.9547302118405
0.6	9.27930087732966	10.8258510235513	9.27930088532373	10.8258510328777
0.7	9.53705923503326	10.6969718446995	9.53705924324938	10.6969718539149
0.8	9.79481759273686	10.5680926658477	9.79481760117504	10.5680926749520
0.9	10.0525759504405	10.4392134869959	10.0525759591007	10.4392134959892
1.0	10.3103343081441	10.3103343081441	10.3103343170264	10.3103343170264

TABLE 7: Exact solution in Example 2.

α	Exact solution	
	$\underline{Y}_H(t_i; \alpha)$	$\bar{Y}_h(t_i; \alpha)$
0	7.73275073803317	11.5991261070497
0.1	7.99050909596760	11.4702469280825
0.2	8.24826745390204	11.3413677491153
0.3	8.50602581183648	11.2124885701481
0.4	8.76378416977092	11.0836093911809
0.5	9.02154252770536	10.9547302122137
0.6	9.27930088563980	10.8258510332464
0.7	9.53705924357424	10.6969718542792
0.8	9.79481760150867	10.5680926753120
0.9	10.0525759594431	10.4392134963448
1.0	10.3103343173776	10.3103343173776

TABLE 8: Error in sixth-order RK-Butcher method and sixth-order RK-Huta method in Example 2.

α	Sixth-order RK-Butcher method		Sixth-order RK-Huta method	
	$\underline{Y}_H(t_i; \alpha)$	$\bar{Y}_H(t_i; \alpha)$	$\underline{Y}_H(t_i; \alpha)$	$\bar{Y}_h(t_i; \alpha)$
0	6.92512×10^{-9}	1.03876×10^{-8}	2.63400×10^{-10}	3.95001×10^{-10}
0.1	7.15595×10^{-9}	1.02722×10^{-8}	2.72171×10^{-10}	3.90699×10^{-10}
0.2	7.38678×10^{-9}	1.01568×10^{-8}	2.80950×10^{-10}	3.86299×10^{-10}
0.3	7.61762×10^{-9}	1.00414×10^{-8}	2.89729×10^{-10}	3.81910×10^{-10}

TABLE 8: Continued.

α	Sixth-order RK-Butcher method		Sixth-order RK-Huta method	
	$\underline{Y}_H(t_i; \alpha)$	$\bar{Y}_H(t_i; \alpha)$	$\underline{Y}_H(t_i; \alpha)$	$\bar{Y}_h(t_i; \alpha)$
0.4	7.84846×10^{-9}	9.92600×10^{-9}	2.98510×10^{-10}	3.77600×10^{-10}
0.5	8.07930×10^{-9}	9.81060×10^{-9}	3.07290×10^{-10}	3.73200×10^{-10}
0.6	8.31014×10^{-9}	9.69510×10^{-9}	3.16071×10^{-10}	3.68699×10^{-10}
0.7	8.54098×10^{-9}	9.57970×10^{-9}	3.24858×10^{-10}	3.64300×10^{-10}
0.8	8.77181×10^{-9}	9.46430×10^{-9}	3.33630×10^{-10}	3.60000×10^{-10}
0.9	9.00260×10^{-9}	9.34890×10^{-9}	3.42400×10^{-10}	3.55600×10^{-10}
1.0	9.23350×10^{-9}	9.23350×10^{-9}	3.51200×10^{-10}	3.51200×10^{-10}

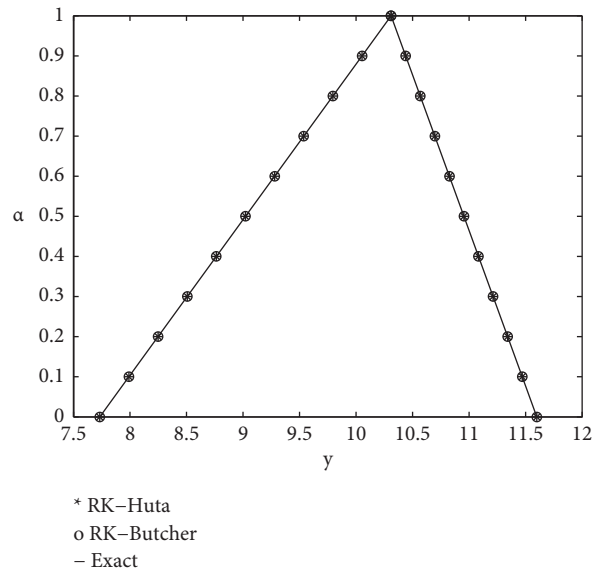


FIGURE 5: Comparison of approximate solution with exact solution (for $h = 0.1$) in Example 2.

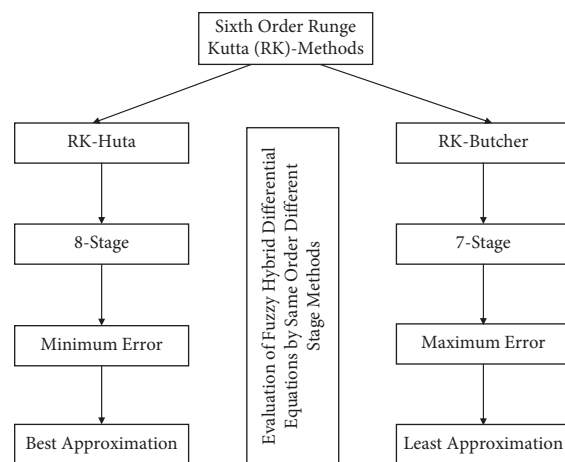


FIGURE 6: Flowchart of Conclusion: maximum stage maximum accuracy.

Therefore,

$$y(1; \alpha) = [(0.75 + 0.25\alpha)e, (1.125 - 0.125\alpha)e],$$

$$y(2; \alpha) = \left(\frac{\pi}{\pi^2 + 1} + e \left(1 + \frac{\pi}{\pi^2 + 1} \right) \right) y(1; \alpha). \quad (54)$$

Then, $y(2.0; 1)$ is nearly approximate to 10.310334317377553, whereas $y_1(2.0; 1)$ is nearly approximate to 10.310334317026362. The approximate solution by RK-Huta is plotted at $t \in [0, 2]$, $\alpha \in [0, 1]$ (see Figure 4), and the error analysis has also been shown (see Table 6). The comparison of approximately obtained solutions by sixth order methods and exact solutions are plotted at $t = 2$, $\alpha \in [0, 1]$ (see Tables 7 and 8 and Figure 5).

4. Conclusion

We can show our conclusion simply via the flow chart in Figure 6.

For clarifying the readers about convergence of numerical results, we stated the theorem by means of consistency. We solved famous-two problems of fuzzy hybrid systems and found numerical solution by sixth order eight stage RK-Huta method and sixth order seven stage RK-Butcher method and generalized them for both the problems by which the future readers can extend the numerical solution to next stage even without solving the problem. Comparison of solutions shows that sixth order RK-Huta method gives better results than sixth order RK-Butcher method for solving any fuzzy hybrid differential equations by the application of error analysis study (see Tables 3 and Table 6). As a part of our study, we are also arriving at the following results:

- (1) When comparing two numerical methods of different order, the higher order will give better accuracy. For example, fourth order Runge-Kutta method will give better accuracy of approximation than Euler method.
- (2) When comparing two numerical methods of same order, the higher stage will give better accuracy. The result was obtained by our research in this paper as we had shown sixth order 8 stage method (RK-Huta method) gives better accuracy than sixth order 7 stage method (RK-Butcher method) in numerical solutions.
- (3) Previously many authors did their work on fuzzy hybrid systems found big errors in accuracy [16–21]. These errors are highly reduced by the above-given two sixth-order methods.
- (4) As far as the numerical solution is concerned, these two methods are better than any other existing numerical methods, in fact RK-Huta of order 6-stage 8 is still best from our study but the thing may change when compare them with approximate analytical methods which will be our future work.

Data Availability

Data sharing is not applicable to this article as no data sets were generated or analyzed during the current study.

Conflicts of Interest

The authors declare that they have no conflicts of interest.

Authors' Contributions

All authors contributed equally and significantly in writing this paper and typed, read, and approved the final manuscript.

References

- [1] L. A. Zadeh, "Fuzzy sets," *Information and Control*, vol. 8, no. 3, pp. 338–353, 1965.
- [2] M. Ma, M. Friedman, and A. Kandel, "Numerical solutions of fuzzy differential equations," *Fuzzy Sets and Systems*, vol. 105, no. 1, pp. 133–138, 1999.
- [3] O. Kaleva, "Fuzzy differential equations," *Fuzzy Sets and Systems*, vol. 24, no. 3, pp. 301–317, 1987.
- [4] R. Goetschel and W. Voxman, "Elementary fuzzy calculus," *Fuzzy Sets and Systems*, vol. 18, no. 1, pp. 31–43, 1986.
- [5] A. Kandel, "Fuzzy dynamical systems and the nature of their solutions," in *Fuzzy Sets: Theory and Application to Policy Analysis and Information Systems*, P. P. Wang and S. K. Chang, Eds., pp. 93–122, Plenum Press, New York, NY, USA, 1980.
- [6] D. Prasantha Bharathi, T. Jayakumar, and S. Vinoth, "Numerical solutions of fuzzy multiple hybrid single neutral delay differential equations," *International Journal of Scientific & Technology Research*, vol. 8, no. 9, pp. 520–523, 2019.
- [7] V. Lakshmikantham and X. Z. Liu, "Impulsive hybrid systems and stability theory," *International Journal of Nonlinear Differential Equations*, vol. 5, pp. 9–17, 1999.
- [8] V. Lakshmikantham and R. N. Mohapatra, *Theory of Fuzzy Differential Equations and Inclusions*, Taylor & Francis, Oxfordshire, UK, 2003.
- [9] M. Paripour, E. Hajilou, A. Hajilou, and H. Heidari, "Application of Adomian decomposition method to solve hybrid fuzzy differential equations," *Journal of Taibah University for Science*, vol. 9, no. 1, pp. 95–103, 2015.
- [10] P. B. Dhandapani, D. Baleanu, J. Thippan, and V. Sivakumar, "Fuzzy type RK4 solutions to fuzzy hybrid retarded delay differential equations," *Frontiers in Physics*, vol. 7, no. 168, pp. 1–6, 2019.
- [11] S. Pederson and M. Sambandham, "Numerical solution of hybrid fuzzy differential equation IVPs by a characterization theorem," *Information Sciences*, vol. 179, no. 3, pp. 319–328, 2009.
- [12] D. P. Bharathi, T. Jayakumar, and S. Vinoth, "Numerical solution of hybrid fuzzy mixed delay differential equation by fourth order Runge-Kutta method," *The interdisciplinary journal of Discontinuity, Nonlinearity, and Complexity*, vol. 10, no. 1, pp. 77–86, 2021.
- [13] P. Prakash and V. Kalaiselvi, "Numerical solution of hybrid fuzzy differential equations by predictor-corrector method," *International Journal of Computer Mathematics*, vol. 86, no. 1, pp. 121–134, 2009.
- [14] D. P. Bharathi, T. Jayakumar, T. Muthukumar, and S. Vinoth, "Existence and uniqueness of solutions for fuzzy mixed type of delay differential equations," *Journal of Applied Nonlinear Dynamics*, vol. 10, no. 1, pp. 187–196, 2021.
- [15] P. B. Dhandapani, J. Thippan, C. Martin-Barreiro, V. Leiva, and C. Chesneau, "Numerical solutions of a differential system considering a pure hybrid fuzzy neutral delay theory," *Electronics*, vol. 11, no. 9, p. 1478, 2022.

- [16] S. Pederson and M. Sambandham, "Numerical solution to hybrid fuzzy systems," *Mathematical and Computer Modelling*, vol. 45, pp. 1133–1144, 2007.
- [17] S. Pederson and M. Sambandham, "The Runge-Kutta method for hybrid fuzzy differential equations," *Nonlinear Analysis Hybrid Systems*, vol. 2, pp. 626–634, 2008.
- [18] T. Jayakumar and K. Kanagarajan, "Numerical solution for hybrid fuzzy system by Runge-Kutta method of order five," *International Journal of Applied Mathematical Sciences*, vol. 6, pp. 3591–3606, 2012.
- [19] T. Jayakumar and K. Kanagarajan, "Numerical solution for hybrid fuzzy system by Runge-Kutta Fehlberg method," *International Journal of Mathematical Analysis*, vol. 6, pp. 2619–2632, 2012.
- [20] A. Ahmadian, S. Salahshour, and C. S. Chan, "A Runge-Kutta method with reduced number of function evaluations to solve hybrid fuzzy differential equations," *Soft Computing*, vol. 19, no. 4, pp. 1051–1062, 2015.
- [21] T. Allahviranloo and S. Salahshour, "Euler method for solving hybrid fuzzy differential equation," *Soft Computing*, vol. 15, no. 7, pp. 1247–1253, 2011.
- [22] F. Saberiad, S. M. Karbassi, M. Heydari, and S. M. M. Hosseini, "Application of homotopy perturbation method for solving hybrid fuzzy differential equations," *Journal of Mathematical Extension*, vol. 12, no. 1, pp. 113–145, 2018.
- [23] S. Seikkala, "On the fuzzy initial value problem," *Fuzzy Sets and Systems*, vol. 24, no. 3, pp. 319–330, 1987.
- [24] A. Sepahvandzadeh and B. Ghazanfari, "Variational iteration method for solving hybrid fuzzy differential equations," *Journal of Mathematical Extension*, vol. 10, no. 4, pp. 75–85, 2016.
- [25] M. K. Jain, *Numerical Solution of Differential Equations*, Wiley Eastern, Hoboken, NJ, USA, 1984.

Research Article

Convergence Analysis of Two Parallel Methods for Common Variational Inclusion Problems Involving Demicontractive Mappings

Thanasak Mouktonglang,^{1,2} Kanyuta Pochinapan,^{1,2} Pariwate Varnakovida,^{3,4} Raweerote Suparatulorn ⁵ and Sompop Moonchai^{1,2}

¹Advanced Research Center for Computational Simulation, Chiang Mai University, Chiang Mai 50200, Thailand

²Department of Mathematics, Faculty of Science, Chiang Mai University, Chiang Mai 50200, Thailand

³KMUTT Geospatial Engineering and Innovation Center, Faculty of Science, King Mongkut's University of Technology Thonburi, Thung Khru, Bangkok 10140, Thailand

⁴Department of Mathematics, Faculty of Science, King Mongkut's University of Technology Thonburi, Thung Khru, Bangkok 10140, Thailand

⁵Elementary Education Program, Faculty of Education, Suan Dusit University Lampang Center, Lampang 52100, Thailand

Correspondence should be addressed to Raweerote Suparatulorn; raweerote.s@gmail.com

Received 22 September 2022; Revised 16 January 2023; Accepted 6 April 2023; Published 30 May 2023

Academic Editor: Mohammad W. Alomari

Copyright © 2023 Thanasak Mouktonglang et al. This is an open access article distributed under the Creative Commons Attribution License, which permits unrestricted use, distribution, and reproduction in any medium, provided the original work is properly cited.

The main objective of this article is to propose two novel parallel methods for solving common variational inclusion and common fixed point problems in a real Hilbert space. Strong convergence theorems of both methods are established by allowing for some mild conditions. Moreover, numerical studies of the signal recovery problem consisting of various blurred filters demonstrate the computational behavior of the proposed methods and other existing methods.

1. Introduction

Throughout this article, a real Hilbert space is denoted by \mathcal{H} with inner product $\langle \cdot, \cdot \rangle$ and associated norm $\|\cdot\|$. It is defined that $[K] := \{1, 2, \dots, K\}$ is the index set for any positive integer K . Let \mathbb{R} and \mathbb{N} be the sets of real numbers and nonnegative integers, respectively. The problem of identifying a point $v \in \mathcal{H}$ such that

$$0 \in (F_i + G_i)v, \quad (1)$$

is called the common variational inclusion problem (CVIP), where $F_i: \mathcal{H} \rightarrow \mathcal{H}$ is a single valued mapping and $G_i: \mathcal{H} \rightarrow 2^{\mathcal{H}}$ is a multivalued mapping for all $i \in [K]$. If $[K] = \{1\}$, then the CVIP (1) becomes the variational inclusion problem (VIP). The VIP is widely acknowledged as a fundamental aspect of nonlinear analysis, and it plays a pivotal role in numerous mathematical models, such as

composite minimization problems, variational inequality problems, split feasibility problems, and convex programming. Its broad range of applications extends to various areas, including machine learning, signal and image recovery, and beyond (see [1–7]). To solve the VIP, several splitting algorithms have been created and refined; one of the most prominent splitting algorithms is the forward-backward splitting method (see [8, 9] for more information). Chen and Rockafellar [10] used this method in 1997 to obtain a weak convergence result. Later, Tseng [11] created a modification of the forward-backward splitting method, known as the forward-backward-forward method or Tseng's method. This approach makes use of an adaptive line-search rule and relaxes the assumptions of [10] in order to prove weak convergence. In 1964, Polyak [12] introduced the inertial extrapolation technique as a means to expedite the convergence of iterative algorithms, commonly known

as the heavy ball method. This powerful optimization algorithm has since demonstrated its efficacy in accelerating the rate of convergence of the classical gradient descent method and found applications in various fields, such as machine learning, computer vision, and control theory. Padcharoen et al. [13] recently presented a splitting method for solving the VIP in \mathcal{H} , which was developed from Tseng's method with the inertial extrapolation technique. Weak convergence of this method was established under usual assumptions. This method also solved the problems of image deblurring and image recovery. Some recent results for the VIP and related problems are stated in the studies of [14–25]. In order to solve the VIP when both the operators are multivalued maximal monotone mappings, two of the most often used splitting algorithms include the Peaceman–Rachford splitting algorithm [26] and the Douglas–Rachford splitting algorithm [27]. These splitting algorithms have been extensively studied, see [28–30].

In many practical situations, it is necessary to identify a solution that satisfies multiple constraints. Such constraints can be expressed in terms of a nonlinear functional model. In this paper, our focus is on the investigation of common variational inclusion and common fixed point problems. The motivation for this study arises from their potential utility in addressing real-world challenges, such as signal and image recovery problems, wherein a diverse set of blur filters may be present, see [31, 32]. Furthermore, in Section 4, we demonstrate the applicability of our proposed method in solving signal recovery problems using a variety of blurred filters. This problem consists of finding a point $\bar{x} \in \mathcal{H}$ such that

$$0 \in (F_i + G_i)\bar{x} \text{ and } \bar{x} = S_i\bar{x}, \quad (2)$$

where $G_i: \mathcal{H} \rightarrow 2^{\mathcal{H}}$ is a multivalued mapping and F_i, S_i are single valued mappings on \mathcal{H} for all $i \in [K]$. Suantai et al. [31] proposed a parallel algorithm based on the shrinking projection method of a finite family of G -nonexpansive mappings in \mathcal{H} with directed graphs to identify a common fixed point. This approach has been applied to solve signal recovery problems in scenarios where the noise type is unknown. Similarly, Suparatulatorn and Chaichana [32] investigated the problem of image recovery using CVIP (1) as the mathematical model, specifically for multiple blurred filters. Chang et al. [33] introduced an algorithm based on the viscosity approximating scheme to obtain strong convergence for solving CVIP in a uniformly convex and q -uniformly smooth Banach space. In a recent study, Mouktonglang et al. [34] proposed a parallel algorithm that utilizes the inertial Mann iteration process to demonstrate a weak convergence result for solving problem (2) subject to certain control conditions in \mathcal{H} . Numerous intriguing findings have been reported in the literature concerning problem (2) and related problems. For further details, see [35–39].

Motivated by these results, we develop two parallel algorithms based on Tseng's method, the viscosity approximating scheme, and the inertial extrapolation technique for solving the problem (2) in \mathcal{H} . Strong convergence results of

the proposed methods are provided under standard and mild conditions. As applications, we apply our algorithms in order to solve the signal recovery problem using a variety of blurred filters.

2. Preliminaries

We refer to \rightharpoonup and \longrightarrow , respectively, as weak and strong convergence. We then gather the definitions and lemmas required to support our key results. Let C be a nonempty, closed, and convex subset of a real Hilbert space \mathcal{H} . The metric projection P_C from \mathcal{H} onto C is defined by the following equation:

$$P_C z := \arg \min_{w \in C} \|z - w\|, \quad (3)$$

for all $z \in \mathcal{H}$. From this definition, it follows that

$$\langle z - P_C z, w - P_C z \rangle \leq 0, \quad (4)$$

for any $z \in \mathcal{H}$ and $w \in C$. It is important to mention that the following equalities and inequality hold true in inner product spaces. Assume $z, w \in \mathcal{H}$,

$$\|z + w\|^2 = \|z\|^2 + 2\langle z, w \rangle + \|w\|^2, \quad (5)$$

$$\|z + w\|^2 \leq \|z\|^2 + 2\langle w, z + w \rangle, \quad (6)$$

$$\|az + (1 - a)w\|^2 = a\|z\|^2 + (1 - a)\|w\|^2 - a(1 - a)\|z - w\|^2, \quad (7)$$

for any $a \in \mathbb{R}$. Assume that $G: \mathcal{H} \rightarrow 2^{\mathcal{H}}$ is a multivalued mapping and $S: \mathcal{H} \rightarrow \mathcal{H}$ is a self-mapping.

Definition 1. S is considered to be

- (i) \mathcal{L} -Lipschitz continuous if there is $\mathcal{L} > 0$ such that for all $z, w \in \mathcal{H}$,

$$\|Sz - Sw\| \leq \mathcal{L}\|z - w\|. \quad (8)$$

- (ii) nonexpansive if S is 1-Lipschitz continuous,
- (iii) μ -demicontractive [40, 41] if $\text{Fix}(S) \neq \emptyset$ and there is $\mu \in (0, 1)$ such that for all $p \in \text{Fix}(S)$ and all $z \in \mathcal{H}$,

$$\|Sz - p\|^2 \leq \|z - p\|^2 + \mu\|z - Sz\|^2. \quad (9)$$

Definition 2. G is considered to be

- (i) monotone if for all $(x, z), (y, w) \in \text{graph}(G)$ (the graph of mapping G), $\langle z - w, x - y \rangle \geq 0$,
- (ii) maximal monotone if for every $(x, z) \in \mathcal{H} \times \mathcal{H}$, $\langle z - w, x - y \rangle \geq 0$ for all $(y, w) \in \text{graph}(G)$ if and only if $(x, z) \in \text{graph}(G)$.

Definition 3 (See [42]). Suppose that $\text{Fix}(S) \neq \emptyset$. Then, $I - S$ is considered to be demiclosed at zero if for any $\{v_k\} \subset \mathcal{H}$, the following statement is valid:

$$(I - S)v_k \longrightarrow 0 \text{ and } v_k \rightharpoonup \bar{v} \implies \bar{v} \in \text{Fix}(S). \quad (10)$$

Lemma 4 (See [43]). $S + G$ is maximal monotone mapping, where S is a Lipschitz continuous and monotone mapping, and G is a maximal monotone mapping.

Lemma 5 (See [44]). Let G be a maximal monotone mapping. If $T_\gamma := (I + \gamma G)^{-1}(I - \gamma S)$ and $\gamma > 0$, then $\text{Fix}(T_\gamma) = (S + G)^{-1}(0)$.

Lemma 6 (See [45]). Suppose that S is a μ -demictractive mapping with $\text{Fix}(S) \neq \emptyset$ and let $S_\alpha = \alpha I + (1 - \alpha)S$, where $\alpha \in (\mu, 1)$. Then $\|S_\alpha z - p\|^2 \leq \|z - p\|^2 - (1 - \alpha)(\alpha - \mu)\|Sz - z\|^2$ for all $p \in \text{Fix}(S)$ and all $z \in \mathcal{H}$.

Lemma 7 (See [46]). Let $\{b_k\}$ denote a sequence of real numbers such that $\limsup_{k \rightarrow \infty} b_k \leq 0$, and let $\{a_k\}$ and $\{c_k\}$ be nonnegative sequences of real numbers such that $\sum_{k=1}^{\infty} c_k < \infty$. If for any $k \in \mathbb{N}$ such that

$$a_{k+1} \leq (1 - \gamma_k)a_k + \gamma_k b_k + c_k, \quad (11)$$

where $\{\gamma_k\}$ is a sequence in $(0, 1)$ such that $\sum_{k=1}^{\infty} \gamma_k = \infty$, then $\lim_{k \rightarrow \infty} a_k = 0$.

Lemma 8. (See [47]) Let $\{\Gamma_k\}$ denote a sequence of real numbers such that there exists a subsequence $\{\Gamma_{k_q}\}_{q \in \mathbb{N}}$ of $\{\Gamma_k\}$ satisfying $\Gamma_{k_q} < \Gamma_{k_q+1}$ for all $q \in \mathbb{N}$. Suppose $\{\psi(k)\}_{k \geq k^*}$ is a sequence of integers defined by

$$\psi(k) := \max\{n \leq k: \Gamma_n < \Gamma_{n+1}\}. \quad (12)$$

Then, $\{\psi(k)\}_{k \geq k^*}$ is a nondecreasing sequence such that $\lim_{k \rightarrow \infty} \psi(k) = \infty$, and for all $k \geq k^*$, we have that $\Gamma_{\psi(k)} \leq \Gamma_{\psi(k)+1}$ and $\Gamma_k \leq \Gamma_{\psi(k)+1}$.

3. Convergence Analysis

This section aims at presenting Algorithms 1 and 2 for coping with the problem (2). Let us begin by introducing some assumptions that will be required for the ensuing convergence analysis, for all $i \in [K]$.

Assumption 9. $F_i: \mathcal{H} \rightarrow \mathcal{H}$ is \mathcal{L}_i -Lipschitz continuous and monotone mapping.

Assumption 10. $G_i: \mathcal{H} \rightarrow 2^{\mathcal{H}}$ is maximal monotone mapping.

Assumption 11. $S_i: \mathcal{H} \rightarrow \mathcal{H}$ is μ_i -demictractive mapping and $\phi: \mathcal{H} \rightarrow \mathbb{R}$ is a differentiable function.

Assumption 12. $\Psi := \cap_{i \in [K]} (F_i + G_i)^{-1}(0) \cap \cap_{i \in [K]} \text{Fix}(S_i)$ is nonempty.

Assumption 13. $\{\theta_k\} \subset (0, 1)$, $\{\xi_k\} \subset (0, \infty)$ and $\{\alpha_k^i\} \subset (\mu_i, \bar{\alpha}_i) \subset (0, 1)$, for some $\bar{\alpha}_i > 0$.

Assumption 14. $\{\tau_k^i\} \subset [\tau_i, \bar{\tau}_i] \subset (0, 1/\mathcal{L}_i)$, for some $\tau_i, \bar{\tau}_i > 0$.

Assumption 15. $I - S_i$ is demiclosed at zero.

Assumption 16. $\lim_{k \rightarrow \infty} \theta_k = \lim_{k \rightarrow \infty} \xi_k/\theta_k \|v_k - v_{k-1}\| = 0$, $\sum_{k=1}^{\infty} \theta_k = \infty$ and $\Phi := \nabla \phi$ is contraction with constant $\rho \in (0, 1)$, where $\{v_k\}$ is defined in Algorithms 1 and 2.

Lemma 17. Let $S_i: \mathcal{H} \rightarrow \mathcal{H}$ be a mapping and $F_i: \mathcal{H} \rightarrow \mathcal{H}$ be a \mathcal{L}_i -Lipschitz continuous mapping for all $i \in [K]$. If Assumption 10 holds, $\tau_k^i > 0$ and $\rho_k = h_k^i = S_i j_k^i$ for all $i \in [K]$ in Algorithms 1, then $\rho_k \in \Psi$.

Proof. From $\rho_k = h_k^i$, we have that, for all $i \in [K]$,

$$\rho_k = (I + \tau_k^i G_i)^{-1} (I - \tau_k^i F_i) \rho_k. \quad (13)$$

Using Lemma 5, we get that $\rho_k \in \cap_{i \in [K]} (F_i + G_i)^{-1}(0)$. Because of the Lipschitz condition of F_i , it is evident that, for all $i \in [K]$,

$$\|h_k^i - j_k^i\| \leq \tau_k^i \mathcal{L}_i \|\rho_k - h_k^i\|. \quad (14)$$

Since $\tau_k^i \mathcal{L}_i > 0$ and $\rho_k = h_k^i$, it follows that $h_k^i = j_k^i$ and so $\rho_k = h_k^i = j_k^i = S_i j_k^i$ for all $i \in [K]$. That is, $\rho_k \in \cap_{i \in [K]} \text{Fix}(S_i)$. Therefore, $\rho_k \in \Psi$. \square

Lemma 18. Assume that Assumptions 9–14 are satisfied. Then, we have

$$\|u_k^i - v\|^2 + (1 - \alpha_k^i)(\alpha_k^i - \mu_i) \|S_i j_k^i - j_k^i\|^2 + [1 - (\bar{\tau}_i \mathcal{L}_i)^2] \|\rho_k - h_k^i\|^2 \leq \|\rho_k - v\|^2, \quad (15)$$

$$\|j_k^i - \rho_k\| \leq (1 + \bar{\tau}_i \mathcal{L}_i) \|\rho_k - h_k^i\|, \quad (16)$$

Initialization: Select arbitrary elements $v_0, v_1 \in \mathcal{H}$ and set $k := 1$.
Iterative Steps: Create $\{v_k\}$ through the following process:
Step 1. Set
 $\rho_k = v_k + \theta_k (\Phi(v_k) - v_k) + \xi_k (v_k - v_{k-1})$
and calculate, for all $i \in [K]$,
 $h_k^i = (I + \tau_k^i G_i)^{-1} (I - \tau_k^i F_i) \rho_k$.
Step 2. Compute, for all $i \in [K]$,
 $j_k^i = h_k^i - \tau_k^i (F_i h_k^i - F_i \rho_k)$ and $u_k^i = S_i j_k^i - \alpha_k^i (S_i j_k^i - j_k^i)$.
If $\rho_k = h_k^i = S_i j_k^i$ for all $i \in [K]$, then stop and $\rho_k \in \Psi$. Otherwise, go to **Step 3**.
Step 3. Evaluate
 $v_{k+1} = \operatorname{argmax}\{\|u_k^i - \rho_k\| : i \in [K]\}$.
Replace k by $k + 1$ and go back to **Step 1**.

ALGORITHM 1: Inertial Tseng Mann parallel algorithm 1.

for all $v \in \Psi$ and $i \in [K]$.

Proof. Let $v \in \Psi$. Using (5) with the conditions of τ_k^i and F_i , it follows that, for all $i \in [K]$,

$$\begin{aligned} \|j_k^i - v\|^2 &= \|h_k^i - v\|^2 - 2\tau_k^i \langle h_k^i - v, F_i h_k^i - F_i \rho_k \rangle + (\tau_k^i)^2 \|F_i h_k^i - F_i \rho_k\|^2 \\ &= \|h_k^i - \rho_k\|^2 - 2\langle h_k^i - \rho_k, h_k^i - \rho_k \rangle + 2\langle h_k^i - \rho_k, h_k^i - v \rangle + \|\rho_k - v\|^2 \\ &\quad - 2\tau_k^i \langle h_k^i - v, F_i h_k^i - F_i \rho_k \rangle + (\bar{\tau}_i \mathcal{L}_i)^2 \|h_k^i - \rho_k\|^2 \\ &\leq \|\rho_k - v\|^2 - [1 - (\bar{\tau}_i \mathcal{L}_i)^2] \|\rho_k - h_k^i\|^2 - 2\langle h_k^i - v, \rho_k - h_k^i - \tau_k^i (F_i \rho_k - F_i h_k^i) \rangle. \end{aligned} \quad (17)$$

The definition of h_k^i implies that for all $i \in [K]$,

$$(I - \tau_k^i F_i) \rho_k \in (I + \tau_k^i G_i) h_k^i. \quad (18)$$

This implies that there is $g_k^i \in G_i h_k^i$ such that

$$g_k^i = \frac{1}{\tau_k^i} (\rho_k - h_k^i - \tau_k^i F_i \rho_k), \quad (19)$$

for all $i \in [K]$. The maximally monotonic nature of $F_i + G_i$ leads us to the conclusion that for all $i \in [K]$,

$$\langle F_i h_k^i + g_k^i, h_k^i - v \rangle \geq 0, \quad (20)$$

implying that for all $i \in [K]$,

$$\langle h_k^i - v, \rho_k - h_k^i - \tau_k^i (F_i \rho_k - F_i h_k^i) \rangle \geq 0. \quad (21)$$

This combined with (17) yields that for all $i \in [K]$,

$$\|j_k^i - v\|^2 \leq \|\rho_k - v\|^2 - [1 - (\bar{\tau}_i \mathcal{L}_i)^2] \|\rho_k - h_k^i\|^2. \quad (22)$$

This follows from Lemma 6 that for all $i \in [K]$,

$$\begin{aligned} \|u_k^i - v\|^2 &\leq \|j_k^i - v\|^2 - (1 - \alpha_k^i) (\alpha_k^i - \mu_i) \|S_i j_k^i - j_k^i\|^2 \\ &\leq \|\rho_k - v\|^2 - [1 - (\bar{\tau}_i \mathcal{L}_i)^2] \|\rho_k - h_k^i\|^2 - (1 - \alpha_k^i) (\alpha_k^i - \mu_i) \|S_i j_k^i - j_k^i\|^2. \end{aligned} \quad (23)$$

Furthermore, using the inequality (14) with the condition of τ_k^i and triangle inequality, we derive that inequality (16) is true. \square

Lemma 19. Assume that Assumptions 9–15 hold. If there is a subsequence $\{\rho_{k_m}\}$ of $\{\rho_k\}$ such that $\rho_{k_m} \rightarrow \bar{r} \in \mathcal{H}$ and $\lim_{m \rightarrow \infty} \|\rho_{k_m} - h_{k_m}^i\| = \lim_{m \rightarrow \infty} \|S_i j_{k_m}^i - j_{k_m}^i\| = 0$ for all $i \in [K]$. Then, $\bar{r} \in \Psi$.

Proof. Applying the inequality (16) with $\lim_{m \rightarrow \infty} \|\rho_{k_m} - h_{k_m}^i\| = 0$ for all $i \in [K]$, we get that $\lim_{m \rightarrow \infty} \|\rho_{k_m} - j_{k_m}^i\| = 0$ for all $i \in [K]$. It follows that $j_{k_m}^i \rightarrow \bar{r}$ for all $i \in [K]$, which together with $\lim_{m \rightarrow \infty} \|S_i j_{k_m}^i - j_{k_m}^i\| = 0$ and Assumption 15 indicates that $\bar{r} \in \bigcap_{i \in [K]} \operatorname{Fix}(S_i)$. Next, we exhibit $\bar{r} \in \bigcap_{i \in [K]} (F_i + G_i)^{-1}(0)$. For all $i \in [K]$, let $(v_i, u_i) \in \operatorname{graph}(F_i + G_i)$ be equivalent to $u_i - F_i v_i \in G_i v_i$. This implies, based on the definition of h_k^i , that $1/\tau_{k_m}^i (\rho_{k_m} -$

$h_{k_m}^i - \tau_{k_m}^i F_i \rho_{k_m}^i) \in G_i h_{k_m}^i$ for all $i \in [K]$. By the maximal monotonicity of G_i , we have that, for all $i \in [K]$,

$$\langle v_i - h_{k_m}^i, u_i - F_i v_i - \frac{1}{\tau_{k_m}^i} (\rho_{k_m}^i - h_{k_m}^i - \tau_{k_m}^i F_i \rho_{k_m}^i) \rangle \geq 0. \quad (24)$$

So, for all $i \in [K]$,

$$\begin{aligned} \langle v_i - h_{k_m}^i, u_i \rangle &\geq \langle v_i - h_{k_m}^i, F_i v_i + \frac{1}{\tau_{k_m}^i} (\rho_{k_m}^i - h_{k_m}^i - \tau_{k_m}^i F_i \rho_{k_m}^i) \rangle \\ &= \langle v_i - h_{k_m}^i, F_i v_i - F_i h_{k_m}^i \rangle + \langle v_i - h_{k_m}^i, F_i h_{k_m}^i - F_i \rho_{k_m}^i \rangle \\ &\quad + \frac{1}{\tau_{k_m}^i} \langle v_i - h_{k_m}^i, \rho_{k_m}^i - h_{k_m}^i \rangle \\ &\geq \langle v_i - h_{k_m}^i, F_i h_{k_m}^i - F_i \rho_{k_m}^i \rangle + \frac{1}{\tau_{k_m}^i} \langle v_i - h_{k_m}^i, \rho_{k_m}^i - h_{k_m}^i \rangle. \end{aligned} \quad (25)$$

This can be deduced from the Lipschitz continuity of F_i , $\lim_{m \rightarrow \infty} \|\rho_{k_m}^i - h_{k_m}^i\| = 0$ and $\tau_{k_m}^i \in [\tau_i, \bar{\tau}_i]$ that

$$\langle v_i - \bar{\tau}, u_i \rangle = \lim_{m \rightarrow \infty} \langle v_i - h_{k_m}^i, u_i \rangle \geq 0, \quad (26)$$

For all $i \in [K]$, when considered together with the maximal monotonicity of $F_i + G_i$, leads to the conclusion that $0 \in (F_i + G_i) \bar{\tau}$ for all $i \in [K]$, is equivalent to $\bar{\tau} \in \cap_{i \in [K]} (F_i + G_i)^{-1}(0)$. As a result, $\bar{\tau} \in \Psi$. \square

Theorem 20. *If Assumptions 9–16 hold, then the sequence $\{v_k\}$ generated by Algorithms 1 converges strongly to $v := (P_\Psi \circ \Phi)v$.*

Proof. Let $p \in \Psi$. From $\lim_{k \rightarrow \infty} \xi_k / \theta_k \|v_k - v_{k-1}\| = 0$, we obtain the following equation:

$$\xi_k \|v_k - v_{k-1}\| \leq \theta_k R_1, \quad (27)$$

for some $R_1 > 0$. Since Φ is contraction with constant $\rho \in [0, 1)$ and using (27), we have to compute the following expression:

$$\begin{aligned} \|\rho_k - p\| &= \|v_k + \theta_k (\Phi(v_k) - v_k) + \xi_k (v_k - v_{k-1}) - p\| \\ &\leq \theta_k \|\Phi(v_k) - p\| + (1 - \theta_k) \|v_k - p\| + \xi_k \|v_k - v_{k-1}\| \\ &\leq \theta_k \|\Phi(v_k) - \Phi(p)\| + \theta_k (\|\Phi(p) - p\| + R_1) + (1 - \theta_k) \|v_k - p\| \\ &\leq (1 - \gamma_k) \|v_k - p\| + \gamma_k R_2 \\ &\leq \max \{ \|v_k - p\|, R_2 \}, \end{aligned} \quad (28)$$

where $\gamma_k = \theta_k (1 - \rho)$ and $R_2 = \|\Phi(p) - p\| + R_1 / (1 - \rho)$. Using the inequality (15) with the definition of v_{k+1} and Assumptions 13 and 14 implies that

$$\|v_{k+1} - p\| \leq \|\rho_k - p\|. \quad (29)$$

Therefore, we can conclude that $\|v_{k+1} - p\| \leq \max \{ \|v_k - p\|, R_2 \}$ for any $k \in \mathbb{N}$. Consequently, $\{v_k\}$ is bounded sequence. Moreover, the sequence $\{\Phi(v_k)\}$ is bounded. Since the set Ψ is nonempty, closed and convex, there is a unique $v \in \Psi$ such that $v = (P_\Psi \circ \Phi)v$. By (4), we also get that for any $y \in \Psi$,

$$\langle \Phi(v) - v, y - v \rangle \leq 0. \quad (30)$$

Now, for each $k \in \mathbb{N}$, set $\Xi_k := \|v_k - v\|^2$. Applying (28), we have the following equation:

$$\begin{aligned} \|\rho_k - v\|^2 &\leq ((1 - \gamma_k) \|v_k - v\| + \gamma_k R_2)^2 \\ &= (1 - \gamma_k)^2 \Xi_k + \gamma_k (2R_2 (1 - \gamma_k) \|v_k - v\| + \gamma_k R_2^2) \\ &\leq \Xi_k + \gamma_k R_3, \end{aligned} \quad (31)$$

for some $R_3 > 0$. This follows from (15) that

Initialization: Let $v_0, v_1 \in \mathcal{H}$, $\lambda_i > 0$ and $\tau_1^i \in (0, 1/\mathcal{L}_i)$ for all $i \in [K]$, and set $k := 1$.

Iterative Steps: Create $\{v_k\}$ through the following process:

Step 1. Set
 $\rho_k = v_k + \theta_k (\Phi(v_k) - v_k) + \xi_k (v_k - v_{k-1})$
and calculate, for all $i \in [K]$,
 $h_k^i = (I + \tau_k^i G_i)^{-1} (I - \tau_k^i F_i) \rho_k$.

Step 2. Compute, for all $i \in [K]$,
 $j_k^i = h_k^i - \tau_k^i (F_i h_k^i - F_i \rho_k)$ and $u_k^i = S_i j_k^i - \alpha_k^i (S_i j_k^i - j_k^i)$.
If $\rho_k = h_k^i = S_i j_k^i$ for all $i \in [K]$, then stop and $\rho_k \in \Psi$. Otherwise, go to **Step 3**.

Step 3. Evaluate
 $v_{k+1} = \operatorname{argmax}\{\|u_k^i - \rho_k\| : i \in [K]\}$
and update, for all $i \in [K]$,
 $\tau_{k+1}^i = \begin{cases} \min\{\lambda_i \|\rho_k - h_k^i\| / \|F_i \rho_k - F_i h_k^i\|, \tau_k^i\}, & \text{if } F_i \rho_k \neq F_i h_k^i, \\ \tau_k^i & \text{otherwise.} \end{cases}$
Replace k by $k + 1$ and go back to **Step 1**.

ALGORITHM 2: Inertial Tseng Mann parallel algorithm 2.

$$(1 - \alpha_k^i)(\alpha_k^i - \mu_i) \|S_i j_k^i - j_k^i\|^2 + [1 - (\bar{\tau}_i \mathcal{L}_i)^2] \|\rho_k - h_k^i\|^2 \leq \Xi_k - \|u_k^i - v\|^2 + \gamma_k R_3. \quad (32)$$

For all $i \in [K]$. It implies by (32) that there is $i_k \in [K]$ such that

$$(1 - \alpha_k^{i_k})(\alpha_k^{i_k} - \mu_{i_k}) \|S_{i_k} j_k^{i_k} - j_k^{i_k}\|^2 + [1 - (\bar{\tau}_{i_k} \mathcal{L}_{i_k})^2] \|\rho_k - h_k^{i_k}\|^2 \leq \Xi_k - \Xi_{k+1} + \gamma_k R_3. \quad (33)$$

□

Case 21. Assume that there exists an integer $N \in \mathbb{N}$ such that $\Xi_{k+1} \leq \Xi_k$ for all $k \geq N$. This together with the boundedness of $\{\Xi_k\}$, it is convergent. Since $\lim_{k \rightarrow \infty} \gamma_k = 0$ and using Assumptions 13 and 14, and by (33),

$$\lim_{k \rightarrow \infty} \|\rho_k - h_k^{i_k}\| = \lim_{k \rightarrow \infty} \|S_{i_k} j_k^{i_k} - j_k^{i_k}\| = 0. \quad (34)$$

This combined with (16) yields that for all $i \in [K]$,

$$\begin{aligned} \|v_{k+1} - \rho_k\| &\leq \|v_{k+1} - j_k^{i_k}\| + \|j_k^{i_k} - \rho_k\| \\ &\leq (1 - \alpha_k^{i_k}) \|S_{i_k} j_k^{i_k} - j_k^{i_k}\| + (1 + \bar{\tau}_{i_k} \mathcal{L}_{i_k}) \|\rho_k - h_k^{i_k}\| \longrightarrow 0 \text{ as } k \longrightarrow \infty. \end{aligned} \quad (35)$$

This can be deduced from the definition of v_{k+1} that

$$\lim_{k \rightarrow \infty} \|\rho_k - u_k^i\| = 0, \quad (36)$$

for all $i \in [K]$. Using (15) again, we have

$$(1 - \alpha_k^i)(\alpha_k^i - \mu_i) \|S_i j_k^i - j_k^i\|^2 + [1 - (\bar{\tau}_i \mathcal{L}_i)^2] \|\rho_k - h_k^i\|^2 \leq \|\rho_k - v\|^2 - \|u_k^i - v\|^2 \leq R_4 \|\rho_k - u_k^i\|, \quad (37)$$

for all $i \in [K]$ and for some $R_4 > 0$. From the combination of this with (35) using Assumptions 13 and 14, we can derive that for all $i \in [K]$,

$$\lim_{k \rightarrow \infty} \|\rho_k - h_k^i\| = \lim_{k \rightarrow \infty} \|S_i j_k^i - j_k^i\| = 0. \quad (38)$$

From the definition of ρ_k , the inequality (27) and $\lim_{k \rightarrow \infty} \theta_k = 0$, we have

$$\begin{aligned} \|\rho_k - v_k\| &\leq \theta_k \|\Phi(v_k) - v_k\| + \xi_k \|v_k - v_{k-1}\|, \\ &\leq \theta_k (\|\Phi(v_k) - v_k\| + R_1) \longrightarrow 0 \text{ as } n \longrightarrow \infty. \end{aligned} \quad (39)$$

This together with (35) implies that

$$\lim_{k \rightarrow \infty} \|v_{k+1} - v_k\| = 0. \quad (40)$$

Moreover, because $\{v_k\}$ is bounded, there is $\bar{r} \in \mathcal{R}$ such that $v_{k_m} \rightarrow \bar{r}$ as $m \rightarrow \infty$ for some subsequence $\{v_{k_m}\}$ of $\{v_k\}$. From (39), we get $\rho_{k_m} \rightarrow \bar{r}$ as $m \rightarrow \infty$. Then using (38) with

Lemma 19 implies that $\bar{r} \in \Psi$. By (30), it is easy to demonstrate that

$$\limsup_{k \rightarrow \infty} \langle \Phi(v) - v, v_k - v \rangle = \lim_{m \rightarrow \infty} \langle \Phi(v) - v, v_{k_m} - v \rangle = \langle \Phi(v) - v, \bar{r} - v \rangle \leq 0. \quad (41)$$

Thus, we have by combining this with (40) that

$$\limsup_{k \rightarrow \infty} \langle \Phi(v) - v, v_{k+1} - v \rangle \leq \limsup_{k \rightarrow \infty} \langle \Phi(v) - v, v_{k+1} - v_k \rangle + \limsup_{k \rightarrow \infty} \langle \Phi(v) - v, v_k - v \rangle \leq 0. \quad (42)$$

Hence, from the assumption on Φ , (6), (7) and (29), we obtain

$$\begin{aligned} \Xi_{k+1} &\leq \|\rho_k - v\|^2 \\ &= \|\theta_k (\Phi(v_k) - \Phi(v)) + (1 - \theta_k)(v_k - v) + \xi_k (v_k - v_{k-1}) + \theta_k (\Phi(v) - v)\|^2 \\ &\leq \|\theta_k (\Phi(v_k) - \Phi(v)) + (1 - \theta_k)(v_k - v)\|^2 + 2\langle \xi_k (v_k - v_{k-1}) + \theta_k (\Phi(v) - v), v_{k+1} - v \rangle \\ &\leq \theta_k \|\Phi(v_k) - \Phi(v)\|^2 + (1 - \theta_k) \Xi_k + 2\xi_k \langle v_k - v_{k-1}, v_{k+1} - v \rangle + 2\theta_k \langle \Phi(v) - v, v_{k+1} - v \rangle \\ &\leq \theta_k \rho^2 \Xi_k + (1 - \theta_k) \Xi_k + 2\xi_k \|v_k - v_{k-1}\| \|v_{k+1} - v\| + 2\theta_k \langle \Phi(v) - v, v_{k+1} - v \rangle \\ &\leq \theta_k \rho \Xi_k + (1 - \theta_k) \Xi_k + 2\theta_k \cdot \frac{\xi_k}{\theta_k} \|v_k - v_{k-1}\| \|v_{k+1} - v\| + 2\theta_k \langle \Phi(v) - v, v_{k+1} - v \rangle \\ &\leq (1 - \gamma_k) \Xi_k + \gamma_k \left[R_5 \frac{\xi_k}{\theta_k} \|v_k - v_{k-1}\| + \frac{2}{1 - \rho} \langle \Phi(v) - v, v_{k+1} - v \rangle \right], \end{aligned} \quad (43)$$

for some $R_5 > 0$. As a consequence of applying this to the inequality (42) with Lemma 7, it can be inferred that $\lim_{k \rightarrow \infty} \Xi_k = 0$.

Case 22. We can find a subsequence $\{\Xi_{k_q}\}$ of $\{\Xi_k\}$ such that $\Xi_{k_q} < \Xi_{k_q+1}$ for all $q \in \mathbb{N}$. The inequality $\Xi_{\psi(k)} \leq \Xi_{\psi(k)+1}$ is derived by applying Lemma 8, where $\psi: \mathbb{N} \rightarrow \mathbb{N}$ is defined by (12), and $k \geq k^*$ for some $k^* \in \mathbb{N}$. By similar arguments as in Case 21, we obtain that

$$\lim_{k \rightarrow \infty} \|\rho_{\psi(k)} - h_{\psi(k)}^i\| = \lim_{k \rightarrow \infty} \|S_i j_{\psi(k)}^i - j_{\psi(k)}^i\| = 0, \quad (44)$$

for all $i \in [K]$ and

$$\limsup_{k \rightarrow \infty} \langle \Phi(v) - v, v_{\psi(k)+1} - v \rangle \leq 0. \quad (45)$$

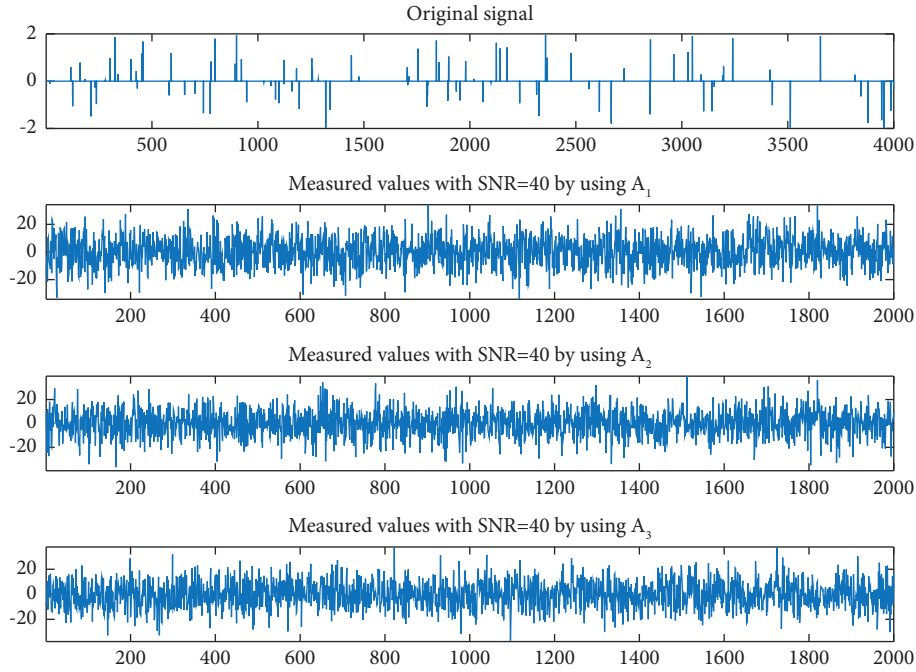
Finally, from $\Xi_{\psi(k)} \leq \Xi_{\psi(k)+1}$ and by (43), for all $k \geq k^*$, we obtain

$$\Xi_{\psi(k)+1} \leq (1 - \gamma_{\psi(k)}) \Xi_{\psi(k)+1} + \gamma_{\psi(k)} \left[R_5 \frac{\xi_{\psi(k)}}{\theta_{\psi(k)}} \|v_{\psi(k)} - v_{\psi(k)-1}\| + \frac{2}{1 - \rho} \langle \Phi(v) - v, v_{\psi(k)+1} - v \rangle \right]. \quad (46)$$

Some simple calculations yield

TABLE 1: Numerical comparison of four algorithms.

		m nonzero elements		
		$m = 100$	$m = 200$	$m = 300$
Algorithm 2.2	Number of iterations	1183	1271	1326
	CPU time (s)	10.0271	10.2887	10.7556
Algorithm 3	Number of iterations	381	433	481
	CPU time (s)	6.3097	6.9989	7.5401
Algorithm 1	Number of iterations	159	180	198
	CPU time (s)	3.9039	4.1992	4.5897
Algorithm 2	Number of iterations	169	193	212
	CPU time (s)	4.1950	4.5258	4.9377

FIGURE 1: From top to bottom: the original signal and the measurement by using A_1 , A_2 , and A_3 , respectively, with $m = 100$.

$$\Xi_{\psi(k)+1} \leq R_5 \frac{\xi_{\psi(k)}}{\theta_{\psi(k)}} \|v_{\psi(k)} - v_{\psi(k)-1}\| + \frac{2}{1-\rho} \langle \Phi(v) - v, v_{\psi(k)+1} - v \rangle. \quad (47)$$

This implies that $\limsup_{k \rightarrow \infty} \Xi_{\psi(k)+1} \leq 0$. Thus, $\lim_{k \rightarrow \infty} \Xi_{\psi(k)+1} = 0$. In addition, by Lemma 8,

$$\lim_{k \rightarrow \infty} \Xi_k \leq \lim_{k \rightarrow \infty} \Xi_{\psi(k)+1} = 0. \quad (48)$$

Therefore, it can be concluded that $v_k \rightarrow v$ as $k \rightarrow \infty$.

Theorem 23. *Assume that Assumptions 9–16 are satisfied. Then, the sequence $\{v_k\}$ generated by Algorithm 2 converges strongly to $v := (P_\Psi \circ \Phi)v$.*

Proof. Employing the same methodology as in the proof of ([48], Lemma 3.1.), we conclude that $\{\tau_k^i\} \subset [\min\{\tau_1^i, \lambda_i/\mathcal{L}_i\}, \tau_1^i] \subset (0, 1/\mathcal{L}_i)$ for all $i \in [K]$, that

is, Assumption 14 holds. The rest is similar to the proof of Theorem 20. \square

4. Application to Signal Recovery Problem

Signal recovery is a fundamental challenge in diverse scientific and engineering domains, and recent developments in signal recovery algorithms have resulted in substantial enhancements in the accuracy and efficacy of signal processing applications. Efficient signal recovery techniques are critical for numerous tasks, such as image and audio analysis, data compression, and communication systems. Consequently, sustained research and development efforts aimed at advancing signal recovery algorithms are

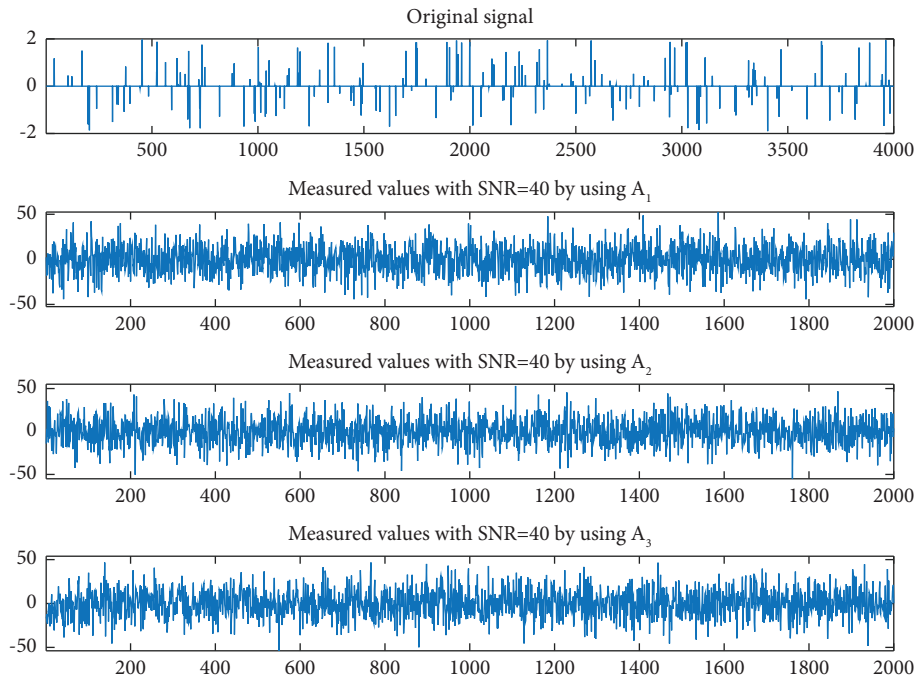


FIGURE 2: From top to bottom: the original signal and the measurement by using A_1 , A_2 , and A_3 , respectively, with $m = 200$.

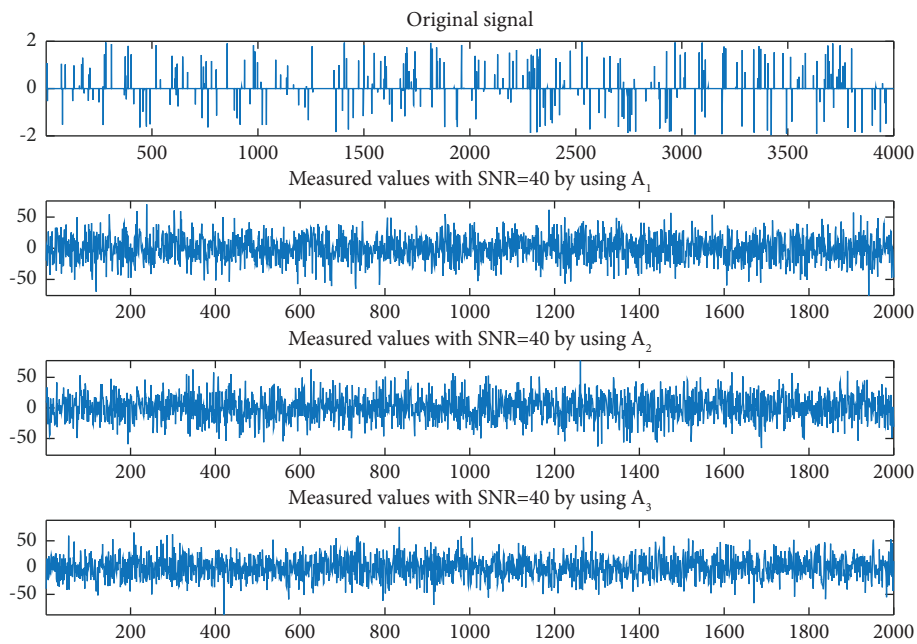


FIGURE 3: From top to bottom: the original signal and the measurement by using A_1 , A_2 , and A_3 , respectively, with $m = 300$.

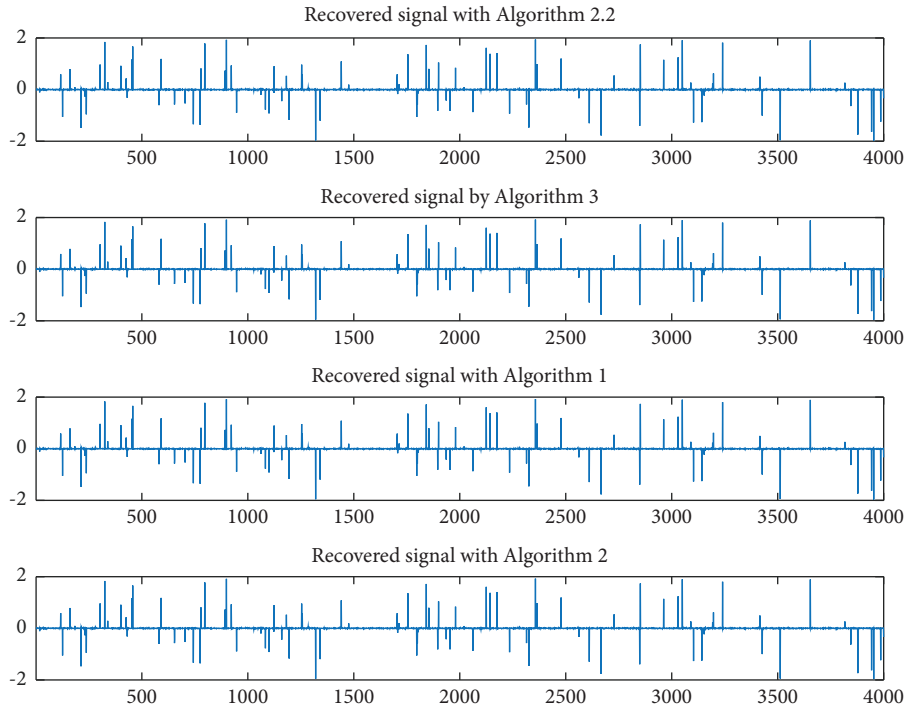


FIGURE 4: From top to bottom: the reconstructed signals by four algorithms for $m = 100$.

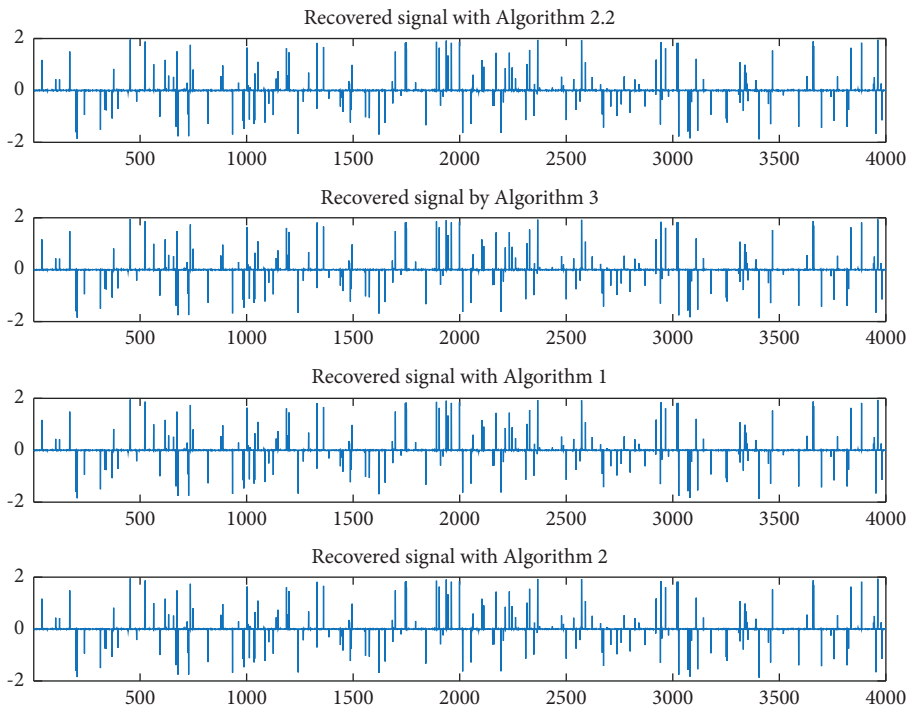


FIGURE 5: From top to bottom: the reconstructed signals by four algorithms for $m = 200$.

imperative to further enhance the performance and capabilities of these applications.

The signal recovery problem involving diverse blurring filters can be mathematically expressed as follows:

$$b_i = A_i x + \varepsilon_i, \quad (49)$$

where $b_i \in \mathbb{R}^M$ is the observed signal with noise ε_i , $x \in \mathbb{R}^N$ is the original signal and $A_i \in \mathbb{R}^{M \times N}$ ($M < N$) is filter matrix

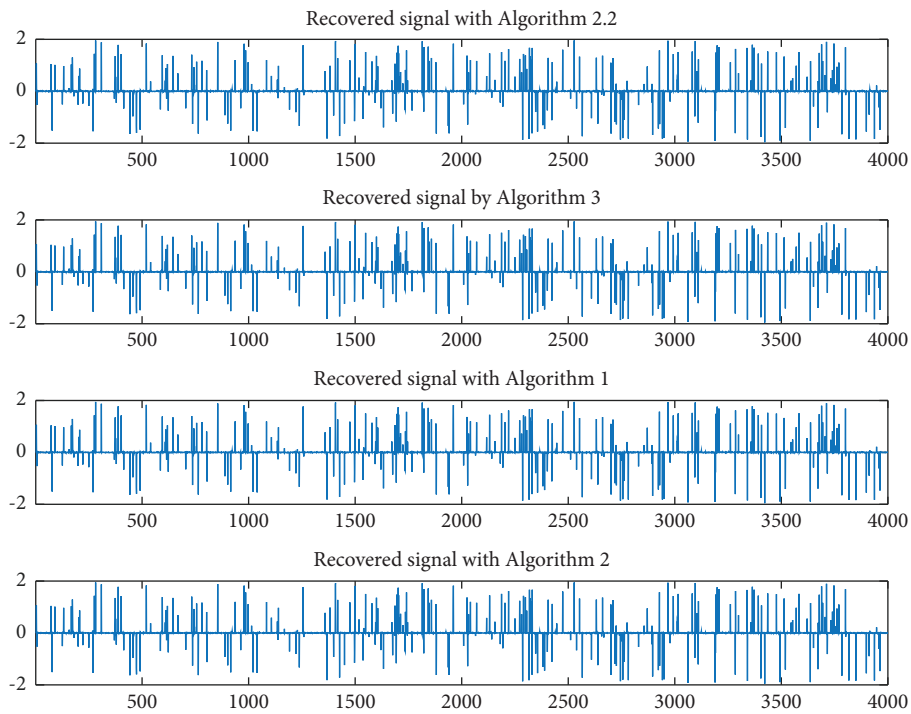


FIGURE 6: From top to bottom: the reconstructed signals by four algorithms for $m = 300$.

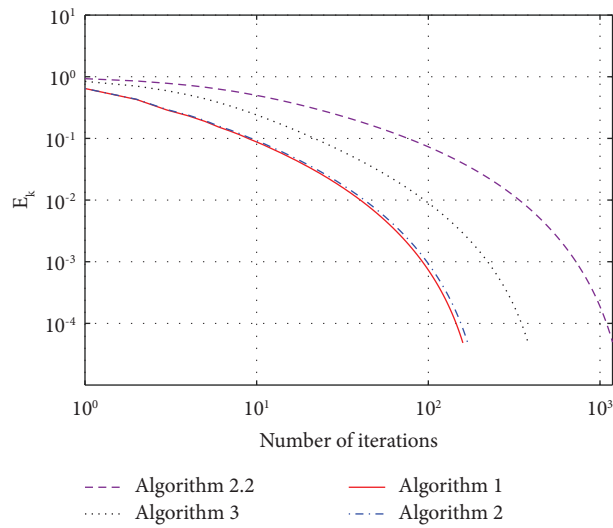


FIGURE 7: Plots of E_k over iter when $m = 100$.

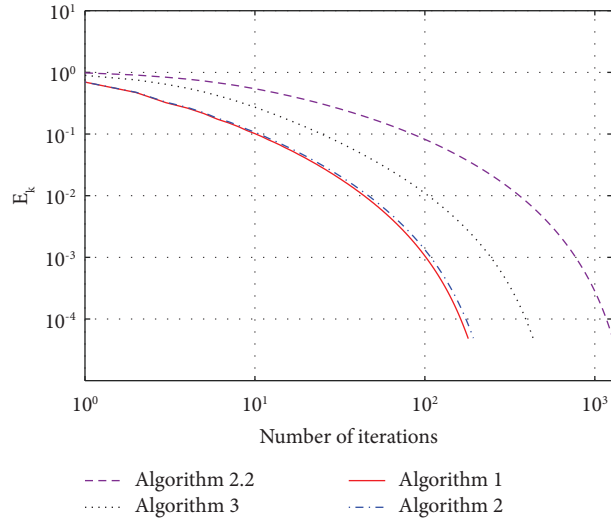


FIGURE 8: Plots of E_k over iter when $m = 200$.

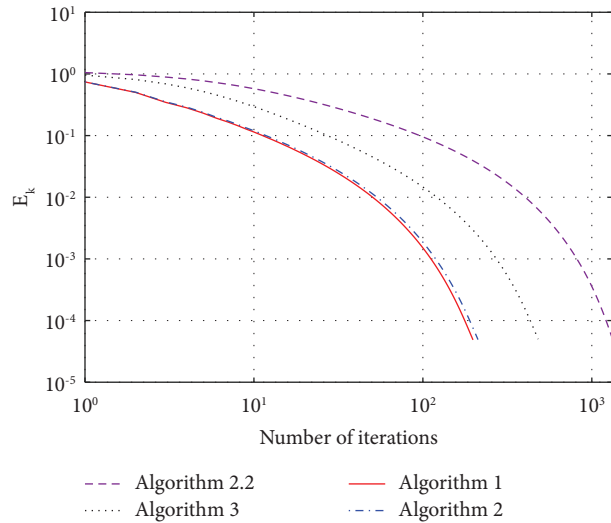


FIGURE 9: Plots of E_k over iter when $m = 300$.

TABLE 2: Numerical results of Algorithms 1.

Inputs		m nonzero elements		
		$m = 50$	$m = 100$	$m = 150$
A_1	Number of iterations	2373	3143	4474
	CPU time (s)	3.4571	4.4129	6.2303
A_2	Number of iterations	2328	3407	4297
	CPU time (s)	3.1495	4.8879	5.8837
A_3	Number of iterations	2334	3162	4316
	CPU time (s)	3.1203	4.2016	6.1732
A_1, A_2	Number of iterations	581	564	762
	CPU time (s)	2.0524	1.9764	2.9730
A_1, A_3	Number of iterations	548	589	685
	CPU time (s)	2.8591	2.0762	3.5921
A_2, A_3	Number of iterations	598	629	644
	CPU time (s)	2.3680	2.1654	2.9194
A_1, A_2, A_3	Number of iterations	138	145	154
	CPU time (s)	0.8413	0.7845	0.8708

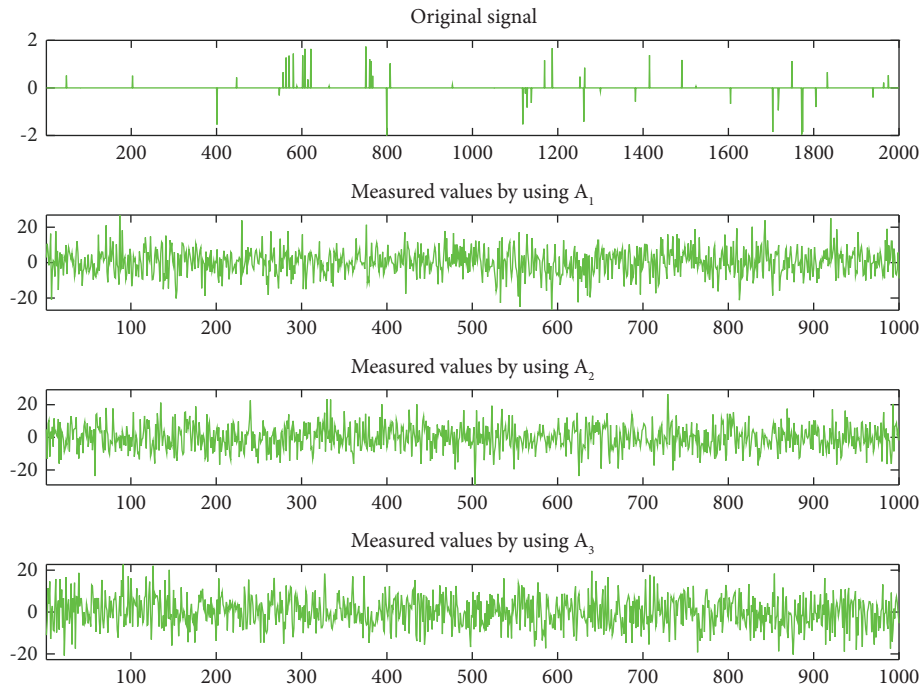


FIGURE 10: From top to bottom: the original signal and the measurement by using A_1 , A_2 , and A_3 , respectively, with $m = 50$.

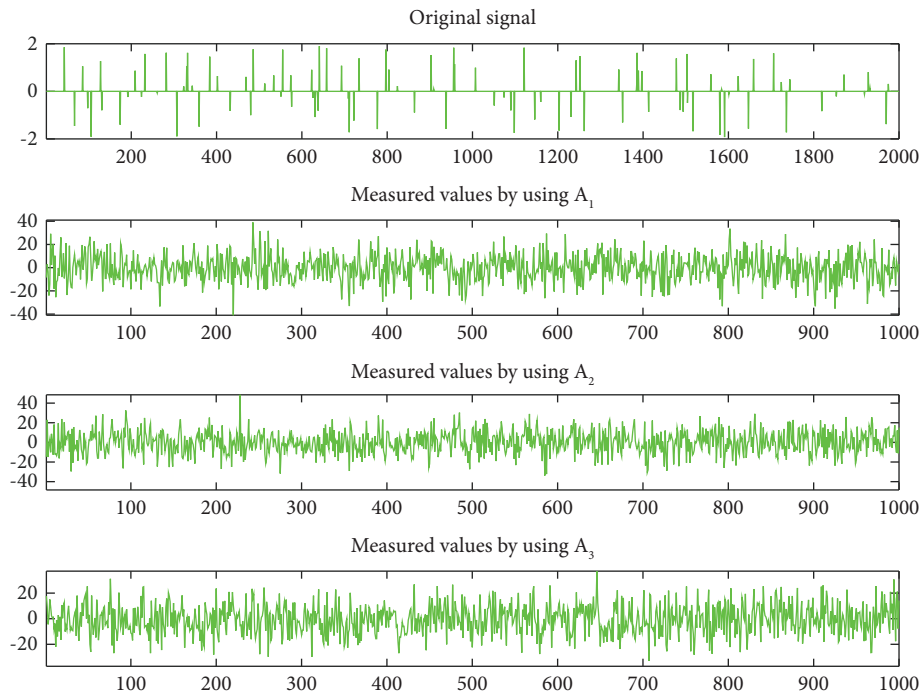


FIGURE 11: From top to bottom: the original signal and the measurement by using A_1 , A_2 , and A_3 , respectively, with $m = 100$.

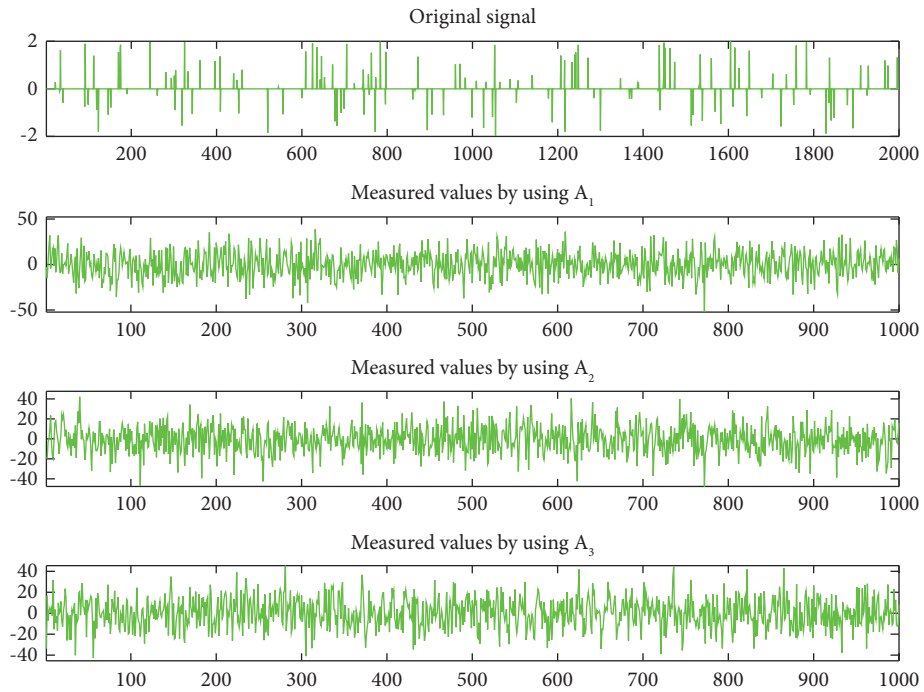


FIGURE 12: From top to bottom: the original signal and the measurement by using A_1 , A_2 , and A_3 , respectively, with $m = 150$.

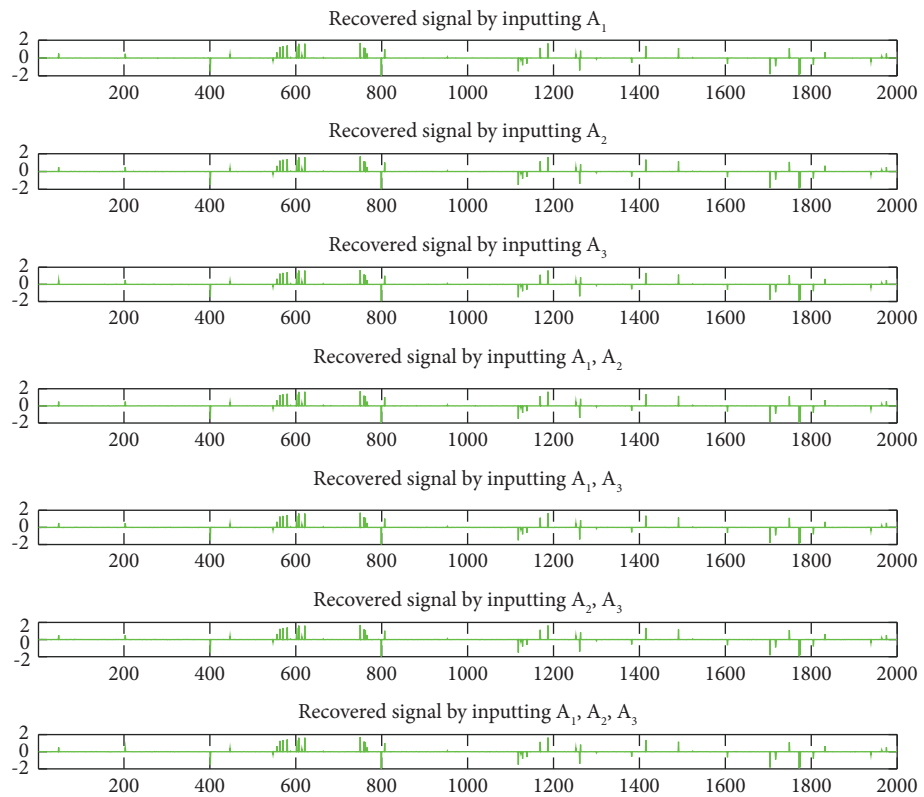


FIGURE 13: From top to bottom: the reconstructed signals by using each input for $m = 50$.

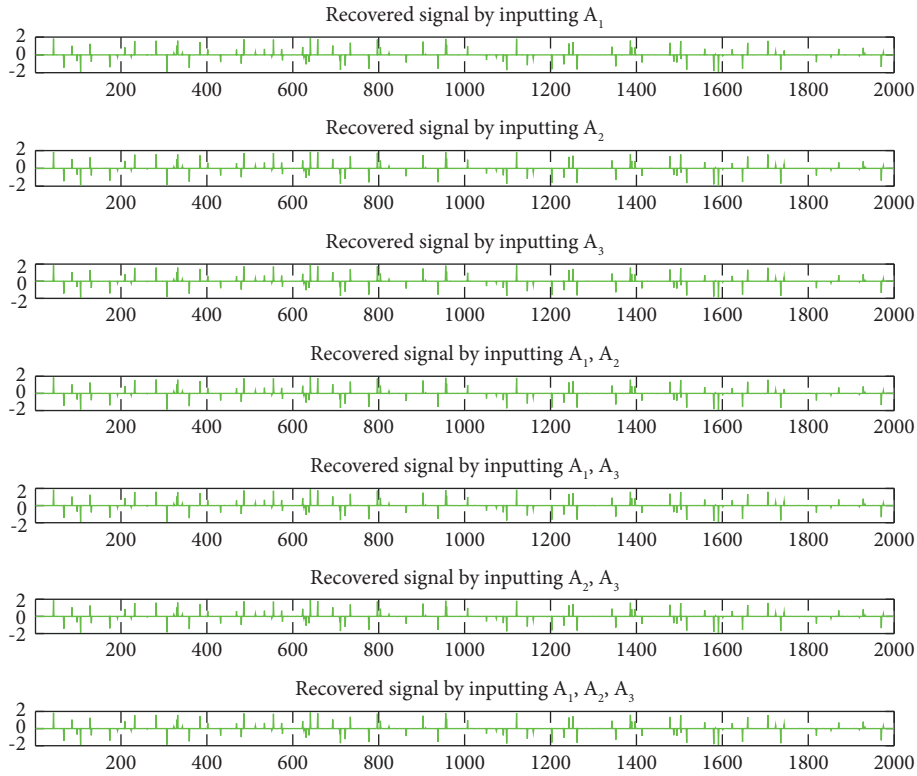


FIGURE 14: From top to bottom: the reconstructed signals by using each input for $m = 100$.

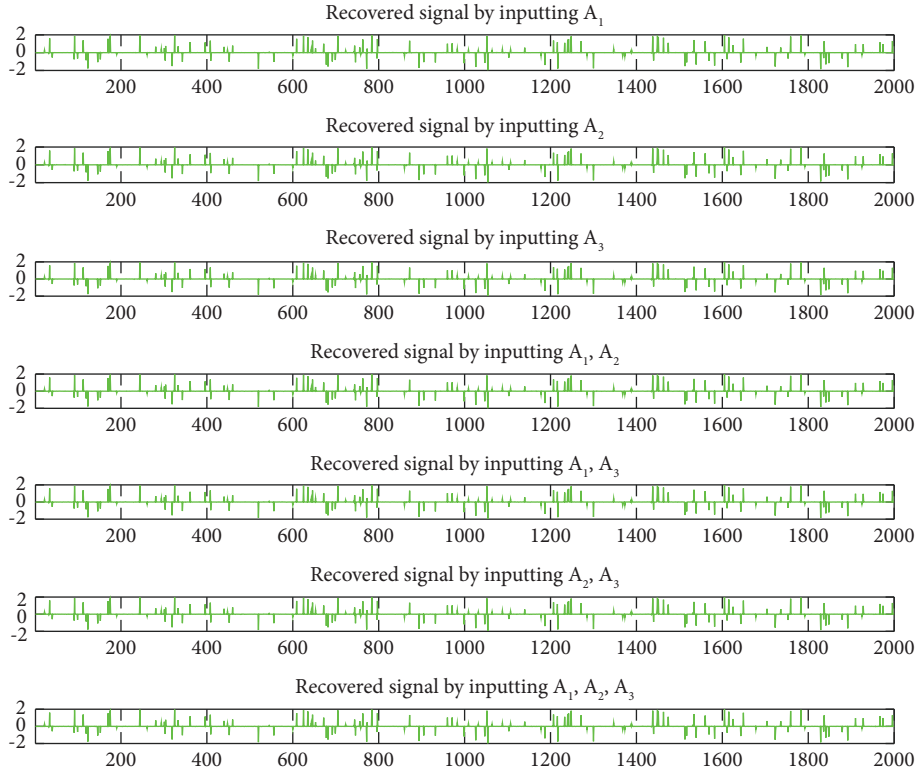


FIGURE 15: From top to bottom: the reconstructed signals by using each input for $m = 150$.

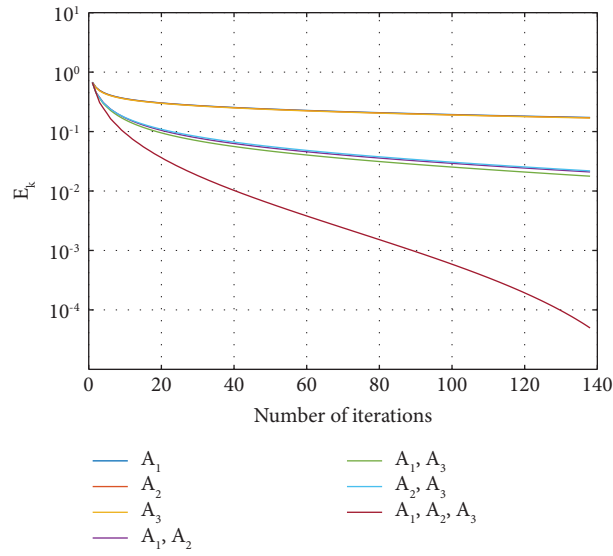


FIGURE 16: Plots of E_k over iter when $m = 50$.

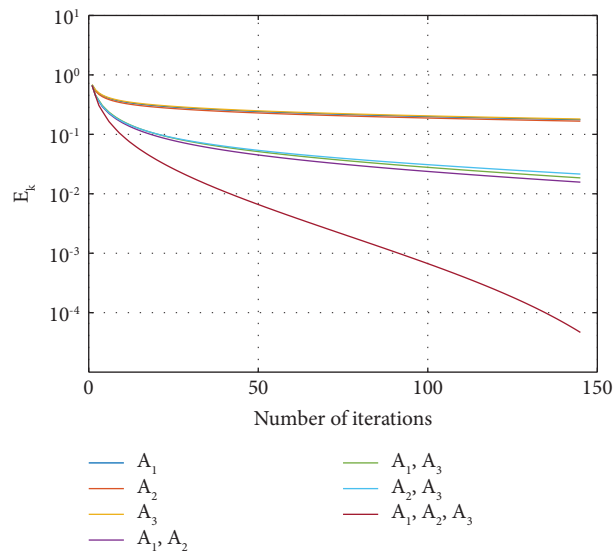


FIGURE 17: Plots of E_k over iter when $m = 100$.

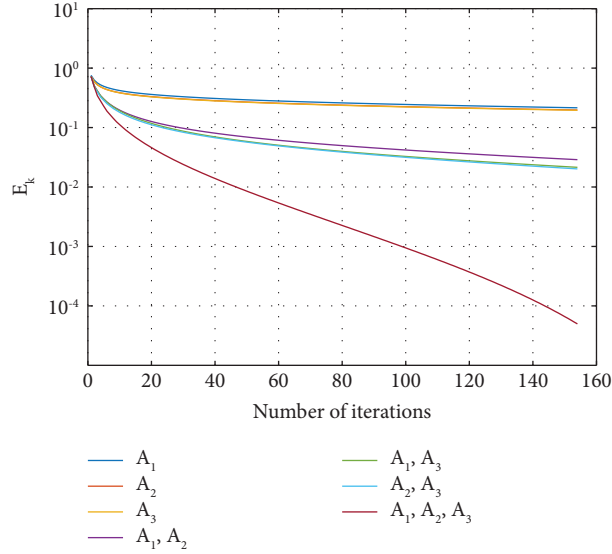


FIGURE 18: Plots of E_k over iter when $m = 150$.

for all $i \in [K]$. Subsequently, we direct our attention toward the following problem:

$$\begin{aligned}
 & \min_{x \in \mathbb{R}^N} \frac{1}{2} \|A_1 x - b_1\|_2^2 + \|x\|_1, \\
 & \min_{x \in \mathbb{R}^N} \frac{1}{2} \|A_2 x - b_2\|_2^2 + \|x\|_1, \\
 & \min_{x \in \mathbb{R}^N} \frac{1}{2} \|A_3 x - b_3\|_2^2 + \|x\|_1, \\
 & \quad \vdots \\
 & \min_{x \in \mathbb{R}^N} \frac{1}{2} \|A_K x - b_K\|_2^2 + \|x\|_1,
 \end{aligned} \tag{50}$$

for all $i \in [K]$. According to Proposition 3.1 (iii) presented in [49], the problem at hand can be recast as problem (2) through the following settings: $\mathcal{H} = \mathbb{R}^N$, $S_i(\cdot) = \text{prox}_{\zeta_i \|\cdot\|_1}(I - \zeta_i \nabla h_i)(\cdot)$, $G_i(\cdot) = \partial(\|\cdot\|_1)$ and $F_i = \nabla h_i$, where $\zeta_i > 0$, $h_i(\cdot) = 1/2 \|A_i(\cdot) - b_i\|_2^2$ for all $i \in [K]$. It is known that S_i is nonexpansive mapping for $\zeta_i \in (0, 2/\|A_i\|_2^2)$ and hence 0-demicontractive. Besides, G_i is maximal monotone mapping, and F_i is monotone and $\|A_i\|_2^2$ -Lipschitz continuous mapping.

In this part, we perform two numerical experiments to present the computational efficiency of Algorithms 1 and 2 for signal recovery problems consisting of various blurring filters. All computations were performed using Matlab R2021a on an iMac equipped with an Apple M1 chip and 16 GB of RAM. Experiment (***) During the first experiment, we provide the numerical comparison of Algorithms 1 and 2 with Algorithm of Corollary 2.2 in [31] (Algorithm 2.2) and Algorithm 3 in [50]. Select the signal size to be $N = 4000$ and $M = 2000$. Set the original signal x is generated by the uniform distribution in $[-2, 2]$ with m nonzero elements

and A_i be the Gaussian matrix generated by command `randn(M, N)`. Let the observation b_i be generated by white Gaussian noise with signal-to-noise ratio $\text{SNR} = 40$, the initial points be the vectors generated randomly and $\zeta_i = 1/\|A_i\|_2^2$ for all $i \in \{1, 2, 3\}$. Measuring the accuracy of the restoration using the mean-squared error, which is defined as: $E_k = 1/N \|v_k - x\|_2^2 < 5 \times 10^{-5}$. The control parameters are defined in the following manner:

- (i) Algorithm 2.2: $\alpha_k^n = 0.5$;
- (ii) Algorithm 3: $\lambda_i = 0.5$, $\varphi(\cdot) = 0.9(\cdot)$, $\gamma_1^i = 9/10 \|A_i\|_2^2$, $a_k = 1/k + 1$, $b_k = 99k/100(k + 1)$ and $\xi_k = \begin{cases} \min\{1/(k+1)^{1.1} \max\{\|u_k - u_{k-1}\|_2, \|u_k - u_{k-1}\|_2^2\}, 0.25\} & \text{if } u_k \neq u_{k-1}; \\ 0.25 & \text{otherwise;} \end{cases}$
- (iii) Algorithm 1: $\alpha_k^i = 0.25$, $\Phi(\cdot) = 0.9(\cdot)$, $\tau_k^i = 9/10 \|A_i\|_2^2$, $\theta_k = 1/k + 1$ and $\xi_k = \begin{cases} \min\{1/(k+1)^{1.1} \max\{\|v_k - v_{k-1}\|_2, \|v_k - v_{k-1}\|_2^2\}, 0.25\} & \text{if } v_k \neq v_{k-1}; \\ 0.25 & \text{otherwise;} \end{cases}$
- (iv) Algorithm 2: $\lambda_i = 0.5$, $\alpha_k^i = 0.25$, $\Phi(\cdot) = 0.9(\cdot)$, $\tau_1^i = 9/10 \|A_i\|_2^2$, $\theta_k = 1/k + 1$ and $\xi_k = \begin{cases} \min\{1/(k+1)^{1.1} \max\{\|v_k - v_{k-1}\|_2, \|v_k - v_{k-1}\|_2^2\}, 0.25\} & \text{if } v_k \neq v_{k-1}; \\ 0.25 & \text{otherwise;} \end{cases}$

The following results are shown.

The numerical results of Experiment (***) clearly demonstrate that both proposed algorithms are more effective than the two previous algorithms, as indicated in Table 1 and Figures 1–9.

Experiment 24. In the second experiment, we present the numerical results obtained via Algorithm 1 for solving problem (4.1) with multiple inputs A_i . The signal size is set to be $N = 2000$ and $M = 1000$, with the original signal x being generated via a uniform distribution over the interval $[-2, 2]$, featuring m nonzero elements. The matrices A_i are Gaussian matrices generated using the command `randn(M, N)`. For $i \in \{1, 2, 3\}$, the observations b_i are generated via the addition of white Gaussian noise ε_i with variance σ_i^2 , with initial points being randomly generated

and $\zeta_i = 1/\|A_i\|_2^2$. Measuring the accuracy of the restoration using the mean-squared error, which is defined as follows: $E_k = 1/N\|v_k - x\|_2^2 < 5 \times 10^{-5}$. For Algorithm 1, let $\sigma_i = 0.01$ (i), $\alpha_k^i = 0.25$, $\Phi(\cdot) = 0.9(\cdot)$, $\tau_k^i = 9/10\|A_i\|_2^2$, $\theta_k = 1/k + 1$ and $\xi_k = \begin{cases} \min\{1/(k+1)^{1.1} \max\{\|v_k - v_{k-1}\|_2, \|v_k - v_{k-1}\|_2^2\}, 0.25\} & \text{if } v_k \neq v_{k-1}; \\ 0.25 & \text{otherwise;} \end{cases}$ The ensuing section depicts the results.

Based on the numerical results obtained from Experiment 24, it is evident that incorporating all three Gaussian matrices (A_1, A_2 , and A_3) into Algorithm 1 leads to more effective outcomes in terms of time and number of iterations, as compared to the usage of only one or two of the matrices. These results are presented in Table 2 and Figures 10–18.

5. Conclusions

In this research, we obtain strong convergence results for common variational inclusion and common fixed point problems using two new parallel methods. Our results extend and generalize several previously published findings, and the numerical results indicate that our suggested approaches to the signal recovery problem including multiple blurring filters outperform the two preceding approaches.

Data Availability

The data used to support the findings of the study are available from the corresponding author upon request.

Conflicts of Interest

The authors declare that they have no conflicts of interest.

Acknowledgments

This research project was partially supported by Suan Dusit University Lampang Center, King Mongkut's University of Technology Thonburi, Faculty of Science, Chiang Mai University, and Chiang Mai University.



References

- [1] A. Beck and M. Teboulle, "A fast iterative shrinkage-thresholding algorithm for linear inverse problems," *SIAM Journal on Imaging Sciences*, vol. 2, no. 1, pp. 183–202, 2009.
- [2] Y. Shehu and P. Cholamjiak, "Iterative method with inertial for variational inequalities in Hilbert spaces," *Calcolo*, vol. 56, no. 1, p. 4, 2019.
- [3] S. Suantai, S. Kesornprom, and P. Cholamjiak, "A new hybrid CQ algorithm for the split feasibility problem in Hilbert spaces and its applications to compressed sensing," *Mathematics*, vol. 7, no. 9, p. 789, 2019.
- [4] R. Suparatulorn, P. Charoensawan, and K. Pochinapan, "Inertial self-adaptive algorithm for solving split feasible problems with applications to image restoration," *Mathematical Methods in the Applied Sciences*, vol. 42, no. 18, pp. 7268–7284, 2019.
- [5] S. Kesornprom, N. Pholasa, and P. Cholamjiak, "On the convergence analysis of the gradient-CQ algorithms for the split feasibility problem," *Numerical Algorithms*, vol. 84, no. 3, pp. 997–1017, 2020.
- [6] P. Peeyada, R. Suparatulorn, and W. Cholamjiak, "An inertial Mann forward-backward splitting algorithm of variational inclusion problems and its applications," *Chaos, Solitons & Fractals*, vol. 158, Article ID 112048, 2022.
- [7] S. Kesornprom and P. Cholamjiak, "A modified inertial proximal gradient method for minimization problems and applications," *AIMS Mathematics*, vol. 7, no. 5, pp. 8147–8161, 2022.
- [8] P. L. Lions and B. Mercier, "Splitting algorithms for the sum of two nonlinear operators," *SIAM Journal on Numerical Analysis*, vol. 16, no. 6, pp. 964–979, 1979.
- [9] G. B. Passty, "Ergodic convergence to a zero of the sum of monotone operators in Hilbert space," *Journal of Mathematical Analysis and Applications*, vol. 72, no. 2, pp. 383–390, 1979.
- [10] G. H.-G. Chen and R. T. Rockafellar, "Convergence rates in forward-backward splitting," *SIAM Journal on Optimization*, vol. 7, no. 2, pp. 421–444, 1997.
- [11] P. Tseng, "A modified forward-backward splitting method for maximal monotone mappings," *SIAM Journal on Control and Optimization*, vol. 38, no. 2, pp. 431–446, 2000.
- [12] B. Polyak, "Some methods of speeding up the convergence of iteration methods," *USSR Computational Mathematics and Mathematical Physics*, vol. 4, no. 5, pp. 791–817, 1964.
- [13] A. Padcharoen, D. Kitkuan, W. Kumam, and P. Kumam, "Tseng methods with inertial for solving inclusion problems and application to image deblurring and image recovery problems," *Computational and Mathematical Methods*, vol. 3, no. 3, Article ID e1088, 2021.
- [14] D. A. Lorenz and T. Pock, "An inertial forward-backward algorithm for monotone inclusions," *Journal of Mathematical Imaging and Vision*, vol. 51, no. 2, pp. 311–325, 2015.
- [15] S. Kesornprom and P. Cholamjiak, "Proximal type algorithms involving linesearch and inertial technique for split variational inclusion problem in hilbert spaces with applications," *Optimization*, vol. 68, no. 12, pp. 2369–2395, 2019.
- [16] S. Suantai, S. Kesornprom, and P. Cholamjiak, "Modified proximal algorithms for finding solutions of the split variational inclusions," *Mathematics*, vol. 7, no. 8, p. 708, 2019.
- [17] J. Abubakar, P. Kumam, A. I. Garba, M. S. Abdullahi, A. H. Ibrahim, and K. Sitthithakerngkiet, "An inertial iterative scheme for solving variational inclusion with application to Nash-Cournot equilibrium and image restoration problems," *Carpathian Journal of Mathematics*, vol. 37, no. 3, pp. 361–380, 2021.
- [18] W. Cholamjiak, P. Cholamjiak, and S. Suantai, "An inertial forward-backward splitting method for solving inclusion problems in Hilbert spaces," *Journal of Fixed Point Theory and Applications*, vol. 20, no. 1, p. 42, 2018.

- [19] P. Cholamjiak, D. Van Hieu, and Y. J. Cho, "Relaxed forward-backward splitting methods for solving variational inclusions and applications," *Journal of Scientific Computing*, vol. 88, no. 3, p. 85, 2021.
- [20] A. Gibali and D. V. Thong, "Tseng type methods for solving inclusion problems and its applications," *Calcolo*, vol. 55, pp. 49–54, 2018.
- [21] A. Taiwo, O. T. Mewomo, and A. Gibali, "A simple strong convergent method for solving split common fixed point problems," *Journal of Nonlinear and Variational Analysis*, vol. 5, no. 5, pp. 777–793, 2021.
- [22] C. Zong and Y. Tang, "Dual three-operator splitting algorithms for solving composite monotone inclusion with applications to convex minimization," *Journal of Applied and Numerical Optimization*, vol. 3, no. 3, pp. 533–554, 2021.
- [23] J. Xiao and Y. Wang, "A viscosity method with inertial effects for split common fixed point problems of demicontractive mappings," *Journal of Nonlinear Functional Analysis*, vol. 2022, 2022.
- [24] X. Zhao, J. C. Yao, and Y. Yao, "A proximal algorithm for solving split monotone variational inclusions," *University Politehnica of Bucharest Scientific Bulletin, Series A: Applied Mathematics and Physics*, vol. 82, no. 3, pp. 43–52, 2020.
- [25] R. H. Haghi and N. Bakhshi, "Some coupled fixed point results without mixed monotone property," *Journal of Advanced Mathematical Studies*, vol. 15, no. 4, pp. 456–463, 2022.
- [26] D. W. Peaceman and H. H. Rachford Jr, "The numerical solution of parabolic and elliptic differential equations," *Journal of the Society for Industrial and Applied Mathematics*, vol. 3, no. 1, pp. 28–41, 1955.
- [27] J. Douglas and H. H. Rachford, "On the numerical solution of heat conduction problems in two and three space variables," *Transactions of the American Mathematical Society*, vol. 82, no. 2, pp. 421–439, 1956.
- [28] G. Li and T. K. Pong, "Douglas-Rachford splitting for non-convex optimization with application to non-convex feasibility problems," *Mathematical Programming*, vol. 159, no. 1–2, pp. 371–401, 2016.
- [29] M. N. Dao and H. M. Phan, "Adaptive Douglas-Rachford splitting algorithm for the sum of two operators," *SIAM Journal on Optimization*, vol. 29, no. 4, pp. 2697–2724, 2019.
- [30] C. K. Sim, "Convergence rates for the relaxed Peaceman-Rachford splitting method on a monotone inclusion problem," *Journal of Optimization Theory and Applications*, vol. 196, no. 1, pp. 298–323, 2023.
- [31] S. Suantai, K. Kankam, P. Cholamjiak, and W. Cholamjiak, "A parallel monotone hybrid algorithm for a finite family of G -nonexpansive mappings in Hilbert spaces endowed with a graph applicable in signal recovery," *Computational and Applied Mathematics*, vol. 40, no. 4, 2021.
- [32] R. Suparatulorn and K. Chaichana, "A strongly convergent algorithm for solving common variational inclusion with application to image recovery problems," *Applied Numerical Mathematics*, vol. 173, pp. 239–248, 2022.
- [33] S. S. Chang, C. F. Wen, and J. C. Yao, "Common zero point for a finite family of inclusion problems of accretive mappings in Banach spaces," *Optimization*, vol. 67, no. 8, pp. 1183–1196, 2018.
- [34] T. Mouktonglang, K. Pochinapan, and R. Suparatulorn, "A parallel method for common variational inclusion and common fixed point problems with applications," *Carpathian Journal of Mathematics*, vol. 39, no. 1, pp. 189–200, 2022.
- [35] P. K. Anh and D. Van Hieu, "Parallel and sequential hybrid methods for a finite family of asymptotically quasi ϕ -nonexpansive mappings ϕ -nonexpansive mappings," *Journal of Applied Mathematics and Computing*, vol. 48, no. 1–2, pp. 241–263, 2015.
- [36] W. Cholamjiak, S. A. Khan, D. Yambangwai, and K. R. Kazmi, "Strong convergence analysis of common variational inclusion problems involving an inertial parallel monotone hybrid method for a novel application to image restoration," *Revista de la Real Academia de Ciencias Exactas, Físicas y Naturales, Serie A. Matemáticas*, vol. 1142 pages, 2020.
- [37] M. Eslamian, "Strong convergence theorem for common zero points of inverse strongly monotone mappings and common fixed points of generalized demimetric mappings," *Optimization*, vol. 71, no. 14, pp. 4265–4287, 2021.
- [38] M. Eslamian and A. Kamandi, "A novel algorithm for approximating common solution of a system of monotone inclusion problems and common fixed point problem," *Journal of Industrial and Management Optimization*, vol. 19, no. 2, pp. 868–889, 2023.
- [39] S. Suantai, W. Cholamjiak, and P. Cholamjiak, "Strong convergence theorems of a finite family of quasi-nonexpansive and Lipschitz multi-valued mappings," *Afrika Matematika*, vol. 26, no. 3–4, pp. 345–355, 2015.
- [40] T. L. Hicks and J. D. Kubicek, "On the Mann iteration process in a Hilbert space," *Journal of Mathematical Analysis and Applications*, vol. 59, no. 3, pp. 498–504, 1977.
- [41] Ş. Mâruşter, "The solution by iteration of nonlinear equations in Hilbert spaces," *Proceedings of the American Mathematical Society*, vol. 63, no. 1, pp. 69–73, 1977.
- [42] H. Y. Zhou and X. L. Qin, *Fixed Points of Nonlinear Operators. Iterative Methods*, De Gruyter, Berlin, Germany, 2020.
- [43] H. Brézis, "Opérateurs Maximaux Monotones et Semigroupes de Contractions dans les Espaces de Hilbert," *Math. Studies 5*, North-Holland, Amsterdam, Netherlands, 1973.
- [44] H. H. Bauschke and P. L. Combettes, "Convex analysis and monotone operator theory in hilbert spaces," *CMS Books in Mathematics*, Springer, New York, NY, USA, 2011.
- [45] B. Tan, Z. Zhou, and S. Li, "Viscosity-type inertial extragradient algorithms for solving variational inequality problems and fixed point problems," *Journal of Applied Mathematics and Computing*, vol. 68, no. 2, pp. 1387–1411, 2022.
- [46] H. K. Xu, "Iterative algorithms for nonlinear operators," *Journal of the London Mathematical Society*, vol. 66, no. 1, pp. 240–256, 2002.
- [47] P. E. Maingé, "Strong convergence of projected subgradient methods for nonsmooth and nonstrictly convex minimization," *Set-Valued Analysis*, vol. 16, no. 7–8, pp. 899–912, 2008.
- [48] J. Yang and H. Liu, "Strong convergence result for solving monotone variational inequalities in Hilbert space," *Numerical Algorithms*, vol. 80, no. 3, pp. 741–752, 2019.
- [49] P. L. Combettes and V. R. Wajs, "Signal recovery by proximal forward-backward splitting," *Multiscale Modeling and Simulation*, vol. 4, pp. 1168–1200, 2005.
- [50] R. Suparatulorn, W. Cholamjiak, A. Gibali, and T. Mouktonglang, "A parallel Tseng's splitting method for solving common variational inclusion applied to signal recovery problems," *Advances in Difference Equations*, vol. 2021, no. 1, p. 492, 2021.

Research Article

Bifurcations in a Plant-Pollinator Model with Multiple Delays

Long Li ¹, Yanxia Zhang ¹, Jianfei Yao,² and Xiuxing Wu²

¹*School of Mathematics and Big Data, Chongqing University of Education, Chongqing 400065, China*

²*Chongqing No. 2 Foreign Language School, Chongqing 400065, China*

Correspondence should be addressed to Yanxia Zhang; zhangyx@cque.edu.cn

Received 10 October 2022; Revised 1 February 2023; Accepted 6 April 2023; Published 17 May 2023

Academic Editor: Watcharaporn Cholamjiak

Copyright © 2023 Long Li et al. This is an open access article distributed under the Creative Commons Attribution License, which permits unrestricted use, distribution, and reproduction in any medium, provided the original work is properly cited.

The plant-pollinator model is a common model widely researched by scholars in population dynamics. In fact, its complex dynamical behaviors are universally and simply expressed as a class of delay differential-difference equations. In this paper, based on several early plant-pollinator models, we consider a plant-pollinator model with two combined delays to further describe the mutual constraints between the two populations under different time delays and qualitatively analyze its stability and Hopf bifurcation. Specifically, by selecting different combinations of two delays as branch parameters and analyzing in detail the distribution of roots of the corresponding characteristic transcendental equation, we investigate the local stability of the positive equilibrium point of equations, derive the sufficient conditions of asymptotic stability, and demonstrate the Hopf bifurcation for the system. Under the condition that two delays are not equal, some explicit formulas for determining the direction of Hopf bifurcation and some conditions for the stability of periodic solutions of bifurcation are obtained for delay differential equations by using the theory of norm form and the theorem of center manifold. In the end, some examples are presented and corresponding computer numerical simulations are taken to demonstrate and support effectiveness of our theoretical predictions.

1. Introduction

It is estimated that there are about 3,50,000 plant species in the nature world, which are classified as seed plants, bryophytes, ferns, and algae. Until 2004, almost certainly over 2,87,655 species had been identified, including 2,58,650 flowering plants, 16,000 bryophytes, 11,000 ferns, and 8000 green algae. Obviously, the flowering plants, accounting for about 90%, make up the majority of the identified plants. It indicated that most of flowering plants rely on some certain medium to transmit pollen, and 90% of medium are animals, especially insects, except for a few by wind and water. Therefore, the research on the interaction between plants and pollinators has important application value in biodiversity conservation and agriculture.

Pollinators are an important part of the ecosystem; their species composition, quantity change, and pollination objects directly or indirectly reflect the ecological environment and its development trend. In addition, they also provide important ecological services for the ecosystem, which plays an important role in maintaining the dynamic balance and

relative stability of the ecosystem. The plant pollinator population system, as an important branch of population ecology, has been a hot issue in the field of biomathematics for half a century. Discussing about the dynamic characteristics between plants and pollinators has real significance in biodiversity conservation, species origin and formation mechanism, and agricultural production. It suggested that the species categories and ecological evolution processes of organisms are diverse. There are complex interactive relationships between plants and pollinators, including reciprocity, hostility, and defense that are generally expressed by differential equation models.

It is a hot topic on the plant-pollinator population dynamics for a half century. As early as 1976, considering about saturation effects of the benefits that the plant derives from the pollinator, May proposed a model of an obligate relationship between a plant and its pollinator and discussed the curvilinear isoclines with stabilizing effect [1, 2]. In 1981, Soberon et al. presented a mathematical model describing the dynamics of the plant-pollinator dynamical interaction with function response. They mainly considered the effects

of two parameters on the stability of their system, including the nectar reward provided by plants to pollinators and the specificity of pollinators to plants [3]. In 1955, Lundberg and Ingvarsson [4] generalized an earlier model of the interactions between plants and pollinators and analyzed the equilibrium points of the system. It showed that there is a threshold standard in the system, which would not last long when it is lower than the standard, and the impact of the existence of the threshold standard on the persistence of plants was further discussed.

After then, some dynamic models of three population interactions appeared, such as the herbivore-plant-pollinator interactions proposed by Jang [5] and the plant-pollinator-robber system raised by Wang et al. [6, 7]. In [5], by analyzing the parameter energy reward and the specificity of pollinators to plants, Jang et al. considered the effect of herbivores on the pollinator's flower visiting rate and further discussed the possible mechanism of herbivores accompanying pollinators to increase the pollinator's flower visiting rate. The results showed that this mechanism could promote the persistence of the interaction between the three populations. The literature [6, 7] focused on the factors that led to the widespread occurrence and stability of interaction by analyzing the mathematical model of plant-pollinator-robber coexistence and dynamic properties by using the relevant theory of the dynamic system. Fishman and Hadany formulated and discussed a multigeneration population dynamics model for plants' interaction with central place pollinators [8]. In [9], Wang et al. investigated a plant-pollinator model with diffusion and analyzed the uniqueness and stability of positive steady state solution by using the regular perturbation theorem and the monotone dynamical system theory. However, in these existing mathematical models, most researchers did not consider the time delay factor. Due to its inevitability and importance, the influence of time delay on dynamic behavior has been adequately considered in some models, such as the predator-prey model [10–14], the competition and cooperation model of two enterprises [15–19], the neuron network model [20–22], the competition model of internet [23, 24], the chemical reaction model [25, 26], and the epidemic model [27–31]. The introduction of the delay factor can more accurately reflect the objective facts and development laws of things. Therefore, most of the scholars tend to be more interested in analyzing the delay differential system when analyzing the differential equation model.

In [7], Wang et al. derived a classical plant-pollinator model.

$$\begin{cases} \frac{dN_1}{dt} = r_1 N_1 + \frac{\alpha_{12} N_1 N_2}{1 + aN_1 + bN_2} - \beta_1 N_1 N_2 - d_1 N_1^2, \\ \frac{dN_2}{dt} = \frac{\alpha_{21} N_1 N_2}{1 + aN_1 + bN_2} - d_2 N_2, \end{cases} \quad (1)$$

where $a, b, r_1, \beta_1, d_1, d_2, \alpha_{12}$, and α_{21} are the positive constants. $N_1(t)$ denotes the population densities of plants,

$N_2(t)$ denotes the population densities of pollinators, r_1 represents the intrinsic growth rate of plants, d_1 is the self-incompatible degree, a is the effective equilibrium constant for plant-pollinator interactions, b is the intensity of exploitation competition among pollinators, α_{12} represents the plants efficiency in translation plant-pollinator interactions into fitness, α_{21} is the corresponding value for the pollinators, β_1 denotes the per-capita negative effect of pollinators on plants, and d_2 is the per-capita mortality rate of pollinators.

Recently, Huang et al. [32] considered the following plant-pollinator model with a diffusion term and a time delay:

$$\begin{cases} \frac{\partial N_1}{\partial t} = N_1 \left[r_1 + \frac{\alpha_{12} N_2}{1 + aN_1 + bN_2} - \beta_1 N_2 - d_1 N_1 \right], \\ \frac{\partial N_2}{\partial t} = D_2 \Delta N_2 + N_2 \left[\frac{\alpha_{21} N_1(t - \tau, x)}{1 + aN_1(t - \tau, x) + bN_2(t - \tau, x)} - d_2 \right], \end{cases} \quad (2)$$

where $\tau > 0$ is a time delay, Δ is the Laplacian operator, and $D_2 > 0$ is a diffusion coefficient. By analyzing eigenvalues of the linearized equation, Huang et al. gave some conditions about the stability of the positive constant steady state and existence of spatially homogeneous and spatially inhomogeneous periodic solutions.

Based on (1) and (2), we incorporate two different delays into the model to reflect the dynamical behaviours depending on the histories. We shall consider the following system:

$$\begin{cases} \frac{dN_1}{dt} = r_1 N_1 + \frac{\alpha_{12} N_1 N_2}{1 + aN_1 + bN_2} - \beta_1 N_1 N_2 - d_1 N_1^2, \\ \frac{dN_2}{dt} = N_2 \left[\frac{\alpha_{21} N_1(t - \tau_1)}{1 + aN_1(t - \tau_1) + bN_2(t - \tau_2)} - d_2 \right], \\ N_1(t) = \phi(t), N_2(t) = \psi(t), t \in \left[-\max_{i=1,2} \{\tau_i\}, 0 \right], \end{cases} \quad (3)$$

where $\tau_i \geq 0$ ($i = 1, 2$) denotes the delay effects in the process when the pollinators translate plant-pollinator interactions into the fitness.

The present article is organized as follows: In Section 2, by selecting two different varying delays τ_i ($i = 1, 2$) as the bifurcation parameters and considering the distribution of corresponding characteristic roots, we shall give the conditions on the stability of the positive equilibrium and the existence of Hopf bifurcation of system (3). In Section 3, based on the normal form method and the center manifold reduction used by Hassard et al. in [33], we shall derive some formulas for deciding the stability and the directions of periodic solutions and Hopf bifurcation. In Section 4, some numerical simulations are carried out to illustrate the validity of the main results.

2. Model Description

In this section, we shall mainly analyze the local stability of the positive constant steady state and the existence of Hopf bifurcation of system (3) by using the methods in [32, 34, 35].

According to [32], for the existence and uniqueness of the positive equilibrium of (3), we have the following result:

Lemma 1. Assume that one of the following conditions holds:

(A1) $\alpha_{21} > ad_2, a_1 < 0, a_1^2 - 4a_0a_2 = 0;$

(A2) $\alpha_{21} > ad_2, 4a_0a_2 < 0;$

where $a_0 = b\beta_1/(\alpha_{21} - ad_2) + d_1d_2b^2/(\alpha_{21} - ad_2)^2, a_1 = (\beta_1 - br_1)/(\alpha_{21} - ad_2) + 2d_1d_2b/(\alpha_{21} - ad_2)^2 - \alpha_{12}/\alpha_{21},$ and

$$a_2 = \frac{r_1}{\alpha_{21} - ad_2} + \frac{d_1d_2}{(\alpha_{21} - ad_2)^2}. \tag{4}$$

Then, (3) has two boundary equilibria, $E_0(0, 0)$ and $E_1(r_1/d_1, 0),$ and a unique positive equilibrium, $E^*(N_1^*, N_2^*),$ where

$$N_1^* = \frac{2a_0d_2 - a_1bd_2 + bd_2\sqrt{a_1^2 - 4a_0a_2}}{2a_0(\alpha_{21} - ad_2)}, \tag{5}$$

$$N_2^* = \frac{-a_1 + \sqrt{a_1^2 - 4a_0a_2}}{2a_0}.$$

Let $u_1 = N_1 - N_1^*$ and $u_2 = N_2 - N_2^*,$ then (3) can be rewritten as follows:

$$\begin{cases} \frac{du_1}{dt} = (u_1 + N_1^*) \left[r_1 + \frac{\alpha_{12}(u_2 + N_2^*)}{1 + a(u_1 + N_1^*) + b(u_2 + N_2^*)} - \beta_1(u_2 + N_2^*) - d_1(u_1 + N_1^*) \right], \\ \frac{du_2}{dt} = (u_2 + N_2^*) \left[\frac{\alpha_{21}(u_1(t - \tau_1) + N_1^*)}{1 + a(u_1(t - \tau_1) + N_1^*) + b(u_2(t - \tau_2) + N_2^*)} - d_2 \right], \\ u_1(t) = \phi(t) - N_1^*, u_2(t) = \psi(t) - N_2^*, t \in \left[-\max_{i=1,2}\{\tau_i\}, 0 \right]. \end{cases} \tag{6}$$

Thus, the positive equilibrium point $E^*(N_1^*, N_2^*)$ of system (3) coincides with the zero equilibrium of system (6).

Let

$$f^{(1)}(u_1, u_2) = (u_1 + N_1^*) \left[r_1 + \frac{\alpha_{12}(u_2 + N_2^*)}{1 + a(u_1 + N_1^*) + b(u_2 + N_2^*)} - \beta_1(u_2 + N_2^*) - d_1(u_1 + N_1^*) \right], \tag{7}$$

$$f^{(2)}(u_1, u_2, w) = (w + N_2^*) \left[\frac{\alpha_{21}(u_1 + N_1^*)}{1 + a(u_1 + N_1^*) + b(u_2 + N_2^*)} - d_2 \right].$$

For $i, j, l \in N_0 = \{0, 1, 2, \dots\},$ we define $f_{ij}^{(1)} (i + j \geq 1)$ and $f_{ijl}^{(2)} (i + j + l \geq 1)$ as follows: in particular.

$$f_{ij}^{(1)} = \frac{\partial^{i+j} f^{(1)}(0, 0)}{\partial u_1^i \partial u_2^j}, f_{ijl}^{(2)} = \frac{\partial^{i+j+l} f^{(2)}(0, 0, 0)}{\partial u_1^i \partial u_2^j \partial w^l}, \tag{8}$$

$$\alpha_1 = f_{10}^{(1)} = -d_1N_1^* - \frac{\alpha_{12}aN_1^*N_2^*}{(1 + aN_1^* + bN_2^*)^2} < 0, \alpha_2 = f_{01}^{(1)} = \frac{\alpha_{12}N_1^*(1 + aN_1^*)}{(1 + aN_1^* + bN_2^*)^2} - \beta_1N_1^*, \tag{9}$$

$$\gamma_1 = f_{100}^{(2)} = \frac{\alpha_{21}N_2^*(1 + bN_2^*)}{(1 + aN_1^* + bN_2^*)^2} > 0, \gamma_2 = f_{010}^{(2)} = -\frac{b\alpha_{21}N_1^*N_2^*}{(1 + aN_1^* + bN_2^*)^2} < 0.$$

By Taylor expansion, (6) can become as follows:

$$\begin{cases} \frac{du_1}{dt} = \alpha_1 u_1(t) + \alpha_2 u_2(t) + \sum_{i+j \geq 2} \frac{1}{i!j!} f_{ij}^{(1)} u_1^i(t) u_2^j(t), \\ \frac{du_2}{dt} = \gamma_1 u_1(t - \tau_1) + \gamma_2 u_2(t - \tau_2) + \sum_{i+j+l \geq 2} \frac{1}{i!j!l!} f_{ijl}^{(2)} u_1^i(t - \tau_1) u_2^j(t - \tau_2) u_2^l(t), \end{cases} \quad (10)$$

and $u_1(t) = \phi(t) - N_1^*, u_2(t) = \psi(t) - N_2^*, t \in [-\max\{\tau_i\}, 0]$.

It is easy to see that system (10) about the equilibrium point $(0, 0)$ yields the following linear system:

$$\begin{cases} \frac{du_1}{dt} = \alpha_1 u_1(t) + \alpha_2 u_2(t), \\ \frac{du_2}{dt} = \gamma_1 u_1(t - \tau_1) + \gamma_2 u_2(t - \tau_2). \end{cases} \quad (11)$$

The corresponding characteristic equation of the system (11) is as follows:

$$\lambda^2 - \alpha_1 \lambda - (\gamma_2 \lambda - \gamma_2 \alpha_1) e^{-\lambda \tau_2} - \gamma_1 \alpha_2 e^{-\lambda \tau_1} = 0. \quad (12)$$

We use the following Lemma in [35] to investigate the distribution of roots of the transcendental equation (12).

Lemma 2. For the transcendental equation,

$$\begin{aligned} P(\lambda, e^{-\lambda \tau_1}, \dots, e^{-\lambda \tau_m}) &= \lambda^n + p_1^{(0)} \lambda^{n-1} + \dots + p_{n-1}^{(0)} \lambda + p_n^{(0)} \\ &+ [p_1^{(1)} \lambda^{n-1} + \dots + p_{n-1}^{(1)} \lambda + p_n^{(1)}] e^{-\lambda \tau_1} \\ &+ \dots + [p_1^{(m)} \lambda^{n-1} + \dots + p_{n-1}^{(m)} \lambda + p_n^{(m)}] e^{-\lambda \tau_m} \\ &= 0. \end{aligned} \quad (13)$$

As $(\tau_1, \tau_2, \tau_3, \dots, \tau_m)$ vary, the sum of orders of the zeros of $P(\lambda, e^{-\lambda \tau_1}, \dots, e^{-\lambda \tau_m})$ in the open right half plane can change only if a zero appears on or crosses the imaginary axis.

Now, we shall consider the following different cases:

Case 1. $\tau_1 = \tau_2 = 0$. Then, (12) becomes

$$\lambda^2 - (\alpha_1 + \gamma_2) \lambda + \gamma_2 \alpha_1 - \gamma_1 \alpha_2 = 0. \quad (14)$$

Since $\alpha_1 < 0, \gamma_2 < 0, -(\alpha_1 + \gamma_2) > 0$ holds. It is obvious that when $\tau_1 = \tau_2 = 0$, the condition that all roots of (14) have negative real parts is given in the following form:

$$(H1): \gamma_2 \alpha_1 - \gamma_1 \alpha_2 > 0 \quad (15)$$

Thus, we have the following result:

Lemma 3. Assume that (H1) holds. Then, for $\tau_1 = \tau_2 = 0$, the positive equilibrium point E^* of (3) is asymptotically stable.

Case 2. $\tau_1 > 0, \tau_2 = 0$. Then, (12) becomes

$$\lambda^2 - (\alpha_1 + \gamma_2) \lambda + \gamma_2 \alpha_1 - \gamma_1 \alpha_2 e^{-\lambda \tau_1} = 0. \quad (16)$$

Suppose that $\tau_1 > 0, \tau_2 = 0$ and $\lambda = i\omega_1$ ($\omega_1 > 0$) are roots of (16). Then, we have

$$\begin{aligned} -\omega_1^2 - i\omega_1(\alpha_1 + \gamma_2) + \gamma_2 \alpha_1 \\ - \gamma_1 \alpha_2 (\cos \omega_1 \tau_1 - i \sin \omega_1 \tau_1) = 0. \end{aligned} \quad (17)$$

Separating the real and imaginary parts of (17), we can obtain

$$\begin{cases} \omega_1^2 - \gamma_2 \alpha_1 = -\gamma_1 \alpha_2 \cos \omega_1 \tau_1, \\ \omega_1 (\alpha_1 + \gamma_2) = \gamma_1 \alpha_2 \sin \omega_1 \tau_1. \end{cases} \quad (18)$$

By simple calculation, we can have

$$\omega_1^4 + (\alpha_1^2 + \gamma_2^2) \omega_1^2 + (\gamma_2 \alpha_1)^2 - (\gamma_1 \alpha_2)^2 = 0. \quad (19)$$

Let $z = \omega_1^2$, then (19) becomes

$$z^2 + (\alpha_1^2 + \gamma_2^2) z + (\gamma_2 \alpha_1)^2 - (\gamma_1 \alpha_2)^2 = 0. \quad (20)$$

Notice that $\alpha_1^2 + \gamma_2^2 > 0$. If the following condition (H2): $(\gamma_2 \alpha_1)^2 - (\gamma_1 \alpha_2)^2 > 0$ holds, then (20) has no positive solution. Thus, all solutions of (16) have negative real parts when $\tau_1 > 0$ under (H2). So, we have the following result:

Theorem 1. Let $\tau_2 = 0$ and (A1) or (A2) holds. When (H2) holds, the positive equilibrium point E^* of (3) is asymptotically stable for all $\tau_1 > 0$.

However, if the condition (H3): $(\gamma_2 \alpha_1)^2 - (\gamma_1 \alpha_2)^2 < 0$ holds, then (20) has a unique positive root.

$$z_0 = \omega_{10}^2 = \frac{1}{2} \left[-(\alpha_1^2 + \gamma_2^2) + \sqrt{(\alpha_1^2 - \gamma_2^2)^2 + 4\gamma_1^2 \alpha_2^2} \right]. \quad (21)$$

Thus, $\omega_{10} = \{1/2 [-(\alpha_1^2 + \gamma_2^2) + \sqrt{(\alpha_1^2 - \gamma_2^2)^2 + 4\gamma_1^2 \alpha_2^2}]\}^{1/2}$, and (16) has a pair of purely imaginary roots $\pm i\omega_{10}$. Substituting ω_{10} into (18), we can get

$$\tau_{1j} = \frac{1}{\omega_{10}} \arccos \left\{ \frac{\omega_{10}^2 - \gamma_2 \alpha_1}{-\gamma_1 \alpha_2} \right\} + \frac{2j\pi}{\omega_{10}}, \quad (j \in \mathbb{N}_0). \quad (22)$$

Let

$$F(\lambda, \tau_1) = \lambda^2 - (\alpha_1 + \gamma_2) \lambda + \gamma_2 \alpha_1 + \gamma_1 \alpha_2 e^{-\lambda \tau_1}. \quad (23)$$

Then, $F(\pm i\omega_{10}, \tau_{1j}) = 0$. Suppose $\lambda(\tau_1) = \alpha(\tau_1) + i\omega(\tau_1)$ is a root of (16) near $\tau_1 = \tau_{1j}$ and $\alpha(\tau_{1j}) = 0, \omega(\tau_{1j}) = \omega_{10}$. From the function differential equation (FDE) theory, for every τ_{1j} ($j = 0, 1, 2, \dots$) there exists $\varepsilon > 0$, such that $\lambda(\tau_1)$ is continuously differentiable at τ_1 for $|\tau_1 - \tau_{1j}| < \varepsilon$. Substituting $\lambda(\tau_1)$ into the left-hand side of (16) and differentiating with respect to τ_1 , we can have

$$\left(\frac{d\lambda}{d\tau_1}\right)^{-1} = \frac{[2\lambda - (\alpha_1 + \gamma_2)]e^{\lambda\tau_1}}{-\lambda\gamma_1\alpha_2} - \frac{\tau_1}{\lambda}. \tag{24}$$

Hence,

$$\left(\frac{d\lambda}{d\tau_1}\right)^{-1}\Big|_{\tau_1=\tau_{1j}} = \frac{[2i\omega_{10} - (\alpha_1 + \gamma_2)](\cos \omega_{10}\tau_{1j} + i \sin \omega_{10}\tau_{1j})}{-i\omega_{10}\gamma_1\alpha_2} - \frac{\tau_{1j}}{i\omega_{10}}. \tag{25}$$

Noting that,

$$\left\{\frac{d(\operatorname{Re}\lambda)}{d\tau_1}\right\}^{-1}\Big|_{\tau_1=\tau_{1j}} = \frac{2\omega_{10}^2 + \alpha_1^2 + \gamma_2^2}{(\gamma_1\alpha_2)^2} > 0. \tag{26}$$

From the above discussions, we can get $d(\operatorname{Re}\lambda)/d\tau_1|_{\tau_1=\tau_{1j}} > 0$ and derive the following theorem:

Theorem 2. For $\tau_2 = 0$, we assume that (A1) or (A2) holds. Assume further that (H3) holds. The following conclusions are true:

- (i) If $\tau_1 \in [0, \tau_{10})$, then the positive equilibrium E^* of (3) is asymptotically stable
- (ii) If $\tau_1 > \tau_{10}$, then the positive equilibrium E^* of (3) is unstable
- (iii) If $\tau_1 = \tau_{10}$, then system (3) undergoes a Hopf bifurcation at the positive equilibrium E^*

Case 3. $\tau_1 = 0, \tau_2 > 0$. Then, (12) becomes

$$\lambda^2 - \alpha_1\lambda - \gamma_1\alpha_2 - (\gamma_2\lambda - \gamma_2\alpha_1)e^{-\lambda\tau_2} = 0. \tag{27}$$

Similar to the second case, we suppose that $\tau_1 = 0, \tau_2 > 0$ and $\lambda = i\omega_2$ ($\omega_2 > 0$) is a root of (27). Through some calculations, we can get

$$z^2 + (\alpha_1^2 + 2\gamma_1\alpha_2 - \gamma_2^2)z + (\gamma_1\alpha_2)^2 - (\gamma_2\alpha_1)^2 = 0, \tag{28}$$

where $z = \omega_2^2$. It is easy to see that if the condition (H4): $\alpha_1^2 + 2\gamma_1\alpha_2 - \gamma_2^2 > 0, (\gamma_1\alpha_2)^2 - (\gamma_2\alpha_1)^2 > 0$ holds, (28) has no positive solution. Thus, all solutions of (27) have negative real parts when $\tau_2 > 0$ under (H4).

Theorem 3. Let $\tau_1 = 0$ and (A1) or (A2) holds. When (H4) holds, then the positive equilibrium E^* of system (3) is asymptotically stable for all $\tau_2 > 0$.

However, if the condition

(H5): $\alpha_1^2 + 2\gamma_1\alpha_2 - \gamma_2^2 > 0, (\gamma_1\alpha_2)^2 - (\gamma_2\alpha_1)^2 < 0$ holds, then (28) has a unique positive solution $z_0 = \omega_{20}^2$ and (27) has a pair of purely imaginary roots $\pm i\omega_{20}$, where

$$\omega_{20} = \left\{\frac{1}{2}\left[-(\alpha_1^2 + 2\gamma_1\alpha_2 - \gamma_2^2) + \sqrt{(\alpha_1^2 + 2\gamma_1\alpha_2 - \gamma_2^2)^2 - 4(\gamma_1^2\alpha_2^2 - \gamma_2^2\alpha_1^2)}\right]\right\}^{1/2}. \tag{29}$$

At this time, we have

$$\tau_{2j} = \frac{1}{\omega_{20}} \arccos\left\{\frac{\gamma_1\alpha_1\alpha_2}{\gamma_2(\omega_{20}^2 + \alpha_1^2)}\right\} + \frac{2j\pi}{\omega_{20}}, j \in \mathbb{N}_0. \tag{30}$$

Let $F(\lambda, \tau_2) = \lambda^2 - \alpha_1\lambda + \gamma_1\alpha_2 + (-\gamma_2\lambda + \gamma_2\alpha_1)e^{-\lambda\tau_2}$, then $F(\pm i\omega_{20}, \tau_{2j}) = 0$.

Suppose $\lambda(\tau_2) = \alpha(\tau_2) + i\omega(\tau_2)$ is a root of (27) near $\tau_2 = \tau_{2j}$ and $\alpha(\tau_{2j}) = 0$, then $\omega(\tau_{2j}) = \omega_{20}$. Substituting $\lambda(\tau_2)$ into (27) and differentiating with respect to τ_2 , we can obtain

$$\left(\frac{d\lambda}{d\tau_2}\right)^{-1} = \frac{(2\lambda - \alpha_1)e^{\lambda\tau_2} - \gamma_2 - \tau_2}{(\gamma_2\alpha_1 - \gamma_2\lambda)\lambda},$$

$$\left(\frac{d\lambda}{d\tau_2}\right)^{-1}\Big|_{\tau_2=\tau_{2j}} = \frac{(2i\omega_{20} - \alpha_1)(\cos \omega_{20}\tau_{2j} + i \sin \omega_{20}\tau_{2j}) - \gamma_2 - \tau_{2j}}{(\gamma_2\alpha_1 - i\omega_{20}\gamma_2)i\omega_{20}} - \frac{\tau_{2j}}{i\omega_{20}} \left\{ \frac{d(\operatorname{Re}\lambda)}{d\tau_2} \right\}^{-1}\Big|_{\tau_2=\tau_{2j}} = \frac{2\gamma_1\alpha_2 - \gamma_2^2 + \alpha_1^2 + 2\omega_0^2}{\gamma_2^2(\omega_0^2 + \alpha_1^2)} > 0. \tag{31}$$

Therefore, we can easily get $d(\operatorname{Re}\lambda)/d\tau_2|_{\tau_2=\tau_{2j}} > 0$. Based on the above analysis, we have the following theorem:

Theorem 4. For $\tau_1 = 0$, assume that (A1) or (A2) holds. Assume further that (H5) holds. The following results are true:

- (i) If $\tau_2 \in [0, \tau_{20})$, then the positive equilibrium E^* of (3) is asymptotically stable
- (ii) If $\tau_2 > \tau_{20}$, then the positive equilibrium E^* of (3) is unstable
- (iii) If $\tau_2 = \tau_{20}$, then system (3) undergoes a Hopf bifurcation at the positive equilibrium E^*

Case 4. $\tau_1 > 0, \tau_2 \in [0, \tau_{20}]$. We consider (12) with τ_2 in its stable interval. Regarding τ_1 as a parameter, without loss of

generality, we consider system (3) under assumption (A1) or (A2) and Case 3. Let $i\omega (\omega > 0)$ be a root of (12), by calculating, we can obtain

$$\omega^4 + k_1\omega^3 + k_2\omega^2 + k_3\omega + k_4 = 0, \tag{32}$$

where $k_1 = 2\gamma_2 \sin \omega\tau_2, k_2 = \gamma_2^2 + \alpha_1^2, k_3 = 2\gamma_2\alpha_1^2 \sin \omega\tau_2, k_4 = (\gamma_2\alpha_1)^2 - (\gamma_1\alpha_2)^2$.

Denoting $H(\omega) = \omega^4 + k_1\omega^3 + k_2\omega^2 + k_3\omega + k_4$, we make the assumption that

(H6): equation (32) has finite positive roots $\omega_1, \omega_2, \dots, \omega_n$, and for every fixed $\omega_i, i = 1, 2, \dots, k$, there exists a sequence $\{\tau_{3i}^j | j = 0, 1, 2, \dots\}$, such that (32) holds, where

$$\tau_{3i}^j = \frac{1}{\omega_3^{(i)}} \arccos \frac{-(\omega_3^{(i)})^2 + \gamma_2\alpha_1 \cos \omega_3^{(i)}\tau_2 - \gamma_2\omega_3^{(i)} \sin \omega_3^{(i)}\tau_2}{\alpha_2\gamma_1} + \frac{2\pi j}{\omega_3^{(i)}}. \tag{33}$$

$$i = 1, 2, \dots, k; j = 0, 1, 2, \dots$$

Let

$$\tau_{30} = \min \left\{ \tau_{3i}^j \mid i = 1, 2, \dots, k; j = 0, 1, 2, \dots \right\}. \tag{34}$$

When $\tau_1 = \tau_{30}$, (12) has a pair of purely imaginary roots $\pm i\omega^*$ for $\tau_2 \in [0, \tau_{20}]$. In the following, we further assume that (H7): $[d(\operatorname{Re}\lambda)/d\tau_1]_{\tau_1=\tau_{30}} \neq 0$. By the general Hopf bifurcation theorem for FDE, we have a result on the stability and Hopf bifurcation for system (3).

Theorem 5. For system (3), we assume that (A1) or (A2) holds and assume further that (H5), (H6), and (H7) are satisfied, and $\tau_2 \in [0, \tau_{20})$. Then, the positive equilibrium E^* is asymptotically stable for $\tau_1 \in (0, \tau_{30})$ and is unstable for

$\tau_1 \in (\tau_{30}, +\infty)$. System (3) undergoes a Hopf bifurcation at the E^* for $\tau_1 = \tau_{30}$.

Case 5. $\tau_2 > 0, \tau_1 \in [0, \tau_{10}]$. We consider (12) with τ_1 in its stable interval. Regarding τ_2 as a parameter, without loss of generality, we consider system (3) under assumption (A1) or (A2) and Case 2. Let $i\omega (\omega > 0)$ be a root of (12), by calculating, we can obtain

$$\omega^4 + k_1\omega^2 + k_2\omega + k_3 = 0, \tag{35}$$

where $k_1 = \alpha_1^2 - \gamma_2^2 + 2\gamma_1\alpha_2 \cos \omega\tau_1, k_2 = -2\gamma_1\alpha_1\alpha_2 \sin \omega\tau_1, k_3 = (\gamma_1\alpha_2)^2 - (\gamma_2\alpha_1)^2$. Denoting $H(\omega) = \omega^4 + k_1\omega^2 + k_2\omega + k_3$, we make the assumption that (H8): equation (35) has finite positive roots $\omega_1, \omega_2, \dots, \omega_n$, and for every fixed $\omega_i, i = 1, 2, \dots, k$, there exists a sequence $\{\tau_{4i}^j | j = 0, 1, 2, \dots\}$ such that (35) holds, where

$$\tau_{4i}^j = \frac{1}{\omega_4^{(i)}} \arccos \frac{-(\omega_4^{(i)})^2 + \gamma_2 \alpha_1 \cos \omega_4^{(i)} \tau_2 - \gamma_2 \omega_4^{(i)} \sin \omega_4^{(i)} \tau_2}{\alpha_2 \gamma_1} + \frac{2\pi j}{\omega_4^{(i)}}. \tag{36}$$

$$i = 1, 2, \dots, k; j = 0, 1, 2, \dots$$

Let

$$\tau_{40} = \min \left\{ \tau_{4i}^j \mid i = 1, 2, \dots, k; j = 0, 1, 2, \dots \right\}. \tag{37}$$

When $\tau_2 = \tau_{40}$, (12) has a pair of purely imaginary roots $\pm i\omega^*$ for $\tau_1 \in [0, \tau_{10}]$. In the following, we further assume that (H9): $[d(\text{Re}\lambda)/d\tau_2]_{\tau_2=\tau_{40}} \neq 0$. Similarly, we have a result on the stability and Hopf bifurcation for system (3).

Theorem 6. *For system (3), assume that (A1) or (A2) holds and further assume that (H8) and (H9) are satisfied, and $\tau_1 \in [0, \tau_{10})$. Then, the positive equilibrium E^* is asymptotically stable for $\tau_2 \in (0, \tau_{40})$ and is unstable for $\tau_2 \in (\tau_{40}, +\infty)$. System (3) undergoes a Hopf bifurcation at the E^* for $\tau_2 = \tau_{40}$.*

3. Direction of Hopf Bifurcation and Stability of Bifurcating Periodic Solution

In the previous section, we have obtained stability and existence of Hopf bifurcation of system (3) at the positive

equilibrium E^* by taking delay τ_i ($i = 1, 2$) as the bifurcation parameter and applying the linearization method. In the present section, we will discuss the direction of Hopf bifurcation and the stability of bifurcation periodic solutions by employing the normal form method and the center manifold theorem by Hassard et al. [33]. We always assume that system (3) undergoes Hopf bifurcation at the positive equilibrium E^* for $\tau_2 = \tau_{20}$, and $\pm i\omega^*$ denotes the corresponding purely imaginary roots of the characteristic equation at E^* .

Without loss of generality, we assume $\tau_1^* < \tau_{40}$, where $\tau_1^* \in (0, \tau_{40})$ and τ_{40} is defined by (37). For convenience, let $\bar{u}_i(t) = u_i(\tau t)$, $u_i(t) = N_i(t) - N_i^*$, ($i = 1, 2$), $\tau_2 = \tau_{40} + \mu$, and $\mu \in \mathbb{R}$, then $\mu = 0$ is the Hopf bifurcation value of (3). Thus, (3) can be rewritten as an FDE in $C = C([-1, 0], \mathbb{R}^2)$ as follows:

$$\dot{u}(t) = L_\mu(u_t) + F(\mu, u_t), \tag{38}$$

where $u(t) = (u_1(t), u_2(t))^T \in C$ and $u_t(\theta) = u(t + \theta)$.

Define the linear operator $L_\mu: C \rightarrow \mathbb{R}$ by

$$L_\mu(\phi) = (\tau_{40} + \mu) \left[B \begin{pmatrix} \phi_1(0) \\ \phi_2(0) \end{pmatrix} + C \begin{pmatrix} \phi_1\left(-\frac{\tau_1^*}{\tau_{40}}\right) \\ \phi_2\left(-\frac{\tau_1^*}{\tau_{40}}\right) \end{pmatrix} + D \begin{pmatrix} \phi_1(-1) \\ \phi_2(-1) \end{pmatrix} \right], \tag{39}$$

and nonlinear operator $F(\mu, \cdot): \mathbb{R} \times C \rightarrow \mathbb{R}$ by

$$F(\mu, \phi) = (\tau_{40} + \mu)(f_1, f_2)^T, \tag{40}$$

where $\phi(\theta) = (\phi_1(\theta), \phi_2(\theta))^T \in C$, $B = \begin{pmatrix} \alpha_1 & \alpha_2 \\ 0 & 0 \end{pmatrix}$,

$C = \begin{pmatrix} 0 & 0 \\ 0 & \gamma_2 \end{pmatrix}$, $D = \begin{pmatrix} 0 & 0 \\ \gamma_1 & 0 \end{pmatrix}$, and

$$f_1 = \sum_{i+j \geq 2} \frac{1}{i!j!} f_{ij}^{(1)} \phi_1^i(0) \phi_2^j(0), \tag{41}$$

$$f_2 = \sum_{i+j+l \geq 2} \frac{1}{i!j!l!} f_{ijl}^{(2)} \phi_1^i(-1) \phi_2^j\left(-\frac{\tau_1^*}{\tau_{40}}\right) \phi_2^l(0).$$

Based on the Riesz representation theorem, we know that there is a matrix function with bounded variation components $\eta(\theta, \mu)$ and $\theta \in [-1, 0]$, such that

$$L_\mu(\phi) = \int_{-1}^0 d\eta(\theta, \mu)\phi(\theta), \phi(\theta) \in C([-1, 0], \mathbb{R}^2). \quad (42)$$

In fact, we can take

$$\eta(\theta, \mu) = \begin{cases} (\tau_{40} + \mu)(B + C + D), & \theta = 0 \\ (\tau_{40} + \mu)(C + D), & \theta \in \left[-\frac{\tau_1^*}{\tau_{40}}, 0\right] \\ (\tau_{40} + \mu)D, & \theta \in \left(-1, -\frac{\tau_1^*}{\tau_{40}}\right) \\ 0, & \theta = -1. \end{cases} \quad (43)$$

In the sequel, we define the operators $A(\mu)$ and $R(\mu)$ by

$$A(\mu)\phi = \begin{cases} \frac{d\phi(\theta)}{d\theta}, \theta \in [-1, 0) \\ \int_{-1}^0 d\eta(s, \mu)\phi(s), \theta = 0 \end{cases}, R(\mu)\phi = \begin{cases} 0, \theta \in [-1, 0) \\ F(\mu, \phi), \theta = 0 \end{cases}. \quad (44)$$

Then, (38) can be further rewritten into the following equation:

$$\dot{u}(t) = A(\mu)u_t + R(\mu)u_t, \quad (45)$$

where $u_t(\theta) = u(t + \theta), \theta \in [-1, 0]$. For $\psi \in C([0, 1], (\mathbb{R}^2)^*)$, we define

$$A^*\psi(s) = \begin{cases} -\frac{d\psi(s)}{ds}, s \in (0, 1], \\ \int_{-1}^0 d\eta^T(t, 0)\psi(-t), s = 0. \end{cases} \quad (46)$$

For $\phi \in C([-1, 0], (\mathbb{R}^2)^*)$ and $\psi \in C([0, 1], (\mathbb{R}^2)^*)$, we define the bilinear inner product.

$$\langle \psi(s), \phi(\theta) \rangle = \bar{\psi}(0)\phi(0) - \int_{-1}^0 \int_{\xi=0}^\theta \bar{\psi}(\xi - \theta)d\eta(\theta)\phi(\xi)d\xi, \quad (47)$$

where $\eta(\theta) = \eta(\theta, 0)$. Let $A = A(0)$, then A and A^* are a pair of adjoint operators. Since $\pm i\omega^* \tau_{40}$ is a pair of eigenvalues of $A(0)$, it follows that they are also a pair of eigenvalues of A^* .

Suppose that $q(\theta) = (1, \alpha)^T e^{i\omega^* \tau_{40} \theta}$ is an eigenvector of the operator $A(0)$ corresponding to the eigenvalues $i\omega^* \tau_{40}$ and $q^*(s) = M(1, \alpha^*) e^{i\omega^* \tau_{40} s}$ is an eigenvector of $A^*(0)$ corresponding to $-i\omega^* \tau_{40}$, where $M = 1/K$. From the definitions of $A, L_\mu \phi$, and $\eta(\theta, \mu)$, we can obtain

$$\begin{pmatrix} i\omega^* - \alpha_1 & -\alpha_2 \\ -\gamma_1 e^{-\lambda \tau_1} & i\omega^* - \gamma_2 e^{-\lambda \tau_2} \end{pmatrix} \begin{pmatrix} 1 \\ \alpha \end{pmatrix} = \begin{pmatrix} 0 \\ 0 \end{pmatrix}. \quad (48)$$

Based on discussions in the last section, we can see

$$\det \begin{pmatrix} i\omega^* - \alpha_1 & -\alpha_2 \\ -\gamma_1 e^{-\lambda \tau_1} & i\omega^* - \gamma_2 e^{-\lambda \tau_2} \end{pmatrix} = 0. \quad (49)$$

Therefore, we can take $\alpha = (i\omega^* - \alpha_1)/\alpha_2$ and $\alpha^* = (-)(i\omega^* + \alpha_1)/\gamma_1 e^{-i\omega^* \tau_{40}}$.

Let $K \in C$ and $q^*(s) = M(1, \alpha^*) e^{i\omega^* \tau_{40} s}$ such that $\langle q^*(s), q(\theta) \rangle = 1$. Then, we can see that $q^*(s)$ is still an eigenvector of the operator A^* corresponding to the eigenvalue $-i\omega^* \tau_{40}$.

From the bilinear inner product of (47), we can get

$$\begin{aligned}
 \langle q^*(s), q(\theta) \rangle &= \bar{q}^*(0)q(0) - \int_{-1}^0 \int_{\xi=0}^{\theta} \bar{q}^*(\xi - \theta) d\eta(\theta) q(\xi) d\xi \\
 &= \bar{M}(1, \bar{\alpha}^*)(1, \alpha)^T - \int_{-1}^0 \int_{\xi=0}^{\theta} \bar{M}(1, \bar{\alpha}^*) e^{-i\omega^* \tau_{40}(\xi - \theta)} d\eta(\theta) (1, \alpha)^T e^{i\omega^* \tau_{40} \xi} d\xi \\
 &= \bar{M}(1, \bar{\alpha}^*)(1, \alpha)^T - \bar{M}(1, \bar{\alpha}^*) \int_{-1}^0 \int_{\xi=0}^{\theta} d\eta(\theta) (1, \alpha)^T e^{i\omega^* \tau_{40} \theta} d\xi \\
 &= \bar{M}(1, \bar{\alpha}^*)(1, \alpha)^T - \bar{M}(1, \bar{\alpha}^*) \int_{-1}^0 \theta e^{i\omega^* \tau_{40} \theta} d\eta(\theta) (1, \alpha)^T \tag{50} \\
 &= \bar{M}(1, \bar{\alpha}^*)(1, \alpha)^T - \bar{M}(1, \bar{\alpha}^*) \left[\tau_{40} B \phi(0) + \tau_{40} C \phi\left(-\frac{\tau_1^*}{\tau_{40}}\right) + \tau_{40} D \phi(-1) \right] (1, \alpha)^T \\
 &= \bar{M}(1, \bar{\alpha}^*)(1, \alpha)^T - \bar{M}(1, \bar{\alpha}^*) \left[\tau_{40} \begin{pmatrix} 0 & 0 \\ 0 & \gamma_2 \end{pmatrix} \begin{pmatrix} -\tau_1^* \\ \tau_{40} \end{pmatrix} e^{-i\omega^* \tau_1^*} - \tau_{40} \begin{pmatrix} 0 & 0 \\ \gamma_1 & 0 \end{pmatrix} e^{-i\omega^* \tau_{40}} \right] (1, \alpha)^T \\
 &= \bar{M}(1 + \alpha \bar{\alpha}^*) + \bar{M} \tau_1^* \gamma_2 \alpha \bar{\alpha}^* e^{-i\omega^* \tau_1^*} + \bar{M} \tau_{40} \gamma_1 \bar{\alpha}^* e^{-i\omega^* \tau_{40}}.
 \end{aligned}$$

Thus, we can choose \bar{K} as follows:

$$\begin{aligned}
 \bar{K} &= 1 + \alpha \bar{\alpha}^* + \tau_1^* \gamma_2 \alpha \bar{\alpha}^* e^{-i\omega^* \tau_1^*} + \tau_{40} \gamma_1 \bar{\alpha}^* e^{-i\omega^* \tau_{40}}, \\
 K &= 1 + \bar{\alpha} \alpha^* + \gamma_2 \bar{\alpha} \alpha^* \tau_1^* e^{i\omega^* \tau_1^*} + \gamma_1 \tau_{40} \alpha^* e^{i\omega^* \tau_{40}}. \tag{51}
 \end{aligned}$$

In addition, from $\langle \psi, A\phi \rangle = \langle A^* \psi, \phi \rangle$ and $A\bar{q}(\theta) = -i\omega^* \bar{q}(\theta)$, we can get

$$\begin{aligned}
 -i\omega^* \langle q^*, \bar{q} \rangle &= \langle q^*, A\bar{q} \rangle = \langle A^* q^*, \bar{q} \rangle = \langle -i\omega^* q^*, \bar{q} \rangle \\
 &= i\omega^* \langle q^*, \bar{q} \rangle. \tag{52}
 \end{aligned}$$

Hence, $\langle q^*(\theta), \bar{q}(\theta) \rangle = 0$.

Next, using the algorithms given in [4], we can calculate the projection system of (3) on the center manifold C_0 when $\mu = 0$. For the solution u_t of (38), let $z(t) = \langle q^*, u_t \rangle$, and then by (45) and (47), we can have

$$\begin{aligned}
 \dot{z}(t) &= \langle q^*, \dot{u}_t \rangle = \langle q^*, A(0)u_t + R(0)u_t \rangle = \langle q^*, A(0)u_t \rangle + \langle q^*, R(0)u_t \rangle \\
 &= \langle A^*(0)q^*, u_t \rangle + \bar{q}^*(0)F(0, u_t) \\
 &= i\omega^* \tau_{40} z + g(z, \bar{z}), \tag{53}
 \end{aligned}$$

where $g(z, \bar{z}) = \bar{q}^*(0)F(0, u_t) = g_{20}(\theta)z^2/2 + g_{11}(\theta)z\bar{z} + g_{02}(\theta)\bar{z}^2/2 + g_{21}(\theta)z^2\bar{z}/2 \dots$.

Let

$$\begin{aligned}
 W(t, \theta) &= u_t(\theta) - z(t)q(\theta) - \bar{z}(t)\bar{q}(\theta) \\
 &= u_t(\theta) - 2\text{Re}\{z(t)q(\theta)\}. \tag{54}
 \end{aligned}$$

Then, on the center manifold C_0 , we can have

$$W(t, \theta) = W(z(t), \bar{z}(t), \theta), \tag{55}$$

where

$$\begin{aligned}
 W(z, \bar{z}, \theta) &= W_{20}(\theta) \frac{z^2}{2} + W_{11}(\theta) z\bar{z} + W_{02}(\theta) \frac{\bar{z}^2}{2} \\
 &\quad + W_{30}(\theta) \frac{z^3}{6} + \dots, \tag{56}
 \end{aligned}$$

where z and \bar{z} are local coordinates for the center manifold C_0 in the directions of q^* and \bar{q}^* . Noting that W is real if u_t is real. We consider only real solution. From (54), we can see

$$\begin{aligned}
u_t(\theta) &= W(t, \theta) + 2\operatorname{Re}\{z(t)q(\theta)\} = W(t, \theta) + z(t)q(\theta) + \bar{z}(t)\bar{q}(\theta) \\
&= (1, \alpha)^T e^{i\omega^* \tau_{40} \theta} z + (1, \bar{\alpha})^T e^{-i\omega^* \tau_{40} \theta} \bar{z} + W_{20}(\theta) \frac{z^2}{2} + W_{11}(\theta) z\bar{z} \\
&\quad + W_{02}(\theta) \frac{\bar{z}^2}{2} + W_{30}(\theta) \frac{z^3}{6} + \dots
\end{aligned} \tag{57}$$

Therefore, $u_{1t}(0)$, $u_{2t}(0)$, $u_{1t}(-1)$, $u_{2t}(-1)$, $u_{1t}(-\tau_1^*/\tau_{40})$, and $u_{2t}(-\tau_1^*/\tau_{40})$ can be obtained.

$$\begin{aligned}
u_{1t}(0) &= z + \bar{z} + W_{20}^{(1)}(0) \frac{z^2}{2} + W_{11}^{(1)}(0) z\bar{z} + W_{02}^{(1)}(0) \frac{\bar{z}^2}{2} + \dots, \\
u_{2t}(0) &= z\alpha + \bar{z}\bar{\alpha} + W_{20}^{(2)}(0) \frac{z^2}{2} + W_{11}^{(2)}(0) z\bar{z} + W_{02}^{(2)}(0) \frac{\bar{z}^2}{2} + \dots, \\
u_{1t}(-1) &= ze^{-i\omega^* \tau_{40}} + \bar{z}e^{i\omega^* \tau_{40}} + W_{20}^{(1)}(-1) \frac{z^2}{2} + W_{11}^{(1)}(-1) z\bar{z} + W_{02}^{(1)}(-1) \frac{\bar{z}^2}{2} + \dots, \\
u_{2t}(-1) &= z\alpha e^{-i\omega^* \tau_{40}} + \bar{z}\bar{\alpha} e^{i\omega^* \tau_{40}} + W_{20}^{(2)}(-1) \frac{z^2}{2} + W_{11}^{(2)}(-1) z\bar{z} + W_{02}^{(2)}(-1) \frac{\bar{z}^2}{2} + \dots, \\
u_{1t}\left(\frac{-\tau_1^*}{\tau_{40}}\right) &= ze^{-i\omega^* \tau_1^*} + \bar{z}e^{i\omega^* \tau_1^*} + W_{20}^{(1)}\left(\frac{-\tau_1^*}{\tau_{40}}\right) \frac{z^2}{2} + W_{11}^{(1)}\left(\frac{-\tau_1^*}{\tau_{40}}\right) z\bar{z} + W_{02}^{(1)}\left(\frac{-\tau_1^*}{\tau_{40}}\right) \frac{\bar{z}^2}{2} + \dots, \\
u_{2t}\left(\frac{-\tau_1^*}{\tau_{40}}\right) &= z\alpha e^{-i\omega^* \tau_1^*} + \bar{z}\bar{\alpha} e^{i\omega^* \tau_1^*} + W_{20}^{(2)}\left(\frac{-\tau_1^*}{\tau_{40}}\right) \frac{z^2}{2} + W_{11}^{(2)}\left(\frac{-\tau_1^*}{\tau_{40}}\right) z\bar{z} + W_{02}^{(2)}\left(\frac{-\tau_1^*}{\tau_{40}}\right) \frac{\bar{z}^2}{2} + \dots.
\end{aligned} \tag{58}$$

Furthermore, we can get $g(z, \bar{z})$, g_{20} , g_{11} , g_{02} , and g_{21} as follows:

$$g(z, \bar{z}) = \bar{q}^*(0)F(0, u_t) = \bar{M}(1, \bar{\alpha}^*)F(0, u_t)$$

$$= \bar{M}(1, \bar{\alpha}^*)\tau_{40} \begin{pmatrix} \frac{1}{2}f_{20}^{(1)}u_{1t}^2(0) + \frac{1}{2}f_{02}^{(1)}u_{2t}^2(0) + f_{11}^{(1)}u_{1t}(0)u_{2t}(0) \\ \frac{1}{2}f_{200}^{(2)}u_{1t}^2(-1) + \frac{1}{2}f_{020}^{(2)}u_{2t}^2\left(-\frac{\tau_1^*}{\tau_{40}}\right) + \frac{1}{2}f_{002}^{(2)}u_{2t}^2(0) + f_{110}^{(2)}u_{1t}(-1) \\ u_{2t}\left(-\frac{\tau_1^*}{\tau_{40}}\right) + f_{101}^{(2)}u_{1t}(-1)u_{2t}(0) + f_{011}^{(2)}u_{2t}(0)u_{2t}\left(-\frac{\tau_1^*}{\tau_{40}}\right) \end{pmatrix}$$

$$g_{20} = 2\bar{M}\tau_{40} \left[\frac{1}{2}f_{20}^{(1)} + \frac{1}{2}f_{02}^{(1)}\alpha^2 + f_{11}^{(1)}\alpha + \bar{\alpha}^* \left(\frac{1}{2}f_{200}^{(2)}e^{-2i\omega^*\tau_{40}} + \frac{1}{2}f_{020}^{(2)}\alpha^2 e^{-2i\omega^*\tau_1^*} + \frac{1}{2}f_{002}^{(2)}\alpha^2 + f_{110}^{(2)}\alpha e^{-i\omega^*\tau_{40}} e^{-i\omega^*\tau_1^*} + f_{101}^{(2)}\alpha e^{-i\omega^*\tau_{40}} + f_{011}^{(2)}\alpha^2 e^{-i\omega^*\tau_1^*} \right) \right];$$

$$g_{11} = \bar{M}\tau_{40} \left[f_{20}^{(1)} + f_{02}^{(1)}\alpha\bar{\alpha} + f_{11}^{(1)}(\alpha + \bar{\alpha}) + \bar{\alpha}^* \left(f_{200}^{(2)} + f_{020}^{(2)}\alpha\bar{\alpha} + f_{002}^{(2)}\alpha\bar{\alpha} + f_{110}^{(2)}(\bar{\alpha}e^{-i\omega^*\tau_{40}}e^{i\omega^*\tau_1^*} + \alpha e^{i\omega^*\tau_{40}}e^{-i\omega^*\tau_1^*}) + f_{101}^{(2)}(\bar{\alpha}e^{-i\omega^*\tau_{40}} + \alpha e^{i\omega^*\tau_{40}}) + f_{011}^{(2)}(\alpha\bar{\alpha}e^{-i\omega^*\tau_1^*} + \bar{\alpha}\alpha e^{i\omega^*\tau_1^*}) \right) \right];$$

(59)

$$g_{02} = 2\bar{M}\tau_{40} \left[\frac{1}{2}f_{20}^{(1)} + \frac{1}{2}f_{02}^{(1)}\bar{\alpha}^2 + f_{11}^{(1)}\bar{\alpha} + \bar{\alpha}^* \left(\frac{1}{2}f_{200}^{(2)}e^{2i\omega^*\tau_{40}} + \frac{1}{2}f_{020}^{(2)}\bar{\alpha}^2 e^{2i\omega^*\tau_1^*} + \frac{1}{2}f_{002}^{(2)}\bar{\alpha}^2 + f_{110}^{(2)}\bar{\alpha}e^{i\omega^*\tau_{40}}e^{i\omega^*\tau_1^*} + f_{101}^{(2)}\bar{\alpha}e^{i\omega^*\tau_{40}} + f_{011}^{(2)}\bar{\alpha}^2 e^{i\omega^*\tau_1^*} \right) \right]$$

$$g_{21} = 2\bar{M}\tau_{40} \left[f_{20}^{(1)} \left(\frac{1}{2}W_{20}^{(1)}(0) + W_{11}^{(1)}(0) \right) + f_{02}^{(1)} \left(\frac{1}{2}\bar{\alpha}W_{20}^{(2)}(0) + \alpha W_{11}^{(2)}(0) \right) + f_{11}^{(1)} \left(\frac{1}{2}W_{20}^{(1)}(0) + \bar{\alpha} + \frac{1}{2}W_{20}^{(2)}(0) + W_{11}^{(1)}(0)\alpha + W_{11}^{(2)}(0) \right) + \bar{\alpha}^* \left(f_{200}^{(2)} \left(\frac{1}{2}W_{20}^{(1)}(-1)e^{i\omega^*\tau_{40}} + W_{11}^{(1)}(-1)e^{-i\omega^*\tau_{40}} \right) + f_{020}^{(2)} \left(\frac{1}{2}W_{20}^{(2)}\left(-\frac{\tau_1^*}{\tau_{40}}\right)\bar{\alpha}e^{i\omega^*\tau_1^*} + W_{11}^{(2)}\left(-\frac{\tau_1^*}{\tau_{40}}\right)\alpha e^{-i\omega^*\tau_1^*} \right) + f_{002}^{(2)} \left(\frac{1}{2}\bar{\alpha}W_{20}^{(2)}(0) + \alpha W_{11}^{(2)}(0) \right) + f_{110}^{(2)} \left(\frac{1}{2}W_{20}^{(2)}\left(-\frac{\tau_1^*}{\tau_{40}}\right)e^{i\omega^*\tau_{40}} + W_{11}^{(2)}\left(-\frac{\tau_1^*}{\tau_{40}}\right)e^{-i\omega^*\tau_{40}} + \frac{1}{2}W_{20}^{(1)}(-1)\bar{\alpha}e^{i\omega^*\tau_1^*} + \alpha W_{11}^{(1)}(-1) \cdot e^{-i\omega^*\tau_1^*} \right) + f_{101}^{(2)} \left(W_{11}^{(2)}(0)e^{-i\omega^*\tau_{40}} + \frac{1}{2}W_{20}^{(2)}(0)e^{i\omega^*\tau_{40}} + \frac{1}{2}\bar{\alpha}W_{20}^{(1)}(-1) + \alpha W_{11}^{(1)}(-1) \right) + f_{011}^{(2)} \cdot \left(\alpha W_{11}^{(2)}(0)e^{-i\omega^*\tau_1^*} + \frac{1}{2}\bar{\alpha}W_{20}^{(2)}(0)e^{i\omega^*\tau_1^*} + \frac{1}{2}\bar{\alpha}W_{20}^{(2)}\left(-\frac{\tau_1^*}{\tau_{40}}\right) + \alpha W_{11}^{(2)}\left(-\frac{\tau_1^*}{\tau_{40}}\right) \right) \right].$$

Next, we compute $W_{20}(\theta)$ and $W_{11}(\theta)$ in g_{21} by using the method in [8, 9, 32]. From (38) and (53), we have

$$\dot{W} = \dot{u}_t - \dot{z}q - \dot{\bar{z}}\bar{q} = \begin{cases} AW - 2\text{Re}\{\bar{q}^*(0)F(0, u_t)q(\theta)\}, & \theta \in [-1, 0) \\ AW - 2\text{Re}\{\bar{q}^*(0)F(0, u_t)q(0)\} + F(0, u_t), & \theta = 0 \end{cases} \triangleq AW + H(z, \bar{z}, \theta), \quad (60)$$

where

$$H(z, \bar{z}, \theta) = H_{20}(\theta)\frac{z^2}{2} + H_{11}(\theta)z\bar{z} + H_{02}(\theta)\frac{\bar{z}^2}{2} + \dots \quad (61)$$

Thus, we have

$$AW(t, \theta) - \dot{W} = -H(z, \bar{z}, \theta) = -H_{20}(\theta)\frac{z^2}{2} - H_{11}(\theta)z\bar{z} - H_{02}(\theta)\frac{\bar{z}^2}{2} - \dots \quad (62)$$

From (56), we can get

$$AW(t, \theta) = AW_{20}(\theta)\frac{z^2}{2} + AW_{11}(\theta)z\bar{z} + AW_{02}(\theta)\frac{\bar{z}^2}{2} + AW_{30}(\theta)\frac{z^3}{6} + \dots, \quad (63)$$

and

$$\dot{W} = W_z \dot{z} + W_{\bar{z}} \dot{\bar{z}} = W_{20}(\theta)z\dot{z} + W_{11}(\theta)(\dot{z}\bar{z} + z\dot{\bar{z}}) + \dots = 2i\omega^* \tau_{40} W_{20}(\theta)\frac{z^2}{2} + \dots \quad (64)$$

Therefore, we can get

$$(A - 2i\omega^* \tau_{40})W_{20}(\theta) = -H_{20}(\theta), \quad AW_{11}(\theta) = -H_{11}(\theta). \quad (65)$$

For $\theta \in [-1, 0)$, we have

$$\begin{aligned} H(z, \bar{z}, \theta) &= -\bar{q}^*(0)F(0, u_t)q(\theta) - q^*(0)\bar{F}(0, u_t)\bar{q}(\theta) \\ &= -g(z, \bar{z})q(\theta) - \bar{g}(z, \bar{z})\bar{q}(\theta). \end{aligned} \quad (66)$$

Comparing coefficients of (66) with (61), we can obtain

$$H_{20}(\theta) = -(g_{20}q(\theta) + \bar{g}_{02}\bar{q}(\theta)), \quad (67)$$

$$H_{11}(\theta) = -(g_{11}q(\theta) + \bar{g}_{11}\bar{q}(\theta)). \quad (68)$$

From (66) and (68), and the definition of A , we can get

$$\dot{W}_{20}(\theta) = 2i\omega^* \tau_{40} W_{20}(\theta) + g_{20}q(\theta) + \bar{g}_{02}\bar{q}(\theta). \quad (69)$$

Noticing that $q(\theta) = q(0)e^{i\omega^* \tau_{40}\theta} = (1, \alpha)^T e^{i\omega^* \tau_{40}\theta}$.

By computing (69), we can get

$$\begin{aligned} W_{20}(\theta) &= \frac{ig_{20}}{\omega^* \tau_{40}} q(0)e^{i\omega^* \tau_{40}\theta} + \frac{i\bar{g}_{02}}{3\omega^* \tau_{40}} \bar{q}(0)e^{-i\omega^* \tau_{40}\theta} \\ &\quad + E_1 e^{2i\omega^* \tau_{40}\theta}, \end{aligned} \quad (70)$$

where $E_1 = (E_1^{(1)}, E_1^{(2)}) \in \mathbb{R}^2$ is a constant vector.

Similarly, from (66) and (68) and the definition of A , we can get

$$\dot{W}_{11}(\theta) = g_{11}q(\theta) + \bar{g}_{11}\bar{q}(\theta), \quad (71)$$

$$\begin{aligned} W_{11}(\theta) &= -\frac{ig_{11}}{\omega^* \tau_{40}} q(0)e^{i\omega^* \tau_{40}\theta} \\ &\quad + \frac{i\bar{g}_{11}}{\omega^* \tau_{40}} \bar{q}(0)e^{-i\omega^* \tau_{40}\theta} + E_2, \end{aligned} \quad (72)$$

where $E_2 = (E_2^{(1)}, E_2^{(2)}) \in \mathbb{R}^2$ is a constant vector.

In what follows, we shall seek appropriate E_1, E_2 in (70) and (72), respectively. From the definition of A and (65), we can have

$$\int_{-1}^0 d\eta(\theta)W_{20}(\theta) = 2i\omega^* \tau_{40} W_{20}(0) - H_{20}(0), \quad (73)$$

$$\int_{-1}^0 d\eta(\theta)W_{11}(\theta) = -H_{11}(0). \quad (74)$$

Thus,

$$H_{20}(0) = -g_{20}q(0) - \bar{g}_{02}\bar{q}(0) + 2\tau_{40}(P_1, P_2)^T, \quad (75)$$

$$H_{11}(0) = -g_{11}q(0) - \bar{g}_{11}\bar{q}(0) + \tau_{40}(Q_1, Q_2)^T, \quad (76)$$

where $P_1 = 1/2f_{20}^{(1)} + 1/2f_{02}^{(1)}\alpha^2 + f_{11}^{(1)}\alpha$ and

$$\begin{aligned}
 P_2 &= \frac{1}{2}f_{200}^{(2)}e^{-2i\omega^*\tau_{40}} + \frac{1}{2}f_{020}^{(2)}\alpha^2e^{-2i\omega^*\tau_1^*} + \frac{1}{2}f_{002}^{(2)}\alpha^2 + f_{110}^{(2)}\alpha e^{-i\omega^*\tau_{40}}e^{-i\omega^*\tau_1^*} \\
 &\quad + f_{101}^{(2)}\alpha e^{-i\omega^*\tau_{40}} + f_{011}^{(2)}\alpha^2e^{-i\omega^*\tau_1^*}, \\
 Q_1 &= f_{20}^{(1)} + f_{02}^{(1)}\alpha\bar{\alpha} + f_{11}^{(1)}(\alpha + \bar{\alpha}), \\
 Q_2 &= f_{200}^{(2)} + f_{020}^{(2)}\alpha\bar{\alpha} + f_{002}^{(2)}\alpha\bar{\alpha} + f_{110}^{(2)}(\bar{\alpha}e^{-i\omega^*\tau_{40}}e^{i\omega^*\tau_1^*} + \alpha e^{i\omega^*\tau_{40}}e^{-i\omega^*\tau_1^*}) \\
 &\quad + f_{101}^{(2)}(\bar{\alpha}e^{-i\omega^*\tau_{40}} + \alpha e^{i\omega^*\tau_{40}}) + f_{011}^{(2)}(\alpha\bar{\alpha}e^{-i\omega^*\tau_1^*} + \bar{\alpha}\alpha e^{i\omega^*\tau_1^*}).
 \end{aligned} \tag{77}$$

Noting that,

$$\left(i\omega^*\tau_{40}I - \int_{-1}^0 e^{i\omega^*\tau_{40}\theta}d\eta(\theta) \right)q(0) = 0, \left(-i\omega^*\tau_{40}I - \int_{-1}^0 e^{-i\omega^*\tau_{40}\theta}d\eta(\theta) \right)\bar{q}(0) = 0. \tag{78}$$

Substituting (71) and (75) into (73), we can have

$$\left(2i\omega^*\tau_{40}I - \int_{-1}^0 e^{2i\omega^*\tau_{40}\theta}d\eta(\theta) \right)E_1 = 2\tau_{40}(P_1, P_2)^T, \tag{79}$$

$$\text{i.e., } \begin{pmatrix} 2i\omega^* - \alpha_1 & -\alpha_2 \\ -\gamma_1 e^{-2i\omega^*\tau_1^*} & 2i\omega^* - \gamma_2 e^{-2i\omega^*\tau_{40}} \end{pmatrix} E_1 = 2 \begin{pmatrix} P_1 \\ P_2 \end{pmatrix}.$$

It follows that,

$$E_1^{(1)} = \frac{\Delta_{11}}{\Delta_1}, E_1^{(2)} = \frac{\Delta_{12}}{\Delta_1}, \tag{80}$$

$$\text{where } \Delta_1 = \det \begin{pmatrix} m_1 & m_2 \\ m_3 & m_4 \end{pmatrix}, \quad \Delta_{11} = 2 \det \begin{pmatrix} P_1 & m_2 \\ P_2 & m_4 \end{pmatrix},$$

$$\Delta_{12} = 2 \det \begin{pmatrix} m_1 & P_1 \\ m_3 & P_2 \end{pmatrix}, \quad m_1 = 2i\omega^* - \alpha_1, \quad m_2 = -\alpha_2,$$

$$m_3 = -\gamma_1 e^{-2i\omega^*\tau_1^*}, \text{ and } m_4 = 2i\omega^* - \gamma_2 e^{-2i\omega^*\tau_{40}}.$$

Similarly, substituting (72) and (74) into (76), we can have

$$\int_{-1}^0 d\eta(\theta)E_2 = -\tau_{40}(Q_1, Q_2)^T, \tag{81}$$

$$\text{i.e., } \begin{pmatrix} \alpha_1 & \alpha_2 \\ \gamma_1 & \gamma_2 \end{pmatrix} E_2 = \begin{pmatrix} Q_1 \\ Q_2 \end{pmatrix}.$$

It follows that,

$$E_2^{(1)} = \frac{\Delta_{21}}{\Delta_2}, E_2^{(2)} = \frac{\Delta_{22}}{\Delta_2}, \tag{82}$$

$$\text{where } \Delta_2 = \det \begin{pmatrix} \alpha_1 & \alpha_2 \\ \gamma_1 & \gamma_2 \end{pmatrix}, \quad \Delta_{21} = 2 \det \begin{pmatrix} Q_1 & \alpha_2 \\ Q_2 & \gamma_2 \end{pmatrix}, \text{ and}$$

$$\Delta_{22} = 2 \det \begin{pmatrix} \alpha_1 & Q_1 \\ \gamma_1 & Q_2 \end{pmatrix}.$$

From (70), (72), (75), and (83), we can calculate g_{21} and derive the following values:

$$\begin{cases} c_1(0) = \frac{i}{2\omega^*\tau_{40}} \left(g_{20}g_{11} - 2|g_{11}|^2 - \frac{1}{3}|g_{02}|^2 \right) + \frac{1}{2}g_{21}, \\ \mu_2 = -\frac{\text{Re}\{c_1(0)\}}{\text{Re}\{\lambda'(\tau_{40})\}}, \\ \beta_2 = 2\text{Re}\{c_1(0)\}, \\ T_2 = -\frac{1}{\omega^*\tau_{40}} \left(\text{Im}\{c_1(0)\} + \mu_2 \text{Im}\{\lambda'(\tau_{40})\} \right). \end{cases} \tag{83}$$

Now, the main result in this section is given.

Theorem 7. For system (3), suppose that (A1) or (A2) holds, and conditions (H1), (H3), (H8), and (H9) hold. The periodic solution is supercritical (resp. subcritical) if $\mu_2 > 0$ (resp. $\mu_2 < 0$). The bifurcating periodic solutions are orbitally asymptotically stable with an asymptotical phase (resp. unstable) if $\beta_2 < 0$ (resp. $\beta_2 > 0$). The period of the bifurcating periodic solutions increases (resp. decreases) if $T_2 > 0$ (resp. $T_2 < 0$).

4. Numerical Simulations

In this section, we shall present some examples and corresponding numerical simulations to verify above mentioned theoretical results.

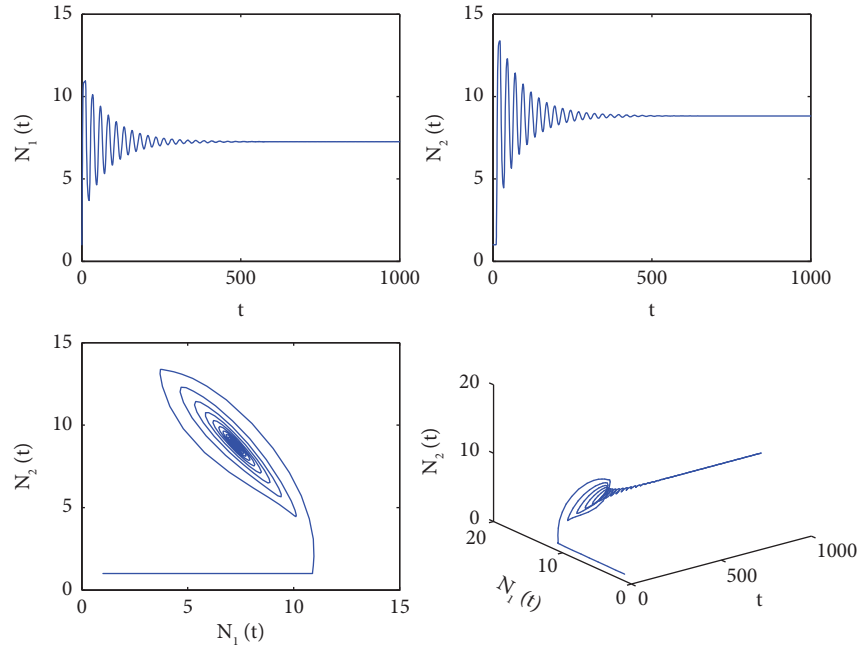


FIGURE 1: Behavior and phase portrait of the system (84) with $\tau_2 = 0, \tau_1 = 10$ ($\alpha_{21} = 6$).

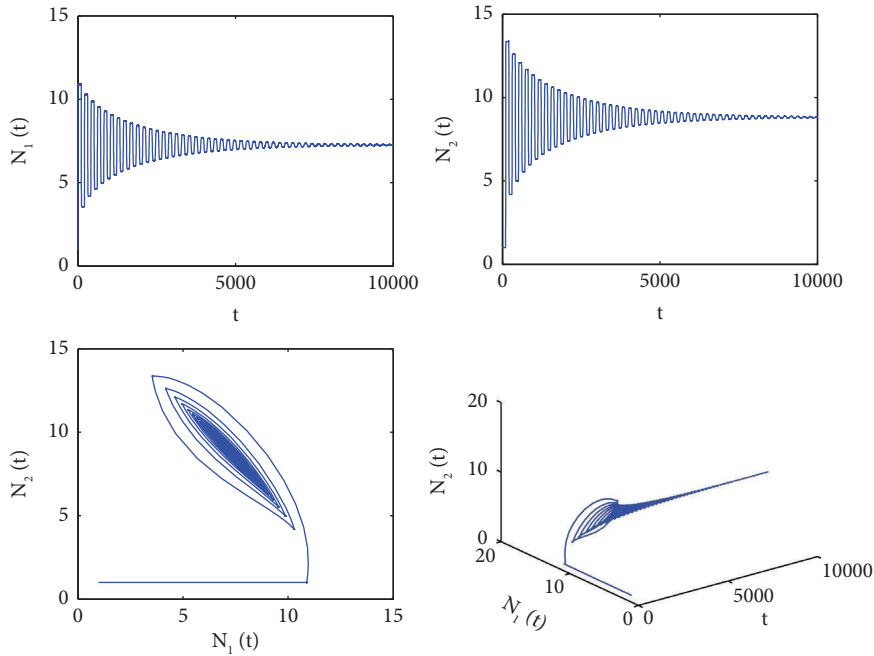


FIGURE 2: Behavior and phase portrait of the system (84) with $\tau_2 = 0, \tau_1 = 100$ ($\alpha_{21} = 6$).

Example 1. We consider system (3) under Case (2). First, we choose $a = 1, b = 4, r_1 = d_2 = 1, d_1 = \beta_1 = 0.1,$ and $\alpha_{12} = 3,$ and then the system (3) is

$$\begin{cases} \frac{dN_1}{dt} = N_1 + \frac{3N_1N_2}{1 + N_1 + 4N_2} - 0.1N_1N_2 - 0.1N_1^2, \\ \frac{dN_2}{dt} = \frac{\alpha_{21}N_1(t - \tau_1)N_2}{1 + N_1(t - \tau_1) + 4N_2(t - \tau_2)} - N_2, \end{cases}$$

(84)

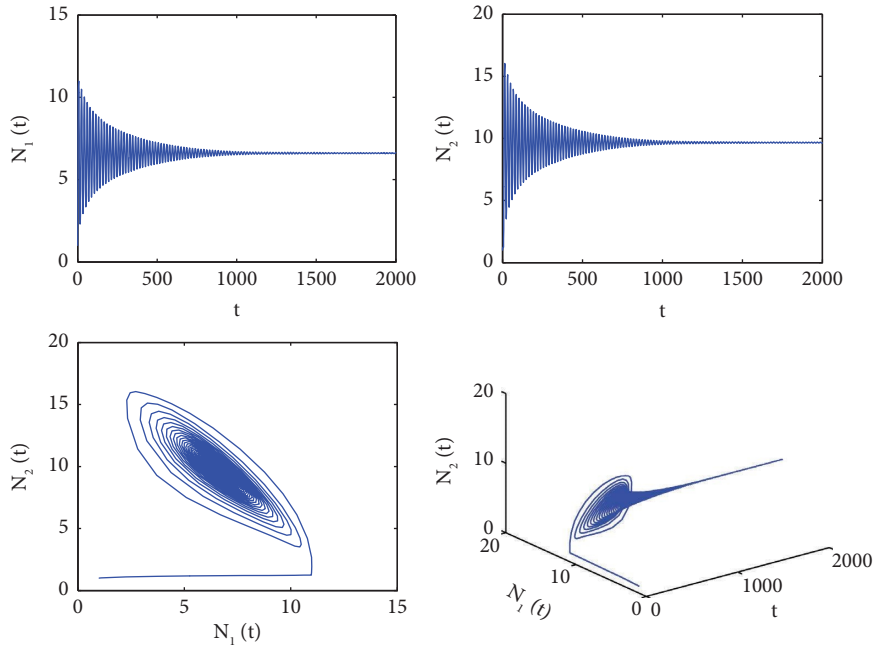


FIGURE 3: Behavior and phase portrait of the system (84) with $\tau_2 = 0, \tau_1 = 6.5$ ($\alpha_{21} = 7$).

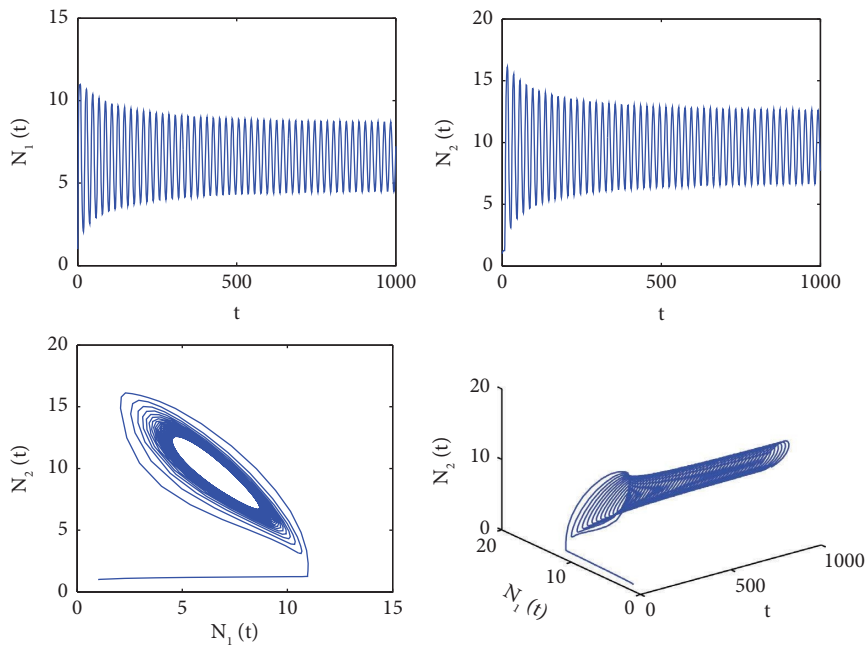


FIGURE 4: Behavior and phase portrait of the system (84) with $\tau_2 = 0, \tau_1 = 7.5$ ($\alpha_{21} = 7$).

where the initial value is $(1, 1)$. Let $\alpha_{21} = 6$, and by computations, we can obtain the unique positive equilibrium $E^* = (7.2568, 8.8210)$ of system (84). When $\tau_1 > 0, \tau_2 = 0$, (A1) or (A2) and (H2) hold, i.e. the conditions of Theorem 1 are satisfied, the positive equilibrium E^* of (84) is asymptotically stable for all $\tau_1 > 0$. In particular, we set $\tau_1 = 10$ and $\tau_1 = 100$, and the corresponding numerical simulation results are given in Figures 1 and 2.

Then, we consider system (84) with $\alpha_{21} = 7$ and keep other parameters unchanged when $\tau_1 > 0, \tau_2 = 0$, (A1) or (A2), and (H3) hold, i.e. the conditions of the Theorem 2 are satisfied. By computations, we can get the unique positive equilibrium $E^* = (6.6066, 9.6598)$, $\omega_{10} = 0.3351$, and $\tau_{10} = 6.9828$. If $\tau_1 \in [0, \tau_{10})$, then the positive equilibrium E^* of (84) is locally asymptotic stable under $\tau_2 = 0$, while it becomes unstable when τ_1 is gradually greater than this

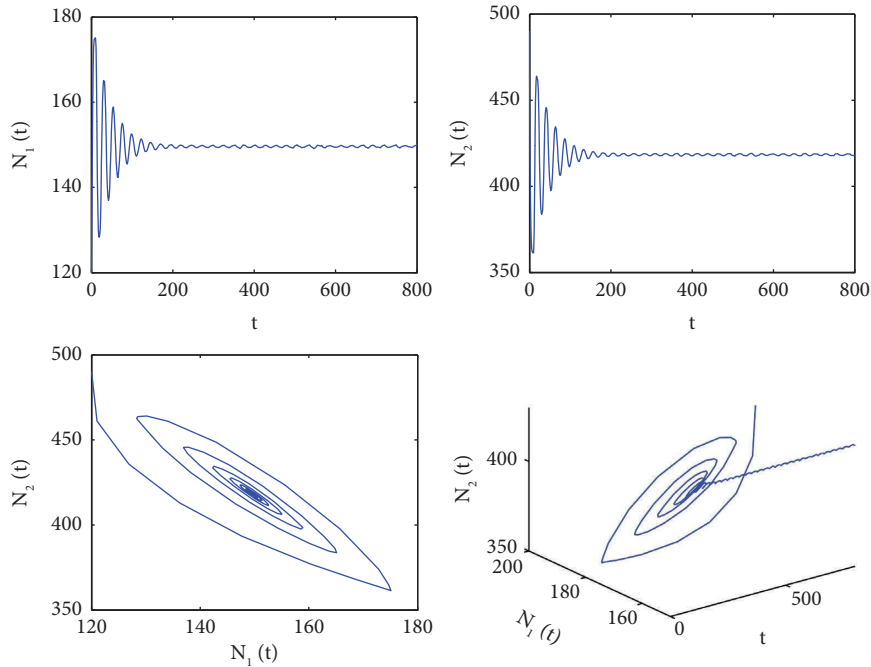


FIGURE 5: Behavior and phase portrait of the system (85) with $\tau_1 = 0, \tau_2 = 10$ ($\alpha_{21} = 3.8$).

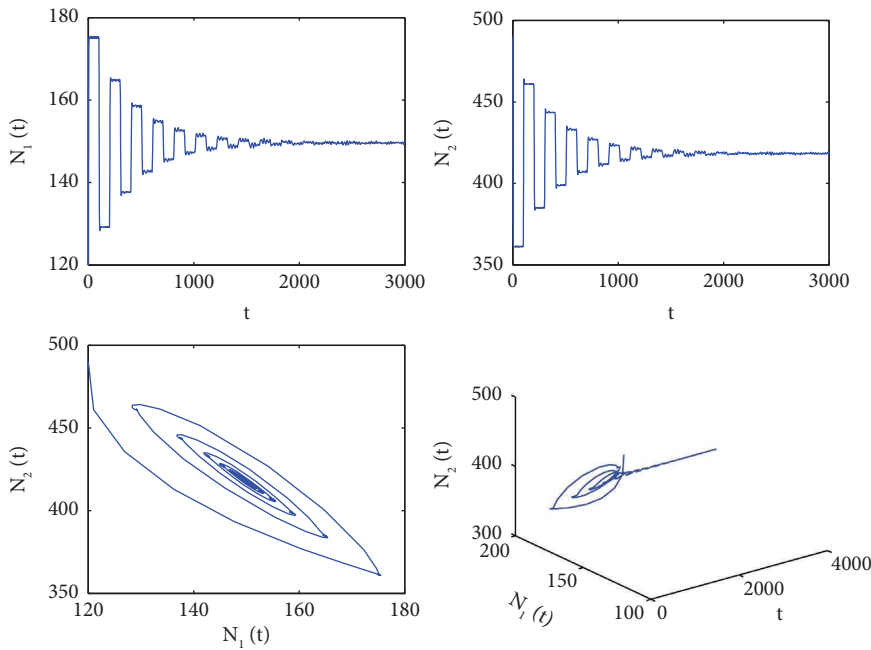


FIGURE 6: Behavior and phase portrait of the system (85) with $\tau_1 = 0, \tau_2 = 100$ ($\alpha_{21} = 3.8$).

critical value through Hopf bifurcation. The corresponding numerical simulation results are given in Figures 3 and 4.

Example 2. We consider system (3) under Case (3) and Case (4). First, we choose $a = b = 2, r_1 = 1, d_1 = \beta_1 = 0.005, d_2 = 0.5,$ and $\alpha_{12} = 5,$ and then the system (3) is

$$\begin{cases} \frac{dN_1}{dt} = N_1 + \frac{5N_1N_2}{1 + 2N_1 + 2N_2} - 0.005N_1N_2 - 0.005N_1^2, \\ \frac{dN_2}{dt} = \frac{\alpha_{21}N_1(t - \tau_1)N_2}{1 + 2N_1(t - \tau_1) + 2N_2(t - \tau_2)} - 0.5N_2, \end{cases} \tag{85}$$

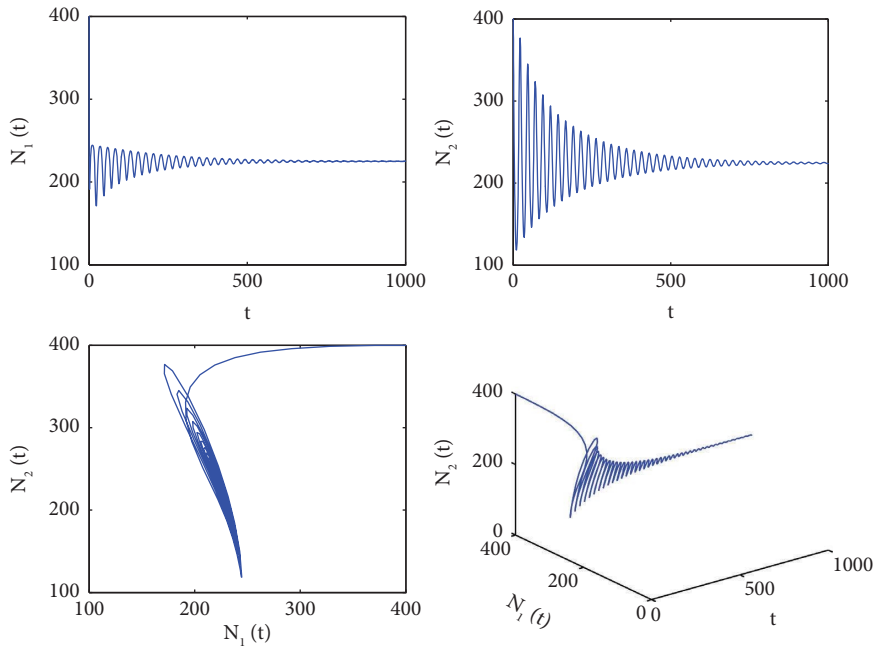


FIGURE 7: Behavior and phase portrait of the system (85) with $\tau_1 = 0, \tau_2 = 7$ ($\alpha_{21} = 2$).

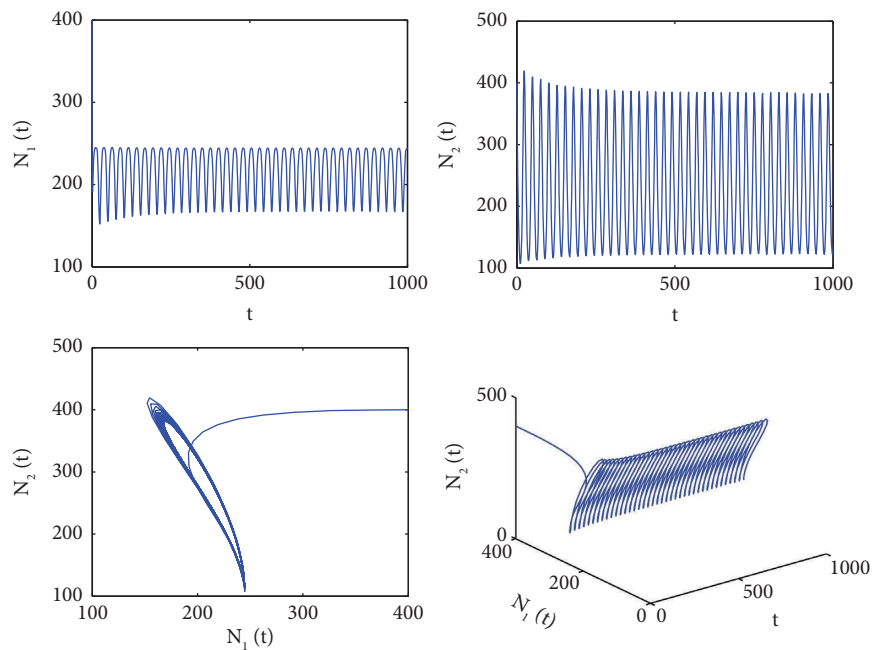


FIGURE 8: Behavior and phase portrait of the system (85) with $\tau_1 = 0, \tau_2 = 7.8$ ($\alpha_{21} = 2$).

where the initial value is $(120, 490)$. Let $\alpha_{21} = 3.8$, and by computations, we can obtain the unique positive equilibrium $E^* = (149.6003, 418.3809)$ of system (85). When $\tau_1 = 0, \tau_2 > 0$, (A1) or (A2), and (H4) hold, i.e. the conditions of the Theorem 3 are satisfied, the positive equilibrium E^* of (85) is asymptotically stable for all $\tau_2 > 0$. In particular, we set $\tau_2 = 10$ and $\tau_2 = 100$, and the corresponding numerical simulation results are given in Figures 5 and 6.

Then, we consider system (85) with $\alpha_{21} = 2$, whose initial value is $(400, 400)$ and keep other parameters unchanged. When $\tau_1 = 0, \tau_2 > 0$, (A1) or (A2), and (H5) hold, the conditions of the Theorem 4 are satisfied. By computations, we can get the unique positive equilibrium $E^* = (224.9722, 224.4722)$, $\omega_{20} = 0.2495$, and $\tau_{20} = 7.4321$. If $\tau_2 \in [0, \tau_{20})$, then the positive equilibrium E^* of (85) is locally asymptotic stable, while it becomes unstable when τ_2

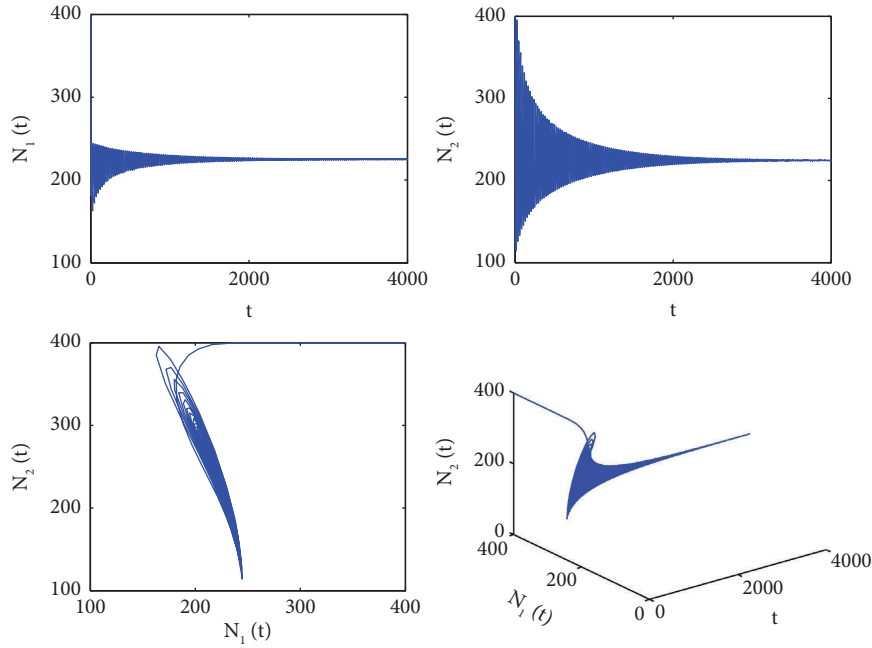


FIGURE 9: Behavior and phase portrait of the system (85) with $\tau_1 = 0.5 < \tau_{30}, \tau_2 = 7$ ($\alpha_{21} = 2$).

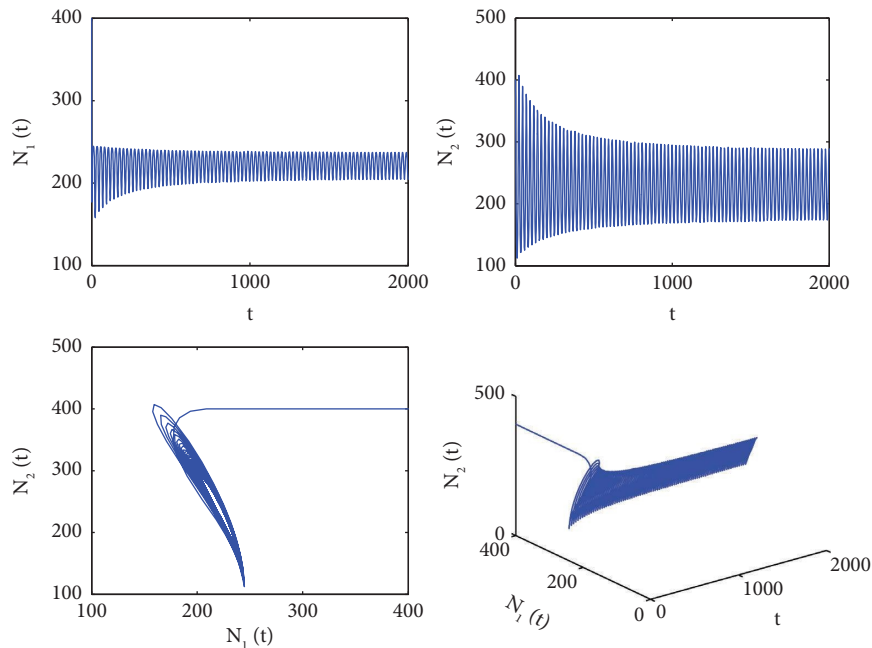


FIGURE 10: Behavior and phase portrait of the system (85) with $\tau_1 = 0.75 > \tau_{30}, \tau_2 = 7$ ($\alpha_{21} = 2$).

is gradually greater than this critical value through Hopf Bifurcation. The corresponding numerical simulation results are given in Figures 7 and 8.

Furthermore, we consider Case (4) of system (85) with $\alpha_{21} = 2$. We fix $\tau_2 = 7 < \tau_{20}$, and take τ_1 as a parameter. By computations, these parameters satisfied conditions (A1) or (A2), (H5), (H6), and (H7) of the Theorem 5, and we can get $\tau_{30} = 0.6768$. If $\tau_1 \in [0, \tau_{30})$, then the positive equilibrium

E^* of (85) is locally asymptotic stable, while it becomes unstable when τ_1 is gradually greater than this critical value through Hopf bifurcation. The corresponding numerical simulation results are given in Figures 9 and 10.

Example 3. We consider system (3) under Case (5). Based on system (84) with $\alpha_{21} = 7$ in example 1, we further fix $\tau_1 = 6.5 < \tau_{10}$, and take τ_2 as a parameter. By computations,

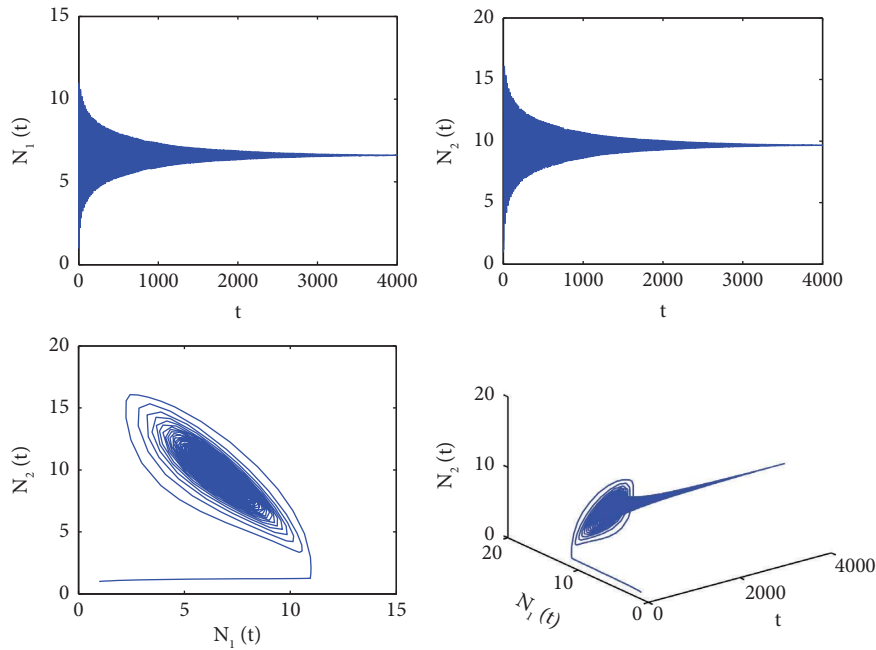


FIGURE 11: Behavior and phase portrait of the system (84) with $\tau_1 = 6.5, \tau_2 = 0.16 < \tau_{40}$ ($\alpha_{21} = 7$).

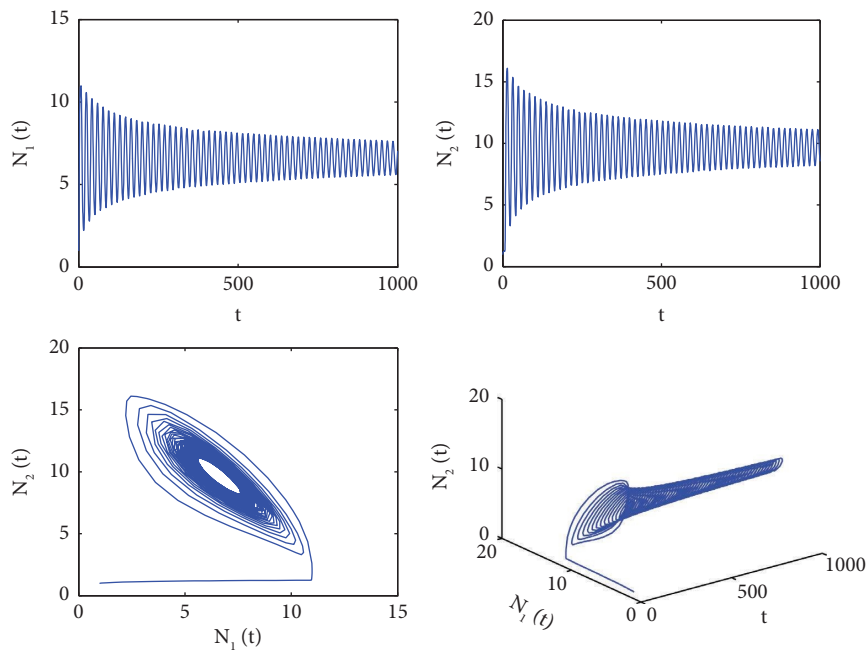


FIGURE 12: Behavior and phase portrait of the system (84) with $\tau_1 = 6.5, \tau_2 = 0.2 > \tau_{40}$ ($\alpha_{21} = 7$).

these parameters satisfied conditions of Theorem 6, and we can get $\tau_{40} = 0.1740$. If $\tau_2 \in [0, \tau_{40})$, then the positive equilibrium E^* of (84) is locally asymptotic stable, while it becomes unstable when τ_2 is gradually greater than this critical value τ_{40} through Hopf bifurcation (see Figures 11 and 12). In addition, we can get $c_1(0) = -0.0431 - 1.9649i$, $\mu_2 = 12.9315 > 0$, and $\beta_2 = -0.0862 < 0$. Hence, when $\tau_1 > 0$ and $\tau_2 \in (0, \tau_{40})$, the Hopf bifurcation of system (84) is

supercritical and the corresponding bifurcation periodic solutions are asymptotically stable.

Remark 1. In this paper, the dynamic properties of a plant-pollinator model with multiple delays are discussed by regarding different delays as bifurcating parameters; particularly, the theory of stability for its equilibrium point is analyzed in detail. The results of these aspects are

comprehensive and satisfactory. We admit that only one case is implemented in the analysis of Hopf bifurcation for the reason that the remaining cases are similar to the one we discussed.

Remark 2. The main novel contributions are reflected as follows:

- (1) The existing problems of bifurcations mainly focus on differential systems with unique delay or multiple identical delays owing to the fact that the stable regions with multiple different delays are difficult to determine. What merits further study in this work is that the dynamic properties of differential systems with multiple opposite delays are discussed in detail, which will stimulate us to further explore the bifurcating problems of the systems with multiple different delays.
- (2) The bifurcating theories about the same delay in [32] are extended to multiple versions of different delays. The results are more accurate and less conservative.
- (3) The exact bifurcating conditions caused by two different delays are derived by breaking through the difficulty of analyzing the characteristic equation.

Meanwhile, the challenges that accompany us in the future are how to design an appropriate controller to improve the stability for systems with multiple delays and how to extend the available system with integral order to the fractional order and continue to consider its dynamic properties, especially regarding the order as a bifurcating parameter, what may be a very meaningful topic.

5. Conclusions

In this paper, we considered the stability and Hopf bifurcation of a kind of a plant-pollination model with two delays. Taking the different combinations of the two delays τ_1 and τ_2 as the bifurcation parameters, we obtained the sufficient conditions for the local asymptotic stability and Hopf bifurcation of the positive equilibrium point E^* of the system model by using the Hopf bifurcation theorem. When $\tau_2 = 0$ and the parameters satisfy (H2) or $\tau_1 = 0$ and the parameters satisfy (H4), the positive equilibrium E^* of the model is asymptotically stable for any delay $\tau_1 > 0$ or $\tau_2 > 0$. It is found that when $\tau_2 = 0$ and the parameters satisfy (H3), there exists a critical value τ_{10} so that the positive equilibrium of the system is stable for $\tau_1 \in [0, \tau_{10})$, and it would be unstable for $\tau_1 \in (\tau_{10}, +\infty)$ and Hopf bifurcation at occurs E^* for $\tau_1 = \tau_{10}$. Similarly, when $\tau_1 = 0$ and the parameters satisfy (H5), there exists a critical value τ_{20} so that the positive equilibrium of the system is stable for $\tau_2 \in [0, \tau_{20})$, and it would be unstable for $\tau_2 \in (\tau_{20}, +\infty)$ and Hopf bifurcation occurs at E^* for $\tau_2 = \tau_{20}$. Furthermore, when $\tau_2 \in [0, \tau_{20})$ is fixed and τ_1 is taken as the bifurcation parameter, we obtain that there exists a critical value τ_{30} such that the positive equilibrium E^* of the system is stable for

$\tau_1 \in [0, \tau_{30})$, and it would be unstable for $\tau_1 \in (\tau_{30}, +\infty)$ and undergoes Hopf bifurcation at E^* for $\tau_1 = \tau_{30}$. Analogously, when $\tau_1 \in [0, \tau_{10})$ is fixed and τ_2 is taken as the bifurcation parameter, we gain that there exists a critical value τ_{40} such that the positive equilibrium E^* of the system is stable for $\tau_2 \in [0, \tau_{40})$, and it would be unstable for $\tau_2 \in (\tau_{40}, +\infty)$ and undergoes Hopf bifurcation at E^* for $\tau_2 = \tau_{40}$. In a word, when τ crosses through a series of critical values including the above, the system can bifurcate a series of nontrivial periodic solutions from the positive equilibrium point. In addition, according to the normal form theory and the central manifold theorem of delay differential equations, some explicit formulas for determining Hopf bifurcation direction and stability of bifurcation periodic solutions are achieved. At last, some numerical simulations are conducted to demonstrate corresponding theoretical results. Our future work will focus on the following meaningful and promising aspects of researches:

- (1) Extending the integral-order model to the fractional-order model. Fractional calculus has more advantages in describing some materials and processes with memory and genetic properties and can describe complex systems more concisely and clearly which has more potential to achieve some results that cannot be achieved by integral calculus.
- (2) Further studying the dynamic properties of the fractional-order system with delays, which is a colorful project. As a bifurcation parameter, the bifurcating behavior caused by delay is worthy of our study, which is also a hot issue in recent years. So what results will be produced when order is used as a bifurcation parameter to study the bifurcation problem of the fractional-order model with delay? This is a topic worthy of our further discussion, and of course, it is also a challenging frontier issue.

Data Availability

The data used to support the findings of the current study are available from the corresponding author.

Conflicts of Interest

The authors declare that there are no conflicts of interest.

Acknowledgments

This work was supported by the Chongqing Big Data Engineering Laboratory for Children, the Chongqing Electronics Engineering Technology Research Center for Interactive Learning, the West China Institute of Children's Brain and Cognition, the Chongqing University Innovation Research Group, the Chongqing Key Discipline of Electronic Information, the Chongqing Natural Science Foundation Project (CSTC2021-msxm1993), and the Science and Technology Research Program of the Chongqing Education Commission of China (KJQN201901601).

References

- [1] R. M. May, *Studies in Mathematical Biology*, American Mathematical Society, Providence, RI, USA, 1976.
- [2] R. M. May, "Theoretical Ecology," *Principles And Applications*, Blackwell Scientific, Oxford, UK, 1976.
- [3] J. M. Soberon and C. Martinez Del Rio, "The dynamics of a plant-pollinator interaction," *Journal of Theoretical Biology*, vol. 91, no. 2, pp. 363–378, 1981.
- [4] S. Lundberg and P. Ingvarsson, "Population dynamics of resource limited plants and their pollinators," *Theoretical Population Biology*, vol. 54, no. 1, pp. 44–49, 1998.
- [5] S. R. Jang, "Dynamics of herbivore-plant-pollinator models," *Journal of Mathematical Biology*, vol. 44, no. 2, pp. 129–149, 2002.
- [6] Y. Wang, "Dynamics of plant-pollinator-robber systems," *Journal of Mathematical Biology*, vol. 66, no. 6, pp. 1155–1177, 2013.
- [7] Y. Wang, D. L. DeAngelis, and J. N. Holland, "Uni-directional interaction and plant-pollinator-robber coexistence," *Bulletin of Mathematical Biology*, vol. 74, no. 9, pp. 2142–2164, 2012.
- [8] M. A. Fishman and L. Hadany, "Plant-pollinator population dynamics," *Theoretical Population Biology*, vol. 78, no. 4, pp. 270–277, 2010.
- [9] L. Wang, H. Jiang, and Y. Li, "Positive steady state solutions of a plant-pollinator model with diffusion," *Discrete and Continuous Dynamical Systems*, vol. 20, no. 6, pp. 1805–1819, 2015.
- [10] C. J. Xu, M. X. Liao, and X. He, "Stability and Hopf bifurcation analysis for a Lotka-Volterra predator-prey model with two delays," *International Journal of Applied Mathematics and Computer Science*, vol. 21, no. 1, pp. 97–107, 2011.
- [11] Y. Song and J. Wei, "Local Hopf bifurcation and global periodic solutions in a delayed predator-prey system," *Journal of Mathematical Analysis and Applications*, vol. 301, pp. 1–21, 2005.
- [12] Z. Jiang and L. Wang, "Global hopf bifurcation for a predator-prey system with three delays," *International Journal of Bifurcation and Chaos in Applied Sciences and Engineering*, vol. 27, no. 07, Article ID 1750108, 2017.
- [13] S. Djilali, "Impact of prey herd shape on the predator-prey interaction," *Chaos, Solitons and Fractals*, vol. 120, pp. 139–148, 2019.
- [14] Y. Guo, N. Ji, and B. Niu, "Hopf bifurcation analysis in a predator-prey model with time delay and food subsidies," *Advances in Differential Equations*, vol. 2019, no. 1, p. 99, 2019.
- [15] C. Xu, P. Li, Q. Xiao, and S. Yuan, "New results on competition and cooperation model of two enterprises with multiple delays and feedback controls," *Boundary Value Problems*, vol. 2019, no. 1, p. 36, 2019.
- [16] L. Li, C. H. Zhang, and X. P. Yan, "Stability and Hopf bifurcation analysis for a two enterprise interaction model with delays," *Communications in Nonlinear Science and Numerical Simulation*, vol. 30, no. 1-3, pp. 70–83, 2016.
- [17] M. X. Liao, C. J. Xu, and X. H. Tang, "Stability and Hopf bifurcation for a competition and cooperation model of two enterprises with delay," *Communications in Nonlinear Science and Numerical Simulation*, vol. 19, no. 10, pp. 3845–3856, 2014.
- [18] M. X. Liao, C. J. Xu, and X. H. Tang, "Dynamical behaviors for a competition and cooperation model of enterprises with two delays," *Nonlinear Dynamics*, vol. 75, no. 1-2, pp. 257–266, 2014.
- [19] Y. X. Zhang and L. Li, "Dynamic analysis on a diffusive two-enterprise interaction model with two delays," *Journal of Mathematics*, vol. 2022, Article ID 3466954, 20 pages, 2022.
- [20] Q. Lv and X. Liao, "Local and global Hopf bifurcation analysis in a neutral-type neuron system with two delays," *Modern Physics Letters B*, vol. 32, no. 08, Article ID 1850049, 2018.
- [21] S. Tyagi, S. K. Jain, S. Abbas, S. Meherrem, and R. K. Ray, "Time-delay-induced instabilities and Hopf bifurcation analysis in 2-neuron network model with reaction-diffusion term," *Neurocomputing*, vol. 313, pp. 306–315, 2018.
- [22] Y. X. Zhang and L. Li, "Stability and hopf bifurcation analysis of a continuous neural network with mixed delays," *IEEE Access*, vol. 10, 2022.
- [23] C. J. Xu, M. X. Liao, and P. Li, "Bifurcation control for a fractional-order competition model of Internet with delays," *Nonlinear Dynamics*, vol. 95, no. 4, pp. 3335–3356, 2019.
- [24] L. Zhao, J. Cao, C. Huang, M. Xiao, A. Alsaedi, and B. Ahmad, "Bifurcation control in the delayed fractional competitive web-site model with incommensurate-order," *International Journal of Machine Learning and Cybernetics*, vol. 10, no. 1, pp. 173–186, 2019.
- [25] C. H. Zhang and Y. He, "Multiple stability switches and hopf bifurcations induced by the delay in a lengyel-epstein chemical reaction system," *Applied Mathematics and Computation*, vol. 378, Article ID 125201, 2020.
- [26] L. Li and Y. X. Zhang, "Dynamic analysis and hopf bifurcation of a lengyel-epstein system with two delays," *Journal of Mathematics*, vol. 2021, Article ID 5554562, 18 pages, 2021.
- [27] J. Liu, "Hopf bifurcation analysis for an SIRS epidemic model with logistic growth and delays," *Journal of Applied Mathematics and Computing*, vol. 50, no. 1-2, pp. 557–576, 2016.
- [28] Z. Wang and X. Wang, "Stability and hopf bifurcation analysis of a fractional-order epidemic model with time delay," *Mathematical Problems in Engineering*, vol. 2018, Article ID 2308245, 8 pages, 2018.
- [29] Y. X. Zhang, L. Li, J. J. Huang, and Y. J. Liu, "Stability and hopf bifurcation analysis of a vector-borne disease model with two delays and reinfection," *Computational and Mathematical Methods in Medicine*, vol. 2021, Article ID 6648959, 18 pages, 2021.
- [30] Z. Zhang, S. Kundu, J. P. Tripathi, and S. Bugalia, "Stability and Hopf bifurcation analysis of an SVEIR epidemic model with vaccination and multiple time delays," *Chaos, Solitons and Fractals*, vol. 131, Article ID 109483, 2020.
- [31] M. Radha and S. Balamuralitharan, "A study on COVID-19 transmission dynamics: stability analysis of SEIR model with Hopf bifurcation for effect of time delay," *Advances in Difference Equations*, vol. 2020, no. 1, p. 523, 2020.
- [32] J. Huang, Z. Liu, and S. Ruan, "Bifurcation and temporal periodic patterns in a plant-pollinator model with diffusion and time delay effects," *Journal of Biological Dynamics*, vol. 11, no. 1, pp. 138–159, 2016.
- [33] B. D. Hassard, N. D. Kazarinoff, and Y. H. Wan, *Theory and Applications of Hopf Bifurcation*, Cambridge University Press, Cambridge, UK, 1981.
- [34] K. L. Cooke and Z. Grossman, "Discrete delay, distributed delay and stability switches," *Journal of Mathematical Analysis and Applications*, vol. 86, no. 2, pp. 592–627, 1982.
- [35] S. Ruan and J. Wei, "On the zero of some transcendental functions with applications to stability of delay differential equations with two delay," *Dynamics of Continuous, Discrete and Impulsive Systems*, vol. 10, pp. 863–874, 2003.

Research Article

Mann Hybrid Deepest-Descent Extragradient Method with Linear-Search Process for Hierarchical Variational Inequalities for Countable Nonexpansive Mappings

Yun-Ling Cui, Lu-Chuan Ceng , Fang-Fei Zhang, Liang He, Jie Yin, Cong-Shan Wang, and Hui-Ying Hu

Department of Mathematics, Shanghai Normal University, Shanghai 200234, China

Correspondence should be addressed to Lu-Chuan Ceng; zenglc@shnu.edu.cn

Received 7 August 2022; Revised 2 October 2022; Accepted 26 November 2022; Published 15 May 2023

Academic Editor: Rehan Ali

Copyright © 2023 Yun-Ling Cui et al. This is an open access article distributed under the Creative Commons Attribution License, which permits unrestricted use, distribution, and reproduction in any medium, provided the original work is properly cited.

In real Hilbert spaces, let the CFPP indicate a common fixed-point problem of asymptotically nonexpansive operator and countably many nonexpansive operators, and suppose that the HVI and VIP represent a hierarchical variational inequality and a variational inequality problem, respectively. We put forward Mann hybrid deepest-descent extragradient approach for solving the HVI with the CFPP and VIP constraints. The proposed algorithms are on the basis of Mann's iterative technique, viscosity approximation method, subgradient extragradient rule with linear-search process, and hybrid deepest-descent rule. Under suitable restrictions, it is shown that the sequences constructed by the algorithms converge strongly to a solution of the HVI with the CFPP and VIP constraints.

1. Introduction

Suppose that P_C is the nearest point projection from H onto C , where H is a real Hilbert space with the inner product $\langle \cdot, \cdot \rangle$ and induced norm $\| \cdot \|$, and C is a convex closed set with $\emptyset \neq C \subset H$. Let $\text{Fix}(T)$ be the fixed-point set of an operator $T: C \rightarrow H$ and \mathbf{R} be the real-number set. We use the notations \rightharpoonup and \rightarrow to denote the weak convergence and strong one in H , respectively. A self-mapping T on C is said to be of asymptotical nonexpansivity iff $\exists \{\theta_k\} \subset [0, +\infty)$ s.t. $\lim_{k \rightarrow \infty} \theta_k = 0$ and

$$(1 + \theta_k)\|u - v\| \geq \|T^k u - T^k v\|, \forall u, v \in C, k \geq 1. \quad (1)$$

In case $\theta_k = 0$ for each k , T is said to be of nonexpansivity. Given an operator $A: H \rightarrow H$. We consider problem of seeking $x^* \in C$ such that $\langle Ax^*, y - x^* \rangle \geq 0, \forall y \in C$, which is called the classical variational inequality one (VIP). We denote by $\text{VI}(C, A)$ the solution set of the VIP. In particular, if the VIP is defined

over C which is the solution set of another problem, then the VIP is called the hierarchical variational inequality (for short, HVI) over the solution set C . It is well known that the extragradient approach is one of the most effective methods for settling the VIP, which is proposed in Korpelevich [1], that is, for any starting $p_0 \in C$, $\{p_k\}$ is fabricated below:

$$\begin{cases} q_k = P_C(p_k - \mu A p_k), \\ p_{k+1} = P_C(p_k - \mu A q_k), \forall k \geq 0, \end{cases} \quad (2)$$

where $\mu \in (0, 1/L)$ and L is the Lipschitzian coefficient of A . In case $\text{VI}(C, A)$ is nonempty, $\{p_k\}$ converges weakly to an element in $\text{VI}(C, A)$. At present, the vast literature on Korpelevich's extragradient technique reveals that numerous scholars have given wide attention to it and improved it in different manners (refer to [1–28]).

In 2018, Thong and Van Hieu [20] first invented the inertial-type subgradient extragradient rule, i.e., for any starting $p_0, p_1 \in H$, $\{p_k\}$ is fabricated below:

$$\begin{cases} w_k = p_k + \alpha_k(p_k - p_{k-1}), \\ v_k = P_C(w_k - \mu Aw_k), \\ C_k = \{v \in H: \langle w_k - \mu Aw_k - v_k, v_k - v \rangle \geq 0\}, \\ p_{k+1} = P_{C_k}(w_k - \mu Av_k), \forall k \geq 1, \end{cases} \quad (3)$$

where $\mu \in (0, 1/L)$ and L is the Lipschitzian coefficient of A . Via mild assumptions, they showed that $\{p_k\}$ converges weakly to a point in $\text{VI}(C, A)$. Besides, due to the importance and applicability of inertial technique, some new inertial iterative algorithms were recently introduced and analyzed (see [29–32] for more details). Recently, the hybrid inertial-type subgradient extragradient rule with linear-search process in [23] was proposed for settling the VIP with the operator A satisfying both pseudomonotonicity and Lipschitz continuity and the common fixed-point problem (CFPP) of finite nonexpansive operators $\{T_i\}_{i=1}^N$ and asymptotically nonexpansive operator T in H . Let $f: H \rightarrow H$ be a contractive map with coefficient $\delta \in [0, 1]$, and $F: H \rightarrow H$ be an operator satisfying both η -strong monotonicity and κ -Lipschitz continuity, such that $\delta < \tau := 1 - \sqrt{1 - \rho(2\eta - \rho\kappa^2)}$ for $0 < \rho < 2\eta/\kappa^2$. Suppose that $\{\alpha_k\} \subset [0, 1]$ and $\{\beta_k\}, \{\gamma_k\} \subset (0, 1)$ s.t. $\beta_k + \gamma_k < 1, \forall k$. Besides, one writes $T_k := T_{k \bmod N}$ for each $k \geq 1$ with the mod function taking values in $\{1, 2, \dots, N\}$, i.e., in case $k = jN + q$ for some $j \geq 0$ and $0 \leq q < N$, one has that $T_k = T_{\overline{N}}$ for $q = 0$ and $T_k = T_q$ for $0 < q < \overline{N}$.

Under suitable assumptions, they proved the strong convergence of the sequence $\{x_k\}$ to a point in $\Omega = \text{VI}(C, A) \cap (\cap_{i=0}^N \text{Fix}(T_i))$ where $T_0 := T$. On the other hand, Reich et al. [25] put forth the modified projection-type rule for handling the VIP with the operator A satisfying both pseudomonotonicity and uniform continuity. Let $\{\alpha_k\} \subset (0, 1)$ and suppose that $f: C \rightarrow C$ is a contractive map with coefficient $\delta \in [0, 1]$.

Under mild assumptions, they proved strong convergence of the sequence $\{x_k\}$ to an element of $\text{VI}(C, A)$.

In real Hilbert spaces, let the CFPP stand for a common fixed-point problem of asymptotically nonexpansive operator and countably many nonexpansive operators. Let the HVI indicate a hierarchical variational inequality. We put forward Mann hybrid deepest-descent extragradient approach for solving the HVI with the CFPP and VIP constraints. The proposed algorithms are on the basis of Mann's iterative technique, viscosity approximation method, subgradient extragradient rule with linear-search process, and hybrid deepest-descent rule. Under suitable restrictions, it is shown that the sequences constructed by the algorithms converge strongly to a solution of the HVI with the CFPP and VIP constraints.

The structure of the article is arranged as follows. Basic notions and tools are given in Section 2. The convergence analysis of the suggested algorithms is discussed in Section 3. Section 4 provides an illustrated instance to demonstrate the applicability and implementability of our suggested algorithms. It is worth pointing out that the theorems in this article enhance and develop those associated results with [21, 23, 25] because our algorithms involve solving the VIP

with the operator satisfying both pseudomonotonicity and uniform continuity and the CFPP of asymptotically nonexpansive operator and countably many nonexpansive operators.

2. Basic Concepts and Tools

Assume $\emptyset \neq C \subset H$, where C is convex and closed in a real Hilbert space H . For given sequence $\{u_n\} \subset H$, the notations $u_n \rightarrow u$ and $u_n \rightharpoonup u$ indicate the weak convergence and strong convergence of $\{u_n\}$ to u , respectively. For each $y, z \in C$, a mapping $T: C \rightarrow H$ is said to be

- (1) κ -Lipschitzian (or of κ -Lipschitz continuity) iff $\exists \kappa > 0$ s.t. $\|Ty - Tz\| \leq \kappa\|y - z\|$
- (2) Of monotonicity iff $\langle Ty - Tz, y - z \rangle \geq 0$
- (3) Of pseudomonotonicity iff $\langle Ty, z - y \rangle \geq 0 \Rightarrow \langle Tz, z - y \rangle \geq 0$
- (4) Of η -strong monotonicity iff $\exists \eta > 0$ s.t. $\langle Ty - Tz, y - z \rangle \geq \eta\|y - z\|^2$
- (5) Of sequentially weak continuity iff for each $\{y_n\}$ in C , one has that $y_n \rightharpoonup y \Rightarrow Ty_n \rightarrow Ty$

Note that the class of pseudomonotone operators properly includes the class of monotone operators. Given any y in H , we know that $\exists!$ (nearest point) $z \in C$, written as $z = P_C y$, s.t. $\|y - z\| \leq \|y - x\|$ for each x in C . P_C is called a nearest point (or metric) projection from H onto C . According to [33], for each $y, z \in H$, the statements below are valid:

- (1) $\langle y - z, P_C y - P_C z \rangle \geq \|P_C y - P_C z\|^2$
- (2) $\langle y - P_C y, x - P_C y \rangle \leq 0, \forall x \in C$
- (3) $\|y - x\|^2 \geq \|y - P_C y\|^2 + \|x - P_C y\|^2, \forall x \in C$
- (4) $\|y - z\|^2 = \|y\|^2 - \|z\|^2 - 2\langle y - z, z \rangle$
- (5) $\|\lambda y + (1 - \lambda)z\|^2 = \lambda\|y\|^2 + (1 - \lambda)\|z\|^2 - \lambda(1 - \lambda)\|y - z\|^2, \forall \lambda \in [0, 1]$

Definition 1 (see [34]). Let $\{\xi_n\}_{n=1}^\infty \subset [0, 1]$ and suppose that $\{T_n\}_{n=1}^\infty$ is a sequence of nonexpansive operators of C into itself. For each n , the operator $W_n: C \rightarrow C$ is constructed below:

$$\begin{cases} U_{n,n+1} = I, \\ U_{n,n} = \xi_n T_n U_{n,n+1} + (1 - \xi_n)I, \\ U_{n,n-1} = \xi_{n-1} T_{n-1} U_{n,n} + (1 - \xi_{n-1})I, \\ \dots \\ U_{n,i} = \xi_i T_i U_{n,i+1} + (1 - \xi_i)I, \\ \dots \\ U_{n,2} = \xi_2 T_2 U_{n,3} + (1 - \xi_2)I, \\ W_n = U_{n,1} = \xi_1 T_1 U_{n,2} + (1 - \xi_1)I. \end{cases} \quad (4)$$

Such an operator W_n is nonexpansive and is known as the W -mapping constructed by T_1, \dots, T_n and ξ_1, \dots, ξ_{n-1} .

Initialization: Given any starting $x_1, x_0 \in H$. Let $\mu \in (0, 1), \ell \in (0, 1), \gamma > 0$.

Iterations: Compute x_{k+1} below:

Step 1. Put $w_k = T_k x_k + \alpha_k (T_k x_k - T_k x_{k-1})$ and calculate $v_k = P_C(w_k - \tau_k A w_k)$, with τ_k being picked to be the largest $\tau \in \{\gamma, \gamma \ell, \gamma \ell^2, \dots\}$ s.t. $\tau \|A w_k - A v_k\| \leq \mu \|w_k - v_k\|$.

Step 2. Calculate $z_k = P_{C_k}(w_k - \tau_k A v_k)$ with $C_k := \{v \in H: \langle w_k - \tau_k A w_k - v_k, v_k - v \rangle \geq 0\}$.

Step 3. Calculate $x_{k+1} = \beta_k f(x_k) + \gamma_k x_k + ((1 - \gamma_k)I - \beta_k \rho F) T^k z_k$.

Again set $k := k + 1$ and go to Step 1.

ALGORITHM 1: Hybrid inertial subgradient extragradient rule (see [23]).

Initialization: Given any starting $x_1 \in C$. Let $\lambda \in (0, 1/\mu), \ell \in (0, 1), \mu > 0$.

Iterations: Compute x_{k+1} below:

Step 1. Calculate $v_k = P_C(x_k - \lambda A x_k)$ and $r_\lambda(x_k) := x_k - v_k$. In case $r_\lambda(x_k) = 0$, one stops; x_k lies in $\text{VI}(C, A)$. In case $r_\lambda(x_k) \neq 0$, one goes to Step 2.

Step 2. Calculate $w_k = x_k - \tau_k r_\lambda(x_k)$, with $\tau_k := \ell^{j_k}$ and j_k is the smallest nonnegative integer j satisfying $\langle A x_k - A(x_k - \ell^j r_\lambda(x_k)), r_\lambda(x_k) \rangle \leq \mu/2 \|r_\lambda(x_k)\|^2$.

Step 3. Calculate $x_{k+1} = \alpha_k f(x_k) + (1 - \alpha_k) P_{C_k}(x_k)$, with $C_k := \{v \in C: \hat{h}_k(v) \leq 0\}$ and $\hat{h}_k(v) = \langle A w_k, v - x_k \rangle + \tau_k/2 \lambda \|r_\lambda(x_k)\|^2$.

Again set $k := k + 1$ and go to Step 1.

ALGORITHM 2: Modified projection-type rule (see [25]).

Proposition 1 (see [34]). Let $[\{\xi_n\}_{n=1}^\infty \subset (0, 1)]$ and suppose that $\{T_n\}_{n=1}^\infty$ is a sequence of nonexpansive operators of C into itself such that $\bigcap_{n=1}^\infty \text{Fix}(T_n) \neq \emptyset$. Then,

(a) W_n is of nonexpansivity and $\text{Fix}(W_n) = \bigcap_{i=1}^\infty \text{Fix}(T_i), \forall n$

(b) $\lim_{n \rightarrow \infty} U_{n,i} u$ exists for all $u \in C$ and $i \geq 1$

(c) The mapping W defined by $Wu := \lim_{n \rightarrow \infty} W_n u = \lim_{n \rightarrow \infty} U_{n,1} u, \forall u \in C$ is nonexpansive operator such that $\text{Fix}(W) = \bigcap_{n=1}^\infty \text{Fix}(T_n)$, and W is known as the W -operator constructed by T_1, T_2, \dots and ξ_1, ξ_2, \dots

Proposition 2 (see [35]). Let $\{\xi_n\}_{n=1}^\infty \subset (0, \varsigma)$ for certain $\varsigma \in (0, 1)$ and suppose $\{T_n\}_{n=1}^\infty$ is a sequence of nonexpansive operators of C into itself such that $\bigcap_{n=1}^\infty \text{Fix}(T_n) \neq \emptyset$. Then, $\lim_{n \rightarrow \infty} \sup_{u \in D} \|W_n u - W u\| = 0, \forall$ (bounded) $D \subset C$.

In what follows, one always assumes that $\{\xi_n\}_{n=1}^\infty \subset (0, \varsigma)$ for certain $\varsigma \in (0, 1)$. Using the subdifferential inequality of $\|\cdot\|^2/2$, we have the relation below:

$$\|y + z\|^2 \leq \|y\|^2 + 2\langle z, y + z \rangle, \forall y, z \in H. \quad (5)$$

Later, we will exploit the lemmas below to derive our main theorems.

Lemma 1 (see [26]). Let H_1 and H_2 be two real Hilbert spaces. Suppose that $A: H_1 \rightarrow H_2$ is uniformly continuous on bounded subsets of H_1 and M is a bounded subset of H_1 . Then, $A(M)$ is bounded.

Lemma 2 (see [36]). Let h be a real-valued function on H and define $K := \{x \in C: h(x) \leq 0\}$. If K is nonempty and h is Lipschitz continuous on C with modulus $\theta > 0$, then $\text{dist}(x, K) \geq \theta^{-1} \max\{h(x), 0\}, \forall x \in C$, where $\text{dist}(x, K)$ denotes the distance of x to K .

Lemma 3. Suppose that $A: C \rightarrow H$ is of both pseudomonotonicity and continuity. Given a point $z^* \in C$. Then, $\langle A z^*, y - z^* \rangle \geq 0 \forall y \in C \Leftrightarrow \langle A y, y - z^* \rangle \geq 0 \forall y \in C$.

Proof. It is easy to check that the conclusion is valid. \square

Lemma 4 (see [8]). Suppose that $\{\bar{a}_n\} \subset [0, \infty]$ such that $\bar{a}_{n+1} \leq (1 - \zeta_n) \bar{a}_n + \zeta_n \bar{b}_n, \forall n \geq 1$, with $\{\zeta_n\}$ and $\{\bar{b}_n\}$ both being real sequences satisfying the conditions: (i) $\{\zeta_n\} \subset [0, 1]$ and $\sum_{n=1}^\infty \zeta_n = \infty$, and (ii) $\limsup_{n \rightarrow \infty} \bar{b}_n \leq 0$ or $\sum_{n=1}^\infty |\zeta_n \bar{b}_n| < \infty$. Then, $\lim_{n \rightarrow \infty} \bar{a}_n = 0$.

Lemma 5 (see [37]). Suppose that $\emptyset \neq C \subset X$ where C is convex and closed in a Banach space X admitting a weakly continuous duality mapping. Let the operator $T: C \rightarrow C$ be of asymptotical nonexpansivity such that $\text{Fix}(T) \neq \emptyset$. Then, $I - T$ is of demiclosedness at zero, that is, for each $\{u_n\} \subset C$ with $u_n \rightarrow u \in C$, the relation holds: $(I - T)u_n \rightarrow 0 \Rightarrow (I - T)u = 0$, with I being the identity mapping of X .

Lemma 6 (see [38]). Suppose that $\{\Gamma_m\}$ is a real sequence which does not decrease at infinity in the sense that $\exists \{\Gamma_{m_j}\} \subset \{\Gamma_m\}$ s.t. $\Gamma_{m_j} < \Gamma_{m_{j+1}}, \forall j \geq 1$. Let $\{\eta(m)\}_{m \geq m_0}$ be formulated by $\eta(m) = \max\{j \leq m: \Gamma_j < \Gamma_{j+1}\}$, with $m_0 \geq 1$ s.t. $\{m \leq m_0: \Gamma_m < \Gamma_{m+1}\} \neq \emptyset$. Then, the statements below are valid:

- (i) $\eta(m_0) \leq \eta(m_0 + 1) \leq \dots$ and $\eta(m) \rightarrow \infty$
- (ii) $\Gamma_{\eta(m)} \leq \Gamma_{\eta(m)+1}$ and $\Gamma_m \leq \Gamma_{\eta(m)+1}, \forall m \geq m_0$

Lemma 7 (see [7, Lemma 8]). Suppose that λ lies in $(0, 1]$, T is a nonexpansive self-mapping on C , and $T^\lambda: C \rightarrow H$ is the mapping formulated by $T^\lambda x := (I - \lambda \rho F) T x, \forall x \in C$, with $F: C \rightarrow H$ being of both κ -Lipschitz continuity and η -strong

monotonicity. Then, T^λ is a contractive map for $\rho \in (0, 2\eta/\kappa^2)$, i.e., $\|T^\lambda y - T^\lambda z\| \leq (1 - \lambda\tau)\|y - z\|, \forall y, z \in C$, with $\tau = 1 - \sqrt{1 - \rho(2\eta - \rho\kappa^2)} \in (0, 1)$.

3. Algorithms and Convergence Analysis

Let $\emptyset \neq C \subset H$, with the feasible set C being convex and closed in a real Hilbert space H .

Condition 1. The following conditions are valid.

(C1) $\{T_n\}_{n=1}^\infty$ is a sequence of nonexpansive operators of C into itself and $T: C \rightarrow C$ is asymptotical nonexpansivity operator with $\{\theta_n\}$.

(C2) W_n is the W -mapping constructed by T_1, \dots, T_n and ξ_1, \dots, ξ_n , with $\{\xi_n\}_{n=1}^\infty \subset [0, \varsigma]$ for certain $\varsigma \in (0, 1)$.

(C3) $A: H \rightarrow H$ is of both pseudomonotonicity and uniform continuity on C , s.t. $\|Az\| \leq \liminf_{n \rightarrow \infty} \|Au_n\|$ for each $\{u_n\} \subset C$ with $u_n \rightarrow z$.

(C4) $f: C \rightarrow H$ is a contractive map with coefficient $\delta \in [0, 1]$, and $F: C \rightarrow H$ is of both η -strong monotonicity and κ -Lipschitz continuity s.t. $\tau = 1 - \sqrt{1 - \rho(2\eta - \rho\kappa^2)} > \delta$ with $0 < \rho < 2\eta/\kappa^2$.

(C5) $\Omega = \text{VI}(C, A) \cap (\cap_{n=1}^\infty \text{Fix}(T_n)) \neq \emptyset$ where $T_0 := T$.

(C6) $\{\gamma_n\}, \{\beta_n\} \subset (0, 1)$ and $\{\sigma_n\} \subset [0, 1]$ s.t.

- (i) $1 > \gamma_n + \beta_n$ and $\sum_{n=1}^\infty \beta_n = \infty$.
- (ii) $\beta_n \rightarrow 0$ and $\theta_n/\beta_n \rightarrow 0$ as $n \rightarrow \infty$.
- (iii) $1 > \limsup_{n \rightarrow \infty} \sigma_n \geq \liminf_{n \rightarrow \infty} \sigma_n > 0$.
- (iv) $1 > \limsup_{n \rightarrow \infty} \gamma_n \geq \liminf_{n \rightarrow \infty} \gamma_n > 0$.

Lemma 8. *The Armijo-type search process (Algorithm 1) is formulated well, and the relation is valid: $\|r_\lambda(w_n)\|^2 \leq \lambda \langle Aw_n, r_\lambda(w_n) \rangle$.*

Proof. Using the uniformly continuity of A on C , from $l \in (0, 1)$, one has $\lim_{j \rightarrow \infty} \langle Aw_n - A(w_n - l^j r_\lambda(w_n)), r_\lambda(w_n) \rangle = 0$. In case $r_\lambda(w_n) = 0$, it is clear that $j_n = 0$. In case

$r_\lambda(w_n) \neq 0$, there exists $j_n \geq 0$ meeting (Algorithm 1). Since P_C is firmly nonexpansive, we obtain that $\langle u - P_C v, u - v \rangle \geq \|u - P_C v\|^2, \forall u \in C, v \in H$. Setting $u = w_n$ and $v = w_n - \lambda A w_n$, one gets $\lambda \langle A w_n, w_n - P_C(w_n - \lambda A w_n) \rangle \geq \|w_n - P_C(w_n - \lambda A w_n)\|^2$, which attains the desired result. \square

Lemma 9. *Let $p \in \Omega$ and h_n be formulated as in (Algorithm 1). Then, $h_n(p) \leq 0$ and $h_n(w_n) = \tau_n/2\lambda \|r_\lambda(w_n)\|^2$. Particularly, in case $r_\lambda(w_n) \neq 0$, one has $h_n(w_n) > 0$.*

Proof. It is clear that $h_n(w_n) = \tau_n/2\lambda \|r_\lambda(w_n)\|^2$. In what follows, we claim $h_n(p) \leq 0$. Indeed, in terms of Lemma 3, one gets $\langle At_n, t_n - p \rangle \geq 0$. Hence, one has $h_n(p) = \langle At_n, t_n - w_n \rangle + \langle At_n, p - t_n \rangle + \tau_n/2\lambda \|r_\lambda(w_n)\|^2 \leq -\tau_n \langle At_n, r_\lambda(w_n) \rangle + \tau_n/2\lambda \|r_\lambda(w_n)\|^2$. Using (Algorithm 1) and Lemma 8, one gets $\langle At_n, r_\lambda(w_n) \rangle \geq \langle A w_n, r_\lambda(w_n) \rangle - \mu/2 \|r_\lambda(w_n)\|^2 \geq (1/\lambda - \mu/2) \|r_\lambda(w_n)\|^2$, which hence arrives at $h_n(p) \leq -\tau_n/2(1/\lambda - \mu) \|r_\lambda(w_n)\|^2$. Therefore, the claim is valid. \square

Lemma 10. *Suppose that the sequences $\{z_n\}, \{y_n\}, \{x_n\}, \{w_n\}$ fabricated in Algorithm 3, are of boundedness. Assume that $x_{n+1} - x_n \rightarrow 0, x_n - w_n \rightarrow 0, y_n - w_n \rightarrow 0, z_n - w_n \rightarrow 0$ and $T^{n+1}x_n - T^n x_n \rightarrow 0$. Then, $\omega_w(\{x_n\}) \subset \Omega$, with $\omega_w(\{x_n\}) = \{z \in H: x_{n_k} \rightarrow z \text{ for certain } \{x_{n_k}\} \subset \{x_n\}\}$.*

Proof. Take a fixed $z \in \omega_w(\{x_n\})$ arbitrarily. Then, $\exists \{x_{n_k}\} \subset \{x_n\}$ s.t. $x_{n_k} \rightarrow z \in H$. Owing to $x_n - w_n \rightarrow 0$, one knows that $\exists \{w_{n_k}\} \subset \{w_n\}$ s.t. $w_{n_k} \rightarrow z \in H$. In what follows, we claim $z \in \Omega$. In fact, observe that $x_n - w_n = \sigma_n(x_n - W_n x_n), \forall n$. Thus, $\|x_n - w_n\| = \sigma_n \|x_n - W_n x_n\|$. Using the assumptions $\liminf_{n \rightarrow \infty} \sigma_n > 0$ and $x_n - w_n \rightarrow 0$, we have

$$\lim_{n \rightarrow \infty} \|x_n - W_n x_n\| = 0. \tag{6}$$

Putting $v_n := \beta_n f(x_n) + \gamma_n x_n + ((I - \gamma_n)I - \beta_n \rho F)T^n z_n$, by Algorithm 3 we obtain that $x_{n+1} = P_C v_n$ and $v_n - T^n z_n = \beta_n f(x_n) + \gamma_n(x_n - T^n z_n) - \beta_n \rho F T^n z_n$, which immediately yields

$$\begin{aligned} \|x_n - T^n z_n\| &\leq \|x_n - x_{n+1}\| + \|x_{n+1} - T^n z_n\| \leq \|x_n - x_{n+1}\| + \|v_n - T^n z_n\| \\ &\leq \|x_n - x_{n+1}\| + \beta_n \|f(x_n)\| + \gamma_n \|x_n - T^n z_n\| + \beta_n \|\rho F T^n z_n\|. \end{aligned} \tag{7}$$

Hence, one gets $\|x_{n+1} - x_n\| + \beta_n(\|f(x_n)\| + \|\rho F T^n z_n\|) \geq (1 - \gamma_n)\|T^n z_n - x_n\|$. Since $x_{n+1} - x_n \rightarrow 0, \beta_n \rightarrow 0, \liminf_{n \rightarrow \infty} (1 - \gamma_n) > 0$ and $\{x_n\}, \{z_n\}$ are of boundedness,

one gets $\lim_{n \rightarrow \infty} \|T^n z_n - x_n\| = 0$. We claim that $\lim_{n \rightarrow \infty} \|x_n - T x_n\| = 0$. Indeed, since T is of asymptotical nonexpansivity, we obtain

Initial Step: Given any starting $x_1 \in C$. Let $\mu > 0, \lambda \in (0, 1/\mu), l \in (0, 1)$.

Iterations: Given the current iterate x_n , calculate x_{n+1} below:

Step 1. Compute $w_n = (1 - \sigma_n)x_n + \sigma_n W_n x_n$, $y_n = P_C(w_n - \lambda A w_n)$ and $r_\lambda(w_n) := w_n - y_n$.

Step 2. Compute $t_n = w_n - \tau_n r_\lambda(w_n)$, where $\tau_n := l^{j_n}$ and the integer j_n is the smallest nonnegative one j s.t. $\mu/2 \|r_\lambda(w_n)\|^2 \geq \langle A(w_n - l^j r_\lambda(w_n)) - A w_n, y_n - w_n \rangle$

Step 3. Calculate

$$x_{n+1} = P_C[\beta_n f(x_n) + \gamma_n x_n + ((1 - \gamma_n)I - \beta_n \rho F)T^n z_n]$$

with $z_n = P_{C_n}(w_n)$, $C_n := \{u \in C: h_n(u) \leq 0\}$ and $h_n(u) = \langle A t_n, u - w_n \rangle + \tau_n/2\lambda \|r_\lambda(w_n)\|^2$.

Set $n := n + 1$ and go to Step 1.

ALGORITHM 3: The 1st Mann hybrid deepest-descent extragradient rule.

$$\begin{aligned} \|x_n - T x_n\| &\leq \|x_n - T^n z_n\| + \|T^n z_n - T^n x_n\| + \|T^n x_n - T^{n+1} x_n\| + \|T^{n+1} x_n - T^{n+1} z_n\| \\ &\quad + \|T^{n+1} z_n - T x_n\| \\ &\leq (2 + \theta_1) \|x_n - T^n z_n\| + (2 + \theta_n + \theta_{n+1}) \|z_n - x_n\| + \|T^n x_n - T^{n+1} x_n\| \\ &\leq (2 + \theta_1) \|x_n - T^n z_n\| + (2 + \theta_n + \theta_{n+1}) (\|z_n - w_n\| + \|w_n - x_n\|) + \|T^n x_n - T^{n+1} x_n\|. \end{aligned} \quad (8)$$

Noticing $x_n - w_n \rightarrow 0$, $z_n - w_n \rightarrow 0$, and $x_n - T^n z_n \rightarrow 0$, we obtain

$$\lim_{n \rightarrow \infty} \|x_n - T x_n\| = 0. \quad (9)$$

Also, we claim $\lim_{n \rightarrow \infty} \|W x_n - x_n\| = 0$. In fact, it is clear that $\|x_n - w_n\| = \sigma_n \|x_n - W_n x_n\|$. Since $\liminf_{n \rightarrow \infty} \sigma_n > 0$ and $x_n - w_n \rightarrow 0$, one has $\lim_{n \rightarrow \infty} \|W_n x_n - x_n\| = 0$. Note that $\|W x_n - x_n\| \leq \|W x_n - W_n x_n\| + \|W_n x_n - x_n\| \leq \sup_{u \in D} \|W u - W_n u\| + \|W_n x_n - x_n\|$, where $D = \{x_n: n \geq 1\}$. Using Proposition 2, we obtain

$$\lim_{n \rightarrow \infty} \|W x_n - x_n\| = 0. \quad (10)$$

Now, we claim $z \in \text{VI}(C, A)$. Indeed, because C is of both convexity and closedness, using $\{w_n\} \subset C$ and $w_{n_k} \rightarrow z$, one has that z lies in C . In case $Az = 0$, it is easily known that $z \in \text{VI}(C, A)$ due to $\langle Az, x - z \rangle \geq 0, \forall x \in C$. In case $Az \neq 0$, combining $w_n - y_n \rightarrow 0$ and $w_{n_k} \rightarrow z$ yields $y_{n_k} \rightarrow z$ as $k \rightarrow \infty$. By the condition imposed on A , one gets $0 < \|Az\| \leq \liminf_{k \rightarrow \infty} \|A y_{n_k}\|$. So, we may presume $\|A y_{n_k}\| \neq 0, \forall k$. In addition, using $y_n = P_C(w_n - \lambda A w_n)$, one has $\langle w_n - \lambda A w_n - y_n, x - y_n \rangle \leq 0, \forall x \in C$, and hence

$$\begin{aligned} \langle A w_n, x - w_n \rangle &\geq \langle A w_n, y_n - w_n \rangle \\ &\quad + \frac{1}{\lambda} \langle w_n - y_n, x - y_n \rangle, \forall x \in C. \end{aligned} \quad (11)$$

Since A is uniformly continuous on C , $\{A w_n\}$ is of boundedness (owing to Lemma 1). Note that $\{y_n\}$ is bounded as well. Thus, using (11), one gets $\liminf \langle A w_{n_k}, x - w_{n_k} \rangle \geq 0, \forall x \in C$. It is clear that $\langle A y_n, x - y_n \rangle \stackrel{k \rightarrow \infty}{\cong} \langle A y_n - A w_n, x - w_n \rangle + \langle A w_n, x - w_n \rangle + \langle A y_n, w_n - y_n \rangle$. Thus, using $y_n - w_n \rightarrow 0$, one gets $A w_n - A y_n \rightarrow 0$ and hence attains $\liminf_{k \rightarrow \infty} \langle A y_{n_k}, x - y_{n_k} \rangle \geq 0, \forall x \in C$.

In what follows, one picks $\{\zeta_j\} \subset (0, 1)$ s.t. $\zeta_j \downarrow 0$ ($j \rightarrow \infty$). For any $j \geq 1$, one writes by m_j the smallest natural number s.t.

$$\langle A y_{n_k}, x - y_{n_k} \rangle + \zeta_j \geq 0, \forall k \geq m_j. \quad (12)$$

Noticing the fact that $\{\zeta_j\}$ is decreasing, we can readily see that $\{m_j\}$ is increasing. From $A y_{m_j} \neq 0, \forall j$ (owing to $\{A y_{m_j}\} \subset \{A y_{n_j}\}$), one puts $v_{m_j} = A y_{m_j} / \|A y_{m_j}\|^2$, and one has $\langle A y_{m_j}, v_{m_j} \rangle = 1, \forall j$. Thus, using (12), one gets $\langle A y_{m_j}, x + \zeta_j v_{m_j} - y_{m_j} \rangle \geq 0, \forall j$. Also, since A is pseudo-monotone, one has $\langle A(x + \zeta_j v_{m_j}), x + \zeta_j v_{m_j} - y_{m_j} \rangle \geq 0, \forall j$, which hence yields

$$\begin{aligned} \langle A x, x - y_{m_j} \rangle &\geq \langle A x - A(x + \zeta_j v_{m_j}), x + \zeta_j v_{m_j} - y_{m_j} \rangle \\ &\quad - \zeta_j \langle A x, v_{m_j} \rangle. \end{aligned} \quad (13)$$

Let us show $\lim_{j \rightarrow \infty} \zeta_j v_{m_j} = 0$. In fact, using $w_{n_j} \rightarrow z \in C$ and $y_n - w_n \rightarrow 0$, one obtains $y_{n_j} \rightarrow z$. Noticing

$\{y_{m_j}\} \subset \{y_{n_j}\}$ and $\zeta_j \downarrow 0$, one deduces that $0 \leq \limsup_{j \rightarrow \infty} \|\zeta_j v_{m_j}\| = \limsup_{j \rightarrow \infty} \zeta_j / \|A y_{m_j}\| \leq$

$\limsup_{j \rightarrow \infty} \zeta_j / \liminf_{j \rightarrow \infty} \|A y_{n_j}\| = 0$. Hence, we get $\zeta_j v_{m_j} \rightarrow 0$ as $j \rightarrow \infty$. So, it follows that the right-hand side of (13) tends to zero by the uniform continuity of A and the boundedness of $\{y_{m_j}\}, \{v_{m_j}\}$, and $\lim_{j \rightarrow \infty} \zeta_j v_{m_j} = 0$. Therefore,

$\langle A x, x - z \rangle = \liminf_{j \rightarrow \infty} \langle A x, x - y_{m_j} \rangle \geq 0, \forall x \in C$. Using Lemma 3, one has $z \in \text{VI}(C, A)$. Last, we claim $z \in \Omega$. In fact, using $x_n - w_n \rightarrow 0$ and $w_{n_j} \rightarrow z$, one gets $x_{n_j} \rightarrow z$. Note that (9) guarantees $x_{n_j} - T x_{n_j} \rightarrow 0$. By Lemma 5, one knows that $I - T$ is of demiclosedness at zero. Thus, using $x_{n_j} \rightarrow z$, one gets $(I - T)z = 0$, that is, $z \in \text{Fix}(T)$. Besides, we claim $z \in \text{Fix}(W) = \bigcap_{n=1}^{\infty} \text{Fix}(T_n)$. Actually, noticing $x_{n_j} \rightarrow z$ and $x_{n_j} - W x_{n_j} \rightarrow 0$ (due to (10)), from Proposition 1 and

Lemma 5, we obtain that $I - W$ is demiclosed at zero. This hence yields $z \in \text{Fix}(W) = \bigcap_{n=1}^{\infty} \text{Fix}(T_i)$. Consequently, $z \in \text{VI}(C, A) \cap (\bigcap_{n=1}^{\infty} \text{Fix}(T_i)) = \Omega$. \square

Lemma 11. Let $\{w_n\}$ be the sequence fabricated in Algorithm 3. Then,

$$\tau_n \|r_\lambda(w_n)\|^2 \longrightarrow 0 \Rightarrow y_n - w_n \longrightarrow 0. \quad (14)$$

Proof. Assume $\limsup_{n \rightarrow \infty} \|y_n - w_n\| = \alpha > 0$. Picking $\{n_k\} \subset \{n\}$, one has $\lim_{k \rightarrow \infty} \|w_{n_k} - y_{n_k}\| = \alpha > 0$. Note that $\lim_{k \rightarrow \infty} \tau_{n_k} \|r_\lambda(w_{n_k})\|^2 = 0$. Consider two cases. If $\liminf_{k \rightarrow \infty} \tau_{n_k} > 0$, one may presume that $\exists d > 0$ s.t. $\tau_{n_k} \geq d > 0, \forall k$. So, one knows that $\|w_{n_k} - y_{n_k}\|^2 = 1/\tau_{n_k} \tau_{n_k} \|w_{n_k} - y_{n_k}\|^2 \leq 1/d \cdot \tau_{n_k} \|w_{n_k} - y_{n_k}\|^2 = 1/d \cdot \tau_{n_k} \|r_\lambda(w_{n_k})\|^2$, which immediately leads to $0 < d^2 = \lim_{k \rightarrow \infty} \|w_{n_k} - y_{n_k}\|^2 \leq \lim_{k \rightarrow \infty} \{1/d \cdot \tau_{n_k} \|r_\lambda(w_{n_k})\|^2\} = 0$. This reaches a contradiction.

If $\liminf_{k \rightarrow \infty} \tau_{n_k} = 0$, there exists a subsequence of $\{\tau_{n_k}\}$, still denoted by $\{\tau_{n_k}\}$, s.t. $\lim_{k \rightarrow \infty} \tau_{n_k} = 0$. We now put $q_{n_k} := 1/\tau_{n_k} y_{n_k} + (1 - 1/\tau_{n_k}) w_{n_k} = w_{n_k} - 1/\tau_{n_k} (w_{n_k} - y_{n_k})$. Then, from $\lim_{k \rightarrow \infty} \tau_{n_k} \|r_\lambda(w_{n_k})\|^2 = 0$, we deduce that $\lim_{k \rightarrow \infty} \|q_{n_k} - w_{n_k}\|^2 = \lim_{k \rightarrow \infty} 1/l^2 \tau_{n_k} \cdot \tau_{n_k} \|y_{n_k} - w_{n_k}\|^2 = 0$. Using (6), one obtains $\langle Aw_{n_k} - Aq_{n_k}, w_{n_k} - y_{n_k} \rangle > \mu/2 \|w_{n_k} - y_{n_k}\|^2$. Since A is uniformly continuous on bounded subsets of C , this ensures that $\lim_{k \rightarrow \infty} \|Aw_{n_k} - Aq_{n_k}\| = 0$, which hence yields $\lim_{k \rightarrow \infty} \|y_{n_k} - w_{n_k}\| = 0$. This reaches a contradiction. Therefore, $y_n - w_n \longrightarrow 0$ as $n \longrightarrow \infty$. \square

Theorem 1. Let $\{x_n\}$ be the sequence fabricated in Algorithm 3. Assume $T^{n+1}x_n - T^n x_n \longrightarrow 0$. Then, $\{x_n\}$ converges strongly to $x^* \in \Omega$, which is only a solution to the VIP: $\langle (f - \rho F)x^*, x - x^* \rangle \leq 0, \forall x \in \Omega$.

Proof. Thanks to $1 > \limsup_{n \rightarrow \infty} \sigma_n \geq \liminf_{n \rightarrow \infty} \sigma_n > 0$ and $\theta_n/\beta_n \longrightarrow 0$, one may presume that $(0, 1) \supset [a, b] \supset \{\sigma_n\}$ and $\beta_n(\tau - \delta)/2 \geq \theta_n, \forall n$. It is easy to check that $P_\Omega(I - \rho F + f): C \longrightarrow C$ is a contractive map. Thus, $\exists! x^* \in C$ s.t. $x^* = P_\Omega(I - \rho F + f)x^*$. Hence, $\exists! x^* \in \Omega$ satisfying the VIP:

$$\langle (f - \rho F)x^*, x - x^* \rangle \leq 0, \forall x \in \Omega. \quad (15)$$

Next in the rest of the proof, we divide it into a few steps. \square

Step 1. One claims that $\{x_n\}$ is of boundedness. Indeed, choose any $p \in \Omega = \text{VI}(C, A) \cap (\bigcap_{n=1}^{\infty} \text{Fix}(T_i))$. Then, $Tp = p$ and $W_n p = p, \forall n$. Let us show the relation below:

$$-\text{dist}^2(w_n, C_n) + \|w_n - p\|^2 \geq \|z_n - p\|^2, \forall p \in \Omega. \quad (16)$$

In fact, one has $\|z_n - p\|^2 = \|P_{C_n} w_n - p\|^2 \leq \|w_n - p\|^2 - \text{dist}^2(w_n, C_n)$, which hence yields

$$\|z_n - p\| \leq \|w_n - p\|, \forall n \geq 1. \quad (17)$$

Using the formulation of w_n , one gets $\|w_n - p\| \leq (1 - \sigma_n) \|x_n - p\| + \sigma_n \|W_n x_n - p\| \leq \|x_n - p\|$, which together with (17) yields

$$\|z_n - p\| \leq \|w_n - p\| \leq \|x_n - p\|, \forall n \geq 1. \quad (18)$$

Noticing $1 > \gamma_n + \beta_n$, from (18) and Lemma 7, we obtain

$$\begin{aligned} \|x_{n+1} - p\| &\leq \|\beta_n f(x_n) + \gamma_n x_n + ((1 - \gamma_n)I - \beta_n \rho F)T^n z_n - p\| \\ &= \|\beta_n (f(x_n) - f(p)) + \gamma_n (x_n - p) + (1 - \gamma_n) \\ &\quad \times [(I - \beta_n/1 - \gamma_n \rho F)T^n z_n - (I - \beta_n/1 - \gamma_n \rho F)p] + \beta_n (f - \rho F)p\| \\ &\leq \beta_n \delta \|x_n - p\| + \gamma_n \|x_n - p\| + (1 - \gamma_n) \\ &\quad \times (1 - \beta_n/1 - \gamma_n \tau) (1 + \theta_n) \|z_n - p\| + \beta_n \| (f - \rho F)p \| \\ &\leq [\beta_n \delta + \gamma_n + (1 - \gamma_n - \beta_n \tau) + \theta_n] \|x_n - p\| + \beta_n \| (f - \rho F)p \| \\ &\leq \max \{ \|x_n - p\|, 2 \| (f - \rho F)p \| / \tau - \delta \}. \end{aligned} \quad (19)$$

Using the induction, we get $\|x_n - p\| \leq \max \{ \|x_1 - p\|, 2 \| (f - \rho F)p \| / \tau - \delta \}, \forall n \geq 1$. Hence, $\{x_n\}$ is of boundedness. Therefore, the sequences $\{w_n\}, \{y_n\}, \{z_n\}, \{f(x_n)\}, \{A_t n\}, \{W_n x_n\}, \{T^n z_n\}$ are of boundedness as well.

Step 2. One claims that $\|v_n - x_{n+1}\|^2 \leq -\|x_{n+1} - p\|^2 + \|x_n - p\|^2 + \beta_n M_1$ for certain $M_1 > 0$. In fact, using Lemma 7 and the convexity of $g(s) = s^2, \forall s \in \mathbf{R}$, we obtain that

$$\begin{aligned}
\|x_{n+1} - p\|^2 &\leq \|v_n - p\|^2 - \|v_n - x_{n+1}\|^2 = \|\beta_n(f(x_n) - f(p)) + \gamma_n(x_n - p) + (1 - \gamma_n) \\
&\quad \times \left[\left(I - \frac{\beta_n}{1 - \gamma_n} \rho F \right) T^n z_n - \left(I - \frac{\beta_n}{1 - \gamma_n} \rho F \right) p \right] + \beta_n(f - \rho F)p\|^2 - \|v_n - x_{n+1}\|^2 \\
&\leq \{\beta_n\|f(x_n) - f(p)\| + \gamma_n\|x_n - p\| + (1 - \gamma_n) \\
&\quad \times \left\| \left(I - \frac{\beta_n}{1 - \gamma_n} \rho F \right) T^n z_n - \left(I - \frac{\beta_n}{1 - \gamma_n} \rho F \right) p \right\|^2 + 2\beta_n \langle (f - \rho F)p, v_n - p \rangle - \|v_n - x_{n+1}\|^2 \\
&\leq \|x_n - p\|^2 + \gamma_n\|x_n - p\|^2 + [(1 - \gamma_n - \beta_n\tau) + \theta_n]\|z_n - p\|^2 \\
&\quad + 2\beta_n \langle (f - \rho F)p, v_n - p \rangle - \|v_n - x_{n+1}\|^2,
\end{aligned} \tag{20}$$

where $v_n := \beta_n f(x_n) + \gamma_n x_n + ((1 - \gamma_n)I - \beta_n \rho F)T^n z_n$ and $x_{n+1} = P_C(v_n)$. Furthermore, according to Algorithm 3, we obtain

Substituting (21) into (20), one gets

$$\begin{aligned}
\|z_n - p\|^2 \|w_n - p\|^2 - \|w_n - z_n\|^2 &= (1 - \sigma_n)\|x_n - p\|^2 \\
+ \sigma_2 \|W_n x_n - p\|^2 - \sigma_n(1 - \sigma_n)\|W_n x_n - x_n\|^2 - \|w_n - z_n\|^2.
\end{aligned} \tag{21}$$

$$\begin{aligned}
\|x_{n+1} - p\|^2 &\leq \beta_n \delta \|x_n - p\|^2 + \gamma_n \|x_n - p\|^2 + [(1 - \gamma_n - \beta_n\tau) + \theta_n] \left\{ \|x_n - p\|^2 \right\} \\
&\quad - \sigma_n(1 - \sigma_n)\|W_n x_n - x_n\|^2 - \|w_n - z_n\|^2 \Big\} + 2\beta_n \langle (f - \rho F)p, v_n - p \rangle - \|v_n - x_{n+1}\|^2 \\
&\leq [1 - \beta_n(\tau - \delta)/2] \|x_n - p\|^2 - [(1 - \gamma_n - \beta_n\tau) + \theta_n] \left\{ \sigma_n(1 - \sigma_n)\|W_n x_n - x_n\|^2 \right. \\
&\quad \left. + \|w_n - z_n\|^2 \right\} + 2\beta_n \langle (f - \rho F)p, v_n - p \rangle - \|v_n - x_{n+1}\|^2 \\
&\leq \|x_n - p\|^2 - [(1 - \gamma_n - \beta_n\tau) + \theta_n] \left\{ \sigma_n(1 - \sigma_n)\|W_n x_n - x_n\|^2 \right. \\
&\quad \left. + \|w_n - z_n\|^2 \right\} + \beta_n M_1 - \|v_n - x_{n+1}\|^2.
\end{aligned} \tag{22}$$

where $\sup_{n \geq 1} 2\|(f - \rho F)p\| \|v_n - p\| \leq M_1$ for some $M_1 > 0$. This immediately attains the claim.

$$\|z_n - p\|^2 \leq \|w_n - p\|^2 - \left[\frac{\tau_n}{2\lambda L} \|r_\lambda(w_n)\|^2 \right]^2. \tag{23}$$

Step 3. One claims that $[(1 - \gamma_n - \beta_n\tau) + \theta_n][\tau_n / 2\lambda L \|r_\lambda(w_n)\|^2]^2 \leq \|x_n - p\|^2 - \|x_{n+1} - p\|^2 + \beta_n M_1$. In fact, let us show that $\exists L > 0$ s.t.

Since the sequence $\{At_n\}$ is bounded, there exists $L > 0$ such that $\|At_n\| \leq L, \forall n \geq 1$. This ensures that $|h_n(u) - h_n(v)| = |\langle At_n, u - v \rangle| \leq L\|u - v\| \forall u, v \in C_n$, which hence implies that $h_n(\cdot)$ is L -Lipschitz continuous on C_n . By Lemmas 2 and 9, we obtain

$$\text{dist}(w_n, C_n) \geq \frac{1}{L} h_n(w_n) = \frac{\tau_n}{2\lambda L} \|r_\lambda(w_n)\|^2. \quad (24)$$

Combining (16) and (24), we get $\|z_n - p\|^2 \leq \|w_n - p\|^2 - [\tau_n/2\lambda L \|r_\lambda(w_n)\|^2]^2$. From (18), (20), and (23), it follows that

$$\begin{aligned} \|x_{n+1} - p\|^2 &\leq \beta_n \|\delta x_n - p\|^2 + \gamma_n \|x_n - p\|^2 + [(1 - \gamma_n - \beta_n \tau) + \theta_n] \|z_n - p\|^2 \\ &\quad + 2\beta_n \langle (f - \rho F)p, v_n - p \rangle \\ &\leq \beta_n \delta \|x_n - p\|^2 + \gamma_n \|x_n - p\|^2 + [(1 - \gamma_n - \beta_n \tau) + \theta_n] \left\{ \|w_n - p\|^2 - \left[\frac{\tau_n}{2\lambda L} \|r_\lambda(w_n)\|^2 \right]^2 \right\} \\ &\quad + 2\beta_n \langle (f - \rho F)p, v_n - p \rangle \\ &\leq \|x_n - p\|^2 - [(1 - \gamma_n - \beta_n \tau) + \theta_n] \left[\frac{\tau_n}{2\lambda L} \|r_\lambda(w_n)\|^2 \right]^2 + \beta_n M_1. \end{aligned} \quad (25)$$

This immediately yields the claim.

Step 4. We show that

$$\|x_{n+1} - p\|^2 \leq [1 - \beta_n(\tau - \delta)] \|x_n - p\|^2 + \beta_n(\tau - \delta) \left[\frac{2\langle (f - \rho F)p, v_n - p \rangle}{\tau - \delta} + \frac{\theta_n}{\beta_n} \cdot \frac{M}{\tau - \delta} \right], \quad (26)$$

for some $M > 0$. In fact, from (20), one obtains

$$\begin{aligned} \|x_{n+1} - p\|^2 &\leq \|v_n - p\|^2 \leq \beta_n \delta \|x_n - p\|^2 + \gamma_n \|x_n - p\|^2 + (1 - \gamma_n - \beta_n \tau + \theta_n) \\ &\quad \times \|z_n - p\|^2 + 2\beta_n \langle (f - \rho F)p, v_n - p \rangle \\ &\leq [1 - \beta_n(\tau - \delta)] \|x_n - p\|^2 + \beta_n(\tau - \delta) \left[2 \frac{\langle (f - \rho F)p, v_n - p \rangle}{\tau - \delta} + \frac{\theta_n}{\beta_n} \cdot \frac{M}{\tau - \delta} \right], \end{aligned} \quad (27)$$

where $\sup_{n \geq 1} \|z_n - p\|^2 \leq M$ for some $M > 0$.

Step 5. One claims that $x_n \rightarrow x^* \in \Omega$, which is only a solution of the VIP (15).

In fact, setting $p = x^*$ in (26), one obtains

$$\beta_n(\tau - \delta) \left[\frac{2\langle (f - \rho F)x^*, v_n - x^* \rangle}{\tau - \delta} + \frac{\theta_n}{\beta_n} \cdot \frac{M}{\tau - \delta} \right] + (1 - \beta_n(\tau - \delta)) \|x_n - x^*\|^2 \geq \|x_{n+1} - x^*\|^2. \quad (28)$$

Setting $\Gamma_n = \|x_n - x^*\|^2$, we demonstrate the convergence of $\{\Gamma_n\}$ to zero via the two cases below.

Case 1. Presume that $\exists n_0 \geq 1$ s.t. $\{\Gamma_n\}$ is nonincreasing. Then, $\lim_{n \rightarrow \infty} \Gamma_n = \hat{h} < +\infty$ and $\Gamma_n - \Gamma_{n+1} \rightarrow 0$ ($n \rightarrow \infty$). Setting $p = x^*$, from Step 2 and $\{\sigma_n\} \subset [a, b] \subset (0, 1)$, we obtain

$$\begin{aligned} &[(1 - \gamma_n - \beta_n \tau) + \theta_n] \left\{ (1 - b)a \|x_n - W_n x_n\|^2 + \|z_n - w_n\|^2 \right\} + \|v_n - x_{n+1}\|^2 \\ &\leq \|x_n - x^*\|^2 - \|x_{n+1} - x^*\|^2 + \beta_n M_1 = \Gamma_n - \Gamma_{n+1} + \beta_n M_1. \end{aligned} \quad (29)$$

Because $\liminf_{n \rightarrow \infty} (1 - \gamma_n) > 0$, $\theta_n \rightarrow 0$, $\beta_n \rightarrow 0$, and $\Gamma_{n+1} - \Gamma_n \rightarrow 0$, one has

Initial Step: Given any starting $x_1 \in C$. Let $\mu > 0, \lambda \in (0, 1/\mu), l \in (0, 1)$.

Iterations: Given the current iterate x_n , calculate x_{n+1} below:

Step 1. Compute $w_n = (1 - \sigma_n)x_n + \sigma_n W_n x_n$, $y_n = P_C(w_n - \lambda A w_n)$ and $r_\lambda(w_n) = w_n - y_n$.

Step 2. Compute

$t_n = w_n - \tau_n r_\lambda(w_n)$, with $\tau_n = l^{j_n}$ and integer j_n being the smallest nonnegative j

s.t. $\mu/2 \|r_\lambda(w_n)\|^2 \geq \langle A(w_n - l^j r_\lambda(w_n)) - A w_n, y_n - w_n \rangle$

Step 3. Calculate

$x_{n+1} = P_C[\beta_n f(x_n) + \gamma_n w_n + ((1 - \gamma_n)I - \beta_n \rho F)T^n z_n]$

with $z_n = P_{C_n}(w_n)$, $C_n = \{u \in C: h_n(u) \leq 0\}$ and $h_n(u) = \langle A t_n, u - w_n \rangle + \tau_n/2\lambda \|r_\lambda(w_n)\|^2$.

Put $n = n + 1$ and return to Step 1.

It is worthy to mention that Lemmas 8–11 remain true for Algorithm 4.

ALGORITHM 4: The 2nd Mann hybrid deepest-descent extragradient rule.

$$\lim_{n \rightarrow \infty} \|x_n - W_n x_n\| = \lim_{n \rightarrow \infty} \|z_n - w_n\| = \lim_{n \rightarrow \infty} \|v_n - x_{n+1}\| = 0. \quad (30)$$

Also, noticing $\beta_n(f(x_n) - \rho FT^n z_n) + (1 - \gamma_n)(T^n z_n - x^*) + \gamma_n(x_n - x^*) = v_n - x^*$, one gets

$$\begin{aligned} \|x_{n+1} - x^*\|^2 &= \|x_{n+1} - v_n + v_n - x^*\|^2 \\ &= \|\gamma_n(x_n - x^*) + (1 - \gamma_n)(T^n z_n - x^*) + \beta_n(f(x_n) - \rho FT^n z_n) + x_{n+1} - v_n\|^2 \\ &= \|x_n - x^*\|^2 + (1 - \gamma_n)[1 + (2 + \theta_n)\theta_n]\|x_n - x^*\|^2 - (1 - \gamma_n)\gamma_n\|T^n z_n - x_n\|^2 \\ &\quad + 2\{\beta_n(\|f(x_n)\| + \|\rho FT^n z_n\|) + \|x_{n+1} - v_n\|\}\|x_{n+1} - x^*\| \\ &= \|x_n - x^*\|^2 + (2 + \theta_n)\theta_n\|x_n - x^*\|^2 - (1 - \gamma_n)\gamma_n\|T^n z_n - x_n\|^2 \\ &\quad + 2\{\beta_n(\|f(x_n)\| + \|\rho FT^n z_n\|) + \|x_{n+1} - v_n\|\}\|x_{n+1} - x^*\|, \end{aligned} \quad (31)$$

which immediately arrives at

$$\begin{aligned} &\gamma_n(1 - \gamma_n)\|x_n - T^n z_n\|^2 \\ &\leq \Gamma_n - \Gamma_{n+1} + \theta_n(2 + \theta_n)\Gamma_n + 2\{\beta_n(\|f(x_n)\| + \|\rho FT^n z_n\|) + \|x_{n+1} - v_n\|\}\Gamma_{n+1}^{1/2}. \end{aligned} \quad (32)$$

Because $1 > \liminf_{n \rightarrow \infty} \gamma_n \geq \liminf_{n \rightarrow \infty} \gamma_n > 0$, $\theta_n \rightarrow 0, \beta_n \rightarrow 0, \Gamma_{n+1} - \Gamma_n \rightarrow 0$, and $v_n - x_{n+1} \rightarrow 0$, from the boundedness of $\{T^n z_n\}, \{f(x_n)\}$, one obtains $\lim_{n \rightarrow \infty} \|T^n z_n - x_n\| = 0$. So, we know from Algorithm 3

and (30) that $\|x_n - w_n\| = \sigma_n \|x_n - W_n x_n\| \leq \|x_n - W_n x_n\| \rightarrow 0$ ($n \rightarrow \infty$), and

$$\begin{aligned} \|x_{n+1} - x_n\| &\leq \|x_{n+1} - v_n\| + \|v_n - x_n\| \\ &= \|x_{n+1} - v_n\| + \|\beta_n f(x_n) + (1 - \gamma_n)(T^n z_n - x_n) - \beta_n \rho FT^n z_n\| \\ &\leq \|x_{n+1} - v_n\| + \|T^n z_n - x_n\| + \beta_n(\|f(x_n)\| + \|\rho FT^n z_n\|) \rightarrow 0 \quad (n \rightarrow \infty). \end{aligned} \quad (33)$$

Setting $p = x^*$, in terms of Step 3, one has $[(1 - \gamma_n - \beta_n \tau) + \theta_n][\tau_n/2\lambda L \|r_\lambda(w_n)\|^2] \leq \Gamma_n - \Gamma_{n+1} + \beta_n M_1$. Since $0 < \liminf_{n \rightarrow \infty} (1 - \gamma_n)$, $\theta_n \rightarrow 0$, $\beta_n \rightarrow 0$, and $\Gamma_{n+1} - \Gamma_n \rightarrow 0$, one gets $\lim_{n \rightarrow \infty} [\tau_n/2\lambda L \|r_\lambda(w_n)\|^2] = 0$. Hence, by Lemma 11, we deduce that

$$\lim_{n \rightarrow \infty} \|y_n - w_n\| = 0. \tag{34}$$

Since $\{x_n\}$ is bounded, we deduce that $\exists \{x_{n_k}\} \subset \{x_n\}$ s.t.

$$\limsup_{n \rightarrow \infty} \langle (f - \rho F)x^*, x_n - x^* \rangle = \lim_{k \rightarrow \infty} \langle (f - \rho F)x^*, x_{n_k} - x^* \rangle. \tag{35}$$

According to the reflexivity of H and boundedness of $\{x_n\}$, one may presume that $x_{n_k} \rightarrow \tilde{x}$. Hence, by (35), one gets

$$\limsup_{n \rightarrow \infty} \langle (f - \rho F)x^*, x_n - x^* \rangle = \langle (f - \rho F)x^*, \tilde{x} - x^* \rangle. \tag{36}$$

So, we know from $x_{n_k} \rightarrow \tilde{x}$ and $x_n - w_n \rightarrow 0$ that $w_{n_k} \rightarrow \tilde{x}$. Because $x_{n+1} - x_n \rightarrow 0$, $x_n - w_n \rightarrow 0$, $y_n - w_n \rightarrow 0$,

$0, z_n - w_n \rightarrow 0$, and $T^{n+1}x_n - T^n x_n \rightarrow 0$, from Lemma 10, we infer that \tilde{x} lies in Ω . Consequently, using (15) and (36), we obtain

$$\limsup_{n \rightarrow \infty} \langle (f - \rho F)x^*, x_n - x^* \rangle = \langle (f - \rho F)x^*, \tilde{x} - x^* \rangle \leq 0. \tag{37}$$

This along with (30)–(33) arrives at

$$\begin{aligned} & \limsup_{n \rightarrow \infty} \langle (f - \rho F)x^*, v_n - x^* \rangle \\ &= \limsup_{n \rightarrow \infty} [\langle (f - \rho F)x^*, v_n - x_{n+1} + x_{n+1} - x_n \rangle + \langle (f - \rho F)x^*, x_n - x^* \rangle] \leq 0. \end{aligned} \tag{38}$$

Note that $\beta_n(\tau - \delta) \in [0, 1] \forall n$, $\sum_{n=1}^\infty \beta_n(\tau - \delta) = \infty$, and $\limsup_{n \rightarrow \infty} [2\langle (f - \rho F)x^*, v_n - x^* \rangle / \tau - \delta + \theta_n / \beta_n \cdot M / \tau - \delta] \leq 0$. So, using Lemma 4 to (28), we have $\lim_{n \rightarrow \infty} \|x_n - x^*\|^2 = 0$.

Case 2. Suppose that $\exists \{\Gamma_{n_k}\} \subset \{\Gamma_n\}$ s.t. $\Gamma_{n_k} < \Gamma_{n_k+1}, \forall k \in \mathcal{N}$, with \mathcal{N} being the set of all natural numbers. Let $\eta: \mathcal{N} \rightarrow \mathcal{N}$ be defined as $\eta(n) := \max \{j \leq n: \Gamma_j < \Gamma_{j+1}\}$. Using Lemma 6, one obtains that $\Gamma_n \leq \Gamma_{\eta(n)+1}$ and $\Gamma_{\eta(n)} \leq \Gamma_{\eta(n)+1}$. Putting $p = x^*$, from Step 2, we have

$$\begin{aligned} & [(1 - \gamma_{\eta(n)} - \beta_{\eta(n)} \tau) + \theta_{\eta(n)}] \left\{ (1 - b)a \|x_{\eta(n)} - W_{\eta(n)} x_{\eta(n)}\|^2 \right. \\ & \quad \left. + \|z_{\eta(n)} - w_{\eta(n)}\|^2 \right\} + \|v_{\eta(n)} - x_{\eta(n)+1}\|^2 \\ & \leq \|x_{\eta(n)} - x^*\|^2 - \|x_{\eta(n)+1} - x^*\|^2 + \beta_{\eta(n)} M_1 \leq \Gamma_{\eta(n)} - \Gamma_{\eta(n)+1} + \beta_{\eta(n)} M_1. \end{aligned} \tag{39}$$

This hence leads to $\lim_{n \rightarrow \infty} \|x_{\eta(n)} - W_{\eta(n)} x_{\eta(n)}\| = \lim_{n \rightarrow \infty} \|z_{\eta(n)} - w_{\eta(n)}\| = \lim_{n \rightarrow \infty} \|v_{\eta(n)} - x_{\eta(n)+1}\| = 0$. Setting $p = x^*$, in terms of Step 3, one gets

$$[(1 - \gamma_{\eta(n)} - \beta_{\eta(n)} \tau) + \theta_{\eta(n)}] \left[\frac{\tau_{\eta(n)}}{2\lambda L} \|r_\lambda(w_{\eta(n)})\|^2 \right]^2 \leq \Gamma_{\eta(n)} - \Gamma_{\eta(n)+1} + \beta_{\eta(n)} M_1, \tag{40}$$

which hence leads to $\lim_{n \rightarrow \infty} [\tau_{\eta(n)} / 2\lambda L \|r_\lambda(w_{\eta(n)})\|^2] = 0$. Using the same inferences as in the proof of Case 1, one obtains that $\lim_{n \rightarrow \infty} \|y_{\eta(n)} - w_{\eta(n)}\| = \lim_{n \rightarrow \infty} \|x_{\eta(n)} - w_{\eta(n)}\| = \lim_{n \rightarrow \infty} \|x_{\eta(n)} - x_{\eta(n)+1}\| = 0$, and

$$0 \geq \limsup_{n \rightarrow \infty} \langle (f - \rho F)x^*, v_{\eta(n)} - x^* \rangle. \tag{41}$$

Furthermore, using (28), one has

$$\begin{aligned} \beta_{\eta(n)}(\tau - \delta)\Gamma_{\eta(n)} &\leq \Gamma_{\eta(n)} - \Gamma_{\eta(n+1)} + \beta_{\eta(n)}(\tau - \delta) \left[\frac{2\langle (f - \rho F)x^*, v_{\eta(n)} - x^* \rangle}{\tau - \delta} + \frac{\theta_{\eta(n)}}{\beta_{\eta(n)}} \cdot \frac{M}{\tau - \delta} \right] \\ &\leq \beta_{\eta(n)}(\tau - \delta) \left[\frac{2\langle (f - \rho F)x^*, v_{\eta(n)} - x^* \rangle}{\tau - \delta} + \frac{\theta_{\eta(n)}}{\beta_{\eta(n)}} \cdot \frac{M}{\tau - \delta} \right], \end{aligned} \tag{42}$$

which hence arrives at

$$\limsup_{n \rightarrow \infty} \Gamma_{\eta(n)} \leq \limsup_{n \rightarrow \infty} \left[\frac{2\langle (f - \rho F)x^*, v_{\eta(n)} - x^* \rangle}{\tau - \delta} + \frac{\theta_{\eta(n)}}{\beta_{\eta(n)}} \cdot \frac{M}{\tau - \delta} \right] \leq 0. \tag{43}$$

Thus, $\lim_{n \rightarrow \infty} \Gamma_{\eta(n)} = 0$. Also, observe that

$$\begin{aligned} &\|x_{\eta(n+1)} - x^*\|^2 \\ &= \|x_{\eta(n+1)} - x_{\eta(n)}\|^2 + 2\langle x_{\eta(n+1)} - x_{\eta(n)}, x_{\eta(n)} - x^* \rangle + \|x_{\eta(n)} - x^*\|^2 \\ &\leq \|x_{\eta(n+1)} - x_{\eta(n)}\|^2 + 2\|x_{\eta(n+1)} - x_{\eta(n)}\| + \|x_{\eta(n)} - x^*\| + \|x_{\eta(n)} - x^*\|^2. \end{aligned} \tag{44}$$

Owing to $\Gamma_n \leq \Gamma_{\eta(n+1)}$, we get

$$\begin{aligned} \|x_n - x^*\|^2 &\leq \|x_{\eta(n+1)} - x^*\|^2 \\ &\leq \|x_{\eta(n+1)} - x_{\eta(n)}\|^2 + 2\|x_{\eta(n+1)} - x_{\eta(n)}\| + \|x_{\eta(n)} - x^*\| + \|x_{\eta(n)} - x^*\|^2 \longrightarrow 0 \quad (n \longrightarrow \infty). \end{aligned} \tag{45}$$

Consequently, $\lim_{n \rightarrow \infty} \|x_n - x^*\|^2 = 0$.

Theorem 2. Suppose that T is a nonexpansive self-mapping on C and $\{x_n\}$ is fabricated by the modification of Algorithm 3, i.e., for any starting $x_1 \in C$,

$$\begin{cases} w_n = (1 - \sigma_n)x_n + \sigma_n W_n x_n, \\ y_n = P_C(w_n - \lambda A w_n), \\ t_n = (1 - \tau_n)w_n + \tau_n y_n, \\ x_{n+1} = P_C[\beta_n f(x_n) + \gamma_n x_n + ((1 - \gamma_n)I - \beta_n \rho F)TP_{C_n}(w_n)], \forall n \geq 1, \end{cases} \tag{46}$$

where for any n , C_n and τ_n are picked as in Algorithm 3. Then, $\{x_n\}$ converges strongly to $x^* \in \Omega$, which is only a solution to the VIP: $\langle (f - \rho F)x^*, x - x^* \rangle \leq 0, \forall x \in \Omega$.

Proof. We write $z_n := P_{C_n}(w_n)$, and divide the proof into a few steps.

Step 1. One claims that $\{x_n\}$ is of boundedness. In fact, via the similar inferences to those in Step 1 of the proof of Theorem 1, one attains the claim.

Step 2. One claims that

$$(1 - \gamma_n - \beta_n \tau) \left\{ (1 - \sigma_n) \sigma_n \|x_n - W_n x_n\|^2 + \|z_n - w_n\|^2 \right\} + \|v_n - x_{n+1}\|^2, \tag{47}$$

$$\leq \|x_n - p\|^2 - \|x_{n+1} - p\|^2 + 2\beta_n \langle (f - \rho F)p, v_n - p \rangle,$$

where $v_n = \beta_n f(x_n) + \gamma_n x_n + ((1 - \gamma_n)I - \beta_n \rho F)Tz_n$. In fact, via the similar inferences to those in Step 2 of the proof of Theorem 1, one attains the claim.

Step 3. One claims that

$$(1 - \gamma_n - \beta_n \tau) \left[\frac{\tau_n}{2\lambda L} \|r_\lambda(w_n)\|^2 \right]^2 \leq \|x_n - p\|^2 - \|x_{n+1} - p\|^2 + 2\beta_n \langle (f - \rho F)p, v_n - p \rangle, \tag{48}$$

In fact, via the similar inferences to those in Step 3 of the proof of Theorem 1, one attains the claim.

Step 4. One claims that

$$\|x_{n+1} - p\|^2 \leq [1 - \beta_n(\tau - \delta)] \|x_n - p\|^2 + \beta_n(\tau - \delta) \cdot \frac{2\langle (f - \rho F)p, v_n - p \rangle}{\tau - \delta}. \tag{49}$$

In fact, via the similar inferences to those in Step 4 of the proof of Theorem 1, one attains the claim.

Proof. Because $1 > \limsup_{n \rightarrow \infty} \sigma_n \geq \liminf_{n \rightarrow \infty} \sigma_n > 0$ and $\theta_n/\beta_n \rightarrow 0$, one may presume that $(0, 1) \supset [a, b] \supset \{\sigma_n\}$ and $\beta_n(\tau - \delta)/2 \geq \theta_n, \forall n$. It is easy to verify that $P_\Omega(I - \rho F + f): C \rightarrow C$ is a contractive map. Hence, $\exists | x^* \in C$ s.t. $x^* = P_\Omega(I - \rho F + f)x^*$. Thus, $\exists | x^* \in \Omega$ satisfying the VIP (15).

Step 5. One claims that $x_n \rightarrow x^* \in \Omega$, which is only a solution of the VIP (15). In fact, via the similar inferences to those in Step 3 of the proof of Theorem 1, one attains the claim.

In what follows, in the rest of the proof, we divide it into some steps.

Next, we introduce modified hybrid deepest-descent extragradient approach. \square

Step 1. One claims that $\{x_n\}$ is of boundedness. In fact, using the similar inferences to those in Step 1 of the proof of Theorem 1, we obtain that relations (16)–(30) hold. Thus, using (30) and $1 > \gamma_n + \beta_n$, one deduces that

Theorem 3. Let $\{x_n\}$ be the sequence fabricated in Algorithm 4. Assume $T^{n+1}x_n - T^n x_n \rightarrow 0$. Then, $\{x_n\}$ converges strongly to $x^* \in \Omega$, which is only a solution to the VIP: $\langle (f - \rho F)x^*, x - x^* \rangle \leq 0, \forall x \in \Omega$.

$$\|x_{n+1} - p\| \leq \|\beta_n(f(x_n) - f(p)) + \gamma_n(w_n - p) + (1 - \gamma_n)$$

$$\times [(I - \beta_n/1 - \gamma_n \rho F)T^n z_n - (I - \beta_n/1 - \gamma_n \rho F)p] + \beta_n(f - \rho F)p\|$$

$$\leq [\beta_n \delta + \gamma_n + (1 - \gamma_n - \beta_n \tau) + \theta_n] \|x_n - p\| + \beta_n \|(f - \rho F)p\| \tag{50}$$

$$\leq \max \left\{ \|x_n - p\|, \frac{2\|(f - \rho F)p\|}{\tau - \delta} \right\}.$$

Using the induction, one obtains $\|x_n - p\| \leq \max \{\|x_1 - p\|, 2\|(f - \rho F)p\|/\tau - \delta\}, \forall n$.

Hence, $\{x_n\}$ is bounded, and so are the sequences $\{w_n\}, \{\gamma_n\}, \{z_n\}, \{f(x_n)\}, \{At_n\}, \{W_n x_n\}, \{T^n z_n\}$.

Step 2. One claims that

$$\begin{aligned}
 & [(1 - \gamma_n - \beta_n \tau) + \theta_n] \{ (1 - \sigma_n) \sigma_n \|x_n - W_n x_n\|^2 + \|z_n - w_n\|^2 \} + \|v_n - x_{n+1}\|^2 \\
 & - \leq -\|x_{n+1} - p\|^2 + \|x_n - p\|^2 + \beta_n M_1.
 \end{aligned} \tag{51}$$

for certain $M_1 > 0$, where $v_n = \beta_n f(x_n) + \gamma_n w_n + ((1 - \gamma_n)I - \beta_n \rho F)T^n z_n$ and $x_{n+1} = P_C v_n$. To prove this, we first note that

$$\begin{aligned}
 \|x_{n+1} - p\|^2 & \leq \beta_n (f(x_n) - f(p)) + \gamma_n (w_n - p) + (1 - \gamma_n) \\
 & \quad \times [(I - \beta_n/1 - \gamma_n \rho F)T^n z_n - (I - \beta_n/1 - \gamma_n \rho F)p] + \beta_n (f - \rho F)p \|^2 - \|v_n - x_{n+1}\|^2 \\
 & \leq \beta_n \delta \|x_n - p\|^2 + \gamma_n \|x_n - p\|^2 + [(1 - \gamma_n - \beta_n \tau) + \theta_n] \|z_n - p\|^2 \\
 & \quad + 2\beta_n \langle (f - \rho F)p, v_n - p \rangle - \|v_n - x_{n+1}\|^2.
 \end{aligned} \tag{52}$$

Furthermore, via the similar reasoning to that in (21), we get

$$\|z_n - p\|^2 \leq \|x_n - p\|^2 - (1 - \sigma_n) \sigma_n \|x_n - W_n x_n\|^2 - \|z_n - w_n\|^2. \tag{53}$$

Substituting (38) into (37), one gets

$$\begin{aligned}
 \|x_{n+1} - p\|^2 & \leq \beta_n \delta \|x_n - p\|^2 + \gamma_n \|x_n - p\|^2 + [(1 - \gamma_n - \beta_n \tau) + \theta_n] \{ \|x_n - p\|^2 \\
 & \quad - (1 - \sigma_n) \sigma_n \|x_n - W_n x_n\|^2 - \|z_n - w_n\|^2 \} + 2\beta_n \langle (f - \rho F)p, v_n - p \rangle - \|v_n - x_{n+1}\|^2 \\
 & \leq \|x_n - p\|^2 - [(1 - \gamma_n - \beta_n \tau) + \theta_n] \{ (1 - \sigma_n) \sigma_n \|x_n - W_n x_n\|^2 + \|z_n - w_n\|^2 \} + \beta_n M_1 \\
 & \quad - \|v_n - x_{n+1}\|^2.
 \end{aligned} \tag{54}$$

with $\sup_{n \geq 1} 2\|(\rho F - f)p\| \|v_n - p\| \leq M_1$ for certain $M_1 > 0$. This immediately arrives at the claim.

Step 3. One claims that

$$[(1 - \gamma_n - \beta_n \tau) + \theta_n] \left[\tau_n / 2\lambda L \|r_\lambda(w_n)\|^2 \right]^2 \leq \|x_n - p\|^2 - \|x_{n+1} - p\|^2 + \beta_n M_1. \tag{55}$$

In fact, via the similar inferences to those in (27), one obtains that for certain $L > 0$,

$$\|z_n - p\|^2 \leq \|w_n - p\|^2 - \left[\tau_n / 2\lambda L \|r_\lambda(w_n)\|^2 \right]^2. \tag{56}$$

From (39), (30), and (43) we know that

$$\begin{aligned}
 \|x_{n+1} - p\|^2 &\leq \beta_n \delta \|x_n - p\|^2 + \gamma_n \|x_n - p\|^2 + [(1 - \gamma_n - \beta_n \tau) + \theta_n] \|z_n - p\|^2 + \beta_n M_1 \\
 &\leq \beta_n \delta \|x_n - p\|^2 + \gamma_n \|x_n - p\|^2 + [(1 - \gamma_n - \beta_n \tau) + \theta_n] \left\{ \|w_n - p\|^2 \right. \\
 &\quad \left. - \left[\tau_n / 2\lambda L \|r_\lambda(w_n)\|^2 \right]^2 \right\} + \beta_n M_1 \\
 &\leq \|x_n - p\|^2 - [(1 - \gamma_n - \beta_n \tau) + \theta_n] \left[\tau_n / 2\lambda L \|r_\lambda(w_n)\|^2 \right]^2 + \beta_n M_1.
 \end{aligned}
 \tag{57}$$

which hence yields the claim.

Step 4. One claims that $\|x_{n+1} - p\|^2 \leq [1 - \beta_n(\tau - \delta)] \|x_n - p\|^2 +$

$\beta_n(\tau - \delta)[2\langle (f - \rho F)p, v_n - p \rangle / \tau - \delta + \theta_n / \beta_n \cdot M / \tau - \delta]$ for some $M > 0$. In fact, using Lemma 7 and (30), one has

$$\begin{aligned}
 \|x_{n+1} - p\|^2 &\leq \|v_n - p\|^2 = \beta_n (f(x_n) - f(p)) + \gamma_n (w_n - p) + (1 - \gamma_n) \\
 &\quad - \times [(1 - \beta_n / 1 - \gamma_n \rho F) T^n z_n - (1 - \beta_n / 1 - \gamma_n \rho F) p] + \beta_n (f - \rho F) p^2 \\
 &\leq \beta_n \delta \|x_n - p\|^2 + \gamma_n \|x_n - p\|^2 + (1 - \gamma_n - \beta_n \tau + \theta_n) \\
 &\quad - \times \|z_n - p\|^2 + 2\beta_n \langle (f - \rho F)p, v_n - p \rangle \\
 &\leq [1 - \beta_n(\tau - \delta)] \|x_n - p\|^2 + \beta_n(\tau - \delta)[2\langle (f - \rho F)p, v_n - p \rangle / \tau - \delta + \theta_n / \beta_n \cdot M / \tau - \delta],
 \end{aligned}
 \tag{58}$$

where $\sup_{n \geq 1} \|x_n - p\|^2 \leq M$ for certain $M > 0$.

Step 5. One claims that $x_n \rightarrow x^* \in \Omega$ which is only a solution of the VIP (15). In fact, setting $p = x^*$, in terms of Step 4, one deduces that

$$\|x_{n+1} - x^*\|^2 \leq [1 - \beta_n(\tau - \delta)] \|x_n - x^*\|^2 + \beta_n(\tau - \delta)[2\langle (f - \rho F)x^*, v_n - x^* \rangle / \tau - \delta + \theta_n / \beta_n \cdot M / \tau - \delta].
 \tag{59}$$

Setting $\Gamma_n = \|x_n - x^*\|^2$, one demonstrates the convergence of $\{\Gamma_n\}$ to zero via the two cases below. \square

Case 3. Presume that $\exists n_0 \geq 1$ s.t. $\{\Gamma_n\}$ is nonincreasing. Then, $\lim_{n \rightarrow \infty} \Gamma_n = \hat{h} < +\infty$ and $\Gamma_n - \Gamma_{n+1} \rightarrow 0$ ($n \rightarrow \infty$). Setting $\overset{n \rightarrow \infty}{p} = x^*$, from Step 2 and $\{\sigma_n\} \subset [a, b] \subset (0, 1)$, we obtain

$$\begin{aligned}
 &[(1 - \gamma_n - \beta_n \tau) + \theta_n] \left\{ (1 - b)a \|x_n - W_n x_n\|^2 + \|z_n - w_n\|^2 \right\} + \|v_n - x_{n+1}\|^2 \\
 &\leq [(1 - \gamma_n - \beta_n \tau) + \theta_n] \left\{ (1 - \sigma_n)\sigma_n \|x_n - W_n x_n\|^2 + \|z_n - w_n\|^2 \right\} + \|v_n - x_{n+1}\|^2 \\
 &\leq \Gamma_n - \Gamma_{n+1} + \beta_n M_1,
 \end{aligned}
 \tag{60}$$

which hence yields

$$\lim_{n \rightarrow \infty} \|x_n - W_n x_n\| = \lim_{n \rightarrow \infty} \|z_n - w_n\| = \lim_{n \rightarrow \infty} \|v_n - x_{n+1}\| = 0.
 \tag{61}$$

Putting $p = x^*$, from Step 3, we obtain $[(1 - \gamma_n - \beta_n \tau) + \theta_n][\tau_n/2\lambda L \|r_\lambda(w_n)\|^2]^2 \leq \Gamma_n - \Gamma_{n+1} + \beta_n M_1$, which immediately leads to $\lim_{n \rightarrow \infty} [\tau_n/2\lambda L \|r_\lambda(w_n)\|^2]^2 = 0$. Using the similar reasoning to that in Case 1 of the proof of Theorem 1, one deduces that $\lim_{n \rightarrow \infty} \|w_n - y_n\| = \lim_{n \rightarrow \infty} \|w_n - x_n\| = \lim_{n \rightarrow \infty} \|x_{n+1} - x_n\| = 0$, and $\limsup_{n \rightarrow \infty} \langle (f - \rho F)x^*, v_n - x^* \rangle \leq 0$. Accordingly, using Lemma 4 to (59), we attain $\lim_{n \rightarrow \infty} \|x_n - x^*\|^2 = 0$.

Case 4. Presume that $\exists \{\Gamma_{n_j}\} \subset \{\Gamma_n\}$ s.t. $\Gamma_{n_j} < \Gamma_{n_j+1}, \forall j \in \mathcal{N}$, with \mathcal{N} being the set of all natural numbers. Let $\eta: \mathcal{N} \rightarrow \mathcal{N}$

be defined as $\eta(n) := \max \{j \leq n: \Gamma_j < \Gamma_{j+1}\}$. Using Lemma 6, one gets $\Gamma_{\eta(n)} \leq \Gamma_{\eta(n)+1}$ and $\Gamma_n \leq \Gamma_{\eta(n)+1}$. In the rest of the proof, applying the similar reasoning to that in Case 2 of the proof of Theorem 1, one obtains the claim.

Theorem 4. Suppose that T is a nonexpansive self-mapping on C and $\{x_n\}$ is fabricated by the modification of Algorithm 4, i.e., for each starting $x_1 \in C$,

$$\begin{cases} w_n = (1 - \sigma_n)x_n + \sigma_n W_n x_n, \\ y_n = P_C(w_n - \lambda A w_n), \\ t_n = (1 - \tau_n)w_n + \tau_n y_n, \\ x_{n+1} = P_C[\beta_n f(x_n) + \gamma_n w_n + ((1 - \gamma_n)I - \beta_n \rho F)TP_{C_n}(w_n)], \forall n \geq 1, \end{cases} \quad (62)$$

where for any n , C_n and τ_n are picked as in Algorithm 4. Then, $\{x_n\}$ converges strongly to $x^* \in \Omega$, which is only a solution to the VIP: $\langle (f - \rho F)x^*, x - x^* \rangle \leq 0, \forall x \in \Omega$.

Proof. One writes $z_n := P_{C_n}(w_n)$ and divides the proof of the theorem into a few steps.

Step 1. One claims that $\{x_n\}$ is of boundedness. In fact, via the similar inferences to those in Step 1 of the proof of Theorem 3, one obtains the claim.

Step 2. One claims that

$$\begin{aligned} & (1 - \gamma_n - \beta_n \tau) \left\{ (1 - \sigma_n) \sigma_n \|x_n - W_n x_n\|^2 + \|z_n - w_n\|^2 \right\} + \|v_n - x_{n+1}\|^2 \\ & \leq \|x_n - p\|^2 - \|x_{n+1} - p\|^2 + 2\beta_n \langle (f - \rho F)p, v_n - p \rangle, \end{aligned} \quad (63)$$

with $v_n = \beta_n f(x_n) + \gamma_n w_n + ((1 - \gamma_n)I - \beta_n \rho F)Tz_n$. In fact, via the similar inferences to those in Step 2 of the proof of Theorem 3, one obtains the claim.

Step 3. One claims that

$$(1 - \gamma_n - \beta_n \tau) \left[\tau_n/2\lambda L \|r_\lambda(w_n)\|^2 \right]^2 \leq \|x_n - p\|^2 - \|x_{n+1} - p\|^2 + 2\beta_n \langle (f - \rho F)p, v_n - p \rangle. \quad (64)$$

In fact, via the similar inferences to those in Step 3 of the proof of Theorem 3, one obtains the claim.

Step 4. One claims that $\|x_{n+1} - p\|^2 \leq [1 - \beta_n(\tau - \delta)]\|x_n - p\|^2 + \beta_n(\tau - \delta) \cdot 2\langle (f - \rho F)p, v_n - p \rangle / \tau - \delta$. Indeed, via the similar inferences to those in Step 4 of the proof of Theorem 3, one obtains the claim.

Step 5. One claims that $x_n \rightarrow x^* \in \Omega$ which is only a solution of the VIP (15). In fact, via the similar

inferences to those in Step 5 of the proof of Theorem 3, one obtains the claim. \square

4. Applicability and Implementability

In this section, we provide an illustrated instance to demonstrate the applicability and implementability of our proposed algorithms. Put $\rho = 2, \lambda = l = \mu = 1/2, \sigma_n = 1/3, \beta_n = 1/3(n + 1)$, and $\gamma_n = 1/3(n + 1)$.

We first provide an example of Lipschitz continuous and pseudomonotone mapping A , asymptotically nonexpansive mapping T , and countably many nonexpansive mappings $\{T_n\}_{n=1}^\infty$ with $\Omega = \text{VI}(C, A) \cap (\cap_{n=1}^\infty \text{Fix}(T_n)) \neq \emptyset$ where $T_0 := T$. Put $C = [-3, 3]$ and $H = \mathbf{R}$ with the inner product $\langle a, b \rangle = ab$ and induced norm $\| \cdot \| = | \cdot |$. The starting point x_1 is arbitrarily selected in C . Put $f(x) = F(x) = 1/2x, \forall x \in C$ s.t.

$$\delta = 1/2 < \tau = 1 - \sqrt{1 - \rho(2\eta - \rho\kappa^2)} = 1. \tag{65}$$

Assume that $A: H \rightarrow H$ and $T, T_n: C \rightarrow C$ are formulated as $Av := 1/1 + |\sin v| - 1/1 + |v|$, $Tv := 3/5 \sin v$, and $T_n v = Sv = \sin v, \forall v \in C, n \geq 1$. We now claim that A is of both pseudomonotonicity and Lipschitz continuity. Indeed, for each $v, u \in H$, one has

$$\begin{aligned} \|Av - Au\| &\leq \left| \frac{\|v\| - \|u\|}{(1 + \|u\|)(1 + \|v\|)} \right| + \left| \frac{\|\sin v\| - \|\sin u\|}{(1 + \|\sin u\|)(1 + \|\sin v\|)} \right| \\ &\leq \frac{\|v - u\|}{(1 + \|u\|)(1 + \|v\|)} + \frac{\|\sin v - \sin u\|}{(1 + \|\sin u\|)(1 + \|\sin v\|)} \leq 2\|v - u\|. \end{aligned} \tag{66}$$

Accordingly, A is of Lipschitz continuity. In what follows, one claims that A is of pseudomonotonicity. For any $v, u \in H$, it is clear that $\langle Av, u - v \rangle = (1/1 + |\sin v| - 1/1 + |v|)(u - v) \geq 0 \Rightarrow \langle Au, u - v \rangle = (1/1 + |\sin u| - 1/1 + |u|)(u - v) \geq 0$. Moreover, it is easy to check that T is of asymptotical

nonexpansivity with $\theta_n = (3/5)^n, \forall n$, s.t. $\|T^n x_n - T^{n+1} x_n\| \rightarrow 0$ as $n \rightarrow \infty$. In fact, one observes that $\|T^n v - T^n u\| \leq 3/5 \|T^{n-1} v - T^{n-1} u\| \leq \dots \leq (3/5)^n \|v - u\| \leq (1 + \theta_n) \|v - u\|$, and

$$\|T^{n+1} x_n - T^n x_n\| \leq (3/5)^{n-1} \|T^2 x_n - T x_n\| = (3/5)^{n-1} \left\| \frac{3}{5} \sin(T x_n) - 3/5 \sin x_n \right\| \leq 2 \left(\frac{3}{5} \right)^n \rightarrow 0. \tag{67}$$

It is clear that $\text{Fix}(T) = \{0\}$ and $\lim_{n \rightarrow \infty} \theta_n / \beta_n = \lim_{n \rightarrow \infty} (3/5)^n / 1/3(n+1) = 0$. Additionally, it is readily known that $T_n = S$ is of nonexpansivity and $\text{Fix}(S) = \{0\}$. Thus, $\Omega = \text{VI}(C, A) \cap \text{Fix}(S) \cap \text{Fix}(T) = \{0\} \neq \emptyset$. So, from $W_n = S$ and $(1 - \gamma_n)I - \beta_n \rho F = (1 - n/3(n+1))I - 1/3(n+1) \cdot 1/2I = 2/3I$, we reduce Algorithm 3 to the following:

$$\begin{cases} w_n = \frac{2}{3}x_n + \frac{1}{3}Sx_n, \\ y_n = P_C\left(w_n - \frac{1}{2}Aw_n\right), \\ t_n = (1 - \tau_n)w_n + \tau_n y_n, \\ x_{n+1} = \frac{1}{3(n+1)} \cdot \frac{1}{2}x_n + \frac{n}{3(n+1)}x_n + \frac{2}{3}T^n P_{C_n}(w_n), \forall n \geq 1, \end{cases} \tag{68}$$

where for any n , C_n and τ_n are picked as in Algorithm 3. Then, by Theorem 1, one deduces that $\{x_n\}$ converges to $0 \in \Omega = \text{VI}(C, A) \cap \text{Fix}(S) \cap \text{Fix}(T)$.

Particularly, noticing the fact that $Tu := 3/5 \sin u$ is of nonexpansivity, we also present the modification of Algorithm 3, i.e.,

$$\begin{cases} w_n = \frac{2}{3}x_n + \frac{1}{3}Sx_n, \\ y_n = P_C\left(w_n - \frac{1}{2}Aw_n\right), \\ t_n = (1 - \tau_n)w_n + \tau_n y_n, \\ x_{n+1} = \frac{1}{3(n+1)} \cdot \frac{1}{2}x_n + \frac{n}{3(n+1)}x_n + \frac{2}{3}TP_{C_n}(w_n), \forall n \geq 1, \end{cases} \tag{69}$$

where for any n , C_n and τ_n are picked as above. Then, by Theorem 2, one infers that $\{x_n\}$ converges to $0 \in \Omega = \text{VI}(C, A) \cap \text{Fix}(S) \cap \text{Fix}(T)$.

5. Concluding Remarks

Compared with the associated theorems of Kraikaew and Saejung [21], Ceng and Shang [23], and Reich et al. [25], our theorems enhance, extend, and develop them in the following ways.

- (i) The issue of seeking a point of $VI(C, A)$ in [21] is developed into our issue of seeking a point of $VI(C, A) \cap (\cap_{i=1}^{\infty} \text{Fix}(T_i))$ with T_n being of nonexpansivity for any n and $T_0 = T$ being of asymptotical nonexpansivity. The Halpern subgradient extragradient rule for settling the VIP in [21] is developed into our Mann hybrid deepest-descent extragradient approach for handling a HVI with the CFPP and VIP constraints, which is on the basis of Mann's iterative technique, viscosity approximation method, subgradient extragradient rule with linear-search process, and hybrid deepest-descent rule.
- (ii) The issue of seeking a point of $VI(C, A)$ in [25] is developed into our issue of seeking a point of $VI(C, A) \cap (\cap_{i=1}^{\infty} \text{Fix}(T_i))$ with T_n being of nonexpansivity for any n and $T_0 = T$ being of asymptotical nonexpansivity. The modified projection-type rule with linear-search process for settling the VIP in [25] is developed into Mann hybrid deepest-descent extragradient approach for settling a HVI with the CFPP and VIP constraints, which is on the basis of Mann's iterative technique, viscosity approximation method, subgradient extragradient rule with linear-search process, and hybrid deepest-descent rule.
- (iii) The issue of seeking a point of $VI(C, A) \cap (\cap_{i=1}^{\infty} \text{Fix}(T_i))$ with Lipschitz continuity and sequentially weak continuity mapping A in [23] is developed into our issue of seeking a point of $VI(C, A) \cap (\cap_{i=1}^{\infty} \text{Fix}(T_i))$ with A being uniform continuity mapping satisfying $\|Az\| \leq \liminf_{n \rightarrow \infty} \|Ax_n\|$ for any $\{x_n\} \subset C$ with $x_n \rightarrow z \in C$. The hybrid inertial-type subgradient extragradient rule with linear-search process in [23] is developed into Mann hybrid deepest-descent extragradient approach, e.g., the original inertial-type iteration " $w_n = T_n x_n + \alpha_n (T_n x_n - T_n x_{n-1})$ " is replaced by Mann-type iteration " $w_n = (1 - \sigma_n)x_n + \sigma_n W_n x_n$ ", and the original viscosity iteration " $x_{n+1} = \beta_n f(x_n) + \gamma_n x_n + ((1 - \gamma_n)I - \beta_n \rho F)T^n z_n$ " is replaced by our hybrid viscosity iteration " $x_{n+1} = P_C [\beta_n f(x_n) + \gamma_n x_n + ((1 - \gamma_n)I - \beta_n \rho F)T^n z_n]$." It is worthy to point out that the definition of z_n in the former formula of x_{n+1} is quite different from the definition of z_n in the latter formula of x_{n+1} .

Data Availability

All data generated or analyzed during this study are included within the article.

Conflicts of Interest

The authors declare that they have no conflicts of interest.

Authors' Contributions

All authors contributed equally to the writing of this paper. All authors have read and approved the final manuscript.

Acknowledgments

This study was partially supported by the 2020 Shanghai Leading Talents Program of the Shanghai Municipal Human Resources and Social Security Bureau (20LJ2006100), the Innovation Program of Shanghai Municipal Education Commission (15ZZ068), and the Program for Outstanding Academic Leaders in Shanghai City (15XD1503100).

References

- [1] G. M. Korpelevich, "The extragradient method for finding saddle points and other problems," *Ekonomikai Matematiczeskie Metody*, vol. 12, pp. 747–756, 1976.
- [2] Y. Yao, Y. C. Liou, and S. M. Kang, "Approach to common elements of variational inequality problems and fixed point problems via a relaxed extragradient method," *Computers and Mathematics with Applications*, vol. 59, pp. 3472–3480, 2010.
- [3] L. O. Jolaoso, Y. Shehu, and J. C. Yao, "Inertial extragradient type method for mixed variational inequalities without monotonicity," *Mathematics and Computers in Simulation*, vol. 192, pp. 353–369, 2022.
- [4] L. C. Ceng, A. Petruşel, J. C. Yao, and Y. Yao, "Hybrid viscosity extragradient method for systems of variational inequalities, fixed points of nonexpansive mappings, zero points of accretive operators in Banach spaces," *Fixed Point Theory*, vol. 19, no. 2, pp. 487–502, 2018.
- [5] L. C. Ceng, A. Petrusel, X. Qin, and J. C. Yao, "Two inertial subgradient extragradient algorithms for variational inequalities with fixed-point constraints," *Optimization*, vol. 70, no. 5-6, pp. 1337–1358, 2021.
- [6] L. C. Ceng, J. C. Yao, and Y. Shehu, "On Mann implicit composite subgradient extragradient methods for general systems of variational inequalities with hierarchical variational inequality constraints," *Journal of Inequalities and Applications*, vol. 2022, no. 1, 78 pages, 2022.
- [7] Y. Yao, N. Shahzad, and J. C. Yao, "Convergence of Tseng-type self-adaptive algorithms for variational

- inequalities and fixed point problems,” *Carpathian Journal of Mathematics*, vol. 37, no. 3, pp. 541–550, 2021.
- [8] H. K. Xu and T. H. Kim, “Convergence of hybrid steepest-descent methods for variational inequalities,” *Journal of Optimization Theory and Applications*, vol. 119, no. 1, pp. 185–201, 2003.
 - [9] L. He, Y. L. Cui, L. C. Ceng, T. Y. Zhao, D. Q. Wang, and H. Y. Hu, “Strong convergence for monotone bilevel equilibria with constraints of variational inequalities and fixed points using subgradient extragradient implicit rule,” *Journal of Inequalities and Applications*, vol. 2021, no. 1, p. 146, 2021.
 - [10] T. Y. Zhao, D. Q. Wang, L. C. Ceng, L. He, C. Y. Wang, and H. L. Fan, “Quasi-inertial Tseng’s extragradient algorithms for pseudomonotone variational inequalities and fixed point problems of quasi-nonexpansive operators,” *Numerical Functional Analysis and Optimization*, vol. 42, no. 1, pp. 69–90, 2021.
 - [11] L. C. Ceng, A. Petruşel, X. Qin, and J. C. Yao, “A modified inertial subgradient extragradient method for solving pseudomonotone variational inequalities and common fixed point problems,” *Fixed Point Theory*, vol. 21, no. 1, pp. 93–108, 2020.
 - [12] L. C. Ceng and Q. Yuan, “Composite inertial subgradient extragradient methods for variational inequalities and fixed point problems,” *Journal of Inequalities and Applications*, vol. 2019, no. 1, p. 274, 2019.
 - [13] J. Yang, H. Liu, and Z. Liu, “Modified subgradient extragradient algorithms for solving monotone variational inequalities,” *Optimization*, vol. 67, no. 12, pp. 2247–2258, 2018.
 - [14] P. T. Vuong, “On the weak convergence of the extragradient method for solving pseudo-monotone variational inequalities,” *Journal of Optimization Theory and Applications*, vol. 176, no. 2, pp. 399–409, 2018.
 - [15] D. V. Thong and D. V. Hieu, “Inertial subgradient extragradient algorithms with line-search process for solving variational inequality problems and fixed point problems,” *Numerical Algorithms*, vol. 80, no. 4, pp. 1283–1307, 2019.
 - [16] Y. Shehu and O. S. Iyiola, “Strong convergence result for monotone variational inequalities,” *Numerical Algorithms*, vol. 76, no. 1, pp. 259–282, 2017.
 - [17] D. V. Thong, Q. L. Dong, L. L. Liu, N. A. Triet, and N. P. Lan, “Two fast converging inertial subgradient extragradient algorithms with variable stepsizes for solving pseudo-monotone VIPs in Hilbert spaces,” *Journal of Computational and Applied Mathematics*, vol. 410, Article ID 114260, 2022.
 - [18] P. T. Vuong and Y. Shehu, “Convergence of an extragradient-type method for variational inequality with applications to optimal control problems,” *Numerical Algorithms*, vol. 81, no. 1, pp. 269–291, 2019.
 - [19] Y. Shehu, Q. L. Dong, and D. Jiang, “Single projection method for pseudo-monotone variational inequality in Hilbert spaces,” *Optimization*, vol. 68, no. 1, pp. 385–409, 2019.
 - [20] D. V. Thong and D. Van Hieu, “Modified subgradient extragradient method for variational inequality problems,” *Numerical Algorithms*, vol. 79, no. 2, pp. 597–610, 2018.
 - [21] R. Kraikaew and S. Saejung, “Strong convergence of the Halpern subgradient extragradient method for solving variational inequalities in Hilbert spaces,” *Journal of Optimization Theory and Applications*, vol. 163, no. 2, pp. 399–412, 2014.
 - [22] L. C. Ceng and C. F. Wen, “Systems of variational inequalities with hierarchical variational inequality constraints for asymptotically nonexpansive and pseudocontractive mappings,” *Revista de la Real Academia de Ciencias Exactas, Físicas y Naturales Serie A Matemáticas*, vol. 113, no. 3, pp. 2431–2447, 2019.
 - [23] L. C. Ceng and M. J. Shang, “Hybrid inertial subgradient extragradient methods for variational inequalities and fixed point problems involving asymptotically nonexpansive mappings,” *Optimization*, vol. 70, no. 4, pp. 715–740, 2021.
 - [24] L. C. Ceng, A. Petruşel, X. Qin, and J. C. Yao, “Pseudomonotone variational inequalities and fixed points,” *Fixed Point Theory*, vol. 22, no. 2, pp. 543–558, 2021.
 - [25] S. Reich, D. V. Thong, Q. L. Dong, X. H. Li, and V. T. Dung, “New algorithms and convergence theorems for solving variational inequalities with non-Lipschitz mappings,” *Numerical Algorithms*, vol. 87, no. 2, pp. 527–549, 2021.
 - [26] A. N. Iusem and M. Nasri, “Korpelevich’s method for variational inequality problems in Banach spaces,” *Journal of Global Optimization*, vol. 50, no. 1, pp. 59–76, 2011.
 - [27] M. Farid, “The subgradient extragradient method for solving mixed equilibrium problems and fixed point problems in Hilbert spaces,” *Journal of Applied and Numerical Optimization*, vol. 1, pp. 335–345, 2019.
 - [28] M. Farid, “Correction to: two algorithms for solving mixed equilibrium problems and fixed point problems in Hilbert spaces,” *Annali dell’Universita di Ferrara*, vol. 68, no. 1, p. 237, 2022.
 - [29] Q. L. Dong, K. R. Kazmi, R. Ali, and X. H. Li, “Inertial Krasnosel’skiĭ–Mann type hybrid algorithms for solving hierarchical fixed point problems,” *Journal of Fixed Point Theory and Applications*, vol. 21, no. 2, p. 57, 2019.
 - [30] M. Alansari, R. Ali, and M. Farid, “Strong convergence of an inertial iterative algorithm for variational inequality problem, generalized equilibrium problem, and fixed point problem in a Banach space,” *Journal of Inequalities and Applications*, vol. 2020, no. 1, p. 42, 2020.
 - [31] M. Farid, R. Ali, and W. Cholamjiak, “An inertial iterative algorithm to find common solution of a split generalized equilibrium and a variational inequality problem in Hilbert spaces,” *Journal of Mathematics*, vol. 2021, Article ID 3653807, 17 pages, 2021.
 - [32] S. F. Aldosary, W. Cholamjiak, R. Ali, and M. Farid, “Strong convergence of an inertial iterative algorithm for generalized mixed variational-like inequality problem and Bregman relatively nonexpansive mapping in reflexive Banach space,” *Journal of Mathematics*, vol. 2021, Article ID 9421449, 25 pages, 2021.
 - [33] K. Goebel and S. Reich, *Uniform Convexity, Hyperbolic Geometry, and Nonexpansive Mappings*, Marcel Dekker, New York, NY, USA, 1984.
 - [34] K. Shimoji and W. Takahashi, “Strong convergence to common fixed points of infinite nonexpansive mappings and applications,” *Taiwanese Journal of Mathematics*, vol. 5, no. 2, pp. 387–404, 2001.
 - [35] S. S. Chang, H. Joseph Lee, and C. K. Chan, “A new method for solving equilibrium problem fixed point problem and variational inequality problem with application to optimization,” *Nonlinear Analysis: Theory, Methods and Applications*, vol. 70, no. 9, pp. 3307–3319, 2009.
 - [36] Y. R. He, “A new double projection algorithm for variational inequalities,” *Journal of Computational and Applied Mathematics*, vol. 185, no. 1, pp. 166–173, 2006.
 - [37] L. C. Ceng, H. K. Xu, and J. C. Yao, “The viscosity approximation method for asymptotically nonexpansive mappings in Banach spaces,” *Nonlinear Analysis: Theory, Methods and Applications*, vol. 69, no. 4, pp. 1402–1412, 2008.
 - [38] P. E. Maingé, “Strong convergence of projected subgradient methods for nonsmooth and nonstrictly convex minimization,” *Set-Valued Analysis*, vol. 16, no. 7–8, pp. 899–912, 2008.

Research Article

Novel Approximations to the Damped Parametric Driven Pendulum Oscillators

Weaam Alhejaili,¹ Alvaro H. Salas ,² and S. A. El-Tantawy ^{3,4}

¹Department of Mathematical Sciences, College of Science, Princess Nourah bint Abdulrahman University, P.O. Box 84428, Riyadh 11671, Saudi Arabia

²Department of Mathematics and Statistics, Universidad Nacional de Colombia, FIZMAKO Research Group, Bogotá, Colombia

³Department of Physics, Faculty of Science, Port Said University, Port Said 42521, Egypt

⁴Research Center for Physics (RCP), Department of Physics, Faculty of Science and Arts, Al-Baha University, Al-Mikhwah, Saudi Arabia

Correspondence should be addressed to S. A. El-Tantawy; tantawy@sci.psu.edu.eg

Received 16 November 2022; Revised 1 April 2023; Accepted 18 April 2023; Published 4 May 2023

Academic Editor: Watcharaporn Cholamjiak

Copyright © 2023 Weaam Alhejaili et al. This is an open access article distributed under the Creative Commons Attribution License, which permits unrestricted use, distribution, and reproduction in any medium, provided the original work is properly cited.

The damped parametric driven nonlinear pendulum equation/oscillator (NPE), also known as the damped disturbed NPE, is examined, along with some associated oscillators for arbitrary angles with the vertical pivot. For analyzing and solving the current pendulum equation, we reduce this equation to the damped Duffing equation (DDE) with variable coefficients. After that, the DDE with variable coefficients is divided into two cases. In the first case, two analytical approximations to the damped undisturbed NPE are obtained. The first approximation is determined using the ansatz method while the second one is derived using He's frequency formulation. In the second case, i.e., the damped disturbed NPE, three analytical approximations in terms of the trigonometric and Jacobi elliptic functions are derived and discussed using the ansatz method. The semianalytical solutions of the two mentioned cases are graphically compared with the 4th-order Runge–Kutta (RK4) approximations. In addition, the maximum error for all the derived approximations is estimated as compared with the RK4 approximation. The proposed approaches as well as the obtained solutions may greatly help in understanding the mysteries of various nonlinear phenomena that arise in different scientific fields such as fluid mechanics, plasma physics, engineering, and electronic chips.

1. Introduction

The complex pendulum is a paradigm for investigating oscillations and numerous other physical problems and nonlinear dynamical phenomena [1, 2]. Several models for the nonlinear pendulum oscillators (NPOs) have been utilized for investigating numerous physical and engineering problems, e.g., the oscillations in chips and electrical circuits, Bose–Einstein condensates, image processing, the movement of satellites, oscillations in different plasma models, and many other problems in several fields [3–5]. Moreover, many evolution equations to the pendulum oscillators have been utilized as a physical model to study several natural problems related to different oscillations, bifurcations, and

chaos [6–8]. For instance, He et al. [9] modified the structure of the pendulum oscillations on a dynamical system by using a device with electromagnetic harvesting to control the kinematics of a spring-pendulum system. Based on Lagrange's equations, the authors derived the governing kinematics equations of the NPOs and solved them analytically using the multiple-scale method (MSM). In that investigation, the authors explained various behaviors, which control the mentioned model, such as the stability of fixed points, amplitudes, phases, and the (in)stability regions. Besides that, they motioned that this model is utilized to control sensors in building transportation and industrial sectors. The auto-parametric system of three degrees of freedom consisting of a damped spring pendulum was

demonstrated in the study of [10]. The analytical solution to the motion equations up to the third approximation was obtained using the MSM. Furthermore, the stability and instability zones were analyzed and investigated. In the study of [11], the authors investigated the periodic property of a rotating pendulum model. The governing equation for this model was solved analytically using He's homotopy perturbation method (He's HPM). The accuracy of the obtained results was verified by comparing the obtained solution with the numerical one based on the 4th-order Runge–Kutta (RK4) method and with He's frequency formulation (He's FF). HPM and its family succeeded more than other methods in analyzing pendulum equations without both linear and negative-linear terms [12] and many other NPOs [13–15]. He's FF has developed rapidly since its inception; where many researchers have developed this method to give good results for many complicated nonlinear problems without any restrictions [16–21]. The hybrid forced Rayleigh–Van der Pol–Duffing oscillator with higher-order nonlinearity has been solved using the Poincaré–Lindstedt approach. The researchers discovered that the approximate solution and the RK4 numerical solution are in good agreement. The authors found that there is a high agreement between the analytical and numerical approximations [22]. Also, the homotopy analysis method (HAM) has been employed for analyzing the damped Duffing oscillator (DDO) [23]. The Laplace transform, modified differential transform method (MDTM), and Padé approximants have been applied for analyzing and investigating the approximations to many NPOs such as the forced DDO and forced damped van der Pol oscillator [24]. Both damped and undamped Helmholtz–Duffing (H–D) oscillators have been studied and analyzed using the ansatz method with the moving boundary technique to obtain high-accurate approximations [25]. The authors [25] made a comparison between both approximate analytic and numeric solutions to prove the accuracy of the analytic approximations, and it was found that the obtained results were in agreement with each other to a large extent. Moreover, the (un)damped quadratic nonlinear Helmholtz oscillator (HO) have been investigated using ansatz method and the exact solution for the undamped oscillator as well as the approximate solution to the damped oscillator have been derived in terms of the Weiersrtrass elliptic functions [26]. There have been few attempts to solve and analyze damped NPOs while taking friction forces into account [27]. The analytical approximations to some damped NPOs have been derived in terms of the Jacobi elliptic functions [27]. There are many other physical forces, such as periodic and perturbed forces in addition to friction force, that can affect the behavior of pendulum oscillators. For instance, the damped parametric nonlinear pendulum equation/oscillator (NPE/NPO) or known as the damped disturbed NPE/NPO has been discussed and solved numerically using implicit discrete mappings [28, 29]. Also, the parametric NPE with both frictional and excited forces has been solved analytically using the ansatz method and He's FF as well as solved numerically via the Galerkin method [30]. The comparison

with the RK4 approximation revealed that the derived analytical and numerical solutions were extremely accurate. Also, utilizing a variety of analytical and numerical techniques, the parametric NPE as well as certain related oscillators have been solved [31]. The authors used the ansatz method for deriving high-accurate approximations to the unforced damped parametric NPE in terms of angular Mathieu functions. Also, the authors applied the ansatz method to find some approximations to the damped (un)forced parametric NPE in terms of trigonometric functions. Moreover, He's FF was applied to obtain some approximations for both undamped and damped parametric NPE. Furthermore, HPM was carried out for analyzing both forced undamped and forced damped parametric NPE. Also, the authors applied the Krylov–Bogoliúbov Mitropolsky method (KBMM) for analyzing forced damped parametric NPE. Finally, the authors made a comparison between all obtained approximations with numerical approximations using both RK4 method and the hybrid Padé–finite difference method. In current work, the parametric (un)disturbed NPE and many other related oscillators will be investigated in detail and some innovative approximations using several effective techniques will be derived using the ansatz method. The present study is divided into two main parts: in the first part, some semianalytical solutions (analytical approximations) to the damped undisturbed NPE will be derived using the ansatz method and He's FF [17, 18, 32]. For the second part, the damped disturbed NPE will be solved analytically via different approaches based on the ansatz method. Furthermore, the comparison between all obtained analytical approximations for the two studied cases and the RK4 numerical approximation will be investigated graphically and numerically.

The rest of the present work is organized as follows. In Section 2, a glimpse about the equation of motion of the parametric pendulum equation and its solution is recovered. In Section 3, two-different analytical approximations (sometimes are called semianalytical solutions) to the damped undisturbed NPO are obtained using a suitable ansatz method and He's FF. In Section 4, some semianalytical solutions to the damped parametric driven NPO are discussed in detail. In this section, three-different formulas for the semianalytical solutions are derived. The results and discussion are introduced in Section 5. We summarized and introduced the most important results in Section 6.

2. The Damped Disturbed NPE and Its Solution

In this section, we construct the differential equation that describes the behavior of the parametric driven NPE on the pivot vertical. A simple mathematical parametric pendulum system is modeled by a point mass m in kg unit, hanging at the end of a massless wire with length l in m unit and fixed to a supporting point “O,” swinging to and from in a vertical plane. It is assumed that the end of the massless wire is moving harmonically with a small harmonic disturbance [28]: $y(t) = \pm \varepsilon \cos(\gamma t)$ (the motion of the vibrating base),

where ε is a dimensionless small parameter and γ represents the frequency of harmonic motion. By analyzing the pendulum motion, we obtain the following equation:

$$\begin{cases} x(t) = l \sin \varphi, \\ y(t) = -l \cos \varphi + \varepsilon \cos(\gamma t), \end{cases} \quad (1)$$

where φ denotes the angular displacement about downward vertical.

Accordingly, the velocities in (x, y) -directions read

$$\begin{cases} \dot{x}(t) = \dot{\varphi} l \cos \varphi, \\ \dot{y}(t) = \pm \dot{\varphi} l \sin \varphi - \varepsilon \gamma \sin(\gamma t). \end{cases} \quad (2)$$

Using the Lagrangian method, the equation of motion could be obtained taking damping force of the medium into account [28]:

$$\mathbb{R}_1 \equiv \ddot{\varphi} + 2\beta\dot{\varphi} + \phi(t) \sin \varphi = 0, \quad (3)$$

where $\phi(t) = \omega_0^2 \pm Q_0 \cos(\gamma t)$, $\omega_0 = \sqrt{g/l}$ denotes the eigenfrequency of the system, $\beta = \mu/(2ml)$ indicates the coefficient of the damping term, $Q_0 = \varepsilon\omega_2$ is the excitation amplitude, and $\omega_2 = \gamma^2/l$. Here, g represents the gravitational acceleration in unit m/s^2 , $g = 9.8m/s^2$. More details about the deriving (3) can be found in the studies of [28, 29].

As a particular case, in the absence of the dissipative (friction) forces, i.e., for $\beta = 0$, the parametric pendulum equation reduces to the undamped disturbed nonlinear pendulum equation:

$$\ddot{\varphi} + \phi(t) \sin \varphi = 0. \quad (4)$$

For $\varepsilon = 0$ and undamping $\beta = 0$, the parametric pendulum equation reduces to the simple pendulum equation:

$$\ddot{\varphi} + \omega_0^2 \sin \varphi = 0. \quad (5)$$

In the following sections, we proceed to solve and analyze all the mentioned cases in detail.

3. Analytical Approximations to the Damped Undisturbed NPE

It is supposed that $\varepsilon = 0$, then (3) reduces into the damped simple pendulum equation:

$$\begin{cases} \mathbb{R}_2 \equiv \ddot{\varphi} + 2\beta\dot{\varphi} + \omega_0^2 \sin \varphi = 0, \\ \varphi(0) = \varphi_0 \text{ and } \dot{\varphi}(0) = \dot{\varphi}_0. \end{cases} \quad (6)$$

For the Chebyshev approximation $\sin \varphi \approx (332/333)\varphi - (13/85)\varphi^3$, the initial value problem (i.v.p.) (6) can be rewritten in the following damped Duffing i.v.p. [33]:

$$\begin{cases} \mathbb{k} \equiv \ddot{\varphi} + 2\beta\dot{\varphi} + p\varphi + q\varphi^3 = 0, \\ \varphi(0) = \varphi_0 \text{ and } \dot{\varphi}(0) = \dot{\varphi}_0. \end{cases} \quad (7)$$

where $p = (332/333)\omega_0^2$ and $q = -(13/85)\omega_0^2$.

3.1. First Formula: Trigonometric Solution. Now, we seek a solution in the following ansatz:

$$\varphi = \exp(-\beta t)[A \sin(f(t)) + B \cos(f(t))], \quad (8)$$

where the coefficients A and B are undetermined coefficients which can be obtained the initial conditions (ICs) $\varphi(0) = \varphi_0$ and $\dot{\varphi}'(0) = \dot{\varphi}_0$ and $f \equiv f(t)$, $f(0) = 0$ is a function to be determined later. Applying the mentioned ICs, the values of A and B are obtained as

$$\begin{cases} A = \pm \sqrt{\pm \frac{4\beta^2 + \sqrt{(-4\beta^2 + 4p + 3q\varphi_0^2)^2 + 48q(\beta\varphi_0 + \dot{\varphi}_0)^2} - 4p - 3q\varphi_0^2}{6q}}, \\ B = \varphi_0. \end{cases} \quad (9)$$

The substitution of (8) into (7) gives us

$$\mathbb{k} = S_1 \sin(f) + S_2 \sin(3f) + S_3 \cos(f) + S_4 \cos(3f), \quad (10)$$

with

$$\begin{aligned}
 S_1 &= \frac{e^{-3\beta t}}{4} \begin{pmatrix} -3A^3q - 3AB^2q + 4A(\dot{f})^2e^{2\beta t} \\ -4Ape^{2\beta t} + 4A\beta^2e^{2\beta t} + 4B\ddot{f}e^{2\beta t} \end{pmatrix}, \\
 S_2 &= -\frac{e^{-3\beta t}}{4} (A^3q - 3AB^2q), \\
 S_3 &= -\frac{e^{-3\beta t}}{4} (-3A^2Bq - 4A\ddot{f}e^{2\beta t} - 3B^3q + 4B(\dot{f})^2e^{2\beta t} - 4Ape^{2\beta t} + 4\beta^2Be^{2\beta t}), \\
 S_4 &= -\frac{e^{-3\beta t}}{4} (3A^2Bq - B^3q).
 \end{aligned} \tag{11}$$

The ODE for the function f could be obtained by eliminating \ddot{f} from the system

$$S_1 = 0 \ \& \ S_3 = 0. \tag{12}$$

The ODE to be solved is

$$\begin{cases} \dot{f} = \sqrt{(3/4)q(A^2 + B^2)e^{-2\beta t} - \beta^2 + p}, \\ f(0) = 0. \end{cases} \tag{13}$$

The solution to the ODE (13) reads

$$f = \frac{1}{2\beta} \left[\sqrt{\Gamma} - \sqrt{\Gamma e^{-2t\beta}} + 2\sqrt{p - \beta^2} (\sinh^{-1}(\Theta) - \sinh^{-1}(\Theta)) \right], \tag{14}$$

with

$$\Theta = 2\sqrt{\frac{p - \beta^2}{3(A^2 + B^2)q}} e^{t\beta} \text{ and } \Gamma = 4p - 4\beta^2 + 3(A^2 + B^2)q. \tag{15}$$

For $\beta \rightarrow 0$, the function f reduces to

$$f = \sqrt{p + (3/4)(A^2 + B^2)}t. \tag{16}$$

Example 1. Let $(\beta, \omega_0) = (0.1, 1)$, then we obtain the following equation:

$$\begin{cases} \ddot{\varphi} + 0.2\dot{\varphi} + \sin \varphi = 0, \\ \varphi(0) = 0 \text{ and } \dot{\varphi}(0) = 0.25. \end{cases} \tag{17}$$

According to the above analysis, the approximate analytical solution reads

$$\varphi_{\text{Approx}} = -0.252583e^{-0.1t} \sin \left(\begin{matrix} 5. \sqrt{3.94799 - 0.0292721e^{-0.2t}} \\ +(-9.93477i)\sin^{-1}(11.6134e^{0.1t}) \\ +(21.3316 + 15.6055i) \end{matrix} \right). \tag{18}$$

The comparison between the approximation (18) and the RK4 numerical approximation is carried out as shown in Figure 1. Also, the maximum distance error (MDE) L_∞ to the approximation (18) as compared to the RK4 approximation is estimated:

$$L_\infty = \max_{0 \leq t \leq 30} |\varphi_{\text{Approx}} - \varphi_{\text{RK}}| = 0.00134826. \tag{19}$$

It is clear from the value of the MDE L_∞ that the analytical approximation (8) is characterized by the high-accuracy as compared to the RK4 numerical approximation, which enhances the effectiveness of this solution.

3.2. Second Approach: He's Frequency Formulation (He's FF). In order to apply He's FF, the following i.v.p.

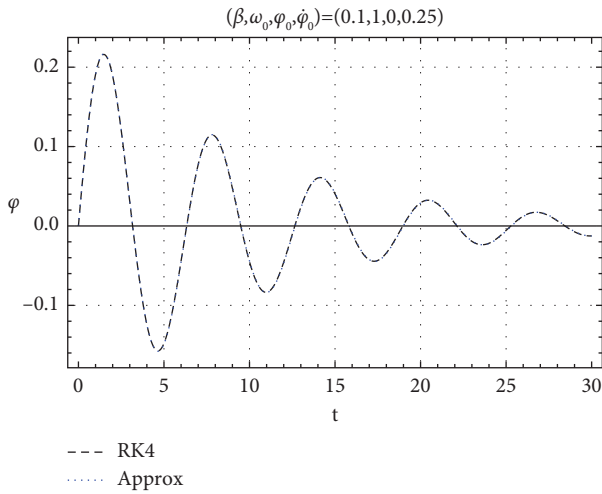


FIGURE 1: A comparison between the approximation (18) and the RK numerical approximation to the i.v.p. (17).

$$\begin{cases} \mathbb{R}_2 \equiv \ddot{\varphi} + 2\beta\dot{\varphi} + \omega_0^2 \sin \varphi = 0, \\ \varphi(0) = \varphi_0 \text{ and } \dot{\varphi}(0) = \dot{\varphi}_0, \end{cases} \quad (20)$$

replaces by the i.v.p.

$$\begin{aligned} \omega(t) &= \mu \int_0^t \sqrt{\left(1 - \frac{3}{26}A^2 e^{-2\rho\tau}\right)} \omega_0^2 d\tau, \\ &= \mu \left(\frac{\sqrt{Y(0)}\omega_0^2 - \sqrt{Y(t)}\omega_0^2}{\sqrt{26}\rho} - \frac{\sqrt{-Y(0)}\omega_0^2 \csc^{-1}(\sqrt{(3/26)}A)}{\rho\sqrt{Y(0)}\omega_0^2} \right. \\ &\quad \left. - \frac{Ae^{\rho t} \sqrt{3A^2 - 26e^{2\rho t}} \sqrt{Y(t)}\omega_0^2 \csc^{-1}(\sqrt{(3/26)}Ae^{-\rho t})}{\rho(3A^2 - 26e^{2\rho t})} \right), \end{aligned} \quad (26)$$

with

$$Y(t) = (26 - 3A^2 e^{-2\rho t}). \quad (27)$$

$$\begin{cases} \ddot{\varphi} + 2\beta\dot{\varphi} + f(\varphi) = 0, \\ \varphi(0) = \varphi_0 \text{ and } \dot{\varphi}(0) = \dot{\varphi}_0, \end{cases} \quad (21)$$

where the function $f(\varphi) \equiv f(x)$ can be obtained from the Chebyshev approximation as

$$f(x) = \omega_0^2 \sin x \approx \omega_0^2 \left(x - \frac{2}{13}x^3\right). \quad (22)$$

According to He's FF, we state

$$\varphi = Ae^{-\rho t} \cos\left(\omega(t) + \arccos\left(\frac{\varphi_0}{A}\right)\right), \quad (23)$$

with

$$\dot{\omega}(t) = \mu\sqrt{(f(x)/x)} \text{ and } x = \frac{\sqrt{a}}{2}Ae^{-\rho t}, \quad (24)$$

which leads to

$$\dot{\omega}(t) = \mu\sqrt{\left(1 - (3/26)A^2 e^{-2\rho t}\right)}\omega_0^2. \quad (25)$$

Solving the ODE (25) using the initial condition (IC) $\omega(0) = 0$, we have

The value of the coefficient A can be obtained by using the value of $\omega(t)$ (given in (26)) and applying the IC $\dot{\varphi}(0) = \dot{\varphi}_0$

$$\Gamma \equiv (-3A^2\varphi_0^2 + 3A^4 - 26A^2 + 26B^2)\mu^2\omega_0^2 + 26\varphi_0^2\rho^2 + 52\varphi_0\rho\dot{\varphi}_0 + 26\dot{\varphi}_0^2 = 0. \quad (28)$$

Using command Solve [$\Gamma == 0, A$] in MATHEMATICA, we finally get the value of A as follows:

$$A = \pm \frac{\sqrt{\pm\left(\sqrt{9\varphi_0^4\mu^2\omega_0^2 - 156\varphi_0^2\mu\omega_0^2 - 312\varphi_0^2\rho^2 - 624\varphi_0\rho\dot{\varphi}_0 + 676\mu^2\omega_0^2 - 312\dot{\varphi}_0^2/\mu\omega_0}\right) + 3\varphi_0^2 + 26}}{\sqrt{6}}. \quad (29)$$

Here, ρ and μ are free parameters that are chosen in order to optimize the approximate solution, i.e., minimize the residual error.

Example 2. We can apply He's FF (23) on Example 1, which is given in equation (20). The approximation (23) and the RK4 numerical approximation are compared with each other as shown in Figure 2 and the error L_∞ is estimated at the best values of $(\rho, \mu) = (0.104, 0.99)$ as

$$\begin{cases} L_\infty = \max_{0 \leq t \leq 30} |\varphi_{\text{Approx}} - \varphi_{\text{RK}}| = 0.00136089. \\ L_\infty = \max_{0 \leq t \leq 30} |\varphi_{\text{He's-FF}}(t) - \varphi_{\text{RK}}(t)| = 0.00531151. \end{cases} \quad (30)$$

It is clear from the errors of both trigonometric solution (8) and He's FF (23) for the same values of parameters that the Trigonometric solution (8) is better than the solution of He's FF (23). However, for higher-order Chebyshev approximation to the function $f(x)$:

$$f(x) = \omega_0^2 \sin x \approx \omega_0^2 \left(x - \frac{1}{6}x^3 - \frac{1}{127}x^5 \right). \quad (31)$$

We cannot get more accuracy but in this case the third-order Chebyshev approximation is better than the fifth-order Chebyshev approximation.

4. Some Analytical Approximations to the Damped Disturbed NPE

Some different formulas to the analytical approximations to the following i.v.p. will be discussed in detail:

$$\begin{cases} \mathbb{R}_1 \equiv \ddot{\varphi} + 2\beta\dot{\varphi} + \phi(t) \sin \varphi = 0, \\ \varphi(0) = \varphi_0 \text{ and } \dot{\varphi}(0) = \dot{\varphi}_0. \end{cases} \quad (32)$$

In the next section, three different formulas with high accuracy are investigated.

4.1. First Formula: Jacobi Elliptic Form. Taking the approximation (13) into account and with the help of the approximation $\sin \varphi \approx (\lambda_0 \varphi - \lambda_1 \varphi^3)$, the i.v.p. (32) reduces to the following variable coefficients damped Duffing i.v.p.:

$$\begin{cases} \mathbb{R} \equiv \ddot{\varphi} + 2\beta\dot{\varphi} + \phi(t)(\lambda_0 \varphi - \lambda_1 \varphi^3) = 0, \\ \varphi(0) = \varphi_0 \text{ and } \dot{\varphi}(0) = \dot{\varphi}_0, \end{cases} \quad (33)$$

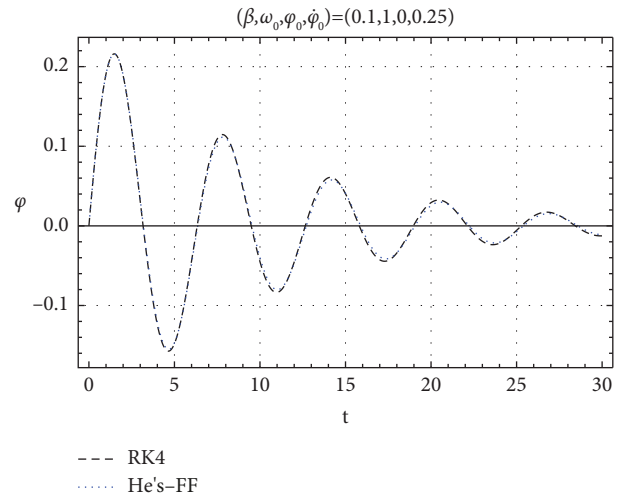


FIGURE 2: A comparison between the He's FF approximation (23) and the RK numerical approximation to the i.v.p. (6).

where $\lambda_0 = (332/333)$ and $\lambda_1 = (13/85)$. Note that the values of $\sin \varphi \approx (\lambda_0 \varphi - \lambda_1 \varphi^3)$ are obtained from the Chebyshev approximation.

Now, we seek approximate analytic solution to the i.v.p. (33) in the following ansatz form:

$$\varphi|_{\text{Approx}(1)} = \exp(-\beta t)\theta(f(t)), \quad (34)$$

where $\theta \equiv \theta(t)$ is a solution to the following i.v.p.:

$$\begin{cases} \ddot{\theta} + \kappa(\lambda_0 \theta - \lambda_1 \theta^3) = 0, \\ \theta(0) = \theta_0 \text{ and } \dot{\theta}(0) = \dot{\theta}_0, \end{cases} \quad (35)$$

where $\kappa = (\omega_0^2 - \varepsilon\omega_2)$.

The solution of the i.v.p. (35) can be expressed in the following form:

$$\theta(t) = \frac{\theta_0 \text{cn}(\sqrt{w}t|m) + \left(\frac{\dot{\theta}_0}{\sqrt{w}}\right) \text{dn}(\sqrt{w}t|m) \text{sn}(\sqrt{w}t|m)}{1 + (p + q\varphi_0^2 - w/2w) \text{sn}(\sqrt{w}t|m)^2}, \quad (36)$$

with

$$p = \lambda_0 \kappa, q = -\lambda_1 \kappa, w = \frac{p}{1 - 2m}, \text{ and } m = \frac{1}{2} \left(1 - \frac{p}{\sqrt{(p + q\theta_0^2)^2 + 2q\dot{\theta}_0^2}} \right). \quad (37)$$

The function $f \equiv f(t)$ is to be determined later, $\text{sn}(\sqrt{w}t|m)$ is the elliptic sine, $\text{cn}(\sqrt{w}t|m)$ is elliptic cosine, $\text{dn}(\sqrt{w}t|m)$ is the delta amplitude, and $0 \leq m \leq 1$.

Inserting solution (8) into the i.v.p. (33), we have the following equation:

$$\beta^2 + \lambda_0 \kappa (\dot{f})^2 + \lambda_0 \varepsilon \omega_2 \cos(\gamma t) - \lambda_0 \omega_0^2 = 0. \quad (38)$$

The solution of (38) gives the value of $f(t)$:

$$f = \pm \frac{\sqrt{333}}{\gamma \sqrt{83\kappa}} \sqrt{\lambda_0 \kappa - \beta^2} E\left(\frac{\gamma}{2} t, \frac{2\lambda_0 \varepsilon \omega_2}{\beta^2 - \lambda_0 \kappa}\right). \quad (39)$$

We can choose the solution with plus sign, then $f(0) = 0$ and $\dot{f}(0) = \sqrt{-(\beta^2/\lambda_0 \kappa) + 1}$.

Now, we must determine the values of θ_0 and $\dot{\theta}_0$ using the conditions $\varphi(0) = \varphi_0$ and $\dot{\varphi}(0) = \dot{\varphi}_0$. The required values are given by the following equation:

$$\theta(f(t)) = \frac{\theta_0 \operatorname{cn}(\sqrt{w} f(t)|m) + (\dot{\theta}_0/\sqrt{w}) \operatorname{dn}(\sqrt{w} f(t)|m) \operatorname{sn}(\sqrt{w} f(t)|m)}{1 + (p + q\varphi_0^2 - w/2w) \operatorname{sn}(\sqrt{w} f(t)|m)^2}. \quad (42)$$

4.2. The Second Formula: Jacobi Elliptic Solution. Here, we can use another approximation to $\sin \varphi \approx (\varphi - 2/13\varphi^3)$, then the i.v.p. (32) reduces to the damped Duffing i.v.p. with variable coefficients:

$$\begin{cases} \mathbb{Q} \equiv \ddot{\varphi} + 2\beta\dot{\varphi} + \phi(t)\left(\varphi - \frac{2}{13}\varphi^3\right) = 0, \\ \varphi(0) = \varphi_0 \text{ and } \dot{\varphi}(0) = \dot{\varphi}_0. \end{cases} \quad (43)$$

Let us consider the solution of the i.v.p. (43) is defined by the following ansatz:

$$\varphi(t)|_{\text{Approx}(2)} = \varphi_0 e^{-t\beta} \operatorname{cn}(\omega(t) + C, m). \quad (44)$$

Inserting the ansatz (44) in the i.v.p (43), we finally obtain the following equation:

$$\begin{cases} 13m\dot{\omega}(t)^2 + \varphi_0^2 e^{-2t\beta} \phi(t) = 0, \\ (2m - 1)\dot{\omega}(t)^2 - \beta^2 + \phi(t) = 0. \end{cases} \quad (45)$$

Eliminating m from system (45), we obtain the following equation:

$$\begin{cases} \dot{\omega}(t) = \sqrt{(\phi(t)(13 - 2\varphi_0^2 e^{-2t\beta}) - 13\beta^2/13)}, \\ \omega(0) = 0. \end{cases} \quad (46)$$

Equation (46) is not integrable, thus it solved numerically in order to get the value of $\omega(t)$.

Furthermore, the solution (44) could be written as

$$\dot{\theta}_0 = \frac{\beta\varphi_0 + \dot{\varphi}_0}{\sqrt{1 - (\beta^2/\lambda_0 \kappa)}}, \theta_0 = \varphi_0. \quad (40)$$

Inserting $f(t)$ given in (39) into solutions (34) and (36), we get the solution of the i.v.p. (33):

$$\varphi|_{\text{Approx}(1)} = \exp(-\beta t) \theta(f(t)), \quad (41)$$

with

$$\begin{aligned} \varphi|_{\text{Approx}(2)} &= \varphi_0 e^{-t\beta} \operatorname{cn}(\omega(t) + C, m) \\ &= \varphi_0 e^{-t\beta} \frac{cn + b_1 \operatorname{sn} \operatorname{dn}}{1 + b_2 \operatorname{sn}^2}, \end{aligned} \quad (47)$$

with

$$\begin{cases} \operatorname{sn} \equiv \operatorname{sn}(\omega(t)|m) = \sqrt{1 - cn^2}, \\ \operatorname{cn} \equiv \operatorname{cn}(\omega(t)|m), \\ \operatorname{dn} \equiv \operatorname{dn}(\omega(t)|m) = \left[\sqrt{1 - m(1 - cn^2)} \right]. \end{cases} \quad (48)$$

By inserting (46) and (47) into the i.v.p. (43) and after straightforward and simply calculations, finally, the values of b_1 and b_2 could be obtained as follows:

$$b_1 = \frac{\sqrt{13}(\beta\varphi_0 + \dot{\varphi}_0)}{\sqrt{-13\beta^2 - \kappa S_1}}, \quad (49)$$

and for $\varphi_0 \neq 0$

$$b_2 = -\frac{\kappa}{2\varphi_0(13\beta^2 + \kappa S_1)^2} \left[\varphi_0 \begin{pmatrix} -169S_2 - 26\beta\dot{\varphi}_0\varphi_0 \\ +4\kappa\varphi_0^4 - 52\kappa\varphi_0^2 \end{pmatrix} + 13 \sin(\varphi_0)(13\beta^2 + \kappa S_1) \right], \quad (50)$$

while $\varphi_0 = 0$, we obtain $b_2 = 0$, where $S_1 = (2\varphi_0^2 - 13)$ and $S_2 = (\beta^2 - \kappa)$.

By substituting equations (49)–(53) into the i.v.p. (43) and solving the obtained solution, we finally obtain the value of “ m ” for $\varphi_0 \neq 0$ as follows:

$$\begin{aligned}
 & -26\kappa\varphi_0\dot{\varphi}_0 \cos(\varphi_0)(13S_2 + 2\kappa\varphi_0^2)^2 \\
 & + 26\kappa \sin(\varphi_0)(26\varphi_0\beta S_2 + 3\dot{\varphi}_0(13S_2 + 2\kappa\varphi_0^2) - 2\beta\kappa\varphi_0^3)(13S_2 + 2\kappa\varphi_0^2) \\
 & + \varphi_0 \left[\begin{array}{c} -156\beta\kappa\varphi_0\dot{\varphi}_0^2(13S_2 + 2\kappa\varphi_0^2) \\ +\beta\varphi_0 \left(\begin{array}{c} -13\gamma^2\varepsilon\omega_2 S_1(13S_2 + 2\kappa\varphi_0^2) + \\ 8\kappa^2\varphi_0^2(78\varphi_0^2 S_2 - 507S_2 + 4\kappa\varphi_0^4) - 8788\kappa S_2^2 \end{array} \right) \\ -\dot{\varphi}_0 \left(\begin{array}{c} 8\kappa\varphi_0^2(507(\beta^4 - \kappa^2) + 2\kappa^2(39 - 2\varphi_0^2)\varphi_0^2) + \\ 13\gamma^2\varepsilon\omega_2 S_1(13S_2 + 2\kappa\varphi_0^2) + \\ 8788\kappa S_2^2 \end{array} \right) \end{array} \right] \\
 m = & \frac{\hspace{10em}}{8\varphi_0(\beta\varphi_0 + \dot{\varphi}_0)(13S_2 + 2\kappa\varphi_0^2)^3}.
 \end{aligned} \tag{51}$$

For $\varphi_0 = 0$, the value of the modulus “ m ” given in (51) reduces to

$$m = \frac{\gamma^2\varepsilon\omega_2}{8(\beta^2 - \kappa)^2}. \tag{52}$$

4.3. *Third Formula: Trigonometric Approach.* Another approximation in terms of trigonometric function to the i.v.p. (43) can be determined by inserting the following ansatz:

$$\varphi|_{\text{Approx}(3)} = A \exp(-\rho t) \cos\left(f + \arccos\left(\frac{\varphi_0}{A}\right)\right), \tag{53}$$

into the i.v.p. (46) which leads to

$$\begin{aligned}
 \mathbb{Q} & \equiv \ddot{\varphi} + 2\beta\dot{\varphi} + \phi(t)\left(\varphi - \frac{2}{13}\varphi^3\right) \\
 & = -\frac{2}{13}A^3 \cos^3(\theta)e^{-3\rho t}\phi(t) + Ae^{-\rho t} \cos(\theta) \\
 & \cdot (\rho^2 - 2\beta\rho + \phi(t) - (\dot{f})^2) \\
 & + Ae^{-\rho t} \sin(\theta) (2(\beta - \rho)\dot{f} + \ddot{f}),
 \end{aligned} \tag{54}$$

where $f \equiv f(t)$, $f(0) = 0$, and ρ is an optimal parameter. For vanishing the coefficient of $\cos(\theta)$, we obtain the following equation:

$$(\rho^2 - 2\beta\rho + \phi(t) - (\dot{f})^2) = 0, \text{ and } f(0) = 0. \tag{55}$$

Solving (55) with $f(0) = 0$ yields

$$f = \int_0^t \sqrt{\rho^2 - 2\beta\rho + \phi(\tau)} d\tau = \frac{2\sqrt{\Pi_0}}{\gamma} E\left(\frac{\gamma}{2}t, -\frac{2Q_0}{\Pi_0}\right), \tag{56}$$

with $\Pi_0 = (\rho^2 - 2\beta\rho + \omega_0^2 - Q_0)$ and $E((\gamma/2)t, -(2Q_0/\Pi_0))$ represents the elliptic integral of the second kind.

Applying the ICs $\varphi(0) = \varphi_0$ and $\dot{\varphi}(0) = \dot{\varphi}_0$, we obtain the following equation:

$$A = \pm \frac{\sqrt{2\rho\varphi_0 \cdot \varphi_0 + \varphi_0^2(\Pi_0 + \rho^2) + \dot{\varphi}_0^2}}{\sqrt{\Pi_0}}. \tag{57}$$

The number ρ is a free arbitrary parameter that we choose in order to get as small residual error as possible.

5. Results and Discussion

In this section, we proceed to analyze all obtained approximations. The discussion can be divided into several cases as follows.

Case 1. For the following numerical example $(\beta, \omega_0, \omega_2, \varepsilon, \gamma, \varphi(0), \dot{\varphi}(0)) = (0.1, 1, 0.5, 0.2, 0.2, 0, 0.1)$

$$\begin{cases} \mathbb{R} \equiv \ddot{\varphi} + 0.2\dot{\varphi} + \phi(t)(\lambda_1\varphi - \lambda_2\varphi^3) = 0, \\ \phi(t) = \omega_0^2 - \varepsilon\omega_2 \cos(\gamma t) = 1 - 0.1 \cos(0.2t), \\ \varphi(0) = 0 \text{ and } \dot{\varphi}(0) = 0.1. \end{cases} \tag{58}$$

The analytical approximations to the damped disturbed NPO (58) according to the first formula (44), second formula (50), and third formula (56) are compared with the RK4 numerical solution and the He’s HPM approximation as illustrated in Figure 3. Also, the MDE L_∞ for the mentioned approximations is estimated:

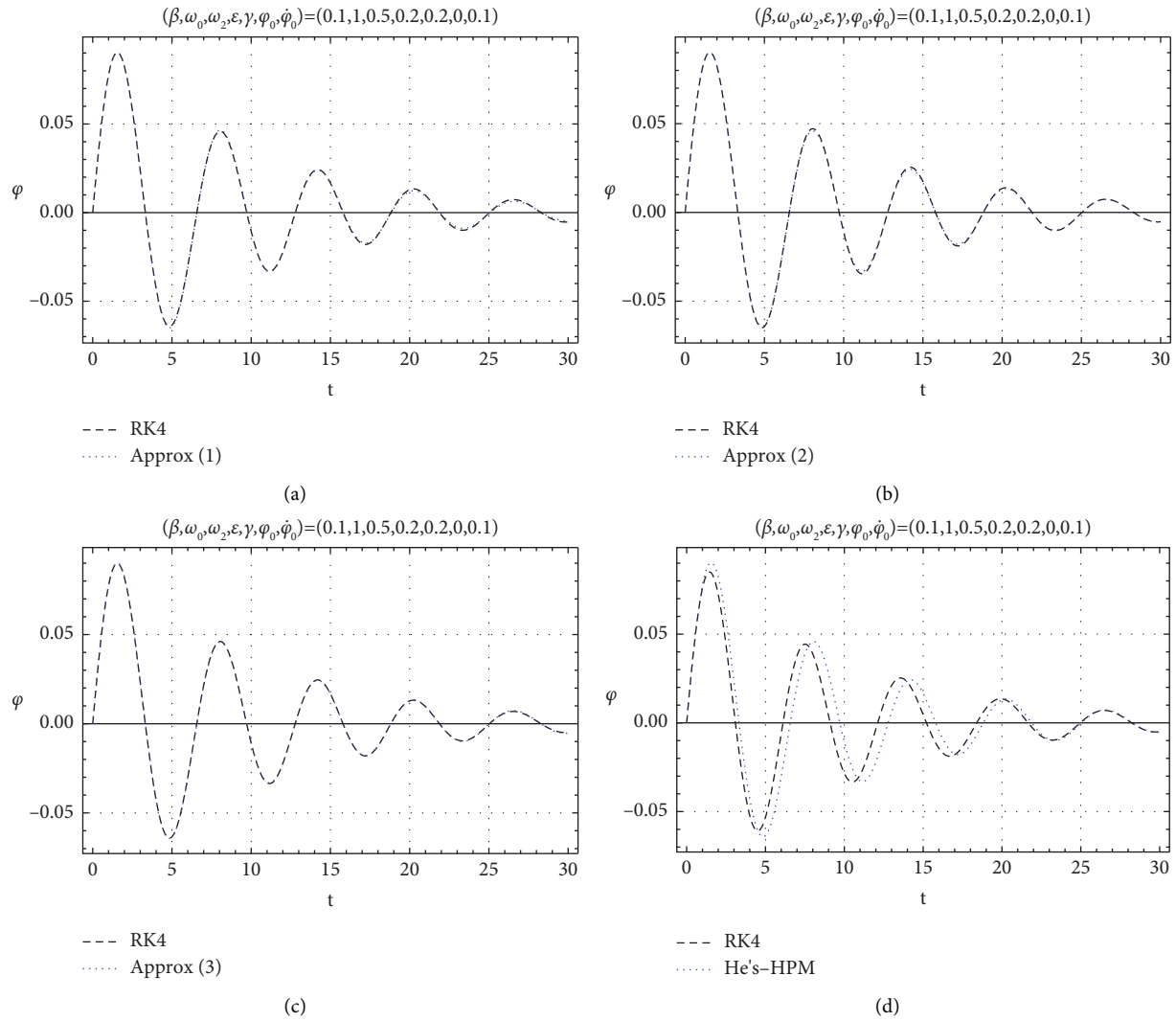


FIGURE 3: A comparison between the RK numerical approximation and the different types of the analytical approximations to the i.v.p. (33): (a) the Jacobi elliptic solution (44), (b) the Jacobi elliptic solution (50), (c) the trigonometric solution (56), and (d) the He’s HPM approximation. Here, $(\omega_2, \varphi_0) = (1, 0)$.

$$\begin{cases} L_{\infty}|_{\text{Approx}(1)} = \max_{0 \leq t \leq 30} |\varphi|_{\text{Approx}(1)} - \varphi_{\text{RK}} = 0.00114366, \\ L_{\infty}|_{\text{Approx}(2)} = \max_{0 \leq t \leq 30} |\varphi|_{\text{Approx}(2)} - \varphi_{\text{RK}} = 0.00139714, \\ L_{\infty}|_{\text{Approx}(3)} = \max_{0 \leq t \leq 30} |\varphi|_{\text{Approx}(3)} - \varphi_{\text{RK}} = 0.000432514, \\ L_{\infty}|_{\text{He's-HPM}} = \max_{0 \leq t \leq 30} |\varphi|_{\text{He's-HPM}} - \varphi_{\text{RK}} = 0.0246647. \end{cases} \tag{59}$$

It is observed that the exact congruence between the analytical approximations (41), (47), (53), and the RK4 numerical solution. Also, it is clear that the derived

approximations show high accuracy as compared to the He’s HPM approximation. Henceforth, for He’s HPM approximation, we used $\lambda_1 = 1$ and $\lambda_2 = 1/6$.

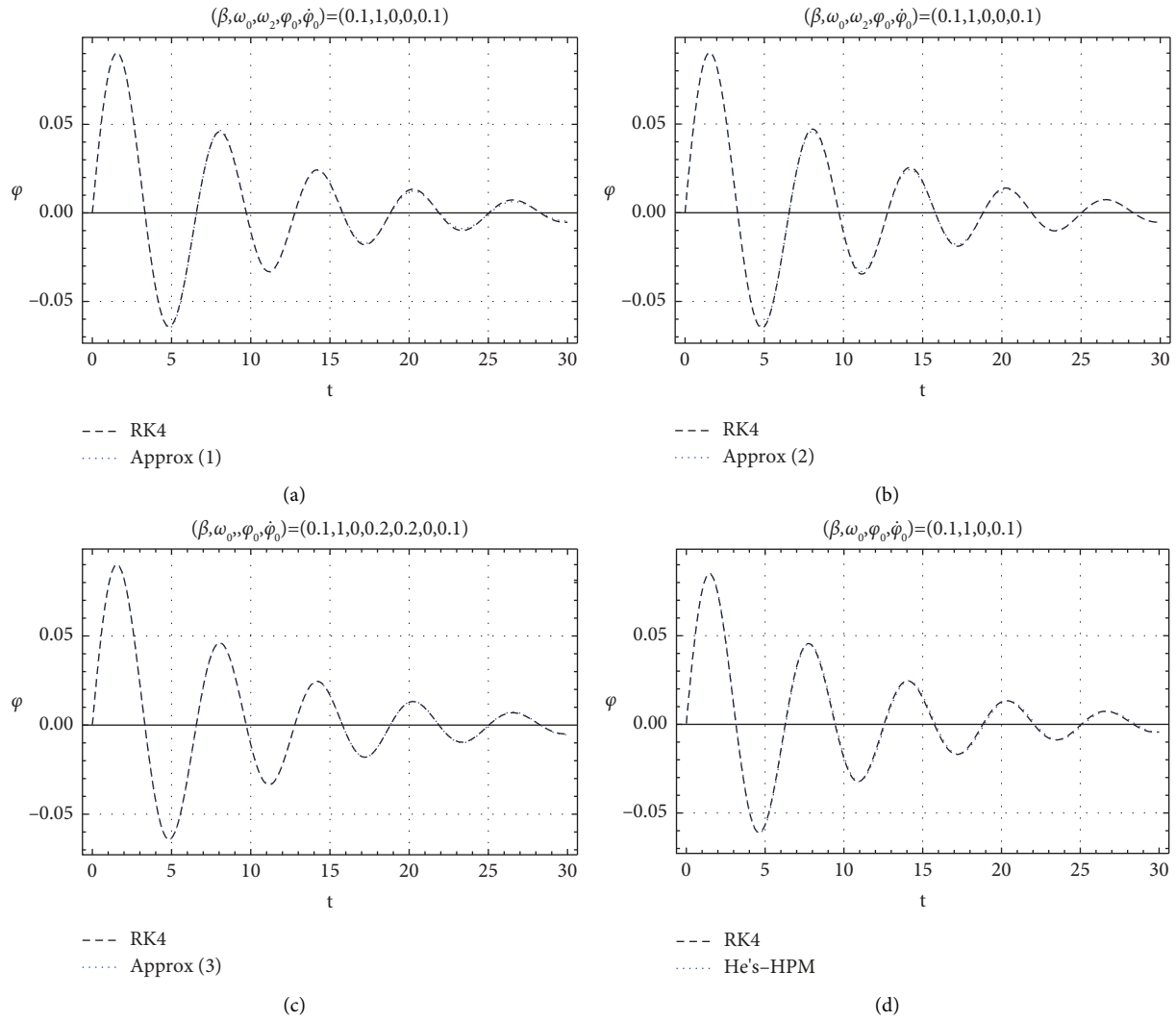


FIGURE 4: A comparison between the RK numerical approximation and the different types of the analytical approximations to the i.v.p. (33): (a) the Jacobi elliptic solution (44), (b) the Jacobi elliptic solution (50), (c) the trigonometric solution (56), and (d) the He's HPM approximation. Here, $(\omega_2, \varphi_0) = (0, 0)$.

Case 2. The approximations (41), (47), and (53) can recover the solutions to the damped undisturbed NPO (32) for $\omega_2 = 0$, i.e., the i.v.p. (7). Now, by considering the values $(\beta, \omega_0, \omega_2, \varphi(0), \dot{\varphi}(0)) = (0.1, 1, 0, 0, 0.1)$, the i.v.p. (7)

$$\begin{cases} \ddot{\varphi} + 0.2\dot{\varphi} + p\varphi + q\varphi^3 = 0, \\ \varphi(0) = 0 \text{ and } \dot{\varphi}(0) = 0.1. \end{cases} \quad (60)$$

The analytical approximations (8), (41), (47), (53), and the RK4 approximation and the He's HPM approximation to the i.v.p. (60) are graphically introduced in Figure 4. Also, the MDE L_∞ is computed for all mentioned approximations

$$\begin{cases} L_\infty|_{\text{Sol. (8)}} = \max_{0 \leq t \leq 30} |\varphi(t)|_{\text{Sol. (8)}} - \varphi_{\text{RK}}(t) = 0.000555229, \\ L_\infty|_{\text{Approx(1)}} = \max_{0 \leq t \leq 30} |\varphi(t)|_{\text{Approx(1)}} - \varphi_{\text{RK}}(t) = 0.000714541, \\ L_\infty|_{\text{Approx(2)}} = \max_{0 \leq t \leq 30} |\varphi(t)|_{\text{Approx(2)}} - \varphi_{\text{RK}}(t) = 0.000121574, \\ L_\infty|_{\text{Approx(3)}} = \max_{0 \leq t \leq 30} |\varphi(t)|_{\text{Approx(3)}} - \varphi_{\text{RK}}(t) = 0.000120303, \\ L_\infty|_{\text{He's-HPM}} = \max_{0 \leq t \leq 30} |\varphi|_{\text{He's-HPM}} - \varphi_{\text{RK}} = 0.00189472. \end{cases} \quad (61)$$

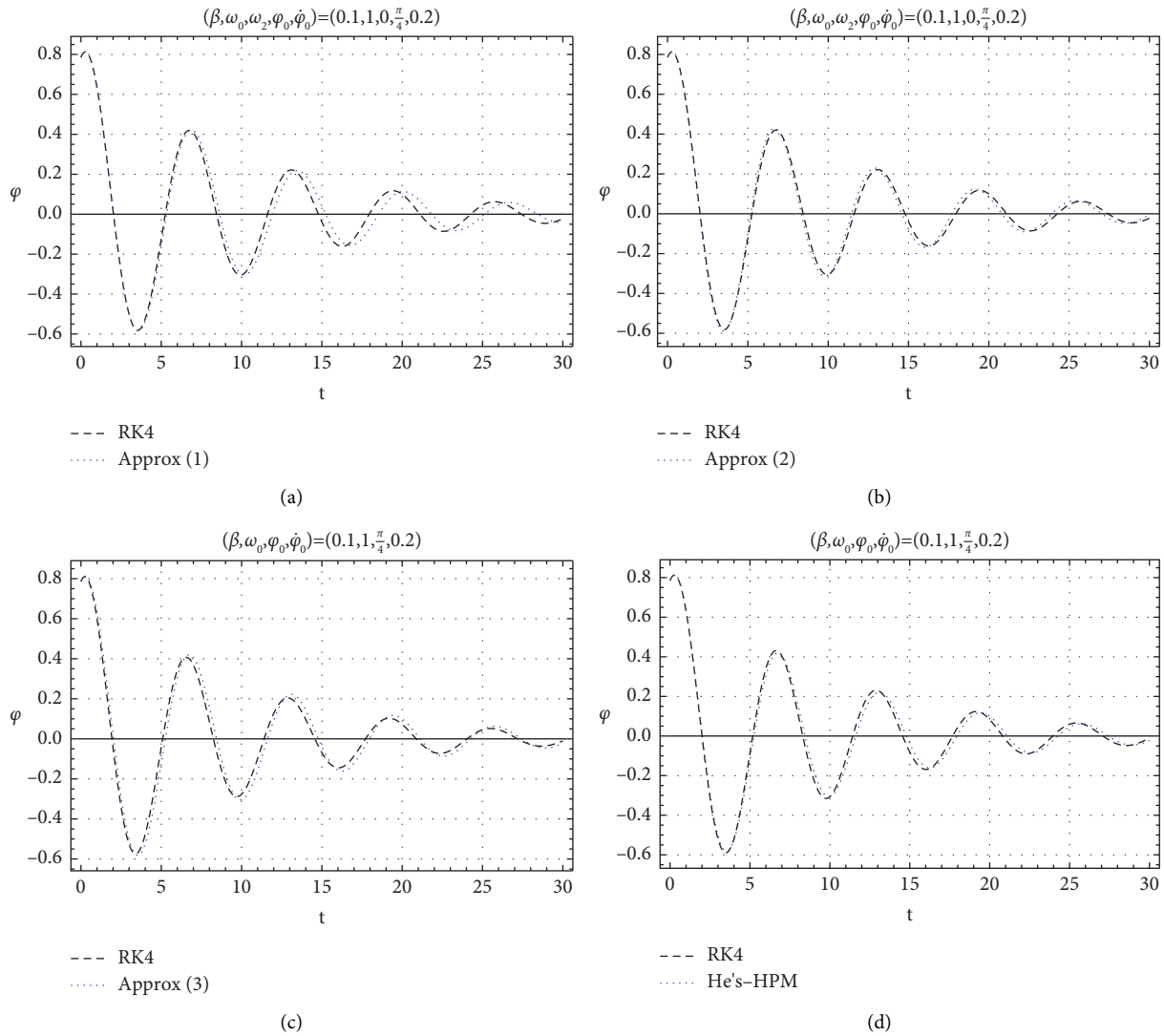


FIGURE 5: A comparison between the RK numerical approximation and the different types of the analytical approximations to the i.v.p. (62): (a) the Jacobi elliptic solution (44), (b) the Jacobi elliptic solution (50), (c) the trigonometric solution (56), and (d) the He's HPM approximation. Here, $(\omega_2, \varphi_0) = (0, \pi/4)$.

Case 3. For $(\beta, \omega_0, \omega_2, \varphi(0), \dot{\varphi}(0)) = (0.1, 1, 0, \pi/4, 0.2)$, the numerical form to the i.v.p. (7) reads

$$\begin{cases} \ddot{\varphi} + 0.2\dot{\varphi} + p\varphi + q\varphi^3 = 0, \\ \varphi(0) = \frac{\pi}{4} \text{ and } \dot{\varphi}(0) = 0.2. \end{cases} \quad (62)$$

The trigonometric solution (8) as well as the Jacobi elliptic solutions (41) and (47) in addition to the RK4 numerical solution and the He's HPM approximation to the i.v.p. (62) are graphically plotted as shown in Figure 5 and their MDE L_∞ is estimated as follows:

$$\left\{ \begin{array}{l} L_{\infty}|_{\text{Sol. (8)}} = \max_{0 \leq t \leq 30} |\varphi(t)|_{\text{Sol. (8)}} - \varphi_{\text{RK}}(t) = 0.0116904, \\ L_{\infty}|_{\text{Approx (1)}} = \max_{0 \leq t \leq 30} |\varphi(t)|_{\text{Approx (1)}} - \varphi_{\text{RK}}(t) = 0.0806987, \\ L_{\infty}|_{\text{Approx (2)}} = \max_{0 \leq t \leq 30} |\varphi(t)|_{\text{Approx (2)}} - \varphi_{\text{RK}}(t) = 0.0422837, \\ L_{\infty}|_{\text{Approx (3)}} = \max_{0 \leq t \leq 30} |\varphi(t)|_{\text{Approx (3)}} - \varphi_{\text{RK}}(t) = 0.0807087, \\ L_{\infty}|_{\text{He's HPM}} = \max_{0 \leq t \leq 30} |\varphi|_{\text{He's-HPM}} - \varphi_{\text{RK}} = 0.0528277. \end{array} \right. \quad (63)$$

It is observed that the trigonometric approximation (8) is better than all other approximations for arbitrary angles with the pivot vertical. Despite this, all the obtained approximations give satisfactory results and have good accuracy.

Furthermore, all analytical approximations (41), (47), and (53) can be recovered the undamped disturbed nonlinear pendulum oscillation ($\beta = 0$ & $\omega_2 \neq 0$) and the undamped undisturbed nonlinear pendulum oscillation ($\beta = \omega_2 = 0$) for arbitrary angles with the vertical pivot. In addition, the obtained solutions can be used for investigation the nonlinear oscillations in different plasma models which most evolutions equations that governed the dynamics of plasma waves and oscillations can be reduced to a pendulum equations (25) and (26).

6. Conclusions

In the current work, the parametric pendulum oscillatory equation and some related oscillatory equations have been solved using different analytical and numerical techniques. In this investigation, two-cases called the damped undisturbed nonlinear pendulum equation/oscillator (NPE/NPO) and the damped disturbed NPE have been discussed. The following list provides a concise summary of the most significant findings:

- (i) For the first oscillator, i.e., damped undisturbed NPO, this oscillator has been reduced to the constant coefficients damped Duffing equation, and its analytical approximations have been derived in terms of the trigonometric functions
 - (a) Both ansatz method and He's frequency formulation were employed to find some approximations for the damped undisturbed NPE
 - (b) The outcomes of comparing the obtained approximations and the numerical solutions revealed the great correctness of the obtained solutions
- (ii) In the second oscillator, i.e., damped disturbed NPO, this oscillator has been reduced to the variable coefficients damped Duffing oscillator in order to facilitate the solution process
 - (a) Three different formulas for the analytical approximations to the damped Duffing equation with variable coefficients in terms of Jacobi elliptic and trigonometric functions have been derived in detail.

- (b) In the first-formula, the modulus of Jacobi elliptic solution has been taken as zero while in the second formula, the modulus of Jacobi elliptic solution was taken as arbitrary value.
- (c) In the third formula, a new ansatz in terms of the trigonometric function was employed to find a high-accurate approximation in terms of trigonometric function.
- (d) It was found that the three-formulas to the analytical approximations to the damped disturbed NPO can be recovered different cases for the pendulum oscillators. Consequently, we discussed several cases for the nonlinear pendulum oscillators for small and arbitrary angles with the vertical pivot, e.g., the damped disturbed NPE ($\beta \neq 0$ & $\omega_2 \neq 0$) and the damped undisturbed nonlinear pendulum oscillation ($\beta \neq 0$ & $\omega_2 = 0$). Also, the obtained approximations can be recovered the undamped disturbed nonlinear pendulum oscillation ($\beta = 0$ & $\omega_2 \neq 0$) and the undamped undisturbed nonlinear pendulum oscillation ($\beta = \omega_2 = 0$) for arbitrary angles with the vertical pivot.

Finally, the obtained results were compared with the RK4 numerical approximation and the He's HPM approximation. It was found that the derived analytical approximations are distinguished by their great precision and more stable across the whole time domain, especially the third formula. Many equations of motions that govern the various pendulum oscillations can be solved using all proposed techniques. In addition, the obtained solutions aid in the investigation of nonlinear oscillations in different plasma physics.

Data Availability

All data generated or analyzed during this study are included within the article and more details are available from the corresponding author upon request.

Additional Points

Future Work. The study of stability analysis to the present pendulum oscillator is one of the most important topics, but it is out of the scope of the present study and it will be addressed in the next work. Also, the differential transform method (DTM) with the Padé approximation in addition can be used for analyzing the present oscillator [34].

Conflicts of Interest

The authors declare that they have no conflicts of interest.

Authors' Contributions

All authors contributed equally and approved the final manuscript.

Acknowledgments

The authors expressed their gratitude to Princess Nourah bint Abdulrahman University Researchers Supporting Project number PNURSP2023R229, Princess Nourah bint Abdulrahman University, Riyadh, Saudi Arabia.





References

- [1] N. Nayfeh and D. T. Mook, *Non-linear Oscillations*, John Wiley, New York, NY, USA, 1973.
- [2] W. Albalawi, A. H. Salas, S. A. El-Tantawy, and A. A. Al-Rahman Youssef, "Approximate analytical and numerical solutions to the damped pendulum oscillator: Newton-Raphson and moving boundary methods," *Journal of Taibah University for Science*, vol. 15, pp. 479–485, 2021.
- [3] A.-M. Wazwaz, *Partial Differential Equations and Solitary Waves Theory, Higher Education*, Springer, Berlin, Germany, 2009.
- [4] Z.-J. Yang, S.-M. Zhang, X.-L. Li, and Z.-G. Pang, "Variable sinh-Gaussian solitons in nonlocal nonlinear Schrödinger equation," *Applied Mathematics Letters*, vol. 82, pp. 64–70, 2018.
- [5] L.-M. Song, Z.-J. Yang, S.-M. Zhang, and X.-L. Li, "Spiraling anomalous vortex beam arrays in strongly nonlocal nonlinear media," *Physical Review A*, vol. 99, no. 6, Article ID 063817, 2019.
- [6] W. Hu and D. J. Scheeres, "Spacecraft motion about slowly rotating asteroids," *Advances in the Astronautical Sciences*, vol. 105, p. 839, 2000.
- [7] W. Lestari and S. Hanagud, "Nonlinear vibration of buckled beams: some exact solutions," *International Journal of Solids and Structures*, vol. 38, no. 26-27, pp. 4741–4757, 2001.
- [8] S. Liu, Z. Fu, S. Liu, and Q. Zhao, "Jacobi elliptic function expansion method and periodic wave solutions of nonlinear wave equations," *Physics Letters A*, vol. 289, no. 1-2, pp. 69–74, 2001.
- [9] C.-H. He, T. S. Amer, D. Tian, A. F. Abolila, and A. A. Galal, "Controlling the kinematics of a spring-pendulum system using an energy harvesting device," *Journal of Low Frequency Noise, Vibration and Active Control*, vol. 41, no. 3, pp. 1234–1257, 2022.
- [10] J. H. He, T. S. Amer, A. F. Abolila, and A. A. Galal, "Stability of three degrees-of-freedom auto-parametric system," *Alexandria Engineering Journal*, vol. 61, no. 11, pp. 8393–8415, 2022.
- [11] J. H. He, T. S. Amer, S. Elnaggar, and A. A. Galal, "Periodic property and instability of a rotating pendulum system," *Axioms*, vol. 10, no. 3, p. 191, 2021.
- [12] Y. Wu and J. H. He, "Homotopy perturbation method for nonlinear oscillators with coordinatedependent mass," *Results in Physics*, vol. 10, pp. 270–271, 2018.
- [13] J. H. He and Y. O. El-Dib, "Homotopy perturbation method for Fangzhu oscillator," *Journal of Mathematical Chemistry*, vol. 58, no. 10, pp. 2245–2253, 2020.
- [14] J. H. He and Y. O. El-Dib, "The reducing rank method to solve third-order Duffing equation with the homotopy perturbation," *Numerical Methods for Partial Differential Equations*, vol. 37, no. 2, pp. 1800–1808, 2020.
- [15] J. H. He and Y. O. El-Dib, "The enhanced homotopy perturbation method for axial vibration of strings," *Facta Universitatis – Series: Mechanical Engineering*, vol. 19, no. 4, p. 735, 2021.
- [16] A. Elías-Zúñiga, L. M. Palacios-Pineda, I. H. Jiménez-Cedeño, D. O. Martínez-Romero, and D. Olvera-Trejo, "Enhanced He's frequency-amplitude formulation for nonlinear oscillators," *Results in Physics*, vol. 19, Article ID 103626, 2020.
- [17] J. H. He, "An improved amplitude-frequency formulation for nonlinear oscillators," *International Journal of Nonlinear Sciences and Numerical Simulation*, vol. 9, no. 2, pp. 211–212, 2008.
- [18] J. H. He, "Amplitude-frequency relationship for conservative nonlinear oscillators with odd nonlinearities," *International Journal of Applications and Computer Math*, vol. 3, no. 2, pp. 1557–1560, 2017.
- [19] C. X. Liu, "A short remark on He's frequency formulation," *Journal of Low Frequency Noise, Vibration and Active Control*, vol. 40, no. 2, pp. 672–674, 2021.
- [20] G. Q. Feng, "He's frequency formula to fractal undamped Duffing equation," *Journal of Low Frequency Noise, Vibration and Active Control*, vol. 40, no. 4, pp. 1671–1676, 2021.
- [21] Y. Wu and Y. P. Liu, "Residual calculation in He's frequency-amplitude formulation," *Journal of Low Frequency Noise, Vibration and Active Control*, vol. 40, no. 2, pp. 1040–1047, 2021.
- [22] C. H. He, D. Tian, G. M. Moatimid, H. F. Salman, and M. H. Zekry, "Hybrid Rayleigh–van der pol–duffing oscillator: stability analysis and controller," *Journal of Low Frequency Noise, Vibration and Active Control*, vol. 41, no. 1, pp. 244–268, 2021.
- [23] M. Turkyilmazoglu, "An effective approach for approximate analytical solutions of the damped Duffing equation," *Physica Scripta*, vol. 86, no. 1, Article ID 015301, 2012.
- [24] H. M. Abdelhafez, "Solution of excited non-linear oscillators under damping effects using the modified differential transform method," *Mathematics*, vol. 4, no. 1, p. 11, 2016.
- [25] A. H. Salas, S. A. El-Tantawy, and M. R. Alharthi, "Novel solutions to the (un) damped Helmholtz-Duffing oscillator and its application to plasma physics: moving boundary method," *Physica Scripta*, vol. 96, no. 10, Article ID 104003, 2021.
- [26] S. A. El-Tantawy, A. H. Salas, and M. R. Alharthi, "A new approach for modelling the damped Helmholtz oscillator: applications to plasma physics and electronic circuits," *Communications in Theoretical Physics*, vol. 73, no. 3, Article ID 035501, 2021.
- [27] K. Johannessen, "An analytical solution to the equation of motion for the damped nonlinear pendulum," *European Journal of Physics*, vol. 35, no. 3, Article ID 035014, 2014.
- [28] Y. Guo, A. C. Luo, and J. Luo, "Bifurcation dynamics of a damped parametric pendulum," *Synthesis Lectures on Mechanical Engineering*, vol. 3, no. 5, pp. 1–98, 2019.
- [29] I. Gabitov, T. Bello, E. Huang, F. Lopez, K. Rumsey, and T. Tao, *Stability Analysis Of Pendulum With Vibrating Base*, University of Arizona, Tucson, AZ, USA, 2014.
- [30] H. A. Alyousef, A. H. Salas, M. R. Alharthi, and S. A. El-Tantawy, "Galerkin method, ansatz method, and He's frequency formulation for modeling the forced damped parametric driven pendulum oscillators," *Journal of Low*

- Frequency Noise, Vibration and Active Control*, vol. 41, no. 4, pp. 1426–1445, 2022.
- [31] H. A. Alyousef, M. R. Alharthi, A. H. Salas, and S. A. El-Tantawy, “Optimal analytical and numerical approximations to the (un)forced (un)damped parametric pendulum oscillator,” *Communications in Theoretical Physics*, vol. 74, no. 10, Article ID 105002, 2022.
- [32] Z.-F. Ren and G.-F. Hu, “He’s frequency–amplitude formulation with average residuals for nonlinear oscillators,” *Journal of Low Frequency Noise, Vibration and Active Control*, vol. 38, no. 3-4, pp. 1050–1059, 2018.
- [33] S. A. El-Tantawy, A. H. Salas, and M. R. Alharthi, “On the analytical solutions of the forced damping duffing equation in the form of weierstrass elliptic function and its applications,” *Mathematical Problems in Engineering*, vol. 2021, Article ID 6678102, 9 pages, 2021.
- [34] A. Zeeshan, M. B. Arain, M. M. Bhatti, F. Alzahrani, and O. A. Bég, “Radiative bioconvection nanofluid squeezing flow between rotating circular plates: semi-numerical study with the DTM-Padé approach,” *Modern Physics Letters B*, vol. 36, no. 03, Article ID 2150552, 2022.

Research Article

An Efficient Iterative Algorithm for Solving the Split Feasibility Problem in Hilbert Spaces Applicable in Image Deblurring, Signal Recovering, and Polynomiography

Lanchakorn Kittiratanawasin ¹, Damrongsak Yambangwai ²,
Chonjaroen Chairatsiripong ² and Tanakit Thianwan ²

¹Department of Mathematics, Faculty of Science, Kasetsart University, Bangkok 10900, Thailand

²Department of Mathematics, School of Science, University of Phayao, Phayao 56000, Thailand

Correspondence should be addressed to Tanakit Thianwan; tanakit.th@up.ac.th

Received 15 November 2022; Revised 23 December 2022; Accepted 28 March 2023; Published 22 April 2023

Academic Editor: Kenan Yildirim

Copyright © 2023 Lanchakorn Kittiratanawasin et al. This is an open access article distributed under the Creative Commons Attribution License, which permits unrestricted use, distribution, and reproduction in any medium, provided the original work is properly cited.

The split feasibility problem (SFP) in Hilbert spaces is addressed in this study using an efficient iterative approach. Under mild conditions, we prove convergence theorems for the algorithm for finding a solution to the SFP. We also present numerical examples to illustrate that the acceleration of our algorithm is effective. Our results are applied to solve image deblurring and signal recovery problems. Furthermore, we show the use of the proposed method to generate polynomiographs.

1. Introduction

Let \mathcal{C} and \mathcal{Q} be nonempty closed convex subsets of real Hilbert spaces \mathcal{H}_1 and \mathcal{H}_2 , respectively. The split feasibility problem (SFP for short) can be formulated as finding a point u^* in \mathcal{C} with the property

$$\mathcal{A}u^* \in \mathcal{Q}, \quad (1)$$

where $\mathcal{A}: \mathcal{H}_1 \rightarrow \mathcal{H}_2$ is a bounded linear operator.

For modeling inverse problems, Censor and Elfving [1] proposed the SFP in finite-dimensional Hilbert spaces. Later on, the SFP can also be applied to medical image reconstruction and signal processing; see, e.g., [2–10].

The SFP (1) can be written as a fixed point problem by using

$$\mathcal{P}_{\mathcal{C}}[\mathcal{I} - \gamma\mathcal{A}^*(\mathcal{I} - \mathcal{P}_{\mathcal{Q}})\mathcal{A}]u^* = u^*, \quad (2)$$

where $\mathcal{P}_{\mathcal{C}}$ and $\mathcal{P}_{\mathcal{Q}}$ are the (orthogonal) projections onto \mathcal{C} and \mathcal{Q} , respectively, $\gamma > 0$ is any positive constant, and \mathcal{A}^* denotes the adjoint of \mathcal{A} . That is, u^* solves the SFP (1) if and only if u^* solves the fixed point equation (2) (see [11]). For

more effective, the readers can see [8, 12–22]. In [7], Byrne proposed the $\mathcal{C}\mathcal{Q}$ algorithm by

$$u_{k+1} = \mathcal{P}_{\mathcal{C}}[\mathcal{I} - \gamma\mathcal{A}^*(\mathcal{I} - \mathcal{P}_{\mathcal{Q}})\mathcal{A}]u_k, k \geq 0, \quad (3)$$

where $0 < \gamma < 2/\|\mathcal{A}\|^2$, $\mathcal{A}^*: \mathcal{H}_2 \rightarrow \mathcal{H}_1$ is the adjoint of \mathcal{A} , and $\mathcal{P}_{\mathcal{C}}$ and $\mathcal{P}_{\mathcal{Q}}$ are the projections onto \mathcal{C} and \mathcal{Q} , respectively. The $\mathcal{C}\mathcal{Q}$ -algorithm (3) has been a useful instrument for solving the SFP due to its own virtues-simple computation, and many variants of the $\mathcal{C}\mathcal{Q}$ -algorithm have been employed in several literature, such as [8, 9], and so on.

The three-step procedures were first introduced by Noor [23]. This method is applied to many problems. For example, see [24–26].

Recently, the following three step iteration method used to solve the SFP was defined by Dang and Gao [27]:

$$\begin{aligned} w_n &= (1 - \gamma_n)u_n + \gamma_n\mathcal{P}_{\mathcal{C}}[(1 - \lambda_n)\mathcal{U}]u_n, \\ \varsigma_n &= (1 - \beta_n)u_n + \beta_n\mathcal{P}_{\mathcal{C}}[(1 - \lambda_n)\mathcal{U}]w_n, \\ u_{n+1} &= (1 - \alpha_n)u_n + \alpha_n\mathcal{P}_{\mathcal{C}}[(1 - \lambda_n)\mathcal{U}]\varsigma_n, \end{aligned} \quad (4)$$

where $\mathcal{U} = \mathcal{F} - \gamma\mathcal{A}^*(\mathcal{F} - \mathcal{P}_{\mathcal{Q}})\mathcal{A}$ and $\{\alpha_n\}, \{\beta_n\}, \{\gamma_n\}, \{\lambda_n\}$ are real sequences in $(0, 1)$. Strong convergence theorems are studied for (4) under some parametric controlling conditions. In addition, Thakur et al. [28] proposed the new three-step iterative method for solving fixed points of nonexpansive mapping.

Motivated by Dang et al., we propose an efficient iterative method which generates a sequence $\{u_n\}$ by

$$\begin{aligned} w_n &= (1 - \gamma_n)u_n + \gamma_n\mathcal{T}u_n, \\ \varsigma_n &= (1 - \beta_n)w_n + \beta_n\mathcal{T}w_n, \\ u_{n+1} &= (1 - \alpha_n)\mathcal{T}u_n + \alpha_n\mathcal{T}\varsigma_n, \end{aligned} \quad (5)$$

where $\mathcal{T} = \mathcal{P}_{\mathcal{C}}[\mathcal{F} - \gamma\mathcal{A}^*(\mathcal{F} - \mathcal{P}_{\mathcal{Q}})\mathcal{A}]$ and $\{\alpha_n\}, \{\beta_n\}, \{\gamma_n\}$ are real sequences in $(0, 1)$.

2. Preliminaries

Let \mathcal{H} be a real Hilbert space with inner product $\langle \cdot, \cdot \rangle$ and induce norm $\|\cdot\|$. I denotes the identity operator in \mathcal{H} . We will denote the set of fixed points of: $\mathcal{H} \rightarrow \mathcal{H}$ by $F(\mathcal{T}) = \{u \in \mathcal{H} : \mathcal{T}u = u\}$. For the sequence $\{u_n\}$ to u in \mathcal{H} , the strong convergence and the weak convergence are denoted by $u_n \rightarrow u$ and $u_n \rightharpoonup u$, respectively. An operator \mathcal{T} on \mathcal{H} is nonexpansive if, for each $u, v \in \mathcal{H}$,

$$\|\mathcal{T}u - \mathcal{T}v\| \leq \|u - v\|, \quad (6)$$

\mathcal{T} is said to be λ -Lipschitz continuous, if each $u, v \in \mathcal{H}$, we have

$$\|\mathcal{T}u - \mathcal{T}v\| \leq \lambda\|u - v\|, \quad (7)$$

for a constant $\lambda > 0$. Assume $\varphi > 0$. Then, \mathcal{T} is called φ -inverse strongly monotone (φ -ism), if each $u, v \in \mathcal{H}$, we have

$$\langle u - v, \mathcal{T}u - \mathcal{T}v \rangle \geq \varphi\|\mathcal{T}u - \mathcal{T}v\|^2. \quad (8)$$

Recall that 1-ism \mathcal{T} is also known as being firmly nonexpansive, that is, for each $u, v \in \mathcal{H}$,

$$\langle u - v, \mathcal{T}u - \mathcal{T}v \rangle \geq \|\mathcal{T}u - \mathcal{T}v\|^2. \quad (9)$$

Let the solution set $\Omega = \{u \in \mathcal{C} : \mathcal{A}u \in \mathcal{Q}\} = \mathcal{C} \cap \mathcal{A}^{-1}\mathcal{Q}$ of the SFP (1) be a closed, convex, and nonempty set. Let $\mathcal{P}_{\mathcal{C}}$ denote the projection from \mathcal{H} onto a nonempty closed convex subset \mathcal{C} of \mathcal{H} that is, $\mathcal{P}_{\mathcal{C}}(u) := \operatorname{argmin}_{v \in \mathcal{C}} \|u - v\|$. Suppose that $d(u, \mathcal{C}) := \inf\{\|u - v\| : v \in \mathcal{C}\}$. We have the following important lemma due to Feng et al. [29]:

Lemma 1. *If $\mathcal{T} = \mathcal{P}_{\mathcal{C}}[\mathcal{F} - \gamma\mathcal{A}^*(\mathcal{F} - \mathcal{P}_{\mathcal{Q}})\mathcal{A}]$, where $0 < \gamma < 2/\|\mathcal{A}\|^2$, then \mathcal{T} is a nonexpansive map.*

Lemma 2 (see [30]). *Let $\{u_n\}$ be a sequence of Hilbert space \mathcal{H} . If $\{u_n\}$ converges weakly to u , then for any $v \in \mathcal{H}$ and $v \neq u$, we have $\lim_{n \rightarrow \infty} \inf\|u_n - u\| < \lim_{n \rightarrow \infty} \inf\|u_n - v\|$.*

Lemma 3 (see [30]). *Let \mathcal{C} be a closed, convex, and nonempty subset of real Hilbert space \mathcal{H} , and $\mathcal{T} : \mathcal{C} \rightarrow \mathcal{C}$ be*

a nonexpansive mapping. Then, $\mathcal{F} - \mathcal{T}$ is demiclosed at zero, i.e., if $u_n \rightharpoonup u \in \mathcal{C}$ and $u_n - \mathcal{T}u_n \rightarrow 0$, then $u = \mathcal{T}u$.

Lemma 4 (see [31]). *Let X be a uniformly convex Banach space and $0 < p \leq t_n \leq q < 1$ for all $n \in \mathbb{N}$. Let $\{u_n\}$ and $\{v_n\}$ be two sequences of X such that $\limsup_{n \rightarrow \infty} \|u_n\| \leq r$, $\limsup_{n \rightarrow \infty} \|v_n\| \leq r$ and $\limsup_{n \rightarrow \infty} \|t_n u_n + (1 - t_n)v_n\| = r$ hold for some $r \geq 0$. Then, $\limsup_{n \rightarrow \infty} \|u_n - v_n\| = 0$.*

3. Convergence Results

Lemma 5. *Let $\{u_n\}$ be generated by (5) and $\mathcal{T} = \mathcal{P}_{\mathcal{C}}[\mathcal{F} - \gamma\mathcal{A}^*(\mathcal{F} - \mathcal{P}_{\mathcal{Q}})\mathcal{A}]$. Then, $\lim_{n \rightarrow \infty} \|u_n - u^*\|$ exists for any $u^* \in F(\mathcal{T})$.*

Proof. Given $u^* \in F(\mathcal{T})$. By nonexpansiveness of \mathcal{T} and using (5), we have

$$\begin{aligned} \|w_n - u^*\| &= \|(1 - \gamma_n)u_n + \gamma_n\mathcal{T}u_n - u^*\| \\ &\leq (1 - \gamma_n)\|u_n - u^*\| + \gamma_n\|\mathcal{T}u_n - u^*\| \\ &\leq (1 - \gamma_n)\|u_n - u^*\| + \gamma_n\|u_n - u^*\| \\ &= \|u_n - u^*\|, \end{aligned} \quad (10)$$

and so

$$\begin{aligned} \|\varsigma_n - u^*\| &= \|(1 - \beta_n)w_n + \beta_n\mathcal{T}w_n - u^*\| \\ &\leq (1 - \beta_n)\|w_n - u^*\| + \beta_n\|\mathcal{T}w_n - u^*\| \\ &\leq (1 - \beta_n)\|w_n - u^*\| + \beta_n\|w_n - u^*\| \\ &= \|w_n - u^*\| \\ &\leq \|u_n - u^*\|. \end{aligned} \quad (11)$$

Using (10) and (11), we have

$$\begin{aligned} \|u_{n+1} - u^*\| &= \|(1 - \alpha_n)\mathcal{T}u_n + \alpha_n\mathcal{T}\varsigma_n - u^*\| \\ &\leq (1 - \alpha_n)\|\mathcal{T}u_n - u^*\| + \alpha_n\|\mathcal{T}\varsigma_n - u^*\| \\ &\leq (1 - \alpha_n)\|u_n - u^*\| + \alpha_n\|\varsigma_n - u^*\| \\ &\leq (1 - \alpha_n)\|u_n - u^*\| + \alpha_n\|u_n - u^*\| \\ &= \|u_n - u^*\|. \end{aligned} \quad (12)$$

Since u^* is chosen arbitrarily in $F(\mathcal{T})$, one deduces that $\{\|u_n - u^*\|\}_n$ is decreasing. It follows that $\lim_{n \rightarrow \infty} \|u_n - u^*\|$ exists for any $u^* \in F(\mathcal{T})$. This completes the proof. \square

Lemma 6. *Let $\{u_n\}$ be generated by (5). and $\mathcal{T} = \mathcal{P}_{\mathcal{C}}[\mathcal{F} - \gamma\mathcal{A}^*(\mathcal{F} - \mathcal{P}_{\mathcal{Q}})\mathcal{A}]$. Then, $\lim_{n \rightarrow \infty} \|u_n - \mathcal{T}u_n\| = 0$.*

Proof. By Lemma 5, we see that $\lim_{n \rightarrow \infty} \|u_n - u^*\|$ exists for any $u^* \in F(\mathcal{T})$. Assume that

$$\lim_{n \rightarrow \infty} \|u_n - u^*\| = c. \quad (13)$$

We take the lim sup of (10) and (11), and we get

$$\limsup_{n \rightarrow \infty} \|w_n - u^*\| \leq c, \tag{14}$$

and

$$\limsup_{n \rightarrow \infty} \|\zeta_n - u^*\| \leq c. \tag{15}$$

In addition, by nonexpensiveness of \mathcal{T} , we have

$$\begin{aligned} \|\mathcal{T}u_n - u^*\| &\leq \|u_n - u^*\|, \|\mathcal{T}w_n - u^*\| \\ &\leq \|w_n - u^*\|, \|\mathcal{T}\zeta_n - u^*\| \leq \|\zeta_n - u^*\|. \end{aligned} \tag{16}$$

Again, by taking the lim sup on both sides, we get

$$\limsup_{n \rightarrow \infty} \|\mathcal{T}u_n - u^*\| \leq c, \tag{17}$$

$$\limsup_{n \rightarrow \infty} \|\mathcal{T}w_n - u^*\| \leq c, \tag{18}$$

and

$$\limsup_{n \rightarrow \infty} \|\mathcal{T}\zeta_n - u^*\| \leq c. \tag{19}$$

In addition,

$$\begin{aligned} c &= \lim_{n \rightarrow \infty} \|u_{n+1} - u^*\| \\ &= \lim_{n \rightarrow \infty} \|(1 - \alpha_n)(\mathcal{T}u_n - u^*) - \alpha_n(\mathcal{T}\zeta_n - u^*)\|. \end{aligned} \tag{20}$$

Using (17)–(19) and Lemma 4, we have

$$\lim_{n \rightarrow \infty} \|\mathcal{T}u_n - \mathcal{T}\zeta_n\| = 0. \tag{21}$$

In addition,

$$\begin{aligned} \|u_{n+1} - u^*\| &= \|(1 - \alpha_n)(\mathcal{T}u_n - u^*) + \alpha_n(\mathcal{T}\zeta_n - u^*)\| \\ &\leq (1 - \alpha_n)\|\mathcal{T}u_n - u^*\| + \alpha_n\|\mathcal{T}\zeta_n - u^*\| \\ &\leq (1 - \alpha_n)\|\mathcal{T}u_n - u^*\| + \alpha_n\|\mathcal{T}u_n - \mathcal{T}\zeta_n\| \\ &\quad + \alpha_n\|\mathcal{T}u_n - u^*\| \\ &= \|\mathcal{T}u_n - u^*\| + \alpha_n\|\mathcal{T}\zeta_n - \mathcal{T}u_n\|, \end{aligned} \tag{22}$$

and taking the lim inf on both sides in this inequality, we have

$$c \leq \liminf_{n \rightarrow \infty} \|\mathcal{T}u_n - u^*\|. \tag{23}$$

Using (17) and (23), we have

$$\lim_{n \rightarrow \infty} \|\mathcal{T}u_n - u^*\| = c. \tag{24}$$

Since,

$$\begin{aligned} \|\mathcal{T}u_n - u^*\| &\leq \|\mathcal{T}u_n - \mathcal{T}\zeta_n\| + \|\mathcal{T}\zeta_n - u^*\| \\ &\leq \|\mathcal{T}u_n - \mathcal{T}\zeta_n\| + \|\zeta_n - u^*\|. \end{aligned} \tag{25}$$

Using (21) and (24) and take the lim inf of (25), and we get

$$c \leq \lim_{n \rightarrow \infty} \inf \|\zeta_n - u^*\|. \tag{26}$$

From (15) and (26), we get

$$\lim_{n \rightarrow \infty} \|\zeta_n - u^*\| = c. \tag{27}$$

In addition,

$$\begin{aligned} c &= \lim_{n \rightarrow \infty} \|\zeta_n - u^*\| \\ &= \lim_{n \rightarrow \infty} \|(1 - \beta_n)(w_n - u^*) + \beta_n(\mathcal{T}w_n - u^*)\|. \end{aligned} \tag{28}$$

By (14), (18), and (28) and Lemma 4, we have

$$\lim_{n \rightarrow \infty} \|\mathcal{T}w_n - w_n\| = 0. \tag{29}$$

In addition,

$$\begin{aligned} \|\zeta_n - u^*\| &= \|(1 - \beta_n)w_n + \beta_n\mathcal{T}w_n - u^*\| \\ &\leq (1 - \beta_n)\|w_n - u^*\| + \beta_n\|\mathcal{T}w_n - u^*\| \\ &\leq (1 - \beta_n)\|w_n - u^*\| + \beta_n\|\mathcal{T}w_n - w_n\| \\ &\quad + \beta_n\|w_n - u^*\| \\ &= \|w_n - u^*\| + \beta_n\|\mathcal{T}w_n - w_n\|. \end{aligned} \tag{30}$$

Using (27) and (29) and take the lim inf of (30), and we get

$$c \leq \liminf_{n \rightarrow \infty} \|w_n - u^*\|. \tag{31}$$

From (14) and (31), we get

$$\lim_{n \rightarrow \infty} \|w_n - u^*\| = c. \tag{32}$$

By using (32), we have

$$\begin{aligned} c &= \lim_{n \rightarrow \infty} \|w_n - u^*\| \\ &= \lim_{n \rightarrow \infty} \|(1 - \gamma_n)(u_n - u^*) + \gamma_n(\mathcal{T}u_n - u^*)\|. \end{aligned} \tag{33}$$

It follows from (13), (17), and (33) and Lemma 4 that

$$\lim_{n \rightarrow \infty} \|\mathcal{T}u_n - u_n\| = 0. \tag{34}$$

Additionally, the solution set, denoted by Ω , is the same as the fixed point set, denoted by \mathcal{F} , i.e., $\Omega = F(\mathcal{F}) = \mathcal{C} \cap \mathcal{A}^{-1}Q \neq \emptyset$ (see [11, 12]) for more details. \square

Theorem 1. Let $\{u_n\}$ be generated (5) and $\mathcal{T} = \mathcal{P}_{\mathcal{C}}[\mathcal{F} - \gamma\mathcal{A}^*(\mathcal{F} - \mathcal{P}_{\mathcal{Q}})\mathcal{A}]$. Then, $\{u_n\}$ converges weakly to a point in Ω .

Proof. Since $\Omega = F(\mathcal{F}) \neq \emptyset$. Then, we only need to show that the sequence $\{u_n\}$ converges weakly to a point in $F(\mathcal{F})$. Taking $u^* \in F(\mathcal{F})$, using Lemma 5, $\lim_{n \rightarrow \infty} \|u_n - u^*\|$ exists. We show that the subsequences of $\{u_n\}$ only have a weak limit in $F(\mathcal{F})$. Suppose that subsequences $\{u_{n_i}\}$ and $\{u_{n_j}\}$ of $\{u_n\}$ converge weakly to ξ and ζ , respectively. From Lemma 6, we have

$$\lim_{n \rightarrow \infty} \|u_{n_i} - \mathcal{T}u_{n_i}\| = 0 = \lim_{n \rightarrow \infty} \|u_{n_j} - \mathcal{T}u_{n_j}\|. \quad (35)$$

It follows from Lemma 3 that $\xi, \varsigma \in F(\mathcal{T})$. Next, we show that the weak limit is unique. Since $\mathcal{T} = \mathcal{P}_{\mathcal{E}}[\mathcal{J} - \gamma\mathcal{A}^*(\mathcal{J} - \mathcal{P}_{\mathcal{Q}})\mathcal{A}]$ is nonexpansive mapping. Using Lemma 5, we have $\lim_{n \rightarrow \infty} \|u_n - u^*\|$ exists. Suppose that $\xi \neq \varsigma$. Using Lemma 2, we have

$$\begin{aligned} \lim_{n \rightarrow \infty} \|u_n - \xi\| &= \lim_{n_i \rightarrow \infty} \|u_{n_i} - \xi\| < \lim_{n_i \rightarrow \infty} \|u_{n_i} - \varsigma\| \\ &= \lim_{n \rightarrow \infty} \|u_n - \varsigma\| = \lim_{n_j \rightarrow \infty} \|u_{n_j} - \varsigma\| \\ &< \lim_{n_j \rightarrow \infty} \|u_{n_j} - \xi\| = \lim_{n \rightarrow \infty} \|u_n - \xi\|. \end{aligned} \quad (36)$$

This is clearly contradictory, hence, $\xi = \varsigma$. Therefore, $\{u_n\}$ converges weakly to a point in $F(\mathcal{T})$. Thus the sequence $\{u_n\}$, converges weakly to a point in Ω .

Mapping \mathcal{T} in \mathcal{H} is called averaged if there exist $\alpha \in (0, 1)$ and a nonexpansive operator S such that $\mathcal{T} = (1 - \alpha)\mathcal{J} + \alpha S$. Set

$$q(u) := \frac{1}{2} \|((\mathcal{J} - \mathcal{P}_{\mathcal{Q}})\mathcal{T})u\|, u \in \mathcal{E}. \quad (37)$$

We consider

$$\text{find } \min_{u \in \mathcal{E}} q(u). \quad (38)$$

By [32], the gradient of q is $\nabla q = \mathcal{T}^*(\mathcal{J} - \mathcal{P}_{\mathcal{Q}})\mathcal{T}$, where \mathcal{T}^* is the adjoint of \mathcal{T} . Since $\mathcal{J} - \mathcal{P}_{\mathcal{Q}}$ is nonexpansive, it follows that ∇q is L -Lipschitzian with $L = \|\mathcal{T}\|^2$. Therefore, ∇q is $1/L$ -ism and for any $0 < \mu < 2/L$, $\mathcal{J} - \mu\nabla q$ is averaged. Therefore, the composition $\mathcal{P}_{\mathcal{E}}(\mathcal{J} - \mu\nabla q)$ is also averaged. Set $\mathcal{T} := \mathcal{P}_{\mathcal{E}}(\mathcal{J} - \mu\nabla q)$. Note that the solution set of SFP is $F(\mathcal{T})$. The following new three-step can be used to find solutions of SFP: \square

Theorem 2. Assume that SFP is consistent. Suppose $\{\alpha_n\}$, $\{\beta_n\}$ and $\{\gamma_n\}$ are sequences in $[\delta, 1 - \delta]$ for all $n \in \mathbb{N}$ and for some δ in $(0, 1)$. Let $\{u_n\}$ be a sequence in \mathcal{E} generated by

$$\begin{aligned} w_n &= (1 - \gamma_n)u_n + \gamma_n\mathcal{P}_{\mathcal{E}}(\mathcal{J} - \mu\nabla q)u_n, \\ \varsigma_n &= (1 - \beta_n)w_n + \beta_n\mathcal{P}_{\mathcal{E}}(\mathcal{J} - \mu\nabla q)w_n, \\ u_{n+1} &= (1 - \alpha_n)\mathcal{P}_{\mathcal{E}}(I - \mu\nabla q)u_n + \alpha_n\mathcal{P}_{\mathcal{E}}(\mathcal{J} - \mu\nabla q)\varsigma_n, n \in \mathbb{N}, \end{aligned} \quad (39)$$

where $0 < \mu < 2/\|\mathcal{T}\|^2$. Then, $\{u_n\}$ converges weakly to a solution of SFP.

Proof. Since $\mathcal{T} := \mathcal{P}_{\mathcal{E}}(\mathcal{J} - \mu\nabla q)$ is nonexpansive, from Theorem 1.

Next, we prove the strong convergence results. \square

Theorem 3. Let $\{u_n\}$ be generated by (5) and $\mathcal{T} = \mathcal{P}_{\mathcal{E}}[\mathcal{J} - \gamma\mathcal{A}^*(\mathcal{J} - \mathcal{P}_{\mathcal{Q}})\mathcal{A}]$. Then, $\{u_n\}$ converges strongly to a point in Ω if and only if $\liminf_{n \rightarrow \infty} d(u_n, \Omega) = 0$.

Proof. If the sequence $\{u_n\}$ has a strong convergence to a point in Ω , then it follows that $\liminf_{n \rightarrow \infty} d(u_n, \Omega) = 0$. To get to the converse, suppose that $\liminf_{n \rightarrow \infty} d(u_n, \Omega) = 0$. Since $F(\mathcal{T}) = \Omega \neq \emptyset$. It follows that $\liminf_{n \rightarrow \infty} d(u_n, F(\mathcal{T})) = 0$. Let $u^* \in F(\mathcal{T})$. Using Lemma 5, we have $\lim_{n \rightarrow \infty} \|u_n - u^*\|$ exists. Thus, $\lim_{n \rightarrow \infty} d(u_n, F(\mathcal{T}))$ exists and $\lim_{n \rightarrow \infty} d(u_n, F(\mathcal{T})) = 0$.

Next, we show that $\{u_n\}$ is a Cauchy sequence in \mathcal{E} . Since $\lim_{n \rightarrow \infty} d(u_n, F(\mathcal{T})) = 0$, given $\varepsilon > 0$, there exists a natural number n_0 such that for all $n \geq n_0$, $d(u_n, F(\mathcal{T})) < \varepsilon/2$. Meanwhile,

$$\inf \left\{ \|u_{n_0} - u^*\| : u^* \in F(\mathcal{T}) \right\} < \frac{\varepsilon}{2}. \quad (40)$$

So, we can find $v^* \in F(\mathcal{T})$ such that $\|u_{n_0} - v^*\| < \varepsilon/2$. For $n \geq n_0$ and $m \geq 1$, we have

$$\begin{aligned} \|u_{n+m} - u_n\| &\leq \|u_{n+m} - v^*\| + \|u_n - v^*\| \\ &\leq \|u_{n_0} - v^*\| + \|u_{n_0} - v^*\| \\ &< \frac{\varepsilon}{2} + \frac{\varepsilon}{2} = \varepsilon. \end{aligned} \quad (41)$$

This shows that $\{u_n\}$ is a Cauchy sequence in \mathcal{E} . From \mathcal{E} is a closed subset in \mathcal{H} . Then, there exists $\xi \in \mathcal{E}$ such that $\lim_{n \rightarrow \infty} u_n = \xi$. Now $\lim_{n \rightarrow \infty} d(u_n, F(\mathcal{T})) = 0$ gives that $d(\xi, F(\mathcal{T})) = 0$. Note that $F(\mathcal{T})$ is closed. Therefore, $\xi \in F(\mathcal{T})$. Again, using $F(\mathcal{T}) = \Omega$, we have $\xi \in \Omega$. Thus, $\{u_n\}$ converges to a point in Ω . This completes the proof.

A mapping \mathcal{T} satisfy Condition A (see [33]) if there exists a nondecreasing function $f: [0, +\infty) \rightarrow [0, +\infty)$ with $f(0) = 0$ and $f(r) > 0$ for all $r \in (0, +\infty)$ such that

$$\|u - \mathcal{T}u\| \geq f(d(u, F(\mathcal{T}))), \quad (42)$$

for all $u \in \mathcal{E}$.

Next, we can prove strong convergence of (5) under Condition A, which is weaker than the compactness of the mappings' domain. \square

Theorem 4. If \mathcal{T} satisfies Condition A, then the sequence $\{u_n\}$ defined by (5) converges strongly to a point in Ω .

Proof. Using Lemma 6, we also get

$$\lim_{n \rightarrow \infty} \|u_n - \mathcal{T}u_n\| = 0. \quad (43)$$

Since \mathcal{T} is a given, it follows that

$$\lim_{n \rightarrow \infty} f(d(u_n, F(\mathcal{T}))) \leq \lim_{n \rightarrow \infty} \|u_n - \mathcal{T}u_n\| = 0. \quad (44)$$

Now $f: [0, +\infty) \rightarrow [0, +\infty)$ with $f(0) = 0$ and $f(r) > 0$ for all $r \in (0, +\infty)$, gives that

$$\lim_{n \rightarrow \infty} d(u_n, F(\mathcal{T})) = 0, \quad (45)$$

and it follows that

$$\lim_{n \rightarrow \infty} d(u_n, \Omega) = 0. \quad (46)$$

From Theorem 3, we have $\{u_n\}$ converges strongly to a point in Ω . This completes the proof. \square

4. Numerical Examples

In this part, we study and compare numerical results of the proposed algorithm (5) with the Dang algorithm (4) to declare that the proposed algorithm is more effective.

Example 1. Suppose that $\mathcal{H}_1 = \mathcal{H}_2 = \mathbb{R}^3$, $\mathcal{C} = \{u \in \mathbb{R}^3: \|u\| \leq 1\}$, $\mathcal{Q} = \{u \in \mathbb{R}^3: \|u\| \leq 2\}$, and $\mathcal{T}u = Mu$.

$$M = \begin{bmatrix} -3 & 1 & 2 \\ -1 & 0 & 1 \\ 1 & 2 & -1 \end{bmatrix}, \quad (47)$$

and take an initial point $u_0 = \{0.6, 0.5, 1.1\}$.

Example 2. Suppose that $\mathcal{H}_1 = \mathcal{H}_2 = \mathbb{R}^3$, $\mathcal{C} = \{u \in \mathbb{R}^3: \|u\| \leq 1\}$, $\mathcal{Q} = \{u \in \mathbb{R}^3: \|u\| \leq 2\}$, and $\mathcal{T}u = Mu$.

$$M = \begin{bmatrix} 2 & -1 & 0 \\ -1 & 2 & -1 \\ 0 & -1 & 2 \end{bmatrix}, \quad (48)$$

and take an initial point $u_0 = \{1.2, 0.6, 0.4\}$.

The projections $\mathcal{P}_{\mathcal{C}}$ and $\mathcal{P}_{\mathcal{Q}}$ of u onto sets \mathcal{C} and \mathcal{Q} are as follows:

$$\mathcal{P}_{\mathcal{C}}(u) = \begin{cases} u, & \|u\| \leq 1, \\ \frac{u}{\|u\|}, & \|u\| \geq 1, \end{cases} \quad (49)$$

$$\mathcal{P}_{\mathcal{Q}}(u) = \begin{cases} u, & \|u\| \leq 2, \\ \frac{u}{\|u\|}, & \|u\| \geq 2. \end{cases}$$

Meanwhile, choose

$$\begin{aligned} \alpha_n &= \beta_n \\ &= \gamma_n \\ &= \frac{n}{n+1} \\ &= 0.99 \quad \text{and} \end{aligned} \quad (50)$$

$$\lambda_n = \frac{1}{\|\mathcal{A}\|_2^2},$$

for Dang and proposed methods. We take $\|u_{n+1} - u_n\| < 10^{-15}$ as the standard of stopping in the process of calculation. All codes were written in MATLAB 2019b. By computing, we obtain the iteration steps and CPU time of these three comparing algorithms in converging to the solution of Examples 1 and 2 as shown in Table 1.

Tables 2 and 3 show the convergence of comparing sequences of Examples 1 and 2 generated by Dang and proposed methods. It can be found from the computing results of Tables 1–3 that, under the same conditions, the results of the proposed method are highly effective compared with Dang method.

5. Applications

This section is devoted to some applications by using the proposed algorithm (5).

5.1. Image Restoration Problems. Assume that B is a matrix with \tilde{m} rows and \tilde{n} columns that represents the degraded representation of the true image X . The restoration model can be obtained by stacking the columns of B and X into two long vectors, \mathbf{b} and \mathbf{u} , both of which have lengths of $n = \tilde{m}\tilde{n}$. The following linear equation system may be used to describe the restoration model as a one-dimensional vector:

$$\mathbf{b} = M\mathbf{u}, \quad (51)$$

where the true image is represented by $\mathbf{u} \in \mathbb{R}^n$, the observed image is represented by $\mathbf{b} \in \mathbb{R}^n$, and the blurring matrix is represented by $M \in \mathbb{R}^{n \times n}$.

Issue (52) is a least squares (LS) problem that needs to be resolved in order to resemble the true image on the restoration model (51).

$$\min_{\mathbf{u}} \frac{1}{2} \|\mathbf{b} - M\mathbf{u}\|_2^2. \quad (52)$$

We will use our key findings for resolving the restoration model (51) by setting the following by using $q(\mathbf{u})$ as above equation. And the following methods are used to resolve the image restoration problem.:

$$\begin{aligned} \mathbf{z}_n &= (1 - \gamma_n)\mathbf{u}_n + \gamma_n(\mathbf{u}_n - \mu M^T(M\mathbf{u}_n - \mathbf{b})), \\ \mathbf{y}_n &= (1 - \beta_n)\mathbf{z}_n + \beta_n(\mathbf{z}_n - \mu M^T(M\mathbf{z}_n - \mathbf{b})), \\ \mathbf{u}_{n+1} &= (1 - \alpha_n)(\mathbf{u}_n - \mu M^T(M\mathbf{u}_n - \mathbf{b})) \\ &\quad + \alpha_n(\mathbf{y}_n - \mu M^T(M\mathbf{y}_n - \mathbf{b})). \end{aligned} \quad (53)$$

The problem (51) is solved using (53), using the parameter (50) and $\mu = 1/\|M^T M\|_2$.

To illustrate the viability of the suggested algorithm, the true RGB (color image) is presented in Figure 1. Peak signal-to-noise ratio (PSNR) is a quantitative metric that is used to assess how well the contrasting algorithms at \mathbf{u}_n work during the image deblurring process. Moreover, we employ the following formula:

$$\frac{\|\mathbf{u}_n - \mathbf{u}\|_{\infty}}{\|\mathbf{u}\|_{\infty}}, \quad (54)$$

to measure the figure error, which is called the relative figure norm.

We then show how to restore photos that have been damaged by the matrices M_G (Gaussian blur of filter size 9×9 with standard deviation $\sigma = 4$), M_O (out focus

TABLE 1: Iteration steps and CPU time of the Dang method (4) and proposed method (5) for the numerical experiment of Examples 1 and 2.

Algorithm	Iterations number		CPU time (sec)	
	Example 1	Example 2	Example 1	Example 2
Dang (4)	111	112	$7.973e-04$	$9.648e-04$
Proposed (5)	2	2	$3.985e-04$	$4.091e-04$

TABLE 2: Comparative sequences of the Dang method (4) and proposed method (5) for the numerical experiment of Example 1 with three decimal places.

Iteration number	Example 1	
	Dang (4)	Proposed (5)
1	(0.600, 0.500, 1.100)	(0.600, 0.500, 1.100)
2	(0.561, 0.467, 1.028)	(0.444, 0.370, 0.815)
3	(0.534, 0.445, 0.979)	
4	(0.514, 0.428, 0.943)	
5	(0.499, 0.416, 0.915)	
⋮	⋮	
29	(0.444, 0.370, 0.815)	
⋮	⋮	
111	(0.444, 0.370, 0.815)	

TABLE 3: Comparative sequences of the Dang method (4) and proposed method (5) for the numerical experiment of Example 2 with three decimal places.

Iteration number	Example 2	
	Dang (4)	Proposed (5)
1	(1.200, 0.600, 0.400)	(1.200, 0.600, 0.400)
2	(1.117, 0.557, 0.979)	(0.857, 0.428, 0.285)
3	(1.054, 0.527, 0.943)	
4	(1.010, 0.505, 0.915)	
5	(0.977, 0.488, 0.815)	
⋮	⋮	
28	(0.857, 0.428, 0.285)	
⋮	⋮	
112	(0.857, 0.428, 0.285)	

blur with radius $r = 6$), and M_M (motion blur specifying with 21 pixels of motion length) (see Figure 2). The reconstructed RGB image shown in Figures 3–5 employs three blurring matrices M_G, M_O , and M_M for 50^{th} , $1,000^{th}$, and $20,000^{th}$ iterations to address the restoration problem. These figures show that the quality of restored images utilizing (53) for solving (51) improve for the three types of degraded images.

Additionally, employing the suggested algorithms with $100,000^{th}$ iterations, the behavior of the relative figure error and the PSNR quality of the deteriorated RGB image are exhibited.

It is interesting to note that the relative errors plot of the suggested technique decreases with the number of iterations. As the number of iterations increases, their graphs also grow, according to the PSNR plots in Figure 6. It can be said that the suggested approach improves the quality of the three distinct types of real RGB images.



FIGURE 1: True images ($243 \times 349 \times 3$).

5.2. *Signal Recovering Problems.* Compressed sensing can be defined in signal processing given by

$$\mathbf{y} = \mathbf{A}\mathbf{u} + \nu, \quad (55)$$

where $\mathbf{u} \in \mathbb{R}^n$ is the original signal, ν is the noise, $\mathbf{y} \in \mathbb{R}^m$ is the observed signal with noisy, and $A \in \mathbb{R}^{m \times n}$ is a degraded matrix. Solving the LASSO problem, (56) can be thought of as finding solutions to previously determined linear equation systems.

$$\min_{\mathbf{u} \in \mathbb{R}^n} \frac{1}{2} \|\mathbf{y} - \mathbf{A}\mathbf{u}\|_2^2 \quad \text{subject to } \|\mathbf{u}\|_1 \leq t, \quad (56)$$

where $t > 0$ is a given constant. We can use our strategy to solve the issue (56) by putting $\mathcal{T} = \mathcal{P}_{\mathcal{C}}(\mathcal{I} - \mu \nabla q)$, where $q(\mathbf{u}) = \frac{1}{2} \|\mathbf{y} - \mathbf{A}\mathbf{u}\|_2^2$ and $\nabla q(\mathbf{u}) = A^T (\mathbf{A}\mathbf{u} - \mathbf{y})$. We demonstrate how to use our approach in signal recovery issues (55). Let $\{\mathbf{u}_n\}$ generated by $C = \{\mathbf{u} \in \mathbb{R}^n: \|\mathbf{u}\|_1 \leq t\}$, we acquire techniques for solving

$$\begin{aligned} \mathbf{w}_n &= (1 - \gamma_n)\mathbf{u}_n + \gamma_n \mathcal{T} \mathbf{u}_n, \\ \mathbf{z}_n &= (1 - \beta_n)\mathbf{w}_n + \beta_n \mathcal{T} \mathbf{w}_n, \\ \mathbf{u}_{n+1} &= (1 - \alpha_n)\mathcal{T} \mathbf{u}_n + \alpha_n \mathcal{T} \mathbf{z}_n, \end{aligned} \quad (57)$$

where $\mu \in (0, 2/\|A^T A\|_2)$ and $\alpha_n, \beta_n, \gamma_n \in (0, 1), \forall n \in \mathbb{N}$.

Following that, various experiments are shown to demonstrate the convergence and usefulness of algorithm (50). $\mathbf{y}_i = A_i \mathbf{u} + \nu_i, i = 1, 2, 3$ with $m = 512$ is generated by \mathbf{u} with $n = 1024$ formed by the uniform distribution in the range $[-2, 2]$ with 70 nonzero items. The original signal is shown in Figure 7.

The procedure begins when the begin data \mathbf{u}_0 with $n = 1024$ is chosen at random and t is the number of nonzero elements (see Figure 8).

The observation signal \mathbf{y}_i is shown in Figure 9.

A_i formed by the normal distribution with mean of zero and variance of one and white Gaussian noise $\nu_i, i = 1, 2, 3$ (see Figure 10).

The convergence features of algorithm (57) with the permutation of the blurring matrices A_1, A_2 , and A_3 are illustrated and analyzed. The relative inaccuracy is calculated by using $\|\mathbf{u}_n - \mathbf{u}_2\|/\|\mathbf{u}_2\|$. The signal-to-noise ratio (SNR) is used to quantify the performance of the recovered signal at the n^{th} iteration (SNR). In addition, the comparative



FIGURE 2: True images are blurred by matrices M_G , M_O , and M_M respectively.



FIGURE 3: Rebuilt images degraded by blurred matrices M_G being 50th, 1,000th, and 20,000th used iterations.



FIGURE 4: Rebuilt images degraded by blurred matrices M_O being 50th, 1,000th, and 20,000th used iterations.



FIGURE 5: Rebuilt images degraded by blurred matrices M_M being 50th, 1,000th, and 20,000th used iterations.

algorithms' parameters α_n, β_n , and γ_n are set to the default parameter (50).

Figure 11 depicts the behavior of relative signal error and SNR quality of the proposed approach with the blurring matrices A_1, A_2 , and A_3 .

The relative signal error plot reduces until it converges to some fixed value, which is impressive. The SNR quality plot of the provided approach shows that the SNR value grows until it also converges to a constant number.

Figures 12–14 demonstrate the recovered signal using the proposed techniques with the group of operator and noise A_i and $\nu_i, i = 1, 2, 3$. The improvement of SNR quality for the recovering signals based on 5,000th, 10,000th, and 20,000th number of iterations are also shown on these figures. As illustrated in Figures 12–14, the proposed algorithms (57) to solve the signal recovery problem have been shown to improve the quality of recovered signals for three different types of degraded signals.

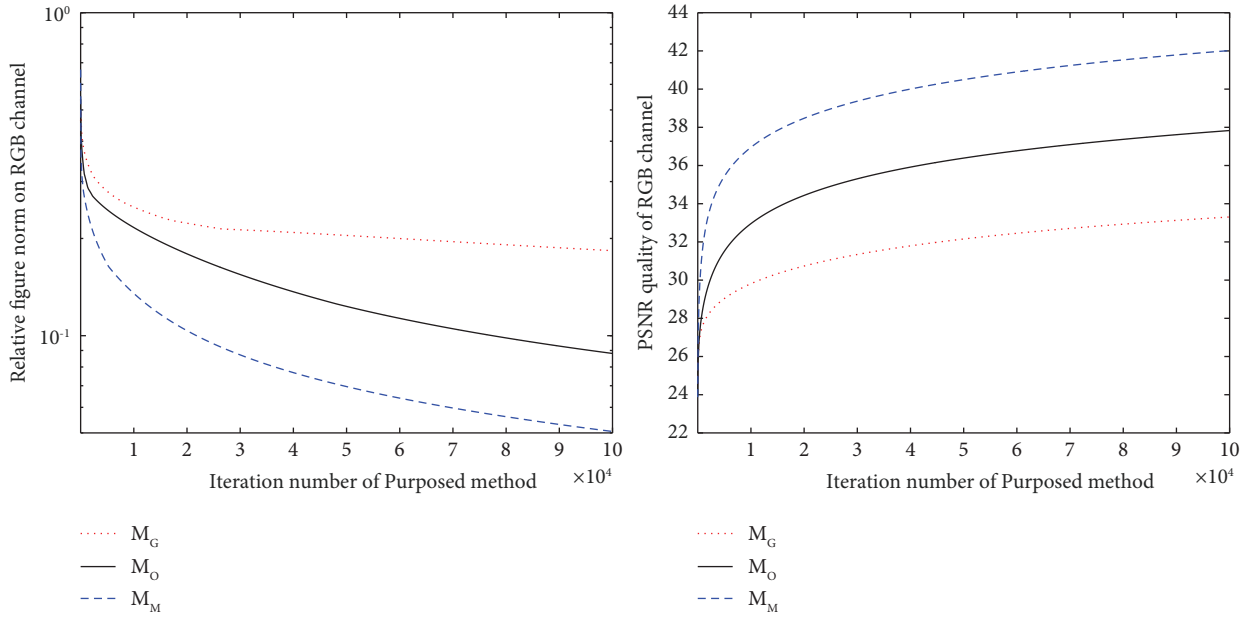


FIGURE 6: The relative figures norm and PSNR plots of the proposed method for all degraded RGB images.

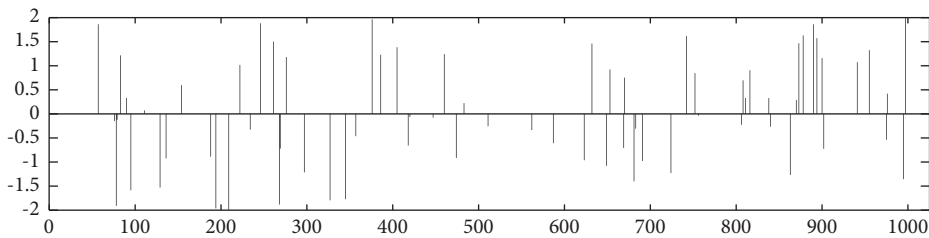


FIGURE 7: The original signal contains 70 nonzero components.

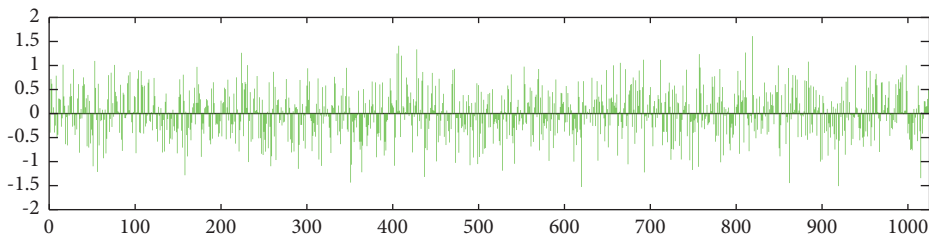


FIGURE 8: Initial signals u_0 .

5.3. *Polynomiography.* In 2005, polynomiography is defined by Kalantari (see, e.g. [34–40]). The formula for Newton’s method of calculating the roots of a complex polynomial P is as follows:

$$z_{n+1} = z_n - \frac{p(z_n)}{p'(z_n)}, n = 0, 1, 2, \dots, \tag{58}$$

where $z_0 \in \mathbb{C}$ is an initial point. Here, we have (59) by using (58). Consider a Hilbert space $\mathcal{H} = \mathbb{C}$, $v_0 = (x_0, y_0)$, and $\{\alpha_n\}, \{\beta_n\}, \{\gamma_n\} \subset (0, 1)$. The following formula generates polynomiographs:

$$\begin{aligned} w_n &= (1 - \gamma_n)v_n + \gamma_n \left(v_n - \frac{p(v_n)}{p'(v_n)} \right), \\ z_n &= (1 - \beta_n)w_n + \beta_n \left(w_n - \frac{p(w_n)}{p'(w_n)} \right), \\ v_{n+1} &= (1 - \alpha_n) \left(v_n - \frac{p(v_n)}{p'(v_n)} \right) + \alpha_n \left(z_n - \frac{p(z_n)}{p'(z_n)} \right), \end{aligned} \tag{59}$$

where $\{\alpha_n\}, \{\beta_n\}, \{\gamma_n\}$ are real sequences in $(0, 1)$.

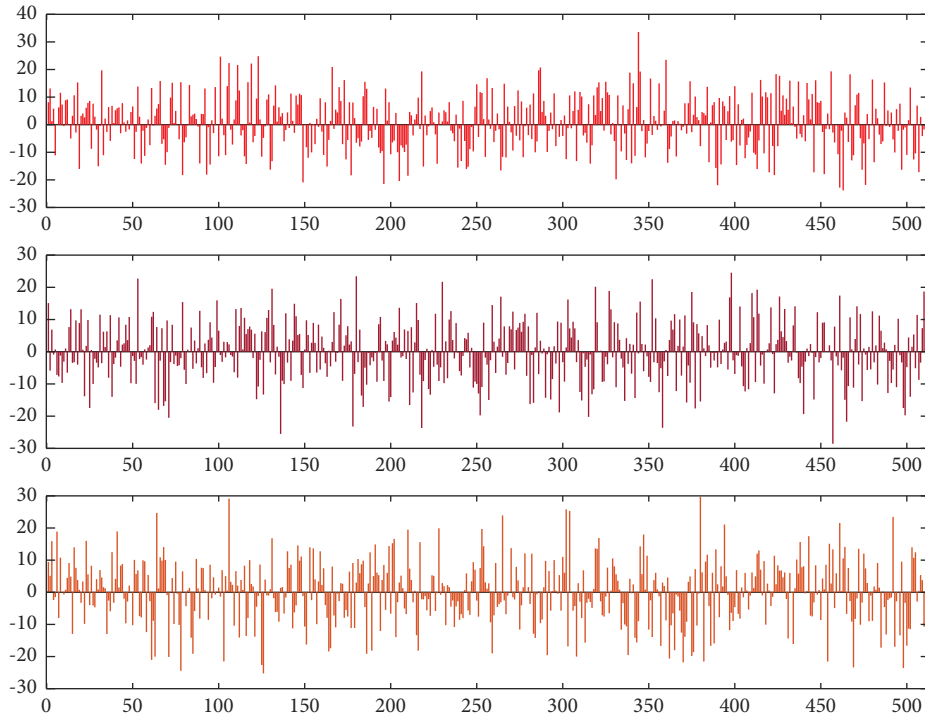


FIGURE 9: Degraded signals y_1 , y_2 , and y_3 .

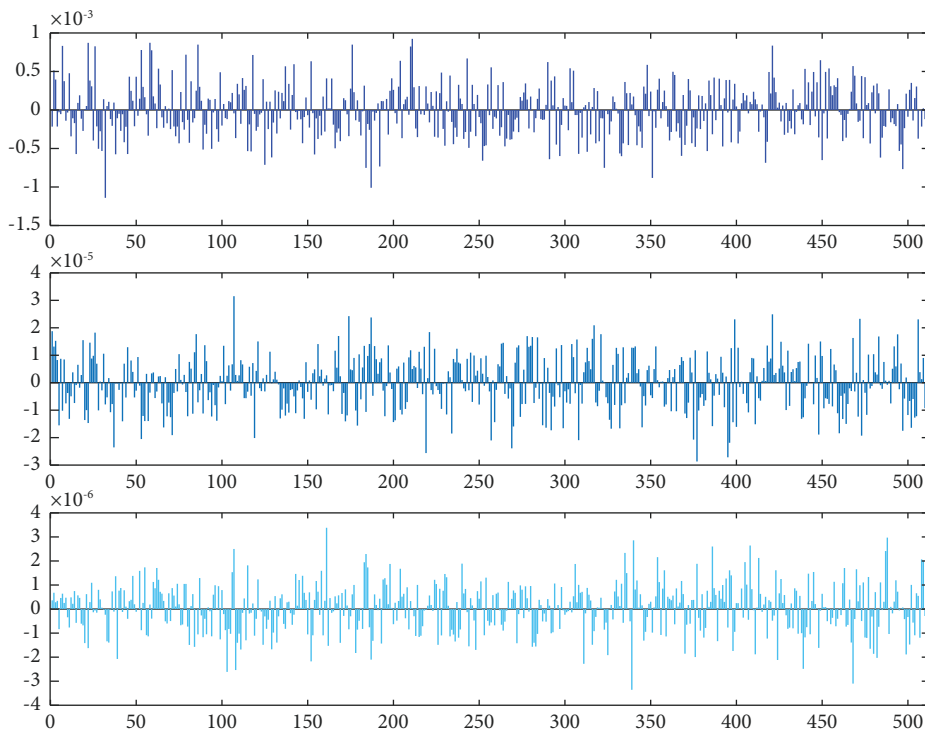


FIGURE 10: Noise signals v_1 , v_2 , and v_3 .

This subsection shows some examples of the polynomiographs obtained by using (59) with real and complex-valued parameters using different color maps.

5.3.1. *Polynomiographs with Real-Valued Parameters of Iterations.* Polynomiographs for complex polynomial equation $p_1(z) = z^3 - 3z^2 + 1$ and $p_2(z) = z^4 + z^2 - 1$ are

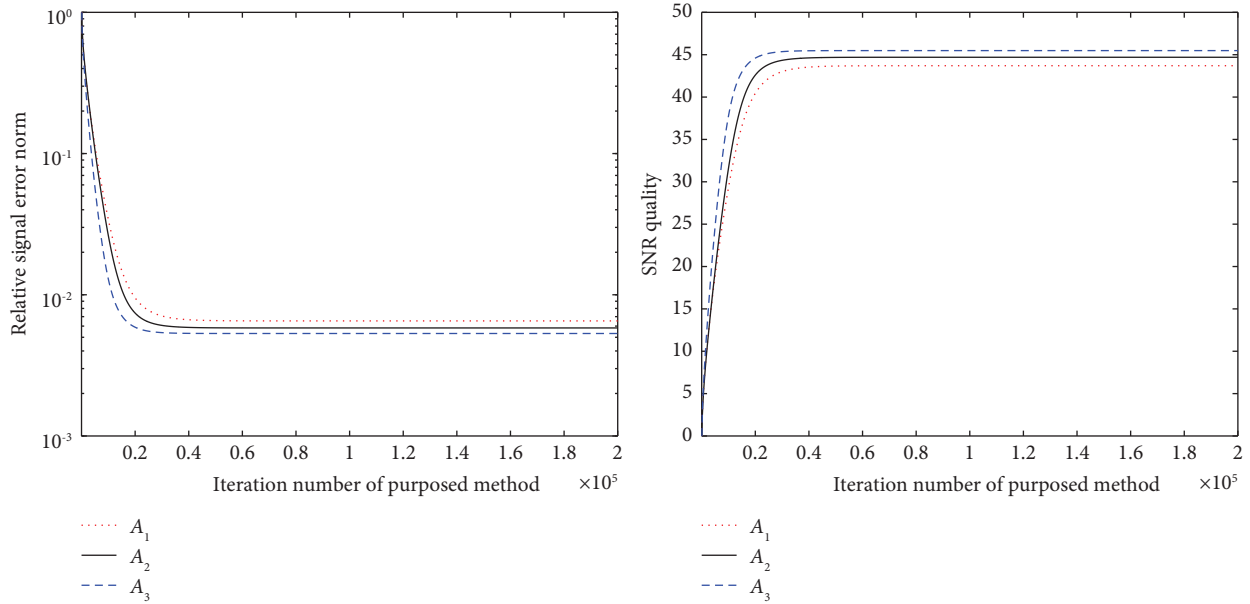


FIGURE 11: The relative signal error and SNR plots of the proposed algorithm with the blurring matrices $A_1, A_2,$ and A_3 in recovering the observed signal with 200,000th iterations.

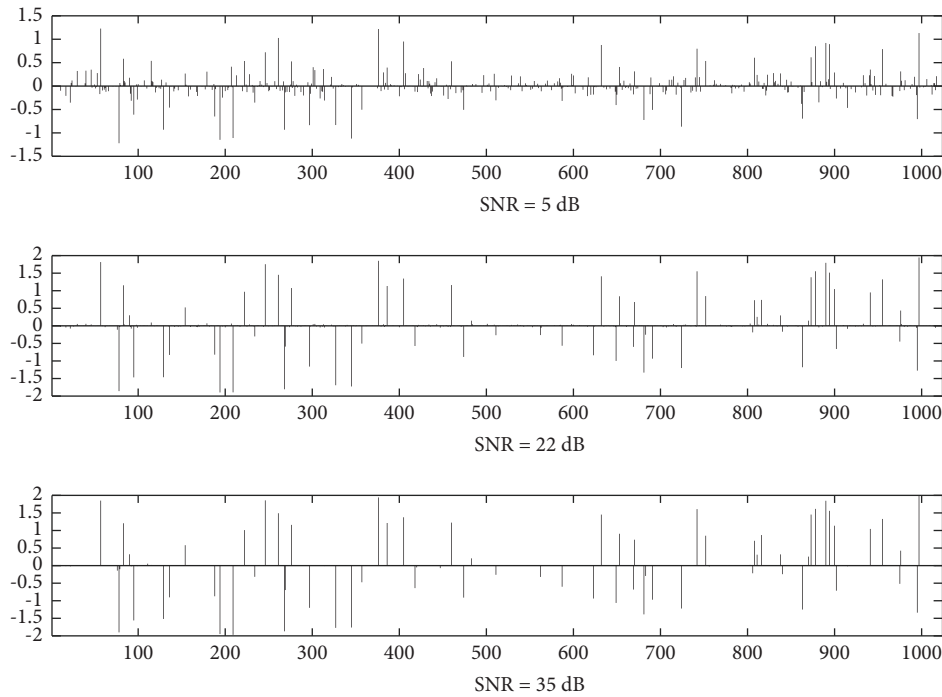


FIGURE 12: Recovering signals based on the SNR quality for the degraded signal with operator A_1 and noise γ_1 .

presented in Figures 15 and 16, respectively. Polynomiographs were generated by resolution 500×500 pixels, number of iterations $n = 15$, accuracy $\epsilon = 0.001$, and $A = [2, 2]^2$. The following parameters were fixed in the iterations: $\alpha_n = 0.35$, $\beta_n = 0.65$, and $\gamma = 0.55$.

5.3.2. Polynomiographs with Complex-Valued Parameters of Iterations. Polynomiographs for complex polynomial

equations, $p_1(z) = z^3 - 3z^2 + 1$ and $p_2(z) = z^4 + z^2 - 1$, are presented in Figures 17 and 18, respectively. Polynomiographs were generated by resolution 500×500 pixels, number of iterations $n = 15$, accuracy $\epsilon = 0.001$, and $A = [2, 2]^2$. The following parameters were fixed in the iterations: $\alpha_n = 0.35 + 0.3i$, $\beta_n = 0.65 + 0.4i$, and $\gamma = 0.55 + 0.75i$.

Figures 15 and 16 show how real parameter components affect symmetry, whereas Figures 17 and 18 show how

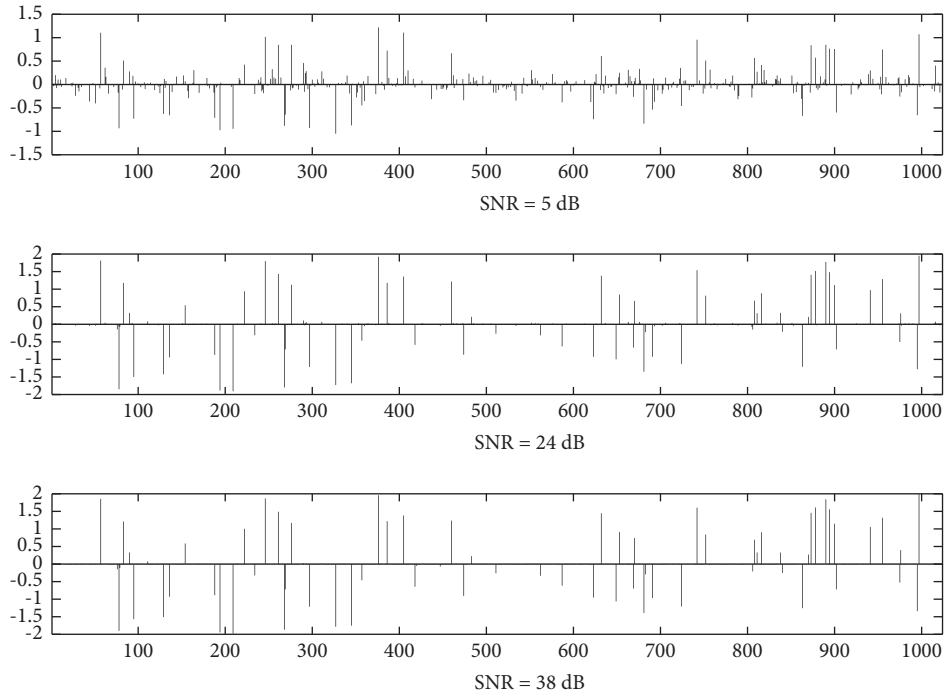


FIGURE 13: Recovering signals based on the SNR quality for the degraded signal with operator A_2 and noise ν_2 .

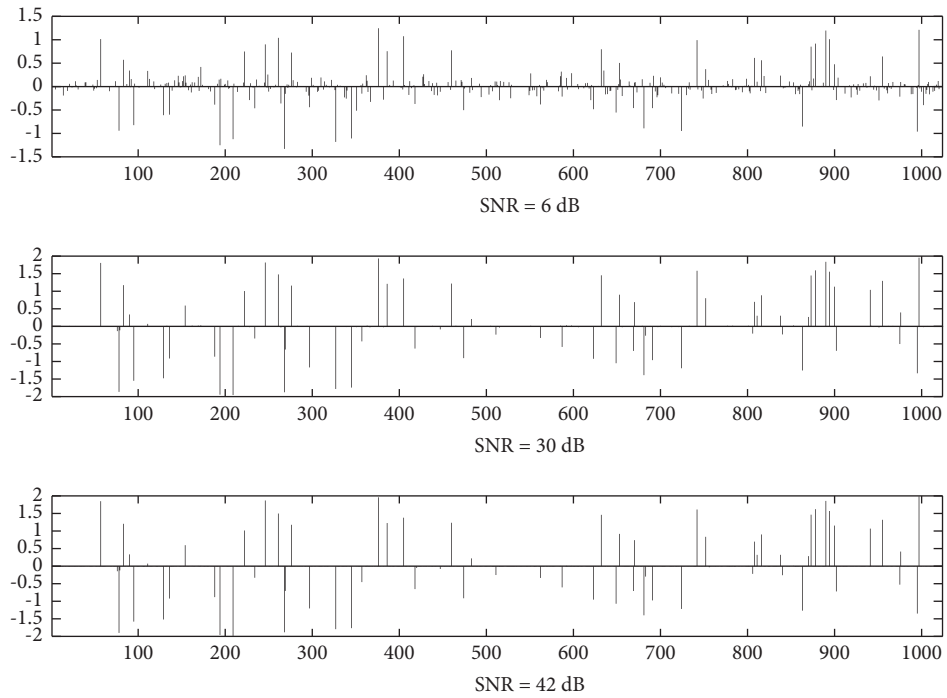


FIGURE 14: Recovering signals based on the SNR quality for the degraded signal with operator A_3 and noise ν_3 .

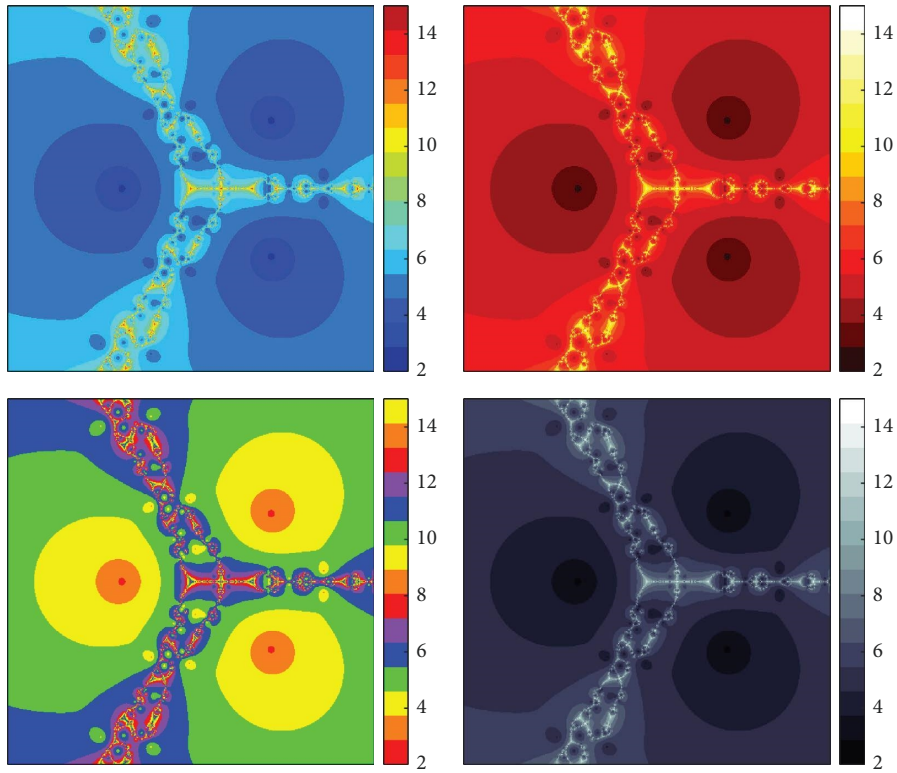


FIGURE 15: Examples of polynomiographs of different color maps for p_1 with real-valued parameters of (59).

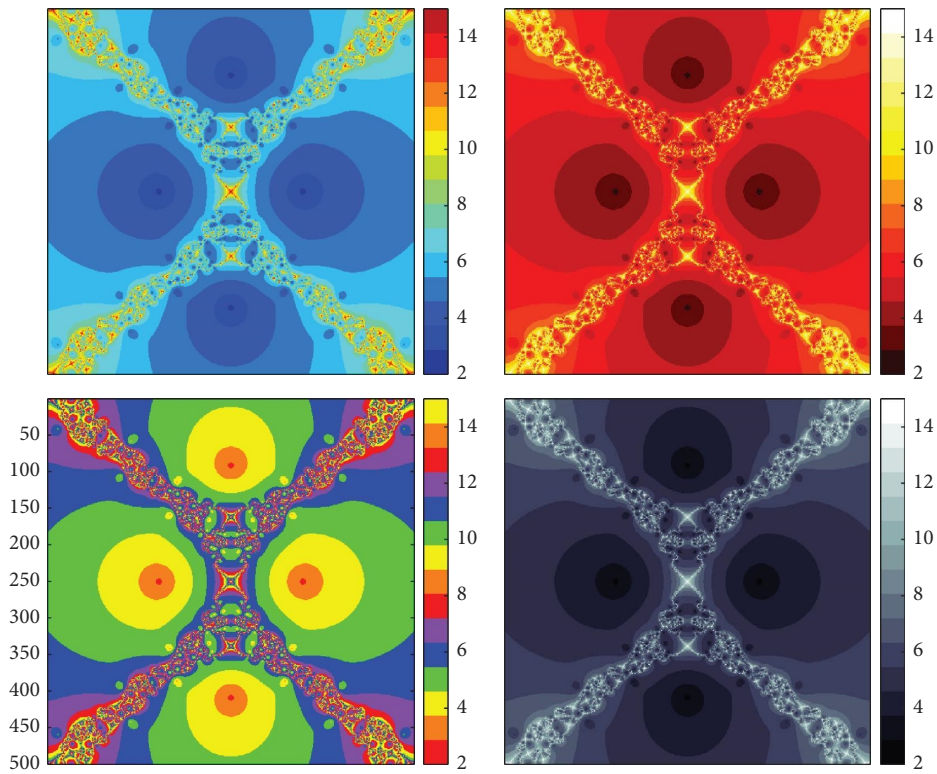


FIGURE 16: Examples of polynomiographs of different color maps for p_2 with real-valued parameters of (59).

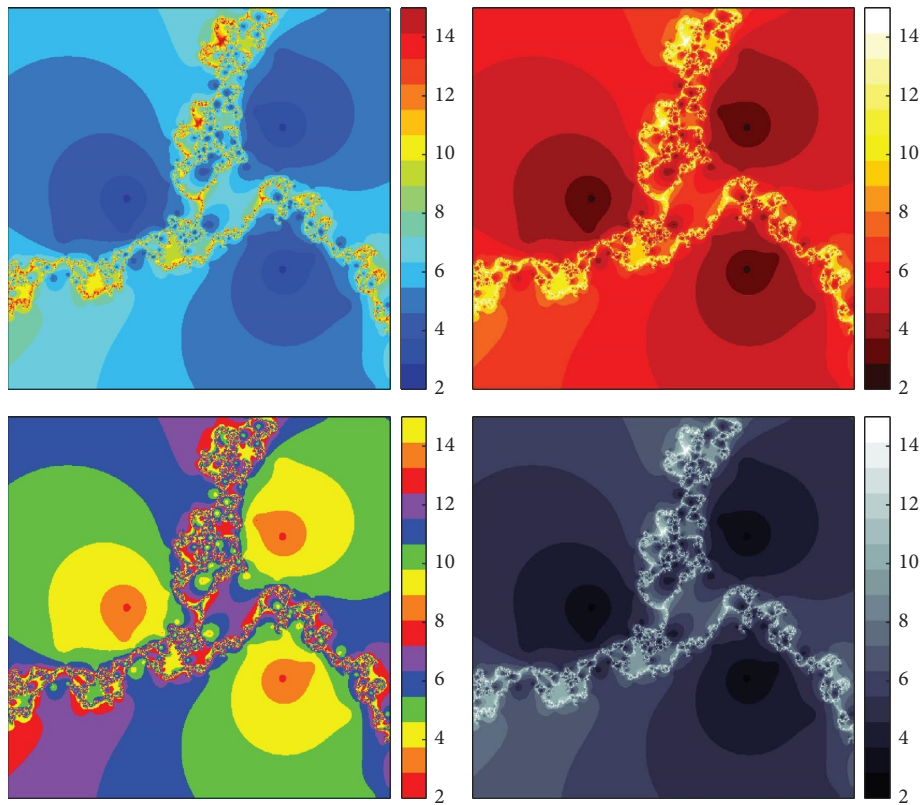


FIGURE 17: Examples of polynomiographs of different color maps for p_1 with complex-valued parameters of (59).

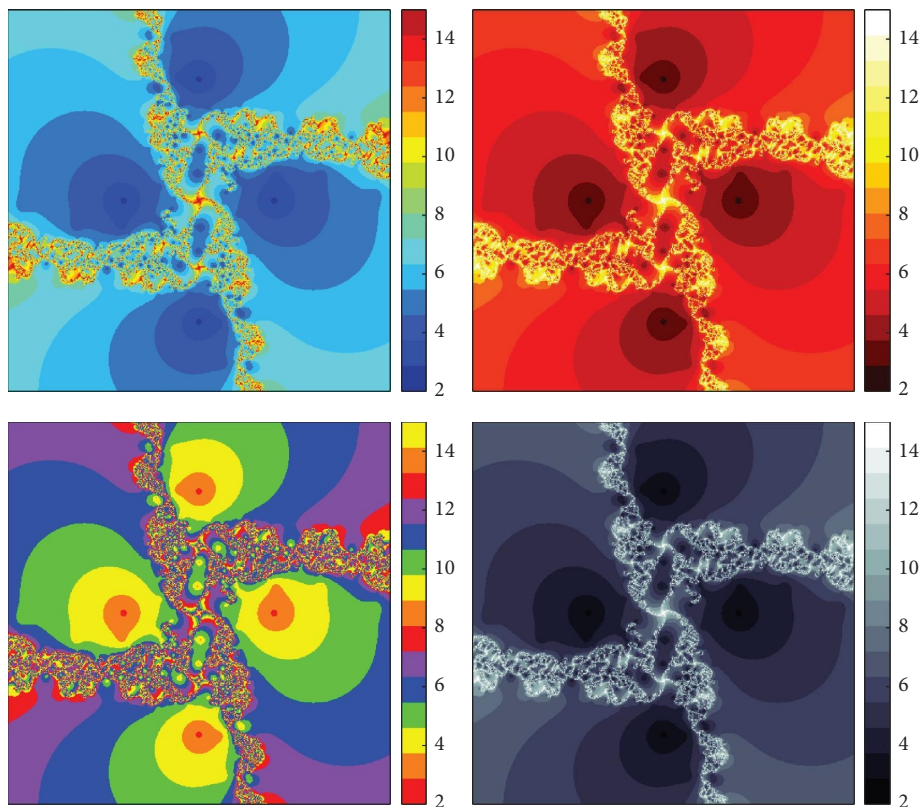


FIGURE 18: Examples of polynomiographs of different color maps for p_2 with complex-valued parameters of (59).

imaginary parameter components produce asymmetric twisting of the polynomiographs and affect the statics or dynamics of the pictures.

Data Availability

No data were used in this manuscript.

Conflicts of Interest

The authors declare that they have no conflicts of interest.

Acknowledgments

The first author acknowledges the financial support provided by the International SciKU Branding (ISB), Faculty of Science, Kasetsart University. C. Chairatsiripong would like to thank the revenue budget for 2021 (PBTSC64001), School of Science, University of Phayao. T. Thianwan would like to thank the Thailand Science Research and Innovation Fund, and University of Phayao (Grant nos. FF65-RIM072 and FF66-UoE015).

References

- [1] Y. Censor and T. Elfving, "A multiprojection algorithm using Bregman projections in a product space," *Numerical Algorithms*, vol. 8, no. 2-4, pp. 221-239, 1994.
- [2] H. He, C. Ling, and H. K. Xu, "An implementable splitting algorithm for the l_1 -norm regularized split feasibility problem," *Journal of Scientific Computing*, vol. 67, pp. 281-298, 2015.
- [3] D. A. Lorenz, F. Sch, S. Wenger, and S. Wenger, "The linearized Bregman method via split feasibility problems: analysis and generalizations," *SIAM Journal on Imaging Sciences*, vol. 7, no. 2, pp. 1237-1262, 2014.
- [4] Y. Censor, T. Elfving, N. Kopf, and T. Bortfeld, "The multiple-sets split feasibility problem and its applications for inverse problems," *Inverse Problems*, vol. 21, no. 6, pp. 2071-2084, 2005.
- [5] Y. Censor, T. Bortfeld, B. Martin, and A. Trofimov, "A unified approach for inversion problems in intensity-modulated radiation therapy," *Physics in Medicine and Biology*, vol. 51, no. 10, pp. 2353-2365, 2006.
- [6] C. Byrne, "A unified treatment of some iterative algorithms in signal processing and image reconstruction," *Inverse Problems*, vol. 20, no. 1, pp. 103-120, 2004.
- [7] C. Byrne, "Iterative oblique projection onto convex sets and the split feasibility problem," *Inverse Problems*, vol. 18, no. 2, pp. 441-453, 2002.
- [8] B. Qu and N. Xiu, "A note on the CQ algorithm for the split feasibility problem," *Inverse Problems*, vol. 21, no. 5, pp. 1655-1665, 2005.
- [9] Q. Yang, "The relaxed CQ algorithm solving the split feasibility problem," *Inverse Problems*, vol. 20, no. 4, pp. 1261-1266, 2004.
- [10] J. Zhao and Q. Yang, "Several solution methods for the split feasibility problem," *Inverse Problems*, vol. 21, no. 5, pp. 1791-1799, 2005.
- [11] H. K. Xu, "Iterative methods for the split feasibility problem in infinite-dimensional Hilbert spaces," *Inverse Problems*, vol. 26, no. 10, Article ID 105018, 2010.
- [12] H. K. Xu, "A variable Krasnosel'skiĭ-Mann algorithm and the multiple-set split feasibility problem," *Inverse Problems*, vol. 22, no. 6, pp. 2021-2034, 2006.
- [13] H. H. Bauschke and J. M. Borwein, "On projection algorithms for solving convex feasibility problems," *SIAM Review*, vol. 38, pp. 367-426, 1996.
- [14] G. Lopez, V. Martín, F. Wang, and H. K. Xu, "Solving the split feasibility problem without prior knowledge of matrix norms," *Inverse Problems*, vol. 28, Article ID 085004, 2012.
- [15] A. Bnouhachem, M. A. Noor, M. Khalfaoui, and S. Zhaoan, "On descent projection method for solving the split feasibility problems," *Journal of Global Optimization*, vol. 54, no. 3, pp. 627-639, 2012.
- [16] H. Zhou and P. Wang, "Adaptively relaxed algorithms for solving the split feasibility problem with a new step size," *Journal of Inequalities and Applications*, vol. 2014, no. 1, 2014.
- [17] H. Cui and F. Wang, "Iterative methods for the split common fixed point problem in Hilbert spaces," *Journal of Fixed Point Theory and Applications*, vol. 2014, no. 1, 2014.
- [18] C. Byrne, Y. Censor, A. Gibali, and S. Reich, "The split common null point problem," *Journal of Nonlinear and Convex Analysis*, vol. 13, pp. 759-775, 2012.
- [19] E. Masad and S. Reich, "A note on the multiple-set split convex feasibility problem in Hilbert space," *Journal of Nonlinear and Convex Analysis*, vol. 8, pp. 367-371, 2007.
- [20] Q. L. Dong, L. Liu, and Y. Yao, "Self-adaptive projection and contraction methods with alternated inertial terms for solving the split feasibility problem," *Journal of Nonlinear and Convex Analysis*, vol. 23, pp. 591-605, 2022.
- [21] K. Saechou and A. Kangtunyakarn, "The method for solving the extension of general of the split feasibility problem and fixed point problem of the cutter," *Journal of Inequalities and Applications*, vol. 2022, no. 1, 2022.
- [22] F. G. Gao, X. X. Liu, and X. C. Li, "Strong Convergence on the Split Feasibility Problem by Mixing w-Mapping," *Journal of Mathematics*, vol. 2021, Article ID 9924937, 6 pages, 2021.
- [23] M. A. Noor, "New approximation schemes for general variational inequalities," *Journal of Mathematical Analysis and Applications*, vol. 251, no. 1, pp. 217-229, 2000.
- [24] R. Glowinski and P. L. Tallec, *Augmented Lagrangian and Operator-Splitting Methods in Nonlinear Mechanics*, SIAM, PA, USA, 1989.
- [25] S. Haubruge, V. H. Nguyen, and J. J. Strodiot, "Convergence analysis and applications of the Glowinski Le Tallec splitting method for finding a zero of the sum of two maximal monotone operators," *Journal of Optimization Theory and Applications*, vol. 97, no. 3, pp. 645-673, 1998.
- [26] D. Yambangwai and T. Thianwan, "Convergence point of G-nonexpansive mappings in Banach spaces endowed with graphs applicable in image deblurring and signal recovering problems," *Ricerche di Matematica*, vol. 2021, pp. 1-28, 2021.
- [27] Y. Z. Dang and Y. Gao, "The strong convergence of a three-step algorithm for the split feasibility problem," *Optimization Letters*, vol. 7, no. 6, pp. 1325-1339, 2013.
- [28] B. S. Thakur, D. Thakur, and M. Postolache, "A new iteration scheme for approximating fixed Points of nonexpensive mapping," *Faculty of Sciences and Math*, vol. 10, pp. 2711-2720, 2016.
- [29] M. Feng, L. Shi, and R. Chen, "A new three-step iterative algorithm for solving the split feasibility problem," *UPB Scientific Bulletin, Series A*, vol. 81, no. 1, pp. 93-102, 2019.
- [30] Z. Opial, "Weak convergence of the sequence of successive approximations for nonexpansive mappings," *Bulletin of the*

- American Mathematical Society*, vol. 73, no. 4, pp. 591–597, 1967.
- [31] J. Schu, “Weak and strong convergence to fixed points of asymptotically nonexpansive mappings,” *Bulletin of the Australian Mathematical Society*, vol. 43, no. 1, pp. 153–159, 1991.
- [32] J. P. Aubin and A. Cellina, *Differential Inclusions: Set-Valued Maps and Viability Theory*, Springer, Berlin, Germany, 1984.
- [33] H. F. Senter and W. G. Dotson, “Approximating fixed points of nonexpansive mappings,” *Proceedings of the American Mathematical Society*, vol. 44, no. 2, pp. 375–380, 1974.
- [34] B. Kalantari, “Method of creating graphical works based on polynomials,” Academic Publications, Ltd, Yorkshire, UK, Patent, US6894705, 2005.
- [35] B. Kalantari, *Polynomial Root-Finding and Polynomiography*, World Scientific Publishing Co. Pte. Ltd, New Jersey, NJ, USA, 2009.
- [36] B. B. Mandelbrot, *The Fractal Geometry of Nature*, W. H. Freeman, New York, NY, USA, 1982.
- [37] Y. C. Kwun, M. Tanveer, W. Nazeer, K. Gdawiec, and S. M. Kang, “Mandelbrot and julia sets via jungck–CR iteration with S -convexity,” *IEEE Access*, vol. 7, pp. 12167–12176, 2019.
- [38] Y. C. Kwun, M. Tanveer, W. Nazeer, M. Abbas, and S. M. Kang, “Fractal generation in modified Jungck–S orbit,” *IEEE Access*, vol. 7, pp. 35060–35071, 2019.
- [39] H. Qi, M. Tanveer, W. Nazeer, and Y. Chu, “Fixed point results for fractal generation of complex polynomials involving sine function via non–standard iterations,” *IEEE Access*, vol. 8, pp. 154301–154317, 2020.
- [40] Y. C. Kwun, A. A. Shahid, W. Nazeer, M. Abbas, and S. M. Kang, “Fractal generation via CR iteration scheme with S -convexity,” *IEEE Access*, vol. 7, pp. 69986–69997, 2019.

Research Article

Oblique Flow of Shear Thinning Fluid through an Absorptive Radiative Medium with Hall Effect

S. Rana,¹ K. Mahmud,² R. Mehmood,² and M. M. Bhatti ^{3,4}

¹Department of Mathematics, Faculty of Basic Sciences, University of Wah, Wah Cantt, Pakistan

²Department of Mathematics, Faculty of Natural Sciences, HITEC University, Taxila Cantt, Pakistan

³College of Mathematics and Systems Science, Shandong University of Science & Technology, Qingdao 266590, Shandong, China

⁴Material Science, Innovation and Modelling (MaSIM) Research Focus Area, North-West University, Mafikeng Campus, Private Bag X2046, Mmabatho 2735, South Africa

Correspondence should be addressed to M. M. Bhatti; mmbhatti@sdust.edu.cn

Received 3 February 2023; Revised 8 March 2023; Accepted 5 April 2023; Published 20 April 2023

Academic Editor: Watcharaporn Cholamjiak

Copyright © 2023 S. Rana et al. This is an open access article distributed under the Creative Commons Attribution License, which permits unrestricted use, distribution, and reproduction in any medium, provided the original work is properly cited.

The assumption of Hall current and ion slip is extremely crucial in several industrial and manufacturing processes, such as MHD (magneto hydrodynamics) accelerators, preservation coils, transmission lines, electric converters, and heating elements. Keeping this in view, the main aim of this article is to present a computational analysis of MHD ion Hall current with nonlinear thermal radiation on the sloping flow of shear thinning fluid through a porous medium on a stretching sheet that allows fluid suction and injection. The major mathematical modelling of governed problems is converted into a system of nonlinear ODEs (ordinary differential equations) by means of appropriate similarity relations. The influence of all relative physical parameters on velocity and temperature is studied through graphs and discussed in a detailed physical manner. Some beneficial mathematical quantities from the practical engineering and industrial point of view, such as skin friction factor and heat transfer rate at the porous surface, are calculated numerically and presented through graphs. It has been observed that flow may become unstable when M is small and the existence of a magnetic field and a porous ground contributes to a highly rough flow over the stretching surface. Suction is actually a resistive force which results in higher skin friction that is beneficial in controlling flow separation. Temperature of the fluid rises with stronger magnetic field and higher thermal radiation effects. The local heat flux decreases as the magnetic field strength and permeability parameter increase.

1. Introduction

Engineers, scientists, and mathematicians face an enormous challenge while dealing with nonlinear rheology of working fluids. There are number of means through which such types of nonlinearity can be confronted. One of the simplest ways in which viscoelastic fluids have been classified is the methodology given by Rivlin and Ericksen [1]. Noll and Truesdell [2] presented stress tensor as a symmetric tensor with velocity gradient and its derivatives in constitutive equations. In this modern era, researchers like [3] have made a lot of contribution in the field of non-Newtonian fluid flows, due their high-tech implication in industries. It is also noteworthy that these types of fluids exhibit very stimulating

mathematical features in their governed flow equations. Oblique stagnation point non-Newtonian fluid flow studies become a more exciting challenge for researchers and investigators due to its wide applications in industries. The fluid flow over a stretched surface is highly significant in so many manufacturing practices. Lok et al. [4] studied time-independent viscid incompressible fluid flow impinging at some arbitrary angles of incidence on a stretching panel. Labropulu et al. [5] developed the study of oblique stagnation-point flow of non-Newtonian fluid towards a stretching surface. Mahapatra et al. [6] analysed a time independent 2D radiative oblique stagnation-point flow with heat transfer characteristics on a shrinking sheet. Sadiq et al. [7] described MHD features of oscillatory oblique

stagnation point flow of micropolar nanofluid. Some more studies developing different physical effects on non-orthogonal stagnation point flows dealing with several non-Newtonian models may be found in [8–10].

The nonlinear radiative electrically conducting fluid flow in manifestation of magnetic field is widely beneficial into electrical control generators, cosmological flows, stellar and lunar power control machinery, planetary automobile re-entry, fissionable production plants, and many other engineering areas. At great operational temperatures, nonlinear thermal radiation becomes more vital and obvious, particularly under nonisothermal conditions. Nonlinear thermal radiation is highly significant when polymer extrusion procedure is monitored by thermally controlled environment. The influence of linear as well as nonlinear thermal radiation on Newtonian as well as non-Newtonian fluid flows in the presence as well as absence of magnetic field has already been discussed by numerous researchers and scientists [11, 12].

Hall and ion currents in influence with magnetic field is the most noteworthy phenomena in modern research due to its intensive, keen-sighted, and immense implications in abundant engineering fields such as power control originators, MHD generators, preservation coils, broadcast ranks, electrical converters, and boiler essentials. By applying Ohm's law directly, mostly the required results are unattainable due to weak magnetic strength but it can be enhanced by adding Hall and ion slip effects in this law. When applied magnetic field is in the direction of magneto hydrodynamics force in combination with Hall ion slip currents, then it becomes tremendously noteworthy in modern research because Hall and ion currents have strong influence on size and track of existing density and subsequently on the magnetic meter.

Ibrahim and Anbessa [13] scrutinized the 3D nanofluid flow of Casson fluid in the presence of applied magnetic field with ion Hall currents and mixed convection over an exponentially stretching surface. Krishna et al. [14] investigated combined effects of Hall and ion slips on MHD spinning stream of ciliary momentum of miniscule bacterium over absorbent intermediate. Rajakumar et al. [15] deliberated the flow of Casson fluid in their research, and they explored the influences of free convection with effects of radiation and viscid indulgence in existence with magnetic fields and Hall ion effects. Kumar and Vishwanath [16] established a scientific arrangement of non-Newtonian fluid flow over a permeable surface with a uniform distribution of magnetic field with Hall current and ion slip effects. Shah et al. [17] defined the flow of micropolar nanofluid in presence of thermally radiative rotating disks for investigation of mass flux and heat flux. Few more related studies on the said topic can be found from the references [18–22].

For continuity of fluid flow, suction/injection is highly recommended, particularly in boundary layer flows. Mainly these types of flows have applications in field of aerodynamics and planetary fields where the use of minimum drag forces is ensured. Suction is used for improvement in efficiency of diffusers. Shojaefard et al. [23] investigated the

control flow of fluid on the surface of a subsonic aircraft by using suction/injection. Braslow [24] showed that fuel ingesting and pollution caused by subsonic aircraft as well as price of commercial aircrafts can be reduced to a good extent only with the help of suction/injection.

Stagnation point flows under influence of suction injection have become one of the great interests for modern researchers. Zeeshan and Majeed [25] inspected the characteristics of Jeffery fluid past a stretched plate under influence of attractive dipole with suction/injection. Similarly, El-Arabawy [26] studied the impact of radiative heat transfer with suction and injection on a constant rotating sheet for a micropolar fluid. Chamkha et al. [27] examined the properties of chemical species and heat and mass transmission on a stretched surface in a permeable medium. Pandey and Kumar [28] categorized the viscid dissipation with the presence of suction/injection on MHD flow of a nanofluid in a porous medium. Rundora and Makinde [29] discussed third-grade fluid with assumptions of time- and temperature-dependent variable viscosity findings in presence of suction/injection in a porous station. Similar type of studies may be seen in [30–36].

The all cited works of numerous researchers and scientists depicted that inclined flow of non-Newtonian fluid in existence with a strong magnetic field with ion and Hall currents and nonlinear thermal radiation in porous medium with suction injection influence is highly suitable in many engineering problems and found to be new in this combination, although many researchers in this modern era of research have explored these types of problem but not yet this one. The novelty of governed fluid problem is stated as follows:

- (i) A picture of the inclined Casson fluid stagnation point flow on a stretched horizontal plate is captured
- (ii) Suction injection phenomenon is taken into consideration, and the horizontal stretched plate is supposed to be permeable.
- (iii) The body force on this bioconvective nanofluid flow is the magneto hydrodynamic force with ion slip and Hall currents
- (iv) Nonlinear thermal radiation is supposed to be added with convective boundary conditions

The current findings and implications are presented by including graphs of fluid distributions that reveal all new impacts of various parameters. Moreover, validation of current results with previously existing literature for Newtonian case is provided.

2. Mathematical Scheme

The mathematical model is constructed by using assumptions of two-dimensional, steady oblique flow of MHD Casson fluid along with Hall and ion slip conditions with suction injection and nonlinear thermal radiation. To keep surface stretched, two equal balanced forces are applied in opposite directions along the x -axis, and the origin is

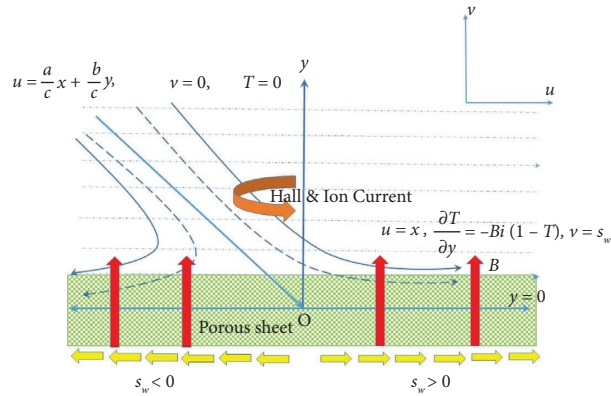


FIGURE 1: Geometrical description of the governed fluid model.

maintained fixed as shown in Figure 1. The basic fundamental laws in component forms as per stated assumptions are [37–39]

$$\frac{\partial u^*}{\partial x^*} + \frac{\partial v^*}{\partial y^*} = 0, \tag{1}$$

$$u^* \frac{\partial u^*}{\partial x^*} + v^* \frac{\partial u^*}{\partial y^*} + \frac{1}{\rho} \frac{\partial p^*}{\partial x^*} = \nu \left(1 + \frac{1}{\beta} \right) \nabla^{*2} u^* + \mathbf{J} \times \mathbf{B} - \frac{\nu}{K_\alpha} u^*, \tag{2}$$

$$u^* \frac{\partial v^*}{\partial x^*} + v^* \frac{\partial v^*}{\partial y^*} + \frac{1}{\rho} \frac{\partial p^*}{\partial y^*} = \nu \left(1 + \frac{1}{\beta} \right) \nabla^{*2} v^*, \tag{3}$$

$$u^* \frac{\partial T^*}{\partial x^*} + v^* \frac{\partial T^*}{\partial y^*} = \alpha \left(\frac{\partial^2 T^*}{\partial y^{*2}} + \frac{\partial^2 T^*}{\partial x^{*2}} \right) - \frac{1}{\rho c_p} \frac{\partial q_r}{\partial y^*}, \tag{4}$$

$$q_r = -\frac{4\delta^* T_\infty^3}{3K^*} \frac{\partial T^*}{\partial y^*}, \tag{5}$$

$$\mathbf{J} = \sigma(\mathbf{E} + \mathbf{V} \times \mathbf{B}) - \frac{\omega_e \tau_e}{\mathbf{B}} (\mathbf{J} \times \mathbf{B}) + \frac{\omega_e \tau_e}{\mathbf{B}^2} \beta_i (\mathbf{J} \times \mathbf{B}) \times (\mathbf{B}). \tag{6}$$

The consistent boundary conditions are [39]

$$\begin{aligned} u^* &= cx^*, \\ v^* &= u_f, \\ -k \frac{\partial T^*}{\partial y^*} &= h_s (T_f - T^*), \\ y^* &= 0, \\ u^* &= ax^* + by^*, \\ v^* &= 0, \\ T^* &= T_\infty, y^* \rightarrow \infty, \end{aligned} \tag{7}$$

$$\begin{aligned} \frac{\partial u}{\partial x} + \frac{\partial v}{\partial y} &= 0, \\ u \frac{\partial u}{\partial x} + v \frac{\partial u}{\partial y} &= \frac{\partial p}{\partial x} + \left(1 + \frac{1}{\beta} \right) \nabla^2 u - \frac{M(1 + \beta_i \beta_e)}{[\beta_e^2 + (1 + \beta_i \beta_e)^2]} u - \Omega u, \end{aligned} \tag{8}$$

where u^* and v^* are the velocity components in x and y directions, and ν , p^* , ρ , T^* , q_r , c_p , T_∞ , k^* , c , a , b , and $\beta =$

$\mu_B (\sqrt{2\pi} c / p_y)$ are the kinematic viscosity, pressure, density, temperature, nonlinear radiative heat flux, specific heat, ambient fluid temperature, thermal coefficient, the constants, and Casson fluid parameter, respectively. $\mathbf{J} \times \mathbf{B}$ is defined as generalised Ohm's law, where \mathbf{J} , σ , and \mathbf{E} are the current density, electrical conductivity, and electric field intensity, respectively. Equations (1)–(8) are transformed into nondimensional form [37–39]:

$$\frac{\partial u}{\partial x} + \frac{\partial v}{\partial y} = 0, \tag{9}$$

$$u \frac{\partial u}{\partial x} + v \frac{\partial u}{\partial y} = \frac{\partial p}{\partial x} + \left(1 + \frac{1}{\beta} \right) \nabla^2 u - \frac{M(1 + \beta_i \beta_e)}{[\beta_e^2 + (1 + \beta_i \beta_e)^2]} u - \Omega u, \tag{10}$$

$$u \frac{\partial v}{\partial x} + v \frac{\partial v}{\partial y} = -\frac{\partial p}{\partial y} + \left(1 + \frac{1}{\beta}\right) \nabla^2 v, \quad (11)$$

$$\left(u \frac{\partial T}{\partial x} + v \frac{\partial T}{\partial y}\right) \text{Pr} = \left(\frac{\partial^2 T}{\partial y^2} + \frac{\partial^2 T}{\partial x^2}\right) + \text{Rd} \frac{\partial}{\partial y} \left((T(\theta_w - 1) + 1)^3 \frac{\partial T}{\partial y} \right), \quad (12)$$

$$\begin{aligned} u &= x, \\ \frac{\partial T}{\partial y} &= -\text{Bi}(1 - T), \\ v &= s_w, \\ \text{at } y &= 0, \end{aligned} \quad (13)$$

$$\begin{aligned} u &= \frac{a}{c}x + \frac{b}{c}y, \\ v &= 0, \\ T &= 0, \\ \text{at } y &\longrightarrow \infty, \end{aligned} \quad (14)$$

where β_e , β_i , Pr , s_w , θ_w , Bi , $M\Omega$, (a/b) , and (b/c) represent the Hall parameter, ion parameter, Prandtl number, suction ($s_w > 0$)/injection ($s_w < 0$) parameter, temperature ratio parameter, Biot number, magnetic field parameter, permeability parameter, stretching ratio parameter, and obliqueness of the flow, respectively.

By stream-function transformation as defined [38] in equations (9)–(14) with $p_{xy} = p_{yx}$,

$$\frac{\partial \psi}{\partial y} \left(\frac{\partial^3 \psi}{\partial x^3} + \frac{\partial^3 \psi}{\partial y^2 \partial x} \right) - \frac{\partial \psi}{\partial x} \left(\frac{\partial^3 \psi}{\partial y^3} + \frac{\partial^3 \psi}{\partial x^2 \partial y} \right) - \left(1 + \frac{1}{\beta}\right) \nabla^4 \psi + \frac{M(1 + \beta_i \beta_e)}{[\beta_e^2 + (1 + \beta_i \beta_e)^2]} \frac{\partial^2 \psi}{\partial y^2} + \Omega \frac{\partial^2 \psi}{\partial y^2}, \quad (15)$$

$$\text{Pr} \left(\frac{\partial \psi}{\partial y} \frac{\partial T}{\partial x} - \frac{\partial \psi}{\partial x} \frac{\partial T}{\partial y} \right) = \left(\frac{\partial^2 T}{\partial x^2} + \frac{\partial^2 T}{\partial y^2} \right) + \text{Rd} \frac{\partial}{\partial y} \left((T(\theta_w - 1) + 1)^3 \frac{\partial T}{\partial y} \right), \quad (16)$$

$$\begin{aligned} \frac{\partial \psi}{\partial y} &= x, \\ \frac{\partial \psi}{\partial x} &= s_w, \\ \frac{\partial T}{\partial y} &= -\text{Bi}(1 - T), \\ y &= 0, \end{aligned} \quad (17)$$

$$\begin{aligned} \frac{\partial \psi}{\partial y} &= \frac{a}{c}x + \frac{b}{c}y, \\ T &= 0, \\ \text{at } y &\longrightarrow \infty. \end{aligned} \quad (18)$$

Over consuming stream-function transformation as defined in [38] into equations (15)–(18) and after integration once,

$$\left(1 + \frac{1}{\beta}\right) f''' + f f'' - (f')^2 - \frac{M(1 + \beta_i \beta_e)}{\beta_e^2 + (1 + \beta_i \beta_e)^2} f' - \Omega f' + B_1 = 0, \quad (19)$$

$$\left(1 + \frac{1}{\beta}\right) g''' + f g'' - f' g' + \frac{M(1 + \beta_i \beta_e)}{\beta_e^2 + (1 + \beta_i \beta_e)^2} g' - \Omega g' + B_2 = 0, \quad (20)$$

$$\theta'' + Pr f\theta' + Rd\left((\theta(\theta_w - 1) + 1)^3\theta'\right)' = 0. \tag{21}$$

The consistent boundary conditions (17) and (18) convert

$$\begin{aligned} f &= -s_w, \\ f' &= 1, \\ g' &= 0, \\ \theta' &= -Bi(1 - \theta(0)), \end{aligned} \tag{22}$$

where B_1 and B_2 can be obtained from B.Cs (23) as

$$\begin{aligned} B_1 &= \frac{a}{c} \left(\frac{M(1 + \beta_i\beta_e)}{\beta_e^2 + (1 + \beta_i\beta_e)^2} + \frac{a}{c} + \Omega \right), \\ B_2 &= \frac{b}{c} \left(A - \frac{M(1 + \beta_i\beta_e)}{\beta_e^2 + (1 + \beta_i\beta_e)^2} y - \Omega y \right). \end{aligned} \tag{24}$$

Defining the transformation

$$g'(y) = \gamma_2 h(y), \tag{25}$$

at $y = 0$,

we get

$$\begin{aligned} f' &= \frac{a}{c}, \\ g' &= \frac{b}{c} y, \\ \theta &= 0, \\ \text{at } y &\longrightarrow \infty, \end{aligned} \tag{23}$$

$$\begin{aligned} \left(1 + \frac{1}{\beta}\right) f''' + ff'' - (f')^2 - \frac{M(1 + \beta_i\beta_e)}{\beta_e^2 + (1 + \beta_i\beta_e)^2} f' \\ + \frac{a}{c} \left(\frac{M(1 + \beta_i\beta_e)}{\beta_e^2 + (1 + \beta_i\beta_e)^2} + \frac{a}{c} + \Omega \right) = 0, \end{aligned} \tag{26}$$

$$\begin{aligned} \left(1 + \frac{1}{\beta}\right) h'' + fh' - f'h - \frac{M(1 + \beta_i\beta_e)}{\beta_e^2 + (1 + \beta_i\beta_e)^2} \\ (h - y) - \Omega(h - y) - A = 0, \end{aligned} \tag{27}$$

$$\theta'' + Pr f\theta' + Rd\left((\theta(\theta_w - 1) + 1)^3\theta'\right)' = 0, \tag{28}$$

$$\begin{aligned} f &= -s_w \\ f' &= 1, \\ h &= 0, \\ \theta' &= -Bi(1 - \theta(0)), \end{aligned} \tag{29}$$

at $y = 0$,

$$\begin{aligned} f' &= \frac{a}{c}, \\ h' &= 1, \\ \theta &= 0, \\ \text{at } y &\longrightarrow \infty. \end{aligned} \tag{30}$$

3. Physical Quantities of Interest

Skin friction coefficients at surface and the local heat flux [37] are the physical quantities of interest that have extensive use in numerous engineering and manufacturing productions.

$$\tau_w = \left(1 + \frac{1}{\beta}\right) \left[x f''(0) + \frac{b}{c} h''(0) \right], \tag{31}$$

$$q_w = -\theta'(0).$$

The stagnation points x_s are

$$x_s = \frac{-(b/c)h'(0)}{f''(0)}. \tag{32}$$

4. Numerical Scheme

The mathematical form of governed problems (26)–(30) is the system of coupled highly nonlinear set of ordinary

differential equations. To solve such system of equations by shooting technique, first of all, make them into set of first-order initial value problem by using following transformation.

$$\begin{pmatrix} f \\ f' \\ f'' \\ f''' \end{pmatrix} = \begin{pmatrix} y_1 \\ y_1' = y_2 \\ y_2' = y_3 \\ y_3' = y_4 \end{pmatrix}, \tag{33}$$

$$\begin{pmatrix} h \\ h' \\ h'' \end{pmatrix} = \begin{pmatrix} y_5 \\ y_5' = y_6 \\ y_6' = y_7 \end{pmatrix},$$

$$\begin{pmatrix} \theta \\ \theta' \\ \theta'' \end{pmatrix} = \begin{pmatrix} y_8 \\ y_8' = y_9 \\ y_9' = y_{10} \end{pmatrix}.$$

We get

$$\begin{aligned} \left(1 + \frac{1}{\beta}\right) y_3' &= -y_1 y_3 + y_2^2 + \frac{M(1 + \beta_i \beta_e)}{\beta_e^2 + (1 + \beta_i \beta_e)^2} y_2 - \frac{a}{c} \left(\frac{M(1 + \beta_i \beta_e)}{\beta_e^2 + (1 + \beta_i \beta_e)^2} + \frac{a}{c} + \Omega \right), \\ \left(1 + \frac{1}{\beta}\right) y_6' &= y_2 y_6 - y_1 y_6 + \left(\frac{M(1 + \beta_i \beta_e)}{\beta_e^2 + (1 + \beta_i \beta_e)^2} + \Omega \right) (y_5 - y) + A, \\ y_9' &= -Pr y_1 y_9 + Rd \{ (y_8 (\theta_w - 1) + 1)^3 y_9 \}', \\ \left. \begin{aligned} y_1(0) &= \alpha_1, y_2(0) = 1, \\ y_3(0) &= \alpha_2, y_5(0) = 0, \\ y_6(0) &= \alpha_3, y_8(0) = 0, \\ y_9(0) &= \alpha_4, \end{aligned} \right\}, \end{aligned} \tag{34}$$

where $\alpha_i, i = 1 \dots 4$, are the shooting factors with assumption of three decimal places tolerance level.

5. Results and Physical Discussion

Comprehensive computational calculations have been conducted and demonstrated by graphs herein segment. The numerical investigation of oblique stagnation point flow of MHD ion Hall current with suction injection of non-Newtonian fluid along with nonlinear thermal radiation in porous medium is presented in this segment. Figures 2–10 are settled to attain the norms and standards of this theoretical research.

Figure 2 is constructed to note the influence of permeability constraint Ω on fluid's normal and tangential velocity $f'(y)$, $h'(y)$, and temperature $\theta(y)$ of fluid with suction/injection. Figure 2(a) presents normal velocity $f'(y)$

shrinkages for rising values of permeability parameter $\Omega = 0.1, 3.0, 5.0, 7.0$, and it is quite evident that the existence of permeable surface becomes the reason of strong restriction to flowing of fluid, so the velocity becomes decelerate. Also, it is worth mentioning here that the magnitude of suction ($s_w > 0$) is greater than the magnitude of injection ($s_w < 0$) for this case, higher suction becomes more effective in porous surface as it delays the boundary layer separation and flow becomes more and more stable. Figure 2(b) indicates other component of velocity $h'(y)$ upswings nearby surface since a high permeability allows fluids to pass through more freely, and after inflection point, it reverses its behaviour and comes to decline far off from sheet because of higher inspiration of porousness parameter $\Omega = 0.1, 3.0, 5.0, 7.0$ and behaves extremely resistive. It is noted in this graph that close to wall injection ($s_w < 0$) is higher than suction but away from the wall effect of suction/

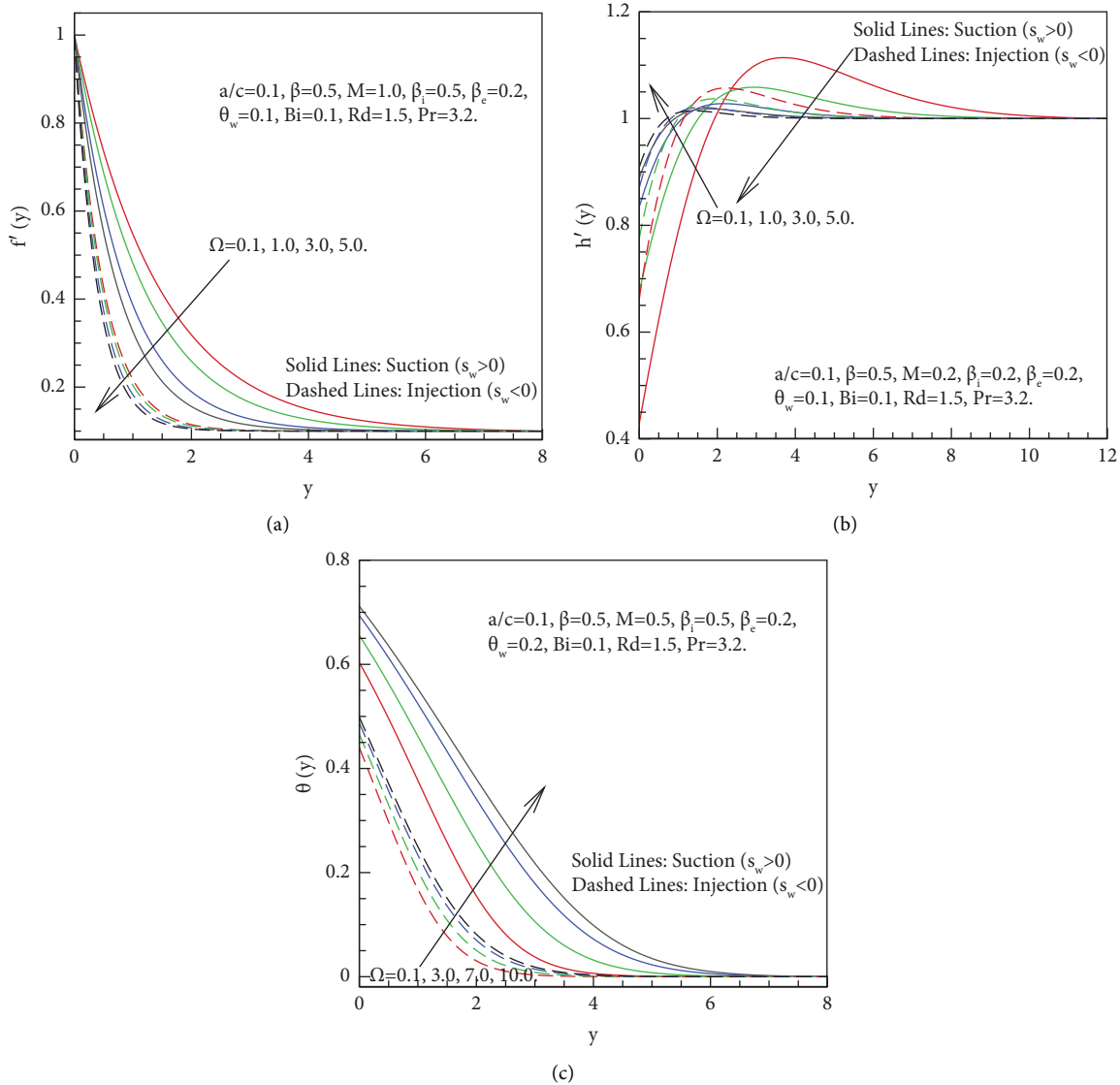


FIGURE 2: (a) Velocity distribution $f'(y)$, (b) velocity distribution $h'(y)$, and (c) temperature distribution $\theta(y)$ for permeability parameter Ω .

injection reversed. Figure 2(c) describes the effect of permeability parameter $\Omega = 0.1, 3.0, 7.0, 10.0$ on temperature of fluid, when permeability parameter Ω rises so that the temperature distribution with thermal boundary layer increases. This happens because permeable surface slows down the motion of fluid flow, and this restriction in flowing of fluid becomes responsible to enhance the temperature of governed fluid. Figure 2(c) also depicts the stronger influence of suction ($s_w > 0$).

Figure 3 describes the impact of ion slip constraint β_i on fluid's velocities $f'(y)$ and $h'(y)$ as well as on temperature $\theta(y)$ of fluid with suction/injection. Conductivity of fluid increases when values of ion slip constraint $\beta_i = 0.1, 3.0, 6.0, 10.0$ escalates and as a reaction, restraining energy comes down and fluid's molecules freely moves and fluid's velocity raises as noted in Figure 3(a). Figure 3(b) is plotted to show similar kind of increasing behaviour for $\beta_i = 0.1, 2.0, 4.0, 6.0$ away from the surface but at surface velocity

reverses its behaviour and declines at wall because at wall fluids have resistance which opposes the flow. Figure 3(c) displays that temperature $\theta(y)$ of fluid declines; also, the thermal boundary layer becomes thinner for ion slip parameter $\beta_i = 0.1, 2.0, 5.0, 8.0$, due to dropping of damping energy in the direction of flow. It is worth mentioning here that velocity profile for suction ($s_w > 0$) is greater than injection ($s_w < 0$). Strong influence of suction is highly useful to reduce the drag in boundary layer flow.

Figure 4 is planned to recognize the enactment of both velocities $f'(y)$, $h'(y)$, and temperature $\theta(y)$ of fluid for Hall parameter β_e . Since the resistance is produced by magnetic field when Lorentz force is strong enough, but due to the presence of Hall parameter β_e , the resistive force becomes weak due to decline in conductivity, so fluid's normal velocity $f'(y)$ proliferates with the rise in Hall parameter $\beta_e = 0.1, 0.3, 0.6, 1.0$ as mentioned in 4(a), and for suction ($s_w > 0$), velocity is greater, but for injection

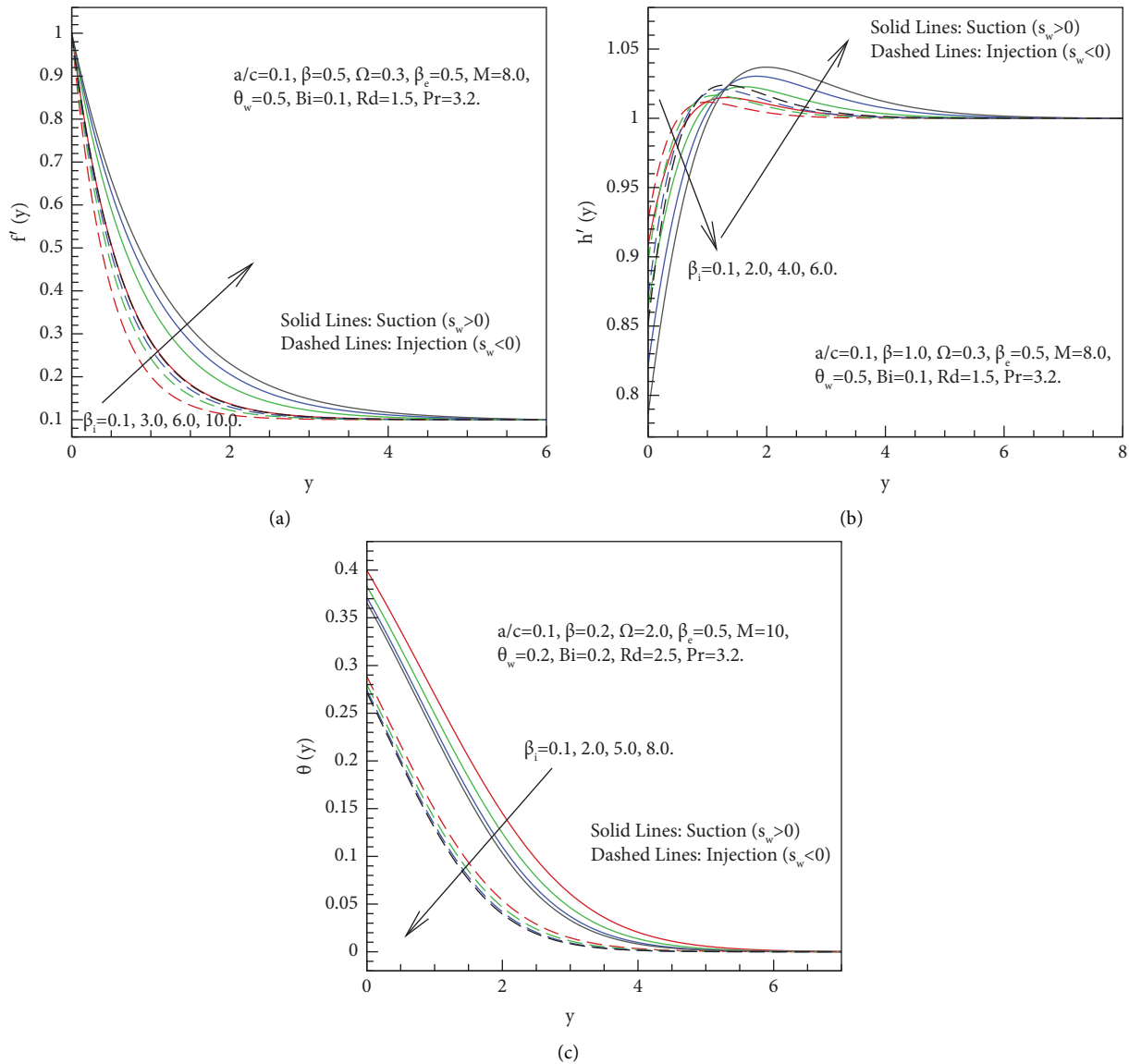


FIGURE 3: (a) Velocity distribution $f'(y)$, (b) velocity distribution $h'(y)$, and (c) temperature distribution $\theta(y)$ for ion slip parameter β_i .

($s_w < 0$), velocity of fluid is smaller. Figure 4(b) expresses the significance of Hall constraint $\beta_e = 0.1, 0.3, 0.6, 1.0$, and it governs when fluid is far away from surface and fluid's tangent component of velocity, $h'(y)$ intensifies away from wall, but near to surface, it takes differing conduct and contracts. Given that the Hall parameter is calculated as the sum of the frequency and the time of electron collisions. An increase in this parameter indicates an increase in the frequency of electrons, the duration of electron collisions, or both. Figure 4(c) shows that temperature $\theta(y)$ drops down when Hall parameter $\beta_e = 0.1, 1.0, 2.0, 5.0$ increases; because of weak resistive force, there is decline in thermal conductivity and as a result the temperature profile declined. The effect of suction ($s_w > 0$) is stronger in these graphs, and it is more applicable in practical world problems/models and useful for situation where to increase output of diffusers of governed fluid through reducing separation drag. Boundary layer suction particular in porous media close to trailing

edge is useful to maximize the lift and minimize the drag force of automobiles, aerofoils, and jet planes.

Figure 5 is intended to show the effect of magnetic field on fluid's velocity and fluid's temperature, every time. The existence of magnetic field means that there is birth of Lorentz strength. Lorentz force is defined as a resistive drag force, so normal velocity $f'(y)$ of fluid descends for $M = 0.1, 1.0, 3.0, 6.0$ as seen in Figure 5(a). But for tangential velocity, $h'(y)$ case is opposite and grows up close to surface but reverses its behaviour when it moves away from the surface for $M = 0.1, 1.0, 3.0, 6.0$, see Figure 5(b). This happens due to the presence of magnetic field. Figure 5(c) contrives to implement the connection of temperature with magnetic field. It shows that temperature $\theta(y)$ increases for higher values of magnetic field $M = 0.1, 3.0, 7.0, 10.0$ because of frictional stress which arise because of Lorentz force, so there occurs increment in thermal conductivity, so in temperature of fluid.

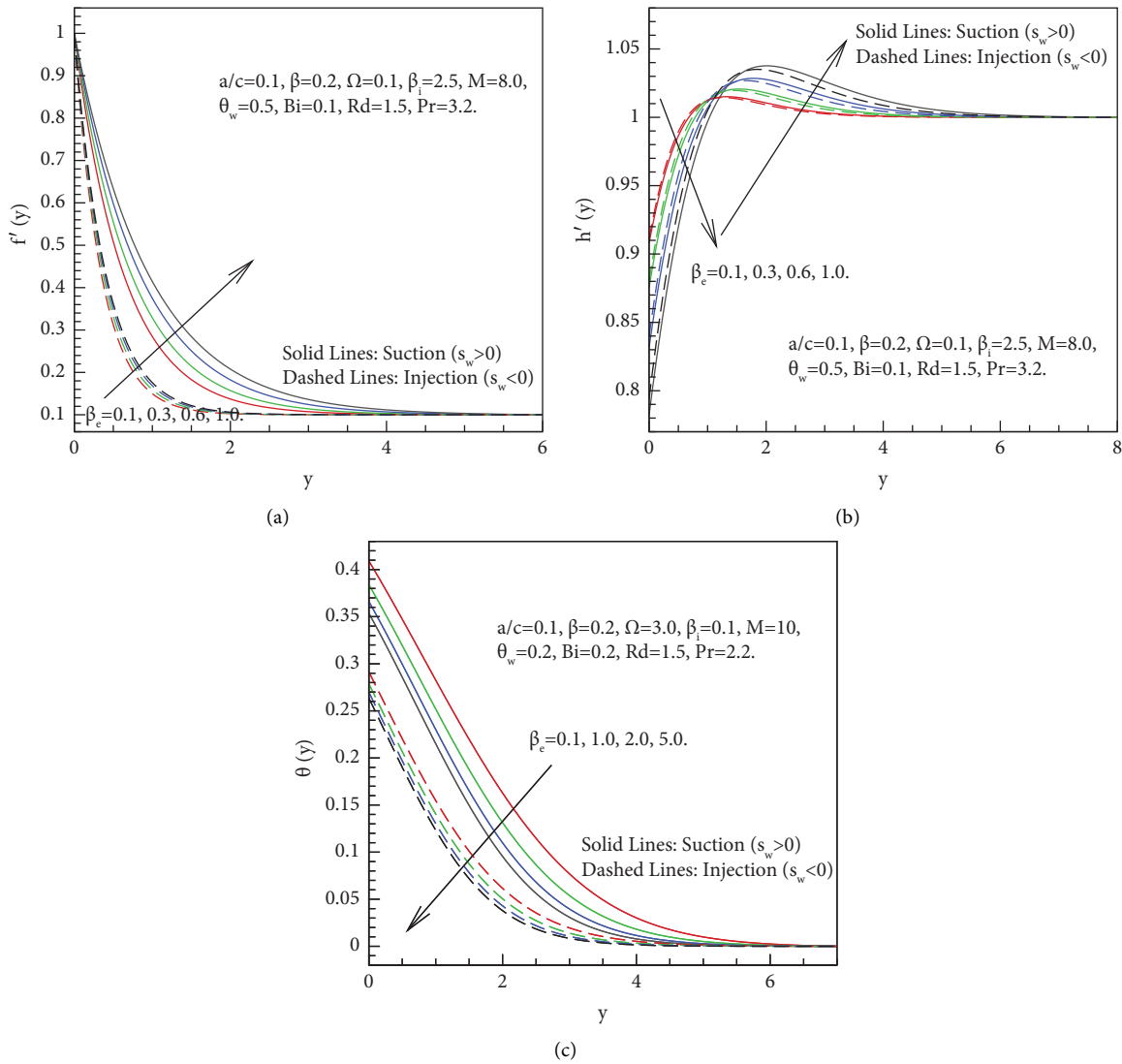


FIGURE 4: (a) Velocity distribution $f'(y)$, (b) velocity distribution $h'(y)$, and (c) temperature distribution $\theta(y)$ for Hall parameter β_e .

Figure 6 is plotted for inspecting the performance of radiation parameter Rd , Biot number Bi , and Prandtl number Pr on temperature distribution. Fluid's temperature $\theta(y)$ enlarged for rising numbers of radiation parameter $Rd = 0.1, 0.5, 1.0, 1.5$ because larger radiation parameter implies more heat is provided to the fluid, so thermal boundary layer becomes thick and temperature of fluid rises as illustrated in Figure 6(a). In addition to being utilised to produce power, radiation is also used in academia, industry, and medical. Radiation is also useful in many other fields, including mining, law enforcement, space exploration, agriculture, archaeology (carbon dating), and many others. Figure 6(b) shows that temperature of fluid becomes higher with growth in Biot number $Bi = 1.0, 1.5, 2.0, 3.0$. Because when convective heat conversation at the surface rises ($Bi \geq 1.0$), then there is enhancement in thermal boundary layer thickness as with a higher heat transfer coefficient, and more heat is transferred from the surface to the fluid. The rate of heat

transmission increases with greater estimates of Bi . Bi can, therefore, be used as a cooling operator in complex operations. Figure 6(c) shows the thermal boundary layer thicknesses shrinkage extremely when there is rise in Prandtl number $Pr = 1.0, 1.5, 2.0, 3.0$; so, there is escalation in the wall temperature gradient. This phenomenon occurs because of higher values Prandtl number, and then, fluid has moderately little thermal conductivity that lessens the occurrence of conduction and reduces the thickness of thermal boundary layer; hence, temperature of fluid declines. Small Prandtl values are a suitable choice for heat-transmitting liquids since they are free-flowing liquids with strong thermal conductivity. Prandtl number ($Pr < 1.0$) specifies fluids with huge thermal conductivity which crops denser thermal boundary layer as compared to the thermal boundary layer for higher Prandtl number ($Pr > 1.0$). Suction is more prominent than injection in all these plots, and it is an efficient source for laminar boundary layer flow, it reduces the contact losses at surface and suction becomes

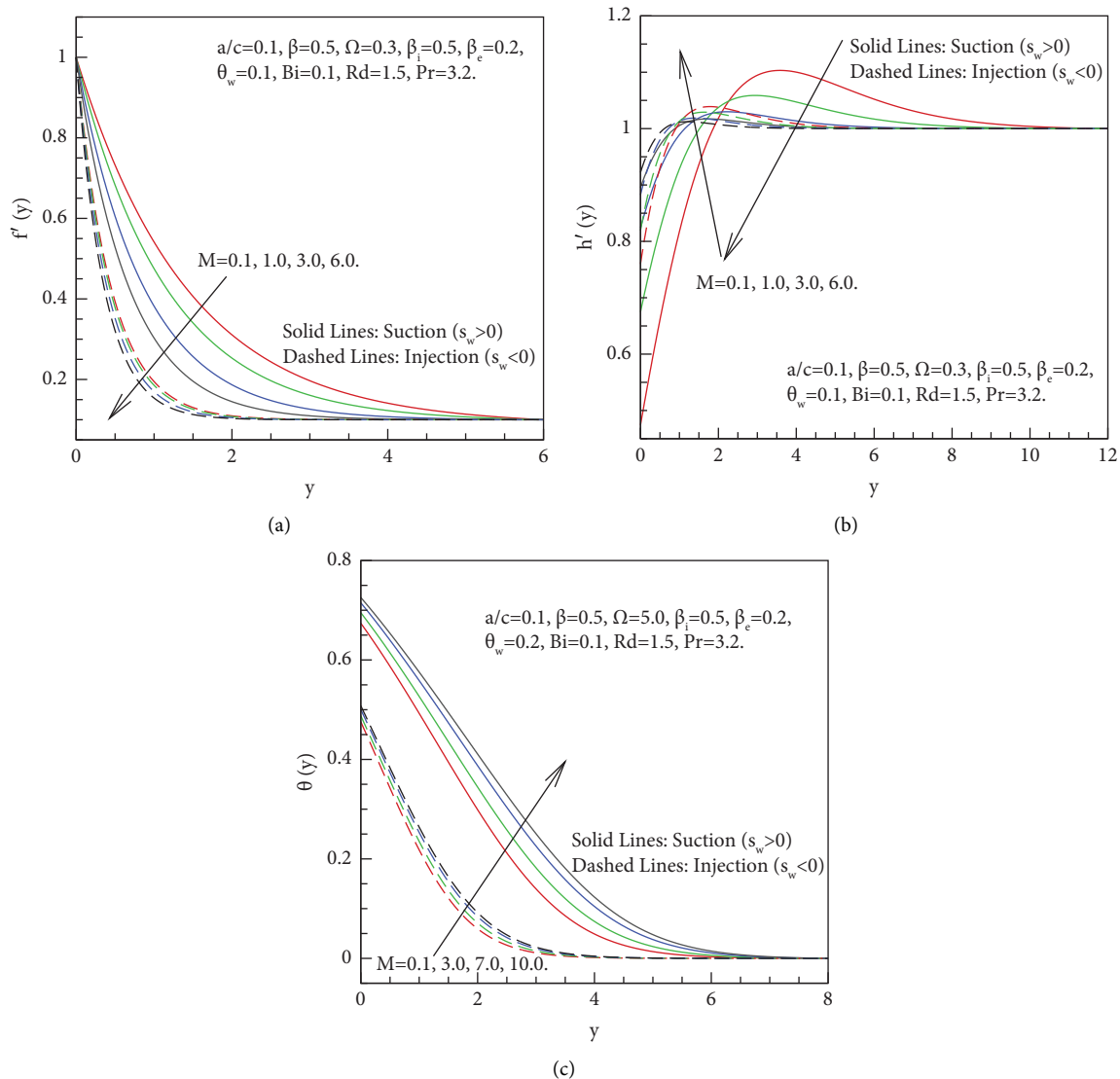


FIGURE 5: (a) Velocity distribution $f'(y)$, (b) velocity distribution $h'(y)$, and (c) temperature distribution $\theta(y)$ for magnetic field parameter M .

more stable in laminar boundary layer, and it becomes thin and remains laminar throughout. These physical quantities are of great worth due to its large and high scales applications in many industrial and engineering arenas, specifically areas of aerodynamics and astronomical, and highly beneficial in controlling flow separation.

Figure 7(a) launches that skin friction coefficient at surface $h'(0)$ increases when permeability parameter $\Omega = 0.1, 0.3, 0.7$ rises with suction ($s_w > 0$) and injection ($s_w < 0$), and also, it upsurges when the values of magnetic field M raised for both cases. It is worth noting in this plot that suction is smaller than injection. Figure 7(b) develops the decreasing influence of local heat transfer rate $-\theta'(0)$ rises for permeability parameter $\Omega = 0.1, 0.3, 0.7$ and for magnetic field parameter M for both cases of suction ($s_w > 0$) as well as for injection ($s_w < 0$). Also, suction ($s_w > 0$) is smaller than injection ($s_w < 0$).

Figure 8(a) indicates skin friction coefficient at wall $h'(0)$ shrinkages when both Hall parameter $\beta_e = 0.1, 0.5, 1.0$ and

ion slip parameter β_i increase. Figure 8(b) displays that local heat flux $-\theta'(0)$ grows up for increasing values of Hall parameter $\beta_e = 0.1, 0.5, 1.0$; on the other hand, it remained fixed for ion slip parameter β_i on local heat flux for both cases of suction as well as for injection but influence of suction is smaller than injection in these two plots.

In Figure 9, it is found that effect of radiation parameter $Rd = 0.1, 0.3, 0.7$ is downward for heat transfer rate at surface $-\theta'(0)$ but have opposite behaviour for Biot number Bi . Also, this figure exhibits that injection is stronger and enhancing than suction. The fluid flow in the channel is controlled by suction or injection phenomenon. Figure 10 shows flow pattern through stream lines for suction ($s_w > 0$) and injection ($s_w < 0$) in the presence and absence of permeability parameter Ω . Figure 10(a) reveals the flow pattern with and without permeability for injection ($s_w < 0$) and for suction ($s_w > 0$) in Figure 10(b). Figure 10(c) simultaneously shows the stream lines pattern for both suction ($s_w > 0$) as

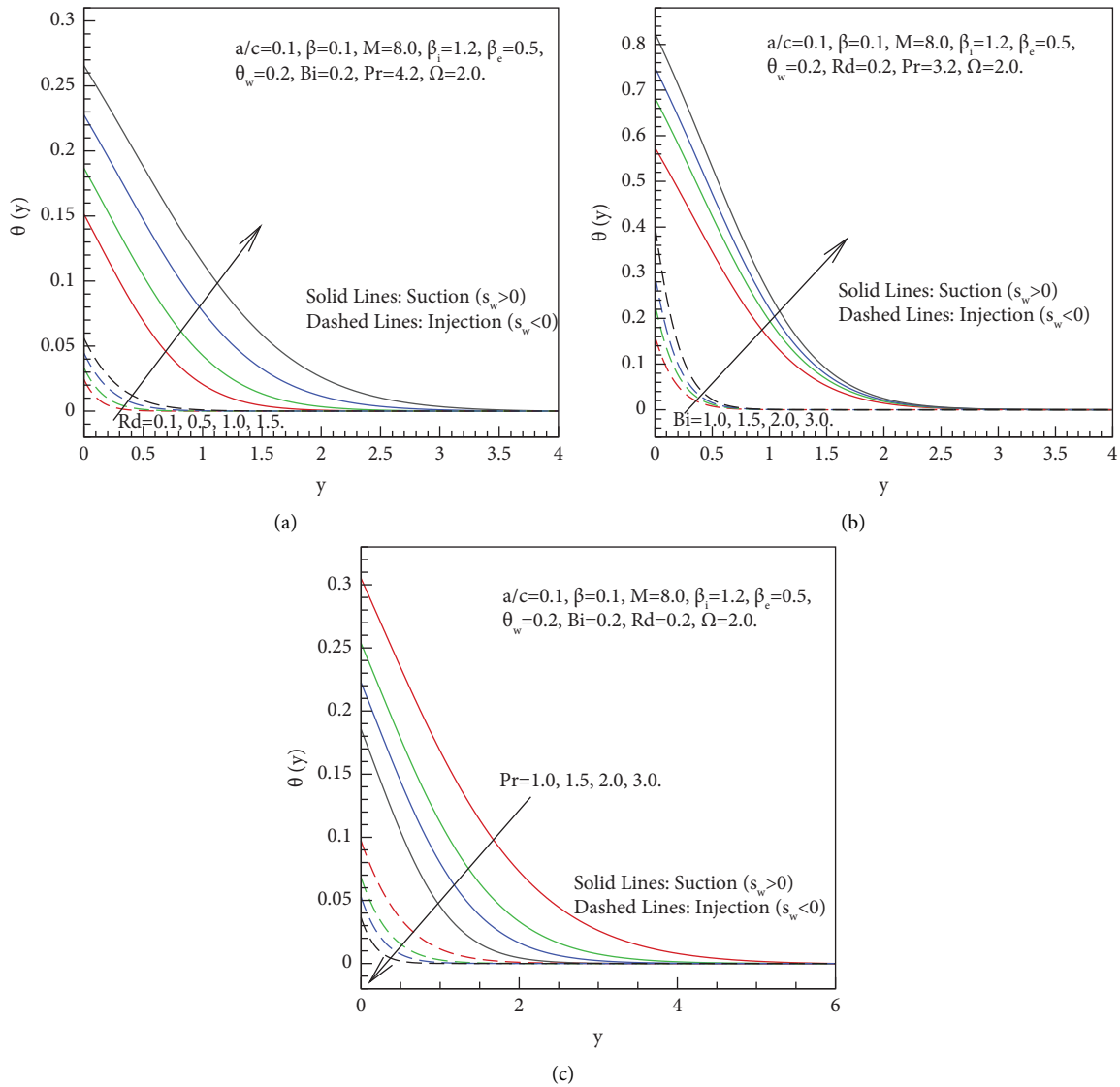


FIGURE 6: (a) Temperature distribution $\theta(y)$ for radiation parameter Rd , (b) temperature distribution $\theta(y)$ for Biot number Bi , and (c) temperature distribution $\theta(y)$ for Prandtl number Pr .

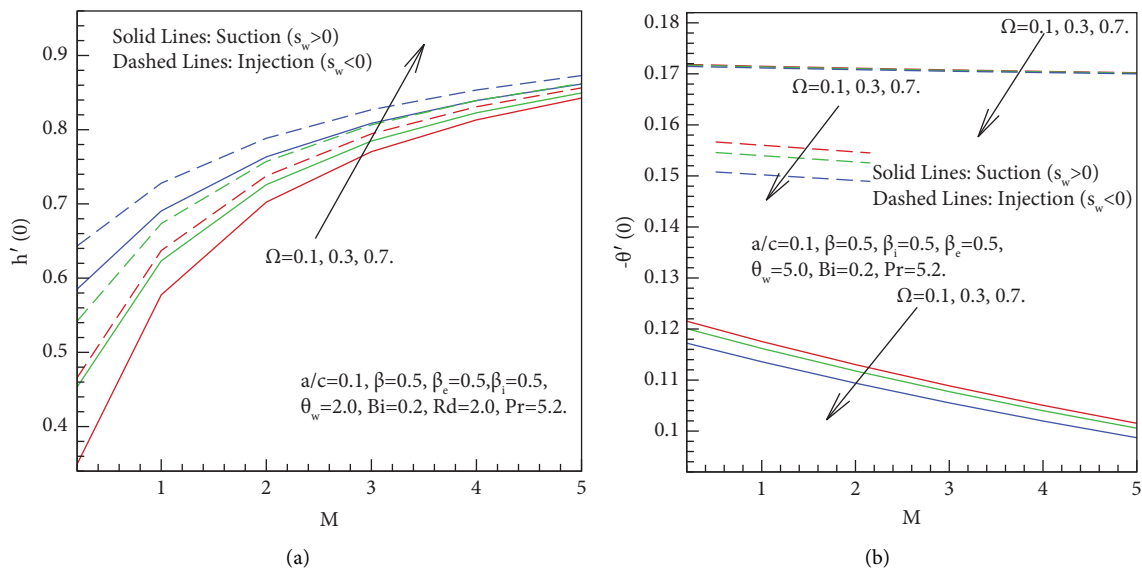


FIGURE 7: (a) Tangential skin friction at surface $-h'(0)$ and (b) heat flux $-\theta'(0)$ for permeability parameter Ω against magnetic field parameter M .

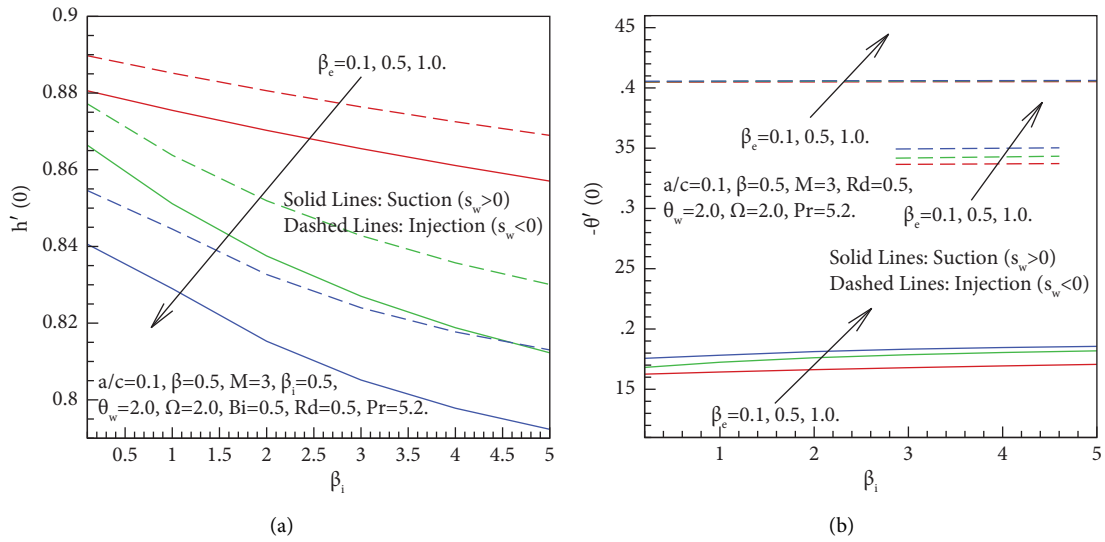


FIGURE 8: (a) Tangential skin friction at surface $-h'(0)$ and (b) heat flux $-\theta'(0)$ for Hall parameter β_e against ion slip parameter β_i .

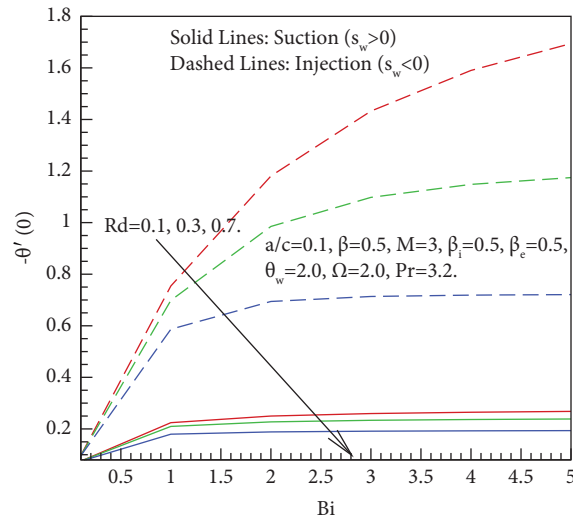


FIGURE 9: Heat flux $-\theta'(0)$ for radiation parameter Rd against number Bi .

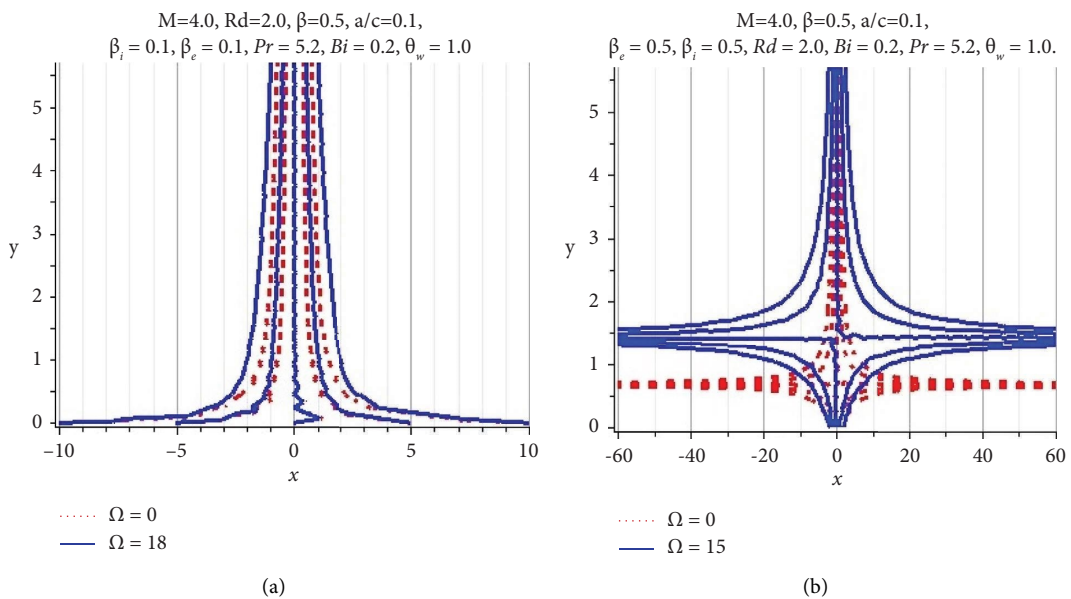


FIGURE 10: Continued.

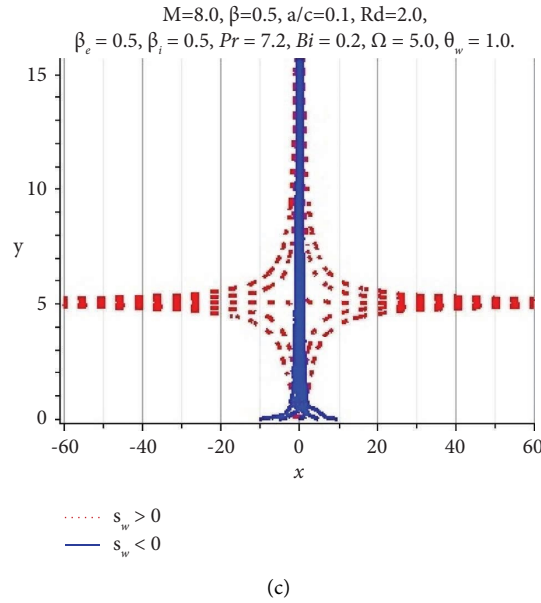


FIGURE 10: Stream lines (a) for permeability parameter with injection, (b) for permeability parameter with suction, and (c) for suction and injection.

TABLE 1: Consequences of local heat flux $-\theta'(0)$ for restrictive case when $Bi \rightarrow \infty$.

Pr	Existing values	Makinde and Aziz [40]	Khan and Pop [41]	Wang [42]
0.2	0.1696	0.1691	0.1691	0.1691
0.7	0.4541	0.4539	0.4539	0.4539
2.0	0.9113	0.9114	0.9113	0.9113
7.0	1.8950	1.8954	1.8954	1.8954
20.0	3.3533	3.3539	3.3539	3.3539
70.0	6.4620	6.4622	6.4621	6.4621

well as injection ($s_w < 0$). The stream contour ψ touches the partition $y = 0$, at stagnation point x , and zero skin friction.

Table 1 provides the comparison of numerical values of local heat flux with previously published results in literature, so that to authenticate the current computational results. For this purpose, the findings of Makinde and Aziz [40], Khan and Pop [41], and Wang [42] are compared with present values of heat transfer rate in Table 1. Here, the assumptions that are made for comparison are fixed temperature with very large Biot number ($Bi \rightarrow \infty$) in BCs also with negligence of permeability parameter and suction/injection effects. These values depicted in the table that the current results of heat flux at surface $-\theta'(0)$ against several numerical figures of Prandtl number Pr took upto 3 decimal places with those values of heat flux presented in [40–42].

6. Concluding Remarks

The major presentation of this type of existing research is particularly in the field of aerodynamics and astral, planetary, cosmological, and astrophysical disciplines so that drag may minimize to reduce the loss of energy. So, in this respect, the prevailing article inspects the blend suction

injection in permeable surface for non-Newtonian fluid with MHD Hall and ion slip effects over a nonlinear thermally radiative stretched surface. The nonlinear radiative electrically conducting fluid flow in manifestation of magnetic field is widely bump into electrical control generators, cosmological flows, stellar and lunar power control machinery, planetary automobile re-entry, fissionable production plants, and many other engineering areas.

- (i) Permeability Ω developed the cause to decline in both velocities but enhances temperature of fluid as this happens in fluids due to high permeability so it allows fluids to pass through more freely. This can be helpful in materials such as aquifers, petroleum reservoirs, cements, and ceramics.
- (ii) Ion and Hall slip parameters β_i and β_e are the causes for rise in velocities. Several engineering issues including those involving power generators, magneto hydrodynamic accelerators, refrigeration coils, transmission lines, electric transformers, and heating used these types of currents.
- (iii) Velocities for magnetic field parameter M falls down for $M > 1$. But for temperature distribution, it rises. Also, both velocities for magnetic field parameter with suction ($s_w > 0$) is recognized more superior than occurrence of injection ($s_w < 0$). The discovery that the interaction of a plasma with a magnetic field could take place at far greater temperatures than were feasible in a spinning mechanical turbine served as the initial catalyst for interest in MHD power generation.
- (iv) Influence of radiation parameter Rd and Biot number Bi on temperature of fluid is more dominant, but for Prandtl number Pr, it became subservient. Several different applications, such as

thermal management, spectroscopy, optoelectronics, and energy-conversion devices, depend on the capacity to control heat radiation.

- (v) Local heat flux is enormous for ion and Hall slip parameter β_i and β_e with injection as compared to suction
- (vi) Heat transfer rate at surface drops down in the presence of radiation parameter Rd , while it flourishes against different values of Biot number Bi , injection in this case is more prominent than suction. Suction/injection is a mechanical phenomenon that is used to control the fluid flow in the channel and reduce surface drag in order to reduce energy losses in the boundary layer region.
- (vii) A solid confirmation is obtained in tabular format of numerical figures with present existing literature. An outstanding agreement is attained for restrictive case.
- (viii) A strong convective boundary condition indicated that for numerous figures of Prandtl number, local heat flux at surface upturns

Nomenclature

u :	x -components of velocity
ν :	Viscosity
ρ :	Density
Ω :	Permeability parameter
T_∞ :	Free stream temperature
c_p :	Specific heat of fluid
q_r :	Nonlinear radiative heat flux
Rd :	Radiation parameter
β_e :	Hall parameter, ion parameter
β_i :	Hall parameter, ion parameter
$Pr = (\nu/a)$:	Prandtl number
BCs:	Boundary conditions
(b/c) :	Obliqueness of fluid flow
ODEs:	Ordinary differential equations
v :	y -components of velocity
p :	Pressure
T :	Temperature
h_s :	Heat transfer coefficient
a, b, c :	Constants
k :	Thermal conductivity
$\beta = \mu_B (\sqrt{2\pi_c} / p_y)$:	Casson fluid parameter
$\theta_w = T_f / T_\infty$:	Temperature ratio parameter
$M = (\sigma / c_p) B_0^2$:	Magnetic field constraint
s_w :	Suction ($s_w > 0$)/injection ($s_w < 0$) parameter
(a/c) :	Stretching ratio constraint
$Bi = -(h/k)\sqrt{\nu}$:	Biot number
A :	Boundary layer displacement constant
PDEs:	Partial differential equations.

Data Availability

No underlying data were collected or produced in this study.

Conflicts of Interest

The authors declare that they have no conflicts of interest with any individual or organization regarding publication of this research.

Acknowledgments

The authors were thankful for technical and financial support from University of Wah, HITEC University, and Shandong University of Science and Technology, Qingdao, China.

References

- [1] R. S. Rivlin and J. L. Ericksen, "Stress-deformation relations for isotropic materials," *Collected Papers of RS Rivlin*, pp. 911–1013, Springer-Verlag New York Inc, Newyork, NY, USA, 1997.
- [2] W. Noll and C. A. Truesdell, *The Non-linear Field Theories of Mechanics*, Springer-Verlag Berlin, Newyork, NY, USA, 1992.
- [3] M. M. Denn, "Fifty years of non-Newtonian fluid dynamics," *AIChE Journal*, vol. 50, no. 10, pp. 2335–2345, 2004.
- [4] Y. Lok, N. Amin, and I. Pop, "Non-orthogonal stagnation point flow towards a stretching sheet," *International Journal of Non-linear Mechanics*, vol. 41, no. 4, pp. 622–627, 2006.
- [5] F. Labropulu, D. Li, and I. Pop, "Non-orthogonal stagnation-point flow towards a stretching surface in a non-Newtonian fluid with heat transfer," *International Journal of Thermal Sciences*, vol. 49, no. 6, pp. 1042–1050, 2010.
- [6] T. R. Mahapatra, S. K. Nandy, and A. S. Gupta, "Oblique stagnation-point flow and heat transfer towards a shrinking sheet with thermal radiation," *Meccanica*, vol. 47, no. 6, pp. 1325–1335, 2012.
- [7] M. A. Sadiq, A. U. Khan, S. Saleem, and S. Nadeem, "Numerical simulation of oscillatory oblique stagnation point flow of a magneto micropolar nanofluid," *RSC Advances*, vol. 9, no. 9, pp. 4751–4764, 2019.
- [8] R. Tabassum, R. Mehmood, O. Pourmehran, N. Akbar, and M. Gorji-Bandpy, "Impact of viscosity variation on oblique flow of Cu–H₂O nanofluid," *Proceedings of the Institution of Mechanical Engineers - Part E: Journal of Process Mechanical Engineering*, vol. 232, no. 5, pp. 622–631, 2018.
- [9] M. N. Sadiq, E. Mahmood, M. Sajid, and N. Ali, "Effects of lubrication on the steady oblique stagnation-point flow of a couple stress fluids," *Physics & Astronomy International Journal*, vol. 2, no. 4, pp. 389–397, 2018.
- [10] P. Pattnaik, M. M. Bhatti, S. R. Mishra, M. A. Abbas, and O. A. Bég, "Mixed convective-radiative dissipative magnetized micropolar nanofluid flow over a stretching surface in porous media with double stratification and chemical reaction effects: ADM-Padé computation," *Journal of Mathematics*, vol. 2022, Article ID 9888379, 19 pages, 2022.
- [11] R. Cortell, "Suction, viscous dissipation and thermal radiation effects on the flow and heat transfer of a power-law fluid past an infinite porous plate," *Chemical Engineering Research and Design*, vol. 89, no. 1, pp. 85–93, 2011.
- [12] Z. Uddin and M. Kumar, "Radiation effect on unsteady MHD heat and mass transfer flow on a moving inclined porous heated plate in presence of chemical reaction," *International Journal of Mathematical Modeling, Simulation and Applications*, vol. 3, no. 2, pp. 155–163, 2010.

- [13] W. Ibrahim and T. Anbessa, "Three-dimensional MHD mixed convection flow of casson nanofluid with Hall and ion slip effects," *Mathematical Problems in Engineering*, vol. 2020, Article ID 8656147, 15 pages, 2020.
- [14] M. V. Krishna, C. Sravanthi, and R. S. R. Gorla, "Hall and ion slip effects on MHD rotating flow of ciliary propulsion of microscopic organism through porous media," *International Communications in Heat and Mass Transfer*, vol. 112, Article ID 104500, 2020.
- [15] K. Rajakumar, K. Balamurugan, M. Umasankara Reddy, and C. V. Ramana Murthy, "Radiation, dissipation and Dufour effects on MHD free convection Casson fluid flow through a vertical oscillatory porous plate with ion-slip current," *International Journal of Heat and Technology*, vol. 36, no. 2, pp. 494–508, 2018.
- [16] S. J. Kumar and S. Vishwanath, "Hall and ion-slip effects on MHD free convective flow of a viscoelastic fluid through porous regime in an inclined channel with moving magnetic field," *Kragujevac Journal of Science*, vol. 42, pp. 5–18, 2020.
- [17] Z. Shah, S. Islam, H. Ayaz, and S. Khan, "Radiative heat and mass transfer analysis of micropolar nanofluid flow of Casson fluid between two rotating parallel plates with effects of Hall current," *Journal of Heat Transfer*, vol. 141, no. 2, 2019.
- [18] K. Ramesh and O. Ojjela, "Entropy generation analysis of natural convective chemically reacting squeezing flow of Casson fluid between parallel disks with Hall and Ion slip currents," *Heat Transfer - Asian Research*, vol. 48, no. 8, pp. 4320–4341, 2019.
- [19] C. RamReddy, O. Surender, and C. V. Rao, "Effects of Soret, Hall and Ion-slip on mixed convection in an electrically conducting Casson fluid in a vertical channel," *Nonlinear Engineering*, vol. 5, no. 3, pp. 167–175, 2016.
- [20] R. Vijayaragavan and S. Karthikeyan, "Hall current effect on chemically reacting MHD Casson fluid flow with dufour effect and thermal radiation," *Asian J Appl Sci Technol*, vol. 2, no. 2, pp. 228–245, 2018.
- [21] M. Abd El-Aziz and A. S. Yahya, "Perturbation analysis of unsteady boundary layer slip flow and heat transfer of Casson fluid past a vertical permeable plate with Hall current," *Applied Mathematics and Computation*, vol. 307, pp. 146–164, 2017.
- [22] W. Ibrahim and T. Anbessa, "Mixed convection flow of nanofluid with Hall and ion-slip effects using spectral relaxation method," *Journal of the Egyptian Mathematical Society*, vol. 27, no. 1, pp. 52–21, 2019.
- [23] M. Shojaefard, "Numerical investigation of flow control by suction and injection on a subsonic airfoil," *American Journal of Applied Sciences*, vol. 2, no. 10, 2005.
- [24] A. Braslow, *History of Suction-type Laminar-Flow Control with Emphasis on Flight Research: Monographs in Aerospace History*, NASA History, Washington, DC, USA, 1999.
- [25] A. Zeeshan and A. Majeed, "Heat transfer analysis of Jeffery fluid flow over a stretching sheet with suction/injection and magnetic dipole effect," *Alexandria Engineering Journal*, vol. 55, no. 3, pp. 2171–2181, 2016.
- [26] H. A. El-Arabawy, "Effect of suction/injection on the flow of a micropolar fluid past a continuously moving plate in the presence of radiation," *International Journal of Heat and Mass Transfer*, vol. 46, no. 8, pp. 1471–1477, 2003.
- [27] A. Chamkha, A. Aly, and M. Mansour, "Similarity solution for unsteady heat and mass transfer from a stretching surface embedded in a porous medium with suction/injection and chemical reaction effects," *Chemical Engineering Communications*, vol. 197, no. 6, pp. 846–858, 2010.
- [28] A. K. Pandey and M. Kumar, "Effect of viscous dissipation and suction/injection on MHD nanofluid flow over a wedge with porous medium and slip," *Alexandria Engineering Journal*, vol. 55, no. 4, pp. 3115–3123, 2016.
- [29] L. Rundora and O. Makinde, "Effects of suction/injection on unsteady reactive variable viscosity non-Newtonian fluid flow in a channel filled with porous medium and convective boundary conditions," *Journal of Petroleum Science and Engineering*, vol. 108, pp. 328–335, 2013.
- [30] N. A. Haroun, P. Sibanda, S. Mondal, and S. S. Motsa, "On unsteady MHD mixed convection in a nanofluid due to a stretching/shrinking surface with suction/injection using the spectral relaxation method," *Boundary Value Problems*, vol. 2015, no. 1, p. 24, 2015.
- [31] S. Hamrelaine, F. Mebarek-Oudina, and M. R. Sari, "Analysis of MHD Jeffery Hamel flow with suction/injection by homotopy analysis method," *J. Adv. Res. Fluid Mech. Therm. Sci.*, vol. 58, no. 2, pp. 173–186, 2019.
- [32] M. Ganapathirao, R. Ravindran, and I. Pop, "Non-uniform slot suction (injection) on an unsteady mixed convection flow over a wedge with chemical reaction and heat generation or absorption," *International Journal of Heat and Mass Transfer*, vol. 67, pp. 1054–1061, 2013.
- [33] R. Tabassum and R. Mehmood, "Crosswise stream of methanol-iron oxide ($\text{CH}_3\text{OH}-\text{Fe}_3\text{O}_4$) with temperature-dependent viscosity and suction/injection effects," *Proceedings of the Institution of Mechanical Engineers - Part E: Journal of Process Mechanical Engineering*, vol. 233, no. 5, pp. 1013–1023, 2019.
- [34] S. Abo-Dahab, M. A. Abdelhafez, F. Mebarek-Oudina, and S. M. Bilal, "MHD casson nanofluid flow over nonlinearly heated porous medium in presence of extending surface effect with suction/injection," *Indian Journal of Physics*, vol. 95, no. 12, pp. 2703–2717, 2021.
- [35] A. K. Pandey and M. Kumar, "Squeezing unsteady MHD Cu-water nanofluid flow between two parallel plates in porous medium with suction/injection," *Computational and Applied Mathematics Journal*, vol. 4, no. 2, pp. 31–42, 2018.
- [36] B. K. Jha, B. Aina, and S. Muhammad, "Combined effects of suction/injection and wall surface curvature on natural convection flow in a vertical micro-porous annulus," *Thermophysics and Aeromechanics*, vol. 22, no. 2, pp. 217–228, 2015.
- [37] S. Rana, R. Mehmood, and N. S. Akbar, "Mixed convective oblique flow of a Casson fluid with partial slip, internal heating and homogeneous-heterogeneous reactions," *Journal of Molecular Liquids*, vol. 222, pp. 1010–1019, 2016.
- [38] R. Mehmood, S. Rana, N. Akbar, and S. Nadeem, "Non-aligned stagnation point flow of radiating Casson fluid over a stretching surface," *Alexandria Engineering Journal*, vol. 57, no. 2, pp. 939–946, 2018.
- [39] K. Mahmud, S. Rana, A. Al-Zubaidi, R. Mehmood, and S. Saleem, "Interaction of Lorentz force with cross swimming microbes in couple stress nano fluid past a porous Riga plate,"

International Communications in Heat and Mass Transfer, vol. 138, Article ID 106347, 2022.

- [40] O. D. Makinde and A. Aziz, "Boundary layer flow of a nanofluid past a stretching sheet with a convective boundary condition," *International Journal of Thermal Sciences*, vol. 50, no. 7, pp. 1326–1332, 2011.
- [41] W. Khan and I. Pop, "Boundary-layer flow of a nanofluid past a stretching sheet," *International Journal of Heat and Mass Transfer*, vol. 53, no. 11-12, pp. 2477–2483, 2010.
- [42] C. Wang, "Free convection on a vertical stretching surface," *ZAMM-Journal of Applied Mathematics and Mechanics/Zeitschrift für Angewandte Mathematik und Mechanik*, vol. 69, no. 11, pp. 418–420, 1989.

Research Article

New Existence and Stability Results for $[\psi, \omega]$ -Caputo–Fabrizio Fractional Nonlocal Implicit Problems

Mohammed S. Abdo ¹, Wafa Shammakh ², and Hadeel Z. Alzumi ²

¹Department of Mathematics, Hodeidah University, Al Hudaydah, Yemen

²University of Jeddah, Faculty of Science, Department of Mathematics, Jeddah, Saudi Arabia

Correspondence should be addressed to Mohammed S. Abdo; msabdo@hoduniv.net.ye

Received 21 September 2022; Revised 26 October 2022; Accepted 24 November 2022; Published 1 March 2023

Academic Editor: Watcharaporn Cholamjiak

Copyright © 2023 Mohammed S. Abdo et al. This is an open access article distributed under the Creative Commons Attribution License, which permits unrestricted use, distribution, and reproduction in any medium, provided the original work is properly cited.

In the context of ψ -weighted Caputo–Fabrizio fractional derivatives, we develop and extend the existence and Ulam–Hyers stability results for nonlocal implicit differential equations. The fixed-point theorems due to Banach and Krasnoselskii are the foundation for the proof of existence and uniqueness results. Additionally, the Ulam–Hyers stability demonstrates the assurance of the existence of solutions via Gronwal inequality. Also, we offer an example as an application to explain and validate the acquired results. Finally, in terms of our outcome, we designate a more general problem for the $[\psi, \omega]$ -Caputo–Fabrizio fractional system that includes analogous problems to the problem at hand.

1. Introduction

It is noteworthy that fractional calculus (FC) has received considerable attention from researchers due to its wide variety of applications in several scientific domains. The significant concepts and definitions of FC have been introduced by Osler [1] and Kilbas et al. [2]. Samko et al. [3] and Diethelm and Ford [4] provided some basic history of FC and its applications in engineering and various fields of science.

Many classes of fractional differential equations (FDEs) have been extensively investigated and analyzed in the past decades; for instance, theories involving the existence of unique solutions have been notarized in [5–7] and references therein. Numerical and analytical methods are developed with the aim of solving such equations then tracked as useful in modeling some real-world problems, as shown in [8–10].

The qualitative properties of solutions address an indispensable piece of the theory of FDEs. The beforehand previously mentioned district has been investigated well for classical DEs. Regardless, for FDEs, there are various aspects and viewpoints that require further investigation and

analysis. The existence and uniqueness have been intensively studied by using Riemann–Liouville (R-L), Caputo, Hilfer, and other FDs, as shown in [11–16] and references therein.

Generalized FDs and integrals and their applications were discussed by several authors. For example, Kilbas et al. [2] introduced some nice properties of ψ -Reiman–Liouville FD. The ψ -Caputo FD has been defined by Almedia [17]. Then, Sousa and Oliveira proposed another generalization in the Hilfer sense [18].

In the previously mentioned derivatives, there exists a singular kernel. In this manner, as of late, some authors presented some new kinds of FDs in which they have supplanted a singular kernel with a nonsingular kernel, as shown in [19–21]. The nonlocal FDs with nonsingular kernels have been demonstrated as a decent tool to model real-world problems in various areas of engineering and science, as shown in [22–25].

On the other hand, Jarad et al. [26] introduced the concept of weighted FDs. Some recent papers dealt with the theory of existence and Ulam–Hyers (UH) (and Generalized Ulam–Hyers (GUH)) stability of different types of FDEs due to their importance in many areas of exploration; for

instance, Shaikh et al. [27] established the existence and uniqueness results of the following CF-type Cauchy problem:

$$\{ {}^{CF}\mathbb{D}_{0^+}^\vartheta v(x) = f(x, v(x)), x \in [0, 1], 0 < \vartheta < 1, v(0) = v_0. \quad (1)$$

The existence and UH stability results in the following CF fractional implicit equation:

$${}^{CF}\mathbb{D}_{0^+}^\vartheta v(x) = f(x, v(x), {}^{CF}\mathbb{D}_{0^+}^\vartheta v(x)), x \in [0, T], 0 < \vartheta < 1. \quad (2)$$

$v(0) = v_0$ and $av(0) + av(T) = c$ were investigated by Abbas et al. [28] in b-metric spaces and by Salim et al. [29] in Banach spaces, respectively. The equation (2) with $0 < \vartheta \leq 2$ was considered by Gul et al. [30].

On the other hand, Abdo et al. [31], considered the following weighted Caputo problem:

$$\{ {}^C\mathbb{D}_{0^+}^{\vartheta; \psi, w} \rho(x) = \varphi(x, \rho(x)), 0 < \vartheta \leq 1, \rho(0) = \rho_0. \quad (3)$$

In this regard, Al-Refai and Jarrah [32], introduced the concept of the $[\psi, w]$ -Caputo–Fabrizio FD, where $\psi(x)$ is a monotone function and $w(x)$ is a weight function. They also obtained the uniqueness result of the Cauchy problem. Motivated by studies [31, 32], we consider the following weighted implicit nonlocal FDE:

$$\{ {}^{CF}\mathbb{D}_{a;w}^\mu \rho(x) = \varphi(x, \rho(x), {}^{CF}\mathbb{D}_{a;w}^\mu \rho(x)), \rho(a) = c + g(\rho), \quad (4)$$

and the following $[\psi, w]$ type implicit nonlocal FDE:

$$\{ {}^{CF}\mathbb{D}_{a;w}^{\mu; \psi} \rho(x) = \varphi(x, \rho(x), {}^{CF}\mathbb{D}_{a;w}^{\mu; \psi} \rho(x)), \rho(a) = c + g(\rho), \quad (5)$$

where $0 < \mu < 1$, $x \in \mathcal{O}: = [a, b]$, $c \in \mathbb{R}$, $g \in C(\mathcal{O})$, $\varphi: \mathcal{O} \times \mathbb{R} \times \mathbb{R} \rightarrow \mathbb{R}$ is a given function, and ${}^{CF}\mathbb{D}_{a;w}^{\mu; \psi}$ is a $[\psi, w]$ -Caputo–Fabrizio FD, and $w, \psi \in C^1(\mathcal{O})$ with $w, w', \psi > 0$ on \mathcal{O} .

We pay attention to the topic of the novel weighted operators with another function. As far as we are aware, no studies using the $[\psi, w]$ -Caputo–Fabrizio FDs have been published that address the qualitative aspects of the aforementioned problems. Consequently, to enhance and enrich the literature on this new trend, which is extremely restricted right now, we develop and extend the existence, and Ulam–Hyers stability results for problems (4) and (5) based on Banach’s fixed point theorem, Krasnoselskii’s fixed point theorem, and Gronwal inequality. Besides, we also give a more general problem as a system, that covers the problems at hand.

Remark 1

- (i) If $\psi(x) = x$, then problem (5) reduces to problem (4)
- (ii) If $\psi(x) = x$, $w = 1$, and $g \equiv 0$, then problem (5) reduces to the implicit problem (2), as shown in [28, 29]
- (iii) If $\psi(x) = x$, $w = 1$, and $g \equiv 0$, then problem (5) reduces to the Cauchy problem (1) without implicit term, as shown in [27]

- (iv) Our current results for the problem (5) stay available on problem (4)
- (v) With different values of ψ , our current problems cover many problems associated with less general operators; for instance, the operator presented by Caputo and Fabrizio [19]

The accessories of this paper are arranged as follows: Section 2 gives some fundamental results about advanced FC. Our key findings for the problems (4) and (5) are obtained in Section 3. A comprehensive example that verifies the validity of the theories is provided in Section 4. Section 5 includes the conclusions of the work.

2. Primitive Results

In this section, we begin by giving some notations and basic nomenclature. Let $\mathcal{O}: = [a, b]$, $a < b < \infty$, and \mathbb{R} be the set of real numbers. $C[a, b]$ and $AC[a, b]$ denote the set of continuous and absolutely continuous functions, respectively, on \mathcal{O} , endowed with the usual supremum norm. Let $\psi(x)$ and $w(x)$ be the monotone and weight function, respectively, with $w, \psi \in C^1(\mathcal{O})$ and $w, w', \psi' > 0$ on \mathcal{O} .

Definition 1 (see [32]). Let $0 < \vartheta < 1$, and $\rho \in AC[\mathcal{O}, \mathbb{R}]$. The left $[\psi, w]$ -Caputo–Fabrizio FD is defined as

$${}^{CF}\mathbb{D}_{a;w}^{\mu; \psi} \rho(x) = \frac{\aleph(\mu)}{1 - \mu} \frac{1}{w(x)} \int_a^x e^{-\lambda_\mu(\psi(x) - \psi(\zeta))} \frac{d}{d\zeta} (w\rho)(\zeta) d\zeta, \quad (6)$$

where $\lambda_\mu = \mu/1 - \mu$, and $\aleph(\mu)$ is a normalization function satisfying $\aleph(0) = \aleph(1) = 1$.

The previous operator can be written as

$${}^{CF}\mathbb{D}_{a;w}^{\mu; \psi} \rho(x) = \frac{\aleph(\mu)}{1 - \mu} \frac{e^{-\lambda_\mu \psi(x)}}{w(x)} \int_a^x e^{\lambda_\mu \psi(\zeta)} \frac{d}{d\zeta} (w\rho)(\zeta) d\zeta. \quad (7)$$

Definition 2 (see [32]). Let $0 < \vartheta < 1$, and $\rho \in AC[\mathcal{O}, \mathbb{R}]$. The left $[\psi, w]$ -Caputo–Fabrizio FI is defined as

$${}^{CF}\mathbb{I}_{a;w}^{\mu; \psi} \rho(x) = \frac{1 - \mu}{\aleph(\mu)} \rho(x) + \frac{\mu}{\aleph(\mu)} \frac{1}{w(x)} \int_a^x \psi'(\zeta) w(\zeta) \rho(\zeta) d\zeta. \quad (8)$$

Lemma 1 (see [32]). *Let $\rho \in AC[\mathcal{O}, \mathbb{R}]$. Then,*

$$\begin{aligned} {}^{CF}\mathbb{D}_{a;w}^{\mu; \psi} {}^{CF}\mathbb{I}_{a;w}^{\mu; \psi} \rho(x) &= \rho(x), \\ {}^{CF}\mathbb{D}_{a;w}^{\mu; \psi} {}^{CF}\mathbb{I}_{a;w}^{\mu; \psi} \rho(x) &= \rho(x) - \frac{w(a)\rho(a)}{w(x)}. \end{aligned} \quad (9)$$

In particular, if $\rho(a) = 0$, we have ${}^{CF}\mathbb{D}_{a;w}^{\mu; \psi} {}^{CF}\mathbb{I}_{a;w}^{\mu; \psi} \rho(x) = \rho(x)$.

Lemma 2 (see [32]). *Let $0 < \vartheta < 1$, and $\rho \in AC[\mathcal{O}, \mathbb{R}]$ with $f(a) = 0$. Then, the following FDE:*

$$\begin{aligned} {}^{CF}\mathbb{D}_{a;w}^{\mu; \psi} {}^{CF}\mathbb{I}_{a;w}^{\mu; \psi} \rho(x) &= f(x), \\ \rho(a) &= c, \end{aligned} \quad (10)$$

has the unique solution

$$\rho(x) = \frac{w(a)}{w(x)}c + \frac{1-\mu}{\aleph(\mu)}f(x) + \frac{\mu}{\aleph(\mu)}\frac{1}{w(x)}\int_a^x \psi'(\zeta)w(\zeta)f(\zeta)d\zeta, x \in \mathcal{O}. \tag{11}$$

For our forthcoming analysis, we need Banach’s contraction map [33] and Krasnoselskii’s fixed point theorem [34].

Lemma 3 (Gronwall’s Lemma [35]). *Let $a, b > 0$, and $d \geq 0$. Let’s assume that functions $z, y: \mathcal{O} \rightarrow \mathbb{R}^+$ are continuous if*

$$z(x) \leq d + \int_a^x y(\zeta)z(\zeta)d\zeta, \forall x \in \mathcal{O}. \tag{12}$$

Then,

$$z(x) \leq d \exp\left(\int_a^x y(\zeta)d\zeta\right), \forall x \in \mathcal{O}. \tag{13}$$

3. Main Results

In this section, we give some qualitative analyses of $[\psi, w]$ -Caputo–Fabrizio type problems (4) and (5).

Lemma 4. *Let $0 < \vartheta < 1$, $\rho \in AC[\mathcal{O}, \mathbb{R}]$ and $g \in C[\mathcal{O}, \mathbb{R}]$ be continuous with $f(a) = 0$. Then, the following ψ -weighted FDE:*

$$\left\{ \begin{aligned} {}^{CF}\mathbb{D}_{a;w}^{\mu;\psi}\rho(x) &= f(x), x \in \mathcal{O}, \rho(a) = c + g(\rho), \end{aligned} \right. \tag{14}$$

has the unique solution

$$\begin{aligned} \rho(x) &= \frac{w(a)}{w(x)}[c + g(\rho)] + a_\mu f(x) \\ &+ \frac{b_\mu}{w(x)}\int_a^x \psi'(\zeta)w(\zeta)f(\zeta)d\zeta, x \in \mathcal{O}, \end{aligned} \tag{15}$$

where $a_\mu = 1 - \mu/\aleph(\mu)$, and $b_\mu = \mu/\aleph(\mu)$.

Proof. Let’s assume that ρ satisfies the first equation of (14). From Corollary 2.1 in [32], the equation ${}^{CF}\mathbb{D}_{a;w}^{\mu;\psi}\rho(x) = f(x)$ implies that

$$\rho(x) = \frac{w(a)\rho(a)}{w(x)} + a_\mu f(x) + \frac{b_\mu}{w(x)}\int_a^x \psi'(\zeta)w(\zeta)f(\zeta)d\zeta. \tag{16}$$

So, by the nonlocal condition $\rho(a) = c + g(\rho)$, we obtain

$$\begin{aligned} \rho(x) &= \frac{w(a)}{w(x)}[c + g(\rho)] + a_\mu f(x) \\ &+ \frac{b_\mu}{w(x)}\int_a^x \psi'(\zeta)w(\zeta)f(\zeta)d\zeta, \end{aligned} \tag{17}$$

which is (15).

Conversely, if ρ satisfies (15), then by Lemma 1, we have

$$\begin{aligned} {}^{CF}\mathbb{D}_{a;w}^{\mu;\psi}\rho(x) &= {}^{CF}\mathbb{D}_{a;w}^{\mu;\psi}\left(\frac{w(a)}{w(x)}[c + g(\rho)]\right) + {}^{CF}\mathbb{D}_{a;w}^{\mu;\psi}\left(a_\mu f(x) + \frac{b_\mu}{w(x)}\int_a^x \psi'(\zeta)w(\zeta)f(\zeta)d\zeta\right) \\ &= {}^{CF}\mathbb{I}_{a;w}^{\mu;\psi}{}^{CF}\mathbb{D}_{a;w}^{\mu;\psi}f(x) \\ &= f(x), \end{aligned} \tag{18}$$

where ${}^{CF}\mathbb{D}_{a;w}^{\mu;\psi}(w(a)/w(x)[c + g(\rho)])(x) = 0$. Moreover, $\rho(a) = c + g(\rho)$. \square

Hence, we can deduce the next corollary:

Corollary 1. *Let $0 < \vartheta < 1$, $\varphi \in AC[\mathcal{O}, \mathbb{R}]$ and $g \in C[\mathcal{O}, \mathbb{R}]$ with $\varphi_\rho(0) = 0$. Then, the problem (5) is equivalent to*

$$\begin{aligned} \rho(x) &= \frac{w(a)}{w(x)}[c + g(\rho)] + a_\mu \varphi_\rho(x) \\ &+ \frac{b_\mu}{w(x)}\int_a^x \psi'(\zeta)w(\zeta)\varphi_\rho(\zeta)d\zeta, x \in \mathcal{O}, \end{aligned} \tag{19}$$

where $\varphi_\rho \in C[\mathcal{O}, \mathbb{R}]$ with $\varphi_\rho(x) := \varphi(x, \rho(x), \varphi_\rho(x))$.

We define the operator $\mathcal{K}: AC[\mathcal{O}, \mathbb{R}] \rightarrow AC[\mathcal{O}, \mathbb{R}]$ by

$$\begin{aligned} (\mathcal{K}\rho)(x) &= \frac{w(a)}{w(x)}[c + g(\rho)] + a_\mu \varphi_\rho(x) \\ &+ \frac{b_\mu}{w(x)}\int_a^x \psi'(\zeta)w(\zeta)\varphi_\rho(\zeta)d\zeta, x \in \mathcal{O}. \end{aligned} \tag{20}$$

Then, the fixed point of operator \mathcal{K} is equivalent to the solution of the $[\psi, w]$ -type problem (5).

The first result is based on Banach FPT [33].

Theorem 1. *assume that:*

(Hy₁): There exists $L_\varphi, M_\varphi > 0$ such that

$$|\varphi(x, v, \omega) - \varphi(x, \bar{v}, \bar{\omega})| \leq L_\varphi|v - \bar{v}| + M_\varphi|\omega - \bar{\omega}|, \tag{21}$$

for each $x \in \mathcal{O}$, $v, \omega, \bar{v}, \bar{\omega} \in \mathbb{R}$.

(Hy₂): There exists $L_g > 0$ such that $0 < L_g < 1$ and $|g(v) - g(\omega)| \leq L_g |v - \omega|$, for $v, \omega \in C[\mathcal{O}, \mathbb{R}]$.

If

$$L_g + \left[a_\mu + b_\mu \frac{w(b)}{w(a)} [\psi(b) - \psi(a)] \right] \frac{L_\varphi}{1 - M_\varphi} < 1. \quad (22)$$

Then, the $[\psi, w]$ -type problem (5) has a unique solution on $AC[\mathcal{O}, \mathbb{R}]$.

Proof. Let $\varphi_\rho(x) = \varphi(x, \rho(x), \varphi_\rho(x))$ and $\varphi_{\bar{\rho}}(x) = \varphi(x, \bar{\rho}(x), \varphi_{\bar{\rho}}(x))$. Then, by (Hy₁), we have

$$|\varphi_\rho(x) - \varphi_{\bar{\rho}}(x)| = |\varphi(x, \rho(x), \varphi_\rho(x)) - \varphi(x, \bar{\rho}(x), \varphi_{\bar{\rho}}(x))| \leq L_\varphi |\rho(x) - \bar{\rho}(x)| + M_\varphi |\varphi_\rho(x) - \varphi_{\bar{\rho}}(x)|, \quad (23)$$

which implies

$$\begin{aligned} |(\mathcal{K}\rho)(x) - (\mathcal{K}\bar{\rho})(x)| &\leq \sup_{x \in \mathcal{O}} \left\{ \frac{w(a)}{w(x)} |g(\rho) - g(\bar{\rho})| + a_\mu |\varphi_\rho(x) - \varphi_{\bar{\rho}}(x)| + \frac{b_\mu}{w(x)} \int_a^x \psi'(\zeta) w(\zeta) |\varphi_\rho(\zeta) - \varphi_{\bar{\rho}}(\zeta)| d\zeta \right\} \\ &\leq L_g \|\rho - \bar{\rho}\| + a_\mu \frac{L_\varphi}{1 - M_\varphi} \|\rho - \bar{\rho}\| + \frac{L_\varphi}{1 - M_\varphi} \|\rho - \bar{\rho}\| \frac{w(b)}{w(a)} b_\mu [\psi(b) - \psi(a)] \\ &= \left[L_g + \left(a_\mu + \frac{w(b)}{w(a)} b_\mu [\psi(b) - \psi(a)] \right) \frac{L_\varphi}{1 - M_\varphi} \right] \|\rho - \bar{\rho}\|. \end{aligned} \quad (27)$$

As the condition (22), \mathcal{K} is a contraction and by the Banach's fixed point theorem, \mathcal{K} has a unique fixed point which is unique solution of (5). \square

Next, we give existence results based on the Krasnoselskii fixed point theorem [34].

Theorem 2. Let $\varphi: \mathcal{O} \times \mathbb{R} \times \mathbb{R} \rightarrow \mathbb{R}$, and $g: C[\mathcal{O}, \mathbb{R}] \rightarrow \mathbb{R}$ be continuous satisfying (Hy₁) and (Hy₂). In addition, we assume that

(Hy₃): There exist constants $n_\varphi, m_\varphi, s_\varphi > 0$ with $0 < s_\varphi < 1$ such that

$$|\varphi(x, \rho_1, \rho_2)| \leq n_\varphi + m_\varphi |\rho_1| + s_\varphi |\rho_2|, \quad (28)$$

for each $x \in \mathcal{O}$, $\rho_1, \rho_2 \in \mathbb{R}$.

(Hy₄): $|g(\rho)| \leq \mu_g |\rho|$, for $\rho \in C[\mathcal{O}, \mathbb{R}]$, and $\mu_g > 0$.

Then, the $[\psi, w]$ -type problem (5) has a least one solution if

$$\mu_g + \left[a_\mu + \frac{w(b)}{w(a)} b_\mu [\psi(b) - \psi(a)] \right] \frac{m_\varphi}{1 - s_\varphi} < 1. \quad (29)$$

$$|\varphi_\rho(x) - \varphi_{\bar{\rho}}(x)| \leq \frac{L_\varphi}{1 - M_\varphi} |\rho(x) - \bar{\rho}(x)|. \quad (24)$$

Since $\psi', w > 0$, and applying the mean value theorem for integrals, we obtain

$$\int_a^x \psi'(\zeta) w(\zeta) d\zeta = w(\kappa) \int_a^x \psi'(\zeta) d\zeta = w(\kappa) [\psi(x) - \psi(a)], \quad (25)$$

for some $a < \kappa < b$, then

$$\int_a^x \psi'(\zeta) w(\zeta) d\zeta \leq w(b) [\psi(b) - \psi(a)]. \quad (26)$$

We suppose $\rho(x), \bar{\rho}(x) \in AC[\mathcal{O}, \mathbb{R}]$, we have from (Hy₂), (24), and (26) that

Proof. From (20), we define the operators $\mathcal{K}_1, \mathcal{K}_2: AC[\mathcal{O}, \mathbb{R}] \rightarrow AC[\mathcal{O}, \mathbb{R}]$ by

$$(\mathcal{K}_1\rho)(x) = \frac{w(a)}{w(x)} [c + g(\rho)] + a_\mu \varphi_\rho(x), \quad x \in \mathcal{O}, \quad (30)$$

and

$$(\mathcal{K}_2\rho)(x) = \frac{b_\mu}{w(x)} \int_a^x \psi'(\zeta) w(\zeta) \varphi_\rho(\zeta) d\zeta, \quad x \in \mathcal{O}, \quad (31)$$

where $(\mathcal{K}_1\rho + \mathcal{K}_2\rho)(x) = (\mathcal{K}\rho)(x)$. Let us define $\mathcal{F}_r = \{\rho \in AC[\mathcal{O}, \mathbb{R}]: \|\rho\| \leq r\}$. We choose

$$r \geq \frac{|c| + (a_\mu + w(b)/w(a) b_\mu [\psi(b) - \psi(a)]) n_\varphi / 1 - s_\varphi}{1 - \mu_g + [a_\mu + w(b)/w(a) b_\mu [\psi(b) - \psi(a)]] m_\varphi / 1 - s_\varphi}. \quad (32)$$

For $\varphi_\rho(\zeta) = \varphi(\zeta, \rho(\zeta), \varphi_\rho(\zeta))$, we use assumption (Hy₃) to get

$$\begin{aligned} |\varphi_\rho(\zeta)| &= |\varphi(\zeta, \rho(\zeta), \varphi_\rho(\zeta))| \\ &\leq n_\varphi + m_\varphi |\rho(\zeta)| + s_\varphi |\varphi_\rho(\zeta)|, \end{aligned} \quad (33)$$

which implies

$$|\varphi_\rho(\zeta)| \leq \frac{n_\varphi + m_\varphi |\rho(\zeta)|}{1 - s_\varphi}. \tag{34}$$

For any $\rho, \rho^* \in \mathcal{F}_r$, we have

$$\begin{aligned} |(\mathcal{K}_1\rho + \mathcal{K}_2\rho^*)(\kappa)| &\leq |(\mathcal{K}_1\rho)(\kappa)| + |(\mathcal{K}_2\rho^*)(\kappa)| \\ &\leq \sup_{\kappa \in \bar{\mathcal{O}}} \left\{ \frac{w(a)}{w(\kappa)} [c + |g(\rho)|] + a_\mu |\varphi_\rho(\kappa)| \right\} \\ &\quad + \sup_{\kappa \in \bar{\mathcal{O}}} \left\{ \frac{b_\mu}{w(\kappa)} \int_a^\kappa \psi'(\zeta) w(\zeta) |\varphi_{\rho^*}(\zeta)| d\zeta \right\} \\ &\leq |c| + \mu_g \|\rho\| + a_\mu \frac{n_\varphi + m_\varphi \|\rho\|}{1 - s_\varphi} + \frac{n_\varphi + m_\varphi \|\rho^*\|}{1 - s_\varphi} \frac{w(b)}{w(a)} b_\mu [\psi(b) - \psi(a)] \\ &\leq \left(\mu_g + \left[a_\mu + \frac{w(b)}{w(a)} b_\mu [\psi(b) - \psi(a)] \right] \frac{m_\varphi}{1 - s_\varphi} \right) r + |c| + \left(a_\mu + \frac{w(b)}{w(a)} b_\mu [\psi(b) - \psi(a)] \right) \frac{n_\varphi}{1 - s_\varphi} \leq r. \end{aligned} \tag{35}$$

Due to (29), we deduce that $\|\mathcal{K}_1\rho + \mathcal{K}_2\rho^*\| \leq r$.

Since φ and g are continuous, we show that \mathcal{K}_1 is a contraction operator. For each $\rho(\kappa), \sigma(\kappa) \in AC[\bar{\mathcal{O}}, \mathbb{R}]$, and for any $\kappa \in \bar{\mathcal{O}}$, we have

$$\begin{aligned} &|\mathcal{K}_1\rho(\kappa) - \mathcal{K}_1\sigma(\kappa)| \\ &\leq \sup_{\kappa \in \bar{\mathcal{O}}} \left\{ \frac{w(a)}{w(\kappa)} [|g(\rho) - g(\sigma)|] + a_\mu |\varphi_\rho(\kappa) - \varphi_\sigma(\kappa)| \right\} \\ &\leq L_g \|\rho - \sigma\| + \frac{a_\mu L_\varphi}{1 - M_\varphi} \|\rho - \sigma\|. \end{aligned} \tag{36}$$

Hence,

$$\|\mathcal{K}_1\rho - \mathcal{K}_1\sigma\| \leq \left(L_g + \frac{a_\mu L_\varphi}{1 - M_\varphi} \right) \|\rho - \sigma\|. \tag{37}$$

From (22), $L_g + a_\mu L_\varphi / 1 - M_\varphi < 1$. So, \mathcal{K}_1 is a contraction.

Next, to prove that \mathcal{K}_2 is a compact and continuous operator, we provide the following steps:

Step 1: \mathcal{K}_2 is continuous. Let $\{\rho_n\}_{n \geq 1}$ be in \mathcal{B}_r such that $\rho_n \rightarrow \rho$ in \mathcal{B}_r . Then, $|\mathcal{K}_2\rho_n(\kappa) - \mathcal{K}_2\rho(\kappa)| \rightarrow 0$, as $n \rightarrow \infty$, due to continuity of φ, ψ and w .

Step 2: \mathcal{K}_2 is uniformly bounded. By (31) we have

$$\begin{aligned} |\mathcal{K}_2\rho(\kappa)| &\leq \sup_{\kappa \in \bar{\mathcal{O}}} |(\mathcal{K}_2\rho)(\kappa)| \\ &\leq \sup_{\kappa \in \bar{\mathcal{O}}} \left\{ \frac{b_\mu}{w(\kappa)} \int_a^\kappa \psi'(\zeta) w(\zeta) |\varphi_\rho(\zeta)| d\zeta \right\}. \end{aligned} \tag{38}$$

From (26) and (34), and for any $\rho \in \mathcal{F}_r$, (38) becomes

$$\begin{aligned} |\mathcal{K}_2\rho(\kappa)| &\leq \sup_{\kappa \in \bar{\mathcal{O}}} \left\{ \frac{b_\mu}{w(\kappa)} \int_a^\kappa \psi'(\zeta) w(\zeta) \frac{n_\varphi + m_\varphi |\rho(\zeta)|}{1 - s_\varphi} d\zeta \right\} \\ &\leq \frac{n_\varphi + m_\varphi \|\rho\|}{1 - s_\varphi} b_\mu \frac{w(b)}{w(a)} [\psi(b) - \psi(a)] \\ &\leq \frac{(n_\varphi + m_\varphi r) b_\mu}{1 - s_\varphi} \frac{w(b)}{w(a)} [\psi(b) - \psi(a)] \leq r^*. \end{aligned} \tag{39}$$

Thus, \mathcal{K}_2 is uniformly bounded on \mathcal{F}_r .

Step 3: \mathcal{K}_2 is compact. Let $\rho \in \mathcal{F}_r$, and $\kappa \in \bar{\mathcal{O}}$ with $\kappa_\epsilon < \kappa_\delta \in \bar{\mathcal{O}}$. Then,

$$\begin{aligned}
 & |(\mathcal{K}_2\rho)(\kappa_\delta) - (\mathcal{K}_2\rho)(\kappa_\epsilon)| \\
 & \leq \left| \frac{b_\mu}{w(\kappa_\delta)} \int_a^{\kappa_\delta} \psi'(\zeta)w(\zeta)\varphi_\rho(\zeta)d\zeta - \frac{b_\mu}{w(\kappa_\epsilon)} \int_a^{\kappa_\epsilon} \psi'(\zeta)w(\zeta)\varphi_\rho(\zeta)d\zeta \right| \\
 & \leq \left| \frac{b_\mu}{w(\kappa_\delta)} - \frac{b_\mu}{w(\kappa_\epsilon)} \right| \int_a^{\kappa_\delta} \psi'(\zeta)w(\zeta)|\varphi_\rho(\zeta)|d\zeta \\
 & \quad + \frac{b_\mu}{w(\kappa_\epsilon)} \int_{\kappa_\epsilon}^{\kappa_\delta} \psi'(\zeta)w(\zeta)|\varphi_\rho(\zeta)|d\zeta \\
 & \leq b_\mu|w(\kappa_\delta) - w(\kappa_\epsilon)| \int_a^{\kappa_\delta} \psi'(\zeta)w(\zeta)|\varphi_\rho(\zeta)|d\zeta \\
 & \quad + \frac{b_\mu}{w(\kappa_\epsilon)} \int_{\kappa_\epsilon}^{\kappa_\delta} \psi'(\zeta)w(\zeta)|\varphi_\rho(\zeta)|d\zeta \\
 & \leq |w(\kappa_\delta) - w(\kappa_\epsilon)| \frac{(n_\varphi + m_\varphi r)b_\mu}{1 - s_\varphi} w(\kappa_\epsilon) [\psi(\kappa_\epsilon) - \psi(a)] \\
 & \quad + \frac{(n_\varphi + m_\varphi r)b_\mu}{1 - s_\varphi} \frac{w(\kappa_\delta)}{w(\kappa_\epsilon)} [\psi(\kappa_\delta) - \psi(\kappa_\epsilon)].
 \end{aligned} \tag{40}$$

Since

$$\begin{aligned}
 \int_{\kappa_\epsilon}^{\kappa_\delta} \psi'(\zeta)w(\zeta)d\zeta & \leq w(\kappa_\delta) [\psi(\kappa_\delta) - \psi(\kappa_\epsilon)], \\
 \int_a^{\kappa_\epsilon} \psi'(\zeta)w(\zeta)d\zeta & \leq w(\kappa_\epsilon) [\psi(\kappa_\epsilon) - \psi(a)],
 \end{aligned} \tag{41}$$

due to mean value theorem for integrals. Consequently, (40) gives

$$|(\mathcal{K}_2\rho)(\kappa_\delta) - (\mathcal{K}_2\rho)(\kappa_\epsilon)| \longrightarrow 0, \text{ as } \kappa_\delta - \kappa_\epsilon \longrightarrow 0. \tag{42}$$

Thus, \mathcal{K}_2 is equicontinuous on \mathcal{F}_r . As per preceding steps, \mathcal{K}_2 is relatively compact on \mathcal{F}_r , and by the Arzela–Ascoli theorem, \mathcal{K}_2 has at least one fixed point. By virtue of Krasnoselskii’s theorem [34], the ψ -weighted problem (5) has a least one solution. \square

3.1. UH Stability Analysis. In this section, we give the UH stability and generalized UH stability results for the ψ -weighted problem (5).

Definition 3. (5) is UH stable if there exists a $\chi_\varphi > 0$ such that for each $\epsilon > 0$ and each solution $\sigma \in AC[\mathcal{O}, \mathbb{R}]$ of the inequality

$$\left| {}^{CF}\mathbb{D}_{a;w}^{\mu;\psi}\sigma(\kappa) - \varphi(\kappa, \sigma(\kappa), {}^{CF}\mathbb{D}_{a;w}^{\mu;\psi}\sigma(\kappa)) \right| \leq \epsilon, \kappa \in \mathcal{O}, \tag{43}$$

there exists a solution $\rho \in AC[\mathcal{O}, \mathbb{R}]$ of (5), satisfying

$$|\sigma(\kappa) - \rho(\kappa)| \leq \chi_\varphi \epsilon. \tag{44}$$

Remark 2. $\sigma \in AC[\mathcal{O}, \mathbb{R}]$ satisfies (44) if and only if there exists $\omega \in AC[\mathcal{O}, \mathbb{R}]$ with

- (i) $|\omega(\kappa)| \leq \epsilon, \kappa \in \mathcal{O}$,
- (ii) For all $\kappa \in \mathcal{O}$,

$${}^{CF}\mathbb{D}_{a;w}^{\mu;\psi}\sigma(\kappa) = \varphi(\kappa, \sigma(\kappa), {}^{CF}\mathbb{D}_{a;w}^{\mu;\psi}\sigma(\kappa)) + \omega(\kappa). \tag{45}$$

Lemma 5. Let $0 < \mu < 1$, and $\sigma \in AC[\mathcal{O}, \mathbb{R}]$ be a solution of (43). Then, σ satisfies

$$\left| \sigma(\kappa) - \mathcal{A}_\sigma(\kappa) - \frac{b_\mu}{w(\kappa)} \int_a^\kappa \psi'(\zeta)w(\zeta)\varphi_\sigma(\zeta)d\zeta \right| \leq \epsilon b_\mu \frac{w(b)}{w(a)} [\psi(b) - \psi(a)], \kappa \in \mathcal{O}, \tag{46}$$

where

$$\mathcal{A}_\sigma(\kappa) := \frac{w(a)}{w(\kappa)} [c + g(\sigma)] + a_\mu \varphi_\sigma(\kappa), \tag{47}$$

and $\varphi_\sigma(\kappa) = \varphi(t, \omega(t), \varphi_\sigma(\kappa))$.

Proof. Let σ be a solution of (43). It follows from (ii) of Remark 2 that

$$\left\{ {}^{CF}\mathbb{D}_{a;w}^{\mu;\psi} \sigma(x) = \varphi(x, \sigma(x), {}^{CF}\mathbb{D}_{a;w}^{\mu;\psi} \sigma(x)) + \omega(x)\sigma(0) = c + g(\sigma). \right. \quad (48)$$

Then, the solution of problem (48) is

$$\sigma(x) = \mathcal{A}_\sigma(x) + \frac{b_\mu}{w(x)} \int_a^x \psi'(\zeta)w(\zeta)[\varphi_\sigma(\zeta) + \omega(\zeta)]d\zeta, x \in \mathcal{O}. \quad (49)$$

Once more by (i) of Remark 2, we get

$$\begin{aligned} & \left| \sigma(x) - \mathcal{A}_\sigma(x) - \frac{b_\mu}{w(x)} \int_a^x \psi'(\zeta)w(\zeta)\varphi_\sigma(\zeta)d\zeta \right| \\ & \leq \frac{b_\mu}{w(x)} \int_a^x \psi'(\zeta)w(\zeta)|\omega(\zeta)|d\zeta \\ & \leq \frac{b_\mu}{w(x)} \varepsilon \int_a^x \psi'(\zeta)w(\zeta)d\zeta \\ & \leq \varepsilon \frac{w(b)}{w(a)} b_\mu [\psi(b) - \psi(a)]. \end{aligned} \quad (50)$$

□

Theorem 3. Assume that the conditions of Theorem 1 are fulfilled. Then, the solution of the ψ -weighted problem (5) is UH and generalized UH stable.

Proof. Let $\sigma \in AC[\mathcal{O}, \mathbb{R}]$ be a solution of (43), and $\rho \in AC[\mathcal{O}, \mathbb{R}]$ be a unique solution of ψ -weighted problem (5)

$$\left\{ {}^{CF}\mathbb{D}_{a;w}^{\mu;\psi} \rho(x) = \varphi(x, \rho(x), {}^{CF}\mathbb{D}_{a;w}^{\mu;\psi} \rho(x)) \rho(a) = \sigma(a). \right. \quad (51)$$

From Corollary 1, we get

$$\rho(x) = \mathcal{A}_\rho(x) + \frac{b_\mu}{w(x)} \int_a^x \psi'(\zeta)w(\zeta)\varphi_\rho(\zeta)d\zeta, x \in \mathcal{O}, \quad (52)$$

where $\mathcal{A}_\rho(x) := w(a)/w(x)[c + g(\rho)] + a_\mu \varphi_\rho(x)$. Clearly, if $\rho(a) = \sigma(a)$, then $g(\rho) = g(\sigma)$. Also, by (Hy₁) and (Hy₂) along with (24), we have

$$\begin{aligned} |\mathcal{A}_\rho(x) - \mathcal{A}_\sigma(x)| & \leq \frac{w(a)}{w(x)} |g(\rho) - g(\sigma)| + a_\mu |\varphi_\rho(x) - \varphi_\sigma(x)| \\ & \leq a_\mu \frac{L_\varphi}{1 - M_\varphi} \|\rho - \sigma\|. \end{aligned} \quad (53)$$

From (22), we get $\mathcal{A}_\rho(x) = \mathcal{A}_\sigma(x)$. Hence, (52) becomes

$$\rho(x) = \mathcal{A}_\sigma(x) + \frac{b_\mu}{w(x)} \int_a^x \psi'(\zeta)w(\zeta)\varphi_\rho(\zeta)d\zeta, x \in \mathcal{O}. \quad (54)$$

Using Lemma 5, (Hy₁), and (Hy₂), we have

$$\begin{aligned} |\sigma(x) - \rho(x)| & = \left| \sigma(x) - \mathcal{A}_\sigma(x) - \frac{b_\mu}{w(x)} \int_a^x \psi'(\zeta)w(\zeta)\varphi_\rho(\zeta)d\zeta \right| \\ & \leq \left| \sigma(x) - \mathcal{A}_\sigma(x) - \frac{b_\mu}{w(x)} \int_a^x \psi'(\zeta)w(\zeta)\varphi_\sigma(\zeta)d\zeta \right| \\ & \quad + \frac{b_\mu}{w(x)} \int_a^x \psi'(\zeta)w(\zeta)|\varphi_\sigma(\zeta) - \varphi_\rho(\zeta)|d\zeta \\ & \leq \varepsilon \frac{w(b)}{w(a)} b_\mu [\psi(b) - \psi(a)] \\ & \quad + a_\mu \frac{L_\varphi}{1 - M_\varphi} \int_a^x \psi'(\zeta)w(\zeta)|\sigma(\zeta) - \rho(\zeta)|d\zeta. \end{aligned} \quad (55)$$

Using Gronwall's Lemma [35], we obtain

$$\begin{aligned} |\sigma(x) - \rho(x)| & \leq \varepsilon \frac{w(b)}{w(a)} b_\mu [\psi(b) - \psi(a)] \exp\left(a_\mu \frac{L_\varphi}{1 - M_\varphi} \int_a^x \psi'(\zeta)w(\zeta)d\zeta \right) \\ & \leq \varepsilon \frac{w(b)}{w(a)} b_\mu [\psi(b) - \psi(a)] \exp\left(a_\mu \frac{L_\varphi}{1 - M_\varphi} \frac{w(b)}{w(a)} b_\mu [\psi(b) - \psi(a)] \right) \\ & = \varepsilon \chi_\varphi, \end{aligned} \quad (56)$$

where

$$\chi_\varphi = \frac{w(b)}{w(a)} b_\mu [\psi(b) - \psi(a)] \exp\left(a_\mu \frac{L_\varphi}{1 - M_\varphi} \frac{w(b)}{w(a)} b_\mu [\psi(b) - \psi(a)] \right). \quad (57)$$

Hence, (5) is UH stable. Moreover, if there exists a nondecreasing function $\phi: \mathbb{R}^+ \rightarrow \mathbb{R}^+$ such that $\phi(\varepsilon) = \varepsilon$. Then, from (56), we have

$$|\sigma(\kappa) - \rho(\kappa)| \leq \chi_\phi \phi(\varepsilon), \kappa \in \mathcal{D}, \tag{58}$$

with $\phi(0) = 0$, which proves (5) is GUH stable. \square

4. Example

Here, we provide an example to illustrate the obtained results.

Example 1. consider the following $[\psi, w]$ -Caputo–Fabrizio type problem:

$$\left\{ \begin{aligned} {}^{CF} \mathbb{D}_{0^+, \kappa/3}^{1/4, \kappa/2} \rho(\kappa) &= \frac{(\kappa - 1)^3}{10} \frac{\sin|\rho(\kappa)| + \sin|{}^{CF} \mathbb{D}_{0^+, \kappa/3}^{1/4, \kappa/2} \rho(\kappa)|}{5 + \kappa} + \frac{(\kappa - 1)^3}{20}, \kappa \in [1, 2], v(1) = \frac{1}{3} + \sum_{i=1}^n d_i \rho(\kappa_i). \end{aligned} \right. \tag{59}$$

Clearly, $\mu = 1/4, \psi(\kappa) = \kappa/2, w(\kappa) = \kappa/3, a = 1, b = 2, c = 1/3, 1 < \kappa_1 = 1.5 < \dots < \kappa_n < 2 = b$, and d_i are positive constants with $\sum_{i=1}^n d_i < 2/5$. Set

$$\varphi(\kappa, \rho, \sigma) = \frac{(\kappa - 1)^3}{10} \left(\frac{\sin|\rho| + \sin|\sigma|}{5 + \kappa} + \frac{1}{2} \right), \tag{60}$$

for $\kappa \in [1, 2], \rho, \sigma \in [0, \infty)$, and

$$g(\rho) = \sum_{i=1}^n d_i \rho(\kappa_i), \rho \in [0, \infty). \tag{61}$$

(I) Application of Theorem 1: Note that $\varphi(1, \rho(1), \sigma(1)) = 0$. Now, let $\kappa \in [1, 2]$, and $\rho, \sigma, \rho^*, \sigma^* \in [0, \infty)$. Then,

$$\begin{aligned} &|\varphi(\kappa, \rho, \sigma) - \varphi(\kappa, \rho^*, \sigma^*)| \\ &= \frac{(\kappa - 1)^3}{10} \left| \frac{\sin|\rho| + \sin|\sigma|}{5 + \kappa} - \frac{\sin|\rho^*| + \sin|\sigma^*|}{5 + \kappa} \right| \\ &\leq \frac{(\kappa - 1)^3}{10} \left| \frac{\sin|\rho| - \sin|\rho^*|}{5 + \kappa} + \frac{\sin|\sigma| - \sin|\sigma^*|}{5 + \kappa} \right| \\ &\leq \frac{1}{70} (|\rho - \rho^*| + |\sigma - \sigma^*|), \end{aligned} \tag{62}$$

$$|g(\rho) - g(\sigma)| = \left| \sum_{i=1}^n d_i \rho(\kappa_i) - \sum_{i=1}^n d_i \sigma(\kappa_i) \right| \leq \sum_{i=1}^n d_i |\rho - \sigma| \leq \frac{2}{5} |\rho - \sigma|.$$

Thus, (Hy₁) and (Hy₂) hold with $L_\varphi = M_\varphi = 1/70$, and $L_g = 2/5$. In addition, the condition (22) holds. Indeed, we have $\aleph(\mu) = 1, a_\mu = 3/4, b_\mu = 1/4$ and

$$L_g + \left[a_\mu + b_\mu \frac{w(b)}{w(a)} [\psi(b) - \psi(a)] \right] \frac{L_\varphi}{1 - M_\varphi} = \frac{143}{345} < 1. \tag{63}$$

Thus, Theorem 1 shows that (59) has a unique solution on $[1, 2]$.

(II) Application of Theorem 3: For $\varepsilon > 0$ with $\chi_\phi = 1/8 \sqrt[7]{\varepsilon} > 0$. It follows from Theorem 3 that (59) is HU and GUH stable.

(III) Application of Theorem 2: For $\kappa \in [1, 2]$, and $\rho, \sigma \in [0, \infty)$, we have

$$\begin{aligned} |\varphi(\kappa, \rho, \sigma)| &= \frac{(\kappa - 1)^3}{10} \frac{\sin|\rho|}{5 + \kappa} + \frac{(\kappa - 1)^3}{10} \frac{\sin|\sigma|}{5 + \kappa} + \frac{(\kappa - 1)^3}{20} \\ &\leq \frac{(\kappa - 1)^3}{20} + \frac{(\kappa - 1)^3}{10(5 + \kappa)} |\rho| + \frac{(\kappa - 1)^3}{10(5 + \kappa)} |\sigma| \\ &\leq \frac{1}{20} + \frac{1}{70} |\rho| + \frac{1}{70} |\sigma|, \\ |g(v)| &= \left| \sum_{i=1}^n d_i \rho(\kappa_i) \right| \leq \sum_{i=1}^n d_i |\rho| \leq \frac{2}{5} |v|. \end{aligned} \tag{64}$$

Consequently, (Hy₃) and ((Hy₄)) hold with $n_\phi = 1/20, m_\phi = s_\phi = 1/70$ and $m_g = 2/5$. Also, we have

$$\mu_g + \left[a_\mu + \frac{w(b)}{w(a)} b_\mu [\psi(b) - \psi(a)] \right] \frac{m_\varphi}{1 - s_\varphi} = \frac{143}{345} < 1. \quad (65)$$

Thus, all the assumptions of Theorem 2 are satisfied. Hence, (59) has a solution on [1, 2].

Remark 3. consider a more general problem as a system that contains a number of problems similar to our current problem (5) as follows:

$$\left\{ \begin{aligned} {}^{CF} \mathbb{D}_{a;w}^{\mu_i; \psi} \rho_i(\chi) &= \varphi_i(\chi, \rho_i(\chi), {}^{CF} \mathbb{D}_{a;w}^{\mu_i; \psi} \rho_i(\chi)), \chi \in \mathcal{O} \rho_i(a) = c_i + g(\rho_i), \quad i = 1, \dots, n \in \mathbb{N}, \end{aligned} \right. \quad (66)$$

where $0 < \mu_i < 1$, ${}^{CF} \mathbb{D}_{a;w}^{\mu_i; \psi}$ is the generalized Caputo–Fabrizio FD of order μ_i .

The system (66) can be written as

$$\left\{ \begin{aligned} {}^{CF} \mathbb{D}_{a;w}^{Y; \psi} \mathcal{P}(\chi) &= \Phi(\chi, \mathcal{P}(\chi), {}^{CF} \mathbb{D}_{a;w}^{\mu_i; \psi} \mathcal{P}(\chi)), \chi \in \mathcal{O}, \mathcal{P}(a) = C + g(\mathcal{P}), \end{aligned} \right. \quad (67)$$

where

$$\begin{aligned} \mathcal{P}(\chi) &= \begin{bmatrix} \rho_1(\chi) \\ \rho_2(\chi) \\ \vdots \\ \rho_n(\chi) \end{bmatrix}, \Phi(\chi, \mathcal{P}(\chi), {}^{CF} \mathbb{D}_{a;w}^{\mu_i; \psi} \mathcal{P}(\chi)) = \begin{bmatrix} \varphi_1(\chi, \rho_1(\chi), {}^{CF} \mathbb{D}_{a;w}^{\mu_i; \psi} \rho_1(\chi)) \\ \varphi_2(\chi, \rho_1(\chi), {}^{CF} \mathbb{D}_{a;w}^{\mu_i; \psi} \rho_1(\chi)) \\ \vdots \\ \varphi_n(\chi, \rho_1(\chi), {}^{CF} \mathbb{D}_{a;w}^{\mu_i; \psi} \rho_1(\chi)) \end{bmatrix}, \\ \mathcal{P}(a) &= \begin{bmatrix} \rho_1(a) \\ \rho_2(a) \\ \vdots \\ \rho_n(a) \end{bmatrix}, C = \begin{bmatrix} c_1 \\ c_2 \\ \vdots \\ c_n \end{bmatrix}, Y = \begin{bmatrix} \mu_1 \\ \mu_2 \\ \vdots \\ \mu_n \end{bmatrix}. \end{aligned} \quad (68)$$

By using Corollary 1, the system (67) has the following solution:

$$\begin{aligned} \mathcal{P}(\chi) &= \frac{w(a)}{w(\chi)} [C + g(\mathcal{P})] + a_Y \Phi_{\mathcal{P}}(\chi) \\ &+ \frac{b_Y}{w(\chi)} \int_a^\chi \psi'(\zeta) w(\zeta) \Phi_{\mathcal{P}}(\zeta) d\zeta, \chi \in \mathcal{O}, \end{aligned} \quad (69)$$

where $\Phi_{\mathcal{P}}(\chi) = \Phi(\chi, \mathcal{P}(\chi), \Phi_{\mathcal{P}}(\chi))$, $a_Y = 1 - Y/\aleph(Y)$, and $b_Y = Y/\aleph(Y)$.

Remark 4. Following the methodology of proof used in the preceding parts, we can obtain the same results (Theorems 1–3) for the nonlinear system (67) in view of the formula (69).

5. Conclusions

In this regard, Al-Refai and Jarrah [32] defined the weighted Caputo–Fabrizio FD of the Caputo sense. As an extra contribution to this topic, we developed and extended the existence, uniqueness, and UH stability results for nonlocal implicit equations involving $[\psi, w]$ -Caputo–Fabrizio FDs.

Our approach has been based on Banach’s and Krasnoselskii’s fixed point theorem. As an application, we have given a convenient example that validates the theoretical results. Finally, in light of our present results, a more general problem for the nonlocal implicit system has been presented that contains similar problems to the problem considered.

In the future direction, it will be interesting to study the current systems under $[\psi, w]$ -Atangana–Baleanu of the Caputo sense, introduced recently in [21, 36].

Data Availability

No data were used to support this study.

Conflicts of Interest

The authors declare that they have no conflicts of interest.

Acknowledgments

This work was conducted during our work at Hodeidah University.

References

- [1] T. J. Osler, "Leibniz rule for fractional derivatives generalized and an application to infinite series," *SIAM Journal on Applied Mathematics*, vol. 18, no. 3, pp. 658–674, 1970.
- [2] A. A. Kilbas, H. M. Srivastava, and J. J. Trujillo, *Theory and Applications of Fractional Differential Equations*, Elsevier B.V, Amsterdam, Netherlands, 2006.
- [3] S. G. Samko, A. A. Kilbas, and O. I. Marichev, *Fractional Integrals and Derivatives, Theory and Applications*, Gordon & Breach, Amsterdam, Netherlands, 1993.
- [4] K. Diethelm and N. J. Ford, "Analysis of fractional differential equations," *Journal of Mathematical Analysis and Applications*, vol. 265, no. 2, pp. 229–248, 2002.
- [5] M. S. Abdo, A. G. Ibrahim, and S. K. Panchal, "Nonlinear implicit fractional differential equation involving-Caputo fractional derivative," *Proc. Jangjeon Math. Soc.*, vol. 22, no. 3, pp. 387–400, 2019.
- [6] F. Jarad, T. Abdeljawad, and Z. Hammouch, "On a class of ordinary differential equations in the frame of Atangana-Baleanu fractional derivative," *Chaos, Solitons & Fractals*, vol. 117, pp. 16–20, 2018.
- [7] S. Abbas, M. Benchohra, and G. M. N'Guérékata, *Topics in Fractional Differential Equations*, vol. 27, Springer Science & Business Media, Berlin, Germany, 2012.
- [8] M. K. Alaoui, R. Fayyaz, A. Khan, R. Shah, and M. S. Abdo, "Analytical investigation of noyes–field model for time-fractional belousov–zhabotinsky reaction," *Complexity*, vol. 2021, pp. 1–21, Article ID 3248376, 2021.
- [9] B. N. Abood, S. S. Redhwan, and M. S. Abdo, "Analytical and approximate solutions for generalized fractional quadratic integral equation," *Nonlinear Funct. Anal. Appl.*, vol. 26, no. 3, pp. 497–512, 2021.
- [10] A. Atangana and J. F. Gómez-Aguilar, "Numerical approximation of Riemann-Liouville definition of fractional derivative: from Riemann-Liouville to Atangana-Baleanu," *Numerical Methods for Partial Differential Equations*, vol. 34, no. 5, pp. 1502–1523, 2018.
- [11] B. Ahmad and S. K. Ntouyas, "Existence results for a coupled system of Caputo type sequential fractional differential equations with nonlocal integral boundary conditions," *Applied Mathematics and Computation*, vol. 266, pp. 615–622, 2015.
- [12] S. K. Ntouyas, "Global existence results for certain second order delay integrodifferential equations with nonlocal conditions," *Dynamic Systems and Applications*, vol. 7, pp. 415–426, 1998.
- [13] V. Lakshmikantham and A. S. Vatsala, "Basic theory of fractional differential equations," *Nonlinear Analysis: Theory, Methods & Applications*, vol. 69, no. 8, pp. 2677–2682, 2008.
- [14] H. Gu and J. J. Trujillo, "Existence of mild solution for evolution equation with Hilfer fractional derivative," *Applied Mathematics and Computation*, vol. 257, pp. 344–354, 2015.
- [15] J. Wang and Y. Zhang, "Nonlocal initial value problems for differential equations with Hilfer fractional derivative," *Applied Mathematics and Computation*, vol. 266, pp. 850–859, 2015.
- [16] L. Zhao and Y. Jiang, "Existence and stability for a coupled hybrid system of fractional differential equations with Atangana-Baleanu-Caputo derivative," *Journal of Mathematics*, vol. 2022, pp. 1–12, Article ID 4741224, 2022.
- [17] R. Almeida, "A Caputo fractional derivative of a function with respect to another function," *Communications in Nonlinear Science and Numerical Simulation*, vol. 44, pp. 460–481, 2017.
- [18] J. V. C. Sousa and E. C. Oliveira, "On the-Hilfer fractional derivative," *Communications in Nonlinear Science and Numerical Simulation*, vol. 60, pp. 72–91, 2018.
- [19] M. Caputo and M. Fabrizio, "New definition of fractional derivative without singular kernel," *Prog. Fract. Differ. Appl.*, vol. 1, no. 2, pp. 73–85, 2015.
- [20] J. Losada and J. Nieto, "Properties of a new fractional derivative without singular kernel," *Prog. Fract. Differ. Appl.*, vol. 1, pp. 87–92, 2015.
- [21] J. Hristov and D. Baleanu, "Transient heat diffusion with a non-singular fading memory: from the Cattaneo constitutive equation with Jeffrey's Kernel to the Caputo-Fabrizio time-fractional derivative," *Thermal Science*, vol. 20, no. 2, pp. 757–762, 2016.
- [22] S. Thabet, M. S. Abdo, and K. Shah, "Theoretical and numerical analysis for transmission dynamics of COVID-19 mathematical model involving Caputo-Fabrizio derivative," *Advances in Differential Equations*, vol. 184, 2021.
- [23] M. S. Abdo, S. K. Panchal, K. Shah, and T. Abdeljawad, "Existence theory and numerical analysis of three species prey-predator model under Mittag-Leffler power law," *Advances in Differential Equations*, vol. 249, 2020.
- [24] A. Atangana and J. F. Gómez-Aguilar, "Fractional derivatives with no-index law property: application to chaos and statistics," *Chaos, Solitons & Fractals*, vol. 114, pp. 516–535, 2018.
- [25] B. Ghanbari, S. Kumar, and R. Kumar, "A study of behaviour for immune and tumor cells in immunogenetic tumour model with non-singular fractional derivative," *Chaos, Solitons & Fractals*, vol. 133, Article ID 109619, 2020.
- [26] F. Jarad, T. Abdeljawad, and K. Shah, "On the weighted fractional operators of a function with respect to another function," *Fractals*, vol. 28, no. 8, Article ID 2040011, 2020.
- [27] A. Shaikh, A. Tassaddiq, K. S. Nisar, and D. Baleanu, "Analysis of differential equations involving Caputo–Fabrizio fractional operator and its applications to reaction–diffusion equations," *Advances in Differential Equations*, vol. 178, 2019.
- [28] S. Abbas, M. Benchohra, and S. Krim, "Initial value problems for Caputo-Fabrizio implicit fractional differential equations in b-metric spaces," *Bulletin of the Transilvania University of Brasov Series III Mathematics and Computer Science*, vol. 1, pp. 1–12, 2021.
- [29] K. Salim, S. Abbas, M. Benchohra, and M. A. Darwish, "Boundary value problem for implicit Caputo-Fabrizio fractional differential equations," *Int. J. Differ. Equ.*, vol. 15, no. 2, pp. 493–510, 2020.
- [30] R. Gul, M. Sarwar, K. Shah, T. Abdeljawad, and F. Jarad, "Qualitative analysis of implicit Dirichlet boundary value problem for Caputo-Fabrizio fractional differential equations," *Journal of Function Spaces*, vol. 2020, pp. 1–9, Article ID 4714032, 2020.
- [31] M. S. Abdo, T. Abdeljawad, S. M. Ali, K. Shah, and F. Jarad, "Existence of positive solutions for weighted fractional order differential equations," *Chaos, Solitons & Fractals*, vol. 141, Article ID 110341, 2020.
- [32] M. Al-Refai and A. M. Jarrah, "Fundamental results on weighted Caputo–Fabrizio fractional derivative," *Chaos, Solitons & Fractals*, vol. 126, pp. 7–11, 2019.
- [33] Y. Zhou, *Basic Theory of Fractional Differential Equations*, World Scientific, Singapore, 2014.

- [34] M. A. Krasnoselskii, "Two remarks on the method of successive approximations," *Usp. Mat. Nauk*, vol. 10, pp. 123–127, 1955.
- [35] T. H. Gronwall, "Note on the derivatives with respect to a parameter of the solutions of a system of differential equations," *Annals of Mathematics*, vol. 20, no. 4, pp. 292–296, 1919.
- [36] K. Hattaf, "A new generalized definition of fractional derivative with non-singular kernel," *Computation*, vol. 8, no. 2, p. 49, 2020.

Research Article

Comparative Analysis of the Time-Fractional Black–Scholes Option Pricing Equations (BSOPE) by the Laplace Residual Power Series Method (LRPSM)

Muhammad Imran Liaqat ¹ and Eric Okyere ²

¹National College of Business Administration & Economics, Lahore 54000, Pakistan

²Department of Mathematics and Statistics, University of Energy and Natural Resources, Sunyani, Ghana

Correspondence should be addressed to Eric Okyere; eric.okyere@uenr.edu.gh

Received 13 September 2022; Revised 12 October 2022; Accepted 25 November 2022; Published 16 February 2023

Academic Editor: Watcharaporn Cholamjiak

Copyright © 2023 Muhammad Imran Liaqat and Eric Okyere. This is an open access article distributed under the Creative Commons Attribution License, which permits unrestricted use, distribution, and reproduction in any medium, provided the original work is properly cited.

The residual power series method is effective for obtaining solutions to fractional-order differential equations. However, the procedure needs the $(n - 1)\omega$ derivative of the residual function. We are all aware of the difficulty of computing the fractional derivative of a function. In this article, we considered the simple and efficient method known as the Laplace residual power series method (LRPSM) to find the analytical approximate and exact solutions of the time-fractional Black–Scholes option pricing equations (BSOPE) in the sense of the Caputo derivative. This approach combines the Laplace transform and the residual power series method. The suggested method just needs the idea of an infinite limit, so the computations required to determine the coefficients are minimal. The obtained results are compared in the sense of absolute errors against those of other approaches, such as the homotopy perturbation method, the Aboodh transform decomposition method, and the projected differential transform method. The results obtained using the provided method show strong agreement with different series solution methods, demonstrating that the suggested method is a suitable alternative tool to the methods based on He's or Adomian polynomials.

1. Introduction

Fractional calculus (FC) deals with fractional derivatives and integrations. The pioneers of FC were two mathematicians, Leibniz and L'Hospital, and the date September 30, 1695, is regarded as its exact birthday. Many scientists and researchers have been drawn to FC in recent decades because it is commonly used in scientific contexts such as engineering, image processing, physics, biochemistry, biology, fluid mechanics, and entropy theory [1–5]. Although fractional derivatives can be defined in a variety of ways, not all of them are generally used. The Atangana–Baleanu, Riemann–Liouville (R-L), Caputo–Fabrizio, Caputo, and conformable operators are the most frequently used [6–12]. In some cases, fractional derivatives are preferable to integer-order derivatives for modeling because they can simulate and analyze complicated systems having complicated

nonlinear processes and higher-order behaviors. There are two main causes of this. First, we can select any order for the derivative operator, rather than being restricted to an integer order. Second, depending on both the past and current circumstances, noninteger order derivatives are advantageous when the system has long-term memory. The primary components of FC, which is the generalized version of classical calculus and has piqued the interest of numerous academics and scientists due to its wide range of applications, are fractional order differential equations (FODEs). The FODEs are frequently used for their logical support in the mathematical framework of physical problems, including technology, healthcare, monetary markets, and decision theory. As a result, the solutions provided by the FODEs are significant and useful. Applications regularly face FODEs that are too complex for close-form solutions. Under the specified initial and boundary conditions, numerical

methods present a potent alternative tool for solving FODEs. Several numerical techniques, including the Shehu decomposition approach [13], the differential transform method [14], the variational iteration method [15], the operational matrix approach [16], the homotopy analysis technique [17], the Aboodh transform decomposition method [18], the finite difference method [19], the fractional power series method [20], the Chebyshev polynomials method [21], the residual power series method [22], and the natural transform homotopy perturbation method [23], have been developed in recent years for solving FODEs.

It is efficient to obtain approximate analytical solutions to FODEs using the residual power series method (RPSM). However, the algorithm requires the $(n - 1)\omega$ derivative of the residual function. We are all aware of how difficult it is to calculate a function's fractional derivative. As a result, the use of conventional RPSM is somewhat constrained. To overcome the limitations of the RPSM, Eriqat et al. introduced a new technique called LRPSM [24]. Several FODEs have been solved through the recommended method [24–29]. The provided equation is transformed into the Laplace transform (LT) space in accordance with the set of rules for this novel approach; the solution to the new form of the problem is established; the solution to the original equation is then achieved by applying the inverse LT.

The pricing of financial derivatives is a topic that has generated a great deal of interest and literature. A financial derivative is an asset whose price is based on the value of another asset. Frequently, a stock or bond serves as the

underlying asset. Financial derivatives are not a completely novel concept. It is generally agreed that Charles Castelly's work, which was published in 1877, was the first attempt at contemporary derivative pricing, despite some historical controversy regarding the exact year of the birth of financial derivatives [30]. Although it lacked mathematical rigor, Castell's book served as a general introduction to ideas such as hedging and speculative trading.

The first widely used mathematical method to calculate the theoretical value of an option contract using prevailing equity markets' predicted dividends, the option's strike price, projected interest rates, time till the cessation, and expected unpredictability was the Black–Scholes (BS) model, developed in 1997 by Fischer Black, Robert Merton, and Myron Scholes. The Pricing of Options and Corporate Liabilities by Black and Scholes, published in the Journal of Political Economy in 1973, provided the initial formulation of the equation. Robert C. Merton contributed to the editing of that document. Later that year, he wrote his own work, "Theory of Rational Option Pricing," expanding the model's mathematical capabilities and applications while also coining the term "BS theory of options pricing" [31]. One of the most significant mathematical representations of a financial market is the BS equation. The value of financial derivatives is controlled by a second-order parabolic partial differential equation. Many different commodities and payout structures have been used in the BS model for pricing stock options. The following equation describes the BS model for the value of an option [32]:

$$\frac{\partial^\omega w(\kappa, \zeta)}{\partial \zeta^\omega} + \frac{\sigma^2 \kappa^2}{2} \frac{\partial^2 w(\kappa, \zeta)}{\partial \kappa^2} + \mathfrak{F}(\zeta) \kappa \frac{\partial w(\kappa, \zeta)}{\partial \kappa} - \mathfrak{F}(\zeta) w(\kappa, \zeta) = 0, \quad (1)$$

where ω is the order of the Caputo derivative (CD), $w(\kappa, \zeta)$ is the European offer's value at the fundamental market cap of κ and time ζ , the fluctuation component of the company's shares, often referred to as σ , quantifies the variance of the stock's return, Y is the expiration date, and $\mathfrak{F}(\zeta)$ is the risk-free interest rate. $w_c(\kappa, \zeta)$ and $w_p(\kappa, \zeta)$, correspondingly, stand for the call and put values on European options. Then, the payoff functions are given by $w_c(\kappa, \zeta) = \max(\kappa - U, 0)$ and $w_p(\kappa, \zeta) = \max(U - \kappa, 0)$, where U indicates the termination price for the option and the function $\max(\kappa, 0)$ gives the larger value between κ and 0. The important financial view of the BS equation is that it minimizes risk by allowing for the prudent selection of purchasing and selling the stock under scrutiny. It is a sign that, according to the BS financial model, there is only one correct price for the option. The important financial view of the BS equation is that it minimizes risk by allowing for the prudent selection of purchasing and selling the stock under scrutiny. It is a sign that, according to the BS financial model, there is only one correct price for the option. In this article, a fractional model that may be used to model the pricing of various financial derivatives is presented.

Numerous techniques have been used to examine the time-fractional BSOPE [33–40]. Each of these techniques has specific restrictions and flaws. These techniques involve a lot of computing work and a long running time. In this article, we considered LRPSM, which is a simple and efficient technique to solve BSOPE. The advantage of the recommended method over the homotopy perturbation method (HPM) and the Adomian decomposition method (ADM) is its strength in handling problems without the use of He's and Adomian polynomials. The advantage of this approach is that the problem does not involve any physical parameter assumptions, no matter how big or small. For a series such as the RPSM, the coefficients must be determined each time using the fractional derivative. Since LRPSM just needs the idea of an infinite limit, the computations required to determine the coefficients are minimal. The LRPSM results are also compared to those of other approaches, including the projected differential transform method (PDTM) [34], the Aboodh transform decomposition method (ATMD) [35], and the homotopy perturbation method (HPM) [36]. The results obtained using the suggested method show strong agreement with numerous methodologies, proving that the

LRPSM is a useful substitute for approaches using He’s or Adomian polynomials. Additionally, error functions are used to compare the exact and approximative solutions graphically and numerically. The higher degrees of accuracy and convergence rates were confirmed by the error analysis, demonstrating the suggested method’s efficacy and reliability. The process is rapid, exact, and simple to use, and it produces excellent results.

The article’s structure is as follows: In Section 2, we use a number of important definitions and conclusions from the theory of FC. The main concept of LRPSM is examined in Section 3 in order to establish and determine the solution of the time-fractional BSOPE. Section 4 investigates the potential, capability, and simplicity of the suggested approach using three numerical models. In Section 5, graphics and tables are used to investigate the numerical outcomes and discussion. Section 6, towards the end, has the conclusion.

2. Preliminaries

In this section, we examine several common definitions, properties, and some useful consequences that we used in this article.

Definition 1 (see [24]). We assume that the function $w(x, \zeta)$ is of exponential order δ and piecewise continuous. Then, the LT of $w(x, \zeta)$ for $\zeta \geq 0$ is formulated as

$$\mathcal{L}[w(x, \zeta)] = W(x, s) = \int_0^\infty w(x, \zeta)e^{-s\zeta}d\zeta, \quad s > \delta, \quad (2)$$

and the inverse LT is defined by

$$\mathcal{L}^{-1}[W(x, s)] = w(x, \zeta) = \int_{h-\infty}^{h+\infty} e^{s\zeta}W(x, s)ds, \quad h = Re(s) > h_0, \quad (3)$$

where h_0 lies in the right half plane of the absolute convergence of the Laplace integral.

Lemma 1 (see [24–29]). Let $w_1(x, \zeta)$ and $w_2(x, \zeta)$ be piecewise continuous on $[0, \infty$ and be of exponential order. We assume that $\mathcal{L}[w_1(x, \zeta)] = W_1(x, s)$, $\mathcal{L}[w_2(x, \zeta)] = W_2(x, s)$, and c_1, c_2 are constants. Then, the properties mentioned as follows are valid:

- (i) $\mathcal{L}[c_1w_1(x, \zeta) + c_2w_2(x, \zeta)] = c_1W_1(x, s) + c_2W_2(x, s)$
- (ii) $\mathcal{L}^{-1}[c_1W_1(x, s) + c_2W_2(x, s)] = c_1w_1(x, \zeta) + c_2w_2(x, \zeta)$
- (iii) $\phi_0(x) = \lim_{s \rightarrow \infty} sW(x, s) = w(x, 0)$

- (iv) $\mathcal{L}[D_\zeta^\omega w(x, \zeta)] = s^\omega W(x, s) - \sum_{j=0}^{n-1} w^{(j)}(x, 0)/s^{j-\omega+1}, n-1 < \omega \leq n, n \in \mathbb{N}$
- (v) $\mathcal{L}[D_\zeta^{n\omega} w(x, \zeta)] = s^{n\omega} W(x, s) - \sum_{j=0}^{n-1} s^{\omega(n-j)-1} D_\zeta^{j\omega} w(x, 0), 0 < \omega \leq 1$

Definition 2 (see [41]). The fractional derivative of $w(x, \zeta)$ I order ω in the CD sense is defined as follows:

$$D_\zeta^\omega w(x, \zeta) = \mathcal{I}_\zeta^{n-\omega} w^{(n)}(x, \zeta), \quad \zeta \geq 0, \quad n-1 < \omega \leq n, \quad (4)$$

where $\mathcal{I}_\zeta^{n-\omega}$ is the R-L integral of $w(x, \zeta)$.

Theorem 1 (see [24]). We assume that the multiple fractional power series (MFPS) representation for the function $\mathcal{L}[w(x, \zeta)] = W(x, s)$ is given by

$$W(x, s) = \sum_{n=0}^\infty \frac{\phi_n(x)}{s^{n\omega+1}}, \quad s > 0, \quad (5)$$

then we have

$$\phi_n(x) = D_\zeta^{n\omega} w(x, 0), \quad (6)$$

where $D_\zeta^{n\omega} = D_\zeta^\omega \cdot D_\zeta^\omega \dots D_\zeta^\omega$ (n – times).

The conditions for the convergence of the MFPS are determined in the following theorem.

Theorem 2 (see [24]). Let $\mathcal{L}[w(x, \zeta)] = W(x, s)$ can be denoted as the new form of MFPS explained in Theorem 1. If $|\mathcal{L}[D_\zeta^{(j+1)\omega} w(x, \zeta)]| \leq \mathcal{L}$, on $0 < s \leq v$ with $0 < \omega \leq 1$, then the remainder $R_j(x, s)$ of the new form of MFPS satisfies the following inequality:

$$|R_j(x, s)| \leq \frac{\mathcal{L}}{s^{(j+1)\omega+1}}, \quad 0 < s \leq v. \quad (7)$$

3. Methodology for the LRPSM for the Time-Fractional BSOPE

This section examines the steps for using the suggested method to find solutions to BSOPEs. Running the LT on the BSOPE and then considering MFPS as the BSOPE’s new space solution constitute the main idea of LRPSM. The way in which the coefficients of this series utilize the limit idea is the main difference between the LRPSM and the RPSM. The generated consequents are then transformed into real space using the inverse LT. The guidelines for using the LRPSM to find solutions are as follows:

Step 1: Equation (1) should be changed as follows:

$$D_\zeta^\omega w(x, \zeta) - f\left(w(x, \zeta), \frac{\sigma^2 x^2 \partial^2 w(x, \zeta)}{2\partial x^2}, \mathfrak{F}(\zeta)x \frac{\partial w(x, \zeta)}{\partial x}, \mathfrak{F}(\zeta)w(x, \zeta)\right) = 0. \quad (8)$$

Step 2: by considering LT on both sides of equation (8), we obtain the following:

$$W(x, s) - \frac{w(x, 0)}{s} - \frac{1}{s^\omega} F(x, s) = 0, \quad (9)$$

where

$$W(\kappa, s) = \mathcal{L}[w(\kappa, \zeta)], \quad (10)$$

and

$$F(\kappa, s) = \mathcal{L}\left[f\left(\frac{\sigma^2 \kappa^2 \partial^2 w(\kappa, \zeta)}{2\partial \kappa^2}, \mathfrak{F}(\zeta)w(\kappa, \zeta), w(\kappa, \zeta), \mathfrak{F}(\zeta)\kappa \frac{\partial w(\kappa, \zeta)}{\partial \kappa}\right)\right]. \quad (11)$$

Step 3: we assume that the solution of equation (9) is the following series:

$$W(\kappa, s) = \sum_{n=0}^{\infty} \frac{\phi_n(\kappa)}{s^{m\kappa+1}}, \quad s > 0. \quad (12)$$

Step 4: we obtained the following as a result of using Lemma 1(iii):

$$\phi_0(\kappa) = \lim_{s \rightarrow \infty} sW(\kappa, s) = w(\kappa, 0) = 0. \quad (13)$$

Step 5: we define the k th-truncated expansion of $W(\kappa, s)$ as

$$W_k(\kappa, s) = \frac{\phi_0(\kappa)}{s} + \sum_{n=1}^k \frac{\phi_n(\kappa)}{s^{n\omega+1}}. \quad (14)$$

Step 6: we introduce Laplace residual function (LRF) of equation (9) and the k th-LRF, respectively, as follows:

$$\mathcal{L}[\text{Res}(\kappa, s)] = W(\kappa, s) - \frac{\phi_0(\kappa)}{s} - \frac{1}{s^\omega} F(s), \quad (15)$$

$$\mathcal{L}[\text{Res}_k(\kappa, s)] = W_k(\kappa, s) - \frac{\phi_0(\kappa)}{s} - \frac{1}{s^\omega} F_k(s). \quad (16)$$

Step 7: we use the expansion form of $W_k(\kappa, s)$ into $\mathcal{L}[\text{Res}_k(\kappa, s)]$.

Step 8: we multiply both sides of $\mathcal{L}[\text{Res}_k(\kappa, s)]$ with $s^{k\omega+1}$.

Step 9: by utilizing the fact in equation (16), we solve the following sequence of algebraic equations for $\phi_n(\kappa)$, where $n = 1, 2, 3, \dots, k$, step by step:

$$\lim_{s \rightarrow \infty} (s^{\omega+1} \mathcal{L}[\text{Res}_k(\kappa, s)]) = 0, \quad k = 1, 2, 3, \dots \quad (17)$$

Step 10: we use the attained values of $\phi_n(\kappa)$ into the k th-truncated expansion of $W(\kappa, s)$ for each $n = 1, 2, 3, \dots, k$ to attain the k th-approximate solution of the algebraic equation in equation (9).

Step 11: we apply the inverse LT on the final form of $W_k(\kappa, s)$ to attain k th-approximate solution, $w_k(\kappa, \zeta)$ of the suggested problem.

4. Some Illustrated Problems

In this section, three time-fractional BSOPE in the CD sense are solved in order to assess the effectiveness and suitability of the suggested approach.

Problem 1. consider the time-fractional BSOPE that follows [34]:

$$\frac{\partial^\omega w(\kappa, \zeta)}{\partial \zeta^\omega} + \kappa^2 \frac{\partial^2 w(\kappa, \zeta)}{\partial \kappa^2} + 0.5\kappa \frac{\partial w(\kappa, \zeta)}{\partial \kappa} - w(\kappa, \zeta) \quad (18)$$

$$= 0, \quad 0 < \omega \leq 1,$$

under the following initial conditions:

$$w(\kappa, 0) = \max(\kappa^3, 0) = \begin{cases} \kappa^3 & \text{for } \kappa > 0, \\ 0 & \text{for } \kappa \leq 0. \end{cases} \quad (19)$$

We will examine the case when $\kappa > 0$. Applying LT on both sides of equation (18), we have

$$\mathcal{L}\left[\frac{\partial^\omega w(\kappa, \zeta)}{\partial \zeta^\omega} + \kappa^2 \frac{\partial^2 w(\kappa, \zeta)}{\partial \kappa^2} + 0.5\kappa \frac{\partial w(\kappa, \zeta)}{\partial \kappa} - w(\kappa, \zeta)\right] = 0. \quad (20)$$

Making use of the process outlined in Section 3, we get the findings from equation (20) as follows:

$$W(\kappa, s) = \frac{\kappa^3}{s} - \frac{1}{s^\omega} \kappa^2 D_{\kappa\kappa} \mathcal{L}[w(\kappa, \zeta)] - \frac{1}{s^\omega} 0.5\kappa D_\kappa \mathcal{L}[w(\kappa, \zeta)] + \frac{1}{s^\omega} \mathcal{L}[w(\kappa, \zeta)]. \quad (21)$$

We suppose that the expansion of $W(\kappa, s)$ is as follows:

$$W(\chi, s) = \sum_{n=0}^{\infty} \frac{\phi_n(\chi)}{s^{n\omega+1}}. \tag{22}$$

The k th-truncated expansion is given as follows:

$$W_k(\chi, s) = \sum_{n=0}^k \frac{\phi_n(\chi)}{s^{n\omega+1}}. \tag{23}$$

We obtained the following as a result of using Lemma 1(iii):

$$\mathcal{L}[\text{Res}(\chi, s)] = W(\chi, s) - \frac{\chi^3}{s} + \frac{1}{s^\omega} \chi^2 D_{\chi\chi} W(\chi, s) + \frac{1}{s^\omega} (0.5) \chi D_\chi W(\chi, s) - \frac{1}{s^\omega} W(\chi, s). \tag{26}$$

The k th-LRF of equation (21) is as follows:

$$\mathcal{L}[\text{Res}_k(\chi, s)] = W_k(\chi, s) - \frac{\chi^3}{s} + \frac{1}{s^\omega} \chi^2 D_{\chi\chi} W_k(\chi, s) + \frac{1}{s^\omega} (0.5) \chi D_\chi W_k(\chi, s) - \frac{1}{s^\omega} W_k(\chi, s). \tag{27}$$

We expand the characteristics of the RPSM to highlight the following details [42, 43]:

- (i) $\mathcal{L}[\text{Res}(\chi, s)] = 0$ and $\lim_{s \rightarrow \infty} \mathcal{L}[\text{Res}_k(\chi, s)]$
- (ii) $\lim_{s \rightarrow \infty} s \mathcal{L}[\text{Res}(\chi, s)] = 0 \Rightarrow \lim_{s \rightarrow \infty} s \mathcal{L}[\text{Res}_k(\chi, s)]$

$$\phi_0(\chi) = \lim_{s \rightarrow \infty} sW(s) = w(\chi, 0) = \chi^3. \tag{24}$$

As a result, the k th-truncate expansion of equation (21) is as follows:

$$W_k(\chi, s) = \frac{\chi^3}{s} + \sum_{n=1}^k \frac{\phi_n(\chi)}{s^{n\omega+1}}. \tag{25}$$

The LRF of equation (21) is as follows:

- (iii) $\lim_{s \rightarrow \infty} s^{k\omega+1} \mathcal{L}[\text{Res}(\chi, s)] = \lim_{s \rightarrow \infty} s^{k\omega+1} \mathcal{L}[\text{Res}_k(\chi, s)] \stackrel{s \rightarrow \infty}{=} 0$, where $k = 1, 2, 3, \dots$. To determine the first unknown co-efficient $\phi_1(\chi)$ in (25), we have to use the 1st truncated series $W_1(\chi, s) = \chi^3/s + \phi_1(\chi)/s^{\omega+1}$ into the 1st-LRF, $\mathcal{L}[\text{Res}_1(\chi, s)]$, to obtain

$$\mathcal{L}[\text{Res}_1(\chi, s)] = \left[\frac{\chi^3}{s} + \frac{\phi_1(\chi)}{s^{\omega+1}} \right] - \frac{\chi^3}{s} + \frac{1}{s^\omega} \chi^2 D_{\chi\chi} \left[\frac{\chi^3}{s} + \frac{\phi_1(\chi)}{s^{\omega+1}} \right] + \frac{1}{s^\omega} (0.5) \chi D_\chi \left[\frac{\chi^3}{s} + \frac{\phi_1(\chi)}{s^{\omega+1}} \right] - \frac{1}{s^\omega} \left[\frac{\chi^3}{s} + \frac{\phi_1(\chi)}{s^{\omega+1}} \right]. \tag{28}$$

$s^{\omega+1}$ is used on both sides of equation (28):

$$s^{\omega+1} \mathcal{L}[\text{Res}_1(\chi, s)] = \phi_1(\chi) + \chi^2 D_{\chi\chi} \left[\chi^3 + \frac{\phi_1(\chi)}{s^\omega} \right] + (0.5) \chi D_\chi \left[\chi^3 + \frac{\phi_1(\chi)}{s^\omega} \right] - \left[\chi^3 + \frac{\phi_1(\chi)}{s^\omega} \right]. \tag{29}$$

We use the fact that

$$\lim_{s \rightarrow \infty} s^{k\omega+1} \mathcal{L}[\text{Res}_k(\chi, s)] = 0, \text{ for } k = 1. \tag{30}$$

As a result, we obtained as follows:

$$\phi_1(\chi) = -6.5\chi^3. \tag{31}$$

Similarly, to find out values of the second undefined coefficient $\phi_2(\chi)$, we have to use the 2nd-truncates series $W_2(\chi, s) = \chi^3/s + \phi_1(\chi)/s^{\omega+1} + \phi_2(\chi)/s^{2\omega+1}$ into the 2nd-LRF to obtain

$$\begin{aligned} \mathcal{L}[\text{Res}_2(\chi, s)] &= \left[\frac{\chi^3}{s} + \frac{\phi_1(\chi)}{s^{\omega+1}} + \frac{\phi_2(\chi)}{s^{2\omega+1}} \right] - \frac{\chi^3}{s} + \frac{1}{s^\omega} \chi^2 D_{\chi\chi} \left[\frac{\chi^3}{s} + \frac{\phi_1(\chi)}{s^{\omega+1}} + \frac{\phi_2(\chi)}{s^{2\omega+1}} \right] \\ &+ \frac{1}{s^\omega} (0.5) \chi D_\chi \left[\frac{\chi^3}{s} + \frac{\phi_1(\chi)}{s^{\omega+1}} + \frac{\phi_2(\chi)}{s^{2\omega+1}} \right] - \frac{1}{s^\omega} \left[\frac{\chi^3}{s} + \frac{\phi_1(\chi)}{s^{\omega+1}} + \frac{\phi_2(\chi)}{s^{2\omega+1}} \right]. \end{aligned} \tag{32}$$

Using $s^{2\omega+1}$ on both sides of equation (32), we get the following equation:

$$s^{2\omega+1} \mathcal{L} [\text{Res}_2(\kappa, s)] = s^\omega \phi_1(\kappa) + \phi_2(\kappa) + s^{\omega+1} \kappa^2 D_{\kappa\kappa} \left[\frac{\kappa^3}{s} + \frac{\phi_1(\kappa)}{s^{\omega+1}} + \frac{\phi_2(\kappa)}{s^{2\omega+1}} \right] + s^{\omega+1} (0.5) D_\kappa \left[\frac{\kappa^3}{s} + \frac{\phi_1(\kappa)}{s^{\omega+1}} + \frac{\phi_2(\kappa)}{s^{2\omega+1}} \right] - s^{\omega+1} \left[\frac{\kappa^3}{s} + \frac{\phi_1(\kappa)}{s^{\omega+1}} + \frac{\phi_2(\kappa)}{s^{2\omega+1}} \right]. \tag{33}$$

Again, we use the fact that

$$\lim_{s \rightarrow \infty} s^{k\omega+1} \mathcal{L} [\text{Res}_k(\kappa, s)] = 0, \text{ for } k = 2. \tag{34}$$

As a result, we obtained the 2nd coefficient $\phi_1(\kappa)$ in the following form:

$$\phi_2(\kappa) = (6.5)^2 \kappa^3. \tag{35}$$

Therefore, the 2nd-approximate LRPS solution of equation (21) is

$$W_2(\kappa, s) = \frac{1}{s} \kappa^3 - \frac{6.5}{s^{\omega+1}} \kappa^3 + \frac{(6.5)^2}{s^{2\omega+1}} \kappa^3. \tag{36}$$

Typically, to find the coefficients $\phi_k(\kappa)$, first we use the k th-truncated series in equation (25), then we utilize it in the k th-LRF, equation (27), we multiply $\mathcal{L} [\text{Res}_k(\kappa, s)]$ by $s^{k\omega+1}$, and then we solve the algebraic equation as follows:

$$\lim_{s \rightarrow \infty} s^{k\omega+1} \mathcal{L} [\text{Res}_k(\kappa, s)] = 0, \text{ for } \phi_k(\kappa). \tag{37}$$

We get the following results by utilizing the previous procedure:

$$\begin{aligned} \phi_3(\kappa) &= -(6.5)^3 \kappa^3, \\ \phi_4(\kappa) &= (6.5)^4 \kappa^3, \\ \phi_5(\kappa) &= -(6.5)^5 \kappa^3. \end{aligned} \tag{38}$$

The approximate solution of equation (21) is obtained by five iterations as follows:

$$W_5(\kappa, s) = \frac{\kappa^3}{s} - \frac{6.5\kappa^3}{s^{\omega+1}} + \frac{(6.5)^2\kappa^3}{s^{2\omega+1}} - \frac{(6.5)^3\kappa^3}{s^{3\omega+1}} + \frac{(6.5)^4\kappa^3}{s^{4\omega+1}} - \frac{(6.5)^5\kappa^3}{s^{5\omega+1}}. \tag{39}$$

By applying the inverse LT to equation (39), we are able to approximate the fifth step solution in the original feature space:

$$w_5(\kappa, \zeta) = \kappa^3 - \frac{6.5\kappa^3\zeta^\omega}{\Gamma(\omega+1)} + \frac{(6.5)^2\kappa^3\zeta^{2\omega}}{\Gamma(2\omega+1)} - \frac{(6.5)^3\kappa^3\zeta^{3\omega}}{\Gamma(3\omega+1)} + \frac{(6.5)^4\kappa^3\zeta^{4\omega}}{\Gamma(4\omega+1)} - \frac{(6.5)^5\kappa^3\zeta^{5\omega}}{\Gamma(5\omega+1)}. \tag{40}$$

When we use $\omega = 1$ in equation (40), we get the following form:

$$w_5(\kappa, \zeta) = \kappa^3 \left[1 + \frac{(-6.5\zeta)}{1!} + \frac{(-6.5\zeta)^2}{2!} + \frac{(-6.5\zeta)^3}{3!} + \frac{(-6.5\zeta)^4}{4!} + \frac{(-6.5\zeta)^5}{5!} \right], \tag{41}$$

which are the first six terms of the expansion $\kappa^3 e^{-6.5\zeta}$ and, thus, is the exact solution of equations (18) and (19) at $\omega = 1$.

Problem 2. consider the following time-fractional BSOPE [35]:

$$\frac{\partial^\omega w(\kappa, \zeta)}{\partial \zeta^\omega} + 0.08(2 + \sin \kappa)^2 \kappa^2 \frac{\partial^2 w(\kappa, \zeta)}{\partial \kappa^2} + 0.06\kappa \frac{\partial w(\kappa, \zeta)}{\partial \kappa} = 0.06w(\kappa, \zeta), \quad 0 < \omega \leq 1, \tag{42}$$

subject to the following initial conditions:

$$w(\varkappa, 0) = \max(\varkappa - 25e^{-0.06}, 0). \tag{43}$$

First, we perform LT on both sides of equation (42), we use the initial condition from equation (43), and then we format the resulting equation as follows:

$$W(\varkappa, s) = \frac{1}{s} \max(\varkappa - 25e^{-0.06}, 0) - \frac{1}{s^{\omega}} 0.08(2 + \sin \varkappa)^2 \varkappa^2 D_{\varkappa \varkappa} W(\varkappa, s) - \frac{0.06 \varkappa}{s^{\omega}} D_{\varkappa} W(\varkappa, s) + \frac{0.06}{s^{\omega}} W(\varkappa, s). \tag{44}$$

We describe the expansion solution of the algebraic equation (44). So, we suppose that the series of $W(\varkappa, s)$ is as follows:

$$W(\varkappa, s) = \sum_{n=0}^{\infty} \frac{\phi_n(\varkappa)}{s^{n\omega+1}}. \tag{45}$$

The k th-truncated series of the expansion of $W(\varkappa, s)$ is as follows:

$$W_k(\varkappa, s) = \sum_{n=0}^k \frac{\phi_n(\varkappa)}{s^{n\omega+1}}. \tag{46}$$

We obtained the following as a result of using Lemma 1(iii):

$$\phi_0(\varkappa) = \lim_{s \rightarrow \infty} sW(\varkappa, s) = w(\varkappa, 0) = \max(\varkappa - 25e^{-0.06}, 0). \tag{47}$$

So, the k th-truncated expansion becomes as follows:

$$W_k(\varkappa, s) = \frac{1}{s} \max(\varkappa - 25e^{-0.06}, 0) + \sum_{n=1}^k \frac{\phi_n(\varkappa)}{s^{n\omega+1}}. \tag{48}$$

The LRF of (44) is as follows:

$$\mathcal{L}[\text{Res}(\varkappa, s)] = W(\varkappa, s) - \frac{1}{s} \max(\varkappa - 25e^{-0.06}, 0) + \frac{1}{s^{\omega}} 0.08(2 + \sin \varkappa)^2 \varkappa^2 D_{\varkappa \varkappa} W(\varkappa, s) + \frac{0.06 \varkappa}{s^{\omega}} D_{\varkappa} W(\varkappa, s) - \frac{0.06}{s^{\omega}} W(\varkappa, s). \tag{49}$$

The k th-LRF of equation (44) is designed as follows:

$$\begin{aligned} \mathcal{L}[\text{Res}_k(\varkappa, s)] &= W_k(\varkappa, s) - \frac{1}{s} \max(\varkappa - 25e^{-0.06}, 0) + \frac{1}{s^{\omega}} 0.08(2 + \sin \varkappa)^2 \varkappa^2 D_{\varkappa \varkappa} W_k(\varkappa, s) \\ &\quad + \frac{0.06 \varkappa}{s^{\omega}} D_{\varkappa} W_k(\varkappa, s) - \frac{0.06}{s^{\omega}} W_k(\varkappa, s). \end{aligned} \tag{50}$$

To determine the first unknown coefficient $\phi_1(\varkappa)$ in equation (46), we have to use 1st-truncated expansion $W_1(\varkappa, s) = 1/s \max(\varkappa - 25e^{-0.06}, 0) + \phi_1(\varkappa)/s^{\omega+1}$ into the 1st-LRF $\mathcal{L}[\text{Res}_1(\varkappa, s)]$, then we multiply by $s^{\omega+1}$ on both sides, and then we use the following fact $\lim_{s \rightarrow \infty} s^{\omega+1} \mathcal{L}[\text{Res}_1(\varkappa, s)] = 0$ to obtain

$$\phi_1(\varkappa) = -0.06[\varkappa - \max(\varkappa - 25e^{-0.06}, 0)]. \tag{51}$$

Similarly, to establish the value of the second undefined coefficient $\phi_2(\varkappa)$, we have to utilize the 2nd truncated expansion $W_2(\varkappa, s) = 1/s \max(\varkappa - 25e^{-0.06}, 0) + \phi_1(\varkappa)/s^{\omega+1} + \phi_2(\varkappa)/s^{2\omega+1}$ into the 2nd-LRF and use the following fact $\lim_{s \rightarrow \infty} s^{2\omega+1} \mathcal{L}[\text{Res}_2(\varkappa, s)] = 0$, we have

$$\phi_2(\varkappa) = -(0.06)^2 \varkappa - \max(\varkappa - 25e^{-0.06}, 0). \tag{52}$$

Therefore, the approximate solution derived from the 2nd iteration of equation (44) is as follows:

$$\begin{aligned} W_2(\varkappa, s) &= \frac{1}{s} (\max(\varkappa - 25e^{-0.06}, 0)) - \frac{0.06}{s^{\omega+1}} (\varkappa - \max(\varkappa - 25e^{-0.06}, 0)) \\ &\quad - \frac{(0.06)^2}{s^{2\omega+1}} (\varkappa - \max(\varkappa - 25e^{-0.06}, 0)). \end{aligned} \tag{53}$$

To determine the 3rd, 4th, and 5th unknown coefficients, we repeat the same process. We get as follows:

$$\begin{aligned}\phi_3(\kappa) &= -(0.06)^3(\kappa - \max(\kappa - 25e^{-0.06}, 0)), \\ \phi_4(\kappa) &= -(0.06)^4(\kappa - \max(\kappa - 25e^{-0.06}, 0)), \\ \phi_5(\kappa) &= -(0.06)^5(\kappa - \max(\kappa - 25e^{-0.06}, 0)).\end{aligned}\quad (54)$$

Therefore, the approximate solution derived from the 5th iteration of equation (44) is as follows:

$$W_5(\kappa, s) = \frac{1}{s}(\max(\kappa - 25e^{-0.06}, 0)) - \left[\frac{0.06}{s^{\varpi+1}} + \frac{(0.06)^2}{s^{2\varpi+1}} + \frac{(0.06)^3}{s^{3\varpi+1}} + \frac{(0.06)^4}{s^{4\varpi+1}} + \frac{(0.06)^5}{s^{5\varpi+1}} \right] (\kappa - \max(\kappa - 25e^{-0.06}, 0)). \quad (55)$$

By utilizing the inverse LT on both sides of equation (55), the approximate solution derived from the 5th iteration by LRPSM of equations (42) and (43) is as follows:

$$w_5(\kappa, \zeta) = \max(\kappa - 25e^{-0.06}, 0) - \left[\frac{(0.06\zeta^\varpi)}{\Gamma(\varpi+1)} + \frac{(0.06\zeta^\varpi)^2}{\Gamma(2\varpi+1)} + \frac{(0.06\zeta^\varpi)^3}{\Gamma(3\varpi+1)} + \frac{(0.06\zeta^\varpi)^4}{\Gamma(4\varpi+1)} + \frac{(0.06\zeta^\varpi)^5}{\Gamma(5\varpi+1)} \right] (\kappa - \max(\kappa - 25e^{-0.06}, 0)). \quad (56)$$

When $\varpi = 1$ is used in equation (56), we get as follows:

$$w_5(\kappa, \zeta) = \max(\kappa - 25e^{-0.06}, 0) - \left[0.06\zeta + \frac{(0.06\zeta)^2}{2!} + \frac{(0.06\zeta)^3}{3!} + \frac{(0.06\zeta)^4}{4!} + \frac{(0.06\zeta)^5}{5!} \right] (\kappa - \max(\kappa - 25e^{-0.06}, 0)). \quad (57)$$

As a result, the following is the exact solution of equations (42) and (43) for $\varpi = 1$:

$$w(\kappa, \zeta) = \max(\kappa - 25e^{-0.06}, 0) + (1 - e^{0.06\zeta})(\kappa - \max(\kappa - 25e^{-0.06}, 0)). \quad (58)$$

subject to the initial condition:

$$w(\kappa, 0) = \max(e^\kappa - 1, 0). \quad (60)$$

First, we perform LT on both sides of equation (59), using the initial condition from equation (60), and then format the resulting equation as follows:

Problem 3. consider the following time-fractional BSOPE [36]:

$$\frac{\partial^\varpi w(\kappa, \zeta)}{\partial \zeta^\varpi} = \frac{\partial^2 w(\kappa, \zeta)}{\partial \kappa^2} + (\lambda - 1) \frac{\partial w(\kappa, \zeta)}{\partial \kappa} \quad (59)$$

$$-\lambda w(\kappa, \zeta), \quad 0 < \varpi \leq 1,$$

$$W(\kappa, s) = \frac{1}{s} \max(e^\kappa - 1, 0) + \frac{1}{s^\varpi} D_{\kappa\kappa} W(\kappa, s) + \frac{(\lambda - 1)}{s^\varpi} D_\kappa W(\kappa, s) - \frac{\lambda}{s^\varpi} W(\kappa, s). \quad (61)$$

We describe the expansion solution of the algebraic equation (61). Therefore, we assume that the expansion of $W(\varkappa, s)$ is as follows:

$$W(\varkappa, s) = \sum_{n=0}^{\infty} \frac{\phi_n(\varkappa)}{s^{n\bar{\omega}+1}}. \tag{62}$$

The k th-truncated expansion of equation (61) is as follows:

$$W_k(\varkappa, s) = \frac{1}{s} \max(e^\varkappa - 1, 0) + \sum_{n=1}^k \frac{\phi_n(\varkappa)}{s^{n\bar{\omega}+1}}. \tag{63}$$

The LRF of equation (61) takes the following form:

$$\mathcal{L}[\text{Res}(\varkappa, s)] = W(\varkappa, s) - \frac{1}{s} \max(e^\varkappa - 1, 0) - \frac{1}{s^{\bar{\omega}}} D_{\varkappa x} W(\varkappa, s) - \frac{(\lambda - 1)}{s^{\bar{\omega}}} D_x W(\varkappa, s) + \frac{\lambda}{s^{\bar{\omega}}} W(\varkappa, s). \tag{64}$$

Accordingly, the k th-LRF takes the following form:

$$\mathcal{L}[\text{Res}_k(\varkappa, s)] = W_k(\varkappa, s) - \frac{1}{s} \max(e^\varkappa - 1, 0) - \frac{1}{s^{\bar{\omega}}} D_{\varkappa x} W_k(\varkappa, s) - \frac{(\lambda - 1)}{s^{\bar{\omega}}} D_x W_k(\varkappa, s) + \frac{\lambda}{s^{\bar{\omega}}} W_k(\varkappa, s). \tag{65}$$

We substitute the k th-truncated series equations (63) into (64), multiply the resulting equation by $s^{k\bar{\omega}+1}$, and then

solve the equation $\lim_{s \rightarrow \infty} s^{k\bar{\omega}+1} \mathcal{L}[\text{Res}_k(\varkappa, s)] = 0$, where $k = 1, 2, 3, 4, 5$, for $\phi_k(\varkappa)$ gives

$$\begin{aligned} \phi_0(\varkappa, s) &= \max(e^\varkappa - 1, 0), \\ \phi_1(\varkappa, s) &= \lambda [\max(e^\varkappa, 0) - \max(e^\varkappa - 1, 0)], \\ \phi_2(\varkappa, s) &= -\lambda^2 [\max(e^\varkappa, 0) - \max(e^\varkappa - 1, 0)], \\ \phi_3(\varkappa, s) &= \lambda^3 [\max(e^\varkappa, 0) - \max(e^\varkappa - 1, 0)], \\ \phi_4(\varkappa, s) &= -\lambda^4 [\max(e^\varkappa, 0) - \max(e^\varkappa - 1, 0)], \\ \phi_5(\varkappa, s) &= \lambda^5 [\max(e^\varkappa, 0) - \max(e^\varkappa - 1, 0)]. \end{aligned} \tag{66}$$

Therefore, the approximate solution derived from the 5th iteration of equation (61) is as follows:

$$\begin{aligned} W_5(\varkappa, s) &= \frac{1}{s} \max(e^\varkappa - 1, 0) + \frac{\lambda}{s^{\bar{\omega}+1}} [\max(e^\varkappa, 0) - \max(e^\varkappa - 1, 0)] - \frac{\lambda^2}{s^{2\bar{\omega}+1}} [\max(e^\varkappa, 0) - \max(e^\varkappa - 1, 0)] \\ &+ \frac{\lambda^3}{s^{3\bar{\omega}+1}} [\max(e^\varkappa, 0) - \max(e^\varkappa - 1, 0)] - \frac{\lambda^4}{s^{4\bar{\omega}+1}} [\max(e^\varkappa, 0) - \max(e^\varkappa - 1, 0)] + \frac{\lambda^5}{s^{5\bar{\omega}+1}} [\max(e^\varkappa, 0) - \max(e^\varkappa - 1, 0)]. \end{aligned} \tag{67}$$

By utilizing the inverse LT on both sides of equation (67), the approximate solution derived from the 5th iteration by LRPSM of equations (59) and (60) is as follows:

$$\begin{aligned}
w_5(\varkappa, \zeta) &= \max(e^\varkappa - 1, 0) + \frac{\lambda \zeta^\omega}{\Gamma(\omega + 1)} [\max(e^\varkappa, 0) - \max(e^\varkappa - 1, 0)] \\
&\quad - \frac{\lambda^2 \zeta^{2\omega}}{\Gamma(2\omega + 1)} [\max(e^\varkappa, 0) - \max(e^\varkappa - 1, 0)] + \frac{\lambda^3 \zeta^{3\omega}}{\Gamma(3\omega + 1)} [\max(e^\varkappa, 0) - \max(e^\varkappa - 1, 0)] \\
&\quad - \frac{\lambda^4 \zeta^{4\omega}}{\Gamma(4\omega + 1)} [\max(e^\varkappa, 0) - \max(e^\varkappa - 1, 0)] + \frac{\lambda^5 \zeta^{5\omega}}{\Gamma(5\omega + 1)} [\max(e^\varkappa, 0) - \max(e^\varkappa - 1, 0)].
\end{aligned} \tag{68}$$

When $\omega = 1$ is used in equation (68), we get as follows:

$$w_5(\varkappa, \zeta) = \max(e^\varkappa - 1, 0) + \left[\frac{\lambda \zeta}{1!} - \frac{\lambda^2 \zeta^2}{2!} + \frac{\lambda^3 \zeta^3}{3!} - \frac{\lambda^4 \zeta^4}{4!} + \frac{\lambda^5 \zeta^5}{5!} \right] [\max(e^\varkappa, 0) - \max(e^\varkappa - 1, 0)]. \tag{69}$$

As a result, the following is the exact solution of equations (59) and (60) for $\omega = 1$:

$$w(\varkappa, \zeta) = \max(e^\varkappa - 1, 0)e^{-\lambda \zeta} + \max(e^\varkappa, 0)(1 - e^{-\lambda \zeta}). \tag{70}$$

5. Numerical Simulation and Discussion

The findings of the results of the models presented in Problems 1–3 are evaluated graphically and numerically in this section. Error functions can be used to evaluate the numerical method's correctness and competency. It is important to provide the errors of the approximation analytical solution that the LRPSM offers in terms of an infinite fractional power series. We used the absolute and recurrence error functions to demonstrate the accuracy and strength of LRPSM.

The 2D graphs of the comparative analysis of the exact and approximative solutions derived by the suggested method in Problems 1–3 are shown in Figures 1(a)–1(c). These figures display the 2D plots of the precise solution and the approximate solution attained from the fifth iteration attained by LRPSM for Examples 1–3 when $\omega = 0.6, 0.7, 0.8, 0.9,$ and 1.0 in the range of $\zeta \in [0, 0.5]$. These graphs indicate that when $\omega \rightarrow 1.0$ is applied, the approximative solution converges to the precise solution. The precise result and the approximation overlap at $\omega = 1.0$, demonstrating the efficacy and accuracy of the recommended method.

Figures 2(a)–2(c) display the 2D curve of calculating the similarity with the help of absolute error of the approximation formed in the fifth step and the precise solution found by the suggested technique for Examples 1–3, respectively, for $\omega = 1.0$ in the range of $\zeta \in [0, 0.5]$. The article has shown that the fifth-step approximation solution of the recommended approach is very close to the exact solution. By showing the absolute error of the precise and approximate outputs on a graph, LRPSM's precision is proven.

The comparison article using the 3D curve is shown in Figures 3(a)–3(c) in the sense of the absolute error of the

approximate finding from the fifth iteration and the exact finding found using the suggested method to Examples 1–3, respectively, at $\omega = 1.0$ in the ranges of $\zeta \in [0, 0.2]$ and $\omega \in [0, 0.2]$. The article has revealed that the fifth-step approximation of the recommended approach is very similar to the precise result. The absolute error of the precise and approximation findings on 3D graphs serves as a demonstration of the precision of LRPSM.

In Tables 1–6, the numerical convergence of the approximation to the precise solution has been demonstrated by $|w^4(\varkappa, \zeta) - w^3(\varkappa, \zeta)|$ and $|w^5(\varkappa, \zeta) - w^4(\varkappa, \zeta)|$ in the range $\zeta \in [0, 0.1]$. Tables 1–6 shows that $w^4(\varkappa, \zeta)$ and $w^5(\varkappa, \zeta)$ obtained by the suggested method quickly approaches the $w(\varkappa, \zeta)$ when $\omega \rightarrow 1.0$. We can see from Tables 1, 3, and 5 that all of the test problems for the fourth stage have very low recurrence errors. The recurrence error will further decrease if we take into account the fifth-step approximation shown in Tables 2, 4, and 6. The approximation is rapidly approaching the exact solution as a result of the accuracy of our suggested strategy being demonstrated by the recurring error process. We arrived at the conclusion that the suggested approach is a feasible and efficient technique for solving particular classes of FODEs with fewer calculations and iteration steps.

For appropriately selected points, $|w(\varkappa, \zeta) - w^6(\varkappa, \zeta)|$ and $|w(\varkappa, \zeta) - w^7(\varkappa, \zeta)|$ in the range $\zeta \in [0, 0.1]$ obtained by LRPSM at $\omega = 1.0$ in Examples 1–3 are displayed in Tables 7–12 for comparison article in the sense of the absolute error of the approximate and the exact finding. We can see from Tables 7, 9, and 11 that approximate solutions derived from the 6th iteration for all of the test problems have very low errors. The absolute error will further decrease if we take into account the 7th-step approximation shown in Tables 8, 10, and 12. By quantitatively comparing the absolute inaccuracy of the precise and approximative findings, LRPSM's precision is shown.

Tables 13–15 also compares the absolute error of the approximations from the fifth iteration obtained by the LRPSM of Examples 1–3 at plausible short-listed grid points in the range $\zeta \in [0, 0.1]$ with the absolute error of the fifth-

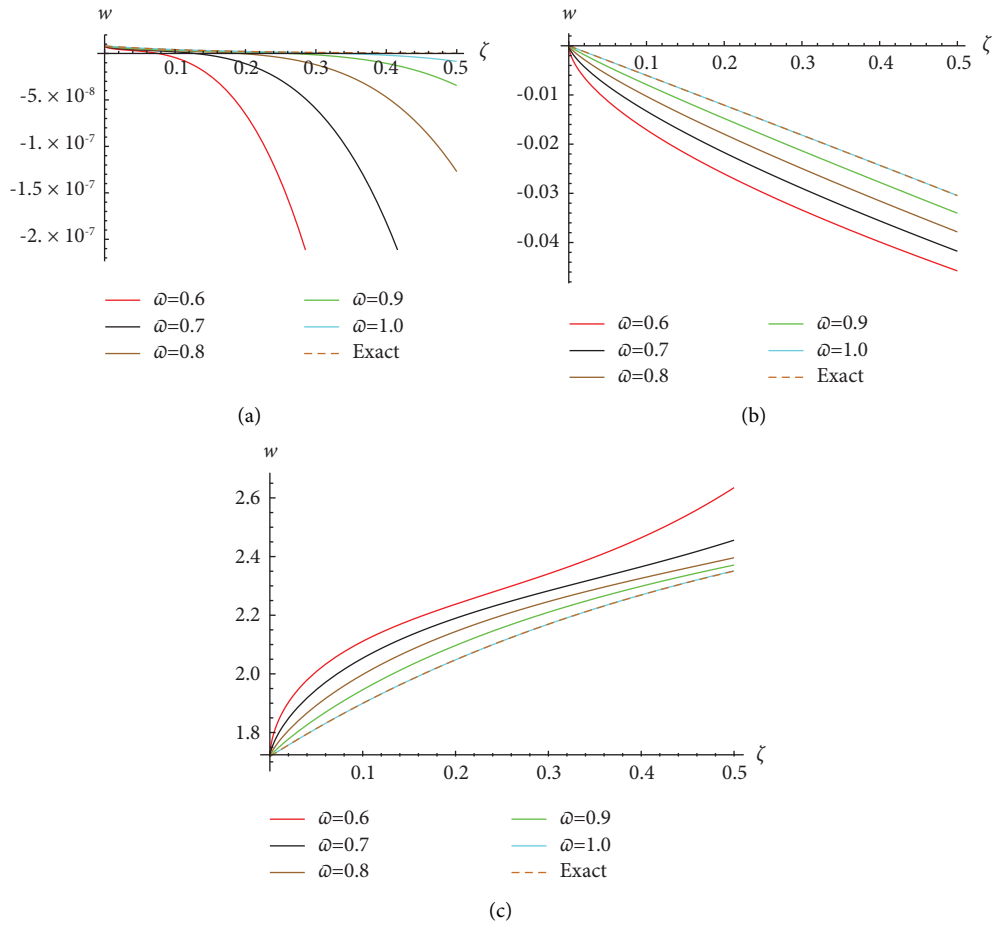


FIGURE 1: The approximate result of five iterations, as well as the exact result of $w(x, \zeta)$ for various values of ω in the range $\zeta \in [0, 0.5]$ for (a) Problem 1, when $\kappa = 0.002$, (b) Problem 2, when $\kappa = 1.0$, and (c) Problem 3, when $\kappa = 1.0$ and $\lambda = 2.0$.

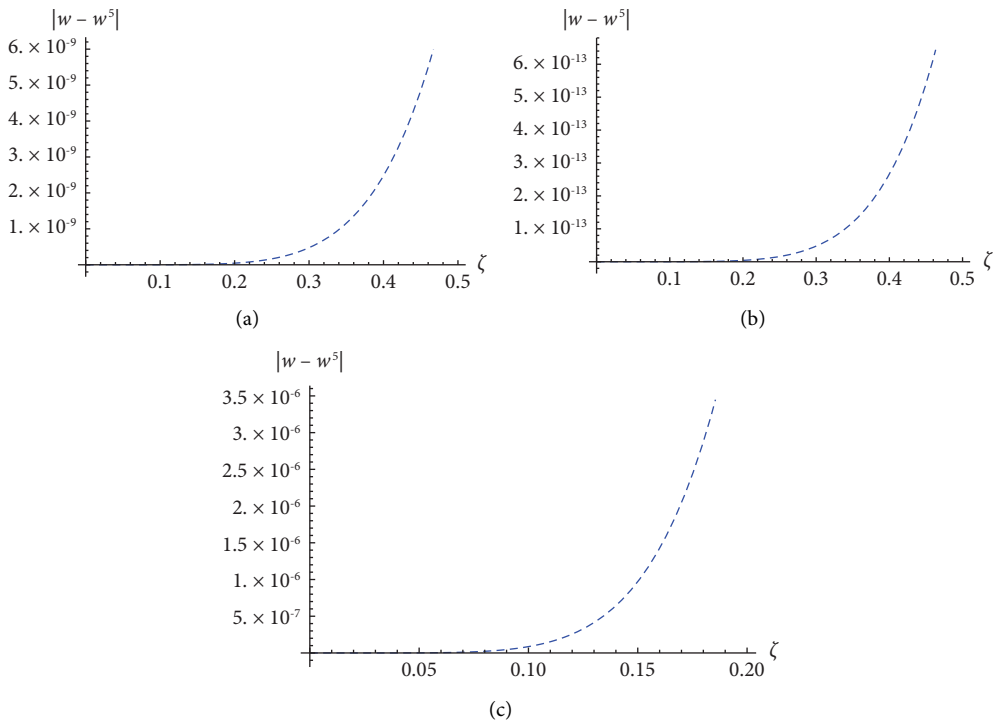


FIGURE 2: In Figure 2, the 2D curve of $|w(x, \zeta) - w^5(x, \zeta)|$ in the range $\zeta \in [0, 0.5]$, when $\omega = 1.0$ for (a) Problem 1, when $\kappa = 0.002$, (b) Problem 2, when $\kappa = 1.0$, and (c) Problem 3, when $\kappa = 1.0$ and $\lambda = 2.0$.

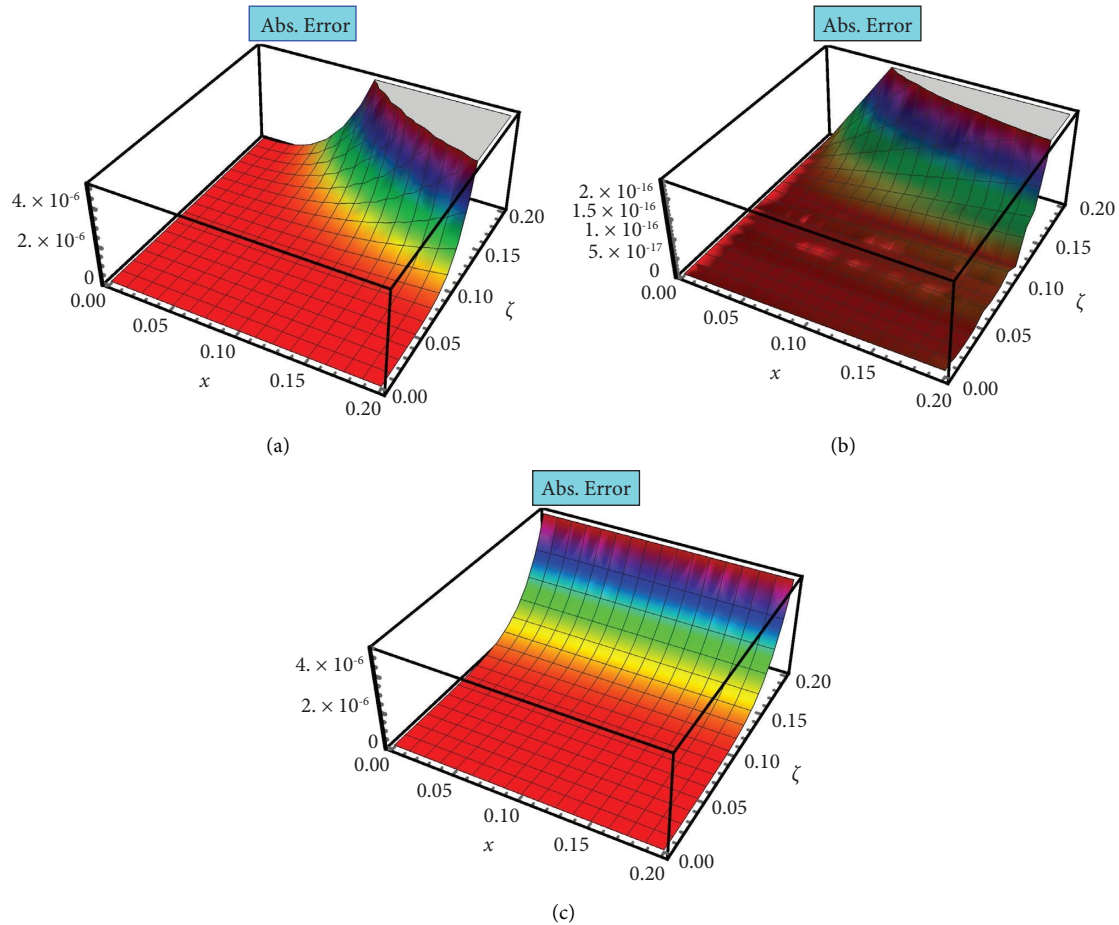


FIGURE 3: In Figure 3, the 3D curve of $|w(x, \zeta) - w^5(x, \zeta)|$ in the ranges $\zeta \in [0, 0.2]$ and $\varpi \in [0, 0.2]$, when $\varpi = 1.0$ for (a) Problem 1, (b) Problem 2, and (c) Problem 3, when $\lambda = 2.0$.

TABLE 1: $|w^4(x, \zeta) - w^3(x, \zeta)|$ of Problem 1 at different values of ϖ at $\kappa = 0.002$ determined by LRPSM at plausible locations in the range $\zeta \in [0, 0.1]$.

ζ	$\varpi = 0.7$	$\varpi = 0.8$	$\varpi = 0.9$	$\varpi = 1.0$
0.01	7.64160×10^{-12}	7.32938×10^{-13}	6.73357×10^{-14}	5.95021×10^{-15}
0.02	5.32192×10^{-11}	6.73539×10^{-12}	8.16495×10^{-13}	9.52033×10^{-14}
0.03	1.65624×10^{-10}	2.46522×10^{-11}	3.51465×10^{-12}	4.81967×10^{-13}
0.04	3.70640×10^{-10}	6.18955×10^{-11}	9.90060×10^{-12}	1.52325×10^{-12}
0.05	6.92309×10^{-10}	1.26407×10^{-10}	2.21074×10^{-11}	3.71888×10^{-12}
0.06	1.15347×10^{-9}	2.26543×10^{-10}	4.26177×10^{-11}	7.71147×10^{-12}
0.07	1.77606×10^{-9}	3.71006×10^{-10}	7.42333×10^{-11}	1.42865×10^{-11}
0.08	2.58129×10^{-9}	5.68794×10^{-10}	1.20052×10^{-10}	2.43721×10^{-11}
0.09	3.58974×10^{-9}	8.29169×10^{-10}	1.83450×10^{-10}	3.90393×10^{-11}
0.1	4.82152×10^{-9}	1.84106×10^{-10}	3.37478×10^{-11}	5.95021×10^{-12}

TABLE 2: $|w^5(x, \zeta) - w^4(x, \zeta)|$ of Problem 1 at different values of ϖ at $\kappa = 0.002$ determined by LRPSM at plausible locations in the range $\zeta \in [0, 0.1]$.

ζ	$\varpi = 0.7$	$\varpi = 0.8$	$\varpi = 0.9$	$\varpi = 1.0$
0.01	7.98018×10^{-13}	3.86764×10^{-14}	1.77337×10^{-15}	7.73527×10^{-17}
0.02	9.02854×10^{-12}	6.18822×10^{-13}	4.01268×10^{-14}	2.47529×10^{-15}
0.03	3.73196×10^{-11}	3.13278×10^{-12}	2.48797×10^{-13}	1.87967×10^{-14}
0.04	1.02146×10^{-10}	9.90115×10^{-12}	9.07967×10^{-13}	7.92092×10^{-14}
0.05	2.23053×10^{-10}	2.41727×10^{-11}	2.47836×10^{-12}	2.41727×10^{-13}
0.06	4.22223×10^{-10}	5.01246×10^{-11}	5.62964×10^{-12}	6.01495×10^{-13}
0.07	7.24195×10^{-10}	9.28619×10^{-11}	1.12653×10^{-11}	1.30007×10^{-12}
0.08	1.15565×10^{-9}	1.58418×10^{-10}	2.05449×10^{-11}	2.53469×10^{-12}
0.09	1.74526×10^{-9}	2.53756×10^{-10}	3.49053×10^{-11}	4.56760×10^{-12}
0.1	2.52355×10^{-9}	3.86764×10^{-10}	5.60790×10^{-11}	7.73527×10^{-12}

TABLE 3: $|w^4(\kappa, \zeta) - w^3(\kappa, \zeta)|$ of Problem 2 at different values of ϖ at $\kappa = 1.0$ determined by LRPSM at plausible locations in the range $\zeta \in [0, 0.1]$.

ζ	$\varpi = 0.7$	$\varpi = 0.8$	$\varpi = 0.9$	$\varpi = 1.0$
0.01	6.93499×10^{-12}	6.65164×10^{-13}	6.11093×10^{-14}	5.40000×10^{-15}
0.02	4.82981×10^{-11}	6.11258×10^{-12}	7.40995×10^{-13}	8.64000×10^{-14}
0.03	1.50309×10^{-10}	2.23726×10^{-11}	3.18965×10^{-12}	4.37400×10^{-13}
0.04	3.36367×10^{-10}	5.61721×10^{-11}	8.98510×10^{-12}	1.38240×10^{-12}
0.05	6.28292×10^{-10}	1.14718×10^{-10}	2.00632×10^{-11}	3.37500×10^{-12}
0.06	1.04681×10^{-9}	2.05595×10^{-10}	3.86769×10^{-11}	6.99840×10^{-12}
0.07	1.61183×10^{-9}	3.36699×10^{-10}	6.73690×10^{-11}	1.29654×10^{-11}
0.08	2.34260×10^{-9}	5.16198×10^{-10}	1.08951×10^{-10}	2.21184×10^{-11}
0.09	3.25780×10^{-9}	7.52497×10^{-10}	2.50264×10^{-9}	3.54294×10^{-11}
0.1	4.37568×10^{-9}	1.05421×10^{-9}	2.43280×10^{-10}	5.40000×10^{-11}

TABLE 4: $|w^5(\kappa, \zeta) - w^4(\kappa, \zeta)|$ of Problem 2 at different values of ϖ at $\kappa = 1.0$ determined by LRPSM at plausible locations in the range $\zeta \in [0, 0.1]$.

ζ	$\varpi = 0.7$	$\varpi = 0.8$	$\varpi = 0.9$	$\varpi = 1.0$
0.01	6.68516×10^{-15}	3.24000×10^{-16}	1.48559×10^{-17}	6.48000×10^{-19}
0.02	7.56340×10^{-14}	5.18400×10^{-15}	3.36151×10^{-16}	2.07360×10^{-17}
0.03	3.12634×10^{-13}	2.62440×10^{-14}	2.08423×10^{-15}	1.57464×10^{-16}
0.04	8.55701×10^{-13}	8.29440×10^{-14}	7.60623×10^{-15}	6.63552×10^{-16}
0.05	1.86856×10^{-12}	2.02500×10^{-13}	2.07618×10^{-14}	2.02500×10^{-15}
0.06	3.53705×10^{-12}	4.19904×10^{-13}	4.71607×10^{-14}	5.03885×10^{-15}
0.07	6.06674×10^{-12}	7.77924×10^{-13}	9.43715×10^{-14}	1.08909×10^{-14}
0.08	9.68115×10^{-12}	1.32710×10^{-12}	1.72109×10^{-13}	2.12337×10^{-14}
0.09	1.46205×10^{-11}	2.12576×10^{-12}	2.92409×10^{-13}	3.82638×10^{-14}
0.1	2.11403×10^{-11}	3.24000×10^{-12}	4.69785×10^{-13}	6.48000×10^{-14}

TABLE 5: $|w^4(\kappa, \zeta) - w^3(\kappa, \zeta)|$ of Problem 3 at different values of ϖ at $\kappa = 0.002$ when $\lambda = 2.0$ determined by LRPSM at plausible locations in the range $\zeta \in [0, 0.1]$.

ζ	$\varpi = 0.7$	$\varpi = 0.8$	$\varpi = 0.9$	$\varpi = 1.0$
0.01	1.71234×10^{-5}	1.64238×10^{-6}	1.50887×10^{-7}	1.33333×10^{-8}
0.02	1.19254×10^{-4}	1.5092810×10^{-5}	1.82962×10^{-6}	2.13333×10^{-7}
0.03	3.71134×10^{-4}	5.52410×10^{-5}	7.87569×10^{-6}	1.08000×10^{-6}
0.04	8.30537×10^{-4}	1.38697×10^{-4}	2.21854×10^{-5}	3.41333×10^{-6}
0.05	1.55134×10^{-3}	2.83255×10^{-4}	4.95386×10^{-5}	8.33333×10^{-6}
0.06	2.58472×10^{-3}	5.07642×10^{-4}	9.54985×10^{-5}	1.72800×10^{-5}
0.07	3.97984×10^{-3}	8.31357×10^{-4}	1.66343×10^{-4}	3.20133×10^{-5}
0.08	5.78419×10^{-3}	1.27456×10^{-3}	2.69015×10^{-4}	5.46133×10^{-5}
0.09	8.04396×10^{-3}	1.85802×10^{-3}	4.11079×10^{-4}	8.74800×10^{-5}
0.1	1.08042×10^{-2}	2.60300×10^{-3}	6.00692×10^{-4}	1.33333×10^{-4}

TABLE 6: $|w^5(\kappa, \zeta) - w^4(\kappa, \zeta)|$ of Problem 3 at different values of ϖ at $\kappa = 0.002$ when $\lambda = 2.0$ determined by LRPSM at plausible locations in the range $\zeta \in [0, 0.1]$.

ζ	$\varpi = 0.7$	$\varpi = 0.8$	$\varpi = 0.9$	$\varpi = 1.0$
0.01	2.75110×10^{-7}	1.33333×10^{-8}	6.11355×10^{-10}	2.66667×10^{-11}
0.02	3.11251×10^{-6}	2.13333×10^{-7}	1.38334×10^{-8}	8.53333×10^{-10}
0.03	1.28656×10^{-5}	1.08000×10^{-6}	8.57707×10^{-8}	6.48000×10^{-9}
0.04	3.52140×10^{-5}	3.41333×10^{-6}	3.13014×10^{-7}	2.73067×10^{-8}
0.05	7.68955×10^{-5}	8.33333×10^{-6}	8.54394×10^{-7}	8.33333×10^{-8}
0.06	1.45558×10^{-4}	1.72800×10^{-5}	1.94077×10^{-6}	2.07360×10^{-7}
0.07	2.49660×10^{-4}	3.20133×10^{-5}	3.88360×10^{-6}	4.48187×10^{-7}
0.08	3.98401×10^{-4}	5.46133×10^{-5}	7.08269×10^{-6}	8.73813×10^{-7}
0.09	6.01665×10^{-4}	8.74800×10^{-5}	1.20333×10^{-5}	1.57464×10^{-6}
0.1	8.69973×10^{-4}	1.33333×10^{-4}	1.93327×10^{-5}	2.66667×10^{-6}

TABLE 7: $|w(\kappa, \zeta) - w^6(\kappa, \zeta)|$ of Problem 1 at $\kappa = 0.003$ when $\varpi = 1.0$ determined by LRPSM at plausible locations in the range $\zeta \in [0, 0.1]$.

ζ	$w(\kappa, \zeta)$	$w^6(\kappa, \zeta)$	$ w^6(\kappa, \zeta) - w(\kappa, \zeta) $
0.01	2.53008×10^{-8}	2.53008×10^{-8}	2.60496×10^{-20}
0.02	2.37086×10^{-8}	2.37086×10^{-8}	3.30768×10^{-18}
0.03	2.22165×10^{-8}	2.22165×10^{-8}	5.60646×10^{-17}
0.04	2.08184×10^{-8}	2.08184×10^{-8}	4.16685×10^{-16}
0.05	1.95082×10^{-8}	1.95082×10^{-8}	1.97128×10^{-15}
0.06	1.82805×10^{-8}	1.82805×10^{-8}	7.00821×10^{-15}
0.07	1.71301×10^{-8}	1.71301×10^{-8}	2.04572×10^{-14}
0.08	1.60521×10^{-8}	1.60521×10^{-8}	5.16919×10^{-14}
0.09	1.50419×10^{-8}	1.50420×10^{-8}	1.16989×10^{-13}
0.1	1.40952×10^{-8}	1.40955×10^{-8}	2.42728×10^{-13}

TABLE 8: $|w(\kappa, \zeta) - w^7(\kappa, \zeta)|$ of Problem 1 at $\kappa = 0.003$ when $\varpi = 1.0$ determined by LRPSM at plausible locations in the range $\zeta \in [0, 0.1]$.

ζ	$w(\kappa, \zeta)$	$w^7(\kappa, \zeta)$	$ w(\kappa, \zeta) - w^7(\kappa, \zeta) $
0.01	2.53008×10^{-8}	2.53008×10^{-8}	2.11758×10^{-22}
0.02	2.37086×10^{-8}	2.37086×10^{-8}	5.38461×10^{-20}
0.03	2.22165×10^{-8}	2.22165×10^{-8}	1.37022×10^{-18}
0.04	2.08184×10^{-8}	2.08184×10^{-8}	1.35902×10^{-17}
0.05	1.95082×10^{-8}	1.95082×10^{-8}	8.0436×10^{-17}
0.06	1.82805×10^{-8}	1.82805×10^{-8}	3.43448×10^{-16}
0.07	1.71301×10^{-8}	1.71301×10^{-8}	1.17061×10^{-15}
0.08	1.60521×10^{-8}	1.60521×10^{-8}	3.38332×10^{-15}
0.09	1.50419×10^{-8}	1.50418×10^{-8}	8.62135×10^{-15}
0.1	1.40952×10^{-8}	1.40952×10^{-8}	1.98913×10^{-14}

TABLE 9: $|w(\kappa, \zeta) - w^6(\kappa, \zeta)|$ of Problem 2 at $\kappa = 1.0$ when $\varpi = 1.0$ determined by LRPSM at plausible locations in the range $\zeta \in [0, 0.1]$.

ζ	$w(\kappa, \zeta)$	$w^6(\kappa, \zeta)$	$ w(\kappa, \zeta) - w^6(\kappa, \zeta) $
0.01	-0.00060018	-0.00060018	2.95987×10^{-17}
0.02	-0.00120072	-0.00120072	4.42354×10^{-17}
0.03	-0.00180162	-0.00180162	7.69784×10^{-17}
0.04	-0.00240288	-0.00240288	7.19910×10^{-17}
0.05	-0.00300450	-0.00300450	5.46438×10^{-17}
0.06	-0.00360649	-0.00360649	1.00614×10^{-16}
0.07	-0.00420883	-0.00420883	5.72459×10^{-17}
0.08	-0.00481154	-0.00481154	3.12250×10^{-17}
0.09	-0.00541461	-0.00541461	7.28584×10^{-17}
0.1	-0.00601804	-0.00601804	5.89806×10^{-17}

TABLE 10: $|w(\kappa, \zeta) - w^7(\kappa, \zeta)|$ of Problem 2 at $\kappa = 1.0$ when $\varpi = 1.0$ determined by LRPSM at plausible locations in the range $\zeta \in [0, 0.1]$.

ζ	$w(\kappa, \zeta)$	$w^7(\kappa, \zeta)$	$ w(\kappa, \zeta) - w^7(\kappa, \zeta) $
0.01	-0.00060018	-0.00060018	2.94903×10^{-17}
0.02	-0.00120072	-0.00120072	4.40186×10^{-17}
0.03	-0.00180162	-0.00180162	7.67615×10^{-17}
0.04	-0.00240288	-0.00240288	7.15573×10^{-17}
0.05	-0.00300450	-0.00300450	5.50775×10^{-17}
0.06	-0.00360649	-0.00360649	1.00614×10^{-16}
0.07	-0.00420883	-0.00420883	5.63785×10^{-17}
0.08	-0.00481154	-0.00481154	3.12250×10^{-17}
0.09	-0.00541461	-0.00541461	7.28584×10^{-17}
0.1	-0.00601804	-0.00601804	5.89806×10^{-17}

TABLE 11: $|w(\varkappa, \zeta) - w^6(\varkappa, \zeta)|$ of Problem 3 at $\varkappa = 1.0$ and $\lambda = 2.0$ when $\varpi = 1.0$ determined by LRPSM at plausible locations in the range $\zeta \in [0, 0.1]$.

ζ	$w(\varkappa, \zeta)$	$w^6(\varkappa, \zeta)$	$ w(\varkappa, \zeta) - w^6(\varkappa, \zeta) $
0.01	1.73808	1.73808	2.22045×10^{-16}
0.02	1.75749	1.75749	3.24185×10^{-14}
0.03	1.77652	1.77652	5.51115×10^{-13}
0.04	1.79517	1.79517	4.11982×10^{-12}
0.05	1.81344	1.81344	1.95961×10^{-11}
0.06	1.83136	1.83136	7.00426×10^{-11}
0.07	1.84892	1.84892	2.05550×10^{-10}
0.08	1.86614	1.86614	5.22144×10^{-10}
0.09	1.88301	1.88301	1.18793×10^{-9}
0.1	1.73808	1.89955	2.47757×10^{-9}

TABLE 12: $|w(\varkappa, \zeta) - w^7(\varkappa, \zeta)|$ of Problem 3 at $\varkappa = 1.0$ and $\lambda = 2.0$ when $\varpi = 1.0$ determined by LRPSM at plausible locations in the range $\zeta \in [0, 0.1]$.

ζ	$w(\varkappa, \zeta)$	$w^7(\varkappa, \zeta)$	$ w(\varkappa, \zeta) - w^7(\varkappa, \zeta) $
0.01	1.73808	1.73808	0.0
0.02	1.75749	1.75749	0.0
0.03	1.77652	1.77652	4.21885×10^{-15}
0.04	1.79517	1.79517	4.10783×10^{-14}
0.05	1.81344	1.81344	2.45359×10^{-13}
0.06	1.83136	1.83136	1.05249×10^{-12}
0.07	1.84892	1.84892	3.60423×10^{-12}
0.08	1.86614	1.86614	1.04659×10^{-11}
0.09	1.88301	1.88301	2.67941×10^{-11}
0.1	1.73808	1.89955	6.21085×10^{-11}

TABLE 13: $|w(\varkappa, \zeta) - w^5(\varkappa, \zeta)|$ in different approaches for Problem 1 at $\varkappa = 0.002$ when $\varpi = 1.0$ at plausible locations in the range $\zeta \in [0, 0.1]$.

ζ	Abs.error [LRPSM]	Abs.error [PDTM] [34]
0.01	8.30269×10^{-19}	8.30269×10^{-19}
0.02	5.26512×10^{-17}	5.26512×10^{-17}
0.03	5.94281×10^{-16}	5.94281×10^{-16}
0.04	3.30894×10^{-15}	3.30894×10^{-15}
0.05	1.25095×10^{-14}	1.25095×10^{-14}
0.06	3.70206×10^{-14}	3.70206×10^{-14}
0.07	9.25270×10^{-14}	9.25270×10^{-14}
0.08	2.04357×10^{-13}	2.04357×10^{-13}
0.09	4.10678×10^{-13}	4.10678×10^{-13}
0.1	7.66068×10^{-13}	7.66068×10^{-13}

TABLE 14: $|w(\varkappa, \zeta) - w^5(\varkappa, \zeta)|$ in different approaches for Problem 2 at $\varkappa = 1.0$ when $\varpi = 1.0$ at plausible locations in the range $\zeta \in [0, 0.1]$.

ζ	Abs.error [LRPSM]	Abs.error [ATDM] [35]
0.01	2.94903×10^{-17}	2.94903×10^{-17}
0.02	4.40186×10^{-17}	4.40186×10^{-17}
0.03	7.67615×10^{-17}	7.67615×10^{-17}
0.04	7.11237×10^{-17}	7.11237×10^{-17}
0.05	5.63785×10^{-17}	5.63785×10^{-17}
0.06	1.03216×10^{-16}	1.03216×10^{-16}
0.07	6.41848×10^{-17}	6.41848×10^{-17}
0.08	1.47451×10^{-17}	1.47451×10^{-17}
0.09	1.07553×10^{-16}	1.07553×10^{-16}
0.1	1.23165×10^{-16}	1.23165×10^{-16}

TABLE 15: $|w(\kappa, \zeta) - w^s(\kappa, \zeta)|$ in different approaches for Problem 3 at $\kappa = 1.0$ and $\lambda = 2.0$ when $\varpi = 1.0$ at plausible locations in the range $\zeta \in [0, 0.1]$.

ζ	Abs.error [LRPSM]	Abs.error [HPM] [36]
0.01	8.88178×10^{-14}	8.88178×10^{-14}
0.02	5.65636×10^{-12}	5.65636×10^{-12}
0.03	6.42488×10^{-11}	6.42488×10^{-11}
0.04	3.59969×10^{-10}	3.59969×10^{-10}
0.05	1.36929×10^{-9}	1.36929×10^{-9}
0.06	4.07716×10^{-9}	4.07716×10^{-9}
0.07	1.02521×10^{-8}	1.02521×10^{-8}
0.08	2.27795×10^{-8}	2.27795×10^{-8}
0.09	4.60513×10^{-8}	4.60513×10^{-8}
0.1	8.64113×10^{-8}	8.64113×10^{-8}

step approximations obtained by various methods, including the PDTM [34], ATDM [35], and HPM [36]. Strong agreement between the results produced using the suggested method and various series solution techniques shows that the LRPSM is a useful substitute for approaches based on He's or Adomian polynomials.

6. Conclusion

In this article, we used the LRPSM to solve time-fractional BSOPE in the sense of CD. The effectiveness of the LRPSM has been demonstrated by results in both graphs and numerically. The approximate solutions achieved using LRPSM are in perfect agreement with the corresponding exact solutions, as can be seen from the graphs and tables. The numerical evidence for the convergence of the approximate solution to the exact solution is presented in Tables 1–6. The comparison article is established in Tables 7–12 in terms of the absolute error of the approximate and exact solutions. The results of these numerical approaches are also compared with the PDTM, ATDM, and HPM in terms of absolute errors in Tables 13–15.

The results obtained using the suggested approach, which demonstrates excellent agreement with PDTM, ATDM, and HPM, show that LRPSM is a suitable replacement tool for He's or Adomian polynomial-based methods used to solve FODEs. When determining the coefficients for a series such as the RPSM, the fractional derivative needs to be determined each time. However, LRPSM just needs the idea of an infinite limit. As a result, the computations required to determine the coefficients are minimal. The results led us to the conclusion that our technique is easy to use, accurate, flexible, and effective.

Data Availability

No data were generated or analyzed during the current study.

Conflicts of Interest

The authors declare that they have no conflicts of interest.

Authors' Contributions

The authors declare that the study was realized in collaboration with equal responsibility. All authors read and approved the final manuscript.

References

- [1] V. V. Kulish and J. L. Lage, "Application of fractional calculus to fluid mechanics," *Journal of Fluids Engineering*, vol. 124, no. 3, pp. 803–806, 2002.
- [2] V. E. Tarasov, "On history of mathematical economics: application of fractional calculus," *Mathematics*, vol. 7, no. 6, p. 509, 2019.
- [3] H. Sun, Y. Zhang, D. Baleanu, W. Chen, and Y. Chen, "A new collection of real world applications of fractional calculus in science and engineering," *Communications in Nonlinear Science and Numerical Simulation*, vol. 64, pp. 213–231, 2018.
- [4] Y. A. Rossikhin and M. V. Shitikova, "Application of fractional calculus for dynamic problems of solid mechanics: novel trends and recent results," *Applied Mechanics Reviews*, vol. 63, no. 1, 2010.
- [5] D. Valério, J. T. Machado, and V. Kiryakova, "Some pioneers of the applications of fractional calculus," *Fractional Calculus and Applied Analysis*, vol. 17, no. 2, pp. 552–578, 2014.
- [6] S. Rezapour, M. I. Liaqat, and S. Etemad, "An effective new iterative method to solve conformable Cauchy reaction-diffusion equation via the Shehu transform," *Journal of Mathematics*, vol. 2022, Article ID 4172218, 12 pages, 2022.
- [7] E. Bas and R. Ozarslan, "Real world applications of fractional models by Atangana-Baleanu fractional derivative," *Chaos, Solitons & Fractals*, vol. 116, pp. 121–125, 2018.
- [8] M. I. Liaqat, A. Khan, A. Akgül, and M. Ali, "A novel numerical technique for fractional ordinary differential equations with proportional delay," *Journal of Function Spaces*, vol. 2022, Article ID 6333084, 21 pages, 2022.
- [9] A. Traore and N. Sene, "Model of economic growth in the context of fractional derivative," *Alexandria Engineering Journal*, vol. 59, no. 6, pp. 4843–4850, 2020.
- [10] A. Khan, M. I. Liaqat, M. Younis, and A. Alam, "Approximate and exact solutions to fractional order Cauchy reaction-diffusion equations by new combine techniques," *Journal of Mathematics*, vol. 2021, Article ID 5337255, 12 pages, 2021.
- [11] R. Hilfer, Y. Luchko, and Z. Tomovski, "Operational method for the solution of fractional differential equations with

- generalized Riemann-Liouville fractional derivatives,” *Fractional Calculus and Applied Analysis*, vol. 12, no. 3, pp. 299–318, 2009.
- [12] M. I. Liaqat and E. Okyere, “The fractional series solutions for the conformable time-fractional swift-hohenberg equation through the conformable shehu daftardar-jafari approach with comparative analysis,” *Journal of Mathematics*, vol. 2022, Article ID 3295076, 20 pages, 2022.
- [13] M. I. Liaqat, A. Khan, M. Alam, M. K. Pandit, S. Etemad, and S. Rezapour, “Approximate and closed-form solutions of Newell-Whitehead-Segel equations via modified conformable Shehu transform decomposition method,” *Mathematical Problems in Engineering*, vol. 2022, Article ID 6752455, 14 pages, 2022.
- [14] B. J. Gireesha and G. Sowmya, “Heat transfer analysis of an inclined porous fin using Differential Transform Method,” *International Journal of Ambient Energy*, vol. 43, no. 1, pp. 3189–3195, 2022.
- [15] M. Nadeem, F. Li, and H. Ahmad, “Modified Laplace variational iteration method for solving fourth-order parabolic partial differential equation with variable coefficients,” *Computers & Mathematics with Applications*, vol. 78, no. 6, pp. 2052–2062, 2019.
- [16] S. M. Aznam and M. S. H. Chowdhury, “Generalized Haar wavelet operational matrix method for solving hyperbolic heat conduction in thin surface layers,” *Results in Physics*, vol. 11, pp. 243–252, 2018.
- [17] P. A. Naik, J. Zu, and M. Ghoreishi, “Estimating the approximate analytical solution of HIV viral dynamic model by using homotopy analysis method,” *Chaos, Solitons & Fractals*, vol. 131, Article ID 109500, 2020.
- [18] M. I. Liaqat, A. Khan, M. Alam, and M. K. Pandit, “A highly accurate technique to obtain exact solutions to time-fractional quantum mechanics problems with zero and nonzero trapping potential,” *Journal of Mathematics*, vol. 2022, Article ID 9999070, 20 pages, 2022.
- [19] D. Baleanu, S. Zibaei, M. Namjoo, and A. Jajarmi, “A non-standard finite difference scheme for the modeling and nonidentical synchronization of a novel fractional chaotic system,” *Advances in Difference Equations*, vol. 2021, no. 1, pp. 1–19, 2021.
- [20] M. I. Liaqat, A. Khan, and A. Akgül, “Adaptation on power series method with conformable operator for solving fractional order systems of nonlinear partial differential equations,” *Chaos, Solitons & Fractals*, vol. 157, Article ID 111984, 2022.
- [21] W. Xiang, S. Yan, J. Wu, and W. Niu, “Dynamic response and sensitivity analysis for mechanical systems with clearance joints and parameter uncertainties using Chebyshev polynomials method,” *Mechanical Systems and Signal Processing*, vol. 138, Article ID 106596, 2020.
- [22] O. Abu Arqub, “Application of residual power series method for the solution of time-fractional Schrödinger equations in one-dimensional space,” *Fundamenta Informaticae*, vol. 166, no. 2, pp. 87–110, 2019.
- [23] M. I. Liaqat and A. Akgül, “A novel approach for solving linear and nonlinear time-fractional Schrödinger equations,” *Chaos, Solitons & Fractals*, vol. 162, Article ID 112487, 2022.
- [24] T. Eriqat, A. El-Ajou, N. O. Moa’ath, Z. Al-Zhour, and S. Momani, “A new attractive analytic approach for solutions of linear and nonlinear neutral fractional pantograph equations,” *Chaos, Solitons & Fractals*, vol. 138, Article ID 109957, 2020.
- [25] M. Alaroud, “Application of Laplace residual power series method for approximate solutions of fractional IVP’s,” *Alexandria Engineering Journal*, vol. 61, no. 2, pp. 1585–1595, 2022.
- [26] M. Alquran, M. Ali, M. Alsukhour, and I. Jaradat, “Promoted residual power series technique with Laplace transform to solve some time-fractional problems arising in physics,” *Results in Physics*, vol. 19, Article ID 103667, 2020.
- [27] M. A. N. Oqielat, T. Eriqat, Z. Al-Zhour, O. Ogilat, and A. El-Ajou, I. Hashim, Construction of fractional series solutions to nonlinear fractional reaction diffusion for bacteria growth model via Laplace residual power series method,” *International Journal of Dynamics and Control*, pp. 1–8, 2022.
- [28] H. Aljarrah, M. Alaroud, A. Ishak, and M. Darus, “Approximate solution of nonlinear time-fractional PDEs by Laplace residual power series method,” *Mathematics*, vol. 10, no. 12, p. 1980, 2022.
- [29] R. Saadeh, A. Burqan, and A. El-Ajou, “Reliable solutions to fractional Lane-Emden equations via Laplace transform and residual error function,” *Alexandria Engineering Journal*, vol. 61, no. 12, pp. 10551–10562, 2022.
- [30] S. M. Nuugulu, F. Gideon, and K. C. Patidar, “A robust numerical solution to a time-fractional Black-Scholes equation,” *Advances in Difference Equations*, vol. 2021, no. 1, pp. 1–25, 2021.
- [31] R. H. De Staelen and A. S. Hendy, “Numerically pricing double barrier options in a time-fractional Black-Scholes model,” *Computers & Mathematics with Applications*, vol. 74, no. 6, pp. 1166–1175, 2017.
- [32] V. P. Dubey, R. Kumar, and D. Kumar, “A reliable treatment of residual power series method for time-fractional Black-Scholes European option pricing equations,” *Physica A: Statistical Mechanics and Its Applications*, vol. 533, Article ID 122040, 2019.
- [33] M. Yavuz and N. Özdemir, “A different approach to the European option pricing model with new fractional operator,” *Mathematical Modelling of Natural Phenomena*, vol. 13, no. 1, p. 12, 2018.
- [34] S. O. Edeki, O. O. Ugbebor, and E. A. Owoloko, “Analytical solution of the time-fractional order Black-Scholes model for stock option valuation on no dividend yield basis,” *IAENG International Journal of Applied Mathematics*, vol. 47, no. 4, pp. 1–10, 2017.
- [35] S. Alfaqeh and T. Ozis, “Solving fractional Black-Scholes European option pricing equations by Aboodh transform Decomposition method,” *Palestine Journal of Mathematics*, vol. 9, no. 2, pp. 915–924, 2020.
- [36] S. Kumar, D. Kumar, and J. Singh, “Numerical computation of fractional Black-Scholes equation arising in financial market,” *Egyptian Journal of Basic and Applied Sciences*, vol. 1, no. 3-4, pp. 177–183, 2014.
- [37] M. A. M. Ghandehari and M. Ranjbar, “European option pricing of fractional Black-Scholes model with new Lagrange multipliers,” *Computational Methods for Differential Equations*, vol. 2, no. 1, pp. 1–10, 2014.
- [38] S. O. Edeki, R. M. Jena, S. Chakraverty, and D. Baleanu, “Coupled transform method for time-space fractional Black-Scholes option pricing model,” *Alexandria Engineering Journal*, vol. 59, no. 5, pp. 3239–3246, 2020.
- [39] M. A. M. Ghandehari and M. Ranjbar, “European option pricing of fractional version of the Black-Scholes model: approach via expansion in series,” *International Journal of Nonlinear Science*, vol. 17, no. 2, pp. 105–110, 2014.

- [40] A. R. Kanth and K. Aruna, "Solution of time fractional Black-Scholes European option pricing equation arising in financial market," *Nonlinear Engineering*, vol. 5, no. 4, pp. 269–276, 2016.
- [41] M. I. Liaqat, S. Etemad, S. Rezapour, and C. Park, "A novel analytical Aboodh residual power series method for solving linear and nonlinear time-fractional partial differential equations with variable coefficients," *AIMS Mathematics*, vol. 7, no. 9, pp. 16917–16948, 2022.
- [42] M. Alquran, "Analytical solutions of fractional foam drainage equation by residual power series method," *Mathematical sciences*, vol. 8, no. 4, pp. 153–160, 2014.
- [43] D. G. Prakasha, P. Veerasha, and H. M. Baskonus, "Residual power series method for fractional Swift-Hohenberg equation," *Fractal and fractional*, vol. 3, no. 1, p. 9, 2019.

Research Article

On a Mathematical Model of Tumor-Immune Interaction with a Piecewise Differential and Integral Operator

Shahram Rezapour ^{1,2}, Chernet Tuge Deressa ³, Robert G. Mukharlyamov,⁴
and Sina Etemad ¹

¹Department of Mathematics, Azarbaijan Shahid Madani University, Tabriz, Iran

²Department of Medical Research, China Medical University Hospital, China Medical University, Taichung, Taiwan

³Department of Mathematics, College of Natural Sciences, Jimma University, Jimma, Ethiopia

⁴Peoples' Friendship University of Russia (RUDN University), 6 Miklukho-Maklaya Street, Moscow, 117198, Russia

Correspondence should be addressed to Shahram Rezapour; rezapourshahram@yahoo.ca, Chernet Tuge Deressa; chernet.deressa@ju.edu.et, and Sina Etemad; sina.etemad@azaruniv.ac.ir

Received 27 July 2022; Revised 7 September 2022; Accepted 20 September 2022; Published 15 October 2022

Academic Editor: Watcharaporn Cholamjiak

Copyright © 2022 Shahram Rezapour et al. This is an open access article distributed under the Creative Commons Attribution License, which permits unrestricted use, distribution, and reproduction in any medium, provided the original work is properly cited.

The representation of mathematical models via piecewise differential and integral operators for dynamic systems has this potential to capture cross-over behaviors such as a passage from deterministic to randomness which can be exhibited by different systems. A 3D mathematical model, similar to the prey-predator system, of tumor-immune interaction with piecewise differential and integral operators is developed and analyzed. Three different scenarios, namely, cross-overs from deterministic to randomness, the Mittag-Leffler law to randomness, and a cross-over behavior from fading memory to the power-law and a random process, are considered. The existence, uniqueness, positivity, and boundedness of the solutions of the systems are proved via the linear growth and Lipschitz conditions. The numerical approximations by Toufik, Atangana, and Araz are used for approximation of solutions and simulation of the piecewise models in different scenarios. From the nondimensionalized version of the 3D model representation, it is shown that the parameter values have an impact on the growth of tumor cells, and activating the proliferation of the resting cells has negatively affected the development of tumor cells. Moreover, the dynamics of tumor-immune interaction exhibited a cross-over behavior, and this behavior is exposed by the piecewise modeling approach used for the representations.

1. Introduction

The classical differential equations (ordinary and partial differential equations) were developed based on the concept of rate of changes, and it has been used and investigated for several decades. They have been used in developing several mathematical models representing real-world problems and are effectively used to make their analysis. Nevertheless, some drawbacks with the classical differential equations were observed. The classical differential equations are not efficient in replicating observed realities. For instance, some cases require randomness and cannot be captured by the classical

differential equations, and as a result, the stochastic differential equations came into being and have been used successfully.

In the same way, there are some problems in real world that cannot be captured by stochastic differential equations, and this led to the development of different concepts of fractional derivatives and integrals. Different concepts of fractional operators have been used to capture trends including nonlocalities, power-law processes, memory effects, fractal processes, and some other real-world problems. Though there are different endeavors made by mathematicians to capture different real-world problems using mathematical models, the issue of capturing dynamic systems that display

multiple behaviors is not fully addressed (see [1] and the references therein). With this understanding and to solve the problem of capturing dynamics of real-world problems with cross-over behaviors, Atangana and Araz [1, 2] developed a novel concept named piecewise modeling that involves differential and integral operators.

In this study, the notion of piecewise modeling is considered to develop different piecewise mathematical models for tumor-immune interaction using the classical, stochastic, and fractional derivative concepts.

There are several studies conducted on tumor-immune interaction by using different mathematical models based on classical and fractional derivative concepts. A few of them are reviewed as follows: Kaur and Ahmad [3] developed a mathematical model of tumor-immune interaction by including the Michaelis-Menten function in the model. The authors used the classical derivative and showed that the inclusion of the Michaelis-Menten function helped in achieving stability of the dynamical system and increased the rate of growth of resting cells. A seven-dimensional dynamical model of the tumor-immune system equipped with the Reimann-Liouville fractal-fractional operator with the Mittag-Leffler-type kernel was considered by Farman et al. [4]. The results showed that the IL-12 cytokine and anti-PD-L1 inhibitor increased the immune system and decreased the cancer cells. Ahmed et al. [5] applied ABC fractal-fractional operators to develop a mathematical model and visualize the tumor-immune relationship. Various mathematical models addressing different cancer treatments such as cytotoxic chemotherapy, immunotherapy, and their combination are investigated by Depillis et al. [6].

Wilkie [7] discussed different mathematical models with the classical derivatives of tumor growth in the presence of an immune response, and the findings suggest that feedback from the tumor to the immune response induces the existence of dormant cancer cells. A mathematical model incorporating three types of immunotherapy and focusing on the inhibitory role of Tregs in the tumor-immune system is developed and analyzed by Zhongtao et al. [8]. A mathematical model describing how cancer cell progresses and survives an encounter with the immune cell population is developed and discussed in [9]. The chaotic dynamics of a tumor-immune interaction model with delay are considered in [10]. Kuznetsov et al. [11] developed a tumor-immune interaction mathematical model and described the response of effector cells to the growth of an immunogenic tumor. There are many other studies made on the tumor-immune interaction (see for instance [12–16]).

As the concept of piecewise differential and integral operators is relatively new, hence, little literature is available. The concept of the piecewise derivative and integral operator is used with different fractional derivatives to investigate an SIR mathematical model of COVID-19 in [17]. Zeb et al. [18] investigated a five-dimensional compartmental model of COVID-19 with the concept of piecewise derivative and integral operators combining the Caputo-Fabrizio, classical, and stochastic differential equations. A mathematical model representing an interaction in a food web is considered, and the concept of piecewise

differential and integral operator is imposed for investigation in [19]. A mathematical model of the third wave of COVID-19 is developed and considered with the concept of piecewise differential and integral operators [2]. The concept of piecewise differentiation and integral operator is applied to a CAR-T cells-SARS-2 virus model [20]. Of course, different concepts of fractional derivatives have been used by several authors for investigation of different dynamical systems and different applications (see for instance [21–28] and the references therein).

To the best of the researchers' knowledge, there is no single study conducted on a Tumor-immune interaction mathematical model in the sense of piecewise differential and integral operators. The concept of piecewise derivatives and integrals in capturing real-world problems with multiple behaviors is a novel result as it empowers researchers in the area to use different concepts of derivative and integral operators at the same time to study multiple behaviors of a given dynamic system which may not otherwise be possible.

This study, therefore, focuses on discovering different cross-over behaviors in a mathematical model of tumor-immune interaction in the sense of the piecewise differential and integral operators developed by Atangana and Seda. The classical differential equations, stochastic differential equations, and different concepts of fractional operators are included in the formation of the piecewise differential and integral operators. Accordingly, three different scenarios of the mathematical models were developed: a cross-over from deterministic to randomness, a cross-over from Mittag-Leffler law to randomness, and a cross-over from exponential decay to power-law and random process.

The remaining part of this paper is organized as follows: The formulation and description of the model, the parameters and their description, and the formulation of three piecewise models representing the system are considered in Section 2. Section 3 is devoted to the existence, uniqueness, positivity, and boundedness of the piecewise models. Numerical approximations of the piecewise models are considered in Section 4 followed by simulations in Section 5. The conclusion is provided in Section 6 followed by the list of references in the last section.

2. Formulation of Models

In this section, the tumor-immune mathematical model used in this study is described. The system comprises three nonlinear differential equations that modify to different concepts of fractional operators and stochastic differential equations. The model involves the concentration of tumor cells at time t , represented by $X(t)$, the concentration of hunting predator cells at time t , represented by $Y(t)$, and the concentration of resting predator cells at time t , represented by $Z(t)$. The hunting and resting predator cells are normal tissue cells. The model is similar to the prey-predator system and originally developed by Kaur and Ahmad [3] describing the growth, death, and interaction among this population and is given as shown in:

$$\begin{aligned} \dot{X} &= \Lambda + r_1 X \left(1 - \frac{X}{k_1}\right) - \alpha_1 XY, \\ \dot{Y} &= \beta YZ - d_1 Y - \alpha_2 YX, \\ \dot{Z} &= r_2 Z \left(1 - \frac{Z}{k_2}\right) - \beta YZ - d_2 Z + \frac{\rho XZ}{X + \eta}, \end{aligned} \tag{1}$$

where all the parameters in (1) are nonnegative and the initial conditions are

$$X(0) > 0, Y(0) > 0, Z(0) > 0, \text{ and } k_1 > k_2. \tag{2}$$

The first equation of (1) describes the rate of growth of concentration of tumor cells. It is assumed that tumor cells follow the logistic growth in the absence of any immune intervention (hunting and resting predator CTL cells). The extinction of hunting cells and tumor cells is proportional to the densities of both the cells, in line with the law of mass action. The proliferation of the resting cells is also assumed to follow the logistic growth function in the absence of tumor cells. The multiplying of the resting cells is enhanced by the tumor cells characterized by the term $\rho XZ/(X + \eta)$ called the Michael-Menten function which indicates the saturation effect of the resting predator cells, with a rate of proliferation ρ and a half-saturation constant η . The resting cells are converted to hunting cells by direct contact with them or by fast diffusing substance (cytokines) produced by hunting cells at the rate β . It is worth mentioning that inactivated hunting cells will not get back to the resting stage once over. The parameters of the model and their description used in this study are summarized in Table 1.

Following the work in [1], let us use the following dimensionless variables in the system:

$$t^* = \Lambda t/k_1, X^* = X/k_1, Y^* = \alpha k_1 Y/\Lambda, Z^* = Z/k_2. \tag{3}$$

After applying the dimensionless variables in (2) to the systems (1), we obtain

$$\begin{cases} \dot{X} = 1 + c_1 X(1 - X) - XY, \\ \dot{Y} = c_2 YZ - c_3 Y - c_4 YX, \\ \dot{Z} = c_5 Z(1 - Z) - c_6 YZ - c_7 Z + \frac{c_8 XZ}{X + K}, \end{cases} \tag{4}$$

where

$$\begin{aligned} c_1 &= \frac{r_1 k_1}{\Lambda}, c_2 = \frac{\beta k_2 k_1}{\Lambda}, c_3 = \frac{d_1 k_1}{\Lambda}, c_4 = \frac{\alpha_2 k_1^2}{\Lambda} \\ c_5 &= \frac{r_2 k_1}{\Lambda}, c_6 = \frac{\beta}{\alpha_1}, c_7 = \frac{d_2 k_1}{\Lambda}, c_8 = \frac{\rho k_1}{\Lambda}, K = \frac{\eta}{k_1}. \end{aligned} \tag{5}$$

In this study, the nondimensionalized mathematical model (4) is considered in the sense of piecewise differential and integral operators using classical, stochastic differential equations and different concepts of fractional and integral operators.

2.1. Preliminaries. The basic definitions of different fractional derivatives and integral operators used in the study are recalled as follows.

Definition 1 (see [30–32]). Let $\mu \in (0, 1]$, and $f \in C^1(0, t)$. The fractional ABC (with Mittag-Leffler kernel), Caputo (with the power-law kernel), and Caputo-Fabrizio (with exponential decay kernel) derivatives are, respectively, defined as follows:

$$\begin{aligned} {}_0^{ABC}D_t^\mu f(t) &= \frac{G(\mu)}{1 - \mu} \int_0^t \frac{d}{d\tau} f(\tau) E_\mu \left[-\frac{\mu}{1 - \mu} (t - \tau)^\mu \right] d\tau, \\ {}_0^cD_t^\mu f(t) &= \frac{1}{\Gamma(1 - \mu)} \int_0^t \frac{d}{d\tau} f(\tau) (t - \tau)^{-\mu} d\tau, \\ {}_0^{CF}D_t^\mu f(t) &= \frac{G(\mu)}{1 - \mu} \int_0^t \frac{d}{d\tau} f(\tau) \exp \left[-\frac{\mu}{1 - \mu} (t - \tau) \right] d\tau, \end{aligned} \tag{6}$$

where $G(\mu) = 1 - \mu + \mu/\Gamma(\mu)$ is the normal operator, $E_\mu(\cdot)$ is the Mittag-Leffler function, and $\Gamma(\cdot)$ is the Euler Gamma function.

The fractional integrals of the Caputo, Caputo-Fabrizio, and ABC types are, respectively, given by

$$\begin{aligned} {}_0^cI_t^\mu f(t) &= \frac{1}{\Gamma(\mu)} \int_0^t (t - \rho)^{\mu-1} f(\rho) d\rho, \\ {}_0^{CF}I_t^\mu f(t) &= \frac{1 - \mu}{G(\mu)} f(t) + \frac{\mu}{G(\mu)} \int_0^t f(\rho) d\rho, \\ {}_0^{ABC}I_t^\mu \{f(t)\} &= \frac{1 - \mu}{G(\mu)} f(t) + \frac{\mu}{G(\mu)\Gamma(\mu)} \int_0^t f(\rho) (t - \rho)^{\mu-1} d\rho. \end{aligned} \tag{7}$$

2.2. Equilibrium Points. Four equilibrium points of the system (4) are given below:

$$E_1 = \left(\frac{1}{2} \left(1 + \sqrt{1 + \frac{4}{c_1}} \right), 0, 0 \right),$$

$$E_2 = (X_2, 0, Z_2),$$

$$\text{where } X_2 = \frac{1}{2} \left(1 + \sqrt{1 + \frac{1}{c_1}} \right), Z_2 = \frac{1}{c_5} \left(c_5 - c_7 + \frac{c_8 X_2}{X_2 + K} \right),$$

$$E_3 = (X_3, Y_3, 0), \text{ where } X_3 = -\frac{c_3}{c_4} < 0,$$

$$E_4 = (X_4, Y_4, Z_4) \text{ is the interior equilibrium point,} \tag{8}$$

where

$$C_3 X_4^3 + C_2 X_4^2 + C_1 X_4 + C_0 = 0, \tag{10}$$

TABLE 1: Parameters of the model and their descriptions.

Parameter	Description	Dimensional values	Source
Λ	The rate of conversion of normal tissue cells to malignant (cancerous) cells (fixed input)	1000000/cell/day	Assumed
r_1	The growth rate of the tumor cells X .	0.18/day	[14]
r_2	The growth rate of the resting cells Z	0.1045/day	[29]
β	The rate of conversion of resting cell Z to hunting cell Y	4.32×10^{-8} /cell/day	
k_1	Carrying capacity of tumor cells X	5×10^6 /cell	
k_2	Carrying capacity of resting cells Z	3×10^6 cell	[14]
ρ	The proliferation rate of resting cell Z	0.49545/day	
η	The value at which the growth rate of resting immune cells Z gets half of its maximum value.	1000000	
d_1	Apoptotic or natural death rate of the hunting cells Y .	0.0412/day	
d_2	Apoptotic or natural death rate of the resting cells Z .	0.0412/day	
α_1	The rate of inactivation of tumor cell T by hunter cells Y .	1.101×10^{-7} /cell/day	[29]
α_2	The rate of inactivation of hunting cell Y by tumor cell X	2.2×10^{-8} /cell/day	

and $C_1 = c_5K - (c_7K + (c_5c_3K/c_2) + c_6(c_1K + 1))$,

$$C_2 = c_5 - c_7 + c_8 - \frac{c_5}{c_2}(c_3 + c_4K) - c_1c_6(1 - K), \quad (11)$$

$$C_3 = c_1c_6 - \frac{c_4c_5}{c_2}, C_0 = -c_6K < 0. \quad (12)$$

2.3. Formulation of Piecewise Model. In this subsection, we formulate three different scenarios of piecewise differential operator representations for the tumor-immune interaction model given in (4).

Scenario 1. In this case, we consider a piecewise model that involves a passage from the deterministic to a random process:

For $0 \leq t \leq t_1, X(0) = X_{11}, Y(0) = Y_{12}, Z(0) = Z_{13}$,

$$\begin{cases} \dot{X} = 1 + c_1X(1 - X) - XY, \\ \dot{Y} = c_2YZ - c_3Y - c_4YX, \\ \dot{Z} = c_5Z(1 - Z) - c_6YZ - c_7Z + \frac{c_8XZ}{X + K}, \end{cases} \quad (13)$$

for $t_1 \leq t \leq T, X(t_1) = X_{21}, Y(t_1) = Y_{22}, Z(t_1) = Z_{23}$,

$$\begin{cases} dX = (1 + c_1X(1 - X) - XY)dt + \sigma_1(X)dB_1(t), \\ dY = (c_2YZ - c_3Y - c_4YX)dt + \sigma_2(Y)dB_2(t), \\ dZ = \left(c_5Z(1 - Z) - c_6YZ - c_7Z + \frac{c_8XZ}{X + K} \right)dt + \sigma_3(Z)dB_3(t). \end{cases} \quad (14)$$

The mathematical model (10) has a deterministic character, and it is extended to the stochastic model described in (11) by adding a white noise-type perturbation to the system. The parameters $\sigma_1, \sigma_2, \sigma_3$ are positive constants and are the intensities of the random disturbances. $B_i = (B_1(t), B_2(t), B_3(t))$ is the white noise process.

Scenario 2. In this case, we have considered a piecewise model involving a passage from the Mittag-Leffler law to a random process:

For $0 \leq t \leq t_1, X(0) = X_{11}, Y(0) = Y_{12}, Z(0) = Z_{13}$,

$$\begin{cases} {}_0^{ABC}D_t^\alpha X = 1 + c_1X(1 - X) - XY, \\ {}_0^{ABC}D_t^\alpha Y = c_2YZ - c_3Y - c_4YX, \\ {}_0^{ABC}D_t^\alpha Z = c_5Z(1 - Z) - c_6YZ - c_7Z + \frac{c_8XZ}{X + K}, \end{cases} \quad (15)$$

for $t_1 \leq t \leq t_2, X(t_1) = X_{21}, Y(t_1) = Y_{22}, Z(t_1) = Z_{23}$,

$$\begin{cases} dX = (1 + c_1X(1 - X) - XY)dt + \sigma_1(X - X_4)dB_1(t), \\ dY = (c_2YZ - c_3Y - c_4YX)dt + \sigma_2(Y - Y_4)dB_2(t), \\ dZ = \left(c_5Z(1 - Z) - c_6YZ - c_7Z + \frac{c_8XZ}{X + K} \right)dt + \sigma_3(Z - Z_4)dB_3(t). \end{cases} \quad (16)$$

Scenario 3. In this case, we consider a piecewise model from fading memory to the power-law and then to a random process:

For $0 \leq t \leq t_1, X(0) = X_{11}, Y(0) = Y_{12}, Z(0) = Z_{13}$

$$\begin{cases} {}_0^{CF}D_t^\alpha X = 1 + c_1X(1 - X) - XY, \\ {}_0^{CF}D_t^\alpha Y = c_2YZ - c_3Y - c_4YX, \\ {}_0^{CF}D_t^\alpha Z = c_5Z(1 - Z) - c_6YZ - c_7Z + \frac{c_8XZ}{X + K}, \end{cases} \quad (17)$$

for $t_1 \leq t \leq t_2, X(t_1) = X_{21}, Y(t_1) = Y_{22}, Z(t_1) = Z_{23}$,

$$\begin{cases} {}_0^C D_t^\alpha X = 1 + c_1X(1 - X) - XY, \\ {}_0^C D_t^\alpha Y = c_2YZ - c_3Y - c_4YX, \\ {}_0^C D_t^\alpha Z = c_5Z(1 - Z) - c_6YZ - c_7Z + \frac{c_8XZ}{X + K}, \end{cases} \quad (18)$$

for $t_2 \leq t \leq T, X(t_2) = X_{31}, Y(t_2) = Y_{32}, Z(t_2) = Z_{33},$

$$\begin{cases} dX = (1 + c_1X(1 - X) - XY)dt + \sigma_1(X)dB_1(t), \\ dY = (c_2YZ - c_3Y - c_4YX)dt + \sigma_2(Y)dB_2(t), \\ dZ = \left(c_5Z(1 - Z) - c_6YZ - c_7Z + \frac{c_8XZ}{X + K} \right)dt + \sigma_3(Z)dB_3(t). \end{cases} \quad (19)$$

3. Existence, Uniqueness, Positivity, and Boundedness of the Solutions

This section proves the existence and uniqueness of a solution to the system in Scenario 3.

Theorem 2. *Let $\Omega = \{(X, Y, Z) \in \mathbb{R}^3 : \max\{|X|, |Y|, |Z|\} \leq L\}$. For each initial condition $U_0 = (X_{11}, Y_{12}, Z_{13}) \in \Omega$, there exists a unique solution of (17) for all $t \geq 0$.*

Proof. Let $0 < t_1 < \infty$. We want to find a sufficient condition for the existence and uniqueness of the solution of (17) in the domain $\Omega \times (0, t_1]$.

Suppose that G is a mapping such that $G(W) = (H_1(W), H_2(W), H_3(W))$, where $W = (X, Y, Z)^T, W' = (X', Y', Z')^T$, and

$$\begin{aligned} H_1(X, Y, Z) &= 1 + c_1X(1 - X) - XY, \\ H_2(X, Y, Z) &= c_2YZ - c_3Y - c_4YX, \\ H_3(X, Y, Z) &= c_5Z(1 - Z) - c_6YZ - c_7Z + \frac{c_8XZ}{X + K}. \end{aligned} \quad (20)$$

Now for any $W, W' \in \Omega$, we have

$$\begin{aligned} \|G(W) - G(W')\| &\leq |XY - X'Y'| + |c_2(YZ - Y'Z')| \\ &\quad + c_3(Y' - Y) + c_4(Y'X' - YX)| \\ &\quad + |c_6|Y'Z' - YZ| + |c_7|Z' - Z| + c_8|Z - Z'| \\ &\quad + \left| \frac{c_8XZ}{X + K} - \frac{c_8X'Z'}{X' + K} \right| \leq |X'Y' - XY| \\ &\quad + c_2|YZ - Y'Z'| + c_3|Y' - Y| + c_4|Y'X' \\ &\quad - YX| + |c_6|Y'Z' - YZ| + |c_7|Z' - Z| \\ &\quad + c_8|Z - Z'| + \left| \frac{c_8X}{X + K} (Z - Z') \right| \\ &\quad + \frac{Kc_8Z'}{(X' + K)(X + K)} (X - X')| \\ &\leq (L + KLc_8)|X' - X| + (c_2L + c_3 + c_4L)|Y \\ &\quad - Y'| + (c_6L + c_7 + 2c_8)|Z - Z'| \\ &\leq Y|W - W'|, \leq Y|W - W'|, \end{aligned} \quad (21)$$

where $Y = \max\{L + KLc_8, c_2L + c_3 + c_4L, c_6L + c_7 + 2c_8\}$.

Thus, the mapping G satisfies the Lipschitz condition with respect to W . This proves that the system (17) has a unique solution. \square

Theorem 3. *The solution of (17) is invariant in the set $\mathbb{R}_+^3 = \{W \in \mathbb{R}^3 : W \geq 0 \text{ and } W(t) = (X, Y, Z)^T\}$.*

Proof. By referring to the system (17), we can observe that ${}^C_0D_t^\alpha X(t)|_{X=0} \geq 0, {}^C_0D_t^\alpha Y(t)|_{Y=0} \geq 0, {}^C_0D_t^\alpha Z(t)|_{Z=0} \geq 0$, and then the mentioned system is nonreducing which proves the invariance of the system in \mathbb{R}_+^3 and the feasible region is $\Omega = \{(X, Y, Z) \in \mathbb{R}^3 : \max\{|X|, |Y|, |Z|\} \leq L > 0\}$.

Thus, in Theorems 2 and 3, we find that the system (17) has a unique solution for each initial condition in the feasible set Ω . The existence and uniqueness of the solution of the system (18) can be shown similarly for the domain $\Omega \times [t_1, t_2]$.

We shall now show the existence and uniqueness of the solution for the stochastic differential equation given in (19) based on Theorem 3. Let us first write the system (19) in a Volterra type of integrals for all t in $[t_2, T]$.

For simplicity, let us write (19) in the form

$$\begin{cases} dX = H_1(X, Y, Z)dt + G_1(t, X)dB_1(t), \\ dY = H_2(X, Y, Z)dt + G_2(t, Y)dB_2(t), \\ dZ = H_3(X, Y, Z)dt + G_3(t, Z)dB_3(t), \end{cases} \quad (22)$$

where $t_2 \leq t \leq T$, and the initial condition is given by $X(t_2) = X_{31}, Y(t_2) = Y_{32}, Z(t_2) = Z_{33}$, $H_i, i = 1, 2, 3$ are defined in (20) and $G_3(t, Z) = \sigma_1(Z), G_2(t, Y) = \sigma_2(Y), G_1(t, X) = \sigma_1(X)$, and $E_4 = (X_4, Y_4, Z_4)$ is the interior equilibrium point of (4).

We shall now show the existence and uniqueness of the solution for all t such that $t \in (t_2, T)$. Indeed, by referring to (19), we want to show the following items:

(I) Lipschitz condition: for all $W, W' \in \mathbb{R}_+^3$ and $t \in [t_2, T]$

$$\max\left\{ |H_i(W, t) - H_i(W', t)|, |G_i(W, t) - G_i(W', t)| \right\} \bar{k} |W - W'|^2, i = 1, 2, 3 \quad (23)$$

for some positive constant \bar{k}

(II) Linear growth condition: for all $(W, t) \in \mathbb{R}_+^3 \times [t_2, T]$

$$\max\{|H_i(W, t)|^2, |G_i(W, t)|^2\} \leq k(1 + |W|^2), i = 1, 2, 3, \quad (24)$$

for some positive constant k , where $W = (X, Y, Z)^T$, $W' = (X', Y', Z')^T$. \square

Proof. From the inequalities

$$|G_1(W) - G_1(W')|^2 = |X - X'|^2 \leq \sigma_1^2 |X - X'|^2,$$

$$|G_2(W) - G_2(W')|^2 = |Y - Y'|^2 \leq \sigma_2^2 |Y - Y'|^2, \tag{25}$$

$$|G_3(W) - G_3(W')|^2 = |Z - Z'|^2 \leq \sigma_3^2 |Z - Z'|^2.$$

We have

$$\begin{aligned} |H_1(X) - H_1(X')|^2 &= |(c_1 X(1 - X) - XY) - (c_1 X'(1 - X') - X'Y)|^2 = |c_1 + Y + c_1(X' + X)|^2 |X - X'|^2 \\ &\leq \left(c_1^2 + 2c_1(\|Y\|_\infty^2 + c_1\|X\|_\infty + c_1\|X'\|_\infty + \|XY\|_\infty + \|YX'\|_\infty) \right. \\ &\quad \left. + c_1^2(\|X\|_\infty^2 + \|X'^2\|_\infty^2 + 2\|XX'\|_\infty^2) \right) |X - X'|^2, \end{aligned} \tag{26}$$

where $\|\Phi\|_\infty^2 = \sup_{t \in [t_2, T]} |\Phi|^2$.

Thus, we have

$$|H_1(X) - H_1(X')|^2 \leq \bar{k}_1 |X - X'|^2, \tag{27}$$

where

$$\begin{aligned} \bar{k}_1 &= c_1^2 + 2c_1(\|Y\|_\infty^2 + c_1\|X\|_\infty + c_1\|X'\|_\infty + \|XY\|_\infty \\ &\quad + \|YX'\|_\infty) + c_1^2(\|X\|_\infty^2 + \|X'^2\|_\infty^2 + 2\|XX'\|_\infty^2). \end{aligned} \tag{28}$$

Similarly

$$\begin{aligned} \bar{k}_2 &= (c_1^2 + 2c_2c_4 + 2c_2c_3)\|Z\|_\infty^2 + 2c_3c_4\|X\|_\infty, \\ \bar{k}_3 &= (c_5 + c_7 + c_8)(1 + c_6^2\|Y\|_\infty^2 + 2c_6\|Y\|_\infty) \\ &\quad + c_5^2(\|Z\|_\infty^2 + \|Z'\|_\infty^2) + 2\|Z\|_\infty\|Z'\|_\infty \\ &\quad + (2c_5(c_5 + c_7 + c_8) + 2c_5c_6\|Y\|_\infty)(\|Z\|_\infty + \|Z'\|_\infty). \end{aligned} \tag{29}$$

Now, by choosing $\bar{k} = \max\{\sigma_i^2, \bar{k}_i, i = 1, 2, 3\}$, we can see that the Lipschitz condition (I) is satisfied. Similarly, we obtain

$$\begin{aligned} |G_1(W)|^2 &= \sigma_1^2 |X - X_4|^2 \leq \sigma_1^2 X_4^2 \left(1 + \frac{1}{X_4^2} |X|^2\right) \\ &\leq \sigma_1^2 X_4^2 (1 + |X|^2), \end{aligned} \tag{30}$$

with the condition of $1/X_4^2 \leq 1$

$$\begin{aligned} |G_2(W)|^2 &= \sigma_2^2 |Y - Y_4|^2 \leq \sigma_2^2 Y_4^2 \left(1 + \frac{1}{Y_4^2} |Y|^2\right) \\ &\leq \sigma_2^2 Y_4^2 (1 + |Y|^2), \end{aligned} \tag{31}$$

with the condition of $1/Y_4^2 \leq 1$, and

$$|G_3(W)|^2 = \sigma_3^2 Z_4^2 |Z - Z_4|^2 \leq \sigma_3^2 \left(1 + \frac{1}{Z_4^2} |Z|^2\right) \leq \sigma_3^2 Z_4^2 (1 + |Z|^2), \tag{32}$$

with the condition of $Z_4^2 \leq 1$.

Moreover, $\|(1 + c_1 X)^2\|_\infty + \|(c_1 X + Y)^2\|_\infty |X|^2 \leq \|(1 + c_1 X)^2\|_\infty + \|(c_1 X + Y)^2\|_\infty |X|^2 \leq \leq \leq$

$$\begin{aligned} |H_1(X, Y, Z)|^2 &= |1 + c_1 X(1 - X) - XY|^2, \\ &\leq 1 + 2c_1 X + c_1^2 X^2 + c_1^2 X^4 + 2c_1 X^3 Y + (XY)^2 \\ &\leq \|(1 + c_1 X)^2\|_\infty + \|(c_1 X + Y)^2\|_\infty |X|^2 \\ &\leq k_1 \left(1 + \frac{\|(c_1 X + Y)^2\|_\infty}{\|(1 + c_1 X)^2\|_\infty} |X|^2\right) \leq k_1 (1 + |X|^2), \end{aligned} \tag{33}$$

where $k_1 = \|(1 + c_1 X)^2\|_\infty$ with the condition $\|(c_1 X + Y)^2\|_\infty / k_1 < 1$. Also

$$\begin{aligned} |H_2(X, Y, Z)|^2 &= |c_2 YZ - c_3 Y - c_4 YX|^2 \leq ((c_2^2 \|Z\|_\infty) \\ &\quad + 2c_3 c_4 \|X\|_\infty + (c_4 \|X^2\|_\infty + c_3^2) |Y|^2) \\ &\leq k_2 (1 + |Y|^2), \end{aligned} \tag{34}$$

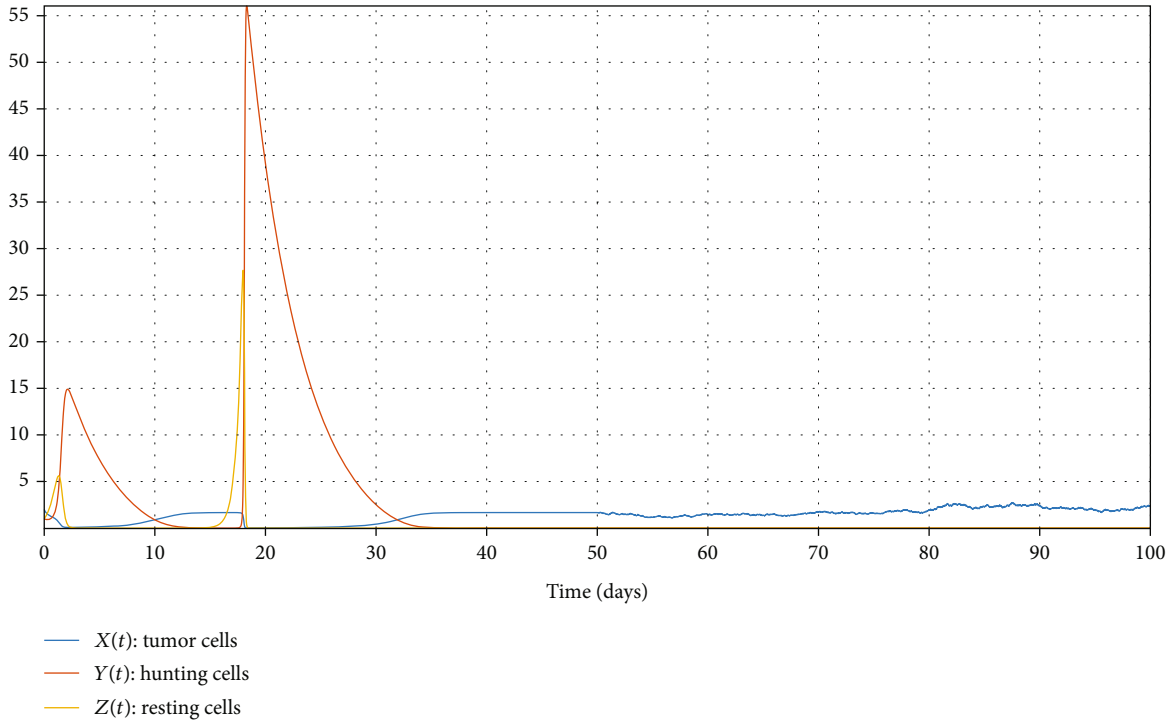


FIGURE 1: Time series trajectories of the piecewise systems (10) and (11) for $c_1 = 0.9, c_2 = 0.65, c_3 = 0.21, c_4 = 0.55, c_5 = 0, c_6 = 0.39, c_7 = 0.21, c_8 = 2.48, K = 0.2$.

where $k_2 = ((c_2^2 \|Z\|_\infty) + 2c_3c_4 \|X\|_\infty + (c_4 \|X^2\|_\infty) + c_3^2)$, and

$$\begin{aligned}
 |H_3(X, Y, Z)|^2 &= \left| c_5 Z(1-Z) - c_6 YZ - c_7 Z + \frac{c_8 XZ}{X+K} \right|^2 \\
 &\leq \left(\begin{aligned} &(c_5 + c_8 - c_7)^2 + c_5^2 \|Z\|_\infty^2 \\ &+ (c_6^2 + 2c_5c_6 + c_8^2 + 2c_2) \|Z\|_\infty + 2c_6c_8 \|Y\|_\infty \end{aligned} \right) |Z|^2 \\
 &\leq k_3 (1 + |Z|^2),
 \end{aligned}
 \tag{35}$$

where $k_3 = (c_5 + c_8 - c_7)^2 + c_5^2 \|Z\|_\infty^2 + (c_6^2 + 2c_5c_6 + c_8^2 + 2c_2) \|Z\|_\infty + 2c_6c_8 \|Y\|_\infty$.

Now, by choosing $k = \max \{ \sigma_1^2 X_4^2, \sigma_2^2 Y_4^2, \sigma_3^2 Z_4^2, k_1, k_2, k_3 \}$, we can see that the linearity condition (II) is satisfied. Thus, the system (19) has a unique solution with the initial conditions $X(t_2) = X_{31}, Y(t_2) = Y_{32}, Z(t_2) = Z_{33}$. We can then conclude that the piecewise differential equation considered in Scenario 3 has a unique solution for all $t \in [0, T]$.

By following the same method, the existence and uniqueness of solutions for the mathematical models described in Scenarios 1 and 2 are proved. \square

4. Numerical Approximations

Based on the work studied in [33], we can show that the numerical approximation of the system in Scenario 1 is given as follows:

For all $t \in [0, t_1]$

$$\begin{aligned}
 W_i(n+1) &= W_i(n) + \frac{23h}{12} H_i(W(n)) + \frac{5h}{12} H_i(W(n-2)) \\
 &\quad - \frac{4h}{3} [H_i(W(n-1))],
 \end{aligned}
 \tag{36}$$

where

$$W = (X, Y, Z), h = \Delta t, W_1 = X, W_2 = Y, W_3 = Z, i = 1, 2, 3,
 \tag{37}$$

and H_1, H_2, H_3 are defined in (20).

For all $t \in [t_1, T]$, we have

$$\begin{aligned}
 X(n+1) &= X(n) + \frac{23h}{12} H_1(X(n), Y(n), Z(n)) \\
 &\quad + \frac{5h}{12} H_1(X(n-2), Y(n-2), Z(n-2)) \\
 &\quad - \frac{4h}{3} [H_1(X(n-1), Y(n-1), Z(n-1))] \\
 &\quad + \frac{5}{12} (B_1(t(n-1)) - B_1(t(n-2))) \sigma_1(X(n-2)) \\
 &\quad - X_4 - \frac{4}{3} (B_1(t(n)) - B_1(t(n-1))) \sigma_1(X(n-1)) \\
 &\quad - X_4 + \frac{23}{12} (B_1(t(n+1)) - B_1(t(n))) \sigma_1(X(n) - X_4),
 \end{aligned}$$

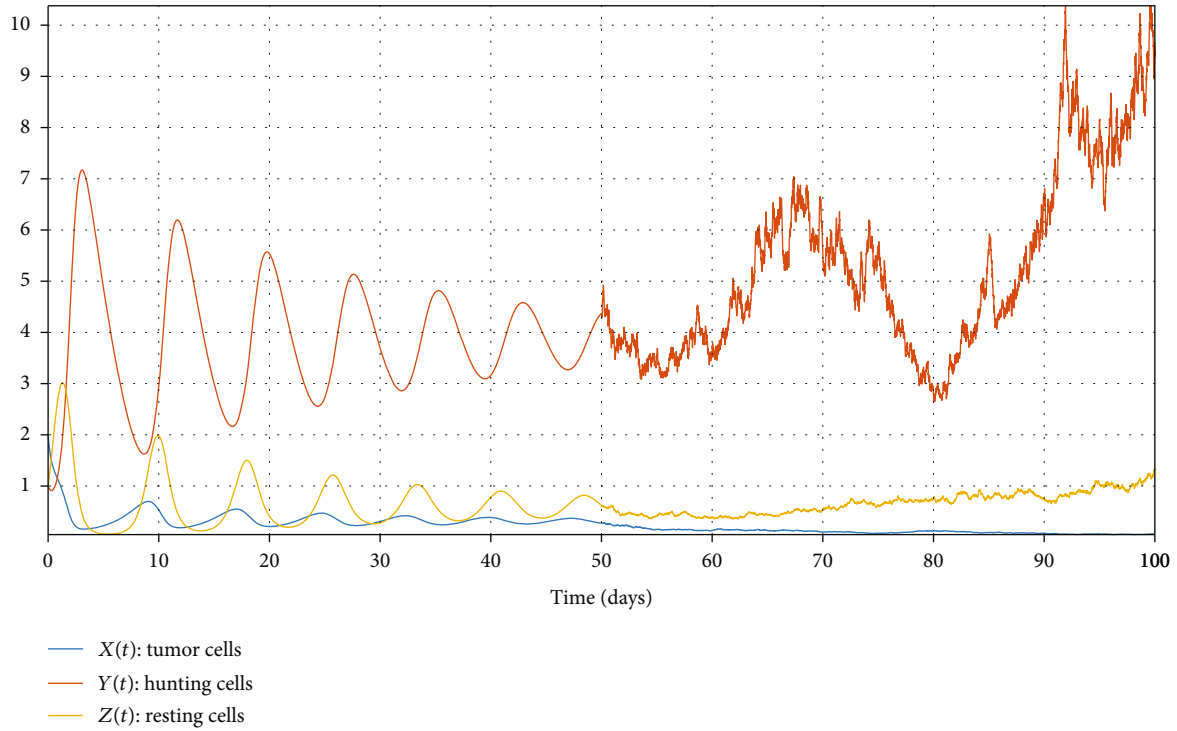


FIGURE 2: Time series trajectories of the piecewise systems (10) and (11) for $c_1 = 0.9$, $c_2 = 0.65$, $c_3 = 0.21$, $c_4 = 0.55$, $c_5 = 0.52$, $c_6 = 0.39$, $c_7 = 0.21$, $c_8 = 2.48$, $K = 0.2$.

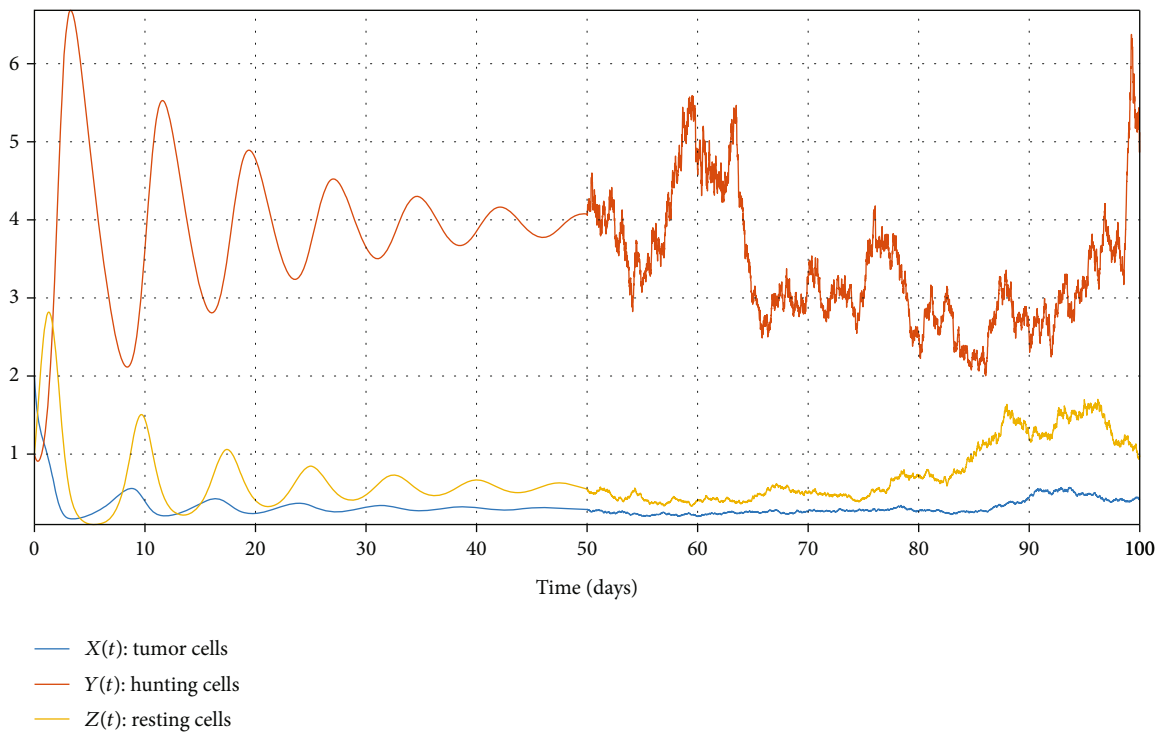


FIGURE 3: Time series trajectories of the piecewise systems (10) and (11) for $c_1 = 0.9$, $c_2 = 0.65$, $c_3 = 0.21$, $c_4 = 0.55$, $c_5 = 0.62$, $c_6 = 0.39$, $c_7 = 0.21$, $c_8 = 2.48$, $K = 0.2$.

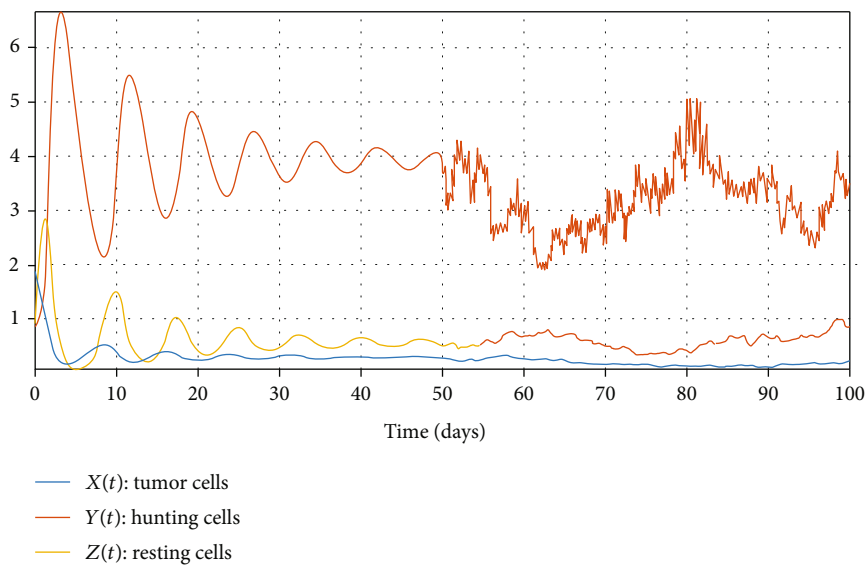


FIGURE 4: Time series trajectories of the piecewise systems (10) and (11) for $c_1 = 0.9, c_2 = 0.65, c_3 = 0.21, c_4 = 0.55, c_5 = 0.92, c_6 = 0.39, c_7 = 0.21, c_8 = 2.48, K = 0.2$.

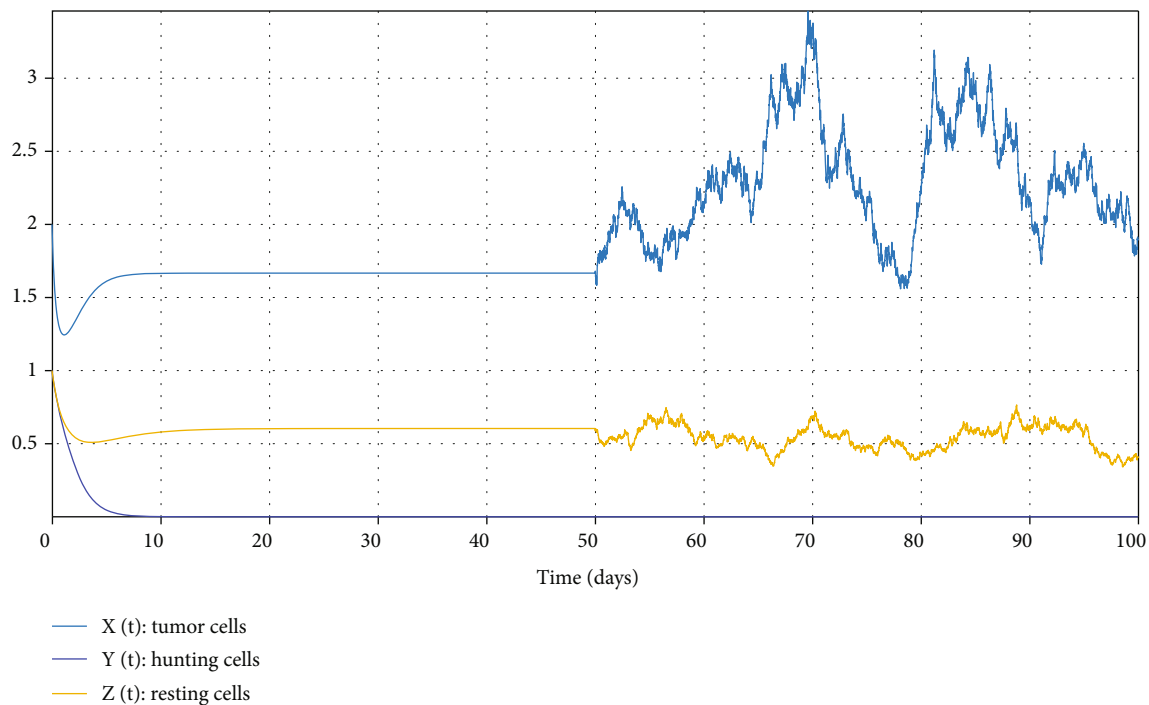


FIGURE 5: Time series trajectories of the piecewise systems (10) and (11) for $c_1 = 0.9, c_2 = 0.65, c_3 = 0.21, c_4 = 0.55, c_5 = 0.52, c_6 = 0.39, c_7 = 0.21, c_8 = 0, K = 0.2$.

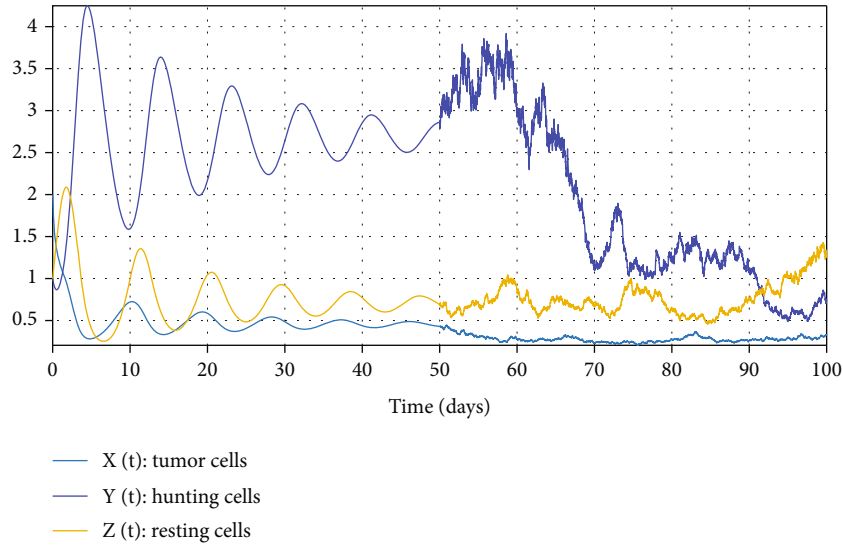


FIGURE 6: Time series trajectories of piecewise systems (10) and (11) for $c_1 = 0.9, c_2 = 0.65, c_3 = 0.21, c_4 = 0.55, c_5 = 0.52, c_6 = 0.39, c_7 = 0.21, c_8 = 1.6, K = 0.2$.

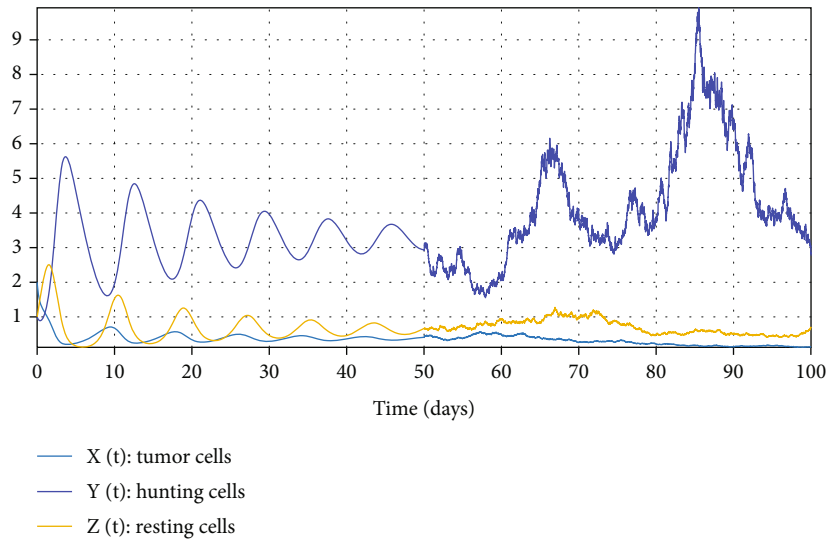


FIGURE 7: Time series trajectories of the piecewise systems (10) and (11) for $c_1 = 0.9, c_2 = 0.65, c_3 = 0.21, c_4 = 0.55, c_5 = 0.52, c_6 = 0.39, c_7 = 0.21, c_8 = 2, K = 0.2$.

$$\begin{aligned}
 Y(n+1) &= Y(n) + \frac{23h}{12}H_2(X(n), Y(n), Z(n)) \\
 &\quad + \frac{5h}{12}H_2(X(n-2), Y(n-2), Z(n-2)) \\
 &\quad - \frac{4h}{3}[H_2(X(n-1), Y(n-1), Z(n-1))] \\
 &\quad + \frac{5}{12}(B_2(t(n-1)) - B_2(t(n-2)))\sigma_2(Y(n-2) \\
 &\quad - Y_4) - \frac{4}{3}(B_2(t(n)) - B_2(t(n-1)))\sigma_2(Y(n-1) \\
 &\quad - Y_4) + \frac{23}{12}(B_2(t(n+1)) - B_2(t(n)))\sigma_2(Y(n) - Y_4), \\
 Z(n+1) &= Z(n) + \frac{23h}{12}H_3(X(n), Y(n), Z(n)) \\
 &\quad + \frac{5h}{12}H_3(X(n-2), Y(n-2), Z(n-2)) \\
 &\quad - \frac{4h}{3}[H_3(X(n-1), Y(n-1), Z(n-1))] \\
 &\quad + \frac{5}{12}(B_3(t(n-1)) - B_3(t(n-2)))\sigma_3(Z(n-2) - Z_4) \\
 &\quad - \frac{4}{3}(B_3(t(n)) - B_3(t(n-1)))\sigma_3(Z(n-1) - Z_4) \\
 &\quad + \frac{23}{12}(B_3(t(n+1)) - B_3(t(n)))\sigma_3(Z(n) - Z_4).
 \end{aligned}
 \tag{38}$$

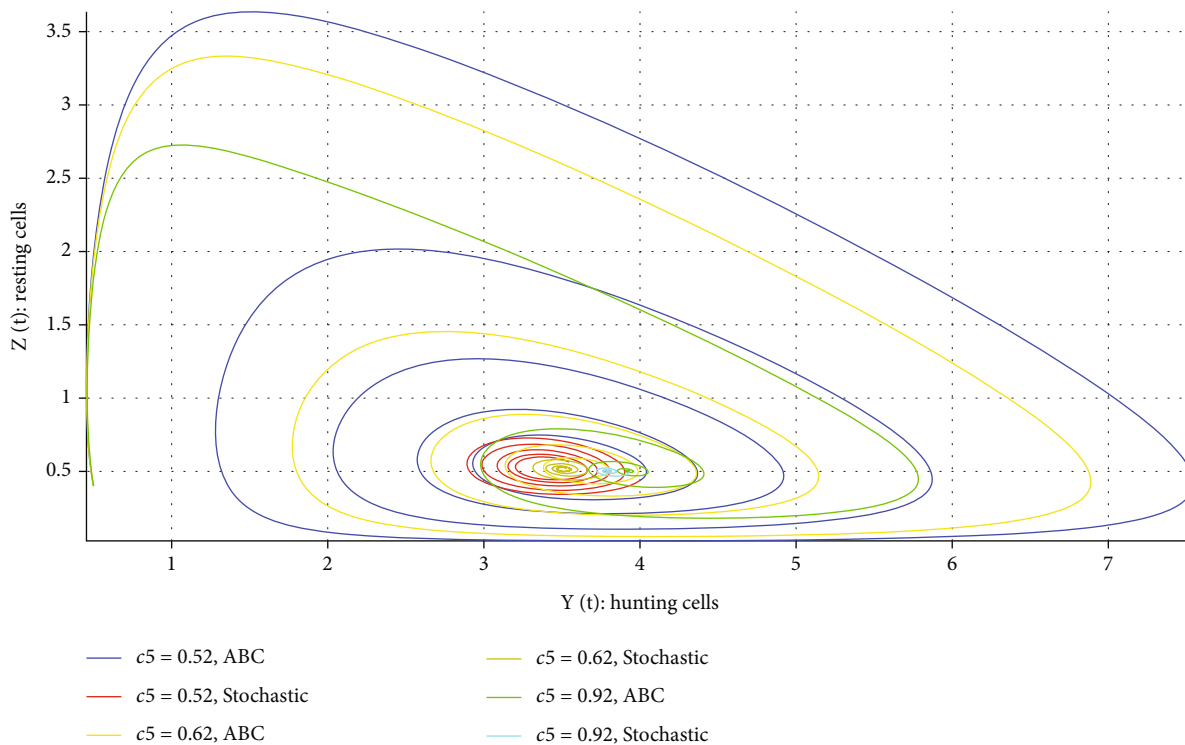


FIGURE 8: Phase portrait of the piecewise systems (15) and (16) projected onto the YZ plane for the parameter values of $c_1 = 0.9, c_2 = 0.65, c_3 = 0.21, c_4 = 0.55, c_6 = 0.39, c_7 = 0.21, c_8 = 2, K = 0.2$, for the derivative order of $\mu = 1$, and the different values of c_5 .

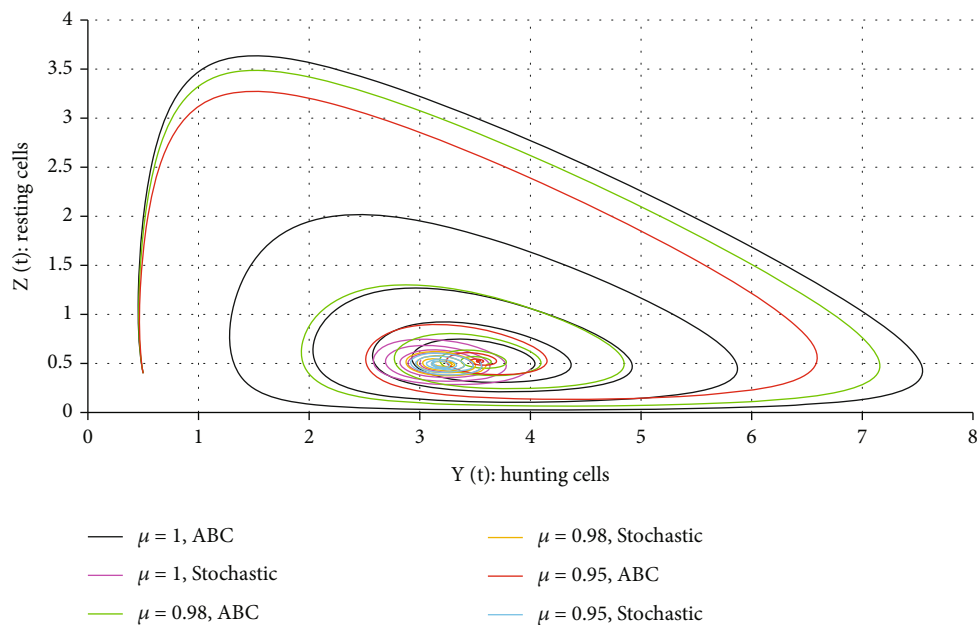


FIGURE 9: Phase portrait of the piecewise systems (15) and (16) projected onto the YZ plane for the parameter values of $c_1 = 0.9, c_2 = 0.65, c_3 = 0.21, c_4 = 0.55, c_5 = 0.52, c_6 = 0.39, c_7 = 0.21, c_8 = 2, K = 0.2$, and different values of fractional order μ .

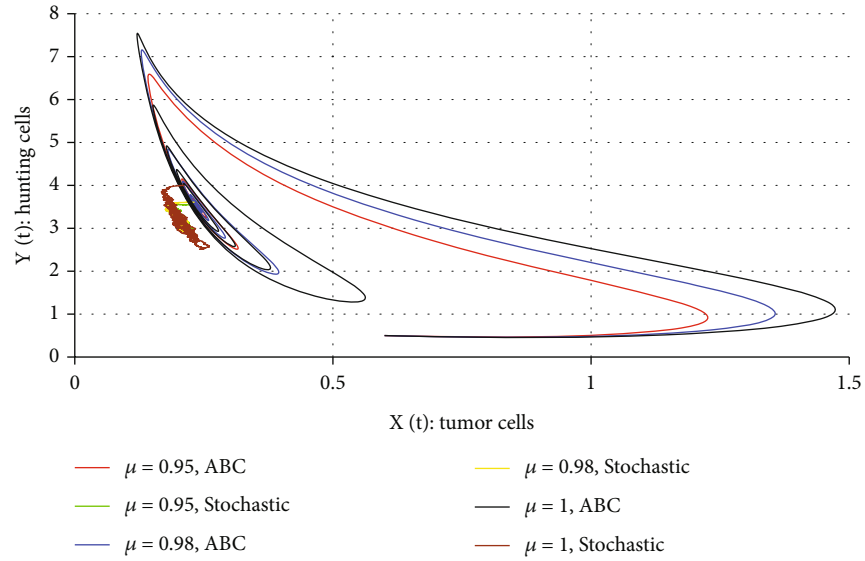


FIGURE 10: Phase portrait of the piecewise systems (15) and (16) projected onto the XY plane for the parameter values of $c_1 = 0.9, c_2 = 0.65, c_3 = 0.21, c_4 = 0.55, c_5 = 0.52, c_6 = 0.39, c_7 = 0.21, c_8 = 2, K = 0.2$, and different values of fractional order μ .

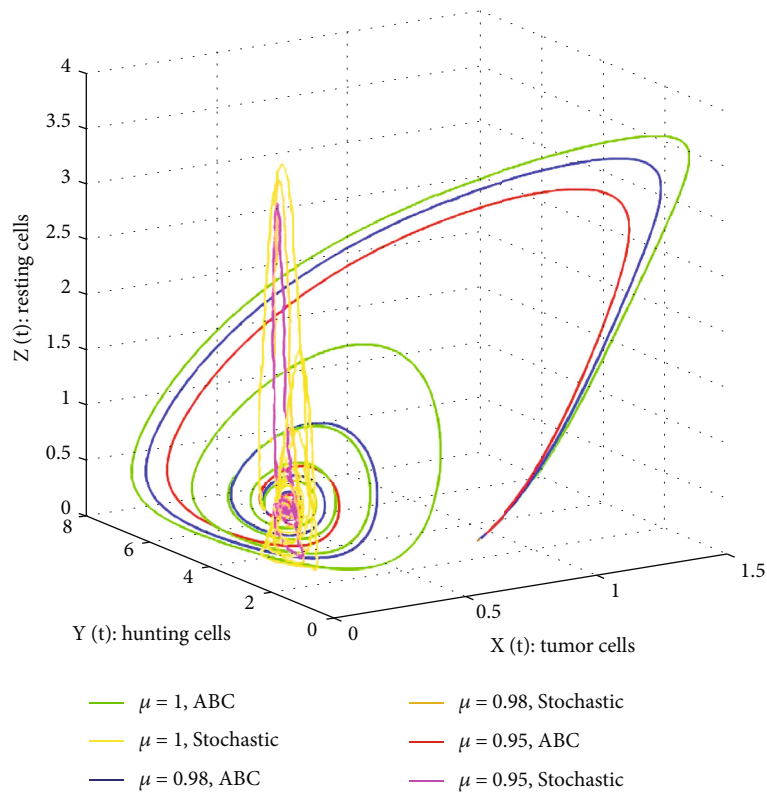


FIGURE 11: Phase portrait of the piecewise system (15) & (16) projected onto the XYZ plane for the parameter values of $c_1 = 0.9, c_2 = 0.65, c_3 = 0.21, c_4 = 0.55, c_5 = 0.52, c_6 = 0.39, c_7 = 0.21, c_8 = 2, K = 0.2$, and different values of fractional order μ .

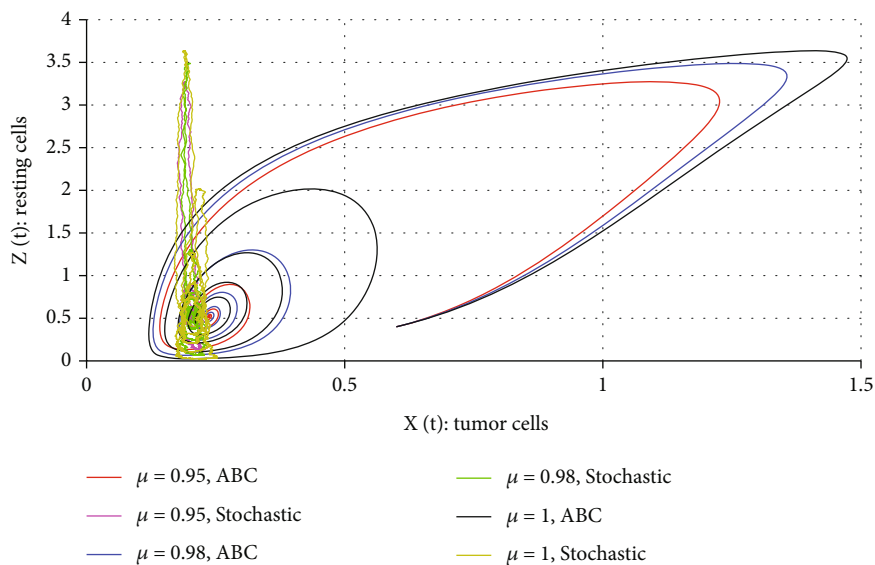


FIGURE 12: Phase portrait of the piecewise systems (15) and (16) projected onto the XZ plane for the parameter values of $c_1 = 0.9, c_2 = 0.65, c_3 = 0.21, c_4 = 0.55, c_5 = 0.52, c_6 = 0.39, c_7 = 0.21, c_8 = 2, K = 0$, and different values of fractional order μ .

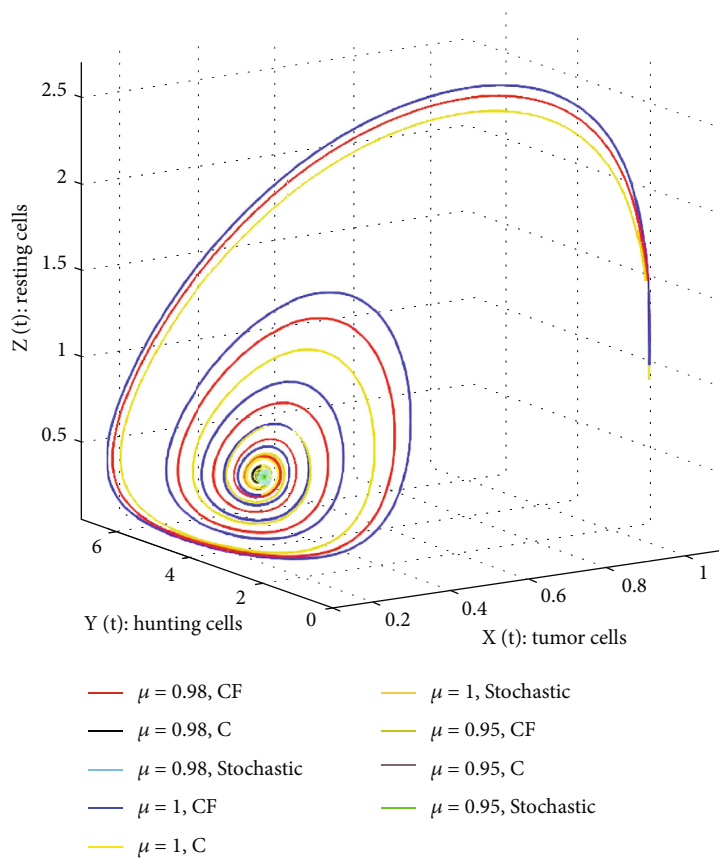


FIGURE 13: Phase portrait of the piecewise systems (17)–(19) projected onto the XYZ plane for the parameter values of $c_1 = 0.9, c_2 = 0.65, c_3 = 0.21, c_4 = 0.55, c_5 = 0.52, c_6 = 0.39, c_7 = 0.21, c_8 = 2, K = 0.2$, and different values of fractional order μ .

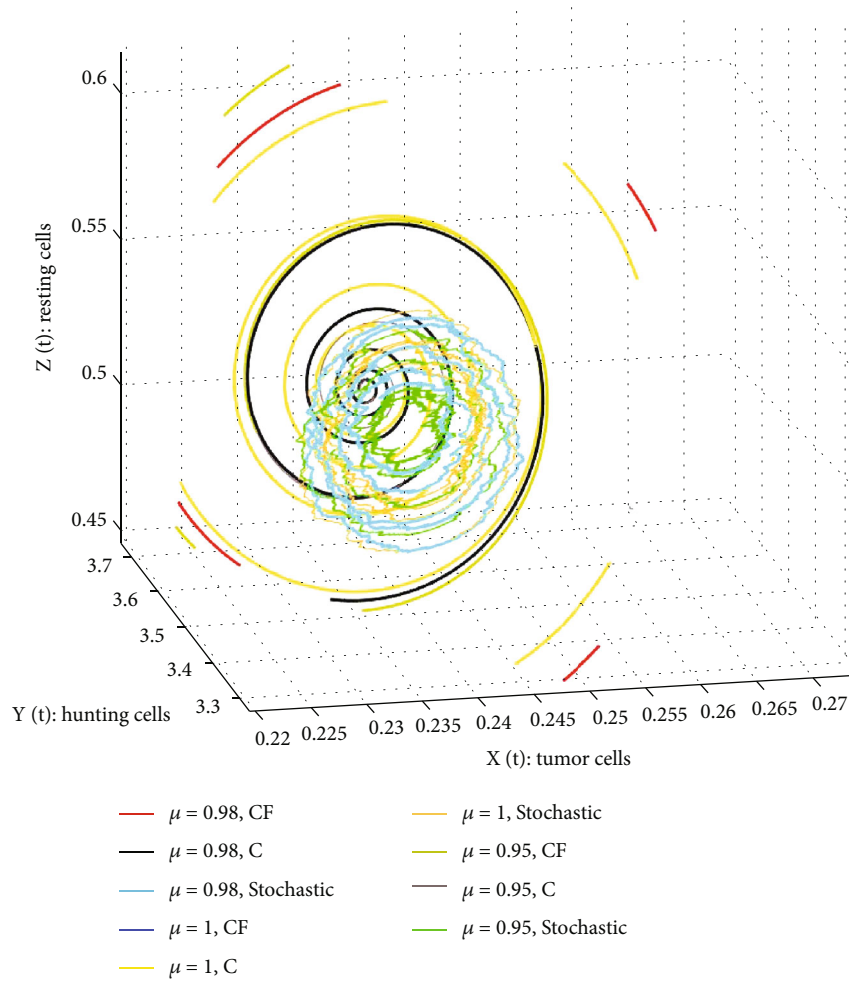


FIGURE 14: Zooming in on the inner part of Figure 13.

By referring to Scenario 2 and applying the numerical method developed in [34], the approximate solution of the ABC fractional derivative part for all $t \in [0, t_1]$ is given by

$$W_i(t_{n+1}) = W_i(0) + \frac{1-\mu}{F(\mu)} H_i(W(t_n)) + \frac{\mu}{F(\mu)\Gamma(\mu)} \sum_{k=1}^n \left(\begin{array}{c} \left(\frac{H_i(W(t_k))}{\Gamma(\mu+2)} \right) \\ \times h^\mu [(n+1-k)^\mu (n-k+2+\mu) - (n-k)^\mu (n-k+2+2\mu)] \\ - \left(\frac{H_i(W(t_{k-1}))}{\Gamma(\mu+2)} \right) \\ \times h^\mu [(n+1-k)^{\mu+1} - (n-k)^\mu (n-j+1+\mu)] \end{array} \right), \quad (39)$$

where

$$W = (X, Y, Z), h = \Delta t, W_1 = X, W_2 = Y, W_3 = Z, i = 1, 2, 3, \quad (40)$$

and H_1, H_2, H_3 are defined in (20).

By referring to Scenario 3 and based on the work studied in [29], we can show that the numerical approximation of

the system for the Caputo-Fabrizio fractional differential equation for $t \in [0, t_1]$ is given as follows:

$$W_i(n+1) = W_i(n) + \frac{1-\mu}{\Gamma(\mu)} (H_i(W(n) - W(n-1))) + \frac{\mu h}{\Gamma(\alpha)} \left[\frac{5}{12} H_i(W(n-2)) - \frac{4}{3} H_i(W(n-1)) + \frac{23}{12} H_i(W(n)) \right], \quad (41)$$

where

$$W = (X, Y, Z), h = \Delta t, W_1 = X, W_2 = Y, W_3 = Z, i = 1, 2, 3, \quad (42)$$

and H_1, H_2, H_3 are defined in (20).

By referring to Scenario 3 and based on the work studied in [29], we can show that the numerical approximation of the system for the Caputo fractional differential equation

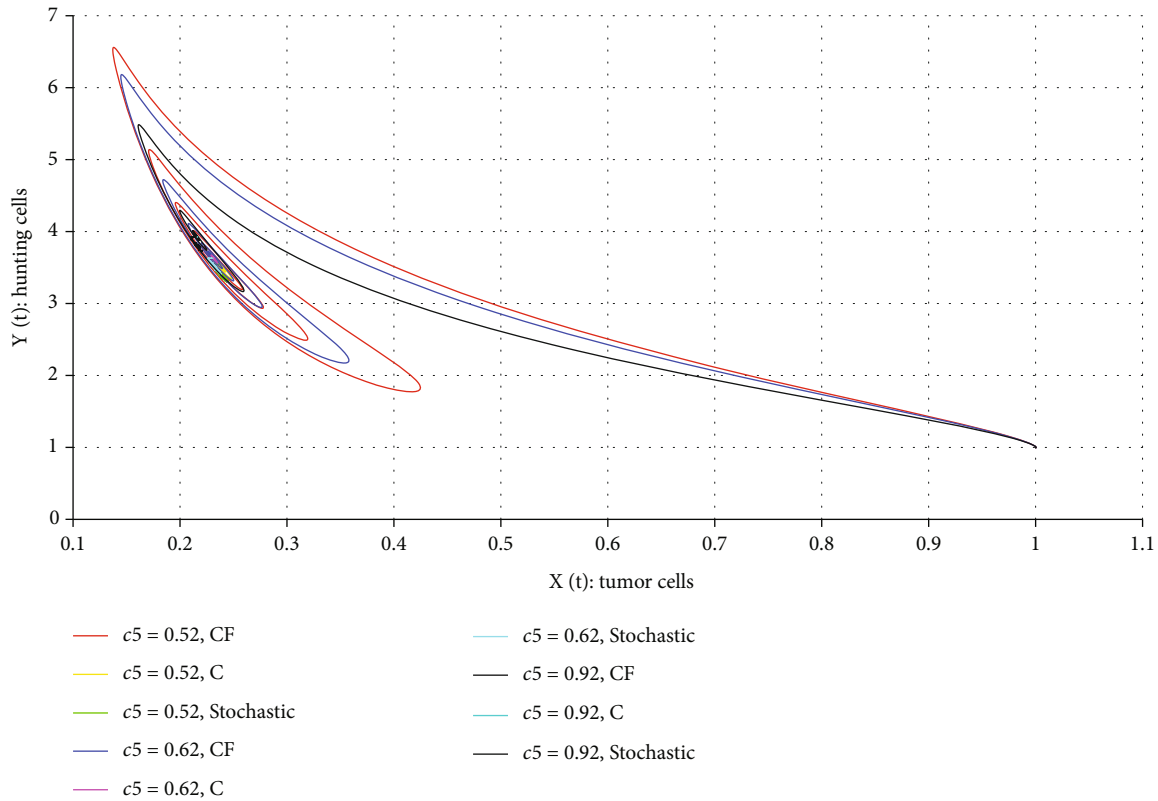


FIGURE 15: Phase portrait of the piecewise systems (15) and (16) projected onto the XZ plane for the parameter values of $c_1 = 0.9, c_2 = 0.65, c_3 = 0.21, c_4 = 0.55, c_6 = 0.39, c_7 = 0.21, c_8 = 2, K 0.2$, different values of the parameter c_5 and fractional order $\mu = 0.98$.

for $t \in [t_1, t_2]$ is given as follows:

$$\begin{aligned}
 W_i(n+1) = & W_i(t_1) + \frac{h^\mu}{\Gamma(\mu+1)} \sum_{j=2}^n H_i(t(j-2), W(j-2))[(n-j+1)^\mu \\
 & - (n-j)^\mu] + \frac{h^\mu}{\Gamma(\mu+2)} \sum_{j=2}^n H_i(t(j-1), W(j-1)) \\
 & - H_i(t(j-2), W(j-2)) \times [(n-j+1)^\mu(n-j+3+2\mu) \\
 & - (n-j)^\mu(n-j+3+3\mu)] + \frac{h^\mu}{2\Gamma(\mu+3)} \sum_{j=2}^n H_i(t(j), W(j)) \\
 & - 2H_i(t(j-1), W(j-1)) + H_i(t(j-2), W(j-2)) \\
 & \times \begin{bmatrix} (n-1)[2(n-j)^2 + (3\mu+10)(n-j) + 2\mu^2 + 9\mu+12] \\ - (n-1)[2(n-j)^2 + (5\mu+10)(n-j) + 6\mu^2 + 18\mu+12] \end{bmatrix}, \tag{43}
 \end{aligned}$$

where

$W = (X, Y, Z), h = \Delta t, W_1 = X, W_2 = Y, W_3 = Z, i = 1, 2, 3,$ and H_1, H_2, H_3 are defined in (20).

5. Numerical Simulations and Discussion

In this section, some of the numerical simulations of three different scenarios are depicted. Based on the dimensional parameter values given in Table 1 and the relationship between parameters given in (5), the following nondimensional parameter values of the system (4) are used for the

numerical simulations: $c_1 = 0.9, c_2 = 0.65, c_3 = 0.21, c_4 = 0.55, c_5 = 0.52, c_6 = 0.39, c_7 = 0.21, c_8 = 2.48, K = 0.2$.

By using the above parameter values, the interior equilibrium point given by expression (9) is calculated to be $E_4 = (X_4, Y_4, Z_4) = (0.308, 3.87, 0.580)$ with the corresponding eigenvalues of the system given by $\{-3.78, -0.22 + 0.88i, -0.22 - 0.88i\}$. Thus, the equilibrium point E_4 is stable.

Let us consider the simulation of Scenario 1 for different values of the parameters $c_5 = r_2 k_1 / \Lambda = 0.52, 0.62, 0.92$ and $c_8 = \rho k_1 / \Lambda = 0, 1, 6, 2$.

It can be observed from Figures 1–4 that when the values of c_5 increase from 0, the hunting cells get activated and seem to increase and continue to oscillate with convergence for the deterministic part and cross-overs to randomness. The hunting cells can increase as indicated in the figures when the value of c_5 is different from zero and gets larger and larger. In Figures 1–4, the tumor cells remain mitigated.

It can be inferred from Figures 5–7 that by increasing the parameter values of c_8 from zero, the number of tumor cells reduces significantly as shown in both deterministic and stochastic parts of the figures. It means that the proliferation of the resting cells enhanced by the tumor cells characterized by the term $c_8 XZ/X + K$ (see Equation (4)) has a positive effect on the mitigation of the tumor cells. It can be inferred from this result that proliferation of the hunting cells has a positive effect on mitigating the tumor cells which seems good news for treating the disease.

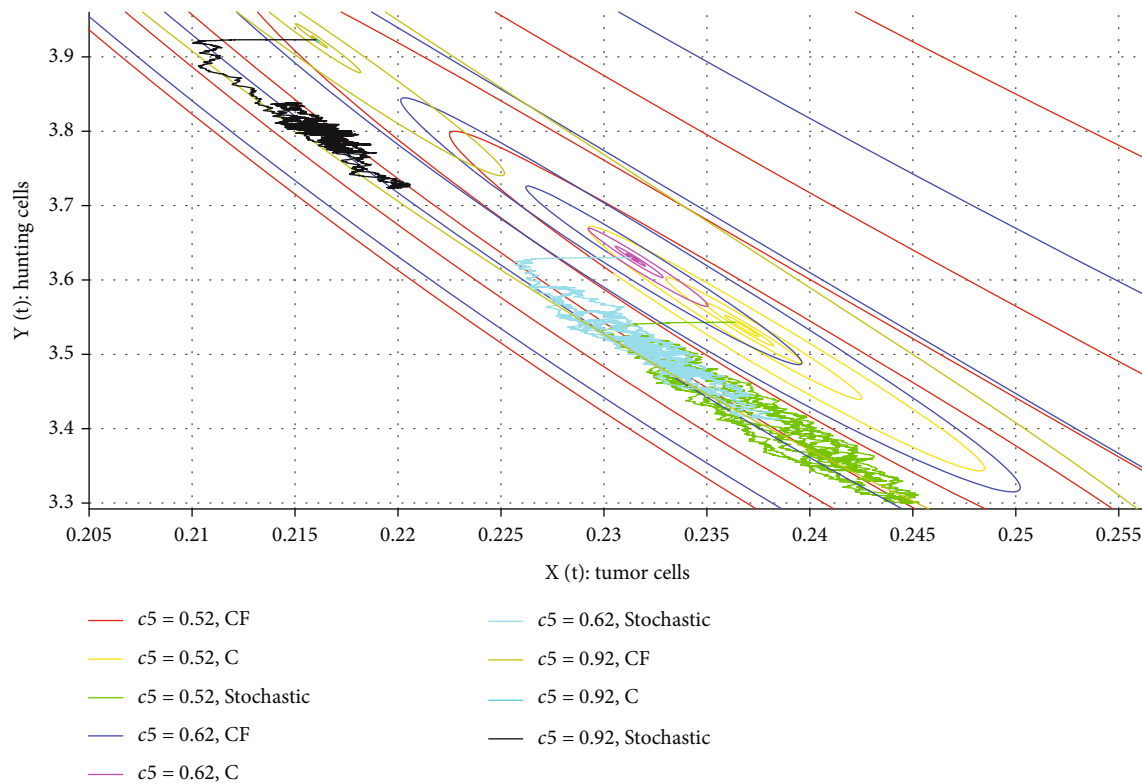


FIGURE 16: Zooming in on the inner part of Figure 15.

Some of the phase portraits for Scenario 2 which is the case for a cross-over from ABC fractional derivatives to the random process of systems in (15) and (16) are depicted in Figures 8–12. In these figures, the effect of different parameter values of c_5 (Figure 8) and the effect of different values of the fractional orders μ (Figures 9–11) are shown.

It can be observed from Figure 8 that by increasing the parameter values of c_5 , the memory effect of the ABC fractional derivative increases. This effect led to a slow increment of the resting cells $Z(t)$, when the number of hunting cells $Y(t)$ is less than one unit, and later on, as the number of hunting cells increased, the number of resting cells decreases until both of them begin decreasing at the same time as shown in Figure 8. This process repeats, and the trajectories spiral inwards and cross-over to randomness.

Some of the simulation results of Scenario 3 are described by piecewise systems (17)–(19); a cross-over from fading memory (Caputo-Fabrizio fractional derivative) to the power-law (Caputo fractional derivative) and then to the random process is depicted in Figures 13–15. These figures show the impact of different fractional orders (Figure 13 and zooming in shown in Figure 14 and different values of the parameter c_5 (Figure 15 and zooming in shown in Figure 16) on the dynamics of the piecewise system described in Scenario 3.

6. Conclusions

The piecewise mathematical model representation of cancer-immune interaction used in this study has exposed a property

that has never been considered or observed in earlier studies using mathematical models based on the classical or different fractional derivatives. The cancer-immune interaction, for instance, showed a cross-over behavior from deterministic to stochastic as shown in the Scenario 1 of this study. We argue that the approach of piecewise mathematical model representation of different real-world dynamic systems is an eye-opener for researchers as the approach has the potential of uncovering hidden properties in the dynamics of a system. In this study, it would have been better to compare the model results with the actual data; it is what the researchers are supposed to consider in future work. It can be contested that the piecewise mathematical model approach is better closer to reality as compared to using only one classical or fractional derivative representation of a dynamic system. This is because of this fact that different dynamical systems have the property that cross-over behaviors cannot be cached without a piecewise mathematical model representation of the system. It is observed from the result of this study that (Scenario 1) the proliferation of the resting cells enhanced by the tumor cells characterized by the term $c_8 XZ/X + K$ is a good target for treatment of the diseases as is shown in Figures 1–5.

Data Availability

No data were generated or analyzed during the current study.

Conflicts of Interest

The authors declare that they have no competing interests.

Authors' Contributions

The authors declare that the study was realized in collaboration with equal responsibility. All authors read and approved the final manuscript.

Acknowledgments

The second author would like to thank Jimma University. Also, the first and fourth authors would like to thank Azarbaijan Shahid Madani University.

References

- [1] A. Atangana and S. I. Araz, "New concept in calculus: piecewise differential and integral operators," *Chaos, Solitons & Fractals*, vol. 145, p. 110638, 2021.
- [2] A. Atangana and S. I. Araz, "Modeling third waves of COVID-19 spread with piecewise differential and integral operators: Turkey, Spain and Czechia," *Results in Physics*, vol. 29, p. 104694, 2021.
- [3] G. Kaur and N. Ahmad, "On study of immune response to tumor cells in prey-predator system," *International Scholarly Research Notices*, vol. 2014, Article ID 346597, 8 pages, 2014.
- [4] M. Farman, A. Ahmad, A. Akgül et al., "Dynamical behavior of tumor-immune system with fractal-fractional operator," *AIMS Mathematics*, vol. 7, no. 5, pp. 8751–8773, 2022.
- [5] S. Ahmad, A. Ullah, T. Abdeljawad, A. Akgül, and N. Mlaiki, "Analysis of fractal-fractional model of tumor-immune interaction," *Results in Physics*, vol. 25, p. 104178, 2021.
- [6] L. G. Depillis, A. Eladdadi, and A. E. Radunskaya, "Modeling cancer-immune responses to therapy," *Journal of Pharmacokinetics and Pharmacodynamics*, vol. 41, no. 5, pp. 461–478, 2014.
- [7] K. P. Wilkie, "A review of mathematical models of cancer-immune interactions in the context of tumor dormancy," *Systems Biology of Tumor Dormancy*, vol. 734, pp. 201–234, 2013.
- [8] Z. Yang, C. Yang, Y. Dong, and Y. Takeuchi, "Mathematical modelling of the inhibitory role of regulatory T cells in tumor immune response," *Complexity*, vol. 2020, Article ID 4834165, 21 pages, 2020.
- [9] K. J. Mahasa, R. Ouifki, A. Eladdadi, and L. de Pillis, "Mathematical model of tumor-immune surveillance," *Journal of Theoretical Biology*, vol. 404, pp. 312–330, 2016.
- [10] S. Khajanchi, "Chaotic dynamics of a delayed tumor-immune interaction model," *International Journal of Biomathematics*, vol. 13, no. 2, p. 2050009, 2020.
- [11] V. A. Kuznetsov, I. A. Makalkin, M. A. Taylor, and A. S. Perelson, "Nonlinear dynamics of immunogenic tumors: parameter estimation and global bifurcation analysis," *Bulletin of Mathematical Biology*, vol. 56, no. 2, pp. 295–321, 1994.
- [12] G. V. Vithanage, H. C. Wei, and S. R. Jang, "Bistability in a model of tumor-immune system interactions with an oncolytic viral therapy," *Mathematical Biosciences and Engineering*, vol. 19, no. 2, pp. 1559–1587, 2022.
- [13] M. A. Dokuyucu and H. Dutta, "Analysis of a fractional tumor-immune interaction model with exponential kernel," *Univerzitet u Nišu*, vol. 35, no. 6, pp. 2023–2042, 2021.
- [14] S. Khajanchi and S. Banerjee, "Stability and bifurcation analysis of delay induced tumor immune interaction model," *Applied Mathematics and Computation*, vol. 248, pp. 652–671, 2014.
- [15] W. Yang, X. Feng, S. Liang, and X. Wang, "Asymptotic behavior analysis of a fractional-order tumor-immune interaction model with immunotherapy," *Complexity*, vol. 2020, Article ID 7062957, 12 pages, 2020.
- [16] N. H. Sweilam, S. M. Al-Mekhlafi, T. Assiri, and A. Atangana, "Optimal control for cancer treatment mathematical model using Atangana–Baleanu–Caputo fractional derivative," *Adv. Difference Equ.*, vol. 2020, no. 1, p. 334, 2020.
- [17] S. Jain and Y. El-Khatib, "Stochastic COVID-19 model with fractional global and classical piecewise derivative," *Results in Physics*, vol. 30, p. 104788, 2021.
- [18] A. Zeb, A. Atangana, Z. A. Khan, and S. Djillali, "A robust study of a piecewise fractional order COVID-19 mathematical model," *Alexandria Engineering Journal*, vol. 61, no. 7, pp. 5649–5665, 2022.
- [19] Y. Cao, S. Alamri, A. A. Rajhi et al., "A novel piece-wise approach to modeling interactions in a food web model," *Results in Physics*, vol. 31, p. 104951, 2021.
- [20] A. Sohail, Z. Yu, R. Arif, A. Nutini, and T. A. Nofal, "Piecewise differentiation of the fractional order CAR-T cells-SARS-2 virus model," *Results in Physics*, vol. 33, p. 105046, 2022.
- [21] M. A. Almalahi, F. Ghanim, T. Botmart, O. Bazighifan, and S. Askar, "Qualitative analysis of Langevin integro-fractional differential equation under Mittag-Leffler functions power law," *Fractal and Fractional*, vol. 5, no. 4, p. 266, 2021.
- [22] D. Zhang, M. S. Saleem, T. Botmart, M. S. Zahoor, and R. Bano, "Hermite–Hadamard-type inequalities for generalized convex functions via the Caputo–Fabrizio fractional integral operator," *Journal of Function Spaces*, vol. 2021, Article ID 5640822, 8 pages, 2021.
- [23] C. T. Deressa and G. F. Duressa, "Analysis of Atangana–Baleanu fractional-order SEAIR epidemic model with optimal control," *Adv. Difference Equ.*, vol. 2021, no. 1, p. 174, 2021.
- [24] S. Rezapour, C. T. Deressa, and S. Etemad, "On a memristor-based hyperchaotic circuit in the context of nonlocal and non-singular kernel fractional operator," *Journal of Mathematics*, vol. 2021, Article ID 6027246, 21 pages, 2021.
- [25] S. Rezapour, C. T. Deressa, A. Hussain, S. Etemad, R. George, and B. Ahmad, "A theoretical analysis of a fractional multi-dimensional system of boundary value problems on the methylpropane graph via fixed point technique," *Mathematics*, vol. 10, no. 4, p. 568, 2022.
- [26] C. T. Deressa, S. Etemad, and S. Rezapour, "On a new four-dimensional model of memristor-based chaotic circuit in the context of nonsingular Atangana–Baleanu–Caputo operators," *Adv. Difference Equ.*, vol. 2021, no. 1, p. 444, 2021.
- [27] S. Etemad, I. Avci, P. Kumar, D. Baleanu, and S. Rezapour, "Some novel mathematical analysis on the fractal-fractional model of the AH1N1/09 virus and its generalized Caputo-type version," *Chaos, Solitons and Fractals*, vol. 162, p. 112511, 2022.
- [28] H. Najafi, S. Etemad, N. Patanarapeelert, J. K. K. Asamoah, S. Rezapour, and T. Sitthiwirattam, "A study on dynamics of CD4⁺ T-cells under the effect of HIV-1 infection based on a mathematical fractal-fractional model via the Adams-Bashforth scheme and Newton polynomials," *Mathematics*, vol. 10, no. 9, p. 1366, 2022.
- [29] R. R. Sarkar and S. Banerjee, "A time delay model for control of malignant tumor growth," in *In National Conference on Non-linear Systems and Dynamics*, vol. 1, pp. 1–5, Riasm, University Of Madras, Chennai, 2006.

- [30] A. Atangana and D. Baleanu, "New fractional derivatives with nonlocal and non-singular kernel: theory and application to heat transfer model," *Thermal Science*, vol. 20, no. 2, pp. 763–769, 2016.
- [31] A. A. Kilbas, H. M. Srivastava, and J. J. Trujillo, *Theory and applications of fractional differential equations*, Elsevier, 2006.
- [32] M. Caputo and M. Fabrizio, "A new definition of fractional derivative without singular kernel," *Progress in Fractional Differentiation & Applications*, vol. 1, no. 2, pp. 73–85, 2015.
- [33] A. Atangana and S. I. Araz, "New numerical approximation for Chua attractor with fractional and fractal-fractional operators," *Alexandria Engineering Journal*, vol. 59, no. 5, pp. 3275–3296, 2020.
- [34] M. Toufik and A. Atangana, "New numerical approximation of fractional derivative with non-local and nonsingular kernel: application to chaotic models," *The European Physical Journal Plus*, vol. 132, no. 10, pp. 1–6, 2017.